The evolution of the Snaefell Volcanic Centre, eastern Iceland.

Hards, Victoria L.

The Evolution of The Snaefell Volcanic Centre, Eastern Iceland.

by

Victoria L. Hards

A Thesis submitted in partial fulfilment of the requirements for the degree of Doctor of Philosophy.

Department of Geological Sciences
University of Durham

July 1995.

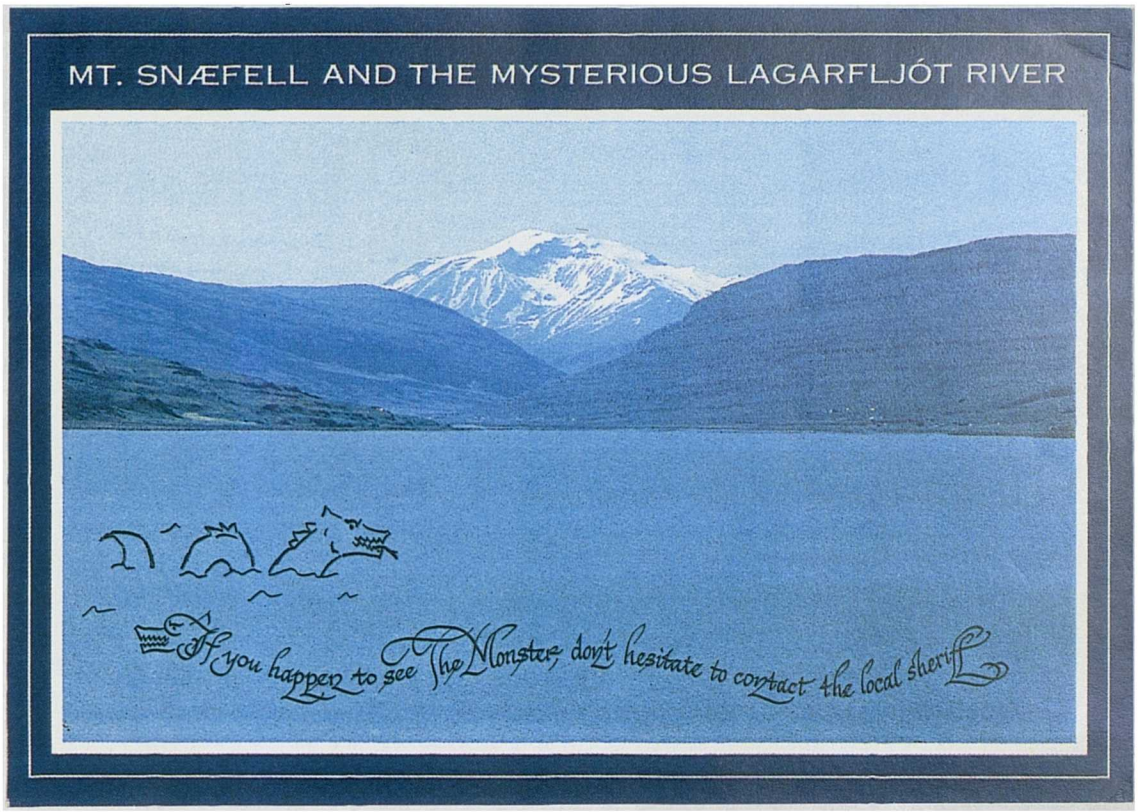

I dedicate this thesis

to

The Lagarfljot Monster.

DECLARATION

I declare that this thesis, which I submit for the degree of Doctor of Philosophy at the University of Durham, is my own work and is not substantially the same as any which has previously been submitted for a degree at this university, or any other university.

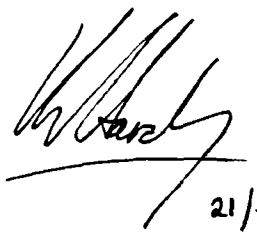

21/7/95.

Victoria L. Hards
University of Durham
July 1995.

ABSTRACT

The Evolution of the Snaefell Volcanic Centre, Eastern Iceland.

Victoria L. Hards, University of Durham.

The Snaefell volcanic centre is located in central-East Iceland, at the northern end of a *flank* or *lateral* volcanic zone, superimposed on the older Tertiary volcanic pile. Snaefell is now considered extinct, although the Bruhnes magnetic signature of its products limits its activity to <0.7Ma. Its activity was dominantly subglacial and most of its products belong to the *moberg* formation of Icelandic geologists. The central mountain was built up by repeated eruptions from an established magma chamber, while the small elongate hills or *tindars* represent single eruptions along the poorly developed fissure swarm of the system. Little or no crustal accretion would have resulted as a result of this activity.

Snaefell is typical of Icelandic flank-zone volcanic centres, in that its products are mildly alkalic and compositionally bimodal, with no true intermediates. Petrographic examination of the series reveals a crystallisation sequence of *ol + Cr spinel, ol + pl, ol + pl + cpx, pl + (ol + cpx), pl + mt (+ cpx),* and finally *alkali feldspar + mt + ol + apatite* in the rhyolites. The first part of this sequence can be quantitatively modelled using the computer program TRACE, although there are some discrepancies, especially in the basalt to basaltic hawaiite range. These can be accounted for by the observation that the Snaefell magmas appear to have fractionated at ~3.5kb (TRACE models crystal fractionation at 1atm) and magma mixing. Magma mixing appears to have been an important process in the evolution of the series, accounting for the ubiquitous presence of complex plagioclase xenocrysts throughout the suite and the linear trends on variation diagrams. There appears to have been little or no crustal involvement in the development of the series.

The alkalic lavas of the Snaefell volcanic system appear to represent the pooled melts of a melting column that extended down into the garnet stability field. The average integrated extent of fusion (i.e. the *point-and-depth average*) ranged from 1 to 5%. The bulk composition of the mantle source appears to have been undepleted or enriched in terms of trace elements, relative to estimates of Bulk Silicate Earth, although not in terms of isotopic character. When Snaefell mafic lavas are compared with examples from the literature of the other mafic lava types in Iceland, correlations between isotopic and trace element enrichment and the degree of melting can be seen. This may be best accounted for in terms of mantle heterogeneity beneath Iceland - i.e. the presence of a relatively depleted MORB-like end member and a more enriched one - and it is proposed that both are integral parts of the Icelandic mantle plume.

Acknowledgements

I would like to thank many individual people and organisations for their help, support, (both moral and financial) that have made this marathon of a job that producing this thesis became, possible at all. If I forget anyone I'll say it now - THANKS!

Firstly, thanks must go to my supervisors; Henry Emeleus, Christine Peirce and Bob Thompson, for support, guidance and putting up with all my strops during the production of this thesis.
To N.E.R.C. for funding.

In Iceland:
To my contacts, Kristjan Saemundsson and Svein Jakobsson for maps, magnetometers, useful discussions and dealing with taxi drivers who can't speak a word of English.
To Karl Gronvold and Niels Oskarsson at the University in Reykjavik, for rescuing me from Snaefell in 1992, and useful discussions and advice in my subsequent visits to Iceland.
To the many wardens - Brynhildur, Ingarossa, Ingeberg to name a few - of the hostel at Snaefell for putting up, ocassionally feeding and generally socialising with (and occasionally mothering!) an eccentric English girl.
Pall Imsland and Armann Hoskuldsson for commiserations on the weather; coffee and tequila.
To Simon Dean, my field assistant over the long, cold summer of 1993. Congratulations on maintaining your sanity after 2 months of my company and all that entailed!
To the Egilsstadir Police for a lift down from Snaefell to Egilsstadir after a rather unfortunate, irreparable incident with the Durham University Lada.

Back in England:
To Ron Hardy, Grand Master of the Durham XRF and XRD machines - you're finally shot of me after 300+ analyses.
To Alan Carr and Gerry for slides and other photographic work.
Julie Southern, Ron Lambert and George Randall (the Dark Lord) for many slides and probe sections.

To Julian Wills, keeper of the ICP-MS at Silwood Park, for help with analyses even when I turned up unexpectedly!
To Tim Hopkins at Manchester, for help and company on two long microprobe sessions.
Dave Stevenson and George Ruth, for resurrecting CG202's computer more times than I can remember.
To those who had the misfortune to share an office with me over the last three years, Mark Wharton, Ian Parkinson (on the night shift), Mehmet Keskin (and for teaching me how to use the computer), Robin Wilson, Nurdane Ilbeyli and Ercan Aldanmaz - thanks for humouring me.
To the other Durham Geology postgrads; Kate, Sue, Sarah, Zoe, Adam, Alun, Wayneee, Chris, Gail, Angus, and anyone else I've omitted(!) for friendship, advice, commiserations, company and drinks at the New Inn, in various measures.
To all my friends, for support, putting up with my long absences and poor communication (and temper) during the production of this thesis.

Lastly, a very special thankyou to my parents for encouragement throughout my studies (and more faith in me than I've ever had in myself!), AND to Andrew Kerr (my second field assistant in addition to everything else!), I don't know what I'd have done without you all.

In God's kitchen

Contents.

Chapter 1 - The Iceland Scenario

Chapter 2 - Physical Volcanology

Appendices

Pocket Contents

Map A1

Topographic map of the Snaefell volcanic centre

Publications (Preprints of):

Hards, V. L., Kempton, P. D. & Thompson, R. N. 1995. The heterogeneous Iceland plume: new insights from the alkali basalts from the Snaefell volcanic centre. *Journal of the Geological Society, London* **152,** in press.

Kerr, A. C., Saunders, A. D., Tarney, J., Berry, N. H. & Hards, V. L. 1995. ,Depleted mantle plume geochemical signatures: no paradox for plume theories. *Geology,* in press.

Units used

Time	
Ma	million years
yrs	years
s	seconds
Distance	
km	kilometres
m	metres
cm	centimetres
mm	millimetres
µm	microns
Å	angstroms
Mass	
Mg	megagrams
kg	kilograms
g	grams
mg	milligrams
Pressure	
Gpa	gigapascals
atm	atmospheres
kb	kilobars
Other	
C	centigrade
K	kelvin
J	joules
mGals	milligals
ppm	parts per million
ml	millilitres
kW	kilowatts
kV	kilovolts
nA	nanoamps
Ω	ohms

Chapter 1
The Iceland Scenario

1.1 Introduction

Iceland is geologically unique; it represents the juxtaposition of a mid-ocean ridge (MOR) spreading centre and a hotspot resulting from the presence of a deep upwelling column of mantle peridotite - a mantle plume (Morgan 1971). It is the longest ridge segment (400km) and largest landmass (103,000km^2) exposed anywhere on a MOR. The presence of the hotspot has resulted in excessive volcanism, producing the anomalously thick (10-15km) Icelandic crust and a divergence from the relative structural simplicity of a normal submarine spreading centre. The subaerial section of the mid-Atlantic plate boundary is wide and complicated, consisting of a series of seismic (*fracture zones* or *transforms*) and volcanic zones - the *axial rift zones* (ARZ) (Einarsson 1991, Saemundsson 1978, 1979). The relative motion of the plate boundary with respect to the stationary hotspot has led to repeated rift jumps (Saemundsson 1974, 1986, Johannesson 1980), propagating rifts and other complexities. The volcanic zones are composed of en-echelon arrays of elongate units called *volcanic systems* (Jakobsson 1979a), each consisting of a *central volcano* - the site of repeated voluminous eruptions - transected by a *fissure swarm.* Volcanism and seismicity are, however, not confined to the plate boundary. There are also superimposed, intraplate volcanic zones known as *flank* or *lateral zones* (Jakobsson 1972, Saemundsson 1978). Magma productivity in these is low and crustal accretion negligible. The Snaefell volcano, on which this study centres, is located in one such zone.

Iceland is distinct from submarine MORs in the diversity of its volcanic products; some 10% of the exposed lava pile is made up of evolved - intermediate and acidic - rocks (Saemundsson 1978). Evolved rocks are rare on normal ocean ridges and at other hotspots such as Hawaii (Marsh et al. 1991). In Iceland they occur mostly in the vicinity of the central volcanoes. Three petrological series are present: tholeiitic, transitional alkalic, and alkalic (Jakobsson 1979a), in order of decreasing volume; the latter two types are extremely rare on normal ocean ridges and limited to Iceland's flank zones. The lavas of Iceland are additionally chemically distinct from those of MORs; they are relatively enriched in incompatible elements, with high $^{87}Sr/^{86}Sr$ $^{206}Pb/^{204}Pb$ $^{3}He/^{4}He$ and low $^{143}Nd/^{144}Nd$. Schilling (1986) and many others have

attributed these features to sources within a deep mantle plume. Regular variations in the geochemistry of the basalts across Iceland led Sigvaldason et al. (1974) to suggest that the hotspot is presently centred on central-east Iceland, which agrees with geophysical studies (e.g. Tryggvason et al. 1983).

1.2 The Iceland hotspot

1.2.1 The plume hypothesis and the North Atlantic region

The excessive volcanism which gave rise to the early Tertiary continental volcanism prior to the opening of the North Atlantic, and subsequently the development of the Iceland transverse ridge, can be explained by the presence of a stationary mantle "hotspot", such as first proposed by Wilson (1963). Morgan (1971) subsequently developed the idea further into the plume hypothesis, which has been extensively applied to Iceland and the N Atlantic (e.g. Schilling 1973, Vogt 1974). It assumes a narrow upwelling plume of hot, relatively primordial material originating at depth from a thermal boundary layer. For stronger upwellings, such as the Iceland plume, this is probably the core-mantle boundary (Loper 1991, Campbell & Griffiths 1992). The plume remains essentially stationary, relative to plate motion, thus producing a volcanic trace on the plates as they move over it. The Iceland plume may have first impinged on the base of the lithosphere at around 64Ma, the onset of the voluminous outpourings in west Greenland (White 1988, White & McKenzie 1989, Eldholm and Grue 1994), with the impact of a so-called "starting plume head" (e.g. Hill 1991). More recently, however, a volcanic track back to ~130Ma has been proposed from reconstruction of plate motions (Lawver & Muller 1994). Nevertheless, it is only the most recent history of the plume with which this study is concerned (figure 1.1).

1.2.2 Consequences of the presence of the hotspot

The proximity of a hotspot to a spreading centre is thought to result in channelling of plume material beneath the section of the ridge closest to the hotspot, thus resulting in excessive volcanism and the production of thicker crust (Vink 1984). Over the last 50Ma, the Iceland transverse ridge was produced. Once the hotspot underlay oceanic lithosphere, heating and thinning it, the spreading ridge appears to have jumped from

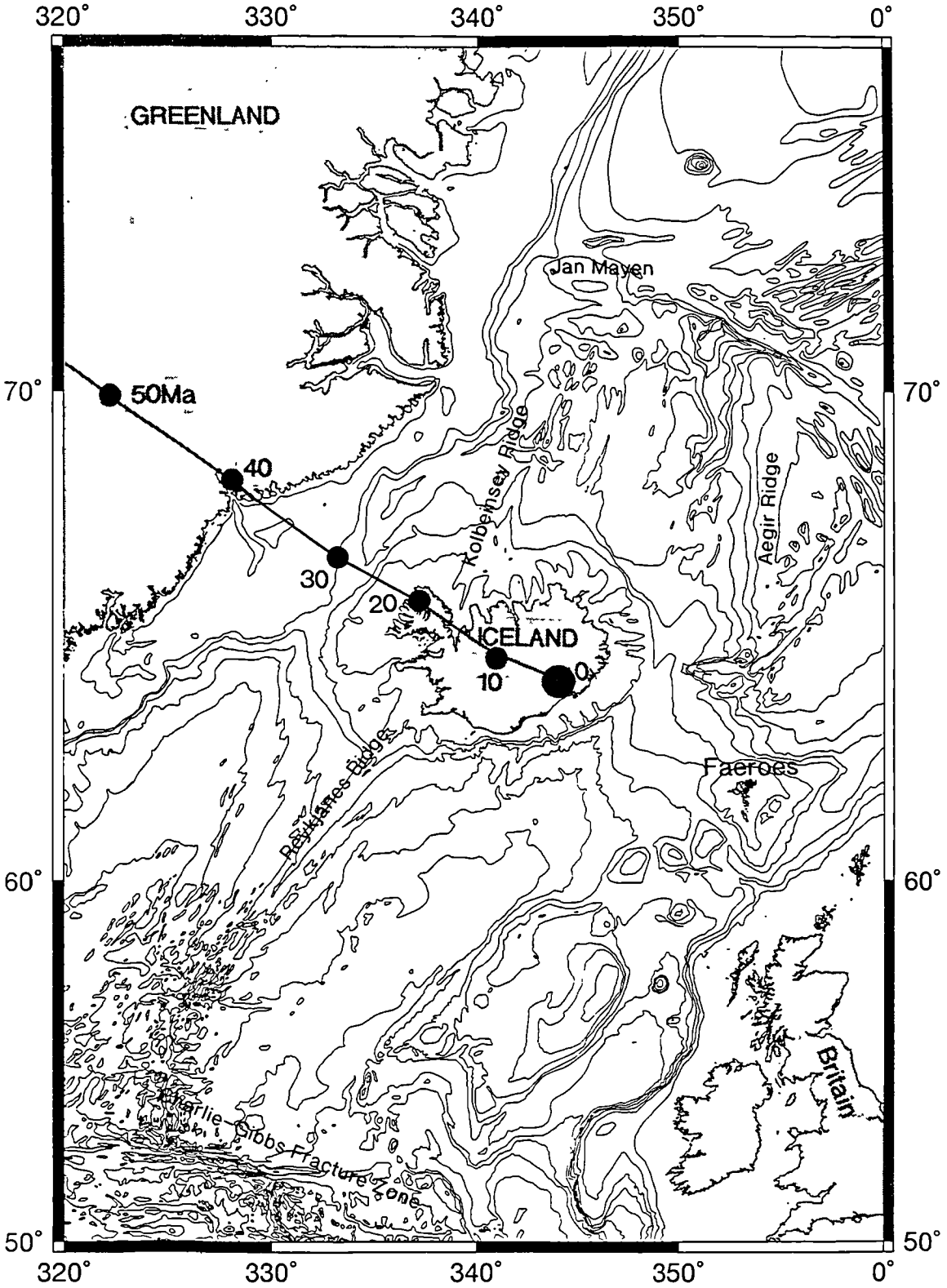

Figure 1.1 Bathymetric map of the North Atlantic region, showing the proposed trace of the Iceland hotspot over the last 50Ma (Lawver & Muller 1994). Contours at 0, 200, 500m and at 500m intervals thereafter. Diagram constructed using GMT (Wessel & Smith 1991) with data from the GEBCO digital atlas (IOC, IHO & BODC 1994).

the Aegir ridge (figure 1.1), westwards, to focus on the hotspot (~chron 13 time, 36Ma). Thus, by at least chron 6 time (20Ma), sea floor spreading was occurring in its present configuration. At some point there appears to have been an increase in volcanic output, initiating the formation of the Iceland block. Estimates for the time at which this occurred range from 19.5 to 35.5Ma (Saemundsson 1986) and it is possible that there is a causative connection between this and the focusing of the spreading axis over the hotspot.

The most obvious indications of the presence of anomalously hot mantle beneath the region throughout its history is the thick crust on the Iceland transverse ridge. It varies in thickness from 30-35km on the Iceland-Faeroe ridge, around 25km on the Greenland-Iceland ridge and around 15km beneath Iceland itself, away from the axial rift zones (Flovenz & Gunnarsson 1991). This contrasts markedly with normal oceanic crust at around 7km. The most extensive feature, however, is the broad swell which produces anomalously shallow bathymetry over most of the Atlantic N of 30°N, attaining a maximum of 2.5km uplift over Iceland (Bott 1988). This swell has been attributed to the presence of abnormally hot mantle. Heat flow measurements across the Cape Verde hotspot are 25% higher than normal oceanic lithosphere of the same age and, from petrological studies of the igneous rocks in Iceland and Hawaii, the plume temperature is calculated to be ~200°C in excess of ambient mantle (Sleep 1990). The buoyancy fluxes of hotspots have been calculated from the swell shape and cross-sectional area (Sleep op. cit.) and the figure obtained for Iceland was $1.4Mgs^{-1}$, similar to that obtained for Cape Verde, but significantly less than Hawaii, the strongest at $8.6Mgs^{-1}$. The N Atlantic region also coincides with a major global geoid high, centred near Iceland, covering a similar region to the uplifted topography (figure 1.2a). A high can also be seen in the global gravity map (figure 1.2b). These anomalies are attributed to dynamically supported mass anomalies associated with mantle convection, caused by mantle flow away from the high pressure hotspot (Bott 1988).

1.2.3 The Icelandic asthenosphere

Detailed geophysical studies have indicated anomalous mantle beneath Iceland and have been used to delineate the three dimensional structure of this. Teleseismic P-wave arrival-time data were subject to a 3D tomographic inversion (Tryggvasson et al. 1983) and revealed a chimney-shaped, low velocity zone extending down to at least 375km (figure 1.3), with a diameter of around 175km at 175-275km depth. This study also indicates that the hotspot is centred on central-east Iceland, corresponding

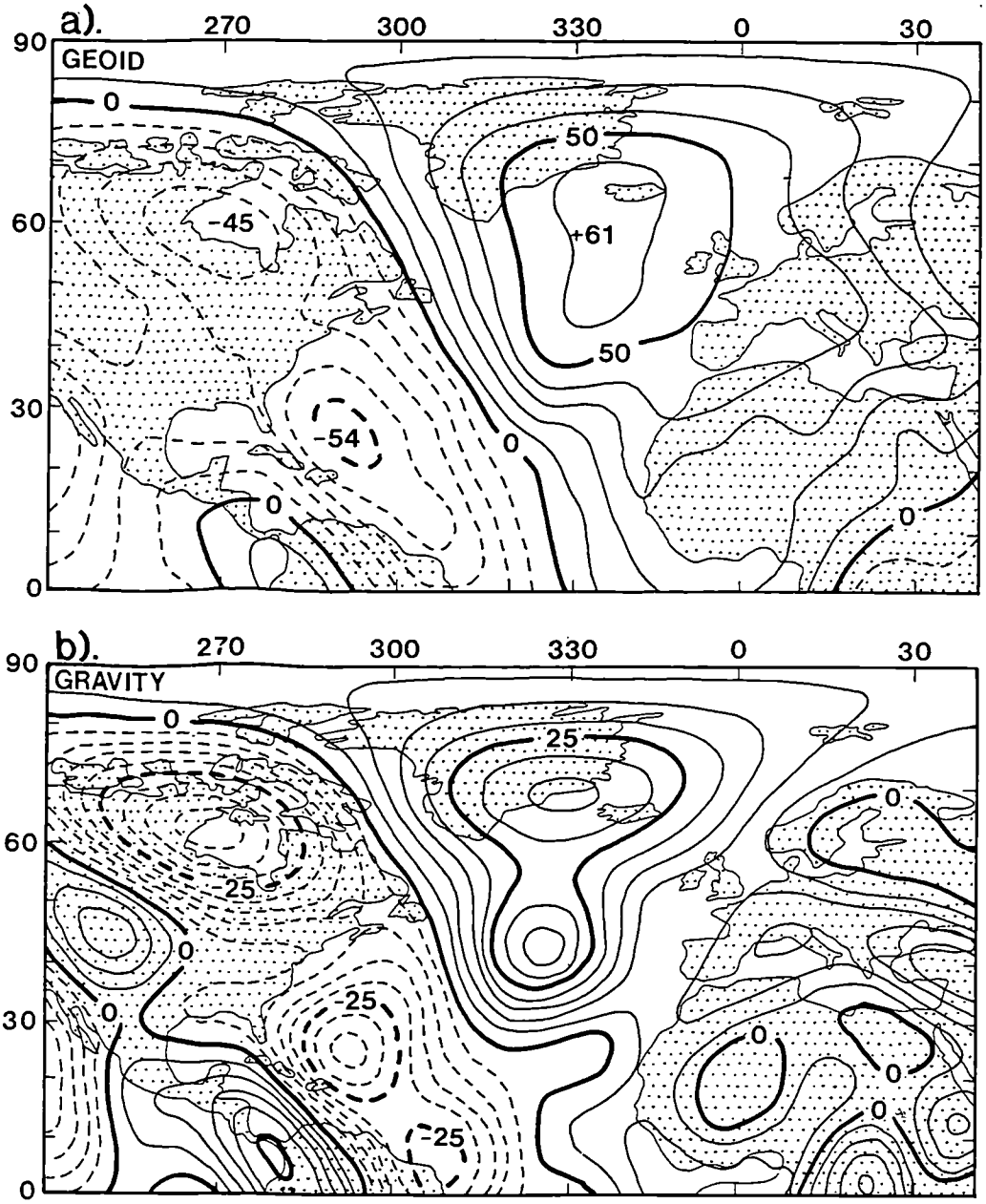

Figure 1.2 (a) The long wave-length geoid anomaly of the North Atlantic and adjacent regions, showing a pronounced high over Iceland and the Azores to the south. Contours at 5m intervals (b) The long-wavelength gravity map of the North Atlantic and adjacent regions. Note the high over the NE Atlantic. Contours at 5mGal intervals. Both maps reproduced from Bott (1988).

to the region of maximum volcanic output along the axial rift zone (Saemundsson 1979). By combining laboratory measurements of seismic velocity and attenuation with depth variations of observed surface wave velocities, Sato et al (1989) estimated temperature and melt fractions present beneath Iceland (table 1.1). An upwelling plume with a potential temperature of 1550°C should cross its solidus at ~110km, to give a cumulative melt fraction of ~30% beneath a mid-ocean ridge, corresponding to a crustal thickness of ~22km, which fits the crustal thickness of the Greenland-Iceland ridge fairly well (Ryan 1990).

Depth (km)	**Temperature** (°C)	**Melt fraction** Xm(%)
30	1260	
45	1310	7*
60	1370	
85	1470	5
100	1530	
>105	1550	<1

*Averaged from 30-60km.

Table 1.1 Temperature and melt fraction estimates for the Icelandic asthenosphere (Sato et al. 1989, Ryan 1990).

The low-velocity zones detected below 110km, therefore pose a problem, and Ryan (op. cit.) has suggested that grain boundary softening and incipient melting triggered by volatiles can account for this. Partial melt accumulation at shallow levels, capping this low-velocity axial region (figure 1.3), is inferred from both magnetotelluric studies (Beblo & Bjornsson 1978, 1980 and Beblo et al. 1983) and the combined interpretation of seismic and resistivity data (Schmeling 1985). The anomalous layer detected is 5km+ thick and has a resistivity of 5-10Ωm, corresponding to a temperature of around 1100°C[1] - within the melting range of basalt. This layer has been shown to rise beneath active central volcanoes (e.g. beneath Krafla it reaches 7km) and descend away from the axial rift, reaching 20-25km depth at 120km distance. Ryan (1990) has equated these geophysically defined, active asthenospheric diapirs in Iceland with the former mantle upwelling zones detected by structural studies in the peridotites of the Oman ophiolite, where they show a regular spacing of ~50km. The major axes of the Oman structures are aligned with the palaeorift zone, and vary from 10-20km in length. The average spacing between the central volcanoes in Iceland's ARZs is about 33km, and probably this may correspond to the optimum wavelength for the rising domes of the low density melt impregnated layer, resulting from *Rayleigh-Taylor instability* (Ryan 1990).

[1]Caution should be exercised in using purely electrical data to estimate mantle temperatures, since modelling such data does not provide a unique solution. Recent work by Menke & Levin (1994) on Icelandic shear-wave data has put the temperature in the lower crust at about 875-950°C.

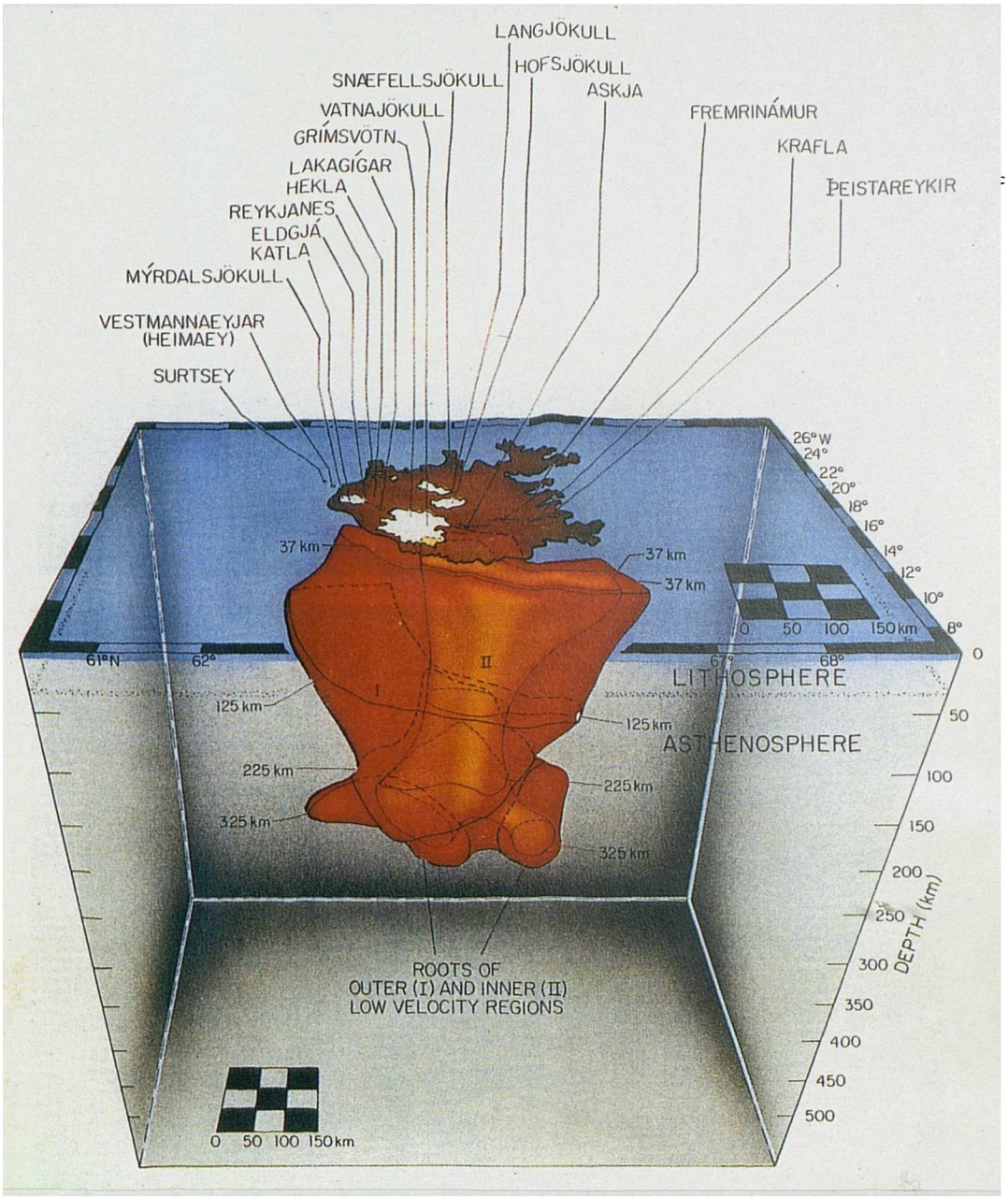

Figure 1.3 Westward view of a three-dimensional representation of the structure of the local anomalous low-velocity zone (the plume) beneath Iceland, from teleseismic compressional-wave tomography (Ryan 1990, Tryggvasson et al. 1983). The outer volume (I, amber to orange), corresponds to compressional wave velocities depressed by up to 2% relative to global means. The brighter yellow inner volume (II) corresponds to velocities depressed by more than 2%. In the upper levels (37-125km) the arcuate structural influence of the mid-Atlantic ridge can be seen. Beneath this (225-325km depth range) the structure becomes more columnar and classically plume-like, with a diameter of ~175km. In the inner zone, melting and the establishment of an interconnected melt network begins at ~110km. This melt rises, driven by positive buoyancy forces within inferred porous media flow, to accumulate at the base of the crust (see text).

1.3 The geology of Iceland

1.3.1 Stratigraphy

In verti cal section ~1500m of extrusives is exposed, and this is thought to be underlain by a further 2000-5000m. The volcanic pile is composed of 80-85% basalt, 10% evolved rocks (acid and intermediate) and 5-10% sediments of volcanic origin in the Tertiary; the sediment fraction increases locally in the Quaternary (Saemundsson 1979). The oldest rocks are found in NW Iceland and are 16Ma (Moorbath et al. 1968), which appears anomalously young when compared with the adjacent sea-floor age as determined from magnetic anomalies. This may be explained by the significant overlaps of subaerial lavas, combined with the fact that the dated sample came from the uppermost 1000m of the exposed pile.

Conventionally the volcanic pile is divided into four stratigraphic units, based on climatic evidence from sedimentary horizons and magnetic reversals, supported by radiometric dating (see timescale of LaBreque et al. 1977). The four groups are:

Postglacial	<13,000yrs.
Upper Pleistocene	13,000yrs-0.7Ma, i.e. the Bruhnes polarity chron.
Plio-Pleistocene	0.7-3.1Ma, including the Matuyama epoch and the Gauss epoch as far back as the Mammoth event.
Tertiary	<3.1Ma.

1.3.2 The Tertiary

Tertiary rocks cover ~50,000km^2 (figure 1.4), and form a monotonous series of subaerial tholeiites displaying little lithological variation. Most of our current knowledge of the structure of the volcanic pile comes from the work of G. P. L. Walker (1955-1965) in eastern Iceland, summarised by Walker (1974). The lavas dip gently towards the axial volcanic zones and appear to thicken down-dip, ranging from around 9° at sea level, to almost horizontal at 700m. They appear to wedge out laterally, away from axis. In gross structure the volcanic pile appears to have grown as a series of lenticular units extruded from the elongate volcanic systems; their greatest thickness being attained in the region of the central volcano. ~55 central volcanoes are known or suspected in the Tertiary lava pile, which given lifespans ranging 0.3->1Ma (Saemundsson 1979), with an average of 0.7Ma which means that only around three would have been active at any one time (Gudmundsson 1986).

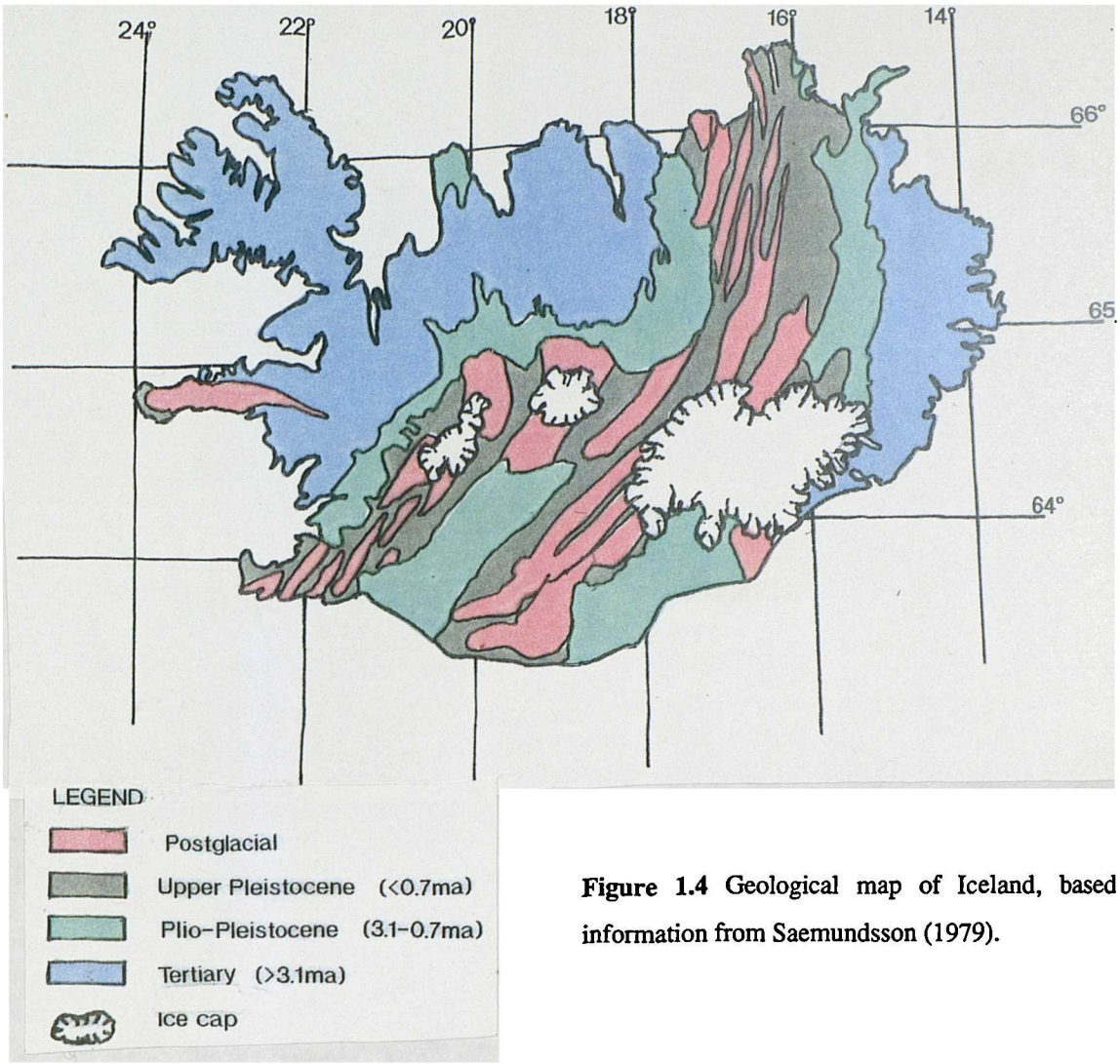

Figure 1.4 Geological map of Iceland, based on information from Saemundsson (1979).

The central volcanoes are characterised by concentrations of acid rocks, high fossil geotherms, hydrothermal alteration and irregular dips in the lava pile, resulting from the rugged palaeotopography (Walker 1974). Large plutons up to 10km^2 in aerial extent occur in the roots of deeply eroded examples. Such magma bodies, tens of cubic kilometres, are unlikely to be able to generate space for themselves at depths of only 1-3km below the surface without the roof failing frequently and magma ascending to the surface. Thus, by implication these plutons must be extinct magma chambers; and indeed many are associated with swarms of inclined sheets, dips ranging 5-90° which appear to have originally acted as feeders to overlying lavas (Gudmundsson 1995). Associated with these intrusions are swarms of sub-parallel, sub-vertical dykes. Swarms reach 10 x >50km in size (Saemundsson 1978), and contain 100's of individual dykes. One profile, Eyjafjordur, examined by Gudmundsson (1995) contained >1,000, ranging in width 0.02m-28.5m (average ~5.4m). Generally, the dyke density increases with depth, and therefore erosion levels, in the crust.

These volcanic systems, described above, are found buried as entities. This indicates that they grew over a stationary magma source, and then moved away, off axis, to become extinct and incorporated into the plate.

1.3.3 The Plio-Pleistocene

Rocks of this age cover ~25,000km^2 (figure 1.4), and appear to have been generated by much the same pattern of volcanism as prevailed in the Tertiary. Interbedded tillites in SE Iceland, however, indicate climatic cooling and the onset of glaciation (Saemundsson 1979). The subglacial environment resulted in an uneven topography of elongate ridges composed of pillows and breccias, collectively referred to as the Palagonite formation (Icelandic *moberg)* and an increase in the amount of detrital material. Volcanism at this time was not confined to the axial rift, but also occurred in two superimposed flank zones. These are the Snaefellsnes zone in the west, which produced alkalic lavas, and the Skagi volcanic zone in the north west, which produced transitional lavas (Sigurdsson et al. 1978).

1.3.4 The Upper Pleistocene

This series covers an area of ~30,000km^2 and is essentially identical to the present-day neovolcanic zones (NVZ). The boundary between this series and the underlying Plio-Pleistocene is, in most places, marked by an unconformity of unknown duration (Saemundsson 1979). The volcanic rocks may be divided into two groups: the first is a series of subaerial basalts formed in the interglacial periods, known as the "grey basalts" (Icelandic *gragryti),* while the second group is the subglacial palagonite formation, (section 2.2). Rocks belonging to this series can mostly be related to presently-active or dormant volcanic systems (figure 1.5). Some 29 systems can be identified[2] in the NVZs, and perhaps 15-20 have developed central volcanoes. This represents an increase by a factor of 5 over the number active during similar periods in the Tertiary. Gudmundsson (1986) proposes that this is due to the presence of thick interbeds of basaltic breccias and other clastics formed during the Plio-Pleistocene which, as they become buried in the volcanic zones may encourage the formation of magma chambers (and thus central volcanoes) due to their differing elastic properties.

[2]Estimates of the number of volcanic systems in the neovolcanic zones, both active and extinct, varies widely from author to author. Saemundsson (1979) put this figure at 30, and subsequently radio echo-soundings appear to have ruled out the existence of volcano at Breidabunga, thus reducing the figure to 29.

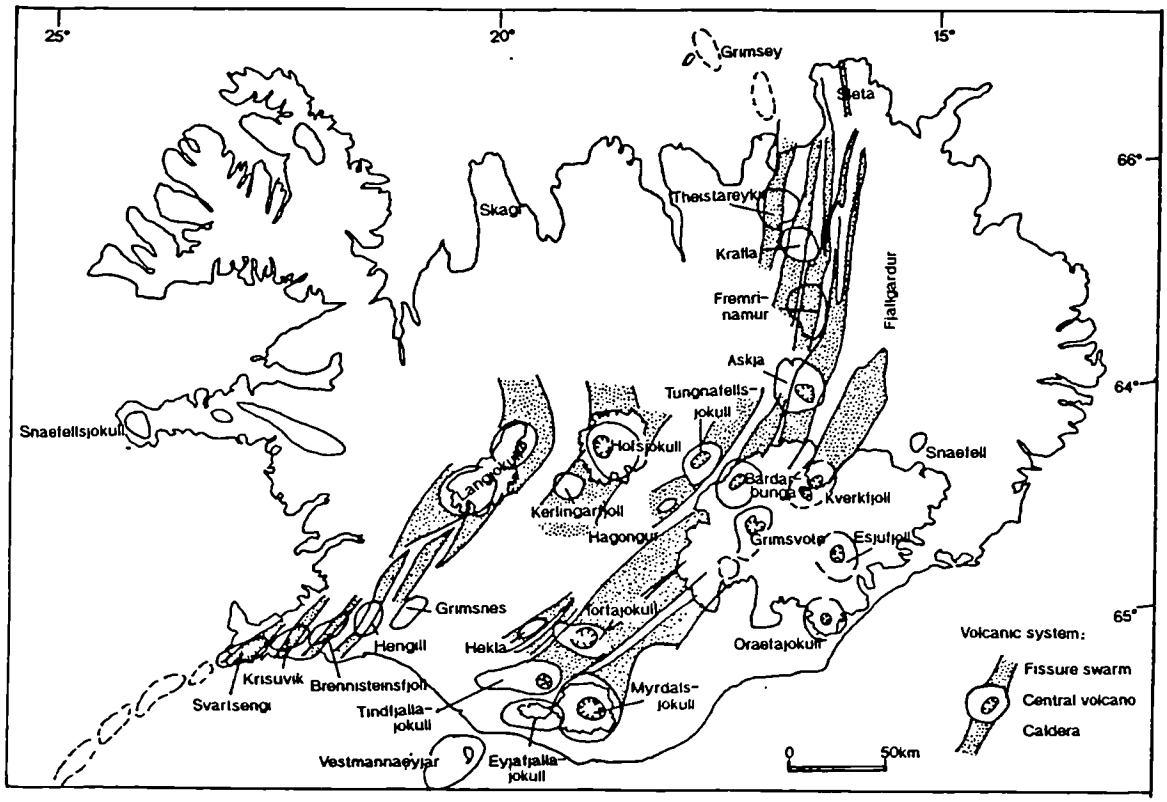

Figure 1.5 Recognised volcanic systems in the neovolcanic zones (NVZs) which have been active in the Upper Pleistocene and postglacial period (<0.7Ma). The locations of well developed central volcanoes and calderas are marked. Stippled areas are fissure swarms, notably absent outside the axial rift zones (ARZs).

1.3.5 The Postglacial

This comprises a series of subaerial lavas, pyroclastics and fluvioglacial outwash deposits. There are possibly 25 active volcanic systems which have produced some 400-500km^3 of lava, covering an area of 12,000km^2 (Saemundsson 1979). Four of those identified in the NVZs - Fjallgardur, **Snaefell,** Geysir and Grafingshalar - are now considered extinct and having no *recorded* postglacial activity. Around 90% of the products are basaltic, and 10% acidic, of which most was erupted in the flank zones. Around 85% of the lava was erupted in the axial rift zone (ARZ), while 15% was erupted in the flank zones (Saemundsson 1978).

1.4 Tectonics

The tectonic regime in Iceland is dominantly controlled by its position on the mid-Atlantic ridge (MAR), with extensional features predominating. The mean half-spreading rate over the last few Ma is around 1cm/yr. in the direction N100°E (Bjornsson 1985). In detail, the tectonic pattern is complicated due to the presence of the hotspot, and the NVZs comprise both ARZs (sites of active rifting) and flank or lateral zones, where rifting is inconspicuous. Fractures offsetting the spreading axis to the east, further complicate the pattern (figure 1.6).

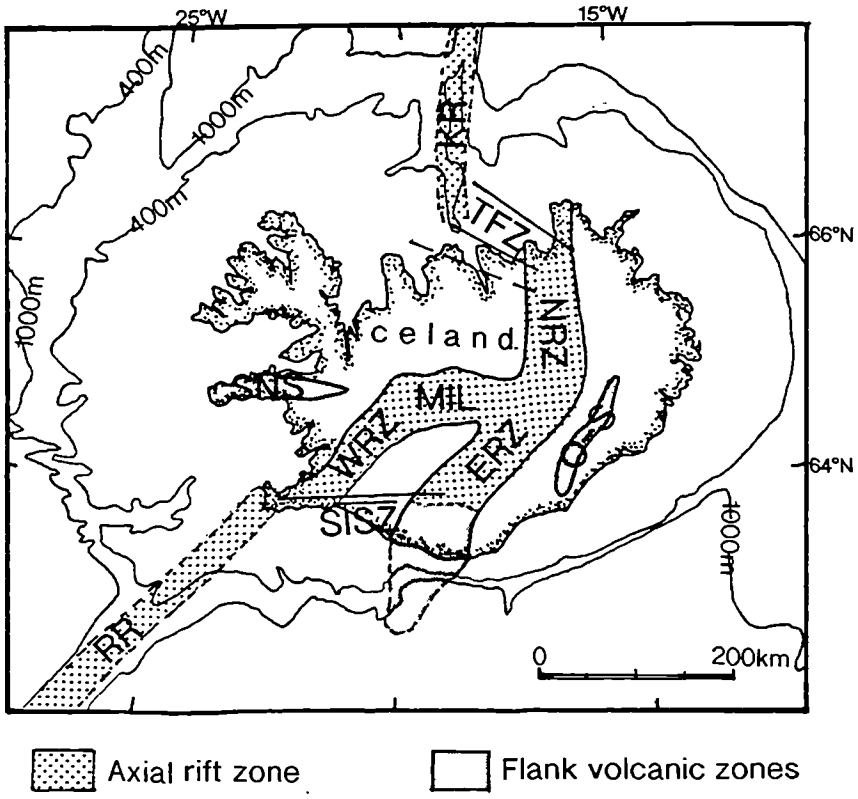

Figure 1.6
Simplified tectonic map of Iceland, showing the neovolcanic zones - axial rift zones (ARZs) and flank zones - and fracture zones. Abbreviations as follows:
RR = Reykjanes Ridge,
SISZ = south Iceland seismic zone,
WRZ = western rift zone,
MIL = mid-Iceland line (a leaky transform),
NRZ = northern rift zone,
ERZ = eastern rift zone,
TFZ = Tjornes fracture zone, KR = Kolbeinsey ridge, SNS = Snaefellsnes volcanic zone and O-S = Oraefajokull-Snaefell zone.

1.4.1 Axial rift zones (ARZs)

The ARZs are defined as comprising rocks formed within the Bruhnes magnetic epoch (Saemundsson 1986) and they mark the present trace of the plate boundary where crustal accretion is occurring. This presently includes the western rift zone (WRZ) and the northern rift zone (NRZ); the northern section of the eastern volcanic zone (ERZ) also, can probably included. These actively rifting segments are linked to each other within Iceland by the central Iceland volcanic zone or mid-Iceland line (MIL), a leaky transform, and to the MAR by two fracture zones, the Tjornes fracture zone (TFZ) to the north and the south Iceland seismic zone (SISZ) to the south.

The ARZs erupt tholeiitic lavas, and the overall discharge rate has been $40km^3/1000yrs$ in postglacial time (Jakobsson 1972, 1979a). The ARZs are characterised by linear extensional features (Saemundsson 1974) and a high geothermal gradient; 100°C/km is indicated from borehole data (Palmason 1981). The flanking lava pile youngs and dips towards them.

Fracturing and deformation is concentrated in the fissure swarms, which can be up to 30km wide and >100km in length (Saemundsson 1978). Their trends vary between branches of the ARZ and they usually form en-echelon arrays that may be either dextral or sinistral. Fissure swarms comprise hundreds of tensional fractures ($\sim10^2m$ long), normal faults with vertical hades ($\sim10^3m$ long) and volcanic fissures of similar length (Gudmundsson 1995). In any particular fissure swarm, the number of tensional fractures exceeds that of either normal faults or volcanic fissures. Most tensional fractures are limited to the uppermost few hundred meters of the crust, and below this down to ~1km, steeply dipping normal faults are the dominant extensional structures. At greater depths, dykes gradually take over as the dominant extensional structures and probably continue down to the base of the crust. Normal faults with hades of up to 60° are also seen, along with rare cross-trending faults of vertical hade and similarly oriented eruptive fissures. Fissure swarms are also the site of continuous subsidence, estimated at 0.5-1cm/yr (Saemundsson 1978) along the trend of the ARZ; and this approximately keeps pace with volcanic extrusion. The subsidence leads to graben formation, with most of the downthrow (up to hundreds of meters), on the marginal faults. Although these show a vertical hade at the surface, many are probably listric at depth. Most fissure swarms focus on a central volcano, the site of maximum productivity; together they constitute a volcanic system (Jakobsson 1979a), many of which are petrologically distinct (Gudmundsson 1995). Some 20 of these have been identified in the ARZ (figure 1.5), (Saemundsson 1986).

The central volcanoes are the foci of frequent eruptions, often of acid and intermediate rocks that are lacking in the fissure swarms. Many central volcanoes, perhaps most, are fed by shallow crustal magma chambers at 1-3km depth, which can be detected by seismic studies (Brandsdottir 1994). These chambers act as traps for upward propagating dykes from a deeper reservoir at the crust/mantle boundary (Gudmundsson 1995). Despite their high productivity, most central volcanoes have low topographic relief and may be classified as composite shield volcanoes (Williams et al. 1983). Around 10 of the central volcanoes in the ARZ have developed calderas (with a diameter of 5-10km) and associated cone-sheet swarms (Saemundsson 1979).

Monogenetic basaltic volcanoes are also present in many volcanic systems, in the form of lava shields in the postglacial, and table mountains formed beneath the Pleistocene ice sheet (Gudmundsson 1995).

1.4.2 Crustal accretion

Rifting and crustal accretion in Iceland occurs in discrete episodes lasting a few years, interspersed with periods of repose lasting >100yrs. (Palmason 1986). Nevertheless, a volcanic eruption occurs every five years or so, although only three since 1724 are thought to have been associated with rifting. Along a single fissure swarm, or part of it, it appears that a rifting episode will occur every 100-150yrs. The most recent such episode occurred in the northern part of the Krafla fissure swarm (1975-1984). It was composed of 21 separate rifting events, 9 of which were accompanied by volcanic eruptions. The total dilation across the fissure swarm was ~9m and the vertical displacement 1-3m (Gudmundsson 1995). Tensional stress builds up in the repose period, in response to continued plate divergence. Crustal separation in these periods is thought to proceed by continuous stretching, which should be detected in long-term gravity changes, tilt variations and geodetic measurements (Saemundsson 1986). It appears to take ~100yrs for tensional stress to build up to the critical level, and that the trigger for rifting may be a magmatic event in a central volcano (Saemundsson 1979).

A quantitative model of the events occuring during a rifting episode was developed, and tested on the results of the recent Krafla rifting episode, by Gudmundsson (1995). He proposes that most of the regional dykes are injected from the deep-seated reservoir at the base of the crust, while most inclined sheets are injected from crustal magma chambers. The loaded crustal segment is much longer than it is thick, so that failure will spread laterally, explaining the observed lateral migration of earthquakes. Magma flows vertically into the failure zone, some of which may meet a crustal chamber in which case it will pond there. At some later time, it may trigger injection of sheets and/or dykes - the observed inflation and deflation events. Failure may begin at any point along the fissure swarm, but, most commonly does so where the crust is thinnest, especially if a magma chamber concentrating stress is present. It appears from the existence of volcanic systems *without* well developed central volcanoes that the presence of a magma chamber is not a pre-requisite for rifting to occur, but the lack of one increases the repose period to up to ~1000yrs (Bjornsson 1985). Rifting events will continue until the (mostly relative) tensile stress in the segment of the divergent plate boundary concerned, is dispersed.

1.4.3 Rift jumping

As a result of the relative movement of the plate boundary over the essentially stationary hotspot - for which rate estimates vary from 0.75cm/yr to 0.3cm/yr, (Johannesson 1980, Steinthorsson et al. 1985) - the Iceland rift system (subaerial section of the MAR, figure 1.5) has never achieved a stable long-term configuration, but has "jumped" repeatedly eastwards. Thus the axial rift currently remains focused on the underlying hotspot, the centre of which is now located about 240km to the east of the logical site of the North American - Eurasian plate boundary, a line connecting the Reykjanes ridge to the south directly with the Kolbeinsey ridge to the north (Lawver & Muller 1994). This "ridge capture" (Sleep 1990) only occurs if, as in the case of Iceland, the hotspot peridotite flux is comparable to or in excess of the material normally supplied to a significant length of the ridge axis (Johannesson 1980, Vink 1984).

It appears that during the last 16Ma rift jumping has occurred on two scales, although these are probably just "end members";

1). Large-scale relocations, 100-200km, leaving the old complex volcanic zone as part of the plate. These appear to have occurred about every 2Ma (e.g. Saemundsson 1974, Johannesson 1980).

2). Small-scale lateral shifts in either direction, ranging from a few hundred metres to ~40km, in the location of the accretion axis, which have occurred more frequently than the large-scale relocations (Helgason 1984,1985, Foulger & Long 1984), figure 1.7.

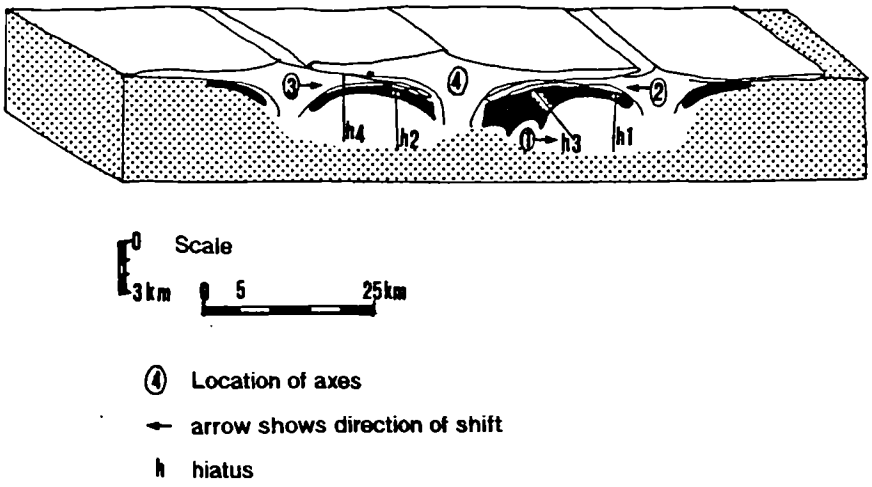

Figure 1.7 Schematic diagram showing the result of frequent small-scale lateral shifts of the volcanic zone, demonstrating the resultant widespread blanketing of older by younger lavas. As a result, these shifts may only be detected by the presence of small anticlinal structures. The location of each axis is marked by numbered circles, of which the most recent is (4). Based on Helgason (1985).

Several features of the Icelandic crust that do not fit Palmason's (1971, 1981) model (which assumes a single, time-averaged plate boundary) can be explained by rift jumping and were summarised by Helgason (1985): **(1).** the irregular depth distribution to seismic layer 3; **(2).** the lack of uniform vertical composition of the crust; **(3).** the abnormal variations in stratigraphic thickness of lavas erupted during chron 5 time in western, northern and eastern Iceland and; **(4).** the relatively shallow burial of extinct Tertiary volcanic centres in eastern Iceland.

The large-scale relocations of the axial rift can be traced by mapping the regional dips in the lava pile, which form shallow synclines and low anticlines (Saemundsson 1974, 1978, 1986, Johannesson 1980). The synclines are interpreted as previous locations of the axial rift, having formed by crustal extension and downsagging.

The suggested evolution of the rift zones and crustal accretion is summarised in figure 1.8, and an account is presented here, based on Johannesson (1980).

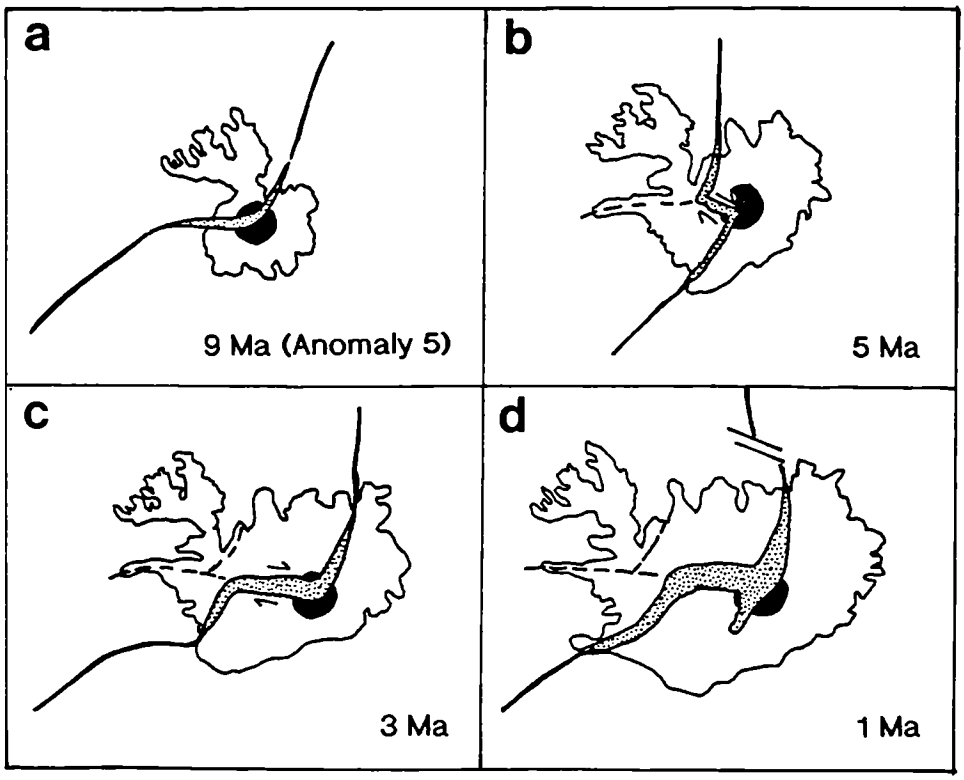

Figure 1.8 Evolution of the Iceland rift system (IRS) over the last 9Ma. Shaded areas indicate active rift zones; heavy lines show their submarine continuations; dashed lines show the sites of extinct rift zones and the black dot shows the location of the hotspot with respect to the IRS. Reconstruction based mainly on the work of Johannesson (1980), together with Saemundsson (1974) and Steinthorsson et al. (1985).

The Snaefellsnes rift zone appears to have been active from around 16Ma to at least 6.7Ma. The southern part appears to have become extinct around 5-6Ma, and a new rift formed further east (the precursor of the WRZ), linked to the northern part of the original rift zone by a fault zone. The northern part of the zone became extinct at

around 3-4Ma and a new rift, the precursor of the present day NRZ, formed 150km to the east. The two rift zones were linked by a leaky transform, the precursor of the MIL. At around 2Ma, rifting and volcanic activity began to propagate southwards from the NRZ, to form what is now the ERZ. Most recently the Kolbeinsey ridge, north of Iceland, jumped westwards to its present position (Saemundsson 1978); a set of en-echelon fissure swarms east of Grimsey Island (figure 1.5) now connects the Kolbeinsey ridge with Iceland's NRZ. At the present day, two rift zones - the WRZ and ERZ - appear to behave in a complementary manner, thus, the WRZ shows low magma productivity, its products being compositionally restricted to primitive olivine tholeiites, while the ERZ produces evolved quartz tholeiites. The tectonics and volcanism here are thought to imply an on-going rift jump (Saemundsson 1986).

Helgason (1984, 1985) proposes the occurrence of small-scale lateral shifts in the rift zone and, from his work in eastern Iceland, suggests that most of the shifts there were westwards. The most recent of these shifts occurred during the Bruhnes polarity chron in NE Iceland. It involved a 40km westwards displacement of the rift axis from the Fjallgardur volcanic system to its present location (figure 1.5). Volcanism here produced a 150km-long subglacial ridge; its lack of a central volcano implying that it was short-lived. Older shifts of this scale are often masked by the blanketing effects of later lava flows (figure 1.7). Small anticlinal structures may be the only clue that remains as to the direction of the shift in a poorly dissected section. Elsewhere in Iceland, a small shift of around 5km in the location of the Hengill central volcano is noted to have occurred at around the same time (Foulger & Long 1984).

1.4.4 Flank zones

Volcanism in Iceland also occurs away from the axes of crustal accretion (the ARZs), in *flank* (Jakobsson 1972) or *lateral* (Saemundsson 1978) volcanic zones with poorly developed extensional features. There are presently three such zones: the Snaefellsnes volcanic zone, the southern tip of the ERZ and the Oraefajokull-Snaefell zone in SE Iceland - about which little is known. Their volcanism appears to extend back only as far as the Plio-Pleistocene; no Tertiary equivalents are known for certain (Saemundsson 1979).

Flank-zone volcanics lie unconformably on the older lava pile that suffered at least minor erosion prior to the deposition of the younger eruptives. Flank zones also contrast petrologically with the ARZ, in that they erupt transitional to alkalic lavas. The volume production decreases markedly with increasing alkalic affinities of the magmas (Jakobsson 1972). In postglacial times, the flank zones account for just 15%

of total volcanic production in the neovolcanic zones, although their production of silicic lavas exceeds that of the ARZs. The production rate is also extremely varied, being lowest in the Snaefellsnes zone and peaking in Myrdalsjokull (Katla), which is estimated to have produced up to 35km^3 in postglacial time (Saemundsson 1978). Most central volcanoes in the flank zones form large stratovolcanoes, cone shaped (e.g. Snaefellsjokull) or elongate parallel to the fissure trend (e.g. Hekla, Eyafallajokull). Many have a large summit crater and sometimes a caldera. The life span of these volcanoes is poorly known. The main structural differences between these zones and the ARZs results from the difference in their tectonic regimes. Large-scale tensional faults and graben formation are absent from the flank-zones, indicating that crustal separation is negligible. As a result they form some of Iceland's most prominent mountains. The extra load of these volcanic edifices appears to be compensated on a regional scale, as is indicated by the regional thickening of seismic layer 2 (Saemundsson 1978).

The Snaefellsnes volcanic zone has an EW trend and is composed of three WNW-ESE volcanic systems (Sigurdsson 1970). It has a very low productivity of ~0.6km^3/1000yrs in postglacial times (Jakobsson 1972). The zone has been interpreted in terms of N-S horizontal extension (Saemundsson 1986), or alternatively a dextral shear zone - a leaky transform (Sigurdsson 1970).

In southern Iceland the tip of the propagating ERZ can be classified as a type of flank zone (Jakobsson 1972). From the rate of rotation of the dying WRZ (the strikes of the ERZ and WRZs differ by 12-16°) a propagation speed of 3.5-5cm/yr has been calculated (Foulger et al. 1993). The two rift zone are connected by the SISZ, which accommodates the differential movement between. It contrasts with typical oceanic transforms, in that it is made up of a broad, complex fault zone (20 x 80km), due to the unstable nature of the stress fields. Broadly, the SISZ shows left-lateral deformation, which results from right-lateral motion on many NS faults. The zone is subject to major earthquake series (M6-7), running from the east to the west, every 80-100yrs as it migrates south in response to the southwards propagation of the ERZ (Foulger et al. op. cit.). The trends of volcanic axes through stratovolcanoes on land (e.g. Hekla and Eyafallajokull), and the tectonic fracture pattern associated with Surtsey, are controlled by the SISZ (Saemundsson 1986).

1.5 The Snaefell volcano

1.5.1 The Oraefajokull-Snaefell volcanic zone

The Oraefajokull-Snaefell zone is a line of stratovolcanoes 40-50km east of the ARZ, in the eastern Vatnajokull region (figure 1.9).

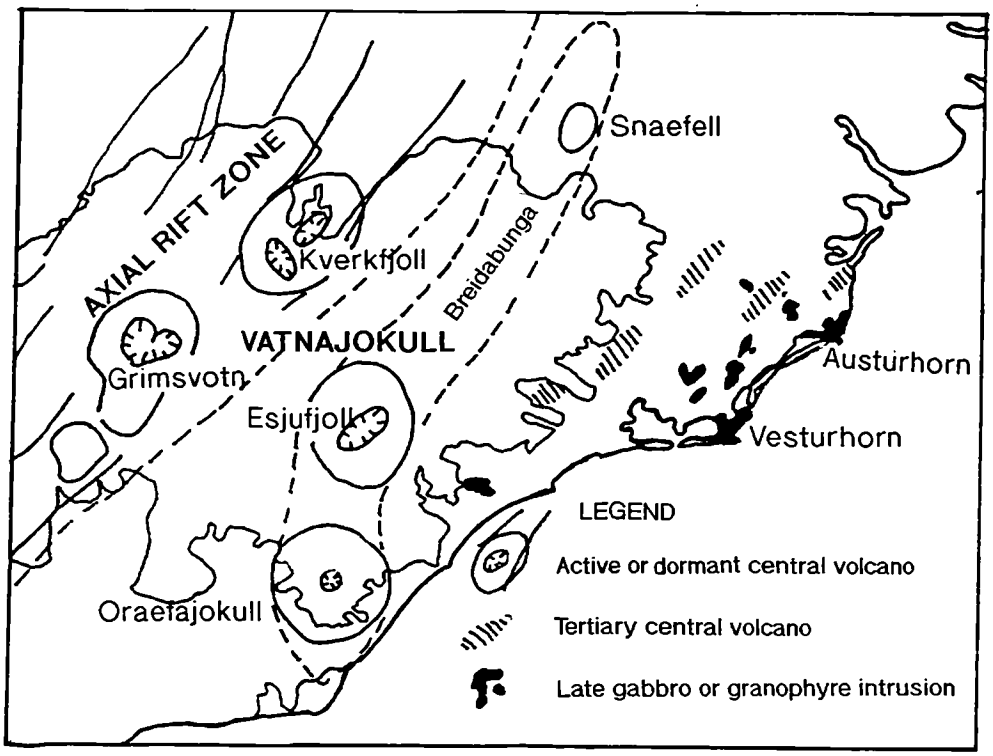

Figure 1.9 Map of the SE Vatnajokull region of Iceland, showing the present day Oraefajokull-Snaefell volcanic zone and major intrusions. These gabbro and granophyre intrusions may have formed in the roots of stratovolcanoes, later superimposed on the lava pile. Their relationship to the axial rift zone at the time of formation was probably similar to that of the Oraefajokull-Snaefell zone today. Modified from Saemundsson (1986).

The existence of the zone was first proposed by Walker (1975), who connected the existence of the historically active Oraefajokull with: **(1).** the young moberg mountains to the north of Vatnajokull (Snaefell) and; **(2).** intraglacial eruptions that occurred between the two, giving rise to the moberg deposits beneath some valley glaciers in SE Iceland. The zone was thought (Saemundsson 1979) to include two volcanoes either partially (Esjufjoll), or wholly (Breidabunga) buried beneath the ice sheet. Subsequently, radio echo-soundings have been carried out across Vatnajokull (Bjornsson & Einarsson 1990) and no support can be found in the topographic data obtained for the existence of a volcano at Breidabunga.

Oraefajokull rises to 2119m, making it the highest point in Iceland, and it is covered by a separate ice cap which merges into the southern edge of Vatnajokull. It is almost circular in shape, with just a slight N-S elongation, and it has a 500m-deep summit caldera (Bjornsson & Einarsson 1990). Eruptive fissures cannot be traced outside the limits of the volcanic cone and no fissure swarm, such as seen in the ARZ, is present (Prestvik 1985). Compositionally the lavas belong to the transitional alkalic series of Jakobsson (1979a). It has been active in the postglacial period and has been the site of two historical eruptions, one in 1362 and a second in 1727, both of which resulted in *jokulhlaups* (glacier floods) on various rivers (Thorarinsson 1958, Bjornsson & Einarsson 1990). At present it is considered quiescent, having a low seismicity.

A caldera has been suggested at Esjufjoll on the basis of a satellite image (Thorarinsson et al. 1973). It appears that the centre is still active, since minor seismicity has been recorded from the area and a jokulhlaup on Jokulsa a Breidamerkursandi in 1927 has also been tentatively linked to Esjufjoll (Bjornsson & Einarsson 1990).

Snaefell itself, has no *recorded* historical activity, is not thought to have erupted postglacially, and is thus considered extinct (Saemundsson 1979). It is a NNE-SSW elongate stratovolcano, surrounded by smaller moberg hills, and rises to 1833m, making it the highest point in Iceland outside Vatnajokull. Aside from a report on the state of its glaciers and small, permanent icecap (Jennings 1952), there is no published work on the centre, so this study starts from scratch!

1.5.2 The origins of the Oraefajokull-Snaefell zone

It has been suggested that a similar line of volcanoes existed in the Tertiary, also offset to the east of the ARZ (Saemundsson 1979, Torfason 1979). Evidence comes from the presence of large gabbro and granophyre intrusions, up to 20km^2 in aerial extent, in SE Iceland (figure 1.9). These are thought to have formed the roots of stratovolcanoes, long since eroded away from the top of the lava pile. They cross-cut the host lavas, have few associated minor intrusions, and appear unrelated to active rifting. Radiometric dating reveals that they are 4-6Ma younger than the bedrock. The latter is around 10-11Ma, which corresponds to the intrusions being formed ~50km offset from the active accretion axis of the time (Torfason 1992). This distance is consistent with the offset of the present-day Oraefajokull-Snaefell zone from the ARZ. It is possible that structural effects (such as the suppression of volcanic activity by the local stress fields associated with ARZ volcanic centres) prevent the development of

further volcanic centres in parallel zones within 50km along each flank of the ARZ (Torfason op. cit.).

This flank zone also closely parallels the ARZ in the zone of maximum volcanic discharge across the Iceland hotspot (Tryggvason et al. 1983) and a causative connection has been suggested (Saemundsson 1979). The transitional nature of the Oraefajokull volcanics suggests a similar tectonic setting to that of volcanic centres in the ERZ, such as Katla. The ERZ is a propagating rift, at the tip of which (Surtsey) more strongly alkalic rocks are erupted. Thus the Oraefajokull-Snaefell zone probably represents a spreading centre frozen in the early stages of development and it is the opinion of the author that this zone represents a relatively small-scale failed rift jump, section 1.4.3. From the plume structure, as delineated by the work of Tryggvason et. al. (1983), it can be seen that the zone lies almost directly over the plume conduit at depth. Thus it is a feasible position for a future spreading axis. One hypothesis (for which there is no real evidence at present) might be that the flux of the plume itself is waning, and thus the rift jump to the Oraefajokull-Snaefell zone failed. The "switching off" of activity at Snaefell, might be connected with the most recent small-scale rift jump, westwards from the Fjallgardur volcanic system (NW of Snaefell) to its present position (Helgason 1985).

1.5.3 The aims of the current study

Since nothing at all is really known about the centre, the first aim is to classify the volcanic rocks and deduce their evolution - in terms of both eruptive environment and chemical composition - and to reconstruct the development of the volcano and its magmatic plumbing. The results will then be used to interpret the development of the centre in terms of the tectonics of Iceland, and to look into the physical and volcanic processes occurring in Iceland as a whole. Finally, it is hoped that this study sheds further light on the composition of the Icelandic asthenosphere (i.e. the mantle plume) and melting processes operating therein.

1.6 Summary

1). Iceland results from the superimposition of a mid-ocean ridge spreading centre over a hotspot or mantle plume. The long-term existence of the latter is signalled most obviously by the abnormally thick crust over Iceland and along the Greenland-Iceland-Faeroes ridge. On a broader scale, there are coincident bathymetric, geoid and gravity anomalies encompassing the whole North Atlantic region, with their maxima around Iceland. On a more localised level, the existence of a mantle plume has been invoked to explain the compositionally anomalous lavas on and around Iceland. Seismic studies on Iceland itself locate a columnar body of anomalous low-velocity material going down to at least 375km. Combined resistivity and seismic studies suggest that this columnar structure is capped by an accumulation of partial melt, lying at the base of the crust.

2). The subaerial portion of the mid-Atlantic ridge is much wider and more complex than its submarine analogue. It consists of a series of volcanically active rifting zones, linked by transform faults. Volcanicity and seismicity are not entirely confined to the plate boundary, but also occur in flank zones. Little crustal widening occurs in these zones, which have poorly developed extensional features and marked topographic expression. Volcanic productivity is also often significantly lower, and the products often have marked alkaline affinities.

3). The Snaefell volcano, the subject of the present study, lies at the northern end of one such zone, 50km to the east of the present site of active rifting. This study aims not only to reconstruct the evolution of this volcano, but also to add to our present understanding of this type of volcanism, and hotspot magmatism in general.

Chapter 2
Physical Volcanology

While the main emphasis of this study was the geochemistry of the lavas from the Snaefell suite, field work on the volcanic system was not limited to sampling alone. Mapping and volcanological studies were an essential part of this project, especially since there has been no previous detailed study on the area. Therefore, the aims of this chapter are to describe and discuss the volcanological structures observed. It intends to focus on the environments and modes of formation of the structures and lithologies at Snaefell, comparing them with examples from the literature. The sampling strategy will also be discussed and the results of mapping presented.

2.1 The Snaefell volcanic system

Snaefell stands 1833m high and as such is the highest peak in Iceland outside the ice cap, Vatnajokull. The Snaefell volcanic system is now considered extinct (Saemundsson 1979), having no *recorded* historical activity, and its activity is confined to the last 0.7-0.8Ma by the Bruhnes magnetic signature (Kristjansson et al. 1988) of its products. These unconformably overlie the Plio-Pleistocene volcanic pile (Johannesson & Saemundsson 1989), which form a plateau at 700-800m dipping gently to the west, - towards the plate accretion axis. The stratigraphic hiatus between is of unknown length, although activity is assumed to have ceased previously within the Matuyama epoch (0.8-2.4Ma); this will be discussed in section 2.5. Thus the bulk of the underlying lavas appear to have reversed magnetic polarity. This provides a simple field distinction between the two lava sequences. Nevertheless, there are exceptions, and lavas were probably erupted during one of the normal-polarity geomagnetic events within the Matuyama epoch, of which there are now thought to have been five (Kristjansson et al. 1988).

The system's volcanic products belong dominantly to the *"moberg"* formation[1] of Icelandic geologists (Kjartansson 1959); for which a subglacial origin has been accepted since early this century (Peacock 1926). Snaefell itself may be classified as a central volcano, since it was both the site of repeated eruptions and produced highly evolved lavas towards the end of its lifetime. These were first observed, although then thought to be a dyke, by Thoroddsen (1905). As is typical of Icelandic volcanics, the system is bimodal. The few compositionally intermediate lavas are banded, streaky hybrids. The small aligned basaltic hills surrounding Snaefell are the products of single eruptions along the system's short, poorly developed fissure swarm. This point has been verified with chemical analysis of samples, as have all subsequent statements that materials are "cogenetic".

Viewed from the south, Snaefell itself (plate 2.1) morphologically resembles the classic *table-mountains* or *stapi* seen in Iceland (such as Herdubreid to the north-west, figure 2.1).

Plate 2.1 Snaefell from the south, the smaller hill in the foreground is Thjofahnjukar. Note the tablemountain-like profile of Snaefell, rising steeply to a platform at ~1600m, then more gently to a small peak. Photograph - H. G. Ljosm, 29/8/1986 (taken from Ferdafelag Islands, Arbok 1987).

It has relatively steep sides rising to a structural platform, consisting of flat-lying sheet flows, at 1550-1650m before rising more gradually to its summit. This appears to consist of a north-south ridge with three small cinder cones(?) along it. The height of

[1]The English term most widely used for this is the "palagonite formation" because of the large amounts of palagonite - hydrated basalt glass - in the tuffs. Rittman (1962) attempted to replace this term with "hyaloclastite" having recognised that many examples contained fresh glass. The term "hyaloclastite", however, has genetic significance, implying that the tuff was formed by non-explosive spallation off the pillow lavas as they formed. As will be demonstrated in later sections, this is not entirely true. Therefore in this study the Icelandic term will be used. All such terms are strictly limited to basaltic material by most authors, and also in this study.

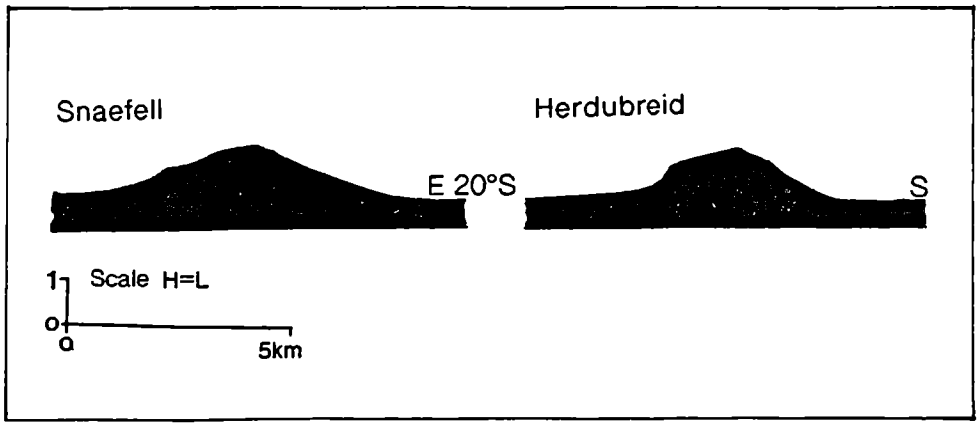

Figure 2.1 Profiles of Snaefell and Herdubreid, constructed from topographic maps (Thorarinson 1958). Note the similarity.

the platform is significant because it indicates the height at which the volcano broke through the ice sheet, thus putting the thickness of the ice sheet at around 1600m during this period. This estimate agrees remarkably well with the topography of the ice sheet as deduced by Walker (1965), shown in figure 2.2.

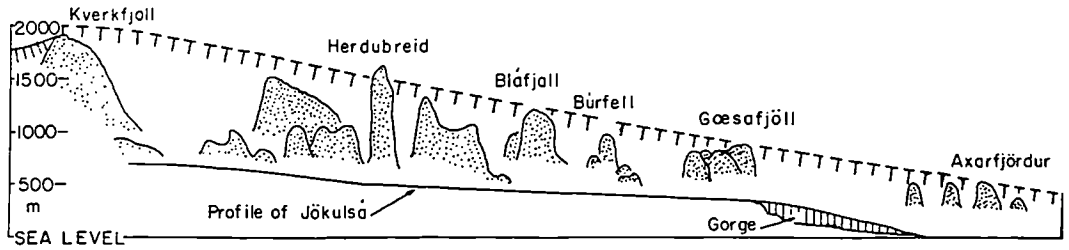

Figure 2.2 Profile from Kverkfjoll north to Axarfjordur showing the present elevation of subglacial volcanoes and how they can be used to define the surface of the Pleistocene ice sheet (from Walker 1965). Snaefell lies to the east of this profile, just south of Herdubreid. The height of the platform in Snaefell's structure indicates that eruption became subaerial at around 1600m, corresponding well with Walker's profile.

Originally, the morphology of Snaefell would have been more uniform, whereas now it has been diversified by glaciation. The summit is covered by a permanent ice cap, and there are four true small glaciers and three further areas mantled by firn (Jennings 1952). Figure 2.3 shows their state in 1937. Over the past half century there appears to have been some glacier retreat but, due to the bad weather and heavy snow cover in the summers of 1993 and 1994, this was difficult to assess. There are two well developed corries, one to the north east and a composite one to the north west (plate 2.2), which cuts deeply into the mountain and provide useful insights into its construction. Erosion over most of the study area is relatively shallow, and thus the majority of the rocks seen are probably extrusives. Glaciation has, however, stripped away the tuffs to a sufficient level to reveal the internal structure of the smaller,

monogenetic hills. Scree and moraines produced by glacial activity mantle many of the slopes, concealing boundaries between eruption units and probably many other features.

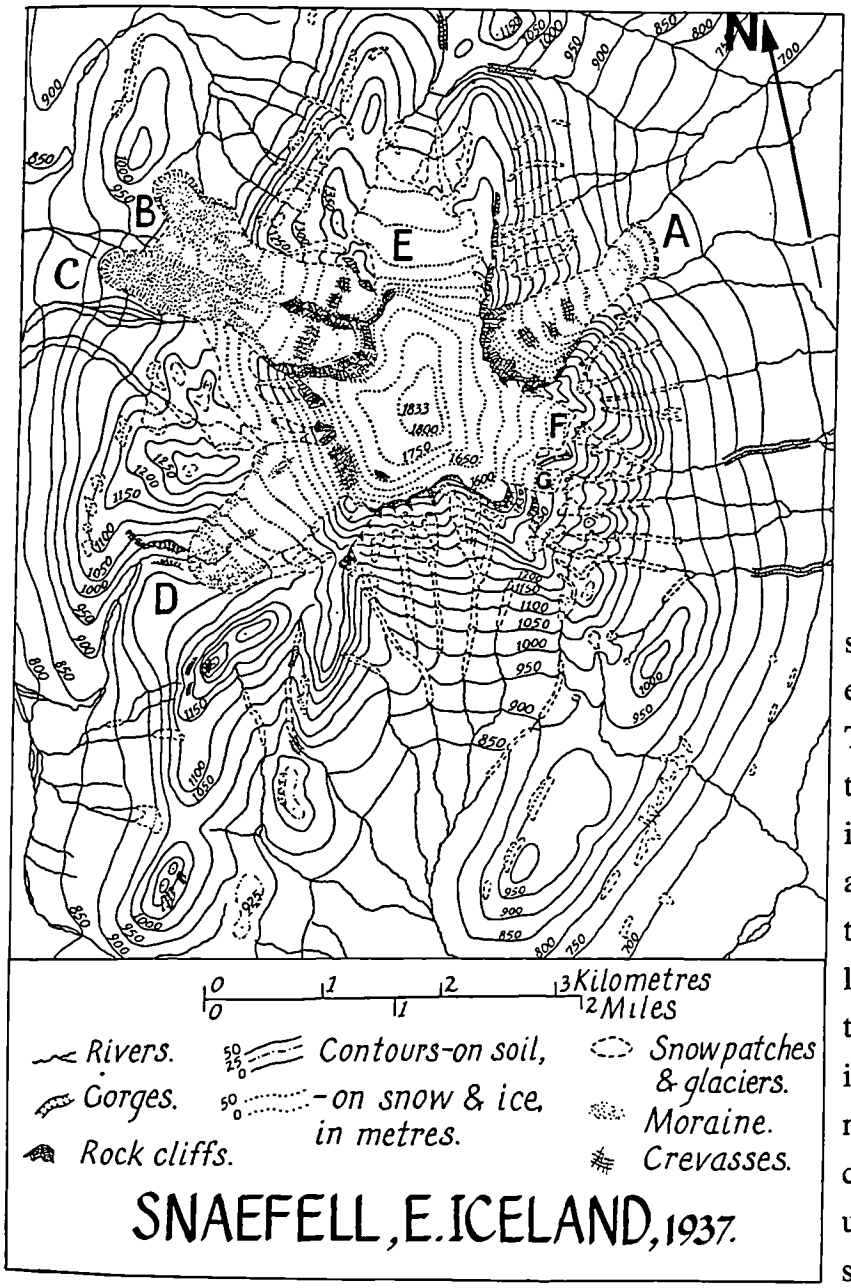

Figure 2.3 Map of the glaciers on Snaefell in 1937, from Jennings (1952). Of the true glaciers A, B and C lie in corries, and C and D feed directly from the permanent summit ice cap. E, F, and G are not true glaciers, E is a *firn* field and F and G are extensions of the summit firn. Today the state of the glaciers is much the same, see text.

Activity in the system was not entirely subglacial. The initial eruptions took place in an interglacial period and produced at least two fairly extensive lava flows. Higher up the succession, intercalated with the more lithologically complex subglacial units, are several subaerial flows (plate 2.3), indicating that the ice sheet varied in thickness over time and at some points may have retreated completely.

A map of the volcanic system (scale ~1:75,000), resulting from work done in this study, is presented (figure 2.4). This distinguishes subglacial, subaerial, basic and acidic extrusives. A stratigraphic column has not been drawn up, since this is very much an example of "heap geology" (K. Gronvold, pers. comm. 1993) and thus a stratigraphy in the classic sense is not present. It should also be noted that *all* boundaries - although

depicted by solid lines are *inferred* - since most are concealed by scree. The overall NE-SW trend of the system is marked.

Plate 2.2 Snaefell from the West, showing the composite corrie divided by a rhyolite buttress, glaciers B and C, with the moraine of glacier C (figure 2.3) in the foreground.

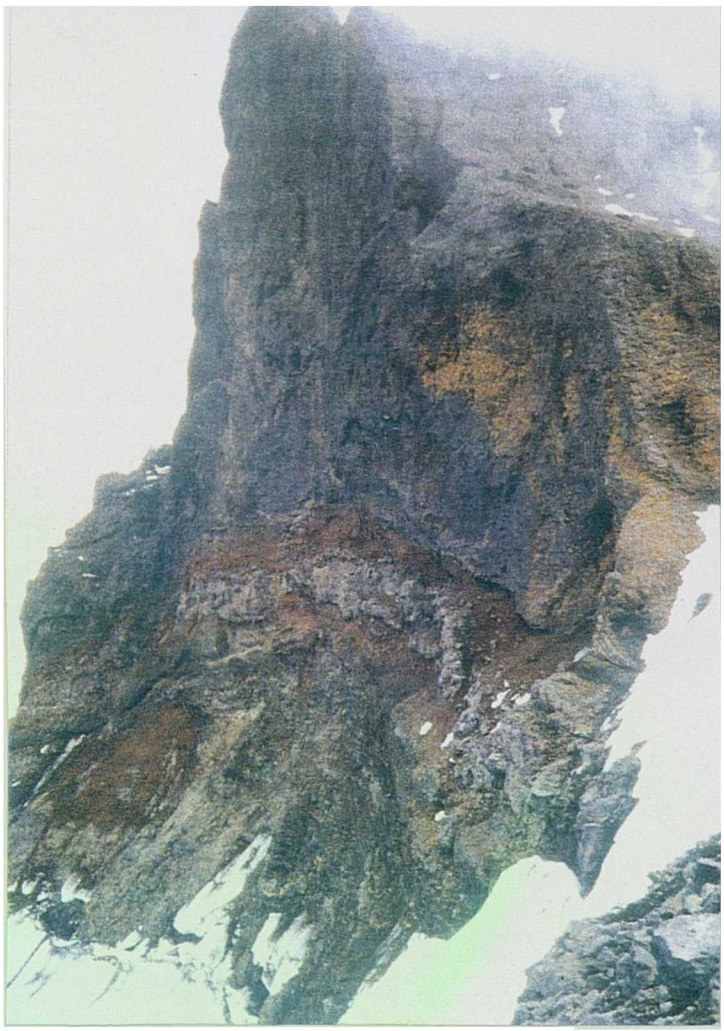

Plate 2.3 Exposure in the backwall of corrie of glacier C; showing a subaerial flow unit intercalated with the more lithologically complex subglacial products. Note the distinctive horizon of reddened (oxidised), bedded scoria which overlies the pale grey subaerial lava flow. (Scale - cliff height ~20m.)

Figure 2.4

Geological map of Snaefell constructed as a result of this study (Scale ~1:75,00). The NE segment was constructed with the help of A. Gudmundsson. Due to the nature of the terrain *all* boundaries, although marked on the map as solid lines, are *inferred.*

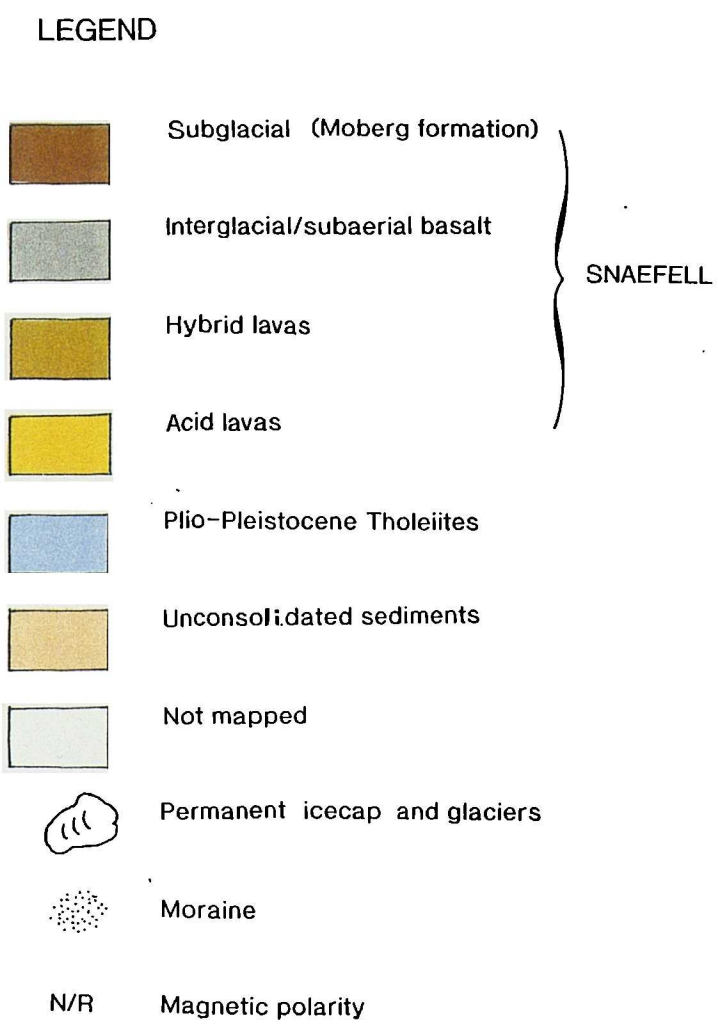

The Snaefell Volcanic System

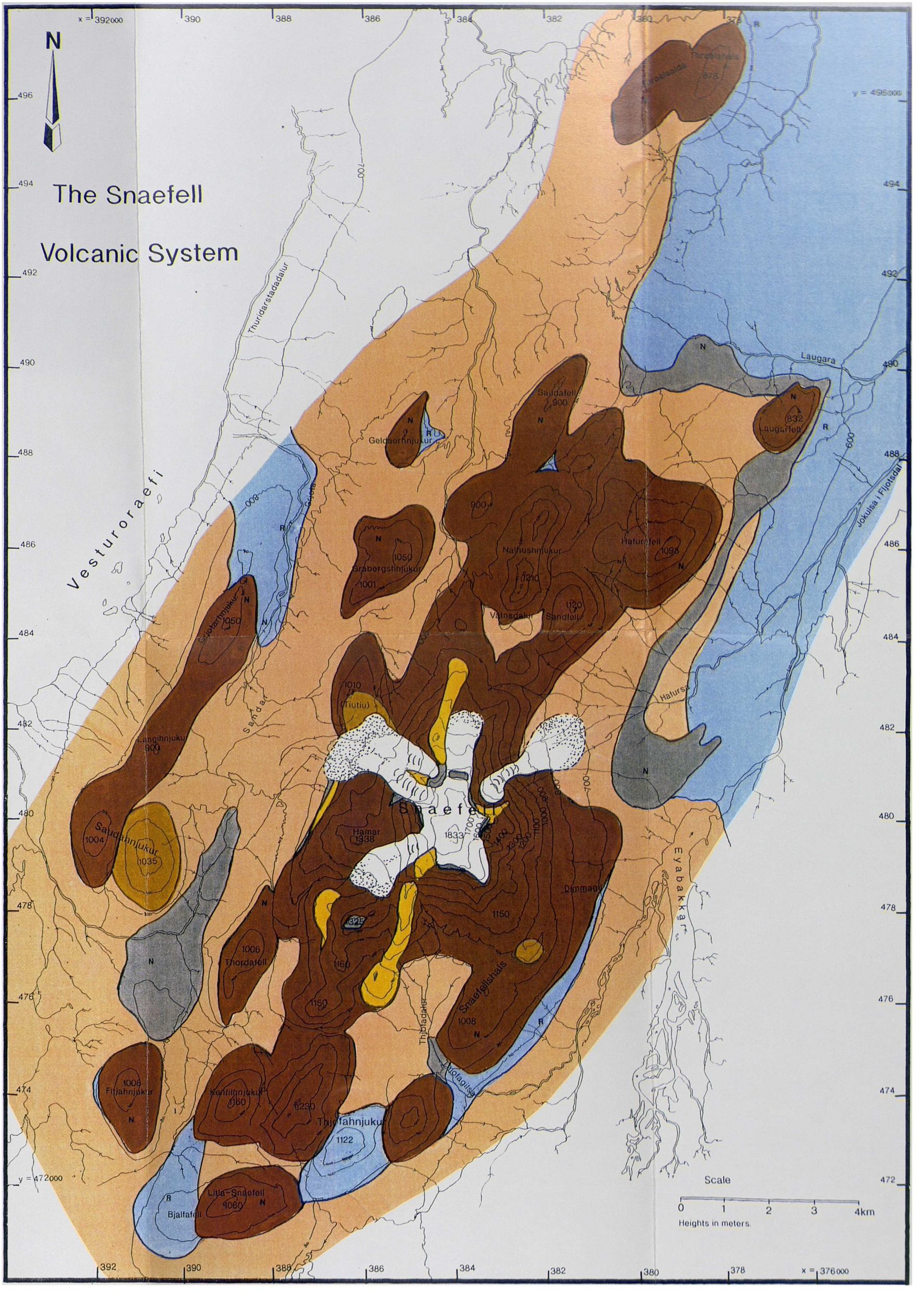

2.2 Subglacial activity

2.2.1 Introduction

As previously mentioned, most of Snaefell's activity occurred beneath the Upper-Pleistocene ice sheet. No subglacial eruption has ever been directly observed, all that usually tells of such an event is a *glacier flood* or *jokulhlaup* (Icelandic), which can represent a serious hazard if the adjacent areas are populated. The sequence of events has been deduced from the study of exposed and dissected volcanic piles. Molten basalt is capable of melting ten time its volume of ice, if allowed to cool. Fissure eruptions, especially, proceed initially at very high extrusion rates and are capable of melting up to $1km^3$ of ice within a few days (Saemundsson 1979). A substantial body of water may therefore accumulate below/within a *thick* (>100m) ice sheet (Smellie et al. 1993), providing a subaqueous environment. The resultant subaquatic volcanic piles show great lithological diversity within a single eruption unit, rendering conventional field mapping a meaningless exercise.

Noe-Nygaard (1940) showed in his study of well-exposed outcrops that regular sequences of lithologies were present. The gross sequence consists of: pillow lava complexes, mantled by breccias and tuffs intruded by cogenetic sills and dykes, and occasionally capped by flat-lying subaerial flows of identical composition. Within the tuffs and breccias, a huge variety of different rock types varying in grainsize, sorting and stratification can be seen. Considering the numerous exogenic forces affecting the primary structure and texture in the resultant loose, water-soaked pile that would result in such an environment, these could be assumed to result from secondary re-working. But, repeated observation of the same major sequences (Sigvaldason 1968) would, however, imply their primary nature, although some deposits have undoubtedly been subject to reworking. In detail there is quite a lot of variation between the sequences observed, and these can be ascribed to factors such as variations in eruption rate, water depth (i.e. hydrostatic pressure) magma composition (especially volatile content), etc.

In the following sections the formation and relationships of the different lithologies observed at Snaefell will be discussed. It was, however, often impossible to trace a complete sequence within a single eruption unit, either because the erosion level was insufficient to reveal the deeper parts, or because the structure was concealed by the mantle of scree (plate 2.4).

Plate 2.4 Scree covered monogenetic subglacial volcano, Nalhushnjukar (382,486), to the north of Snaefell itself (this hill is ~400m high). This thick scree cover made mapping an arduous and frustrating business, defining the base of the unit with any degree of certainty was of course impossible. (All grid references are approximate,and refer to the grid on the map of the volcano presented, figure 2.4.)

2.2.2 Pillow complex

Pillow lava is defined as lava in the form of distorted globular masses which were extruded under water (Whitten & Brooks 1972). The literature on pillow structures in volcanic piles now goes back over a century and a half, and there are many references to the association of pillows and tuffaceous rocks (e.g. Carlisle 1963). Most textbooks discuss only close-packed pillows with just a minor amount of hyaloclastite in the interstices. Nevertheless, in shallow subaqueous conditions there is a gradation from such pillow lavas into fully fragmental material. Therefore in this section I intend to discuss deposits in which the *bulk* consists of complete pillow lavas.

Pillow lavas, referred to as *globular basalts,* have been described in the moberg formation by Peacock (1926) and Noe-Nygaard (1940). The latter considered many pillows to have been formed by intrusion of magma into water-soaked debris, as

opposed to extrusion directly into a subglacial water body. Pillow lavas as such have been reported at the base of subglacial eruption sequences by many subsequent authors (e.g. Mathews 1947, Sigvaldason 1968, Jones 1968, 1969a, 1970.).

Pillow lavas are usually circular or elliptical in cross-section, although more ameoboid ones are seen. They usually show a mutual conformity and curved surfaces are typically convex upwards; radial prismatic jointing is characteristic (Jones 1968, 1970). In three dimensions Jones (1968) describes them beautifully as:

> " having an *entrail-like* aspect, the pillows appearing as swollen protrusions, irregular bulbous digitate cylinders, and vermicular appendixes".

These structures usually have their long-axes aligned down slope.

The same three major factors control the structure of subaqueous lava flows as subaerial ones: slope inclination, viscosity of lava, and extrusion rate. The additional factor to be considered is the rapid chilling that occurs. This results in the formation of pillows. Low viscosity melt extruded on to a gentle slope at an average eruption rate will probably form sausage-like structures, whereas a more viscous melt extruded under the same conditions may form irregular unconnected pillows and/or a breccia (Sigvaldason 1968). The close structural similarity between pillow lavas and pahoehoe toes has long been recognised, and there appears to be nothing incompatible with the former having evolved in a process analogous to the digital advance of a slow-moving pahoehoe flow (Jones 1968). Perhaps the most authoritative account of pillow formation is that of Moore (1975), which was written from both direct observation and the analysis of film showing the growth of Kilauean pillow lavas. These were seen to be composed of interconnected flow lobes, fed from up-slope by larger connected lava tubes. Individual pillows expand, branch - the process of "budding" producing re-entrant selvedges (Cas & Wright 1987) - and lengthen as new lava feeds in, distending and cracking the thin, brittle crust (figure 2.5). New crust is continually formed adjacent to the crack - although chilling is not instant, due to the insulating properties of the leidenfrost layer (Mills 1984) - until the crack stops spreading and a new one forms. Fast spreading (opening at ~5cm s^{-1}) produces zig-zag cracks, resulting in corrugations perpendicular to the cracks. Slow spreading cracks (~0.1cm s^{-1}) produce smaller fault slivers parallel to and tilted away from the crack. Examples of this pattern were observed during fieldwork at Snaefell (plate 2.5) indicat ing a relatively slow rate of pillow growth. Since post-eruption erosion over much of the study area is fairly shallow, good exposures of pillow lavas are rare.

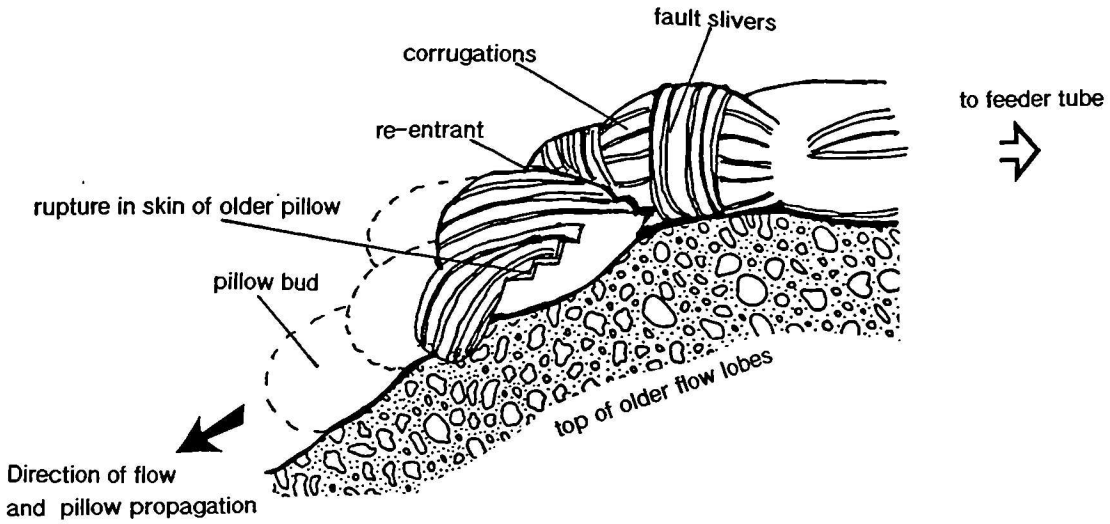

Figure 2.5 Sketch of propagating pillow lavas, modified from Moore (1975). A pillow grows as lava continues to enter from a larger feeder up-slope. Growth of new crust occurs adjacent to cracks, rather than by elastic stretching and continuous growth of crust. Thus new pillow lavas have ridged or corrugated surfaces. New pillows are formed as lava pressure ruptures the skin of an existing pillow, allowing "budding" of a new pillow, resulting in re-entrant angles (Cas & Wright 1987)

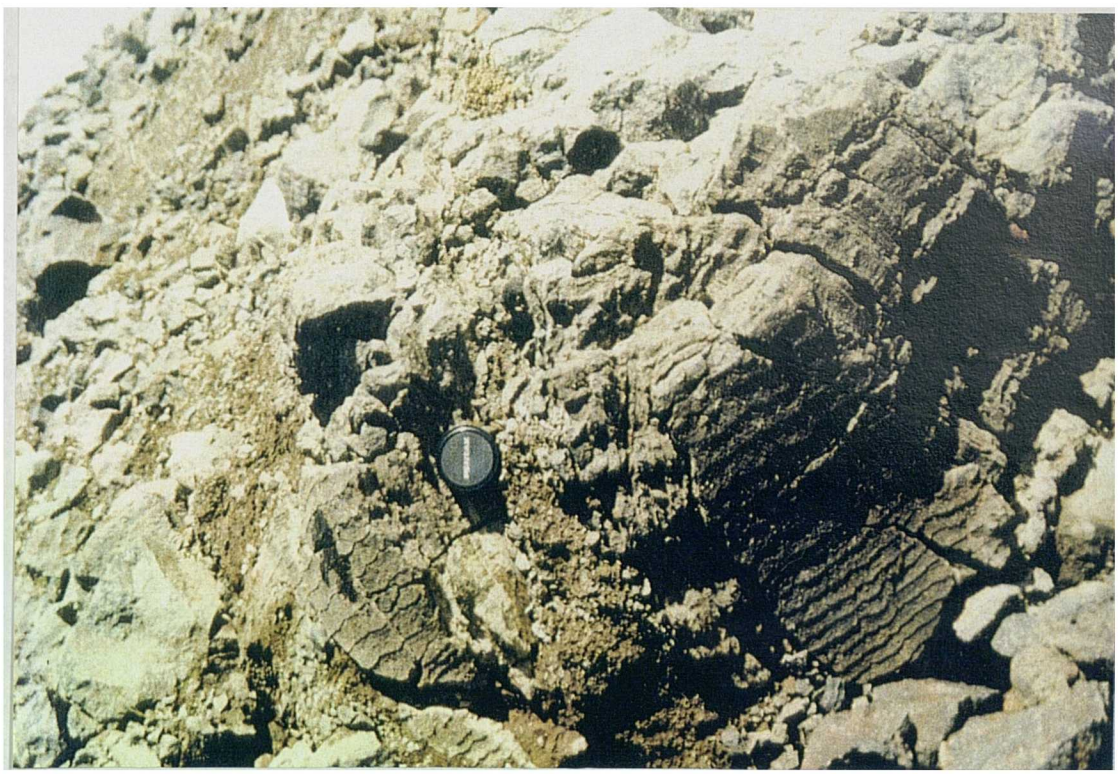

Plate 2.5 Pillow lava with some of its original crust remaining, showing well developed fault slivers dipping away from the growth cracks (383,479).

Pillow lavas at Snaefell vary in size from a few cms to almost 2m in diameter. At the base of the succession they are usually close packed and composed of vesicle-poor basalt with well developed radial jointing (plate 2.6).

Plate 2.6 Probably the best two dimensional exposure of pillow lavas seen, since in only a few places is the volcano sufficiently dissected to expose them (383,479).

Higher up the sequence the amount of tuffaceous matrix increases, as does pillow vesicularity, while the size of individual pillows is reduced. Plate 2.7 shows a cluster of irregularly shaped cindery (highly vesicular) pillow lavas that were probably formed as lava was extruded into the water-saturated fragmental deposit under relatively low hydrostatic pressure (Jones 1969b). Some pillow lavas contain vesicles lined or infilled with a network of dark, fine-grained to glassy material. These are interpreted by the author as the late-stage dregs of melt, drawn into the vesicles as the gas phase cooled and contracted. They were originally termed "segregation vesicles" by (Smith 1967), and will be further discussed petrographically in section 3.1.2. They appear to bear no relationship to the depth at which the magma was extruded (Jones 1969b).

Intrusions - dykes and sills - have also been observed, cutting both tuffs and, in some places, pillow lavas (Peacock 1926). These are now thought to be master channels/tubes or feeders (Jones 1968). Jones (op. cit.) also observed an outward dipping (~20°, locally reaching 40°, Jones 1966) pillow lava pile in direct connection

Plate 2.7 Small, cindery pillow lavas in a matrix of tuff. these pillows in three dimensions are probably still interconnected and it is the author's opinion that these were probably formed on the injection of lava into the water-saturated sediment pile at shallow depths, example from Saudahnjukar West (392,479).

Plate 2.8 Small exposure of columnar jointed basalt in a deeply eroded section of a subglacial volcano - Saudahnjukar West (392,481).

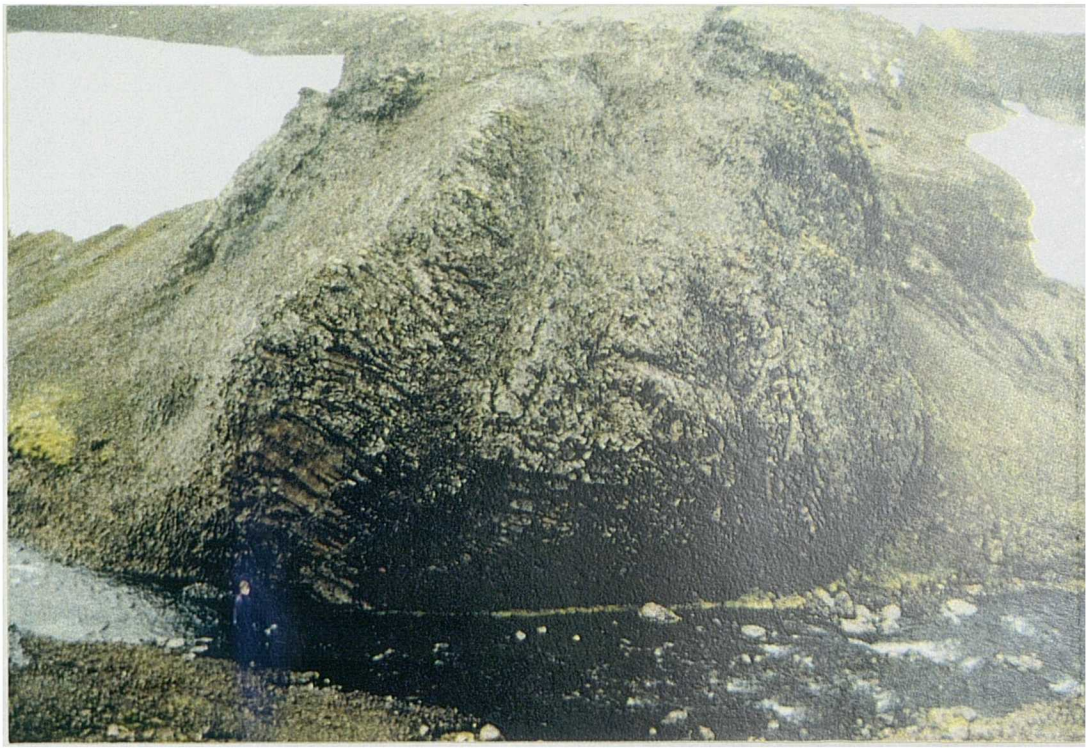

Plate 2.9 Large irregular mass of basalt exposed at the base of a subglacial volcano, interpreted as a feeder, probably lying above the site of the original vent. For scale, see the small figure in the bottom left of the picture (381,487).

Plate 2.10 Large irregular body of basalt (a feeder) overlying a horizon of cogenetic pillow lavas (385,480).

with an axial dyke, and gradations out from columnar jointed basalt masses to pillow structures have also been documented (Walker & Blake 1966). Isolated exposures of columnar jointed basalt (plate 2.8) are fairly common and, in one very deeply eroded unit, a large irregular body of basalt (~6 x 4m) was observed (plate 2.9). This resembles those described in the Cyprus ophiolite (Schminke et al. 1983) and is thought to be a feeder overlying the vent. Such structures do not appear to be confined to the base of the sequence and are also seen overlying pillow lavas (plate 2.10).

Plate 2.11 Good example of a large feeder dyke, ~3m wide, cutting through the tuffs. This one seen in Sandfell (381,485), to the NE of Snaefell.

Large - up to 3m width (plate 2.11) - axial dykes cutting cogenetic bedded tuffs are also very common. These are interpreted as feeders to an upper zone of pillows (or the subaerial capflows seen on some units), resulting from simple build-up of the volcanic pile. Alternatively they may signify an increase in eruption rate, causing a dyke to penetrate through the pre-existing "pillow front" as shown in figure 2.6.

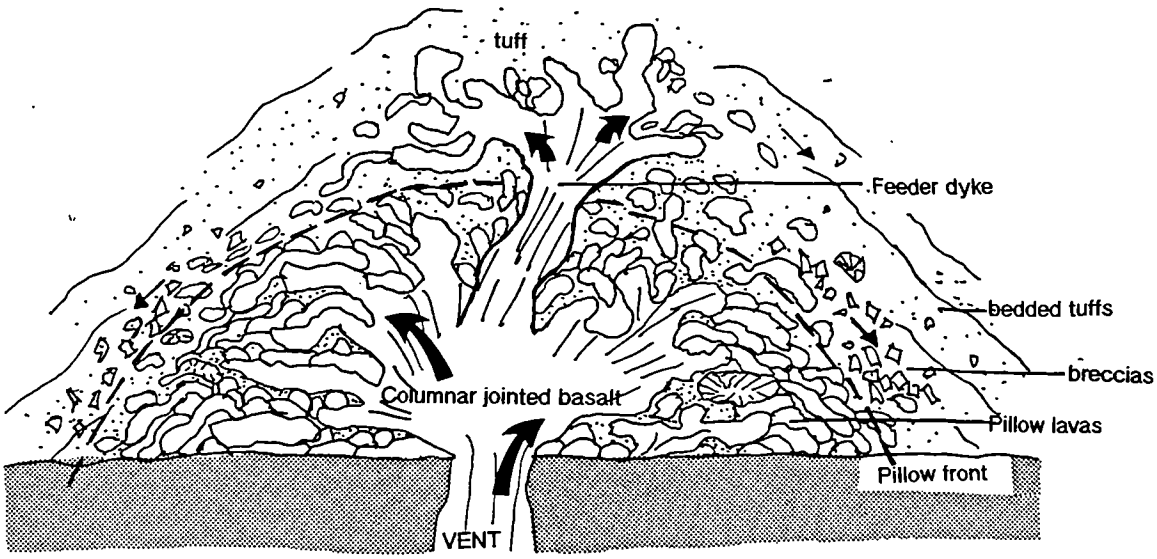

Figure 2.6 A growing pillow volcano, showing the complex feeder zone at the base, the initial pillow front, and the stratified breccias which form by slumping down the volcano's oversteepened flanks. Another pulse in the eruption has sent a feeder dyke up through the initial pillow front, to build a second layer of pillows and (eventually in the end-member case) the subaerial cap-flows.

2.2.3 The Breccias

In the moberg formation, fragmental rocks are as abundant as the basaltic lavas with which they appear in structural continuity. They range in composition from glass-encrusted lava several tens of cm in size - and often highly irregular in outline - to sand-grade material (Jones 1968). Sorting is often extremely poor, indicat ing that the bulk of the deposits are primary and have undergone little re-sedimentation (Sigvaldason 1968). The term *breccia* denotes fragmental rocks composed dominantly of angular clasts >1cm, and this section aims to discuss just the formation of the coarser fragmental deposits. Two broad types of breccia are found, so-called *pillow breccias*, consisting of whole or disagregated pillow lavas in a cogenetic tuffaceous matrix[2], and *flow-foot breccias* (Jones 1970, Jones & Nelson 1970) where lava extruded subaerially flows into water.

In very deep water the pillow breccias are monolithologic, consisting solely of fragments of lithic basalt, cemented either with zeolite and carbonate minerals or welded together during cooling, if fragmentation occurred prior to complete crystallisation (Fisher & Schminke 1984). In shallower water the amount of tuffaceous matrix present increases and fragments are commonly more scoriaceous. Within a unit the breccias usually grade up and outwards into the tuffs, although they are

[2]First used in this sense by Henderson (1953), reported in Carlise (1953).

occasionally completely absent. Several mechanisms by which pillow breccias form have been proposed, on the basis of the varied nature of the clasts:

1). Brecciation often occurs when tube-lava extrudes onto a steep slope; or when the flanks become oversteepened and unstable, resulting in gravitational collapse during the growth of the pillow volcano (Jones 1970, Saemundsson 1979, Fisher & Schminke 1984, Cas & Wright 1987). Such *in-situ* breccias have a similar origin to autoclastic breccias observed in subaerial sequences. This process results in the so-called *joint-block breccias* (common in the moberg formation), composed dominantly of cobble sized (5-25cm) pie-shaped or pyramidal clasts, although occasionally complete pillows, up to tens of cm, may also spall off (Walker & Blake 1966, Sigvaldason 1968, Jones 1970). Glass in these breccias is generally confined to the curved remnant pillow surfaces, unless crystallisation was incomplete when fragmentation occurred.

2). Also directly associated with closely packed pillow assemblages are breccias thought to have formed by lava tube and pillow implosions, resulting from the hydrostatic pressure on the brittle crust - the pressure difference being caused by the cooling contraction of a gas phase (Moore 1975). It is likely that this or a similar process resulted in the *vitric breccias* of Jones (1970) which consist of arcuate plates of glass-encrusted lava.

3). As the volcano grows the vent becomes shallower and the eruption switches from effusive to explosive (discussed in detail in the following section), hence generating fragmental material; both breccias and finer-grained (Sigvaldason 1968).

4). Immediately on top of the pillow lava pile, a distinctive deposit often occurs. This consists of isolated spheroidal to irregular glass-encrusted small pillows, in a matrix of glassy globules, pillow fragments and lapilli-sized glassy clasts (Carlisle 1963, Schminke et al. 1983). This was termed *isolated pillow breccia* by Carlisle (1963), who attributes it to submarine lava fountaining as the eruption reaches shallower water. This is seen to grade into a deposit consisting dominantly of dissaggregated pillows in many instances.

These pillow breccias tend to reside at steeper angles than subaerial basaltic scree, most at greater than 20°, but less than 25° (Jones 1966).

Probably the most abundant type of pillow breccia seen at Snaefell is joint-block breccia, which in places can be traced down into the pillow lava complex, where partially disagregated pillows can be seen (plate 2.12). Where eruption took place from a vent at some height on the flanks of the main massif, resulting in the extrusion

Plate 2.12 Exposure of pillow lavas, the one centre-right appears in the process of brecciation although the fragments (joint-blocks) are still in place and surrounded by the chilled margin.

of lava onto a steep slope, broken ends of tubes and pillow lobes are seen and a talus of breccia would have formed at the base (plate 2.13). These joint-block breccias grade into more tuff-rich deposits (termed *tuff breccias* by Jones 1970), which often appear to have undergone some slumping or flow downslope. In some units, notably Saudahnjukur West (392,479), the pillow complex grades directly into a tuff breccia consisting of fine grained tuff and isolated cindery pillows (plate 2.7). The cindery nature of the pillows indicat ing either that the magma was extremely volatile rich or that extrusion took place in relatively shallow water (Jones 1969a). Isolated-pillow breccias are also seen fairly high up the sequence in a few units; these appear superficially like subaerial spatter deposits and grade into horizons rich in accretionary lapilli.

Flow-foot breccias appear at the top of the sequences, beneath and in structural continuity with the overlying sheet lavas formed when the vent became subaerial (figure 2.7). As the lava flowed into the surrounding water, it would have been quenched and granulated to form "deltas" of breccia which were subsequently overridden by the advancing flows (Mathews 1947). The deposits range from sand-grade glass fragments to boulder-sized clasts (>25cm), which are far more common in these than in the pillow breccias. Flow-foot breccias also display a much greater range in crystallinity, vesicularity and colour; notably reddened (oxidised) clasts are seen

(Jones 1970). The so-called passage zone marks the fossil water level and is marked by attenuated sheets and fingers of lava, and these and similar detached masses characteristically define the steep stratification, which have been likened to foreset bedding (Jones & Nelson 1970). These breccias appear uncommon at Snaefell, where not all eruption units have subaerial capflows. Also subsequent glaciation deprived many units of their tops and added to the screes. One good example (plate 2.14) of the foreset beds was found, although the cap flows have been eroded away. Nevertheless, some of the breccias are undoubtedly the result of secondary reworking of the pillow, breccia and tuff sequences.

Plate 2.13 Broken ends of lava tubes and pillow lobes resulting from extrusion of lava onto a steep slope (387,479).

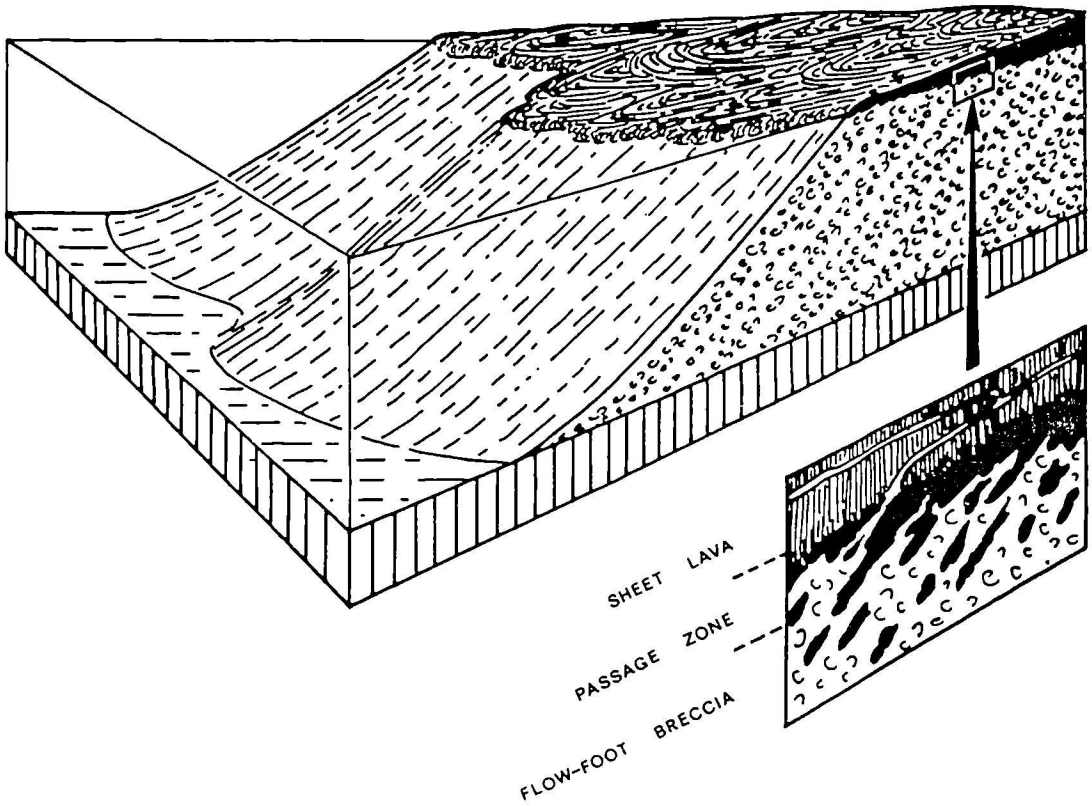

Figure 2.7 Form and structure of a basaltic lava flow that has brecciated on flowing into water. Thickness of breccia unit can reach the order of hundreds of metres (from Jones & Nelson 1970).

Plate 2.14 One of the rare examples of a flow-foot breccia seen at Snaefell (387,477). Height of exposure was estimated to be ~25m. Unfortunately there is no scale on this picture - field assistant was feeling lazy!

2.2.4 Tuffs

According to Cas & Wright (1987) *tuff* denotes the lithified equivalent of a volcanic ash deposit, where the grainsize is dominantly <2mm; when a significant proportion of lapilli (2-64mm) also occur the deposit is called a *lapilli-tuff*. The term is *genetic* and strictly applies only to deposits of material fragmented and laid down by pyroclastic processes. This should not include volcaniclastics derived from either quench-fragmentation or autobrecciation (spallation), and many such aggregates are formed in this manner under subaqueous, especially deep-subaqueous, conditions. These latter aggregates can be coarse and angular, or finely granular, and are called *hyaloclastites* (Honnorez & Kirst 1976, Cas & Wright 1987). The pyroclastic rocks generated by phreatomagmatic and phreatic explosions taking place when eruption occurs in shallow water and on emergence have been called *hyalotuffs* by Honnerez & Kirst (1976). These authors also propose a scheme to differentiate between the clasts formed by quench fragmentation and explosive activity; based on clast morphometry. They suggest that where >20% of the clast perimeter is planar, rather concave or convex, it is assumed to be of quench origin. The weakness of this classification is that it assumes that all quenched debris is derived from non-vesiculated magmas. This assumption is not necessarily valid, and there may be situations where a vesiculated magma is quenched or when quenching and magmatic or phreatomagmatic disruption occur simultaneously (Cas & Wright 1987).

Kokelaar (1986) made a detailed study of the mechanisms whereby volcaniclastics are formed when magma interacts with water in both subaqueous and emergent conditions. He identified four primary processes;

1). *Magmatic explosivity*	- resulting from rapid vesiculation.
2). *Contact-surface steam explosivity*	- explosive expansion and collapse of steam formed at the magma-water interface (the "leidenfrost layer" of Mills, 1984).
3). *Bulk interaction steam explosivity*	- steam explosivity resulting from the enclosure of water in the magma.
4). *Cooling contraction granulation*	- quenching.

These processes may occur together and enhance one another in shallow subaqueous conditions (figure 2.8). At greater depth, prior to the onset of explosive activity, only cooling-contraction granulation will occur. Thus, the percentage of fragmental rocks produced is low, 5-25%; this is the so-called effusive phase. The hyaloclastite produced at this stage will accumulate at the site of formation, or just a short distance away by avalanching (Smellie et al. 1993).

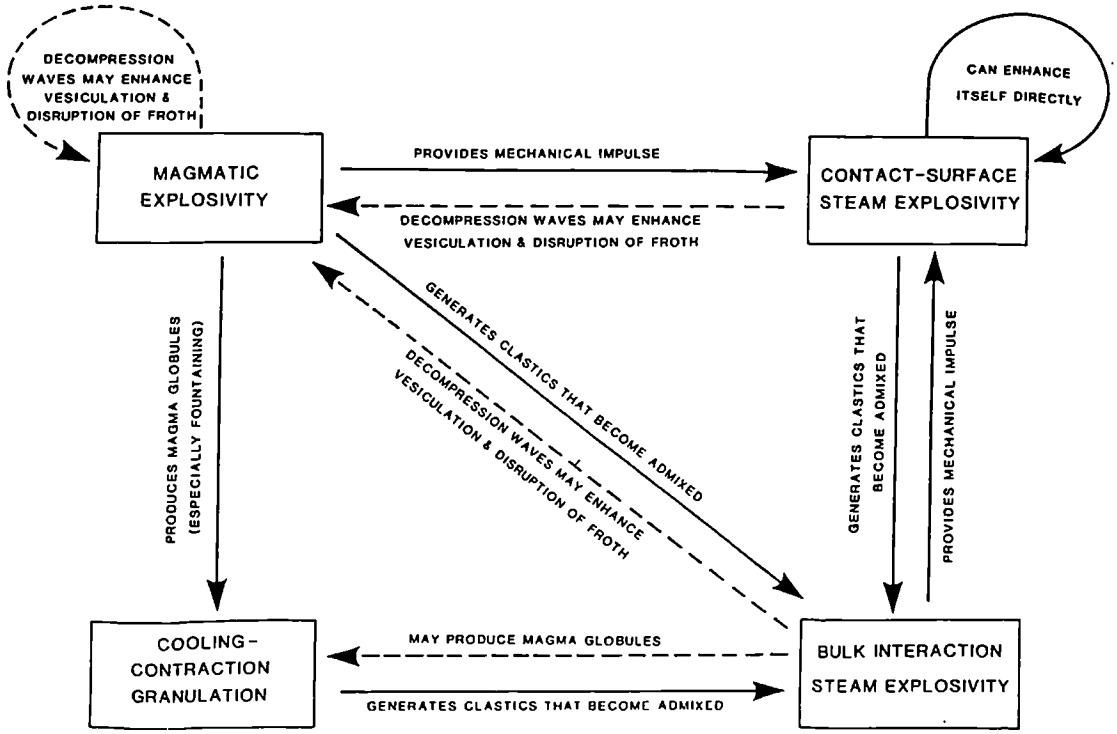

Figure 2.8 Clast forming processes in magma-water interactions at shallow depths, and their possible enhancement interactions (from Kokelaar 1986).

The transition to explosive activity, where fragmental deposits become dominant, is generally assumed to be controlled/initiated by the exsolution of magmatic volatiles, due to the marked increase in clast vesicularity observed at this point (Fisher & Schminke 1984). The depth at which this occurs is referred to as the volatile fragmentation depth or VFD (Fisher & Schminke, op. cit.). For a tholeiitic magma, with ~0.5wt% H_2O, this has been show from field studies (Jones 1970) and theoretical calculations (Allen 1980) to be 100-200m. For an alkalic magma, where the volatile content can reach 1.5%, this is substantially greater; e.g. 780m in the Pliocene basalts of La Palma (Kokelaar 1986). In a recent study (Lackschewitz et al. 1994), vesiculated fragments derived from explosive activity were found on the Kolbeinsey ridge north of Iceland, where the eruptive vent was evidently well below the VFD. They suggest that fragmentation occurred as submarine fire-fountaining produced convection currents, resulting in bombs of still-hot lava being transported up through the VFD and

fragmenting. Thus the transition to explosive activity may occur while the vent is still well below the VFD. Steam explosivity may, however, set in at still greater depths; the limiting factor on this being the hydrostatic pressure. Thus it would seem that the bulk of the fine-grained fragmental deposits at Snaefell - an alkalic volcano - would have been generated explosively, since the water depth attained in most eruptions is unlikely to have been sufficient to inhibit it. Thus the use of the term *tuff* is considered appropriate.

On emergence, surtseyan-type volcanism sets in. This is characterised by intermittent jetting to a continuous uprush of tephra and steam. The deposits are dominantly extremely regular, even and thinly-bedded lapilli and ash deposits, with abundant accretionary lapilli and highly vesicular clasts. Mud flow deposits are also common, indicateing that the primary deposit had a water content of >20% (Kokelaar 1986). The high water content of the deposits leaves them very susceptible to slumping and secondary reworking, resulting in bedded and graded deposits. Bedded deposits of fragmental material may also be produced at this stage in the eruption by quench-granulation, as the lava flows from the now subaerial vent into the surrounding water (as described in the previous section).

In the tuffs at Snaefell, glassy clasts vary in size from <0.1mm to ~10mm; larger clasts are generally almost completely crystalline, often showing well developed chilled margins (plate 2.15).

Plate 2.15 Close-up of coarse-grained tuff, note the well-developed chilled margins on the larger lapilli. The fine, white tracery is the cementing zeolite and carbonate minerals, and the orange/brown colour is due to the palagonite content.

The glassy clasts are dominantly made of clear brown sideromelane, reinforcing their subaqueous origins. This will only form when basaltic magma undergoes drastic chilling, as by eruption into water or ice (Peacock, *in* Peacock & Tyrell 1926) In contrast, on quenching in air, opaque tachylite (heavily charged with finely divided opaques) results. Tachylite becomes a more common component moving up some of the individual Snaefell sequences. Nearer the tops eruption would have been in very shallow water or emergent, but tachylite is still only a minor component. The clasts are very similar to those described by Jones (1970) and clasts described from Surtsey (Fisher & Schminke 1984), in that they are characteristically vesicular, sometimes reaching up to 50% volume; the larger clasts often have scalloped margins (vesicular embayments) and tend to be roughly equant (plate 2.16). Just occasionally they show smooth chilled margins, with any included microlites aligned parallel to them and with an increase in vesicle size inwards. Smaller clasts, closer in size to vesicle diameter, are commonly more shard-like (plate 2.17). Clasts of all sizes often contain small phenocrysts, especially microlites of plagioclase, which often show flow alignment. In addition to the glass and lava fragments, many of the tuffs contain crystal fragments up to 10mm across, indicateing that the magma was porphyritic. The fragments are generally cemented with a fine network of zeolites and carbonate minerals.

Three types of tuff were distinguishable in the Snaefell sequences. The commonest was similar to that described by Jones (1968,1970), which was often homogeneous and poorly sorted. The clasts range in size from ash-grade to larger lapilli, with outcrops up to tens of meters high. Stratification was often poorly formed, although bedding planes were generally fairly obvious. These probably resulted from slumping, which produced turbidite-type deposits contemporaneous with the eruption, as the sides of the volcanic pile became over steepened and unstable. Evidence of the primary nature of the bedding in some of the tuffs was found on Nalhushnjukur (382,486), where lava was seen intruding cogenetic bedded tuff (plate 2.18). These occur within the monogenetic fissure eruption units, which are considered never to have reached emergent state, and additionally in the lower parts of sequences. The other two types resemble those described by Sigvaldason (1968), both of which are believed to be derived from ash showers in the emergent phase. They show stratification which can be related to explosive pulses. The first shows alternating layers of coarse and fine material (plate 2.19), the grain sorting resulting from the ash settling through water. The second type is thought to have been deposited on land and contains abundant accretionary lapilli, the centre of each lappillus consisting of a larger clast, as already described, coated in ~1mm ash. This type is seen in some places, near the top of sequences, to consist of 100% accretionary lapilli, loosely packed with little of no matrix ash.

Plate 2.16 Photomicrograph of one of the lapilli tuffs, sample VH280. The larger lapilli here are composed of fresh, clear brown sideromelane glass, containing fresh olivine phenocrysts indicateing that the magma was porphyritic. Note the scalloped margins (vesicular embayments), indicateing that these lapilli were probably formed explosively. The matrix is composed of more altered, ash grade material. Field of view 6 x 3.7mm, plane polarised light (PPL).

Plate 2.17 Photomicrograph of a fine-grained tuff, VH287. A well sorted deposit consisting of shard-like pieces of sideromelane glass, here containing a few microlites of plagiociase. Field of view 0.66 x 0.4mm, PPL.

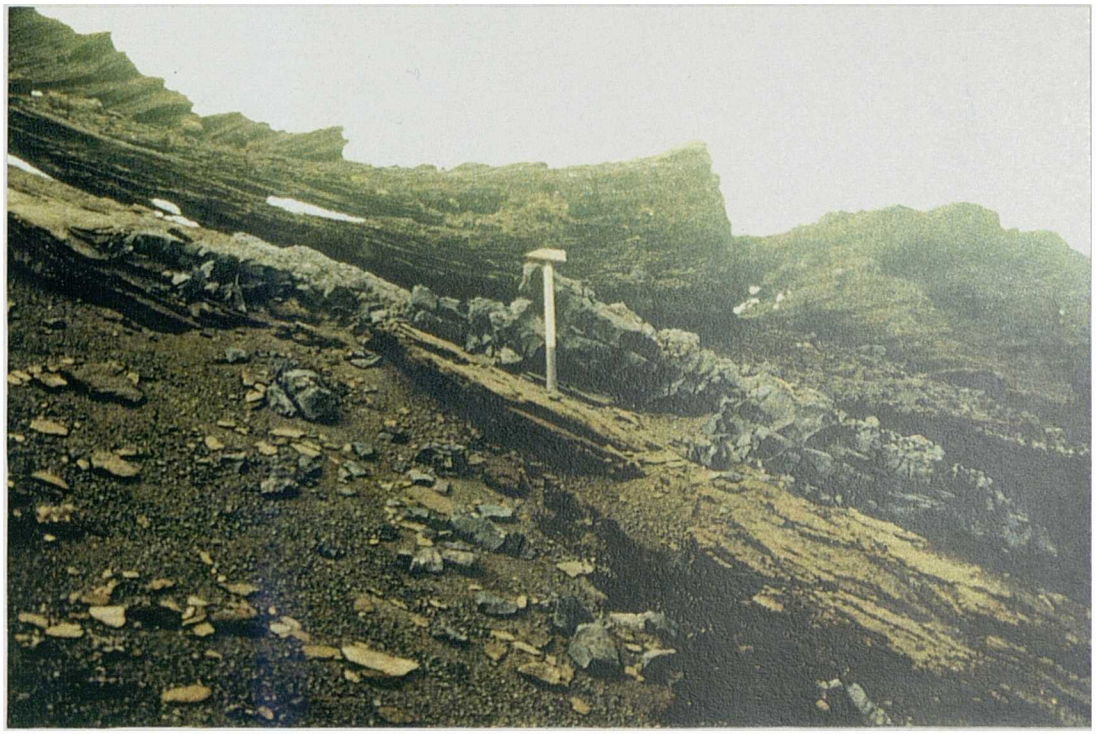

Plate 2.18 Bedded fine grained tuffs intruded by basalt lava extruded in the *same* eruption, indicateing that at least here, the bedding and sorting of the tuff is primary, this example from Nalhushnjukar (383,485).

Plate 2.19 Bedded tuff showing alternating layers of coarse and fine-grained material, the grain-sorting in which is thought to result from settling through water. Note also a small fault running through the deposit to the right of the hammer used for scale (382,480).

Bedded tuffs often undergo further slumping, perhaps as the volcanic pile "inflated" in response to further intrusive activity (plate 2.20).

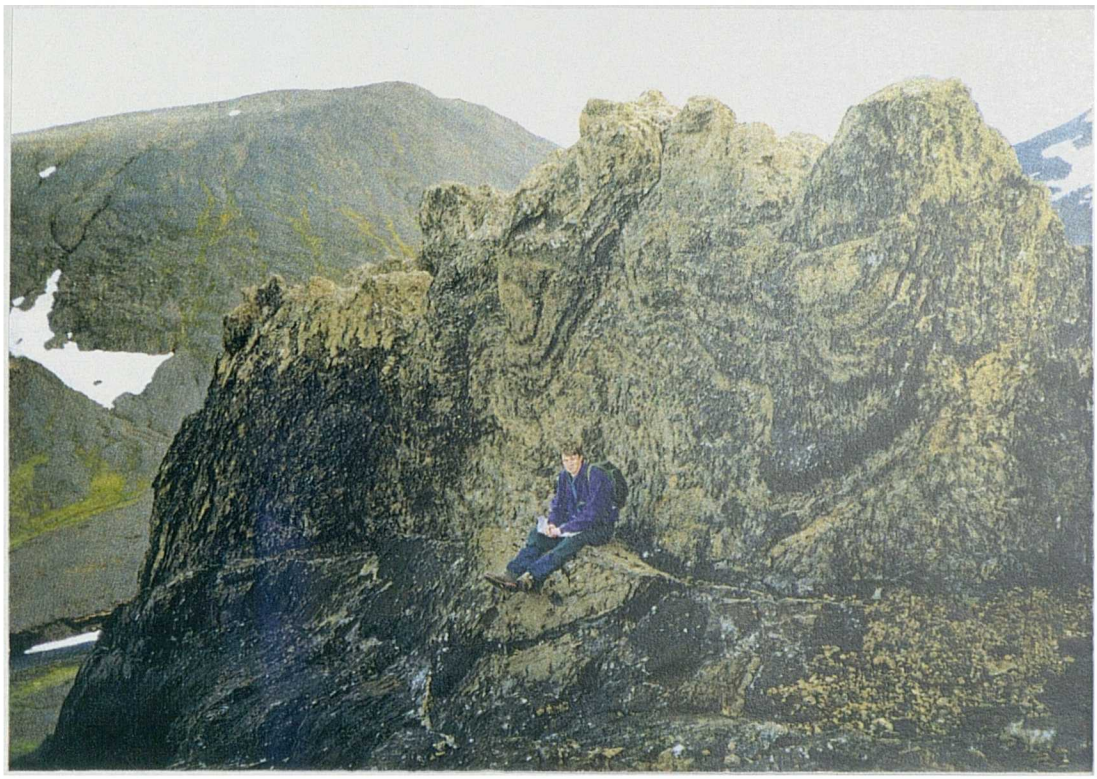

Plate 2.20 Tuff showing beautifully convoluted bedding, possibly resulting from slumping down the side of the volcanic pile in response to inflation resulting from further intrusive activity (382,487).

The degree of alteration through the tuffs is extremely variable, some contain abundant glassy material while others are almost entirely *palagonitised.* Palagonite was initially though to be a mineral species when it was first described in Sicily, although this was disproved before the turn of the century. It was first recognised in Iceland by Bunsen (1847), and has been used since in both mineralogical and stratigraphical (palagonite formation) sense. Peacock (1926) recognised that palagonite was produced by hydration of sideromelane, and identified two distinct forms; amorphous (isotropic) *gel* palagonite and finely fibrous, yellow-red, birefringent *fibro* palagonite. He also noted that tachylite seemed unaffected. A highly palagonitised example from Snaefell is shown in plate 2.21. Sigvaldason (1968) wrote in more detail on the process, concluding that it was essentially a leaching alteration process and occurred in a short-lived hydrothermal system, set up during the eruption and driven by the heat given off by the lava pile underlying the tuffs, as it cooled and crystallised. This accounts for the inhomogeneity of alteration within cogenetic structures, and the process' apparent lack of time-dependence. Two very fine-grained samples, VH2 and VH36, appeared to consist of almost 100% gel palagonite with a few crystals of plagioclase and, on

ignition, were found to contain 30wt% H_2O. XRD revealed that mineralogically they both were poorly crystalline, probably mixed-layer clays, giving a single diffuse peak at $2\theta = 3\text{-}6°$.

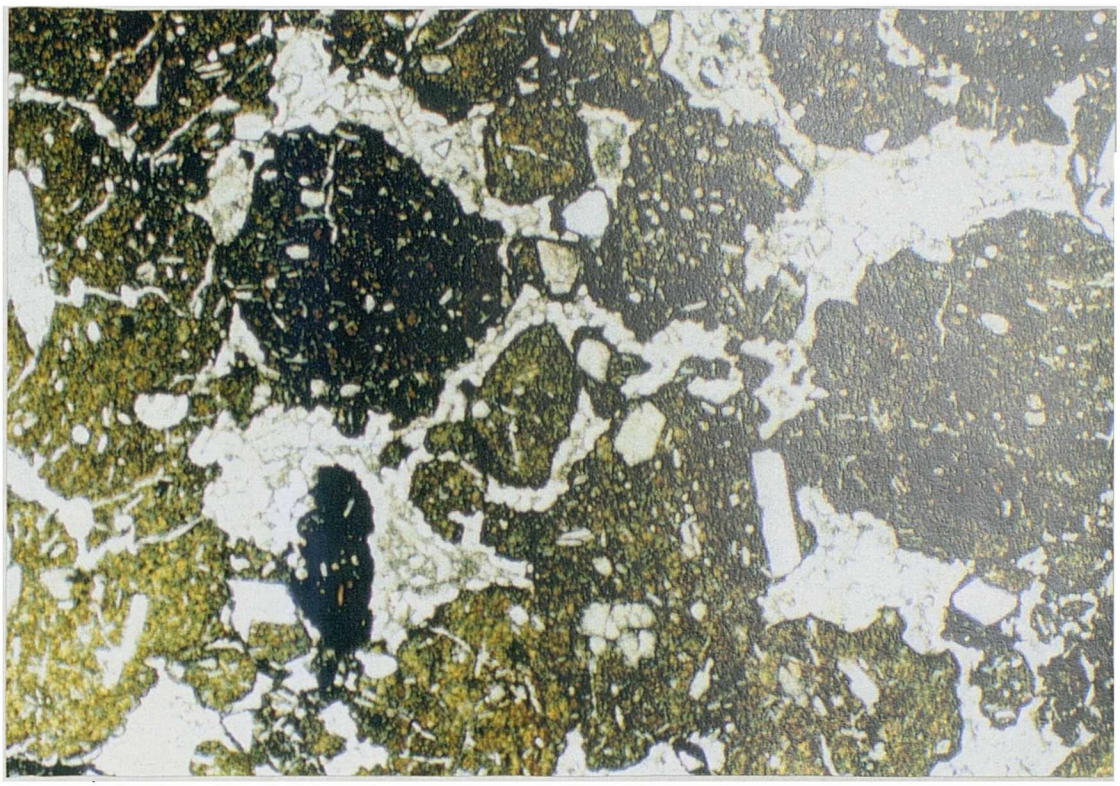

Plate 2.21 Photomicrograph of an example of heavily palagonitized tuff, VH3. The bulk of the lapilli have been replaced by greenish clays, while vesicles are infilled with orange gel palagonite. A few black tachylite lapilli are also present. The clear minerals cementing the lapilli appear to be zeolites. Field of view 6 x 3.7mm, PPL.

2.2.5 Tindars and Tuyas

This section aims to describe and discuss the volcanoes; their shape, structure and genesis. A growth sequence is proposed as a result of field studies and literature survey.

Tindar is Icelandic for peak or pinnacle, and is used to refer to steep-sided linear moberg ridges and mounds, with profiles ranging from smooth to extremely jagged (Jones 1969a).These are considered to be the result of subglacial fissure eruptions (Saemundsson 1979) and often occur in groups, aligned with the volcano-tectonic trend in the Quaternary volcanic zones. Tindars are composed of a basal pillow complex overlain with breccias and mantled by crudely stratified tuffs. Large axial dykes and smaller ones with varied trends are common.

Most of the smaller hills (rising 100-400m above the plateau) surrounding Snaefell itself are considered by the author to be tindars, the results of eruptions along the system's poorly developed fissure swarm. A classic example is Thordafell, plate 2.22.

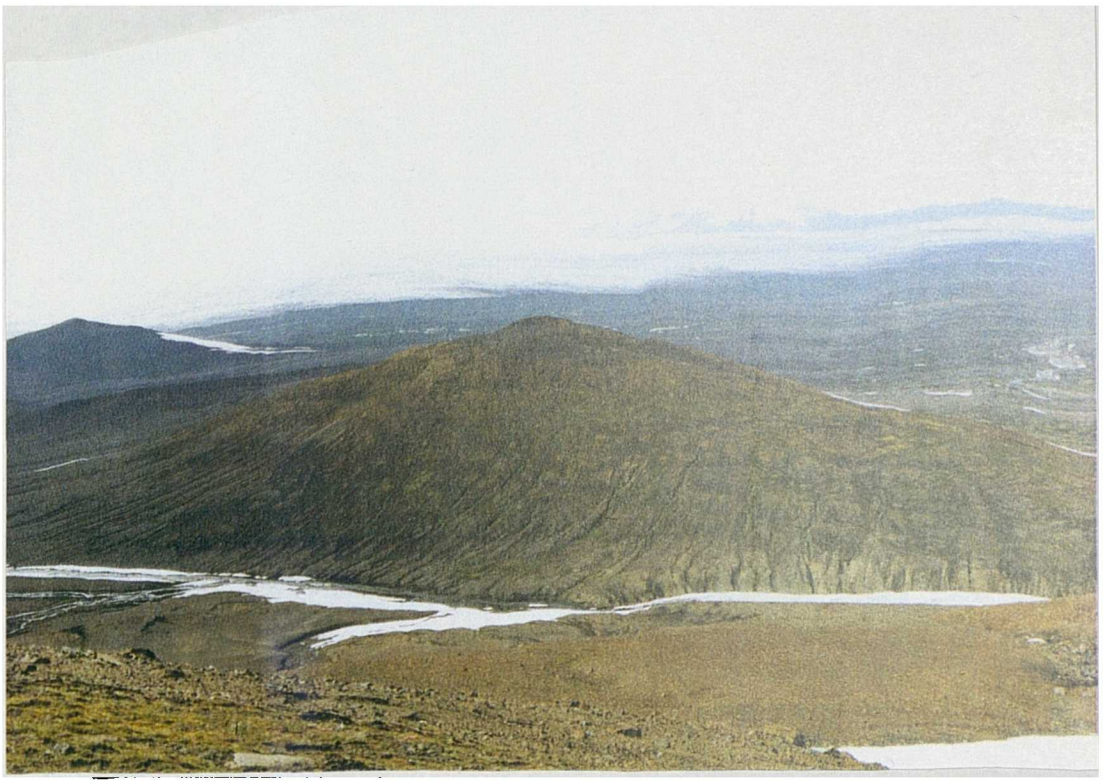

Plate 2.22 Example of a smooth *Tindar* - Thordafell (389,477) - to the SW of Snaefell, ~200m in height.

Flat-topped, steep-sided volcanoes observed in British Columbia were termed *tuyas* by Mathews (1947), and subsequently this term has been adopted for identical structures (table-mountains) in Iceland (Jones 1969a). Tuyas are usually fairly equidimensional, with benched or terraced platforms at the top and steep, scree-covered flanks (debris can extend out up to 1.5 miles, Mathews 1947) and often have summit craters or a row of craterlets, at the top. They are built up on a tindar-like foundation, overlain by steeply dipping deltas of foot-flow breccia and gently dipping (2-3°) subaerial lava flows (Mathews 1947; Jones 1969a). These are the subglacial equivalents of lava shields (Saemundsson 1979).

Few eruption units that could be described as tuyas in the classic sense, were observed at Snaefell, although a deeply dissected one was found and will be described below.

There has been some debate in the literature as to the exact sequence of events that results in these structures, although there is general agreement that eruption took place into *intraglacial lakes* produced by melting of ice by volcanic heat (e.g. Mathews 1947, Kjartansson 1959, Sigvaldason 1968, Jones 1969a). The repeated occurrence of the same successions imply that the controlling factors are external (Sigvaldason 1968). Essentially there are three phases in the growth sequence accepted by the aforementioned list of authors:

An aquatic effusive phase.
An emergent explosive phase.
An aerial effusive phase.

The sequence of formation of the various lithologies is summarised in figure 2.9, which is essential the model of Jones (1968), with minor modifications.

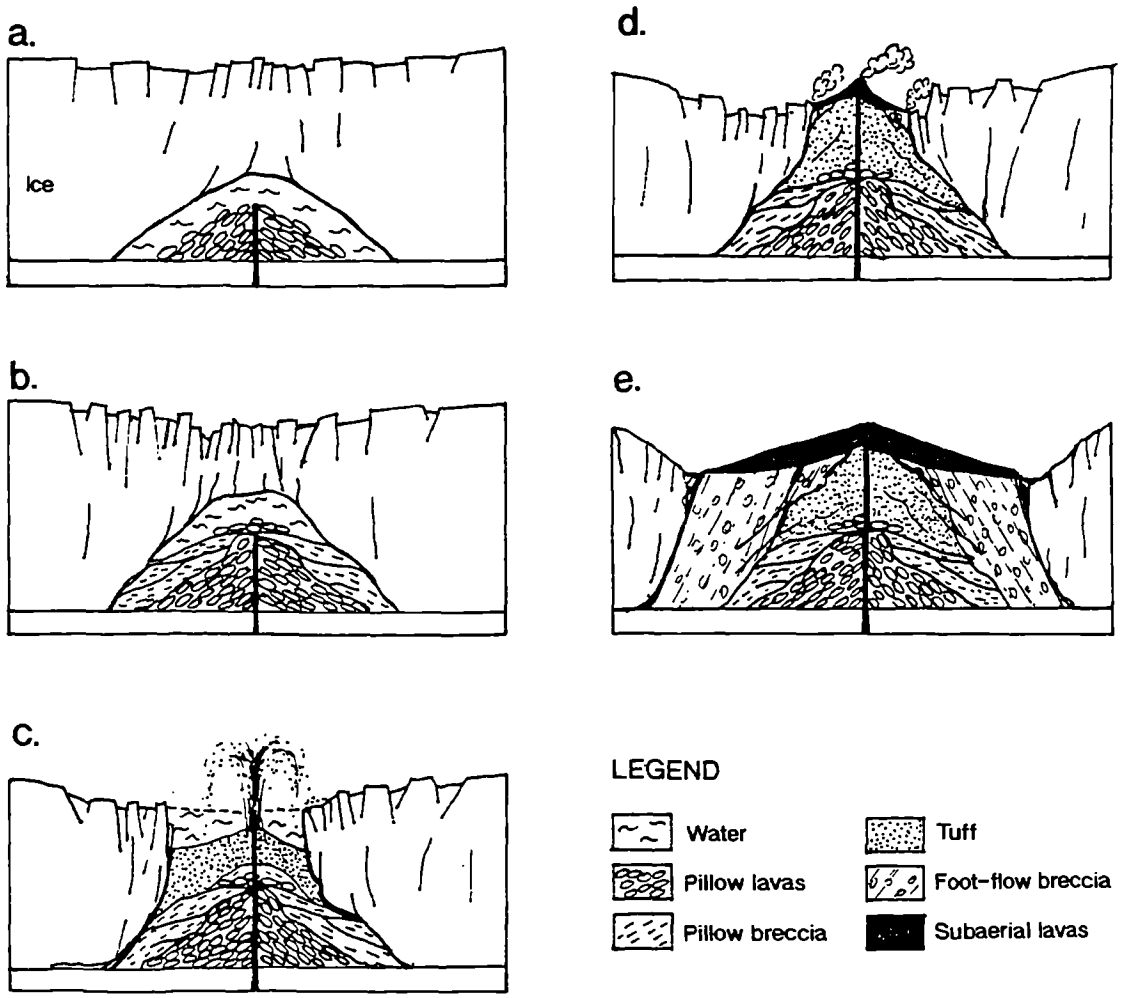

Figure 2.9 Growth sequence of a subglacial monogenetic volcano; ice thickness 300m +. Stage **a**: Quiet effusion of lava into the intraglacial lake formed by magmatic heat, gives rise to a pile of pillow lavas. Stage **b**: The flanks of the pillow lava pile may become oversteepened resulting in slumping and brecciation. Stage **c**: At a depth of <200m, explosive activity sets in, resulting in the production of tuff and more breccias which mantle the pillow lava pile; by now the roof of the vault has probably collapsed. Stage **d:** Some time after emergence of the volcano, explosive activity ceases and effusion of lava is resumed. Stage **e**: Lava flows rapidly encroach on the encircling water and granulate, forming extensive foot-flow breccias which result in steeply dipping deltaic accumulations down the sides of the volcano. Modified from Jones (1968) stage **b** added by Saemundsson (1979).

The initial effusive phase gives rise to pillow lavas and minor amounts of hyaloclastite. As the pillow lava pile grows its flanks often become oversteepened and unstable, resulting in slumping and the formation of pillow breccias. Eventually the volcanic edifice reaches sufficient height, and the roof of the vault collapses, allowing the explosive ("Surtseyan") phase to set in (as previously discussed in section 2.2.3), mantling the volcano with tuff. Sometime after the vent breaches the water's surface, effusive activity resumes. Lava flows spread out until they reach the surrounding water/ice where, on entering they are quenched and granulated. This results in a steep outward dipping deltaic accumulation of breccia - foot-flow breccia (Jones 1969a, Jones & Nelson 1970) - which is subsequently over-ridden by later flows. After the cessation of eruptive activity, the ice gradually returns and erosion sets in.

The growth of a tindar stops at the explosive tuff-producing stage, (c) in figure 2.9. A striking feature of the tuffs is the low bedding dips, some examples even show troughs, Jones (1969a) explains these in terms of banking against the confining walls of ice. This confinement is also thought by Jones (op. cit.) to be responsible for the encircling cliffs of foot-flow breccia, most noticeable in the classic example studied by Jones, Hlodufell.

On tuyas a fossil water level is recorded in the so-called "passage zone" (figure 2.7). The loose, unconsolidated piles of water-saturated debris that comprise these volcanoes, however, are very prone to subsidence. Therefore, if a volcano continues to erupt intermittently during subsidence, successive terraces of lava flows and passage zones result (figure 2.10).

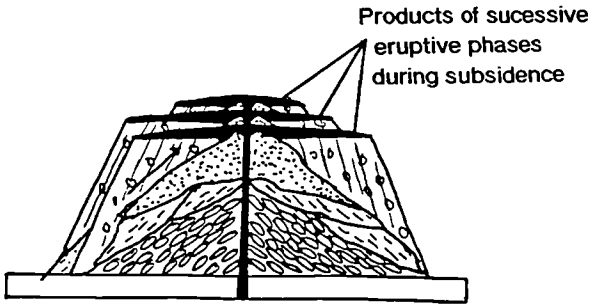

Figure 2.10 Terraced and subsided tuya (Jones 1966, with slight modifications).

This appears to be what happened in the case of the best preserved tuya structure at Snaefell (plate 2.23). It is located on the SE flank of the central mountain and appears to overlie a rhyolitic lava flow. It is therefore is thought by the author to have been formed towards the end of the life of the volcanic system, when ice-cover was relatively shallow - at around 1300m.

At any time during the growth of a subglacial volcano the melt-water lake may escape along channels melted out beneath the ice sheet, especially where it is not frozen to its bedrock. This sudden drainage can result in a *jokulhlaup*.

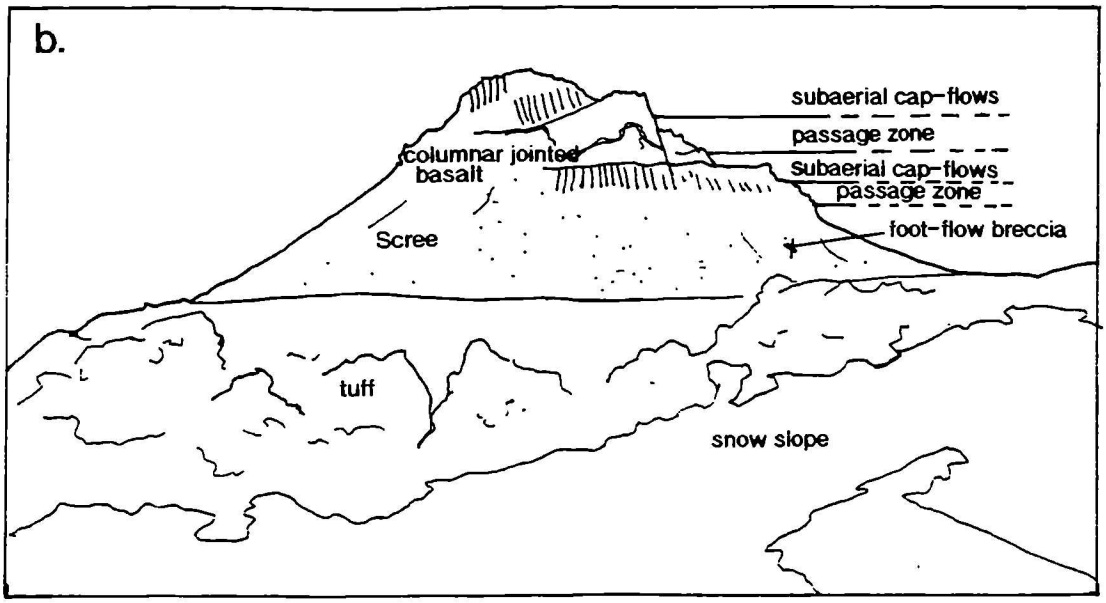

Plate 2.23 **a).** Dissected tuya (~150m high), located on the SE flank of Snaefell (387,477).
b). Line drawing of (a), with the lithological units labelled.

The result of such an event is that lava may flow down over the steep sides of the breccia pile, mantling it (Mathews 1947). This appears to have happened on the upper slopes of mount Snaefell.

2.3 Subaerial activity

As already stated, the bulk of the of the volcanic system's activity took place beneath the Upper-Pleistocene ice sheet. It appears, however, that the initial activity occurred during an interglacial period and that the thickness of the ice sheet varied during the life of the system, resulting in intercalations of subaerial lavas and red oxidised cinder/scoria horizons (plate 2.3). It also appears that all silicic volcanism was subaerial, most of which appears to have occurred late in the life-time of the central volcano.

2.3.1 Basaltic activity

The volcanic rocks of the upper-Pleistocene fall into two categories with regard to morphology and structure. The first is the *moberg formation* (section 2.2) and the second is often referred to as the *grey basalts* or *gragryti* (Icelandic; Saemundsson 1979). These basaltic lavas were erupted in interglacials and subsequently glacial erosion has deprived them of their surface features, revealing their coarser grained interiors. Two fairly extensive examples of such flows represent the initial activity of Snaefell. One, which is ankaramitic, shows a characteristic red/brown weathering (plate 2.24); while the other, which is much more evolved, show a platy weathering. This platy weathering is usually due to the alignment of plagioclase crystals (the so-called *trachytic texture*) within the lava, and can be used in the field as a criterion in the identification of evolved lavas.

Other examples of subaerial volcanism at Snaefell are to be seen at the top of the mountain itself, where the edifice grew up through the ice-sheet; and in the small cap flows on one or two tuyas. The most obvious clues that activity became subaerial are the red (oxidised) horizons of scoria. At around 1600m on Snaefell, reddened cinders and bombs - up to 50cm in length - are encountered. They vary from the classic spindle shape (plate 2.25), to more irregular blocks, sometimes with breadcrusted surfaces. These could have been transported by ice, but the concentration suggests the deposit is primary, although avalanching down-slope could have occurred at any stage. Further up (~1775m), a small outcrop of agglutinated spatter (plate 2.26), containing some small bombs and scoraceous material was found. The top of the mountain culminates in a conical structure, with two smaller cone structures on its northern side. These could be cinder or spatter cones along an originally linear vent. This evidence suggests that the final phase of eruption was hawaiian or strombolian in character.

Plate 2.24 Early subaerial flow unit, deprived of its original surface texture by glaciation and showing well developed N-S glacial striations indicateing northward (arrow) movement of the ice sheet (390,477).

Plate 2.25 Large spindle bomb found at around 1600m on Snaefell.

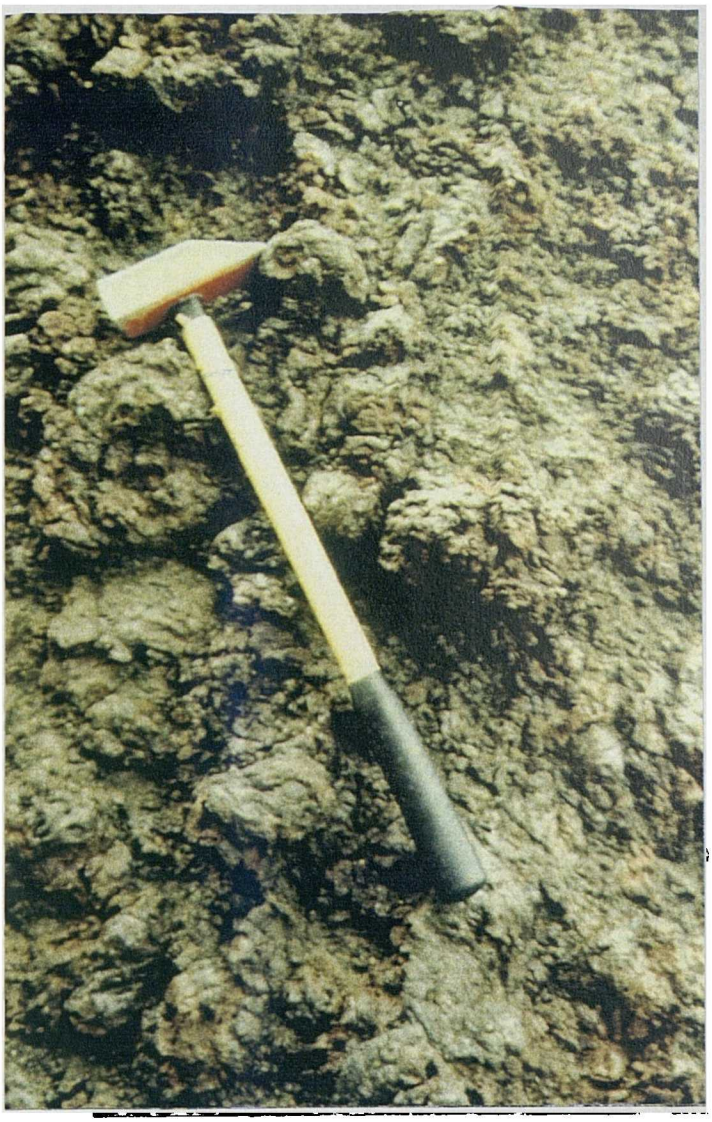

Plate 2.26 Spatter deposit, this particular example was found in a large block brought down by glacier A.

In hawaiian activity the eruption column is essentially a *"fire"* fountain formed when jets of disrupted magma are released almost continuously up to ~200m into the air (Cas & Wright 1987). Strombolian eruptions are more violent, consisting of a series of explosions caused by rapid release of magmatic volatiles (Cas & Wright, op. cit.). Strombolian eruptions therefore have the potential to distribute material over a wider area. Walker (1973) observed that deposits resulting from hawaiian style activity are predominantly composed of agglutinated spatter, while deposits from strombolian eruptions are likely to be composed of loose scoria. He also proposed a scheme to differentiate between the products of these two eruption types based on fragmentation (F) and distribution (D), hawaiian having a D of <0.05km and a low F. Whilst this is a good general guide, considerable variations can occur due to factors such as discharge rate. This then suggests that the eruption at Snaefell showed both eruption styles discussed, possibly proceeding in a similar manner to the 1973 Heimaey eruption (given as an example by Cas & Wright, 1987), which began with lava fountaining from many vents along a fissure, and concluded in strombolian activity from just 3 vents to build a large scoria cone. Snaefell's activity appears to have built one large cinder/spatter cone with two smaller cones on its side.

2.3.2 Silicic volcanism

Acid and intermediate rocks make up around 10% of the exposed volcanic pile in Iceland, and are usually confined to central volcanoes. This is either because only at these sites is volcanic output high enough to trigger anatectic melting (Gustafsson et al. 1989) or because central volcanoes, by definition, overlie long-lived crustal magma chambers where high degrees of fractionation may occur (the origin of the rhyolites will be discussed in detail in chapter 4.)

Subaerial rhyolite flows may take any one of three different forms: symmetrical domes, biscuit-shaped mesa lavas, or coulées - thinner flows which tend to result when a rhyolitic lava is extruded on to a slope (Cas & Wright 1987). Domes are perhaps over-represented in the geological record due to their higher preservation potential. Rhyolitic lava flows tend to be much thicker (ranging from <50 to ~500m, with an average of 60m) than basaltic ones, due to their greater viscosity and higher yield strength. Some Icelandic examples have been found to be substantially thinner; although on closer examination these turned out to be hybrid, the basaltic component reducing the viscosity, and thus the yield strength (Gibson and Walker 1963, reported in Cas & Wright op. cit.). In rhyolite flows a variety of textures and lithologies (the distribution of which is summarised in figure 2.11) can be found.

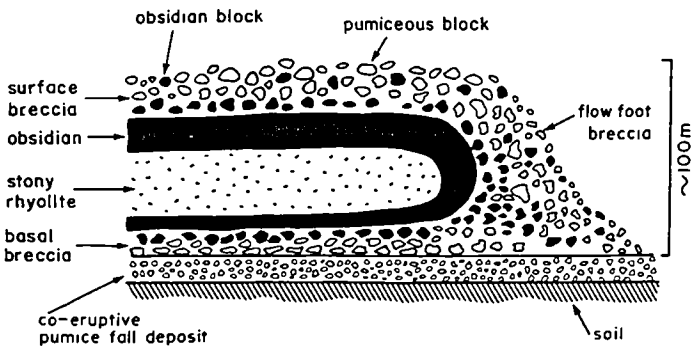

Figure 2.11 Schematic section showing distribution of lithologies in a subaerial rhyolite flow (after Cas & Wright 1987).

The principle component of most older rhyolite flows is foliated, stony (lithic) rhyolite, although in young flows -where erosion is fairly shallow - this is unlikely to be exposed. Where the interior of the flows are exposed, ramp structures are common. This foliation is thought to be due to stretching and shearing during flow, resulting from the interbanding of layers of varying degrees of crystallinity.

A study of subglacial rhyolites was made by Furnes et al. (1980), and their features are summarised below. Subglacial rhyolites consist dominantly of two lithologies; ellipsoidal to irregular lobes (equivalent to basaltic pillow lavas) averaging 7m in diameter, and fragmental material, which Furnes et al. refer to as *hyaloclastite*. Two types of hyaloclastite are described; the first is in intimate association with the lobes,

and the second is pumice-bearing and thought to be generated explosively - this is arguably the acid equivalent of the *hyalotuff* described in section 2.2.3.

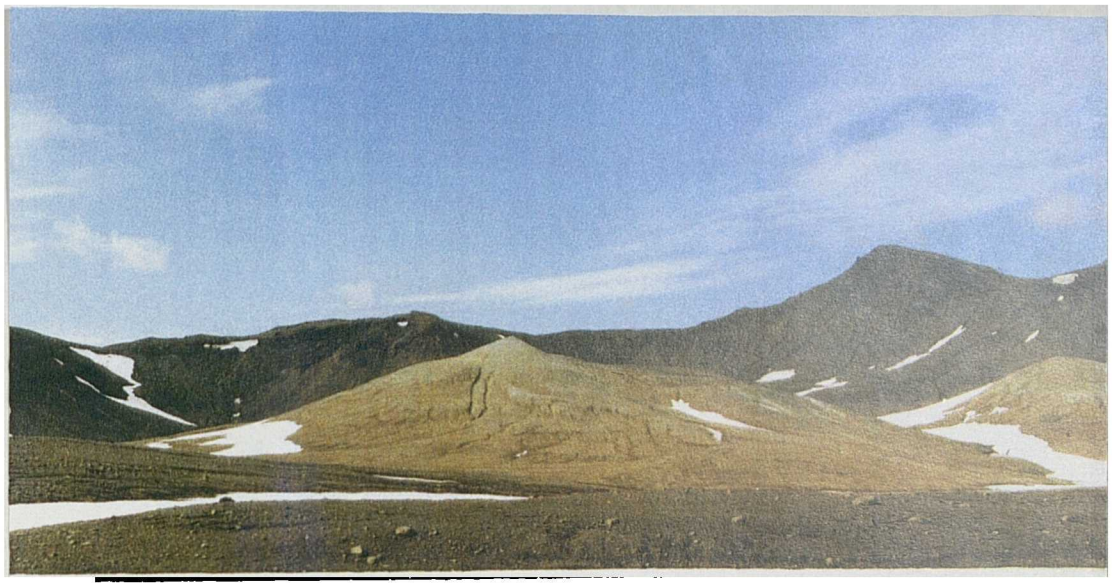

Plate 2.27 Rhyolite dome(?), ~100m high, to the south of Snaefell (385,476).

Most of the acidic lavas at Snaefell are confined to the vicinity of Snaefell itself (i.e. the central volcano), the exceptions are hybrids and will be described in section 2.4. Four separate flows and a ?dome (plate 2.27) can be distinguished with any degree of certainty in the field, three appear to have been extruded from a vent(s) beneath the summit ice cap, while the fourth lies low down to the west. The former three appear to represent almost the last activity of the volcano, although the one on the SW flank is overlain by basaltic material. Close examination suggests that *all* of the rhyolitic lavas were extruded under subaerial conditions and that the magma itself was relatively dry and poor in volatiles, since there is a marked lack of primary *fragmental* material. Eruption probably took place during an interglacial period, since all have suffered glacial erosion subsequently. Erosion has removed all the surface features of these rhyolite flows to reveal their flow-banded, lithic centres, although some loose pieces of obsidian, pumice and lithified obsidian breccias were found in the screes covering most of these flows. Where the lithic rhyolite is exposed some good examples of columnar jointing (plate 2.28), and ramp structures in finer grained examples can be seen. Due to erosion, it is difficult to estimate the original thickness.

Plate 2.28 Rhyolite flow showing well developed curving columnar jointing.

It appears, however, that these flows were unusually thin, certainly the one on the SW flank appears to have been <10m thick! This would imply that these lavas were abnormally fluid on extrusion. Compositionally these lavas are mildly peralkaline (section 4.2.2), and this would certainly result in these lavas having been more fluid than meta-alumnous counterparts, and thus flows would be a little thinner. Another possibility is that the magma was erupted from a zoned magma, a chamber where the cooler, low-density acidic liquid had accumulated above the hotter, higher-density basic liquid, resulting in superheating of the acid liquid (Sigurdsson & Sparks 1981). Such acid magma would be exceedingly fluid, resulting in abnormally thin lava flows. Unlike the Icelandic examples mentioned previously, these do *not* appear to be hybrid in any way (section 3.1.8).

2.4 Magma mixing

As already mentioned above, hybrid lavas were found in the study area (figure 2.4). These were often almost aphyric, streaky or banded rocks which shattered like flint when struck with a hammer. The banding appears to be due to concentrations of finely divided Fe-oxides in the rock, probably precipitated when the two components first mixed. Both discrete exposures of hybrid lavas are present and examples of commingling magmas can be found.

At least two of the hybrid lavas appear to be domes (Saudahnjukar east (391,479), and the example on the SE flank of Snaefell itself), indicateing the relatively high viscosity of the magma. Of possible significance to the magmatic plumbing of the centre, is the peripheral occurrence of these hybrids to the central volcano.

Magma commingling is visible on both outcrop and microscopic (section 3.1.6) scale, and probably occurred as lava was erupted from a *stratified* magma chamber (Blake 1981). Blocks (plate 2.29) and more irregular smeared-out blebs of evolved lava - both pale or glassy rhyolitic compositions and darker, banded hybrids - can be seen as inclusions in a more basaltic host. The blocky shapes of the acid component in some of the aforementioned mixing scenarios illustrates nicely the rheological contrast between the magma types, the more viscous acid magma evidently behaved in a brittle manner on mixing (eruption). Many of these inclusions are also rimmed with highly vesicular basaltic material; the vesiculation probably occurred on mixing, as the basic magma was chilled against the acidic, resulting in rapid exsolution of volatiles.

2.5 The Plio-Pleistocene tholeiites

2.5.1 Lavas

While the aim of this study was to focus on the products of the Snaefell volcanic system, the older, underlying lava pile was looked at in some detail in order differentiate between these lavas and the real subject of this study. Most of the older material is distinct in several ways, and was erupted under dominantly subaerial conditions, although some are intraglacial. It appears that activity in the area previously ceased some 1-2My ago (in the Matuyama magnetic epoch), thus most of the uppermost of the older lavas show reversed magnetic polarity (R), whilst all products of the renewed activity show normal magnetic polarity (N) (A. Gudmundsson pers. com. 1992). A magnetometer was subsequently used in the

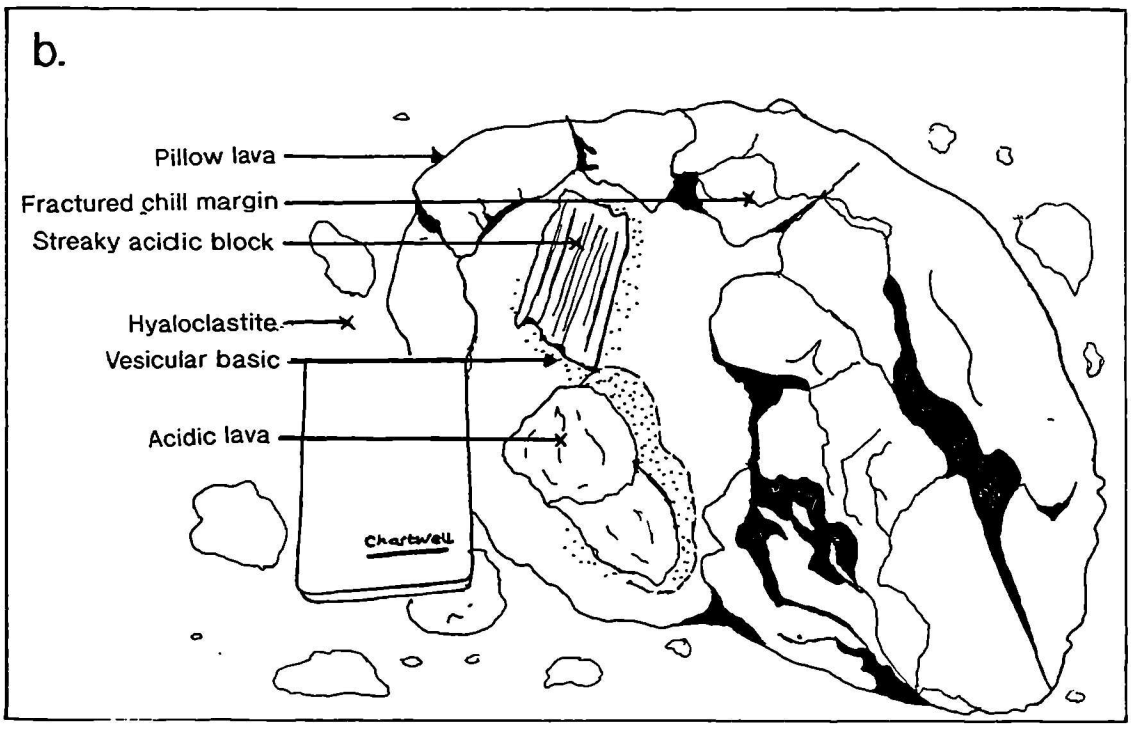

Plate 2.29 a). Co-mingling of magmas at outcrop scale, here demonstrating the rheological contrast between basic and acid end members. The acidic end member seems to have behaved in a brittle manner on mixing. **b).** Line drawing of (a).

field to locate approximately the base of the succession, allowing both sides to be sampled.

Study of the older lavas was begun on a previously studied succession exposed in the bed of the Laurgara river to the NE of Snaefell - the so-called *V profile* (Watkins & Walker 1977). These authors (op. cit.) made an extensive study of a 9000m section of basalts in Eastern Iceland, covering 13.6-2.0Ma, to finally establish a magnetic stratigraphy, tied to previous authors' K-Ar dating. Their study utilised 21 profiles (A-V) through the "flood basalts", of which V is the highest and therefore the youngest. They also observed that there appears to have been a change in climate within the upper third of the section, as cold-climate deposits (tillites etc.) are found. All the lavas also dip gently to the west, the dip angle increasing with age, and being negligible at the top of the section (the V profile). Lava flows V10, V11 and V12[3] were examined and sampled. They are simple subaerial lava flows, probably formed at quite a high extrusion rate (Walker 1971), probably from a fissure eruption. The individual lava flows are separated by intercalations of clastic deposits and thin red horizons. The V-profile itself terminates at V18 (R) in a glaciated surface, below Laugarfell, and is unconformably overlain by the initial products of the renewed activity (N). It thus appears that the hiatus in activity lasted some 1Ma +.

A similar lava succession was observed in the Grjota river to the West, consisting again of simple, basaltic lava flows. They show sparse phenocrysts, mainly of plagioclase and are almost vesicle-free and very hard, indicateing that the magma was probably volatile poor. Columnar jointing is very well developed in many of these flows. The topmost lava here showed normal magnetic polarity, although definitely belonging to the underlying pile.

As previously mentioned, the Plio-Pleistocene climate was cold, and several glaciations occurred (Saemundsson 1979), thus it is unsurprising that some intraglacial eruptions took place. Since the products of such eruptions are much less resistant to the forces of erosion, such deposits are only likely to have been preserved at the top of the succession. Two such tuyas, Bjalfafell and Thjofahnjukar, are present to the south of the Snaefell volcanic system. Both have cap flows characteristic of the older succession and show reversed magnetic polarity. To the east some evolved - andesitic to rhyolitic - flows were found, showing platy weathering.

The base of the Snaefell succession was finally drawn (figure 2.4), however, using compositional criteria: the older lavas are tholeiitic while the later Snaefell volcanics are mildly alkalic (section 4.2.2).

[3]Kindly labelled as such by Walker in a previous visit, with 15cm high numbers in yellow road-paint!

2.5.2 Pyroclastics

A few of the red horizons were examined in detail. In general they are thin, <5cm, and show fairly sharp contacts with the lavas. Occasionally blebs of lava with well developed chill margins, indicateive of rapid cooling, are present (figure 2.12).

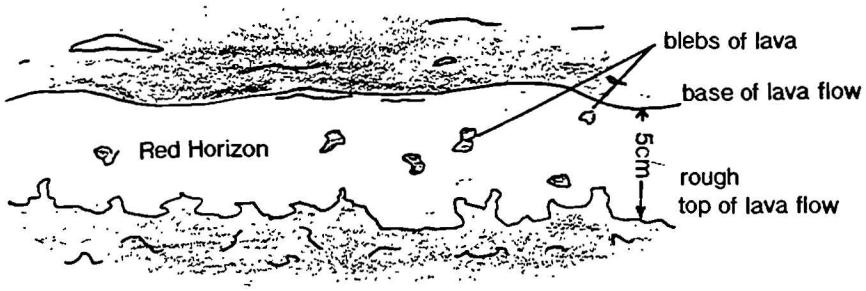

Figure 2.12 Schematic drawing of red horizon intercalated with Plio-Pleistocene tholeiite flow. Note the sharp contacts with both upper and lower flows.

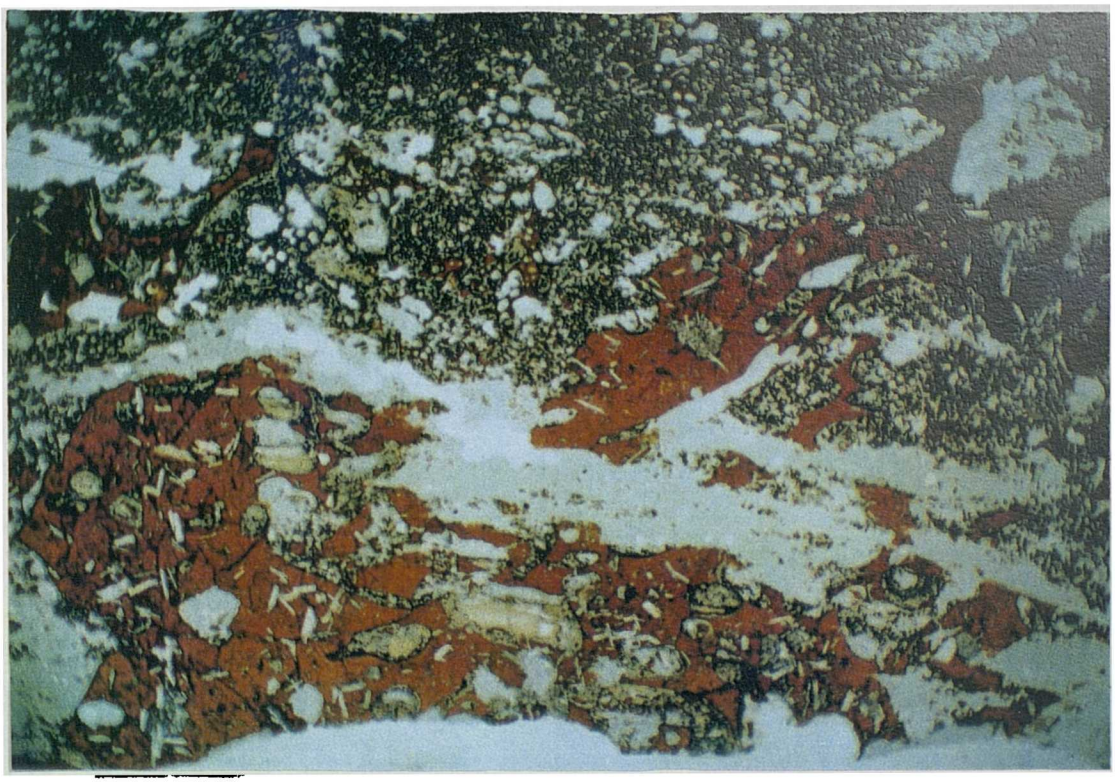

Plate 2.30 Photomicrograph of one of the red (oxidised) pyroclastic flows found intercalated with the Plio-Pleistocene tholeiites. Fragments were evidently originally glassy. Field of view ~12 x 7.2mm, plane polarised light.

These deposits have been interpreted as volcanic dust layers (Watkins & Walker 1977) and fossil soil horizons (Saemundsson 1979). The later seems very unlikely, since the Plio-Pleistocene had a cold climate making deep tropical weathering difficult to envisage.

On examination in thin section (plate 2.30) they can be seen to consist of highly vesicular clasts, often elongate, with scalloped margins (broken vesicles), smaller clasts are highly angular. These clasts are highly oxidised (the red colour of the entire deposit), although it is evident that they were originally glassy; some still contain fresh olivines. It is therefore the opinion of the author that these deposits are pyroclastic in origin, perhaps resulting from an initial explosive phase in the eruption that produced the overlying lava flow. Similar deposits have been described in the British Tertiary by Preston (1982), who assumes them to be wind blown dusts - the glassy spray from lava fountaining - and Kerr (1993).

2.6 Sampling strategy

Since the main focus of this study is the geochemical evolution of the volcanic system, the aim was obviously to obtain a representative sample of each eruption unit for analytical work. This was complicated by several factors: the poor exposure (thick scree cover), the relatively shallow erosion levels and the complex lithological relationships within a single subglacial eruption unit (described in section 2.2.). As previously mentioned also, the central volcano is a classic example of *"heap geology"* with no real stratigraphy; units cannot be traced for any great distance laterally. This meant that the centre could not be sampled representatively by working sections up its flanks. The definition of an eruption unit was verified by taking samples from all lithologies within what was thought to be a single unit on the first visit, thus speeding up the sampling procedure in subsequent visits to the area.

After the initial visit sampling was dominantly restricted to feeder dykes where possible (with the exception of material taken for textural studies from the fragmental deposits). Multiple samples of the same unit were, however, still obtained. Feeder dykes (where exposed) provide samples of clean, fresh rock, are guaranteed to represent that eruption; not incorporated material from previous eruptions (figure 2.13). Some of the pillow lavas and breccias appear to have been affected by hydrothermal solutions, and show vesicles infilled with calcite, indeed calcite veins[4] were observed cutting through many of the tuffs. These were sampled to assess the affects of alteration on one occasion. Loose material derived from previous eruptions can easily be incorporated into the tuffs and breccias (figure 2.13), this was clearly illustrated when samples VH32 and VH33 were collected within a meter of each other from within a tuff breccia unit, which did not show any signs of reworking. VH32 is a

[4]Sampled, and mineral identity verified using XRD analysis.

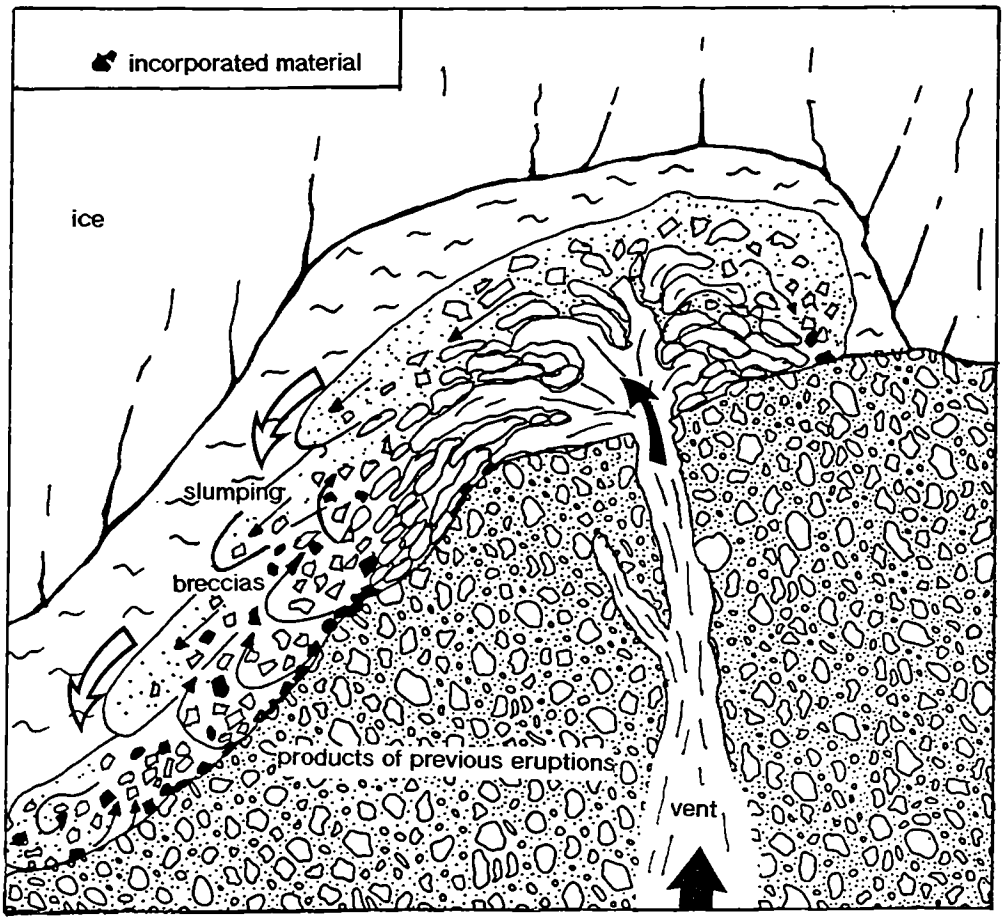

Figure 2.13 Subglacial flank eruption, the vent being located at some elevation so that material is erupted on to a relatively steep slope. The sketch ilustrates how material derived from previous eruptions may become incorporated into the fragmental deposits of the current eruption.

plagioclase phyric mugearite, while VH33 is an olivine basalt; it is obvious that these two samples are derived from separate eruptions.

Obviously in a glaciated terrain such as this, loose material was not collected, except on two occasions (described below); since, even on the top of the smaller tindars, it could have been rafted in by ice. Snaefell's proximity to the glacier, Vatnajokull (<15km), means that the area has extensive deposits of moraine material (figure 2.4) and has probably suffered many local glaciations bringing in yet more material. On the two occasions when loose material was collected, it was taken from the high up in the moraines of two of Snaefell's main glaciers, A (samples prefixed MB) and C (samples prefixed MA) in figure 2.3. This was done in an attempt to ensure that the entire compositional range of the central volcano was represented in the sample collection, since the glacier might have sampled deeper units not otherwise exposed.

2.7 Summary

The results of field mapping and volcanological studies have been presented in this chapter, the main points to come out of this work are summarised below:

1). The Snaefell volcanic system was active within the last 0.7Ma, and is now considered to be extinct. Volcanic activity previously ceased in the area at around 2Ma.

2). Although the onset of activity occurred during an interglacial period, the bulk of the eruptions occurred beneath the Upper-Pleistocene ice sheet, thus most of the products belong to the *moberg formation.*

3). As is typical of Icelandic volcanics, the system is bimodal, the only compositionally intermediate lavas have been proven hybrid by work to be presented in subsequent chapters. The rhyolitic lavas are confined to the central volcano (Snaefell itself).

Chapter 3
Petrography and Mineral Chemistry

In the following section the petrography of the Snaefell suite (and more briefly the underlying Plio-Pleistocene tholeiites) will be described, and genetic implications of phenocryst assemblages and textural features discussed. Subsequently the chemistry of the mineral assemblages will be presented and discussed. The Snaefell series has been divided up using primarily chemical criteria and these are described and discussed fully in section 4.2. Some petrographic divisions within the basaltic end of the series are, however, described and can be related to magma chamber processes such as magma mixing and residence time, and to the bulk chemistry of the samples concerned.

3.1 Petrography

3.1.1 General features of the Snaefell suite

This is a suite of mildly alkaline rocks, ranging from nepheline-normative basalts to peralkaline rhyolites, with corresponding mineralogies.

Both vesicular and non-vesicular examples are found, indicating that either some magmas were more volatile-rich than others, or that the pressure under which they erupted varied. In some lavas two stages of degassing are evident; some vesicles appear very sheared while others appear circular and probably represent late, post-emplacement, degassing. Vesicles in some cases account for nearly 50% by volume of the rock; such samples generally come from either pillows within the *moberg* formation or from spatter deposits.

Phenocryst contents are generally low (<3% by volume; hereafter all modes are given as vol. %), although in some cases they can reach up to 20%, and some completely aphyric samples have been found. The low phenocryst contents are an advantage when it comes to looking at the bulk compositions, in that they should be fairly close to the liquid lines of descent and not confused by crystal accumulation. Pronounced crystal accumulation, most commonly of plagioclase, has occurred in a few samples and is easily detected in both bulk composition and petrography. It is worth noting, however, that the effects on the majority of trace elements (with the

exception of Sr, which is compatible in plagioclase) are minor; trace element ratios certainly may be considered unaffected. In this study microphenocrysts are defined as <0.7mm (Jakobsson 1979a); the distinction between microphenocrysts and groundmass is, however, somewhat gradational. In terms of formation, macrophenocrysts are assumed (Cox et al. 1979) to have formed at depth in an intratelluric environment, and thus are more likely to be euhedral and show complex zoning, while microphenocrysts supposedly formed on quenching, post-extrusion, at cotectic conditions. They are consequently generally subhedral and show little zonation. In the case of some mineral phases, this is not strictly true; early-formed chromites rarely exceed 0.1mm and the spinel phase in general is usually present in the form of euhedral microphenocrysts. Chromites are found enclosed in large euhedral olivine crystals, but, perhaps more convincingly, euhedral magnetites are found in the vitric tuffs enclosed in quenched glass fragments, confirming their intratelluric origins.

Macrophenocrysts of plagioclase feldspar show both normal and, less commonly, reverse zoning as well as oscillatory zoning and mantling with feldspar of different composition and zones of skeletal growth. Normal zoning is what would be expected in a case of simple crystal fractionation, although in a slowly cooled system - where plagioclase is the only phase on the liquidus - reverse zoning can result (Loomis 1982). Oscillatory zoning is thought to result from changes in temperature, and also possibly pressure, during crystallisation; probably caused by periodic convection within the magma chamber on a small scale (Carr 1954, Loomis 1982). Magma mixing can be invoked to explain the occurrence of mantled feldspars (Hibbard 1981). Mixing of a hot mafic magma with a cooler felsic one, both probably charged with crystals, results in undercooling of the mafic one. The result is rapid, dendritic plagioclase growth on any feldspar crystals present and occasionally homogeneous nucleation to produce wholly skeletal phenocrysts. As the system becomes less heterogeneous, and equilibrium approaches, the skeletal growth will be followed by a growth shell of similar composition. At the same time the felsic magma will become superheated, resulting in dissolution of alkali feldspars (and other phenocryst phases) to produce ovoid shapes and sieve textures, such as are observed in some of the basaltic compositions in the Snaefell suite. Care should be taken, however, in the interpretation of sieve-textured plagioclases, since recent experimental work (Nelson & Montana 1992) indicates that these textures can be produced by rapid, isothermal decompression. Extrapolation of their results to apply to geological systems suggests that the resorption could result from depressurization of at least 2-3 kbars, which could occur *in conjunction* with magma mixing. These complex plagioclase phenocrysts are typical of flank zone eruptives, those in the axial rift zones generally contain tabular, euhedral examples (Meyer et al. 1985). This implies that there are

fundamental differences in magma evolution and supply between flank and axial rift zones. Specifically in the flank zones it implies longer residence times in magma chambers, longer time intervals (and therefore greater degrees of fractionation) between magma chamber replenishments in flank zone volcanic systems.

Clinopyroxene also occasionally shows zonation. Both hourglass and sector zoning are present, although these are for the most part poorly developed. Clinopyroxene also often shows undulose extinction and simple twinning. Complex phenocrysts are present right the way through the Snaefell suite, except in the rhyolitic end members; possibly indicating that these evolved in isolation from the more primitive magmas.

Glomeroporphyritic samples are fairly common throughout the series, displaying both monomineralic glomerocrysts and more commonly ones consisting of up to five mineral phases. These can reach several mm across, but more often are 1-2mm in diameter, being made up of many individual microphenocrysts. Glomerocrysts form by secondary nucleation of later mineral phases on early formed ones (Dowty 1980) and can therefore give information about the order of crystallisation operating within the whole suite of rocks, not just within the individual sample. Also seen are intergrowths between two, occasionally more, mineral phases; possibly indicating simultaneous nucleation (Thy 1983) or that there has been secondary nucleation on an earlier mineral phase which has continued to grow along with the later one. The presence of glomerocrysts showing intergrowth between olivine, plagioclase and augite indicates that crystallisation must have occurred under low pressure, cotectic conditions; i.e. in a shallow crustal chamber, implying such basalts cannot be primary.

Gabbroic and acidic xenoliths, distinct from the glomerocrysts, are also found. They appear to be derived from cumulates, although their original textures are masked by their having undergone some degree of partial melting. The gabbroic inclusions resemble those described by Jakobsson et al. (1978) from the Reykjanes peninsula, which they suppose to be autogenic (cognate).

Samples are occasionally *holocrystalline* (following the scheme of MacKenzie et al. 1982), although less often than in the underlying (pre-Snaefell) tholeiites. More commonly the groundmass will show some areas with an *intersertal* texture, still containing fresh glass, or the alteration products thereof. Glass becomes more abundant in the more evolved members of the series (due to nucleation problems in more silicic compositions), culminating at the rhyolitic end of the scale with *hyalophitic* groundmasses in the pitchstones. The grainsize can vary quite significantly across a single unit, from the quenched (*cryptocrystalline* or glassy) material on the pillow rinds to more coarsely crystalline at the centres of the larger feeder dykes, which experienced lesser degrees of undercooling. One important point to note is that grain size does not appear to have any direct correlation with changes in chemistry.

Often the groundmass shows strong signs of oxidation, such as blackening of once glassy regions (seen in segregations of residual dregs of melt - the evidence for which is to be discussed in the following section) and an abundance of divided opaques.

3.1.2 Snaefell basalts (11-6.5 wt% MgO, <4 wt% total alkalis)

There is a wide variation in phenocryst content, from around 15% to <<1%. Although no samples appear to be completely aphyric; close examination generally reveals at least a few microphenocrysts.

The dominant phenocryst phase in the basalts is **olivine** and, in the least evolved ones, the only macrophenocryst phase. It varies in size from ~2mm (although in one or two hand specimens megacryst of ~10mm diameter have been observed) to ~0.1mm in the groundmass. In some cases the distinction between phenocrysts and groundmass is obvious; e.g. sample VH10 (plate 3.1), which constitutes part of a small pillow fragment, and was thus rapidly quenched. In more slowly cooled samples, the distinction can be less clear. Just about all growth forms are observed, from euhedral to anhedral, often showing signs of resorption (previously discussed with reference to feldspars) such as a rounded outline, embayments and sieve textures (plates 3.2). Signs of resorption are seen even in VH10, which is the most primitive sample found (11wt% MgO), perhaps indicating that the phenocrysts at some stage in their growth came into contact with a hotter, presumably more primitive magma. This implies that the parental magmas to the suite are not represented in surface extrusives and contained >11wt% MgO. Glomerophyric clusters are fairly common, consisting sometimes of just small euhedral olivines (plate 3.2), more rarely in other samples of intergrowths of olivine with plagioclase, magnetite and pyroxene which sometimes form spheroids (plate 3.3), where early-formed olivine has presumably provided a nucleus for later plagioclase growth. The samples most commonly showing polyphase glomerocrysts often appear to be hybrid and evidence for this will be discussed subsequently.

Compositionally the olivines show little zoning, although some show slightly more iron-rich rims (visible evidence for this is increasing order of birefringence colours outwards), and this is discussed in section 3.2.1.

Small (<<0.1mm), brown **chrome spinels** are closely associated with, and more often contained within the olivines in less evolved basalts, (plate 3.1). Despite the small size of these, it appears that they crystallised first, although it has been suggested (Thy 1983) that the close spatial relationship of chrome spinel and olivine indicates that the nucleation of chrome spinel is dependant on olivine growth.

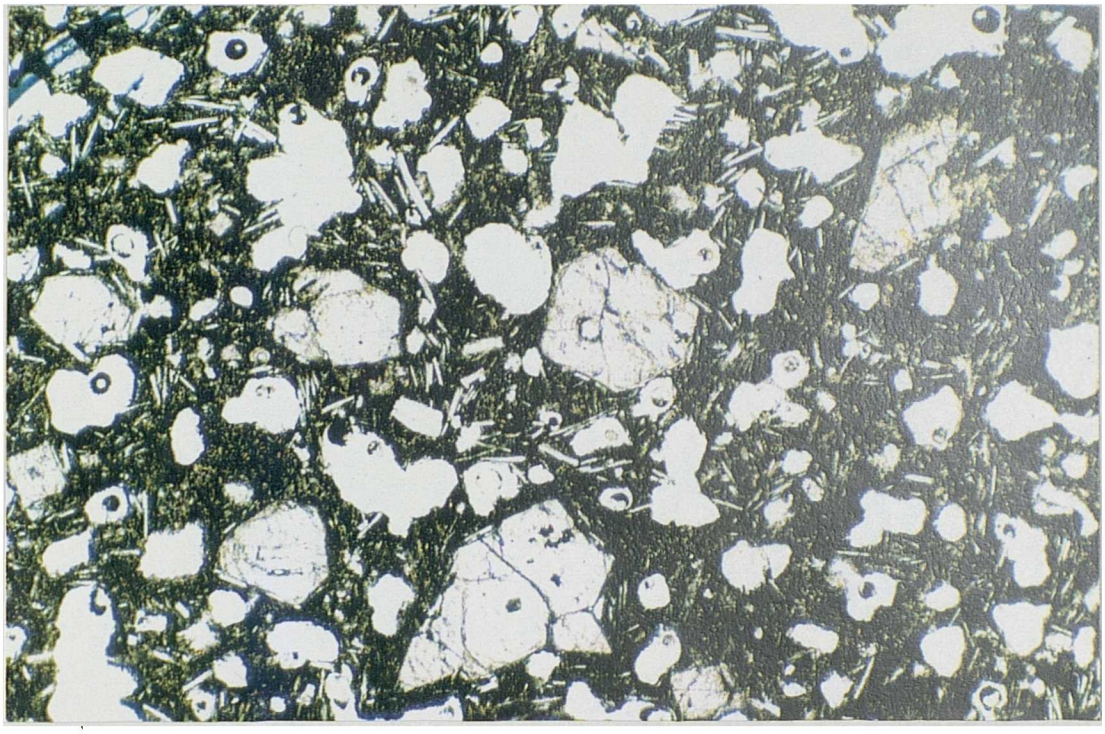

Plate 3.1 VH10, Small euhedral olivine phenocrysts in fine-grained groundmass, note small inclusions of chromite in olivines. Field of view 3 x 1.9mm, shown in plane polarised light. (PPL).

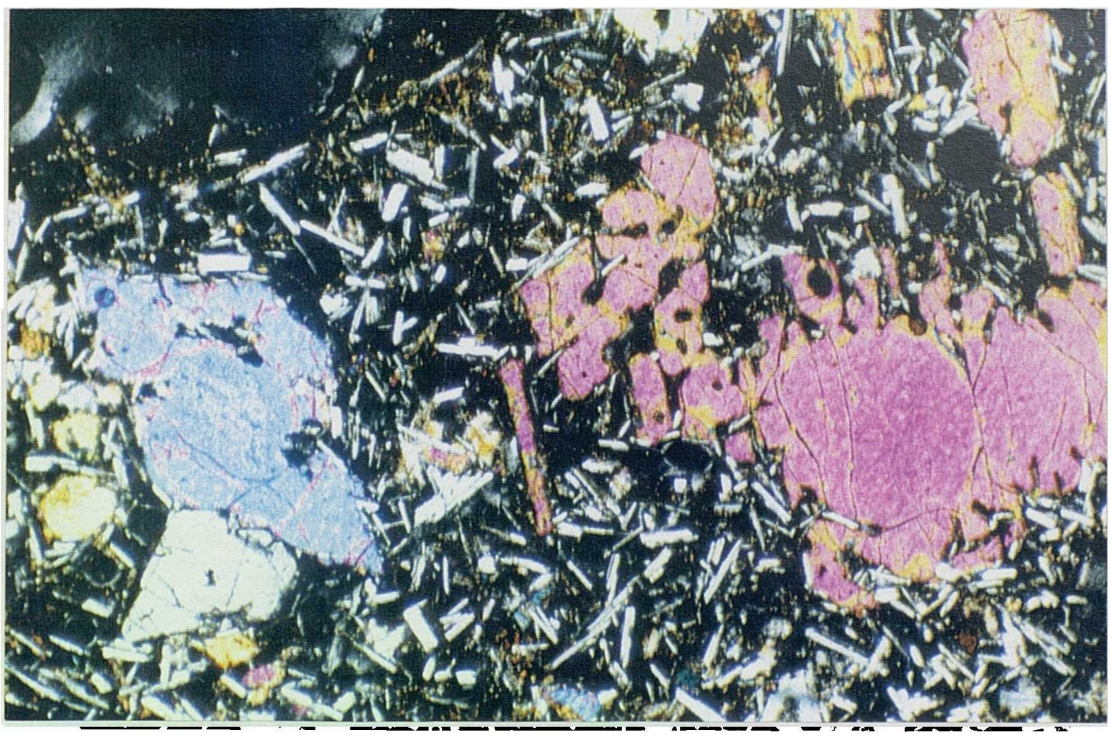

Plate 3.2 Primitive basalt, VH21 containing partially resorbed olivine phenocrysts and small glomerophyric aggregates. 3 x 1.9mm, crossed polars. (XP).

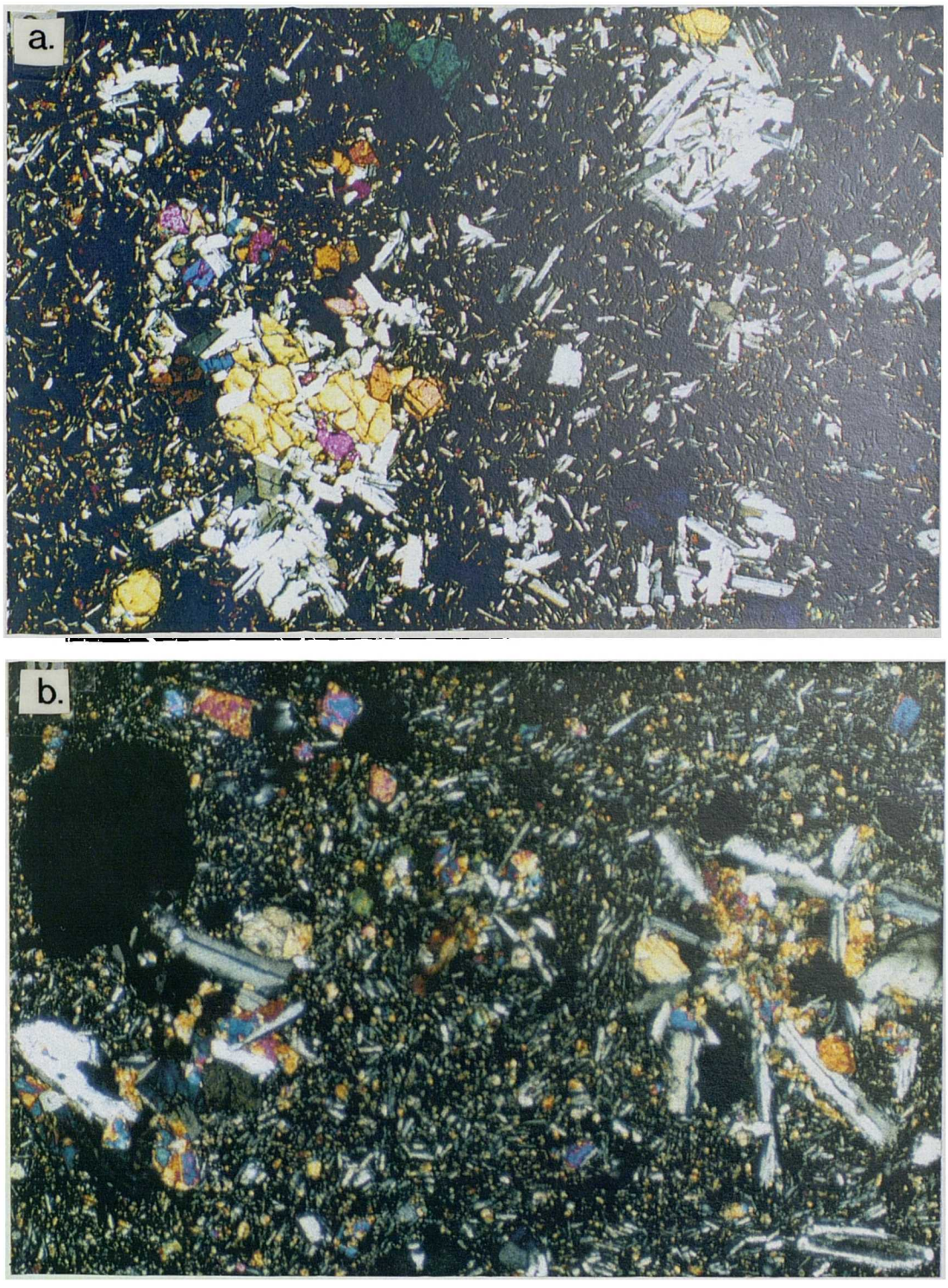

Plate 3.3 Examples of glomerocrysts seen in basalts:

a). VH246, field of view contains two glomerocrysts, one consists of ol, cpx +pl, the second is monomineralic, consisting of just plagioclase. 6 x 3.7mm, XP.

b). VH80, Spheroidal glomerocrysts. 3 x 1.9mm,. XP.

Another possibility is that chrome spinels outside the olivines are resorbed, as the liquid composition becomes increasingly evolved and the temperature falls.

The third phase to appear on the liquidus is **plagioclase** feldspar. This is lacking as a phenocryst phase in the most primitive basalts, although present in the groundmass, where it appears to be compositionally labradorite[1]- typical of basalts with alkaline affinities such as these (Jakobsson 1979a). Phenocrysts reach 4mm in sections examined and all sizes between this and small laths in the groundmass, <0.1mm in length, are seen (in the field megacrysts up to 30mm were seen, but these are rare and were thus not captured in section). The plagioclase varies from euhedral tabular crystals to rounded, evidently resorbed examples with skeletal zones full of glass inclusions (plate 3.4a), indicating magma mixing (Hibbard 1981). This could be due to periodic refilling of the magma chamber with hotter, more primitive magma from source. The simple, euhedral, unzoned examples usually show well developed albite twinning and are compositionally labradorite[1], or around the boundary between andesine and labradorite in slightly more evolved samples. Many of the phenocrysts are, however, are either normally zoned or more complex, resulting from numerous different growth periods in their formation. Often the centres appear to consist of an earlier (more calcic) plagioclase glomerocryst, overgrown with one or more layers of plagioclase of slightly different composition. Oscillatory zoning is also seen, although it is much more common and better developed in more evolved members of the Snaefell suite. Partially resorbed alkali feldspar ovoids can also be seen in some samples.

In some cases the bulk composition of samples classed as basalts is actually rather low in alkalis and MgO; this is due to plagioclase accumulation. One such sample comes from a small eruption unit somewhat displaced to the north from the rest of the complex - Thraelahals - that was probably underlain by a small magma chamber, which reached a high degree of crystallinity prior to eruption. The accumulation of plagioclase could have occurred by flotation, as suggested by Bryan (1983) from his study of MORBs.

The fourth phase to join the crystallising assemblage is clinopyroxene (**augite**). The importance of clinopyroxene as a phenocryst phase is typical of oceanic hotspot basalts (Bryan 1983, Schilling et al. 1983). As a phenocryst it is yellow/brown and can reach 3 mm in size, generally only one cleavage is visible and extinction is at a high angle (up to 45°) to this. The most common form is rounded anhedral, probably partially resorbed and present in samples which appear hybrid, both in terms of texture and bulk composition. These samples contain all rounded phenocrysts, commonly full of melt

[1]Plagioclase compositions in section 3.1 were all determined optically, using the maximum symetrical extinction angles of alternate albite twin lamellae, measured from the fast (α') vibration direction.. For this method to be accurate the section must be cut normal to the {010} plane (Deer et al. 1992).

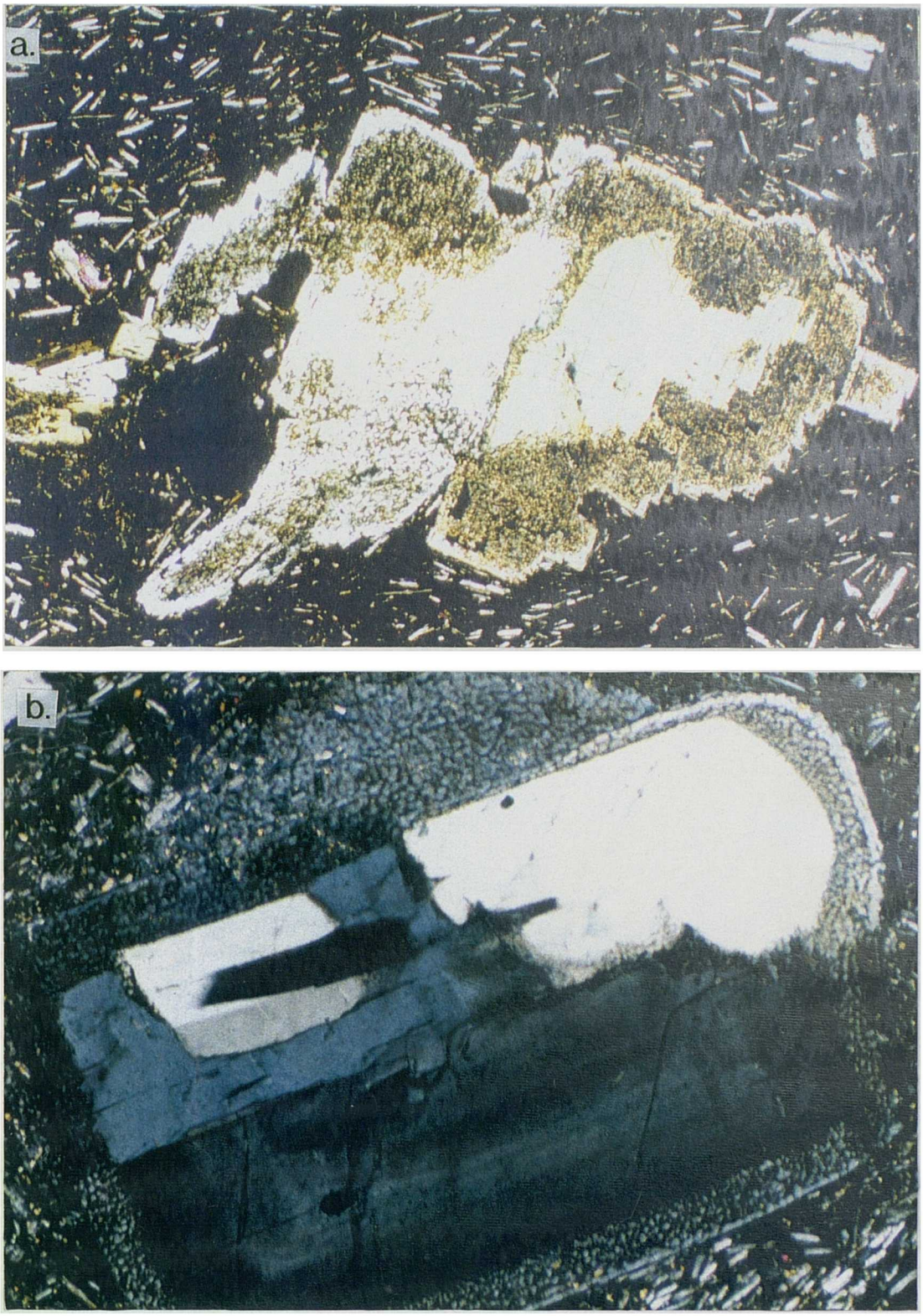

Plate 3.4 Complex plagioclase, showing multiple growth zones and compositional zoning:
(a) VH193, shows dendritic growth zones.
(b) VH43, shows multiple growth zones, compositional zonation, and zones showing a sieve texture. Evidence for open system processes. Field of view 3 x 1.9mm, and 6 x 3.7mm respectively, both shown in XP.

inclusions and a wide variety of feldspar compositions. In terms of composition they are lower in $Fe_2O_3(T)$ than would be expected. Optically there is little evidence of compositional zoning in most cases; a few show patchy extinction that could relate to sector zoning. In more evolved samples microphenocrysts of brown/green pyroxene (which occasionally shows simple twinning) occur. In some instances the clinopyroxene is intergrown with plagioclase.

The **groundmass** in the basalts consists of laths of plagioclase (usually labradorite[1], although reaching andesine[1] in the more evolved basalts) often hollow - swallowtailed - as a result of quenching; clinopyroxene as yellow/brown anhedral grains, or subophitic/ophitic crystals (oikocrysts reaching 2mm in length), or lath shaped and varying widely in colour from yellow to green to brown, (some even appears zoned, plate 3.5); small olivines, euhedral and anhedral magnetite; tiny needles of ilmenite and, more rarely, dendritic growth of oxides; and minor amounts of alteration products replacing glass. Grainsize in the groundmass varies from medium grained (~0.5mm) down to cryptocrystalline. Texturally there is quite considerable variation; a few samples are holocrystaline and are either *ophitic* or *subophitic*, or *intergranular*. The rest show either an intersertal texture, or gradations between intersertal, subophitic and intergranular (plate 3.6). All groundmass textures may be seen within a single sample.

In some samples there is a gradational change in the matrix composition towards the vesicles, with a general decrease in the size of the plagioclase laths and an increase in the abundance of brown pyroxene and opaques, culminating in a opaque lining to the vesicle (plate 3.7) - probably glass that has suffered late-stage deuteric oxidation. In other cases the division is much sharper and laths of groundmass plagioclase may be seen to be arranged tangentially to the edge of the vesicle (also seen in plate 3.7), some are very rich in fresh glass. These features would thus appear to be segregations of the residual dregs of melt drawn into the vesicles, as the gas pressure in them fell with progressive cooling. Some appear to have been sheared, indicating that the rock was still fairly mobile when they formed. These features are not limited to the basalts, but are also seen in the next three groups.

Plate 3.5 VH151. Zoned subophitic clinopyroxene in groundmass. 1.3 x 0.77mm, PPL.

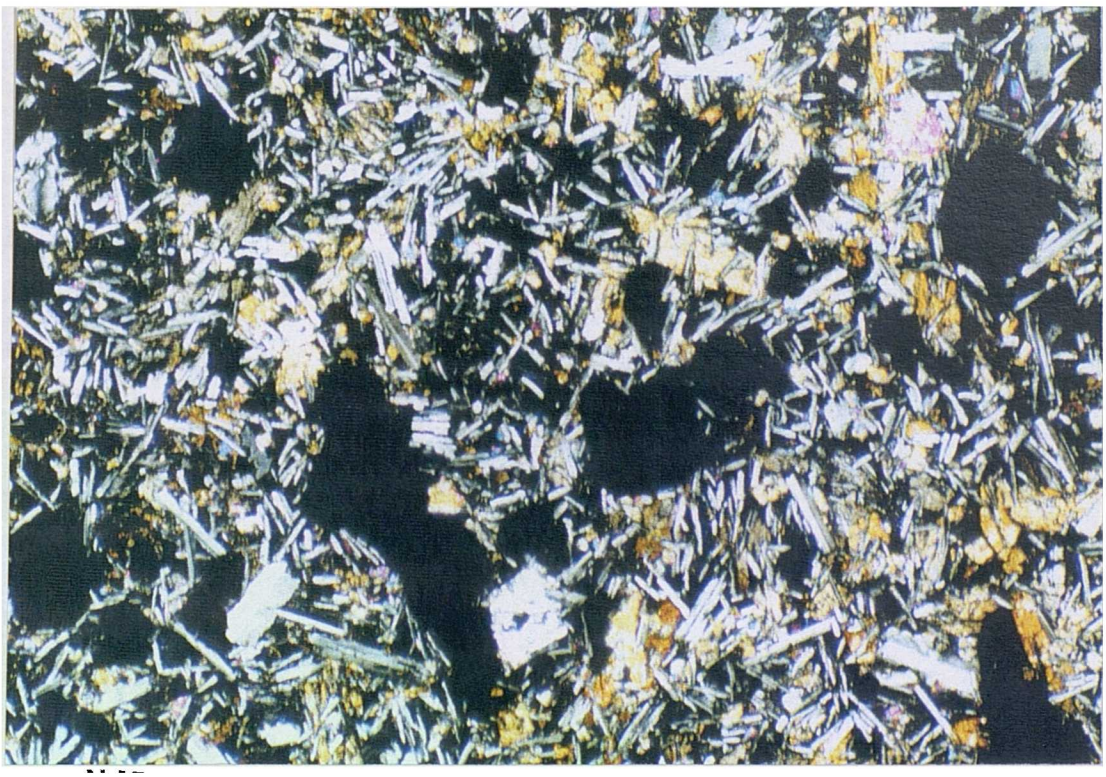

Plate 3.6 Basalt (VH160) displaying groundmass with subophitic, intergranular and intersertal areas. 3 x 1.9mm, XP

Plate 3.7 VH6, Segregations of residual dregs of melt, surrounding and drawn into vesicles. 3 x 1.9mm, PPL.

Ankaramites.

An ankaramite is strictly defined as a porphyritic melanocratic basalt, with abundant phenocrysts of pyroxene and olivine (LeMaitre 1989). In Iceland, they are classified as part of the transitional alkalic series, as basalts containing olivine, augite, plagioclase and magnetite in that order of abundance (Jakobsson 1979a),At Snaefell a single lava flow (sampled several times) has been found that may be classified as ankaramitic. It is rather low in MgO (8%) to be a true ankaramite. It contains up to 20% phenocrysts; macrophenocrysts of augite and olivine (in a ratio of ~3:2) up to ~1mm and microphenocrysts of plagioclase ranging from ~0.4mm down to indistinguishable from the groundmass. The grainsize of the groundmass varies from ~0.3mm to <<0.1mm, and is made up of anhedral to subophitic yellow/brown titan-augite, plagioclase laths and magnetite. Texturally it varies from intergranular to subophitic, depending on the position relative to the surface of the lava flow.

3.1.3 Basaltic hawaiites (7-4.5% MgO, 4-5% total alkalis)

The definition of basaltic hawaiite here is both compositional (given above) and mineralogical. Samples in this category all contain plagioclase which optically appears to be andesine, as opposed to the labradorite seen in the basalts. Most are fine-grained and relatively poor in phenocrysts, if not essentially aphyric.

Olivine is much less common than in the basalts and it is no longer the main phenocryst phase. The crystals are generally <0.5mm in size; exceptionally one unit contains olivines up to 2mm. Most are euhedral or subhedral, although a few samples contain excellent examples of skeletal growth forms; the result of very rapid growth (Drever & Johnson 1957) - not seen in the basalts. They also show a greenish body colour, however this could be simply due to staining; since it appears stronger near the edges and following cracks.

The dominant phenocryst phase in the basaltic hawaiites is **plagioclase**, which ranges in size from ~3mm to tiny laths in the groundmass. As with the basalts, several generations, are visible; larger, including complex macrophenocrysts showing signs of resorption mantling and oscillatory zoning (plate 3.4b); smaller unzoned crystals (andesine) and groundmass laths. While most of the phenocrysts are andesine[1], some of the glomerocrysts contain labradorite[1]. Occasionally, reverse zoned phenocrysts are also found.

Clinopyroxene is more common than it is in the basalt and subhedral to anhedral microphenocrysts are seen in most samples. They are a fairly uniform brown/green colour and have high extinction angles. Some display simple twinning at a high angle to the dominant cleavage and hourglass zoning (made visible by differences in extinction position for the different sectors).

At this stage of fractionation, the spinel phase returns to the liquidus, in the form of **magnetite**. It is very abundant (reflecting the Fe_2O_3(T) enrichment which reaches a maximum somewhere between this group and the hawaiites (section 4.3.4)) as euhedral microphenocrysts, ranging from 0.4mm to crystals indistinguishable from the groundmass. The abundance of magnetite gives many basaltic hawaiites a dark colour.

Glomerocrysts are fairly common, exceptionally reaching 4mm across, but commonly <1.5mm, and dominantly made up of individual microphenocrysts. Occasionally they contain all four phenocryst phases, but more commonly they only contain one of the mafic phases.

The **groundmasses** are generally fine-grained, ranging from 0.3mm to cryptocrystalline; signs of quenching are common. They are composed of: clinopyroxene ranging from yellow/brown titanaugite to browner more iron rich compositions; plagioclase laths (andesine in composition); rare, small, sometimes

euhedral olivines; abundant magnetite and needle-like or dendritic ilmenite and small (<0.1mm) greenish acicular crystals of apatite - not seen in the basalts. The basaltic hawaiites are also much richer in plagioclase and opaque oxides (often increasingly blackened by late-stage oxidation) and often still contain some fresh brown glass in the interstices. Texturally they range from intergranular to ophitic (the oikocrysts imparting an *ophimottled* texture to the sample, plate 3.6), often showing intersertal patches. Some now show a *trachytic* texture, indicative of flowage after crystallisation, despite the fact that many of the plagioclases appear to be the result of quenching, having swallowtail ends. In other samples radiating bundles of plagioclase laths indicate rapid crystallisation from a single nucleus.

3.1.4 Hawaiites (4.5-3.5 %MgO, 5-6% total alkalis)

All the hawaiites are fine grained and phenocryst contents are low (<3%). Mineralogically and texturally this group is very similar to the basaltic hawaiites.

Olivine occurs only as a microphenocryst, up to ~0.5mm, it varies from euhedral to subhedral and often shows embayments and lobate outlines resulting from resorption. A single macrophenocryst was observed; it appeared much stained and had also suffered resorption, indicating its derivation from another magma. Compositionally the olivines are much more iron rich than previously seen (section 3.2.1). They often appear to enclose magnetite and are found intergrown with plagioclase in the so-called "bow-tie" form (plate 3.8).

As in previous groups, complex **plagioclases** are present; unzoned ones are compositionally andesine[1]. Plagioclase is often seen in glomerophyric clusters with clinopyroxene, olivine and magnetite. Occasionally it is poikilitic, containing small, greenish pyroxenes, magnetite and glass inclusions. Both phenocrysts and smaller groundmass laths are often aligned, to give a pronounced trachytic texture.

Clinopyroxenes are usually green/brown subhedral and occur in small clusters <1mm across; a few have hourglass zoning and many show undulose extinction. Occasionally there are more elongate dark brown, more-iron-rich ones in the more-evolved samples.

Magnetite phenocrysts are abundant and can reach 0.5mm; some skeletal examples were also seen.

Small **apatite** microphenocrysts are present in a few sections, reflecting the high P_2O_5 content of this group; up to a maximum of 1.25% (section 4.3.4).

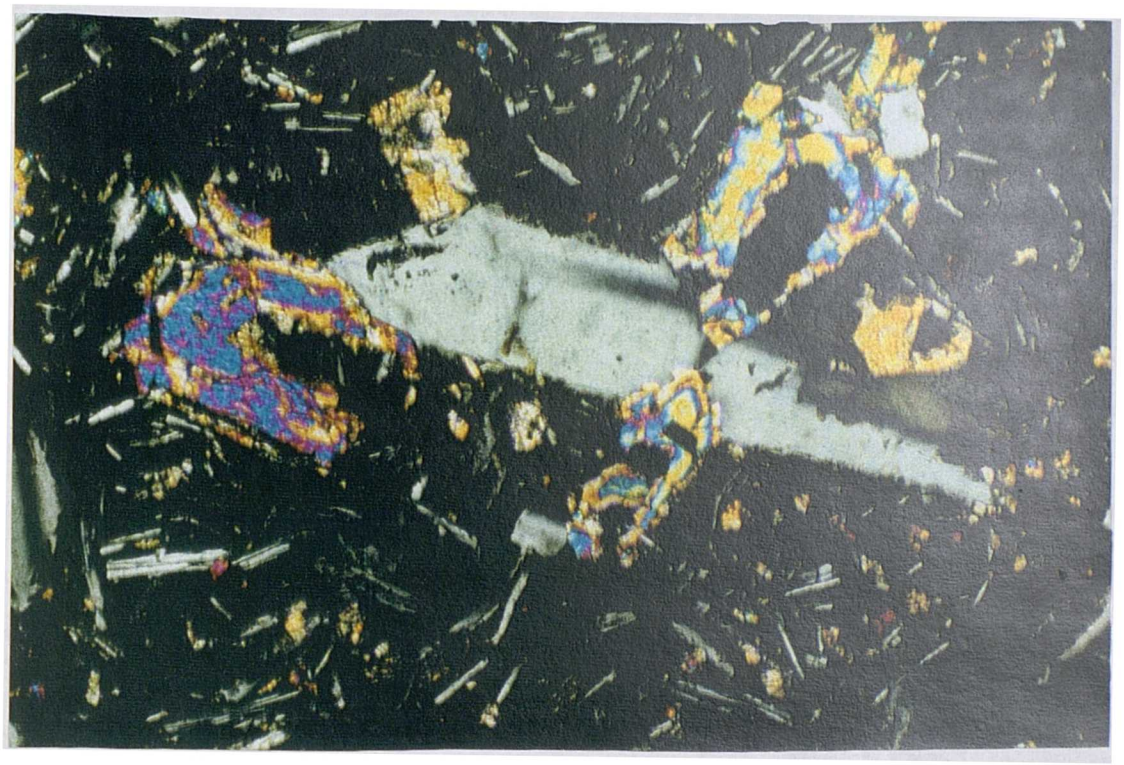

Plate 3.8 "Bow-tie" intergrowth of olivine and plagioclase in a hawaiite, VH156,. 1.3 x 0.77mm, XP.

The **groundmass** consists of laths of plagioclase, ranging from andesine to oligoclase, often with a swallowtail form, indicating quenching; pale brown ophitic/subophitic clinopyroxene; magnetite; ilmenite; and abundant small, green, acicular crystals of apatite (<0.1mm), aligned and in sprays. Again it is very fine grained. Glass becomes much more abundant as the rocks become more evolved, thus no holocrystaline hawaiites were found; most show textural gradation from intergranular or ophitic to intersertal on a scale of <1mm. Some show a completely opaque groundmass which was originally probably completely glassy prior to late-stage deuteric oxidation.

3.1.5 Mugearites (3.5-2 %MgO, 5-7 % total alkalis)

Like the hawaiites, the mugearites are all fine-grained (groundmasses <0.2 mm) and poor in phenocrysts (<3%); some are completely aphyric. Again, they are generally glomeroporphyritic. **Plagioclase** now is dominantly oligoclase[1], although larger (up to 2mm) zoned and mantled examples, some showing sieve textures of varied composition, are still seen. Some larger phenocrysts also show signs that a period of resorption was most recent in their development. Generally, the plagioclases do not exceed 0.5mm and are often flow aligned to give the trachytic texture typical of mugearites (plate 3.9).

Plate 3.9 Mugearite (VH148) showing typical, well developed trachytic texture. 3 x 1.9mm, PPL.

Olivine is present as subhedral skeletal microphenocrysts (<0.3mm) in some, though not all, porphyritic samples. **Clinopyroxene** is fairly abundant, both as a phenocryst phase and making up a large proportion of the groundmass. Clinopyroxene phenocrysts are generally <0.2mm, and usually occurs in glomerophyric clusters with plagioclase and magnetite. In colour they vary from brown to more green and some show oscillatory zoning (plate 3.10). **Magnetite** is still abundant and is usually euhedral, although sometimes skeletal. The crystals can reach 0.4mm across.

Plate 3.10 Clinopyroxene glomerocryst, showing fairly well developed oscillatory zoning, this example from VH99. 0.66 x 0.4mm, XP.

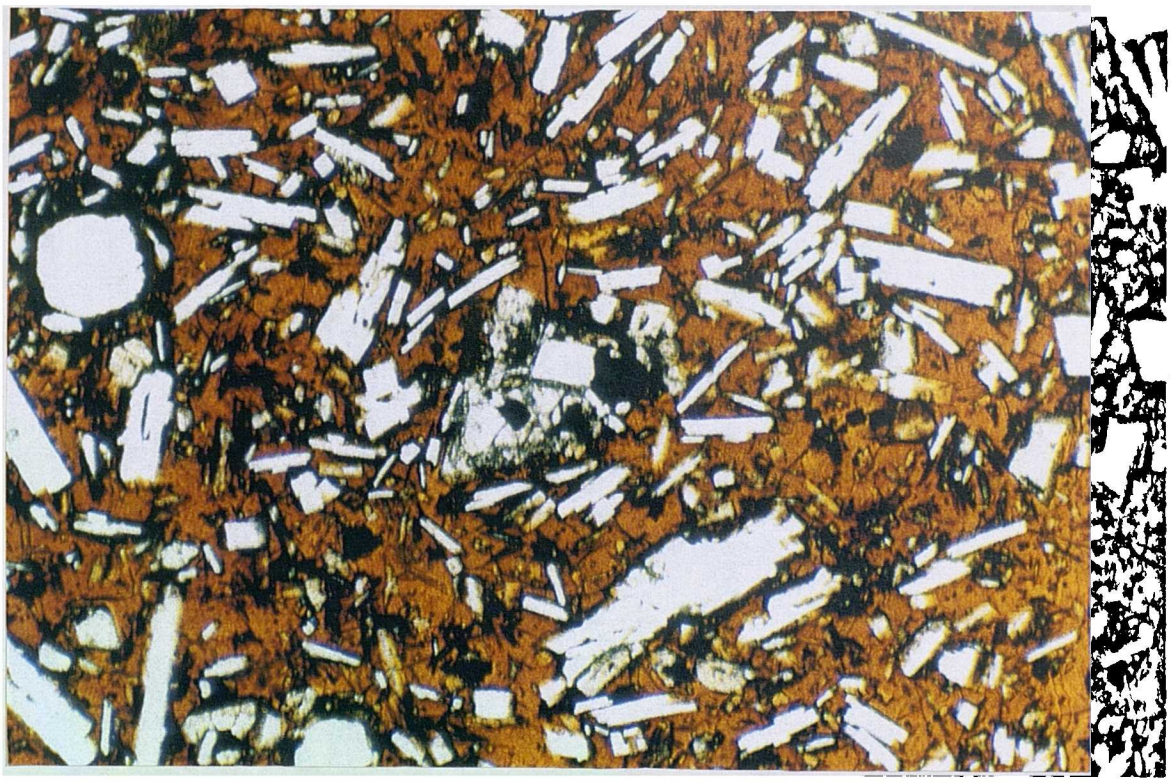

Plate 3.11 Mugearite showing hyalophitic groundmass, VH137, sample from pillow rind. 3. x 1.9mm, PPL.

Brownish **apatite** microphenocrysts are also in evidence in the less evolved members of this group.

The **groundmass** is usually intergranular grading into intersertal with abundant fresh brown glass; some samples have a hyalophitic groundmass (plate 3.11). The groundmass is otherwise very fine grained, mostly <0.2mm, and made up of hollow plagioclase laths (usually with a thin film of glass around them), pale yellow/green anhedral clinopyroxene, euhedral magnetites; occasional ilmenite needles and small acicular apatites.

3.1.6 Benmoreiites (2-0.5% MgO, 7-8% total alkalis)

Samples which classify as benmoreites in terms of bulk composition are fairly rare, and those that do may be divided into two groups. The first group is fine grained and fairly low in phenocrysts (<3%), and members of the second are mixed rocks, being streaky or banded and associated with occurrences of magma co-mingling, sometimes obvious in outcrop. The latter group are very similar to rocks chemically classified as trachytes, see section 3.1.7 for description.

The benmoreiites themselves may be further subdivided on petrographic examination, the first group appear less evolved and are probably true benmoreiites, while the latter show signs of being hybrid in terms of their phenocryst populations.

1. Benmoreiites

These are fairly fine grained and low (<2%) in phenocrysts. The dominant phase is **plagioclase** It rarely exceeds 0.7 mm and is sodic in composition, showing almost symmetrical extinction. Mafic phenocrysts are generally small (~0.2mm), often indistinguishable from the matrix, and rare. **Olivines** are lath-shaped and greenish in colour and **clinopyroxenes** are anhedral, brown/green (ferroaugite) and often occur in glomerophyric clusters. **Opaque oxides** are much less common than in previous groups and often rounded. The **groundmass** in some cases is fairly coarse, reaching ~0.4mm average grainsize, and is texturally fairly uniformly intersertal. It consists of laths of sodic plagioclase and occasionally more equant alkali feldspars, small green anhedral clinopyroxenes, very small equant magnetites and fairly abundant brown glass.

2. "Hybrids"

The dominant phenocryst phase in these is **feldspar**, which is up to 4 mm and shows zones of skeletal growth (plate 3.12a) indicating a magma mixing episode.

The cores of these phenocrysts are of two contrasting types; plagioclases up to andesine in composition and untwinned, or simply-twinned alkali feldspar. Mafic phenocrysts often show strong signs of resorption (plate 3.12b, shows an olivine with

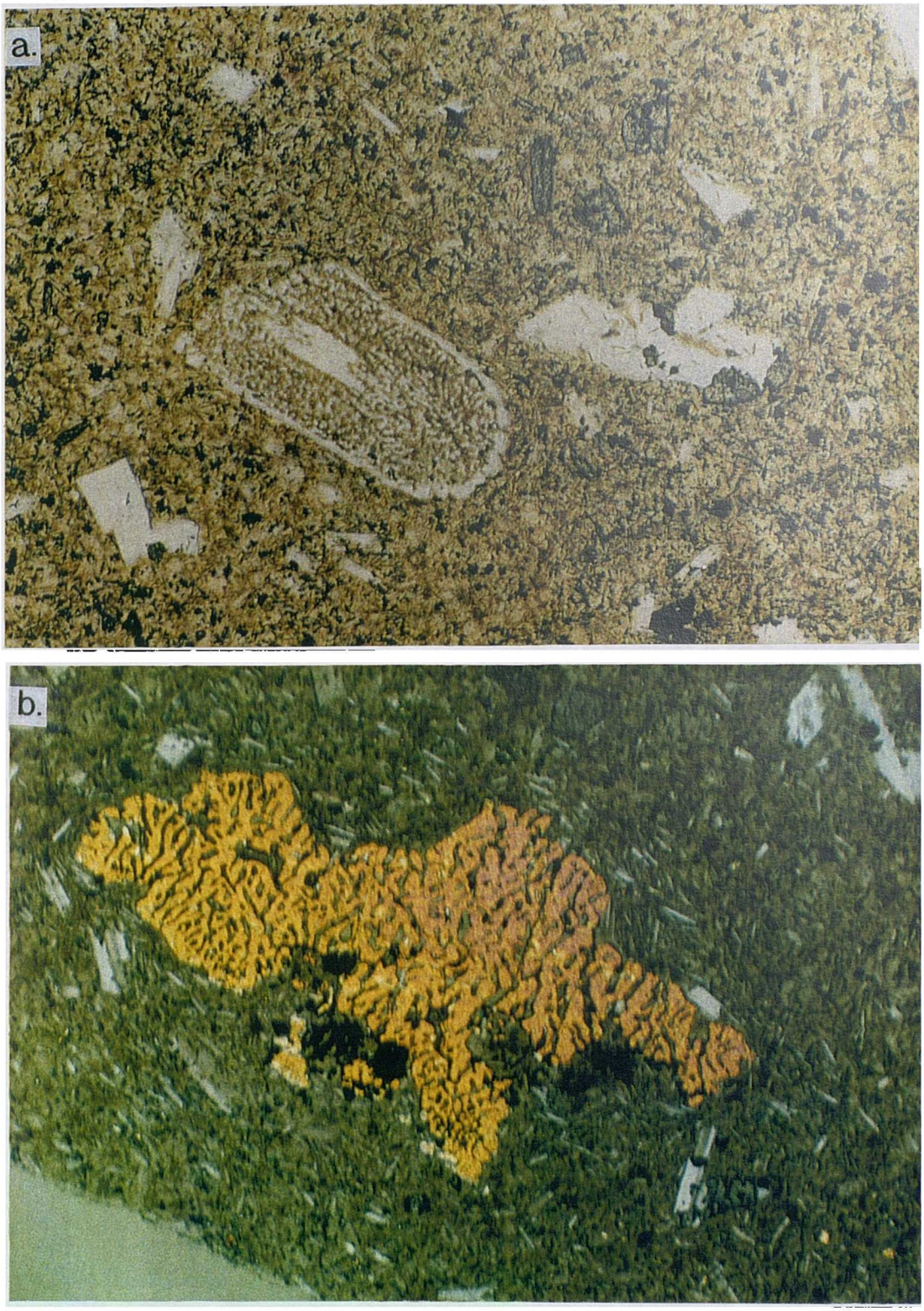

Plate 3.12 VH65, Hybrid of benmoreiitic composition (**a**). Plagioclase showing well developed dendritic growth zone set in hyalophitic groundmass PPL, and (**b**). Excellent example of a sieve textured olivine, polars incompletely crossed. Both fields of view 3 x 1.9mm.

a very well developed sieve texture) from mixing with a hotter magma or one in which they are out of equilibrium, having a rounded or lobate outline with embayments. **Olivines** are up to 0.5mm, and greenish in colour, larger ones are generally anhedral while smaller ones tend to be more euhedral. As with the feldspars, there are two contrasting types of clinopyroxene, yellow/brown augite crystals, probably derived from a basaltic magma, and bright green ferrohedenbergites derived from a more rhyolitic one. Both appear out of equilibrium with their present host. **Magnetite** is also a phenocryst phase and is occasionally euhedral, though more often it has a skeletal appearance. Some are glomeroporphyritic, with clusters of ragged magnetite, green clinopyroxene and partially resorbed sodic plagioclases.

The **groundmasses** are all uniformly hyalophitic, being composed dominantly of brown glass, containing small <0.1mm microlites of green clinopyroxene, blocky alkali feldspars and equant magnetites.

3.1.7 Trachytes (<0.5% MgO, 8-9.5% total alkalis)

Very few trachytes have been found. Most of those that may be classified on the basis of bulk composition as trachytes appear either to be hybrid when examined petrographically, or are so fine grained as to be beyond resolution. Thus it would appear that there is a compositional gap in the suite, between 60 and 69% SiO_2, i.e. there are no true intermediate rocks, as is the case with many Icelandic suites. As with many of the benmoreites, some trachytes are banded and obviously heterogeneous, resulting from mixing of a rhyolitic magma with a basaltic one, (e.g. VH23, plate 3.13a). Magma co-mingling (field occurrences of this are described in section 2.4) can also be seen in a sample taken just adjacent (plate 3.13b). Phenocrysts appear to be dominantly derived from the rhyolitic end-member (sodic alkali feldspar, ferrohedenbergite, fayalitic olivine and magnetite) and are rounded and resorbed. The groundmass is usually very fine grained or glassy, with a banding deriving from uneven distribution of finely divided opaques.

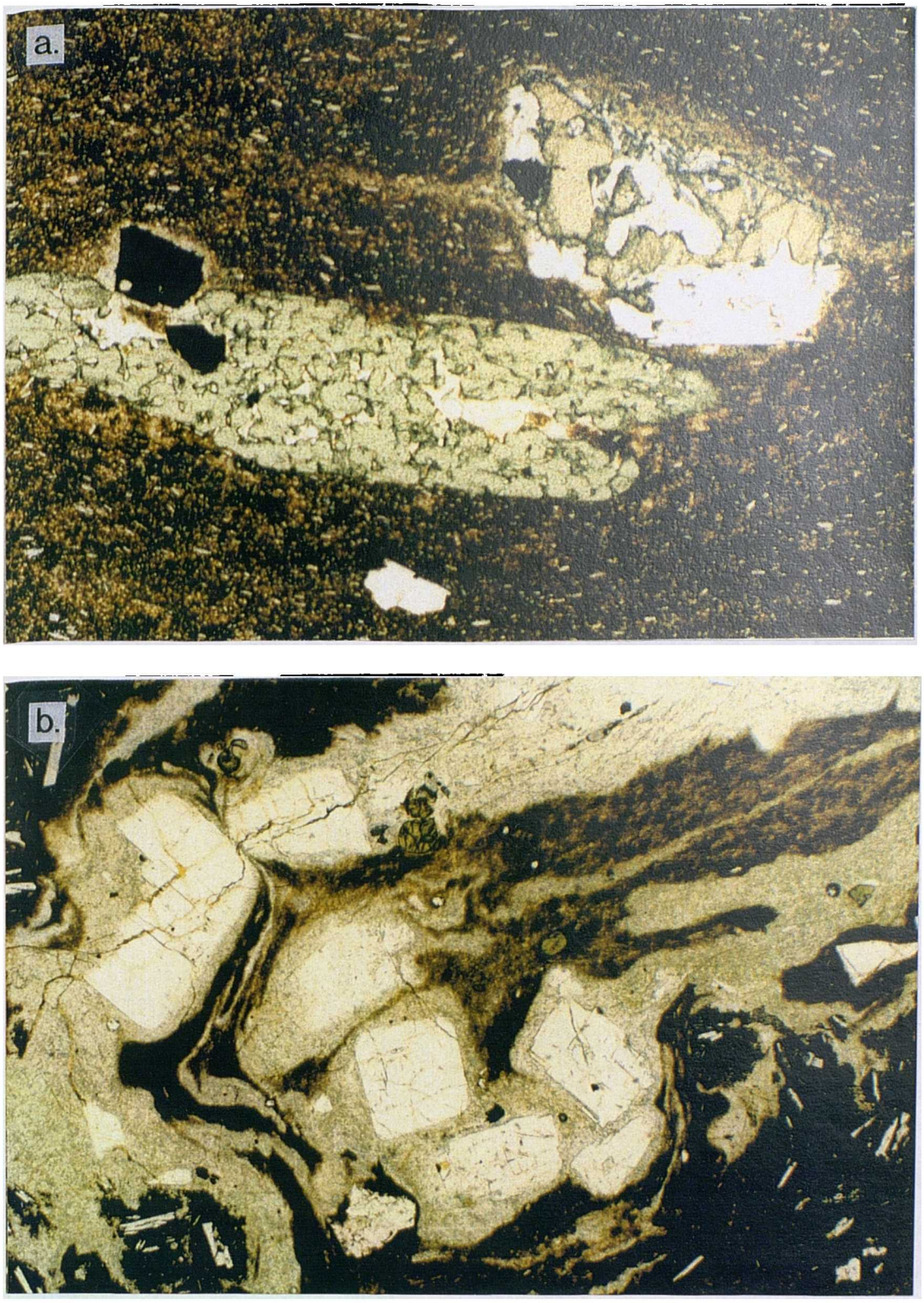

Plate 3.13 (a). VH23, Hybrid of trachytic composition, 3 x 1.9mm, and **(b).** Co-mingling magmas sample VH22, dark, oxidised mugearite and pale rhyolitic magma with brown hybrid (VH23) between. 6 x 3.7mm. Both PPL.

3.1.8 Rhyolites (<0.1% MgO, >9.5% total alkalis)

The rhyolites are mildly peralkaline (molecular $[Na_2O + K_2O]/Al_2O_3$ >1), with a comenditic composition and corresponding mineralogy. Unlike the rest of the suite they show no sign being hybrid (such as complexly zoned and mantled phenocrysts), although they occasionally form one end-member in a mixing scenario. Hybridisation, however, only appears to occur with evolved mafic magmas; the density contrast would prevent mixing directly with more primitive magmas (McBirney 1980).

Generally the rhyolites contain abundant macrophenocrysts (up to 20%) and most are also glomeroporphyritic. The dominant phase is tabular **feldspar**; phenocrysts varying in size from around 4mm down to 0.5mm. Compositionally the feldspars range from sodic plagioclase, with poorly developed polysynthetic twinning showing an almost symmetrical extinction to simply twinned alkali feldspar. Most commonly it is anorthoclase, much of which shows what appears to be very faint cross-hatch twinning. It occurs in both monomineralic glomerocrysts and intergrown with pyroxene, olivine and accessory phases (plate 3.14).

Plate 3.14 VH144, Glomeroporphyritic rhyolite. 3 x1.9mm, PPL.

The next most abundant phase (reaching 2%) is **alkali pyroxene**, which occurs as euhedral or subhedral phenocrysts, up to 1 mm in size. It is commonly bright green in colour although it is occasionally zoned to a paler green either away from or towards

the core of the crystal, and can be pleochroic, from bright green to a more yellow green. In composition it varies from ferrohedenbergite to a more aegerine-rich composition.

In most samples small (<0.4mm), anhedral honey-coloured **fayalites** are also present, although in some samples these are completely pseudomorphed by finely divided opaques.

Accessory phases are magnetite, aenigmatite, apatite and ?kaersutitic amphibole. The **magnetite** occurs as small equant grains (<0.1mm), often enclosed in pyroxene crystals, and is lacking in some of the more evolved samples, where it is replaced by aenigmatite as the Ti host. **Aenigmatite** occurs as small, acicular crystals that could easily be mistaken for pyroxene, but showing the typical pleiochroic scheme of red/brown to almost opaque and reaching up to 0.2mm in length. **Apatite** was found in just one sample, where a small grain was seen to be enclosed within a pyroxene crystal. Similarly just one isolated occurrence of **amphibole** was noted, the ragged crystal was evidently unstable in the extruded rhyolitic magma and was in the process of breaking down. It showed the typical amphibole cleavage intersection of 56° and a pleochroic scheme of orange to almost opaque. Zircon is notably absent here, although it is often present in Icelandic rhyolites, including those from the Austurhorn intrusion (Furman et al. 1992) and the Oraefajokull volcano (Prestvik 1985); both centres very similar in character to Snaefell. This is probably due to the peralkalinity, which increases zircon solubility (Watson 1979). Otherwise Snaefell rhyolites show similar mineralogies to the others mentioned. Phenocrysts in the rhyolites are more often fractured than in the more primitive compositions, indicating an increase in magma viscosity (Gustafsson et al. 1989).

The **groundmass** is often glassy and both pitchstones (1-10 % H_2O) and obsidians (<1 % H_2O) are found. These show classic *hyalophilitic* textures, consisting of fresh isotropic brown glass containing small flow aligned laths of alkali feldspar and microlites of pyroxene (plate 3.15). The remainder of the rhyolites show a more intergranular texture, made up of small hollow alkali feldspars (up to 0.2mm), irregular patches of quartz (absent as a phenocryst, phase as in the Oraefajokull suite (Prestvik 1985)) and hollow needles of green pyroxene (<0.2mm), some of which also contain small spinels.

The general lack of hydrous phases would seem to suggest that the magma was relatively dry.

Plate 3.15 VH51. Obsidian, showing a hyalopilitic texture. 1.3 x 1.9mm, PPL.

3.1.9 Xenoliths

Both gabbroic and leucocratic xenoliths have been found. All appear partially assimilated and out of equilibrium with their host magmas.

1. Gabbros.

These were found in three of the most primitive basaltic units and show a slightly more evolved mineralogy than their hosts. They are medium grained (~4mm) leucogabbros containing three silicate phases, in the following proportions: 75% plagioclase, 10-15% augite, and 15-10% olivine (along with a minor amount of opaques; mostly the result of olivine breakdown). The plagioclase is compositionally labradorite and shows fairly pronounced normal zoning. Where assimilation has occurred to a significant extent, it is rimmed with albite (plate 3.16a). Olivine and augite show fairly uniform compositions within a single sample and are uniformly less magnesian than those of their host magma; they appear to be undergoing preferential assimilation relative to the plagioclase.

Texturally, the xenoliths appear to be cumulates. In some the plagioclases are noticeably aligned, suggesting crystal settling (although this could alternatively result from later diagenetic processes (Hunter 1987)), and also show well developed triple junctions, suggesting they are adcumulates (plate 3.16b).

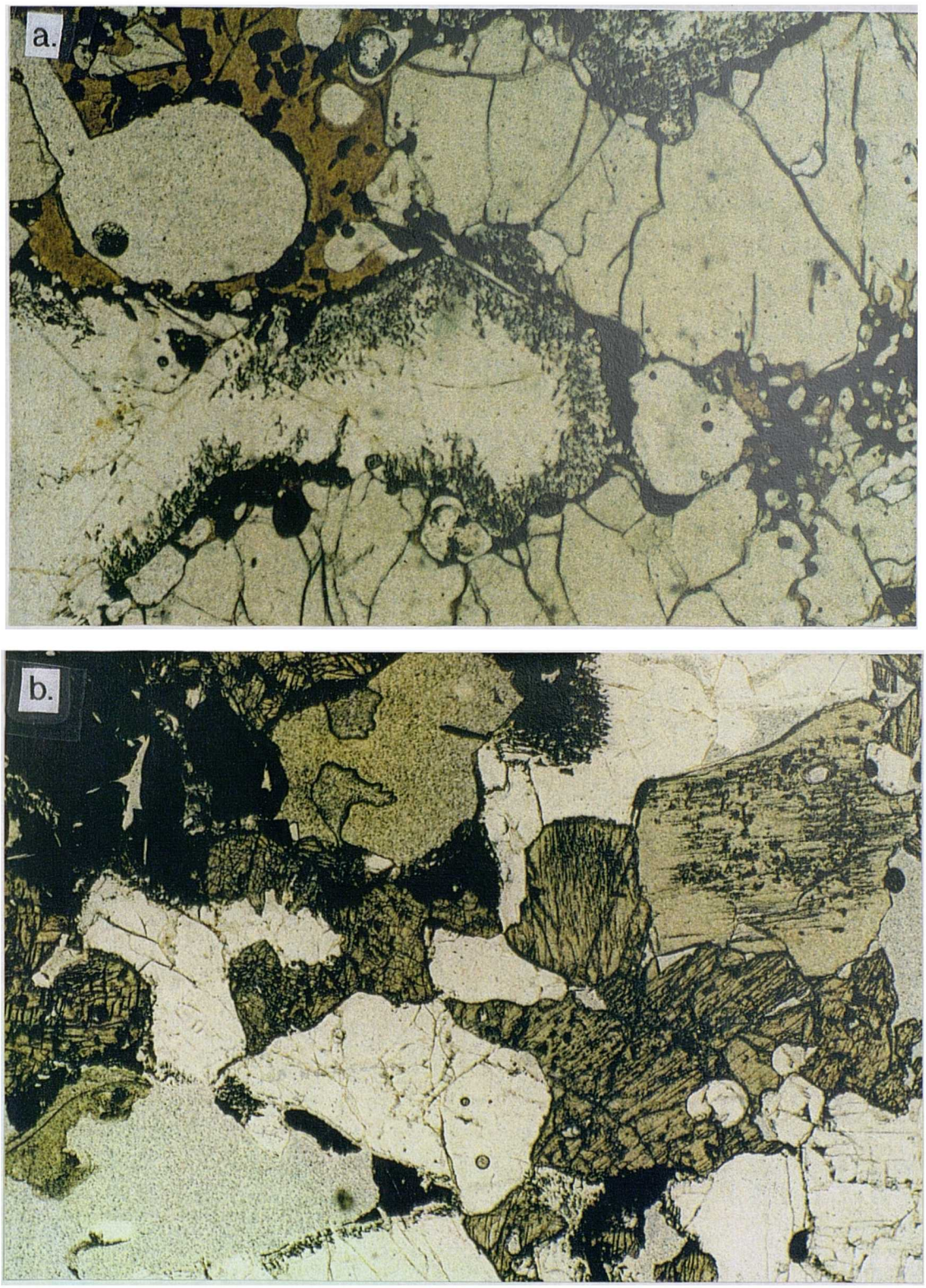

Plate 3.16 (a). VH20, Partially assimilated gabbro xenolith, showing albitic rims on plagioclase and well developed triple points. 3 x 1.9mm, PPL. **(b).** VH81, Gabbro xenolith of slightly more evolved composition, here showing a preferred orientation to the plagioclases. 3 x 1.9,mm, XP.

In most however the original texture has been all but obliterated by assimilation, leaving the rock friable and extremely porous (quenched melt can be seen lining the cavities). Again there are well developed triple junctions and some of the xenoliths appear in the process of disaggregation. Jakobsson (1979a) notes that such gabbroic "nodules" are common in Icelandic basalts, especially tholeiites where they additionally contain orthopyroxene. On the basis of the general mineralogical similarity to their host rocks, he suggests them to be autoliths.

2. Leucocratic xenoliths.

Trondhjemitic xenoliths were found in three different units of either hawaiitic or mugearitic composition, distributed across the complex. As with the gabbros they have a very simple mineralogy, consisting of feldspar (sodic plagioclase with almost symmetrical extinction and untwinned feldspar), quartz, rare granules of opaque oxides and occasionally small globules of secondary carbonate. They are fairly coarse grained (~8mm), and again possibly cumulates. Their texture can give few insights into their origins, since most are in fairly advanced stages of assimilation. They are extremely porous and friable, it is possible some phases have been completely melted out (plate 3.17). The crystals themselves are rounded with lobate outlines, and the feldspars also show altered rims and the whole body generally appears to be in the process of disaggregating.

It is noteworthy that no xenoliths were to be found in the rhyolites. In other Icelandic centres (e.g. Askja, Sigurdsson & Sparks 1981) the presence of similar xenoliths has been used as evidence to support the crustal partial melting theory of the origin of rhyolitic magmas (e.g. Sigurdsson 1977, Marsh et al. 1991).

3.1.10 Alteration

Alteration is not very pronounced in this suite of rocks, most show original mineralogies. It is most pronounced in the lower, earlier units. Olivine, probably the most susceptible mineral to alteration present, is only rarely altered. At the basaltic end of the series it is occasionally stained a brown/green colour, and shows alteration along cracks to the red/brown mineraloid, iddingsite. It also occasionally shows a concentration of divided opaques around the margin and, in a few of the rhyolites, is completely replaced by opaques. The clinopyroxene rarely shows any signs of alteration at all, apart from one or two samples where it appears to be in the process of being replaced by carbonate minerals (probably calcite). The feldspar phase is uniformly unaltered right across the series.

Plate 3.17 VH149, Leucocratic xenolith. 6 x 3.7mm, XP.

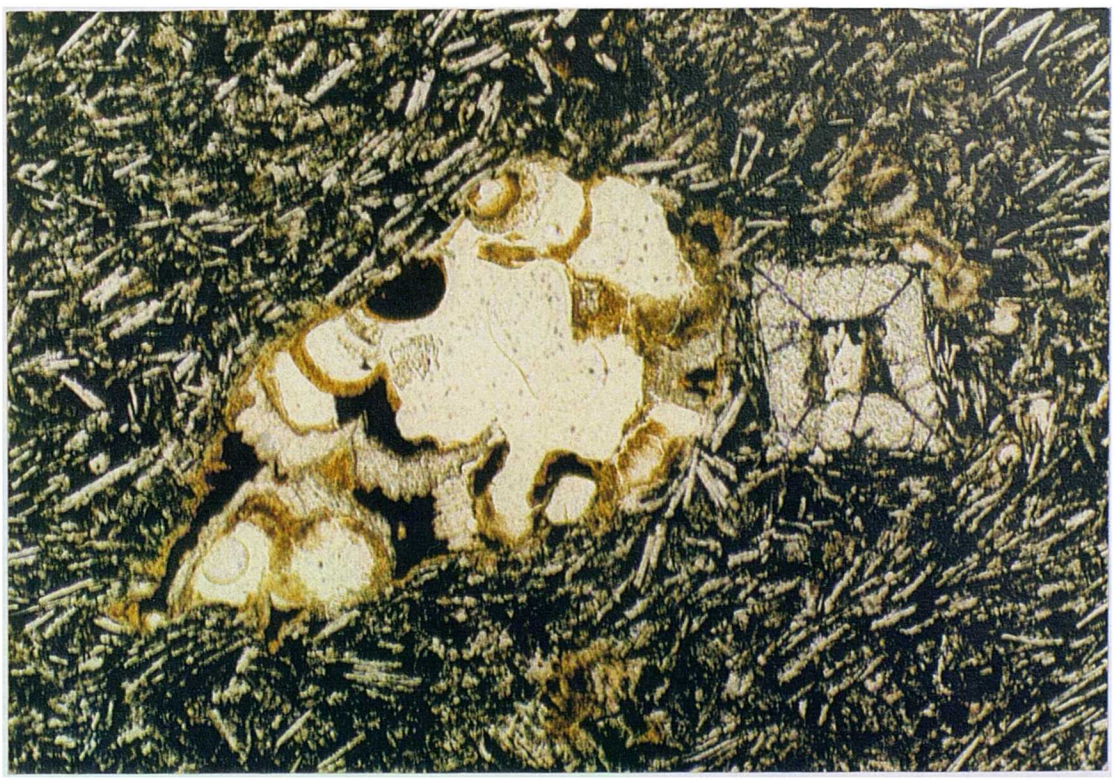

Plate 3.18 VH61, Vug infilled with secondary minerals, carbonates and hydrous iron oxides. Note perfectly fresh olivine adjacent to the vug. 3 x 1.9mm, XP.

In the groundmass alteration is more obvious. Glass has often been replaced by brown/green clay minerals and secondary minerals, such as rusty brown hydrous iron oxides, red hematite, and carbonate are present. Vugs are often infilled with radiating growths of hydrous iron oxides and/or carbonate minerals. It is significant that in many samples where a lot of secondary minerals are present in the groundmass, the olivines are perfectly fresh (plate 3.18), indicating that the fluid circulation was late and at low temperatures.

3.1.11 The underlying Plio-Pleistocene tholeiites

Strictly, these are not really a part of the present study. Nevertheless, quite a few samples were collected (often multiple examples of the same flows) in order to draw a clear division between them and the later products of the Snaefell complex. Thus an overview of their petrography and its contrasts to the Snaefell suite is given here.

The lavas sampled are mostly basaltic, although single examples of basaltic andesite and rhyolite were also collected.

Basalts

These contrast immediately to the overlying Snaefell suite in that they can be easily petrographically subdivided, into the following groupings: (1) Olivine, plagioclase and pyroxene phyric; (2) plagioclase and pyroxene phyric; (3) plagioclase phyric and; (4) essentially aphyric.

The first group is very similar to the Snaefell basalts in many ways, except in the composition of the plagioclase, which spans a greater range, and their texture. They are more often holocrystaline, and the groundmass ranges in grainsize from 1mm (much coarser than anything seen in the Snaefell suite) down to ~0.1mm. The coarser examples also show very well developed ophitic clinopyroxene (plate 3.19).

Lavas from the middle two groups are distinct from the Snaefell suite, the plagioclase-phyric ones are particularly distinctive, with up to 12% phenocrysts ranging from ~0.5mm to 4mm in size, with no gradation down into groundmass. Compositionally these phenocrysts vary from labradorite to andesine, and some show oscillatory zonation. Most are fairly euhedral and there are also abundant glomerocrysts, on which secondary nucleation of a second generation of slightly more evolved crystals is evident, producing a radiating pattern (plate 3.20). They all have a medium grained (~0.3mm) groundmass, consisting of pale brown pyroxene, plagioclase laths and magnetite. Texturally it varies from intergranular to subophitic with intersertal patches.

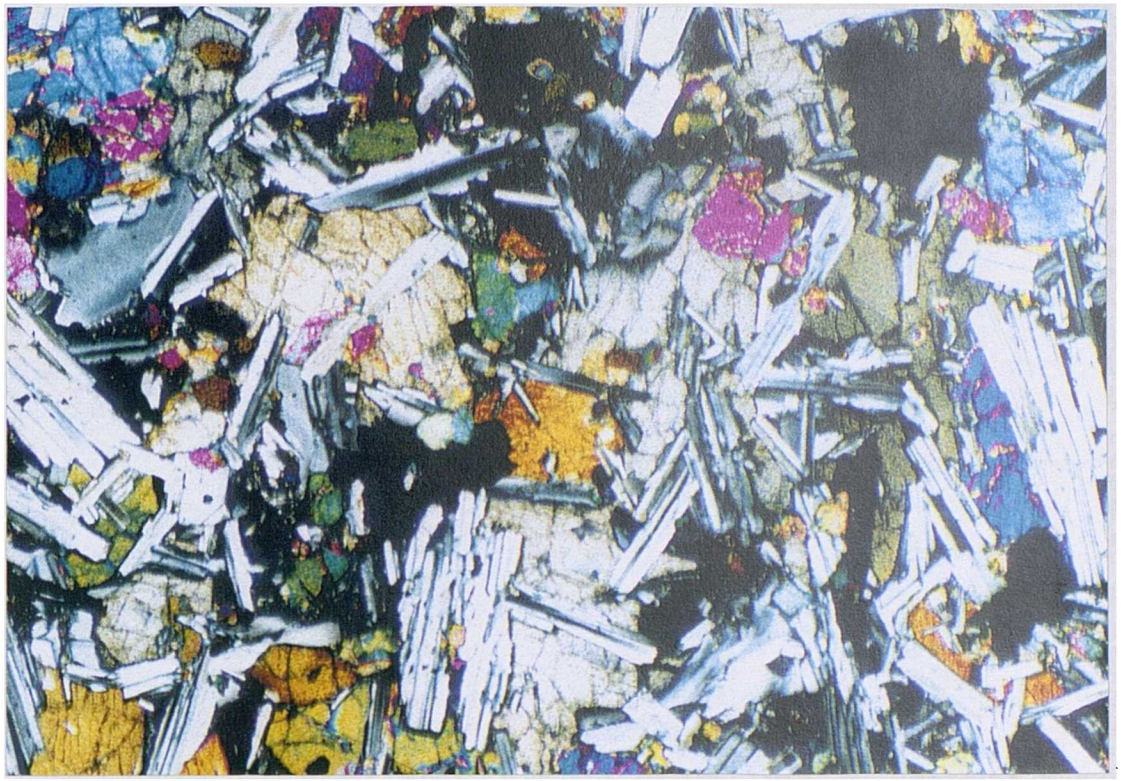

Plate 3.19 VH53 (V11 of Walker profile), Very coarse compared to Snaefell basalts, with a well developed ophitic texture. 3 x 1.9mm, XP.

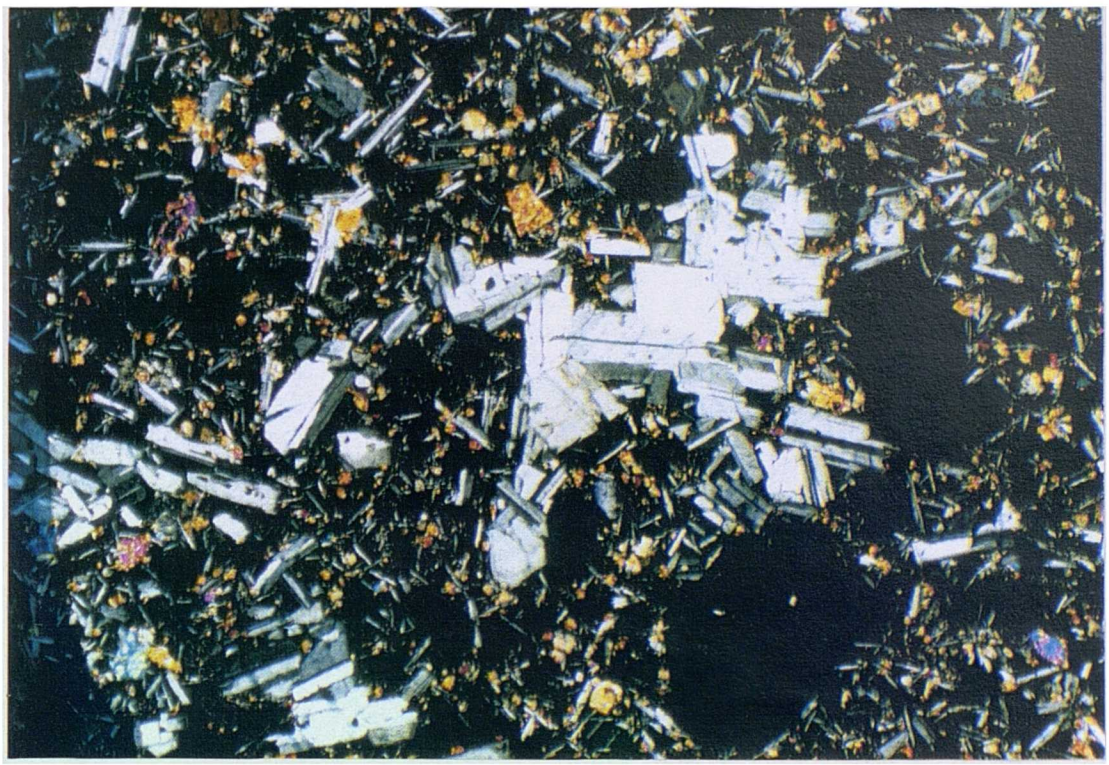

Plate 3.20 VH88, Plagioclase-phyric tholeiitic basalt. 6 x 3.7mm, XP.

The last group is again fairly uniform and contains ~3% microphenocrysts, labradorites up to 0.5mm and euhedral or subhedral yellow/brown pyroxenes up to 0.4mm. A few small glomerocrysts are also present. These generally have a very fine grained to cryptocrystalline groundmass.

Basalts of this age, including some of the lava flows I have actually sampled, are more systematically described in Wood (1978).

Basaltic andesite

This is a very fine grained rock containing sparse phenocrysts of plagioclase (andesine, ~0.8mm) and microphenocrysts of magnetite. The groundmass is made up of tiny (<0.1mm) laths of oligoclase (which are aligned, imparting a trachytic texture to the rock as a whole), small magnetites, yellow/brown titanaugites and an abundance of fresh brown glass. One contrast with rocks in the Snaefell suite that are fractionated to this degree is that it contains *less* spinel.

Rhyolite

The one sample collected is unfortunately not very fresh, but some features of its petrography are still noteworthy. It is flow banded and low in phenocrysts (<2%), most of which are sodic plagioclase with almost symmetrical extinction. These phenocrysts contrast with those seen in Snaefell rhyolites, in that they often show well developed oscillatory zoning. There is also an abundance of the mineraloid iddingsite, which appears to be pseudomorphing either olivine or pyroxene. The groundmass is extremely fine-grained and shows a rusty staining.

3.2 Mineral Chemistry

Analyses were carried out by electron microprobe at both Durham and Manchester, for more details of this and an assessment of data accuracy, see appendix 2. Microprobe work was limited to the Snaefell suite. Samples were selected using both chemical and petrographic criteria, in an attempt to take in all variations within the suite. Efforts were also made to select only fresh material. Lava, xenolith and vitric tuff samples were included, and both mineral grains and glasses were analysed; the data are presented in appendix 5. Olivines, plagioclases, clinopyroxenes and FeTi-oxides were analysed and the chemical variations within each of the mineral groups, along with their petrogenetic significance, are discussed individually in the following sections. The only minerals mentioned in the previous sections which were not analysed are chromite and amphibole. Chromites are generally very small, and amphibole was seen in only a single thin section and, although a probe section was cut from the same sample, none were "captured" in it. Data from the xenoliths will be discussed separately.

3.2.1 Olivine

Olivine is present in some form throughout the entire suite, and ranges in composition from Fo_{89} in VH10 (a high-MgO basalt), to Fo_0 in VH51 (a porphyritic pitchstone). Considering that the accepted compositional range for mantle olivine quoted by Kostopoulos (1991) is Fo_{89-92}, VH10 is compositionally fairly close to a primary magma, but has probably undergone a small amount of olivine fractionation.

Some of the original experimental work on olivine-liquid equilibria in basaltic systems was conducted by Roeder & Emslie (1970), who discovered that the distribution coefficient (K_D) relating the partitioning of Fe and Mg between olivine and liquid, should be equal to 0.3 if equilibrium has been attained:

$$K_D = \frac{(X^{ol}_{FeO})\,(X^{liq}_{MgO})}{(X^{liq}_{FeO})\,(X^{ol}_{MgO})} = 0.3$$

Where X is the mole fraction of the oxide in either the olivine (ol) or the coexisting liquid phase (liq). To apply this to the basalts in this study, whole-rock XRF analyses were taken to represent the composition of the liquid phase, since these samples are all holocrystalline. A mean olivine composition was then calculated for each sample. This reveals (table 3.1), that equilibrium has been established in most cases. The two

exceptions, where K_Ds are too high (indicating that the olivines are too Fe-rich), are both rich in phenocrysts (VH80 ~15% and VH106 ~20%) and therefore may be considered to be cumulates. Olivine is a MgO-rich phase and its accumulation will therefore raise the MgO content in the bulk composition of the lava, although the cumulus olivine need not be as fosterite-rich as the olivine that would be in equilibrium with a magma of that MgO content. Glass compositions were available for a couple of the more evolved samples; one appears to be in equilibrium, while the other (VH65) appears to have excessively Fe-rich olivine. Petrographically this sample appears hybrid; thus the olivine was probably derived from the more evolved end member in a mixing scenario. Data from the vitric tuffs was also considered, a mean glass composition was calculated to represent the liquid composition, along with a mean olivine composition as before. Significantly, most K_Ds are too low, indicating olivines in the tuffs are excessively Mg-rich, suggesting that they could be xenocrystic.

Sample	Rock Type	"Liquid"	K_D
VH1	B	XRF	0.29
VH10	B	XRF	0.27
VH151	B	XRF	0.27
VH262	B	XRF	0.33
VH80	B	XRF	0.42
VH106	B (Ankaramitic)	XRF	0.37
VH137	M	EMP	0.27
VH65	Ben	EMP	0.40
VH11	Vt	EMP	0.22
VH15	Vt	EMP	0.31
VH44	Vt	EMP	0.20
VH84	Vt	EMP	0.15
VH100	Vt	EMP	0.20

Table 3.1. K_Ds calculated using equation of Roeder & Emslie (1970).
B = basalt, M = mugearite, Ben = benmoreite, Vt = Vitric tuff. EMP = electron microprobe data for glass compositions, XRF = X-ray fluorescence whole rock analyses.

Compositional ranges of olivines within lava samples are displayed graphically, using whole-rock MgO content as an index of fractionation, in figure 3.1. These data include phenocryst cores and rims, and smaller groundmass olivines. A general trend may be seen, where Fo of the olivines decreases with MgO content of the whole rock (i.e. with increasing differentiation). Nevertheless, there is quite a lot of scatter, indicating the story is more complicated - even in the basaltic compositions - than

indicated by the "average" K_Ds. The composition of the first olivine to appear on the liquidus of the basaltic magmas was calculated using the computer program TRACE (Nielsen 1988), and these are also shown in figure 3.1.

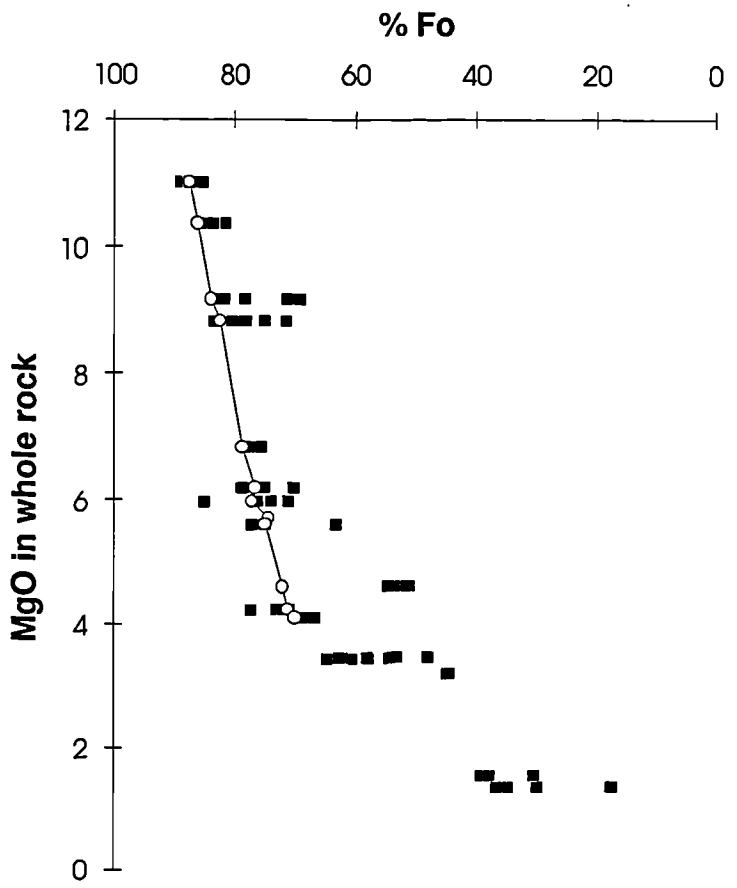

Figure 3.1 Olivine compositions (filled squares) in individual samples, expressed in terms of percentage fosterite (Fo) content plotted against MgO wt% ie. differentiation state of the whole rock. The open circles are the compositions of the first olivine to appear on the liquidus in samples with >4wt% MgO, calculated using the computer program TRACE (Nielson 1988).

A few samples contain olivines with higher MgO content than the calculated equilibrium composition. This could be due to high Fe_2O_3 content in the magma (Larsen et al. 1989) or be explained by magma mixing - these crystals being derived from the more primitive magma - in a periodically replenished magma chamber. That all samples contain less magnesian olivines than the calculated liquidus composition is to be expected (see discussion on crystal zoning below). These can also be accounted for in two additional ways; either they are the result of subsolidus re-equilibration of normally zoned crystals (Moore & Evans 1967), or they were derived from the more differentiated end-member in a magma mixing episode. Magma mixing could also account for the large variations in olivine composition within a single sample.

There also is marked compositional variability within some of the larger olivine crystals, and both normal and reverse zoning is observed. The magnitude of this is tabulated in table 3.2.

Sample	VH1	VH10	VH10	VH80	VH106
Fo% core	75.4	89.0	87.6	78.2	78.0
Fo% rim	77.5	87.3	87.5	69.1	79.2
Zonation	R	N	N	N	R

Table 3.2. Compositional zonation in olivines.

Normal zoning is expected, initially when olivine begins to crystallise in a hot primitive magma it will have a relatively Fo-rich composition. As crystallisation proceeds, the residual magma will become more Fe-rich and the composition of the olivine will reflect this. Reversed zoning is less common and results from magma mixing, when a hot, primitive magma is mixed with a more evolved magma charged with phenocrysts. Thus the resultant host magma will have an intermediate composition and subsequent olivine growth will be more Fo-rich than previously.

Minor elements

Most of the olivines within the Snaefell suite contain detectable amounts of Ca and Na, many also contain Ti, Cr and Ni. Generally Cr_2O_3 and TiO_2 contents are <0.5%, the exceptionally high Ti contents of VH137(5) and VH189(3), and high Cr content of VH89(5) are probably due to tiny included spinels.

The other trace elements are probably held within the olivine, substituting for R" in the structure; $R"_2SiO_4$. In the same way that a solid solution exists between the fosterite and fayalite, a similar solid solution also exists between fayalite and the manganese olivine, tephroite (Mn_2SiO_4). Other recognised minerals within the olivine group are montecellite ($CaMgSiO_4$) and its iron analogue kirschsteinite, although this end member does not occur naturally (Deer et al. 1992). [2]Mg^{2+} = 0.72Å, Fe^{2+}=0.78Å and Mn^{2+}=0.83Å; hence it would be expected that they would be taken up in this order by the olivine structure, and this is approximately what is observed. Mn (Tf) content begins to rise markedly at around Fo_{55} (figure 3.2a), reaching $Tf_{4.8}$, at Fo_0. Ca^{2+}=1.00Å, and thus its uptake into the olivine structure might be expected to occur preferentially in fayalite. However, this is not the case and CaO content is approximately constant with Fo variation (figure 3.2b) between 0.1-0.6wt%. Work by Simkin and Smith (1970), indicates that Ca concentration in olivine is controlled by crystallisation conditions, specifically pressure, rather than differentiation. Na_2O content mirrors that of CaO (figure 3.2c), and varies between 0.2-0.7wt%. Although

[2]All ionic radii taken from Henderson (1982).

there is a charge difference the Na^{+} ion has a very similar radius to the Ca^{2+} ion in octahedral co-ordination at 1.02Å. Simkin and Smith (1970) also report concentrations up to 0.4 wt% NiO, however only a single example containing NiO in a large enough concentration to be measured (>2σ, i.e. > ~0.2wt%) was found, in VH10. Ni^{2+} = 0.69A, and would thus be expected to substitute for Mg^{2+} in the olivine structure.

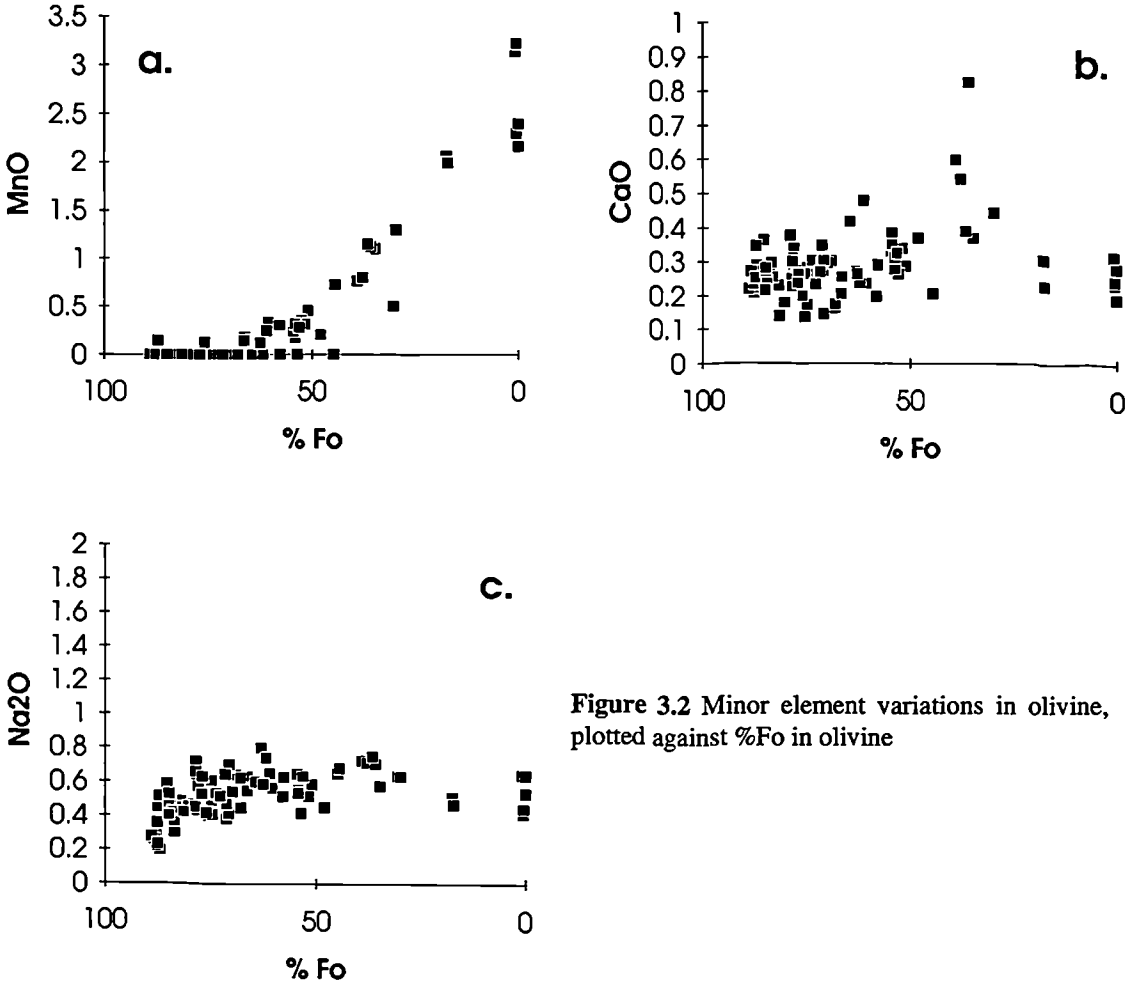

Figure 3.2 Minor element variations in olivine, plotted against %Fo in olivine

3.2.2 Feldspar

Compositionally feldspars vary from $An_{83}Ab_{17}Or_0$ (in a plagioclase phenocryst *core* in sample VH24, a mugearite), to $An_0Ab_{70}Or_{30}$ (in a small anorthoclase phenocryst in VH51, a porphyritic pitchstone). The most primitive (calcic) composition found in a microphenocryst i.e. possibly in equilibrium with the whole rock composition, was $An_{77}Ab_{23}Or_0$ and this was found in a plagioclase lath in VH10, the most primitive sample collected. The compositional range within the suite is summarised in figure 3.3 in terms of An, Ab and Or content, and it can be seen that the bulk of the feldspars analysed lie within the bytownite and labradorite fields.

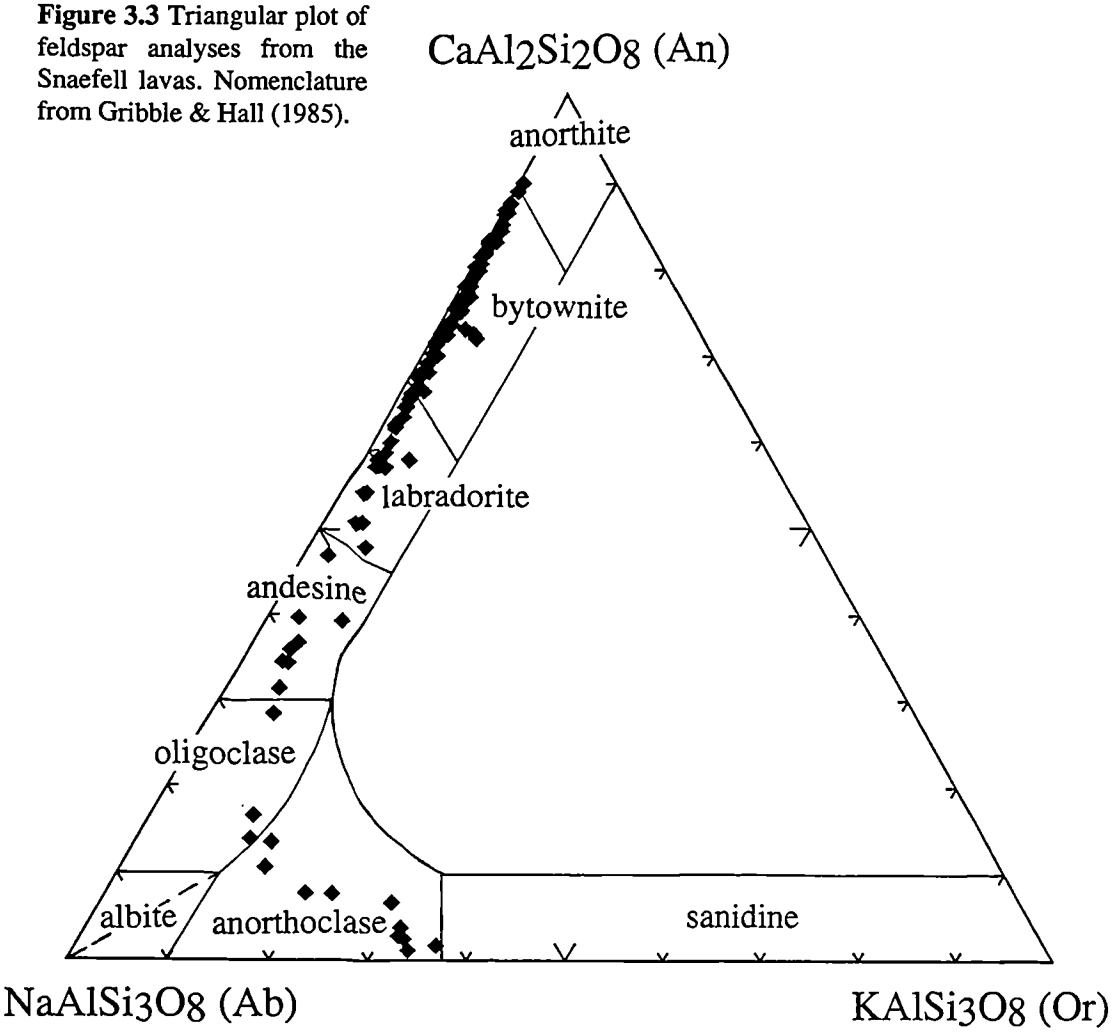

Figure 3.3 Triangular plot of feldspar analyses from the Snaefell lavas. Nomenclature from Gribble & Hall (1985).

This is at odds with the optically[1] determined compositions, discussed in section 3.1, where nothing more primitive than labradorite was indicated. The discrepancy between microprobe analyses and optical determinations of feldspar composition may be accounted for in that the optical technique hinges on the assumption that the viewing plane is normal to the {010} twin planes of the albite twins. The plane of section may be oblique to this and the twinning observed, especially in the groundmass feldspars may be other rarer twin types rather than albite. The K content of the feldspars becomes detectable from around An_{70}, and increases with Na content, finally reaching 4.97wt%. That K-enrichment is not limited to late-stage crystals of low An content indicates that crystallisation occurred rapidly at high temperatures - as would be expected in a volcanic suite of rocks such as this. The most Or-rich composition observed (Or_{30}) is significant, since experimental work (Thompson & MacKenzie 1967) indicates that this represents the feldspar that precipitates from liquids evolving along the temperature minimum in the system SiO_2-Al_2O_3-Na_2O-K_2O in peralkaline liquids; thus further crystallisation should not alter the composition of the feldspar formed.

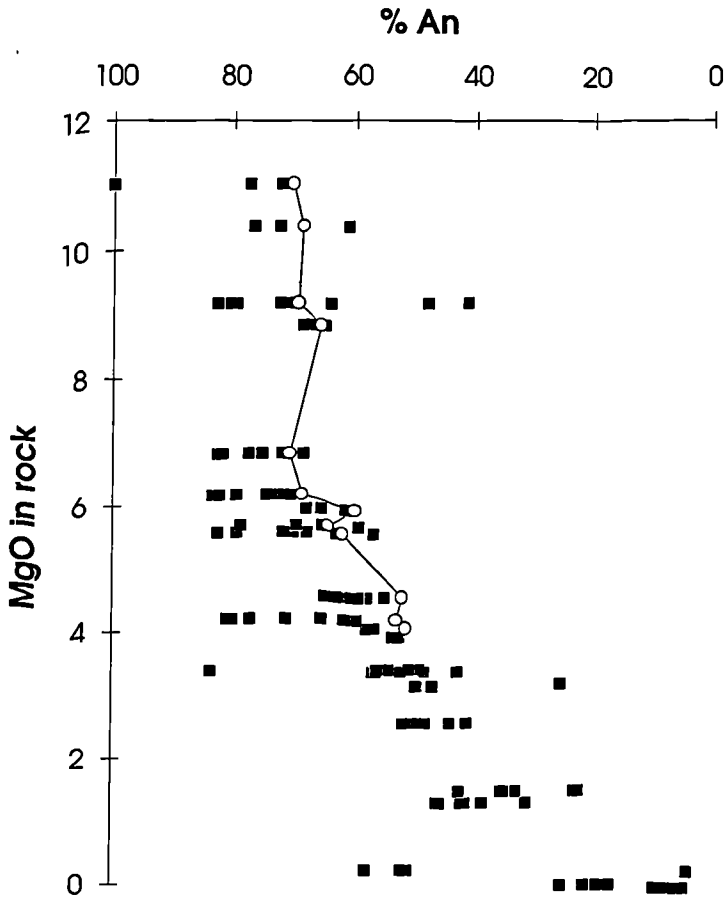

Figure 3.4
Feldspar compositions (filled squares) expressed as percentage anorthite (An) in individual samples, plotted against wt% MgO in whole rocks. Open circles are the composition of the first feldspar to appear on the liquidus, calculated using TRACE (Nielson 1988).

Figure 3.4 show the feldspar compositions plotted against the MgO content of the whole rock, along with the calculated composition of the first feldspar (plagioclase) to appear on the liquidus of the more primitive compositions (in the same way as olivine). It can be seen that there is a lot of scatter in the data, although there is a broad decrease in An content of the feldspar with increasing differentiation, as would be expected. Nearly all the samples appear to contain feldspars with higher An content than calculated, while only a few contain examples with lower An content. This is explicable in terms of mixing two magmas, both charged with feldspar phenocrysts. The resultant magma will be of intermediate composition and possibly substantially hotter than the more evolved end-member; so that resorption of the more evolved feldspar compositions is likely. Magma mixing is also implied when zonation within individual crystals is taken into account (table 3.3). Normal zoning is expected with increasing degree of crystallinity within a sample, such as seen in the rhyolite, VH51. Pronounced reversed zoning coupled with normal zoning in crystals within the same sample (the rims/mantles having similar compositions) suggests, however, that magma mixing occurred, as previously discussed in sections 3.1.1 and 3.2.1.

Sample	Rock Type	Core %An	Rim %An	Range in sample	Calculated	Zoning
VH1	B	81.8	75.2	68-77	70.7	N
VH41	BH	55.0	62.5	60-64	52.1	R
VH50	BH	82.4	71.7	62-71	62.0	N
VH50	BH	56.9	67.8	62-71	62.0	R
VH24	M	83.4	56.3	52-56	-	N
VH65	Ben	46.0	45.9	38-45	-	N
VH65	Ben	31.0	45.5	38-45	-	R
VH51	R	7.7	1.0	0-1.6	-	N

Table 3.3. Compositional zonation in feldspars; the rock-types are as table 3.1, with additionally BH = basaltic hawaiite and R = rhyolite. The "range" refers to the range in composition of small homogeneous feldspars (presumably in equilibrium) within the sample.

Minor elements

Other ions that may be present in small amounts in the feldspar structure, MT_4O_8, include Ti, Fe^{3+}, Fe^{2+}, Mg, Ba and Sr, and Mn in calcic feldspars (Deer et al. 1992). While Ba and Sr were not analysed for and Mn was below detection limit (2σ) in the majority of samples, TiO_2, MgO and [3]FeO were all present in significant quantities, and these are all plotted against An content of the feldspar in figure 3.5.

The M site in the feldspar structure varies from irregular 9-fold co-ordination in the alkali feldspars to 7-fold in calcic plagioclases, the reduction in co-ordination number resulting from distortion of the structure due to an increase in Al^{3+} in the T sites, causing an increase in the T-O bond length (Smith 1974). Therefore ionic radii[2] considered are for 8-fold co-ordination. The radii of ions concerned are: Ca^{2+}=1.12Å, Na^{+}=1.18, K^{+}=1.51, Mg^{2+}=0.89, Ti^{4+}=0.74 and Fe^{2+}=0.92. In tetrahedral co-ordination: Fe^{3+}=0.49, Al^{3+}=0.39 and Si^{4+}=0.26. TiO_2 varies from 0.15 to 0.35wt% and shows no obvious correlation with An content (figure 3.5a). FeO content[3] varies from 0.2 to 3.5wt%, with the majority <1.25wt%. It is probable that most of the Fe is in the higher oxidation state and that up to 0.5wt% oxide is held in the T-site, while the rest is in tiny impurities (Deer et al. 1992). It is however possible that some of the Fe is held in the M-site as Fe^{2+}, in the same way as Mg^{2+} and, considering their small ionic radii, they should replace the Ca^{2+} ion. This is reinforced by the positive correlations with An content (figure 3.5b & c).

[3]Total iron expressed as FeO in the microprobe analyses, no attempt has been made to estimate Fe^{3+} content in the feldspars.

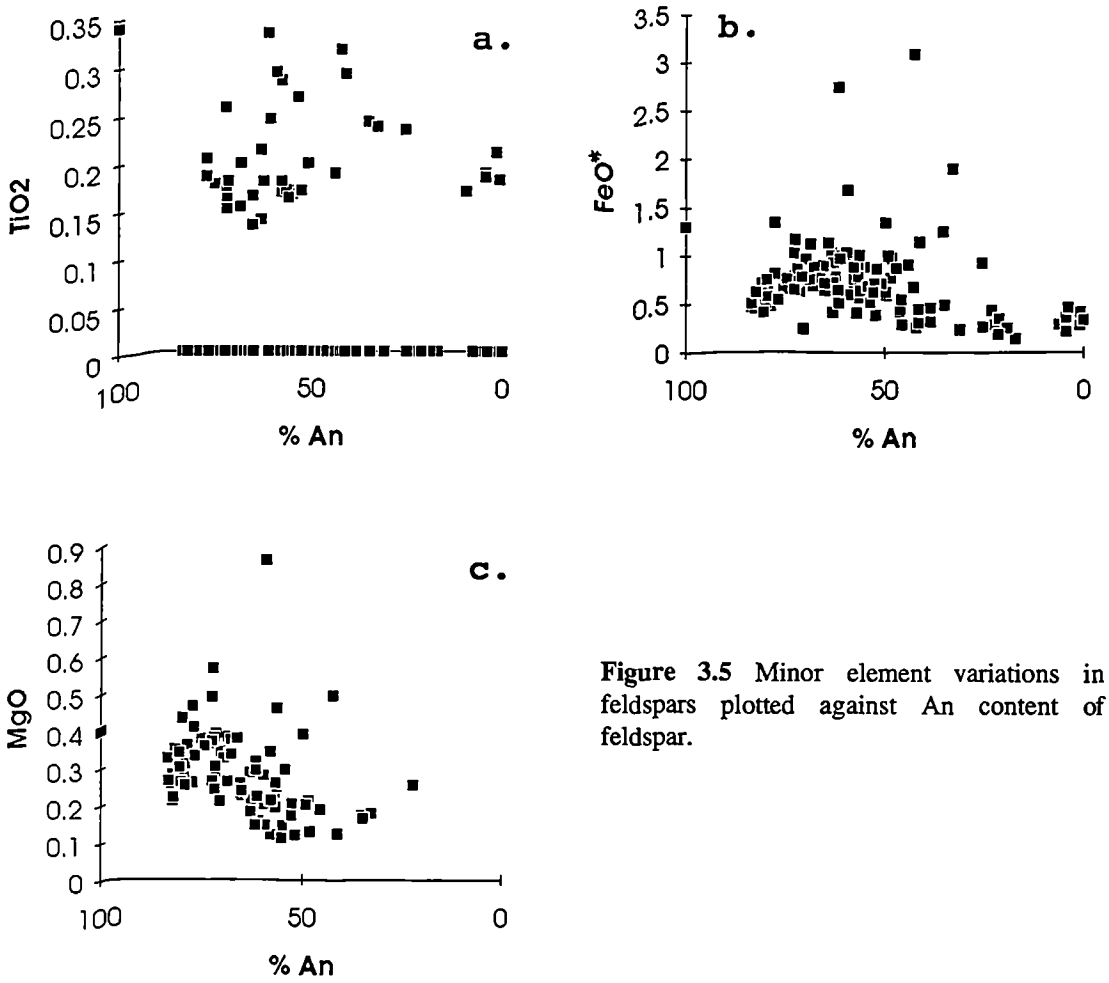

Figure 3.5 Minor element variations in feldspars plotted against An content of feldspar.

3.2.3 Clinopyroxene[4]

Clinopyroxene is the third silicate phase to appear on the liquidus and, in the more primitive basalts, is uncommon as a phenocryst phase. The composition ranges from $En_{46}Wo_{47}Fs_7$ in VH106 (an ankaramitic basalt) to $En_0Wo_{46}Fs_{54}$ in VH51 (a porphyritic pitchstone), and is displayed in the pyroxene quadrilateral, figure 3.6a. Immediately obvious is the compositional gap in the pyroxenes between Fs_{25} and Fs_{45}, suggesting that either pyroxene is unstable at intermediate magma compositions or that the suite is bimodal. The few examples within this zone are all from the obviously hybrid sample, VH65 (figure 3.7c), that was previously discussed in petrographic terms in section 3.1.6(2). Overall the Snaefell suite shows a calcic augite - calcic ferroaugite - hedenbergite trend, similar to that of the Shiant Isles Sill (figure 3.6b), which is typical of mildly alkaline basic magmas (Gibb 1973). The compositional scatter in the Snaefell pyroxenes is probably due to metastable crystallisation

[4]Since the microprobe used did not differentiate between Fe^{2+} and Fe^{3+}, total iron in the raw data was presented as FeO; for the pyroxene and oxide minerals, an estimate of Fe^{3+}/Fe^{2+} was made using the method of Droop (1987).

(discussed below) or magma mixing, already demonstrated to be an important process in the formation of this suite of rocks.

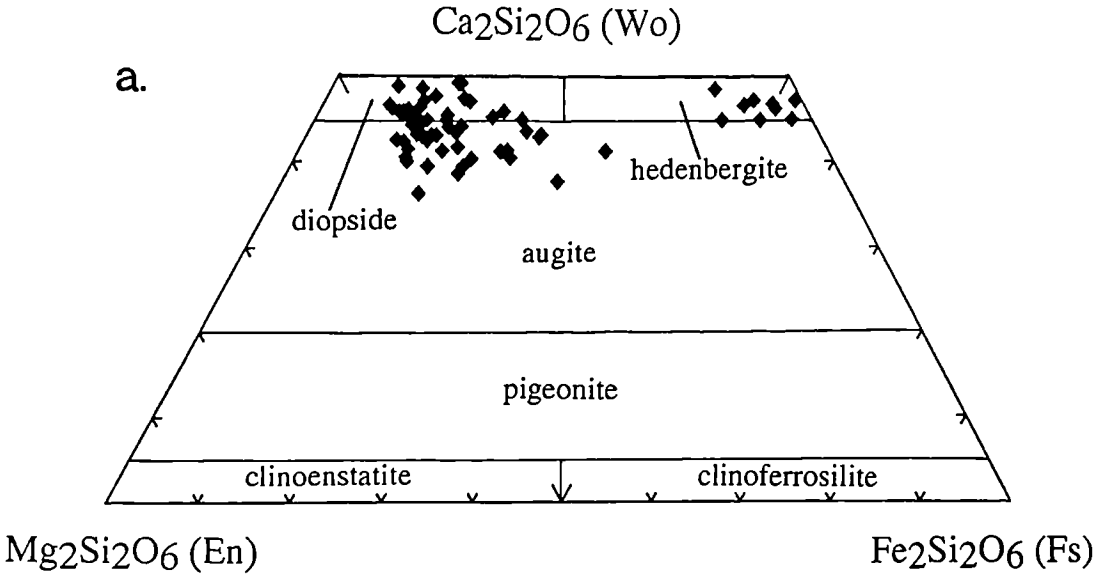

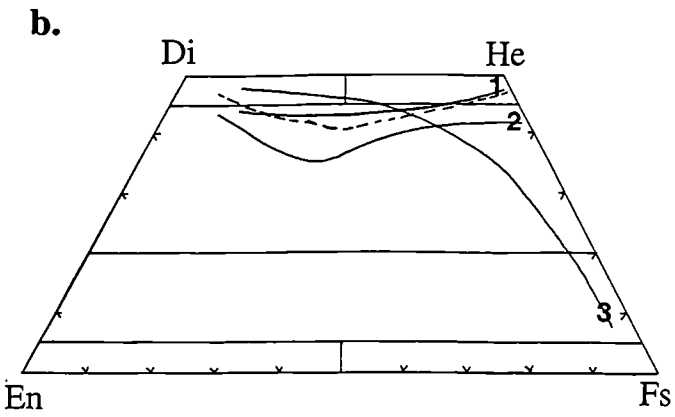

Figure 3.6

(a). Pyroxene compositions plotted on a molar CaMg-CaFe-Mg-Fe quadrilateral. Clinopyroxene nomenclature from Morimoto et al.. 1988.

(b). Trends of clinopyroxene crystallisation:
Dashed line = Snaefell pyroxenes
1 = Shiant Isles Sill (mildly alkaline),
2 = Skaergaard Intrusion (tholeiitic),
3 = Shonkin Sag laccolith (strongly alkaline - soda syenite).
1, 2 & 3 taken from Gibb (1973).

In some cases the individual samples show crystallisation trends (figure 3.7) which illustrate the effect of different rates of cooling. VH9, a relatively coarse grained, therefore relatively slowly cooled, mugearite shows a horizontal trend, normally seen in plutonic rocks such as Skaergaard. Such trends are caused by changes in liquid composition during crystal-liquid fractionation and are thought to reflect stable equilibrium partitioning of Ca, Mg and Fe between crystals and melt (Smith & Lindsley 1971). In contrast VH105, a fine-grained hawaiite, shows a short vertical trend, such as observed by Smith & Lindsley (op. cit.) in the chilled margins of a lava flow. This so-called "quench trend" is thought to be due to either metastable element partitioning between crystals and liquid, or to the presence of a zone of liquid depleted in pyroxene components adjacent to rapidly growing pyroxene crystals.

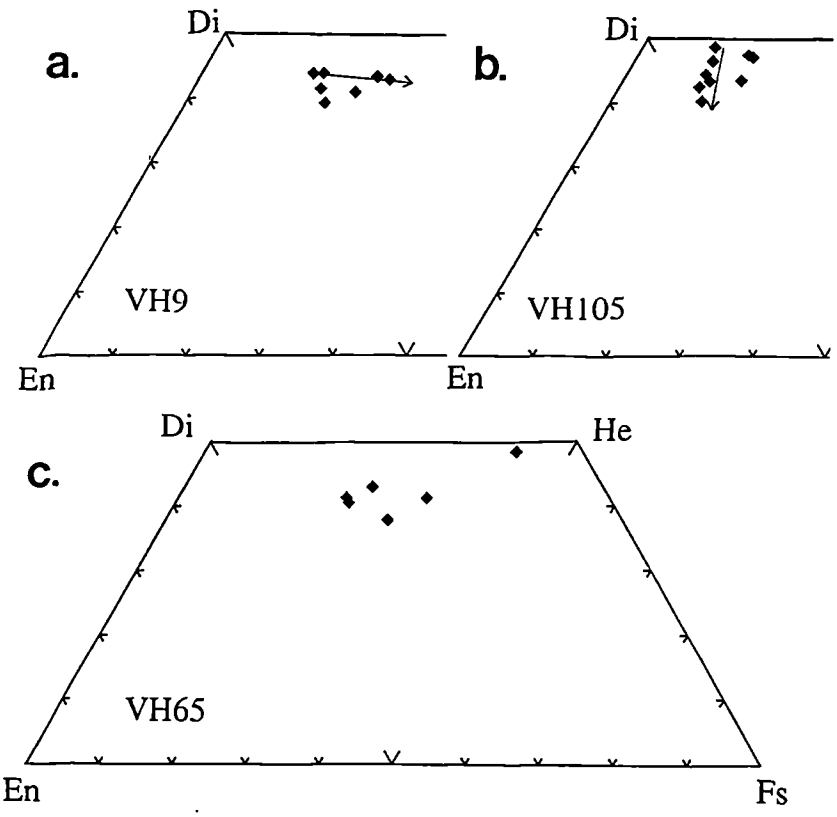

Figure 3.7 Variations in pyroxene composition within individual samples. **(a).** VH9, shows a horizontal trend indicative of equilibrium crystallisation with slow cooling. **(b).** VH105, shows a vertical "quench" trend. **(c.)** VH65, shows a wide variation in compositions, bridging the compositional gap apparent in figure 3.6a.

Minor elements

A wide variety of pyroxene compositions may exist, although the general formula may be expressed as:

$$X_{1-n}^{viii}Y_{1+n}^{vi}Z_2^{iv}O_6.$$

where X = Ca, Na, Y = Mg, $Fe^{2+/3+}$, Ni, Li, Cr, Ti, Mn, and Z = Si, Al. (Gribble & Hall 1985). The substitutions considered in the following sections express the pyroxene formula in this form and apply to the octahedral and tetrahedral sites, since the pyroxenes here are uniformly Ca-rich.

Al_2O_3 and TiO_2

TiO_2 ranges from 0.2-4wt% (figure 3.8a) in the Snaefell pyroxenes, which is within the accepted range for augites - 0.5-0.8wt% - and titanaugites - 3-6wt% (Deer et al. 1992). Al_2O_3 ranges from 0.2-7.5wt% (figure 3.8b.), which is high, since most augites contain <4wt% (op. cit.). The covariance of these two elements shown in figure 3.9, would seem to indicate that a coupled substitution occurs.

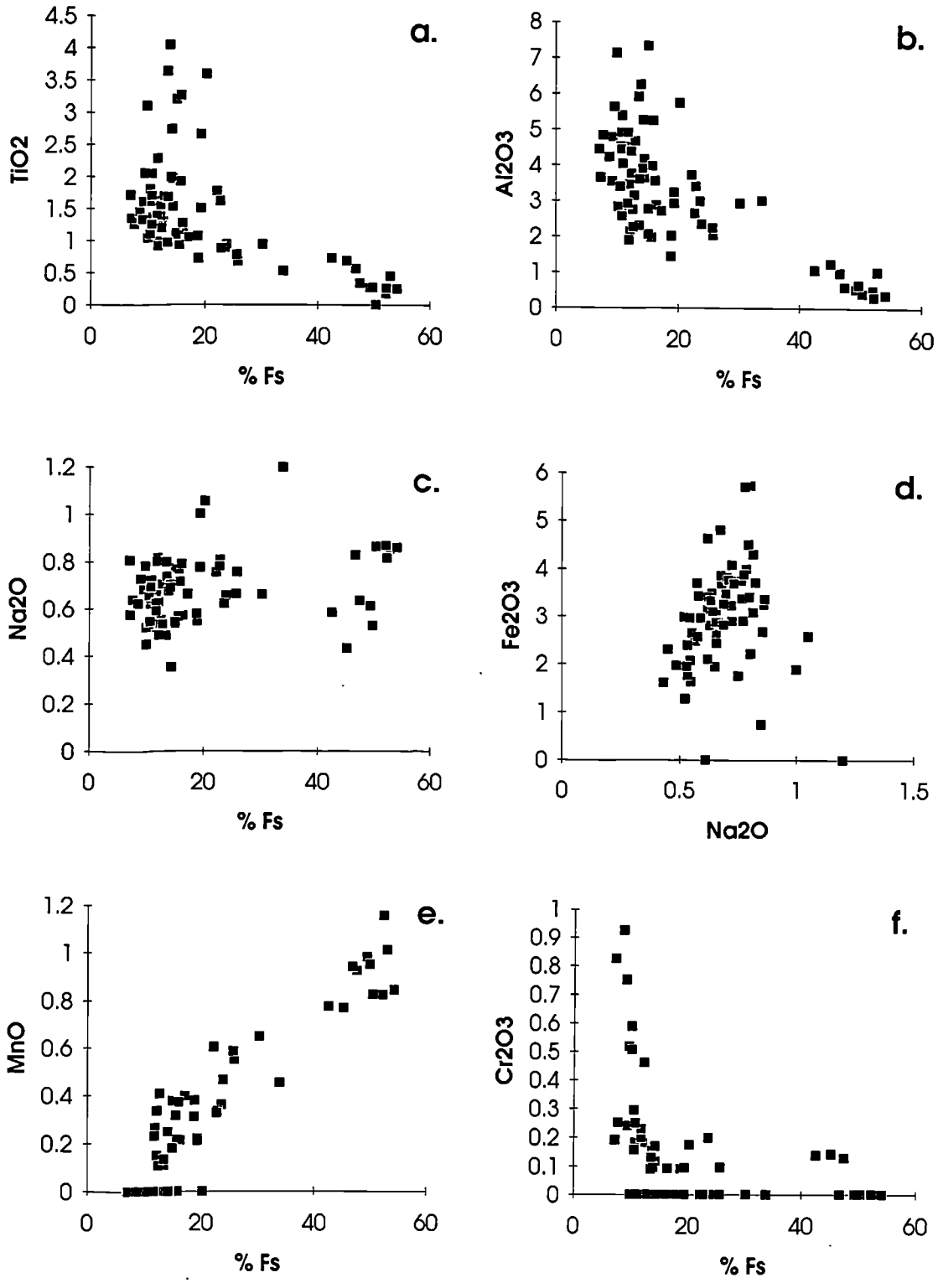

Figure 3.8 Minor element variations in the pyroxenes, plotted against percentage Ferrosilite (Fs) content in pyroxenes.

Most of the Ti can be accounted for in the following substitution:

$$(Mg, Fe)^{vi} + 2Si^{iv} = Ti^{iv} + 2Al^{iv} \qquad \text{Larsen et al. 1989.}$$

The drop in Al_2O_3 with differentiation, as measured by increasing Fs content of the pyroxenes could simply be accounted for by the drop in Al_2O_3 in the magma due to plagioclase fractionation. Nevertheless, it cannot account for the rapid drop at ~Fs_{20}, since plagioclase is always on the liquidus. The trend seen for Al_2O_3 is paralleled by TiO_2, hence it might be assumed that TiO_2 concentration is the controlling factor (Gibb 1973). The last phase to join the crystallising assemblage is Ti-rich magnetite, which precipitates when the Fe^{3+} activity reaches a sufficient level. The drop in TiO_2 in the magma could therefore inhibit both Ti and Al substitution into pyroxene.

There is, however, still an excess of Al to be accounted for in other substitutions, since the ionic ratio of Al to Ti is closer to 4:1 than 2:1 in all but the most titaniferous examples. The excess Al could be incorporated as one of the "tschermakitic" pyroxene components (Gibb 1973, Larsen et al. 1989):

$$(Mg, Fe^{2+})^{vi} + Si^{iv} = Al^{vi} + Al^{iv}$$

or

$$(Mg, Fe^{2+})^{vi} + Si^{iv} = (Fe^{3+}, Cr)^{vi} + Al^{iv}$$

The high tschermakitic component seen in the Snaefell pyroxenes could be the result of high-temperature crystallisation, since the concentration of Al_2O_3 is highest in the early-formed (<20% Fs) pyroxenes. Work by Hertzberg & Chapman (1976) has shown the solubility of the tschermak molecule in clinopyroxene in the CaO-MgO-Al_2O_3-SiO_2 system to vary sympathetically with En content. En content was found to vary with both temperature and pressure, although the former appeared to be the dominant controlling factor. More recent experimental work by Thy (1991) on a mildly alkalic basalt from Surtsey, however, indicates that the pressure of crystallisation is the dominant control on the Al:Ti ratio, which rises with increasing pressure. Looking at figure 3.9, it would appear that the Snaefell basalts crystallised at a pressure intermediate between 1atm and 10kbars.

Na_2O

Na_2O (figure 3.8c) ranges from 0.4-1.2wt%, with the bulk of the analyses falling within the accepted range of 0.5-0.8wt% (Deer et al. 1992). It shows no obvious correlation with percent ferrosilite content.

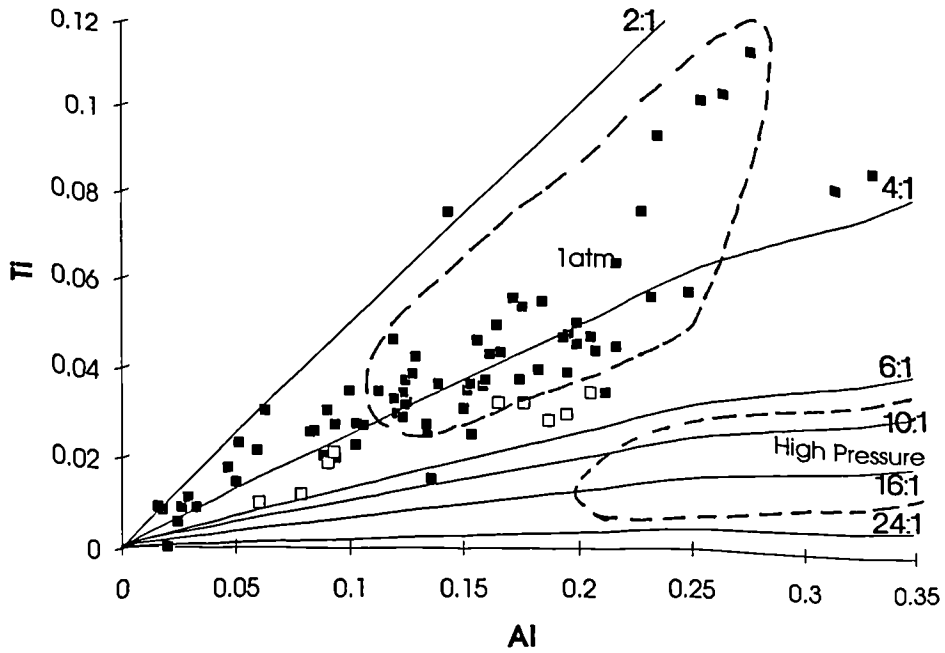

Figure 3.9 Ti vs Al (calculated to 6 oxygens) for pyroxenes, pressure fields are from experimental work on a mildly alkalic basalt from Surtsey (Thy 1991), High pressure = 10-15Kbars. Closed squares - lavas, open squares - gabbro xenoliths.

Na may substitute into augite in either the omphacite molecule or the aegirine molecule as follows:

$$(Mg, Fe^{2+})^{vi} + Si^{iv} = Na^{vi} + Al^{iv}$$

or

$$(Mg, Fe^{2+})^{vi} + Si^{iv} = Na^{vi} + (Fe^{3+})^{iv}$$

Gibb (1973) considers the second substitution more realistic and therefore concludes that the control of Na content is Fe^{3+} activity, and hence oxygen fugacity. In support of this idea, figure 3.8d shows that there is a correlation between Na_2O content and estimated Fe_2O_3. The failure of the pyroxene trend seen here to culminate in aegirine as might be expected for a more strongly alkaline magma, could therefore be due to crystallisation at relatively low oxygen fugacity. Gibb (op. cit.) suggests this to be a result of low initial H_2O in the magma.

MnO and Cr_2O_3

Both MnO and Cr_2O_3 (figure 3.8e & f) correlate with the differentiation state of the magma. MnO shows a strong positive correlation with Fe content, and it can be assumed that it substitutes for Fe^{2+}, reaching 1.2wt% at Fs_{55}. Cr_2O_3 on the other hand varies inversely with Fe content, and Cr appears to be selectively partitioned into

the early Mg rich pyroxenes, along with Al (Gibb 1973); dropping off rapidly at Fs_{15}. It should, however, be noted that this fall in concentration is paralleled by the bulk Cr content of the magma, where it is due to early chromite crystallisation.

3.2.4 Oxide minerals

Two oxide phases, titanomagnetite (ulvospinel-magnetite$_{ss}$) and ferrianilmenite (ilmenite-hematite$_{ss}$), are present in the groundmasses of many samples throughout the suite. Titanomagnetite also occurs as a microphenocryst phase in basaltic hawaiites through to mugearites. Examples large enough for microprobe analysis are, however, limited to the more evolved rocks (<6.5wt% MgO) with one exception, VH106, an ankaramitic rock which probably owes its high MgO content to accumulation of pyroxene and olivine phenocrysts. Ilmenite is often present as very fine needles, and thus was impossible to analyse in all but four samples.

The compositional range of the oxides is displayed in the Fe-Ti-O system, ignoring trace element contents, figure 3.10. This diagram shows that the compositional variation in both oxides is relatively limited and that little oxidation appears to have occurred. (It must be noted here, that the Fe_2O_3 contents used are only estimates[4].) The calculated compositional ranges, based on Fe^{3+} and Ti contents, are $mt_{30}ulv_{70}$ - $mt_{51}ulv_{49}$ and $ilm_{96}hem_4$ - $ilm_{91}hem_9$, and these show no obvious correlation with the differentiation state of the host rocks. Indeed a single sample can show half the entire range in mt-ulv$_{ss}$ (e.g. VH24) and almost the entire range in ilm-hem$_{ss}$ (e.g. VH106). This could be due to changes in temperature or oxygen fugacity (fO_2), on which FeTi-oxide compositions depend.

Minor elements

Extensive substitution by other elements can occur in both oxides, making precise identification difficult.

The magnetite series

Observed concentrations of trace element oxides are show in figure 3.11, plotted against MgO content (differentiation state) of the host rock. Correlations are obvious, and reflect those seen in whole-rock composition across the suite (figure 4.11). Fe^{3+} can be replaced by Al, Cr and V (not analysed for) in the magnetite structure (Deer et al. 1992), and 1-5wt% Al_2O_3 and 1-0.9wt% Cr_2O_3 is present in Snaefell magnetites. Fe^{2+} can be replaced by Ca or Mn (both below detection limits; 2σ here) and a continuous solid solution exists between magnetite and magnesioferrite, $MgFe_2O_4$

Figure 3.10

Triangular diagram for the FeTi-oxides in the Fe-Ti-O system.

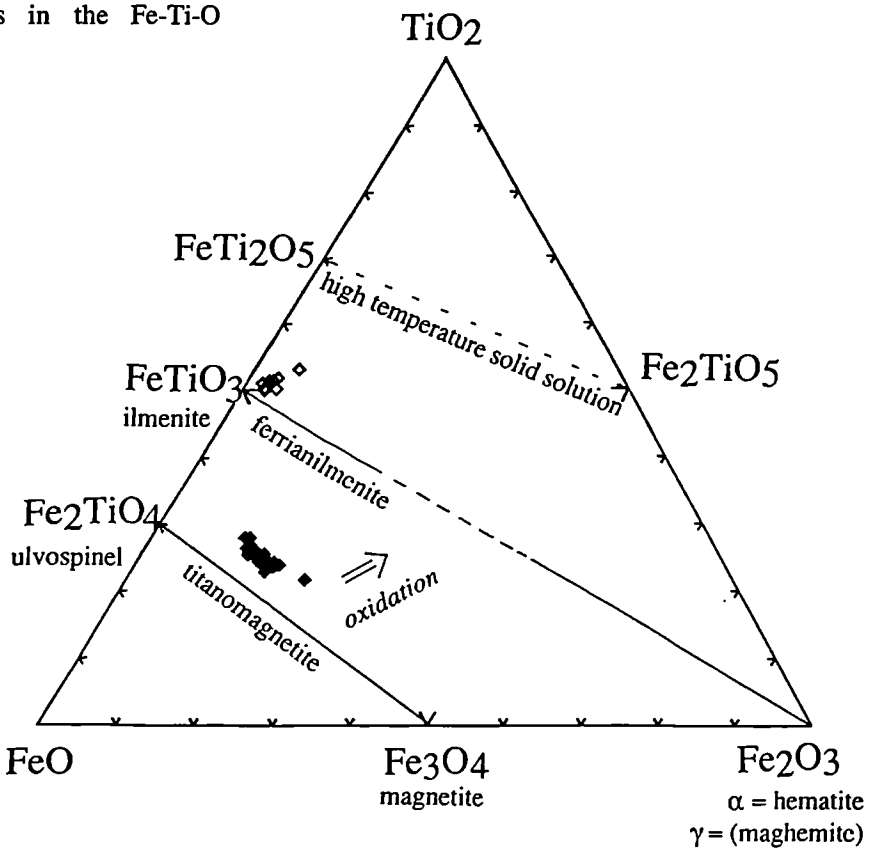

(Deer et al. op. cit.), MgO reaching 5wt%.

Also detected in the Snaefell magnetites were minor amounts of Na_2O and SiO_2, consistently between 0.3-0.9wt% across the series. As noted in section 3.2.1, the Na^+ ion is very close in size to Ca^{2+}, and its single charge could be balanced by a coupled substitution with Si^{4+}. It is unlikely that these last two oxides are merely the result of the microprobe beam hitting the groundmass of the rock surrounding the oxide crystal, since corresponding CaO contents are negligible.

The ilmenite series

Again observed concentrations are shown in figure 3.11, and are much lower than those seen in magnetites. A solid solution exists between ilmenite ($FeTiO_3$), geikielite ($MgTiO_3$) and pyrophanite ($MnTiO_3$); hence small amounts of Mn and Mg are expected to be present and this is the case here. Corundum (Al_2O_3) also has a similar structure, and trace amounts of the three trivalent ions Al, Cr and V are common in ilmenites, but not present in this case.

As with the magnetites, minor amounts of Na_2O and SiO_2 are present.

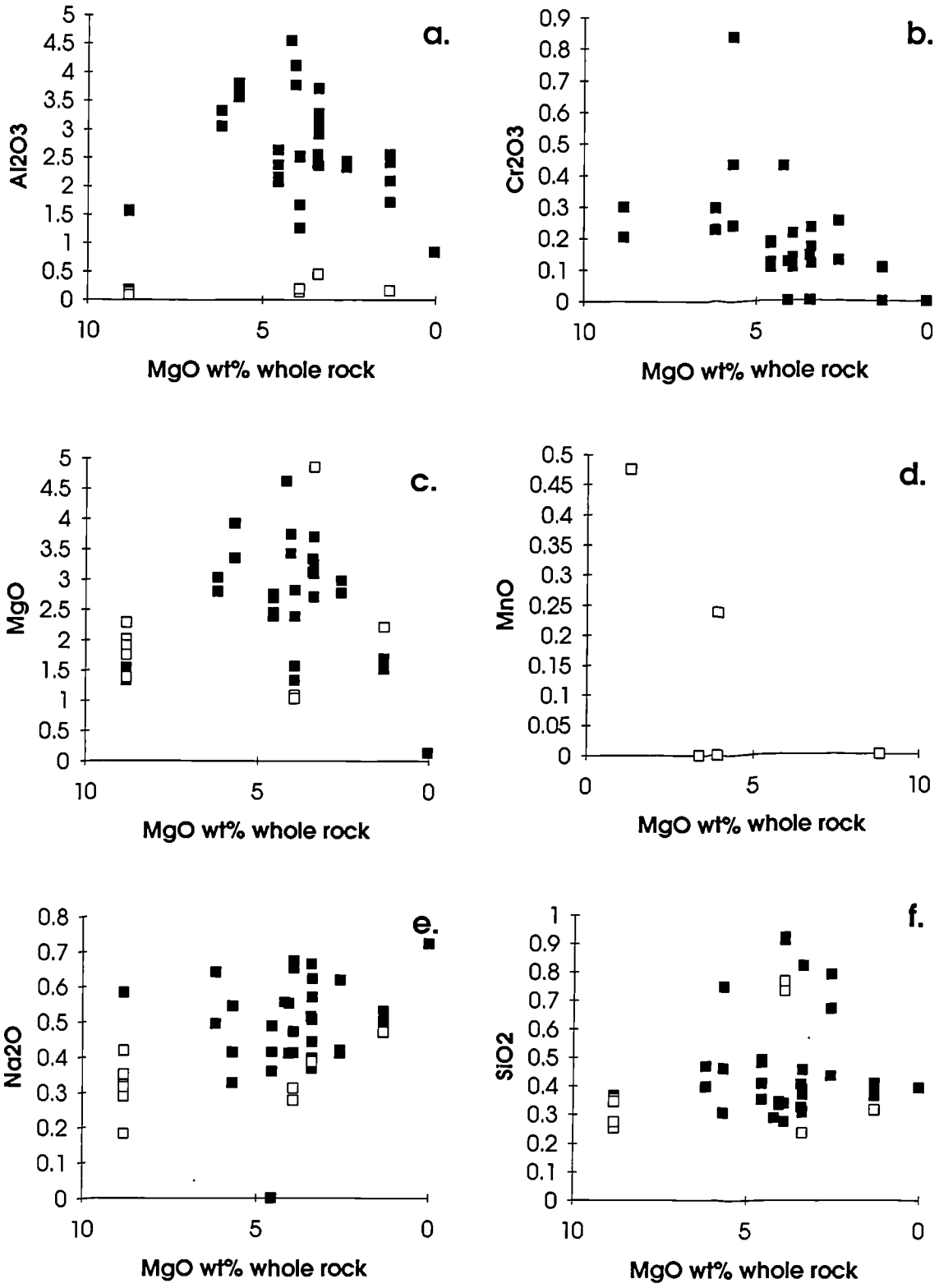

Figure 3.11 Minor element variation in the FeTi-oxides plotted against MgO content (differentiation state) of whole rock. Closed squares - magnetites, open squares - ilmenites.

Geothermometry and oxygen fugacity (fO_2) determinations

Four examples of coexisting magnetite and ilmenite were analysed. The equilibria between the two solid solutions allows both the temperature and fO_2 at the time of crystallisation to be estimated. The following equilibrium reaction is independent of fO_2 and may therefore be used as a geothermometer:

$$FeTiO_3 + Fe_3O_4 = Fe_2O_3 + Fe_2TiO_4$$

The critical equilibrium reaction for determination of fO_2, independent of temperature is:

$$6FeTiO_3 + 2Fe_3O_4 = 6Fe_2TiO_4 + O_2$$

Both equilibria have been experimentally calibrated in the system $FeO\text{-}TiO_2\text{-}Fe_2O_3$ (Buddington & Lindsley 1964) and the results were presented graphically as a series of curves. The application of these curves directly to natural FeTi-oxides, however, results in large uncertainties in calculated temperature and fO_2 since they contain other elements (Al, Mg etc.), sometimes in significant quantities. Powell & Powell (1977) developed equations for calculating temperature and fO_2 of natural FeTi-oxides taking into account impurities, and quantifying the uncertainty they introduce. These equations have been applied to the FeTi-oxides in this study, resulting in huge uncertainties (rendering the results almost meaningless, which is why they are not presented graphically) due to significant quantities of minor elements and variations in oxide composition within samples.

Figure 3.12 shows the results of taking average FeTi-oxide pairs from each of the four samples and reading the temperature and fO_2 from Buddington and Lindsley's original graphs, the "error bars" simply relate to the variation in oxide composition within the individual samples. All four points fall just below the curve of the synthetic quartz-fayalite-magnetite buffer (QFM). These results are similar to those obtained for both Thingmuli (Carmichael 1967) and Krafla (Nicholson 1990). Work on mid-ocean-ridge basalts (MORB) has shown the quenched pillow rinds to be reduced (1-2 $\log_{10}$ units below QFM) relative to the more slowly cooled cores, which lie close to QFM (Christie et al. 1986). This then suggests that oxidation has occurred and that values obtained are unlikely to represent the mantle oxidation state. This process could take place either post-eruption (as appears to happen with MORBs) or while the magma was held in a crustal magma chamber. Oxidation is most likely to be the result of hydrogen loss in either case.

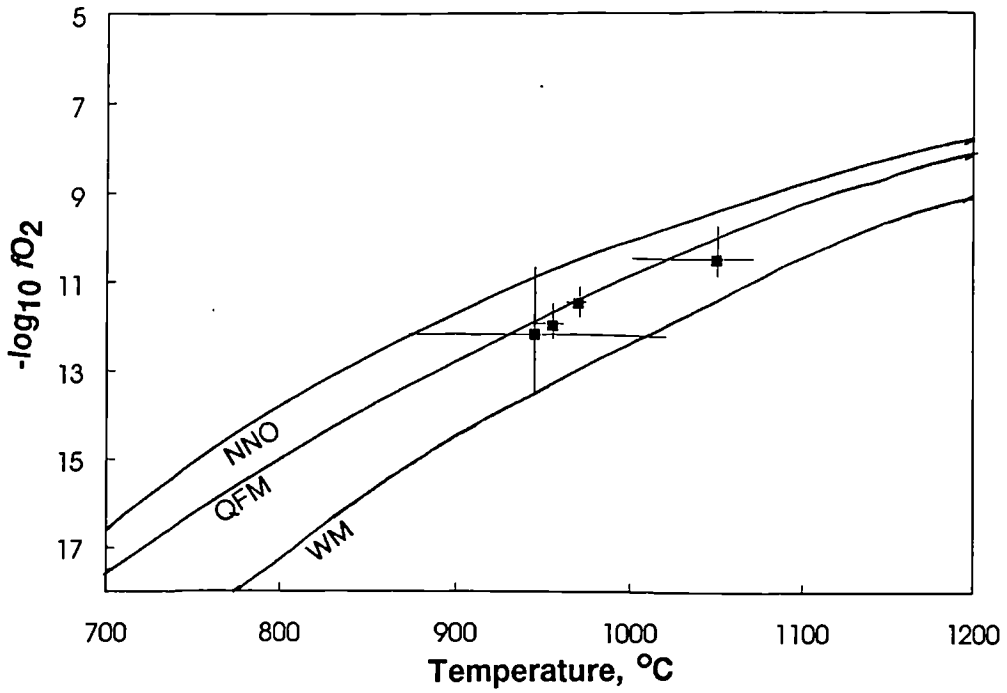

Figure 3.12 FeTi-oxide equilibration temperatures and oxygen fugacities (fO_2) calculated using curves of Buddington & Lindsley (1964). The three labelled curves are the synthetic buffer curves; nickel-nickel oxide (NNO), quartz-fayalite-magnetite (QFM) and wustite-magnetite (WM) respectively (after Carmichael 1967).

3.2.5 Xenoliths

Two of the gabbroic xenoliths (VH20 & VH81) were analysed, and found to contain olivine, plagioclase and clinopyroxene. Neither appears to be in equilibrium with their host lavas, and their differences in mineral composition are shown in figure 3.13. The few mineral analyses from the xenoliths that fall in among those from the host lava are, without exception, small crystals enclosed in glass held within cavities in the xenolith, and which can therefore be assumed to derive from the host lava. It is probable that these xenoliths represent cumulates dredged up from the floor of the magma chamber when more hotter, more primitive magma was injected. It is interesting to notice, from looking at the pyroxene compositions (figure 3.9), that they also appear to have crystallised at greater depth than the associated lavas.

The leucocratic xenoliths contained feldspar ranging in composition from An_{20} in the cores to Or_{17} at the rims where reaction with the host magma had occurred.

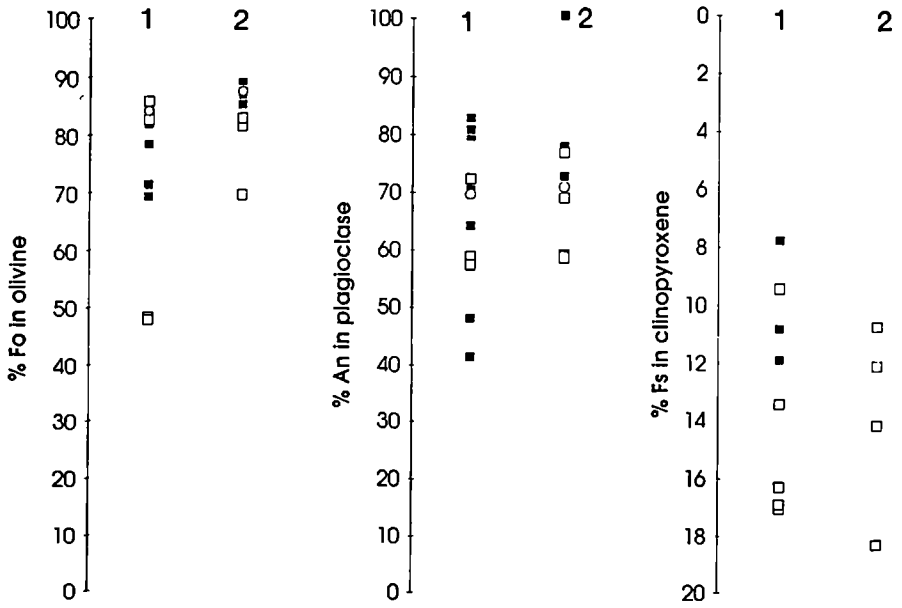

Figure 3.12 Mineral compositions of xenoliths (open squares) compared with those of their host lavas (closed squares). xenolith lava pairs: **1)** - VH81 (x) and VH80 (l), and **2)** - VH20 and VH10. Open circles are the composition of the first to appear on the liquidus of the host lava, further demonstrating the disequilibrium between xenolith and host lava.

3.3 Summary

The petrographic observations and mineral chemistry that have been described and discussed in this chapter allow several conclusions to be drawn as to the petrogenesis of the Snaefell suite:

1). That fractional crystallisation played an important role, and that the sequence of crystallisation was apparently chrome spinel, olivine, plagioclase, clinopyroxene (augite), FeTi-oxides and finally minor phases; apatite and aenigmatite in highly evolved rocks.

2). The story was complicated by magma mixing. Snaefell appears to have been underlain by an established magma chamber which was frequently replenished and from which material was frequently erupted.

3). The suite itself is bimodal, and shows no true intermediates, all samples of intermediate composition appear petrographically to be hybrids.

4). The lack of hydrous mineral phases, pyroxene chemistry and FeTi-oxide equilibria indicate that the fO_2 was relatively low and the magma was fairly dry.

Chapter 4
Petrogenesis I: Magma Chamber Processes

This chapter intends to address the post-generation processes that affected the primary magma(s), in reservoirs - both within and below the Icelandic crust - and post-eruption. The magma chambers and the processes that occurred within them - crystal fractionation and partial assimilation of wall rocks - must be considered, and their effects quantified, *before* the generation processes in the mantle source region(s) can be meaningfully addressed. Also, especially in the case of the rhyolites and highly evolved magmas, it is necessary to consider the question of whether they are heavily crustally contaminated (Sigurdsson & Sparks 1981, Nicholson et al. 1991), or even pure crustal melts (e.g. Oskarsson et al. 1985, Thy et al. 1990). Finally, before any discussion of the composition of the Snaefell magmas can be entered into at all, the results of secondary, post-magmatic alteration processes and associated element mobility need to be assessed.

4.1 Alteration

The Snaefell lavas appear petrographically fresh in general (section 3.1.9), the olivines all remain unaltered. Nevertheless, glass in the interstices of some samples has been replaced by clays and there are signs of secondary minerals, such as carbonates and hydrous Fe-oxides, in the vesicles of others. Zeolites are generally absent, implying that alteration is below zeolite facies. In this respect Snaefell contrasts with all but the topmost few flows in the underlying lava sequence. Nevertheless, palagonite is conspicuous in the subglacial eruption units. Palagonitisation was recognised by Sigvaldason (1968) as essentially a leaching alteration process, that occurs in short-lived hydrothermal cells, set up shortly after eruption. Since most of the samples used in this study were taken from feeder dykes within these subglacial units, element mobility during such hydrothermal alteration must be addressed. Indeed, in any suite of rocks that has been subject to hydrothermal alteration, some degree of element mobility is almost inevitable, and this may affect not only elemental compositions, but also isotope systems. Thus, potential element mobility must be taken into account prior

to any attempt at classification or study of igneous processes; something that is all too frequently ignored, and "mobile elements " used in discriminative plots.

4.1.1 Element mobilities

Controlling factors

Element mobility during hydrothermal alteration is dependant on several factors:

1). The primary composition and mineralogy of the rock. Olivine, for instance is more susceptible to alteration than plagioclase or pyroxene.
2). The crystallisation history. Interstitial glass is the first phase to break down. As it is host to the greatest concentrations of incompatible elements, such as the rare earths (REEs), these elements may be subsequently mobilised (Humphris et al. 1978).
3). The composition of the hydrothermal fluids. The fluid composition during palagonitisation is thought to be initially acidic, becoming more alkaline with time (Furnes 1978).
4). The pressure and temperature at which alteration occurs (i.e. the grade of metamorphism).

The first point implies there may be differences in element mobility within a single suite of rocks, and the second suggests that the more evolved rocks, which are usually more glass-rich due to nucleation problems, will be more susceptible to alteration overall.

In the following assessment, only studies on element mobility in *non-marine* environments have been considered. The reasoning for this is highlighted by Pierce's (1978) work on palagonitisation, where he observes marked differences, specifically that there was greater K, Ca and Sr depletion and Fe, Cr, Mn and Ti enrichment in the palagonites from the subglacial (freshwater) environment, than the examples from the marine environment.

Palagonitisation

Palagonitisation of sideromelane glass has been the subject of several previous studies, which have addressed various aspects; including the rates and temperature dependence (Jakobsson & Moore 1985), the composition, and the element mobilities (Furnes 1978, 1984, Daux et al. 1994). Palagonite is dominantly composed of smectites (Jakobsson & Moore 1985), and most elements show some degree of mobility during its formation (Furnes 1978, 1984). Among the major-element oxides,

only H_2O (H_2O^- and H_2O^+) increases markedly; Al_2O_3 and TiO_2 show some enrichment, and SiO_2, MgO, CaO and Na_2O show depletions relative to the parent sideromelane. The enrichments and depletions correlate fairly well with H_2O increase in the glass. FeO^t shows little variation although Fe_2O_3 increases as a result of oxidation. K_2O shows the largest variations, being strongly depleted in the outermost regions and enriched in the inner regions of the deposit (Furnes 1984). Trace elements behave differently (Furnes 1978), Cr, Co, Cu and Ni are consistently enriched in the palagonite, whereas V, Nb, Zr and LREEs show consistent depletions. Daux et al. (1994) in their study of 11 hyaloclasites, recorded REE losses of up to 40%. Nevertheless, no fractionation among the REEs was observed. Zn, Rb, Sr, Y and Ba show variable trends, with Rb and Sr showing the greatest scatter, indicating that they are the most mobile. Trace elements least affected (<20%) are Zr, Ni, Y, Ba and Nb. The above discussion implies that, unless it is completely certain that glasses are in pristine condition, they are likely to be of very little use in the evaluation of petrogenetic processes.

Whole-rock alteration

In the case of crystalline rocks, as opposed to sideromelane glass, element mobilities might be expected to be much more varied, since elements reside in different sites within the rock-forming minerals. Most studies agree that in all alteration processes, including "carbonatisation and K-metasomatism" (Ludden et al. 1982), the high field strength (HFS) elements Ti, Zr, Y and Nb are relatively immobile (Wood et al. 1976, Smith & Smith 1976, Winchester & Floyd 1977, Ludden et al. 1982) and that their ratios, if not absolute abundances, are unchanged. Absolute abundances of HFS elements are, however, likely to vary as a result of volume changes caused by the addition of metasomatic phases. REEs also appear relatively immobile in most studies, even in chlorite-epidote-actinolite assemblages, although they appear mobile during K-metasomatism (Ludden et al. 1982). In many cases REE mobility cannot, however, be related solely to the metamorphic grade, because the primary distribution of these elements in the rock is critical (Humphris et al. 1978). REEs are highly incompatible in most major rock-forming minerals and thus are hosted dominantly in interstitial glass, which is most susceptible to alteration. Major element oxides appear fairly immobile up to laumontite grade metamorphism (Wood et al. 1976); only Na_2O loss, and K_2O redistribution are observed.

K and Rb especially, along with Sr and Ba, appear mobile at all levels of alteration (Wood et al. 1976, Smith & Smith 1976, Ludden et al 1982). Therefore they should not be used in discriminative plots or to infer igneous processes unless it can be proven that the rocks concerned have not undergone post-magmatic alteration.

Sr and Rb mobility has implications for Sr isotope systematics, since Rb is very mobile, and ^{87}Rb generates ^{87}Sr which will then be only weakly held in Rb sites. This then, could potentially result in selective enrichment of hydrothermal fluids with radiogenic Sr (Wood et al. 1976). Thus Sr isotope data, from older altered lavas especially, must be treated with great caution. LREE mobility could also potentially affect the Nd isotope systematics, but it has been shown that samples from altered and unaltered zones of the same lava flow are analytically indistinguishable (Hawkesworth & Morrison 1978).

Oxygen isotopes

Normal oceanic mantle values for oxygen isotope ratios, measured relative to standard mean ocean water (SMOW), are thought to fall in the range $\delta^{18}O$ = +5.5 to +6‰ (Hemond et al. 1988, Ito et al. 1987). Most Icelandic basalts, however, have abnormally low $\delta^{18}O$ values, outside this range (Hemond et al 1988, Sigmarsson et al. 1992). Fresh lavas from Loihi seamount, Hawaii, also have low $\delta^{18}O$ values averaging +4.9‰ and these have been interpreted as characterising the mantle source within the Hawaiian plume (Garcia et al. 1993). Thus perhaps plumes, such as Iceland, might be characterised by either by low mantle $\delta^{18}O$ values overall, or a greater range of $\delta^{18}O$ than elsewhere, as proposed by Hemond et al. (1988). This explanation alone, however, cannot account for the full extent of the variations in Icelandic basalts (from "normal" $\delta^{18}O$ of +5.5 to <+1‰). A more likely explanation is that these lavas have been subject to post-solidification interaction with meteoric waters - the only natural light oxygen reservoir (Cox et al. 1979) - or have assimilated hydrothermally altered crustal rocks during ascent. $\delta^{18}O$ values reported for hydrothermally altered basalts within drill holes in Iceland are as low as -7.7‰, and the values of $\delta^{18}O$ (as low as -12.7‰) for epidote and low $\delta^{34}S$ (4.8‰) of anhydrite indicate that the altering fluids were of meteoric origin, as expected (Hattori & Muelenbachs 1982).

Therefore it would seem that oxygen isotopes *coupled with other information* can provide a powerful tracer of post-solidification hydrothermal alteration in Icelandic rocks although, taken alone, crustal assimilation cannot be ruled out (discussed in section 4.4).

4.1.2 Effects of alteration on the Snaefell lavas

As has already been noted, the Snaefell lavas show minimal signs of alteration. Their water contents, as measured by loss on ignition (LOI), $H_2O^{+900°C}$, are in general very low, with >95% <3wt% LOI (figure 4.1a). Primary water contents of alkali basalts

such as these (section 4.2) have been calculated at ~0.9% from vesicularity and water solubility in basaltic magmas (Moore 1970). In more acidic magmas, this figure would be expected to increase. LOIs in fresh alkali basalts are found by the same author to vary from 0.49-0.98wt%. Around 21% of the samples analysed in this study actually give negative LOIs; this gain resulting from the oxidation of the FeO present to Fe_2O_3. The lavas from the pile underlying Snaefell (tholeiites, section 4.2), show similarly low LOIs (figure 4.1b), and LOIs from comparable, fresh tholeiitic basalts were found by Moore (1970) to have LOIs varying from 0.31-0.60wt%.

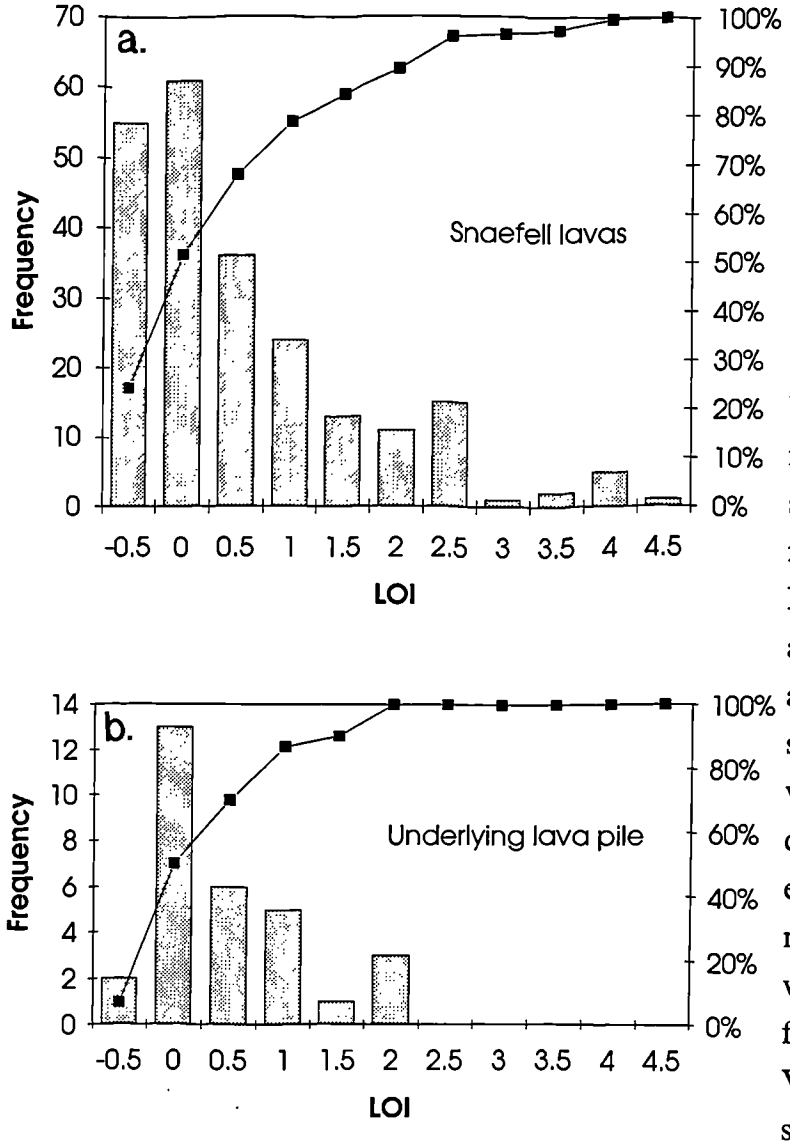

Figure 4.1 Histograms of loss on ignition (LOI),
(a). Snaefell lavas,
(b). Underlying Plio-Pleistocene series.

Glass in the interstices of a few of the basaltic samples appears to have been replaced by clay minerals, and a few show signs of secondary minerals infilling vesicles. In sampling, every attempt was made to avoid rocks where *any* secondary mineralisation was obvious. In order to qualitatively assess the effects of this mineralisation, samples were taken from both fresh rock (a feeder dyke, VH82) and rock showing signs of secondary mineralisation infilling the vesicles (a pillow lava, VH83), both within a single eruption unit (Thordafell). The secondary mineral, on X-ray diffraction analysis (XRD), turned out to be calcite. A vein of secondary calcite in a second unit (Sandfell) was also sampled (VH192) and all three samples were analysed. A spider diagram (figure 4.2) shows that the effects of such mineralisation are minimal, and that element

concentrations in the calcite vein are generally low (with the exception of Sr), indicating that such mineralisation is likely to just result in "dilution" of many elements.

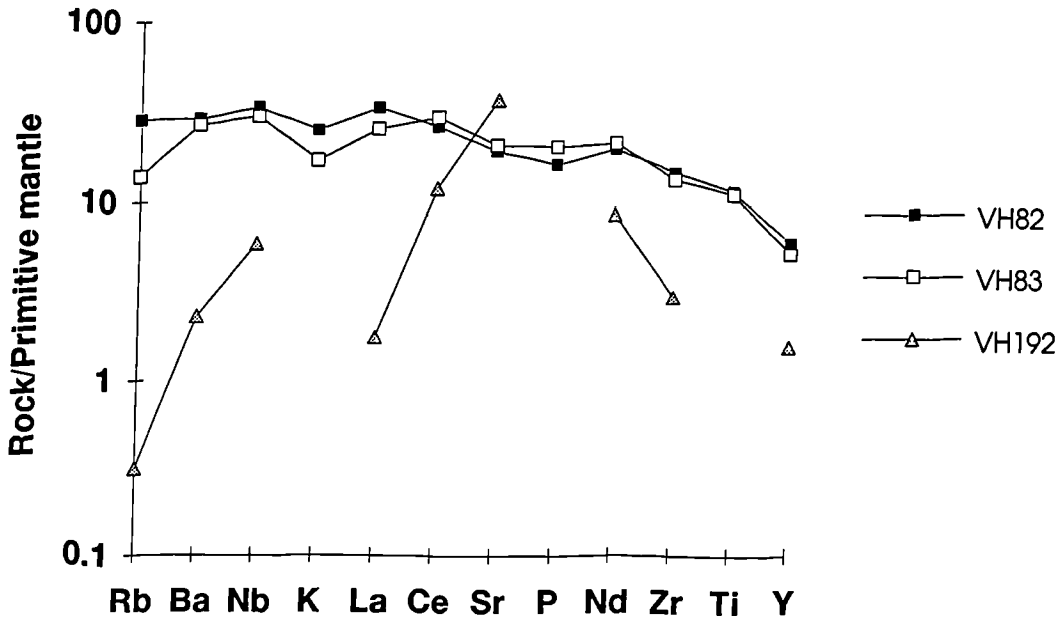

Figure 4.2 Primitive-mantle-normalised (Sun & McDonough 1989) spider diagram, comparing a fresh lava (VH82), with one containing abundant secondary calcite from the same eruptive unit (VH83), Thordafell. VH192 is an example of a calcite vein from another eruptive unit.

In order to assess the mobility of elements in the supposedly fresh material from Snaefell, element/oxide abundances were plotted against Zr, an element which is accepted by all previous studies to be immobile (figure 4.3). Zr is also incompatible in these rocks and thus acts as a fractionation index. Figure 4.3 shows three supposedly immobile elements, Y, Nb and Ce (a LREE) and three supposedly highly mobile elements, Rb, K and Ba. All elements considered here are essentially incompatible (see below), except for Ba and K, which will be taken up by alkali feldspar, (Ba especially is incorporated into *early* alkali feldspar) in highly evolved magmas. Therefore complications in abundances resulting from crystal fractionation or magma mixing are mostly avoided. The plots are almost uniformly coherent, indicating that there has been little post-magmatic redistribution of these elements. The plots of incompatible elements all showing the anticipated fan-shaped arrays resulting from the relatively small initial ranges magnified by crystal fractionation. The underlying lavas (open symbols, figure 4.3) appear similarly unaffected by alteration.

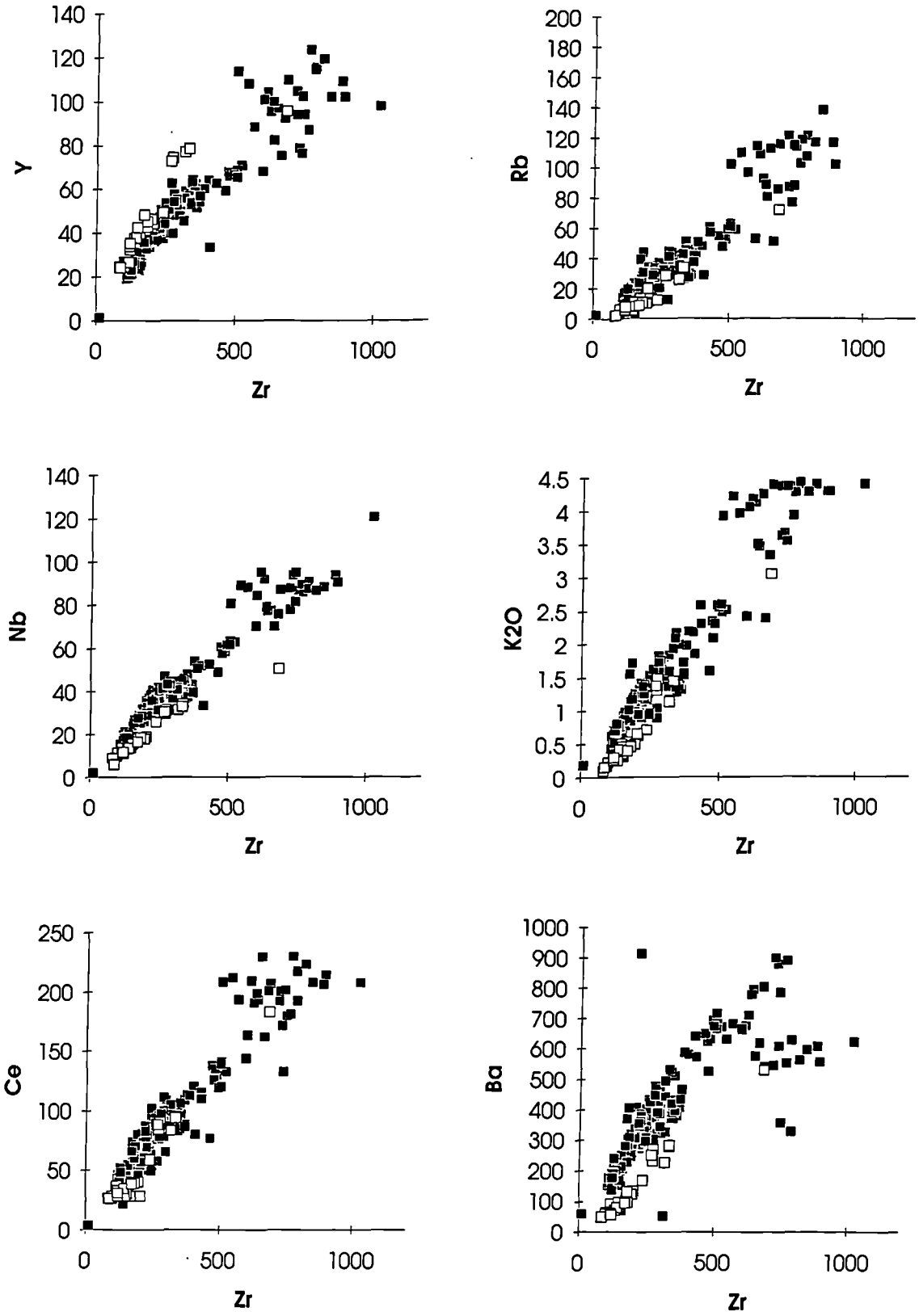

Figure 4.3 Plots of both mobile and immobile incompatible elements against Zr (one of the least mobile trace elements). Note the similar behaviour of all these elements in both series (except Ba; see text), all show a similarly minor amount of scatter. Key to symbols: filled squares = Snaefell data, open squares = underlying Plio-Pleistocene tholeiites

The lack of alteration appears to be confirmed when oxygen isotopes are taken into account (figure 4.4). All the Snaefell samples show values around +5‰, which is within the mantle field discussed previously. This also has implications for the magmatic plumbing and is discussed further below.

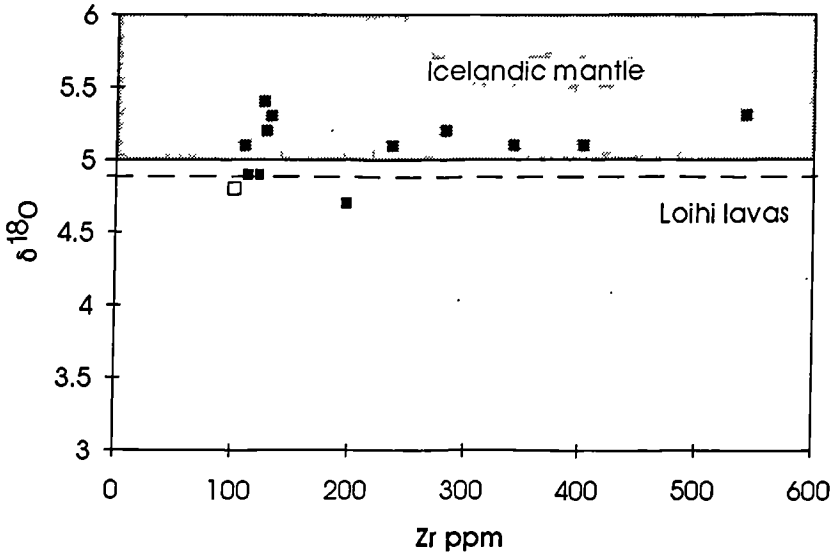

Figure 4.4 Plot of Zr (as a differentiation index) against $\delta^{18}O$. The proposed $\delta^{18}O$ range is taken from Hemond et al. (1988). Key to symbols: filled squares = Snaefell data, open square = an underlying Plio-Pleistocene tholeiite.

To conclude, the affects of alteration appear to be negligible in the two suites of rocks considered here.

4.2 Classification

4.2.1 Review of classification of Icelandic rocks

Classification of Icelandic rock suites over the last couple of decades has varied from author to author, since the recognition that Iceland was *not* petrologically monotonous, and composed solely of tholeiitic lavas (Jakobsson 1972). Probably the most widely accepted division of basaltic and related rocks, in Iceland and elsewhere, is into alkalic and subalkalic (tholeiitic) about the so-called Hawaiian divide on the total alkali:silica (TAS) diagram, proposed by Macdonald & Katsura (1964).

Jakobsson (1979a) divided the Icelandic volcanics into three distinct series: tholeiitic, transitional alkalic and alkalic, on the basis of normative (CIPW) mineralogy. The first series, the tholeiites (e.g. Krafla; Nicholson 1990), are characterised by high Fe and Ti, and low Al; along with normative hypersthene ranging from 10-19 wt%.

These plot below the divide on TAS, and have been divided petrographically into oceanite, tholeiite, icelandite and rhyolite[1]. The second series, the transitional alkalics (e.g. Hekla, Jakobsson 1979b), is still hypersthene normative. The basaltic compositions, however, plot above the divide in TAS, although the evolved compositions plot below. Jakobsson (1979a)divided the series into ankaramite, basalt, basaltic andesite (hawaiite), andesite (mugearite), trachyte(?)[2] and comenditic rhyolite. Finally, the alkalic series (e.g. Vestmanaeyjar) plots consistently above the divide on TAS although it is not very strongly alkalic. Variations appear within these three main series, since each of the volcanic systems show slightly different evolutionary trends. There has subsequently been further debate over the classification of individual systems which do not precisely fit this frame e.g. Oraefajokull (Prestvik 1982). This is particularly significant here, since Snaefell resembles Oraefajokull petrographically and has a similar tectonic setting.

Other aspects of the compositional variability between Icelandic basalt types have been further commented on by many authors (e.g. Hemond et al. 1993). They observed lower SiO_2 and higher Al_2O_3 in alkalic and transitional basalts, in comparison with the tholeiites, along with difference in trace elements and isotopic systematics. The alkalic and transitional alkalic types are relatively enriched in trace elements, and tend to have higher $^{87}Sr/^{86}Sr$ and lower $^{143}Nd/^{144}Nd$.

In order to avoid ambiguity in this study, the recommendations of the IUGS subcommission on the systematics of igneous rocks (LeMaitre 1989, LeBas & Streckiesen 1991) will be adhered to.

4.2.2 Classification of the Snaefell lavas

Since all the rocks are extrusives, the TAS classification has been adopted (figure 4.5). Also marked is the alkalic/subalkalic divide (Miyashiro 1978), which is still widely in use. Thus the Snaefell suite appears to be mildly alkalic, while the underlying lava pile is tholeiitic. The subdivision names hawaiite, mugearite and benmoreite are appropriate here since the series is relatively sodic (Na_2O - 2.0 > K_2O). The rhyolites are actually peralkaline (molecular $[Na_2O + K_2O]/Al_2O_3 > 1$; figure 4.6a), and can be further subdivided into comenditic and pantelleritic (figure 4.6b). Most appear to be comenditic, the few that plot in the pantellerite field on closer inspection appear to be samples previously classed as hybrid on petrographic grounds (chapter 3).

---

[1]Note: some of these names have no firm *compositional* definitions, and may now be virtually obsolete (in the light of IUGS; LeMaitre 1989).

[2]Few examples have been found; Icelandic volcanics are characteristically compositionally bimodal.

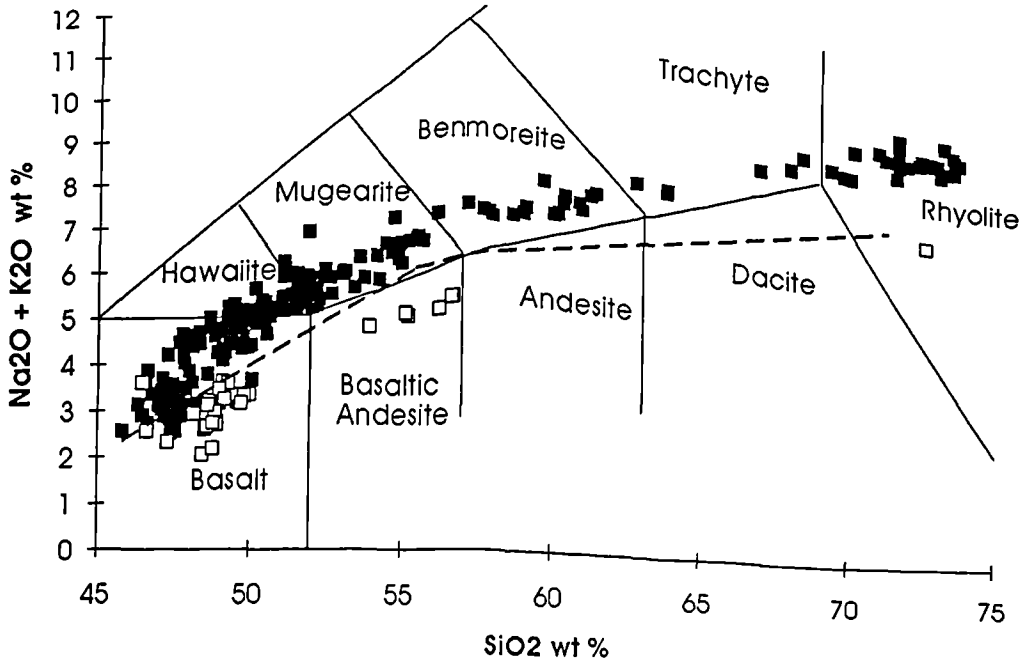

Figure 4.5 Total alkali:silica (TAS) diagram with fields from Le Maitre (1989), showing the Snaefell series (closed symbols) and samples from the underlying lava pile (open symbols). The dashed line is the Hawaiian tholeiitic-alkalic divide (Miyashiro 1978).

The two rock series sampled in the field area can also be separated in terms of incompatible trace element ratios (figure 4.7), These trace element ratios remain fairly constant throughout post-generational processes, implying that they are either a feature of the source composition or the melting processes in operation there. This is especially useful for basaltic compositions, where major element compositions in the two series may be extremely similar.

On further inspection of figure 4.5, the Snaefell suite shows a bimodal distribution, in fact there are probably no true benmoreites or trachytes (i.e. samples which are not mixed magma hybrids; see below), and this is typical of Icelandic suites. The suite is dominated by basic compositions, almost 70% are basalt or hawaiite. Silicic rocks are confined to the central volcano, and represent around 10% of the suite.

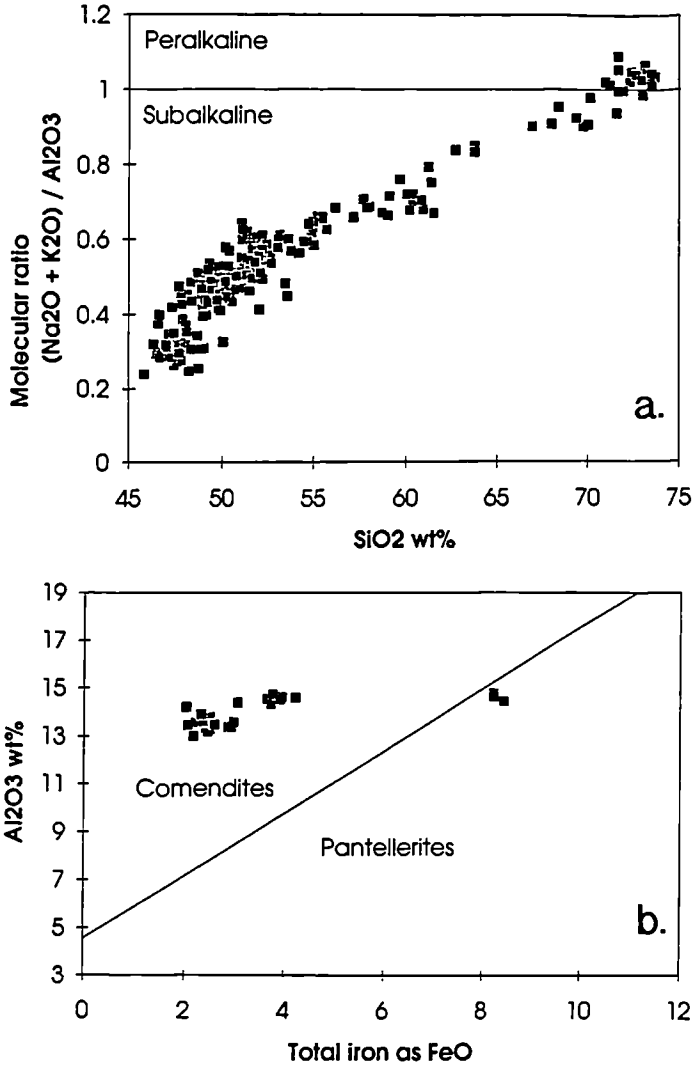

Figure 4.6
Classification of the Snaefell acid rocks.

a). SiO_2 vs Molecular $(Na_2O + K_2O)/Al_2O_3$. Note that although the series as a whole is only mildly alkalic, the rhyolites actually become peralkaline.

b). Al_2O_3 vs total iron as FeO diagram showing the division of the rhyolites (and trachytes) into comenditic and pantelleritic types.

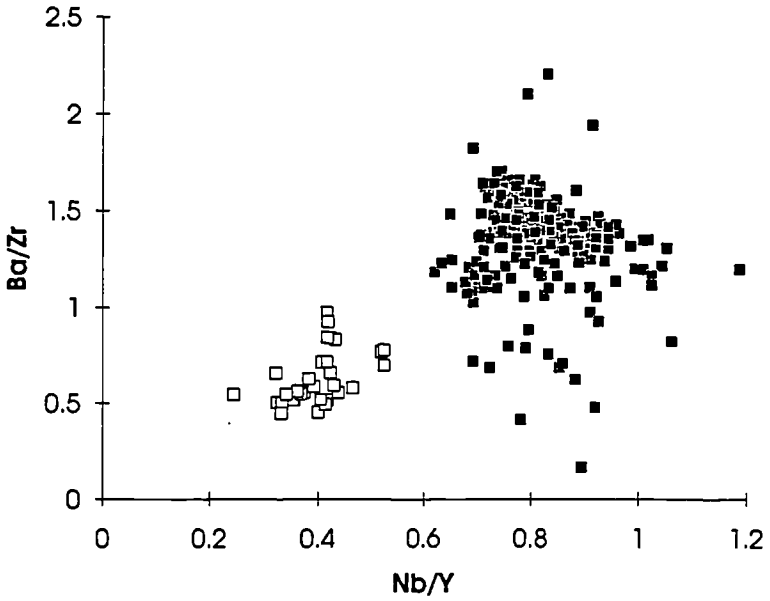

Figure 4.7
Plot of Nb/Y vs Ba/Zr, two ratios altered little by crystal fractionation. Note the clear distinction between the mildly alkalic Snaefell series (closed symbols) from the older, underlying tholeiitic lavas (open symbols).

Thus far, the Snaefell suite appears to fit Jakobsson's (1979a) alkalic series. Nevertheless, most of the basalts are hypersthene normative[3] (figure 4.9, section 4.3.3), and the hawaiites grade into quartz normative compositions. Thus in Jakobsson's (1979a) terms, these rocks fall into the transitional alkalic grouping, although they show fairly strong alkalic affinities.

On figure 4.8 the Snaefell suite is compared with selected suites from other volcanic systems across Iceland in terms of TAS, and falls below Vestmanaeyjar. previously recognised as alkalic, and above Hekla, recognised as transitional. The Snaefell rocks show a remarkably similar trend to those from Oraefajokull and Torfajokull.

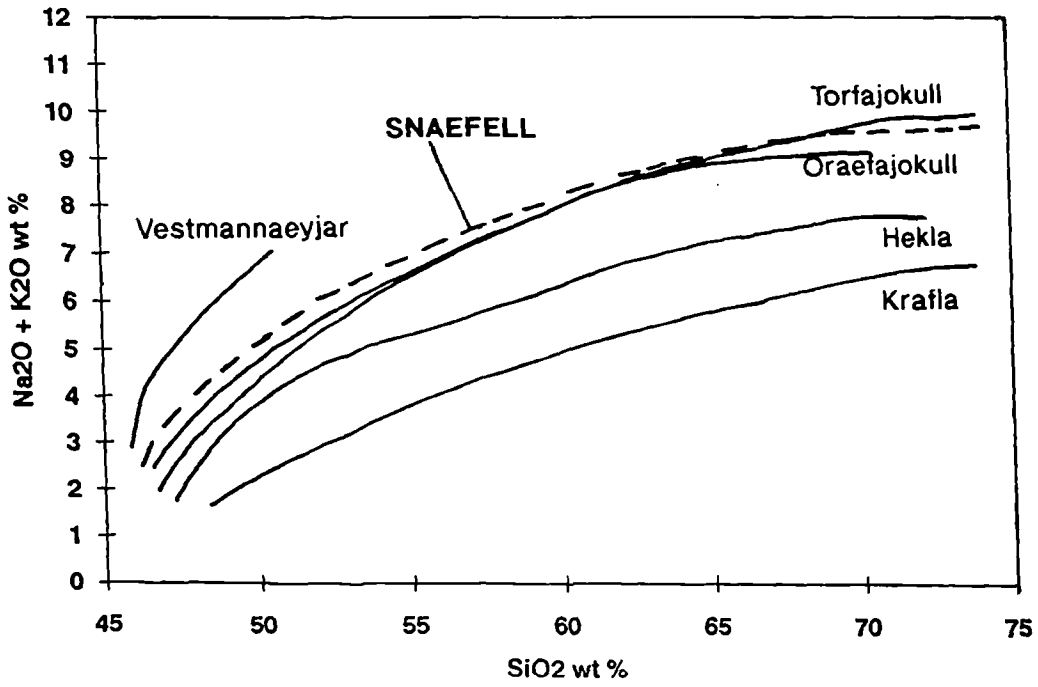

Figure 4.8 TAS diagram comparing the Snaefell suite (dashed line) with a representative selection of other Icelandic lava suites (solid lines) from named volcanic systems. Note the similarity of the Snaefell suite to the Oraefajokull and Torfajokull suites. Data sources: Vestmannaeyjar (Jakobsson 1979b), Torfajokull (MacDonald et al. 1990), Oraefajokull (Prestvik 1985), Hekla (Sigmarsson et al. 1992b), Krafla (Nicholson 1990).

[3]CIPW norms were calculated using IGPET III (M. J. Carr 1990), with Fe_2O_3(T) recast into FeO and Fe_2O_3 following the recommendations of Middlemost (1989). Appeals have been made by several authors for a standardisation of the recasting of Fe_2O_3:FeO in CIPW norms, since they are extremely sensitive to the oxidation state. The first was by Brooks (1976), who suggested a constant value of 0.15. This is not realistic, since the oxygen fugacity of a magma is likely to change as fractionation proceeds, especially for a suite of rocks such as those from Snaefell where a wide variety of compositions is present. Le Maitre (1976), using existing databases of wet chemical analyeses, proposed a scheme dependant on the alkali and silica contents of the rocks concerned, but unfortunately many of these rocks appear to have suffered post-magmatic oxidation. The most recent proposal was made along similar line (Middlemost 1989), using only fresh rocks and has been adopted in this study.

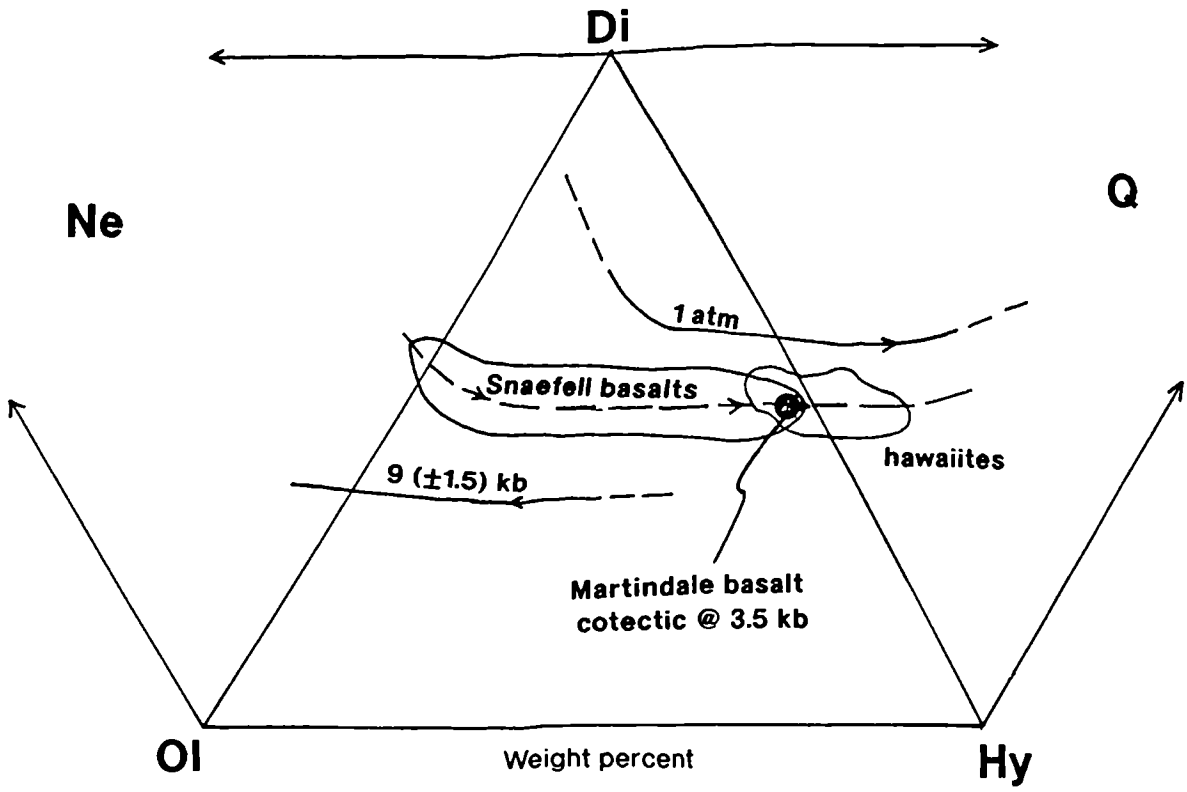

Figure 4.9 Normative Ol-Di-Hy-Ne/Q-plot, showing fields for the Snaefell basalts and hawaiites. The 1atm and 9 kb cotectics are taken from Thompson (1982); Martindale basalt (Helz 1980).

4.3 Fractional crystallisation

4.3.1 Preface

Petrographic work has already revealed that crystal fractionation played a major role in the formation of this suite of rocks. In fact, all the *dominant* trends seen in both major element oxide and trace element abundances (variation diagrams, section 4.3.4) may be accounted for thus. There is, however, much scatter in the data if we assume that, since the rocks are volcanic, such diagrams should show the evolution of liquids or the liquid line of descent (LLD). In actual fact this is most unlikely unless the rocks are very fine grained and relatively phenocryst-free or aphyric (Cox et al. 1979). Crystal accumulation may account for much of the scatter in compatible elements, and must therefore be assessed before any attempt is made to quantify the mineral assemblages crystallising to produce observed trends.

Open-system processes, discussed in subsequent sections, also account for much of the scatter. What is clear, nevertheless, is that a long-lived magma chamber(s) must

have been present throughout much of the centre's life span and its location will be addressed below.

4.3.2 Crystal accumulation

As already described (section 3.1), the bulk of the Snaefell lavas are relatively fine-grained and phenocryst-poor, and therefore the affects of crystal accumulation should be minimal. A few samples, however, have phenocryst contents $\geq$ 15% by volume.

Among the more magnesian basalts, two units show possible evidence of olivine accumulation. One (VH106) is ankaramitic, while the second (VH80) shows three phenocryst phases: olivine, clinopyroxene and plagioclase. Evidence for crystal accumulation comes from both petrographic studies and electron microprobe analysis (section 3.2.1), which indicate that the olivines are too iron-rich to be in equilibrium with the bulk composition of the sample. As explained below, however, VH80 could also be a product of magma mixing.

The most common cumulus phase in the basaltic and intermediate members is plagioclase. Combined petrographic studies and geochemical analysis shows that samples with Al_2O_3 in excess of 16.5 wt% contain cumulus plagioclase, and that this affects around 7% of samples analysed. In the silicic rocks (trachytes and rhyolites), alkali feldspar can reach 20% volume. This could account for some of the scatter seen in the concentration of elements such as Sr and Ba which are compatible in alkali feldspar[4].

Additionally in a few samples (hawaiites and mugearites) containing <5% MgO, there appears to be magnetite accumulation. This is primarily indicated by high TiO_2, V and MnO contents, causing points to fall off the main trend, representing crystal fractionation (figure 4.11). It is, however, not possible to rule out the possibility that all of these samples are of hybrid origin (section 4.5), although in most cases there is little additional evidence for this.

4.3.3 Magma chamber(s)

In the continental setting, primary magmas generated in the mantle tend to collect at the crust-mantle boundary due to the density contrast there (e.g. Cox 1980). In a tensional environment, such as in the early stages of rifting, magmas may proceed into

[4]Estimates of partition coefficients for these elements in alkali feldspar range from 3.6-26 for Sr, and 2.7-12.9 for Ba (Henderson 1982).

the crust and form a chamber there prior to eruption at the surface (Larsen et al. 1989). In the case of Iceland, however, the crust is dominantly basaltic; hence the density contrast between this and the underlying mantle peridotite is probably significantly less than in the continental setting. Nevertheless, evidence discussed below would appear to suggest that magma did indeed accumulate at the crust-mantle boundary at Snaefell.

In a CIPW normative plot of diopside (*di*), hypersthene (*hy*), olivine (*ol*), nepheline (*ne*) and quartz (*Q*)[5] (Figure 4.9) the Snaefell basalts plot mid-way between the one-atmosphere cotectic and the 9kb cotectic. They appear to delineate a cotectic line at some intermediate pressure, following much the same path as the 1atm cotectic, but displaced to lower normative clinopyroxene contents. It can be demonstrated that this is a feature of crystal fractionation, as opposed to an *artefact* of sampling a range of batches of primary magma with differing silica saturations, by using a plot of normative hypersthene (wt% used in phase diagram) against MgO (figure 4.10) as an index of fractionation (the choice of this fractionation index is discussed below).

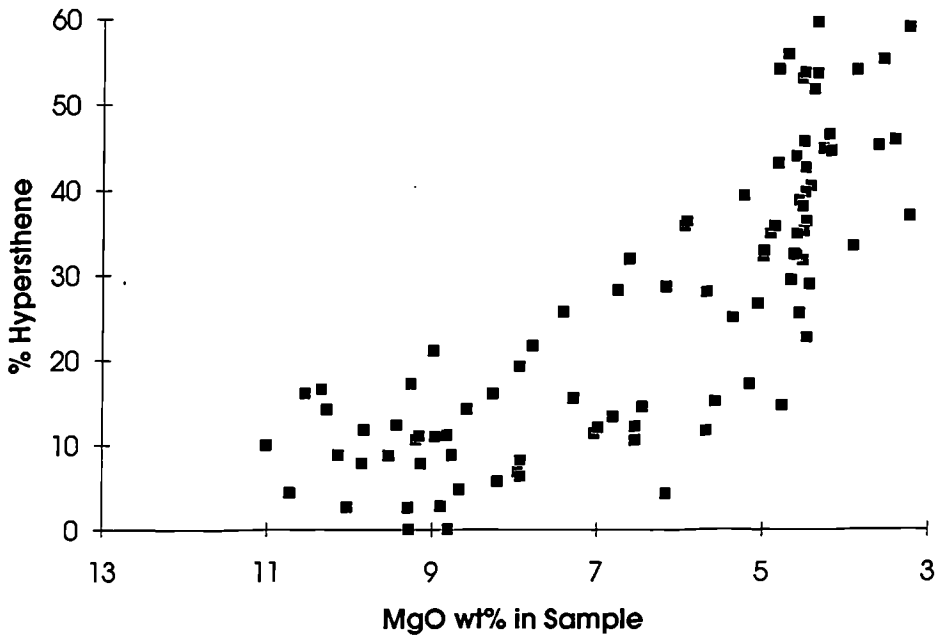

Figure 4.10 MgO vs % Hypersthene as plotted in figure 4.9 (raw CIPW hypersthene data avoided since this is confused by plagioclase accumulation) for Snaefell basalts. Note positive correlation implying that crystal fractionation, as opposed to mantle melting, is responsible for trends seen in figure 4.10.

[5]The advantage of this plot, over other similar phase diagrams that could have been used, is not only its "expanded basalt field" but also its insensitivity to the addition or subtraction of plagioclase (Thompson 1987), the only really notably cumulus mineral in some samples, eg VH151. That the Snaefell basalt field extends just into the nepheline (ne) normative field has no significance because norm calculations are extremely sensitive to oxidation and errors brought in here are over-emphasised by the expanded basalt field.

The percentage of normative hypersthene can be seen to increase systematically with decreasing MgO content. This cotectic delineated by the Snaefell basalts intersects the normative composition of the *Martindale basalt,* a Columbia River basalt containing 6wt% MgO, that was found by phase-equlibria experiments to be in equilibrium with liquidus olivine, plagioclase and clinopyroxene at 3.5kb (Helz 1980), corresponding to around 13km depth. Although crustal thickness is poorly known, a value of ~15km is suggested from seismic studies for off-axis regions (Flovenz & Gunnarsson 1991). Therefore it seems that the Snaefell magmas accumulated and fractionated at the crust-mantle boundary.

The field in figure 4.9 only shows the region in which the majority of the Snaefell basalts lie, a few actually lie closer to the 1 atm cotectic. This suggests that some batches of magma did equilibrate at shallower levels in the crust, prior to eruption at the surface, but that no long-lived magma chambers were established there. The apparent lack of significant crustal assimilation (section 4.4), would also argue against a well-established shallow crustal magma chamber.

The evidence for the lack of a shallow crustal magma chamber sets Snaefell apart from central volcanoes in the present-day axial rift zones. Seismic studies (Brandsdottir 1994), have detected the presence of magma bodies at both Krafla and Askja at depths of around 3km, i.e. the buoyant equilibrium depth of basaltic melt in the Icelandic crust. In *possible* examples of previous flank zones, such as the Austurhorn intrusion (Furman et al. 1992), magma chambers also appear to have been at shallow crustal levels; estimates put the chamber depth here at >2km below the top of the original crust.

4.3.4 Fractional crystallisation from basalt to mugearite

The Snaefell series divides naturally into two sections, being compositionally bimodal and comprising of a series of basalts to mugearites (discussed here) and a small cluster of rhyolites (section 4.3.5). As has been noted in section 4.3.3, the individual basalts and hawaiites appear related by fractional crystallisation, as opposed to differences in partial melting processes.

Selection of an index of differentiation

The choice of differentiation index is important in such studies and must be appropriate to the compositional range of the suite in question. The most commonly used index is SiO_2 (in so-called Harker diagrams), the drawback to this in suites with abundant mafic members is that significant compositional changes can occur while the

silica content is relatively constant. Only at the onset of magnetite crystallisation (a SiO_2-free phase) do any significant changes begin. Previous studies of similar Icelandic suites have used MgO (Furman et al. 1991, Nicholson et al. 1991) or iron:magnesium ratios in various forms (e.g. Wood 1978). MgO is one of the most commonly used alternatives to SiO_2; appropriate to series with a high proportion of mafic compositions, such as in the present study. It is an important component in minerals in equilibrium with mafic magmas, and thus shows much variation with their removal during fractional crystallisation (Rollinson 1993). Using MgO content also has the advantage in that it is *directly* proportional to liquidus temperature of the magma (Thompson 1973). Iron ratio (FeO*/[FeO* + MgO]) or the converse, magnesium number (Mg# = MgO/[FeO* + MgO]) have an advantage over MgO as an index of differentiation, in that MgO content may be buffered (like SiO_2), when a MgO-free phase (e.g. plagioclase) is present in the crystallising assemblage. One specific drawback with iron:magnesium ratios is that they tend to confuse magnesium decrease with iron enrichment, which is pronounced in many Icelandic suites (Jakobsson 1979b).

Major and trace elements analysed by X-ray fluorescence are plotted against MgO content in figure 4.11. Coherent trends can be seen in most cases, with varying amounts of scatter. Since the rocks are volcanic and predominantly fine-grained and phenocryst-poor, these trends arguably represent liquid lines of descent (LLDs); i.e. the path taken by the residual melts in response to removal of mineral phases. Obviously, however, these rocks were erupted in a random time-sequence and therefore the trends seen result from the repeated occurrence of a reproducible differentiation process. Thus what is seen are effectively *bundles* of sub-parallel and overlapping LLDs, which cannot be related to a single *parental magma*, but rather to a series of similar, related magmas (Cox et al. 1979). This would account for some of the scatter, although much is due to the system being open, and subject to repeated tapping, replenishment and magma mixing (section 4.5). Crustal contamination, is also another potential cause (section 4.4).

Inflections present in the apparent LLDs in some of the variation diagrams (figure 4.11) may be interpreted as the entry of a new mineral phase, within which that element is compatible, into the crystallising assemblage (Cox et al. 1979). A few of the trends show more than one apparent inflection (e.g. Fe_2O_3(T), Sc), although scatter may mask more, especially at intermediate MgO contents.

* Total Fe (Fe_2O_3 + FeO) expressed as FeO.

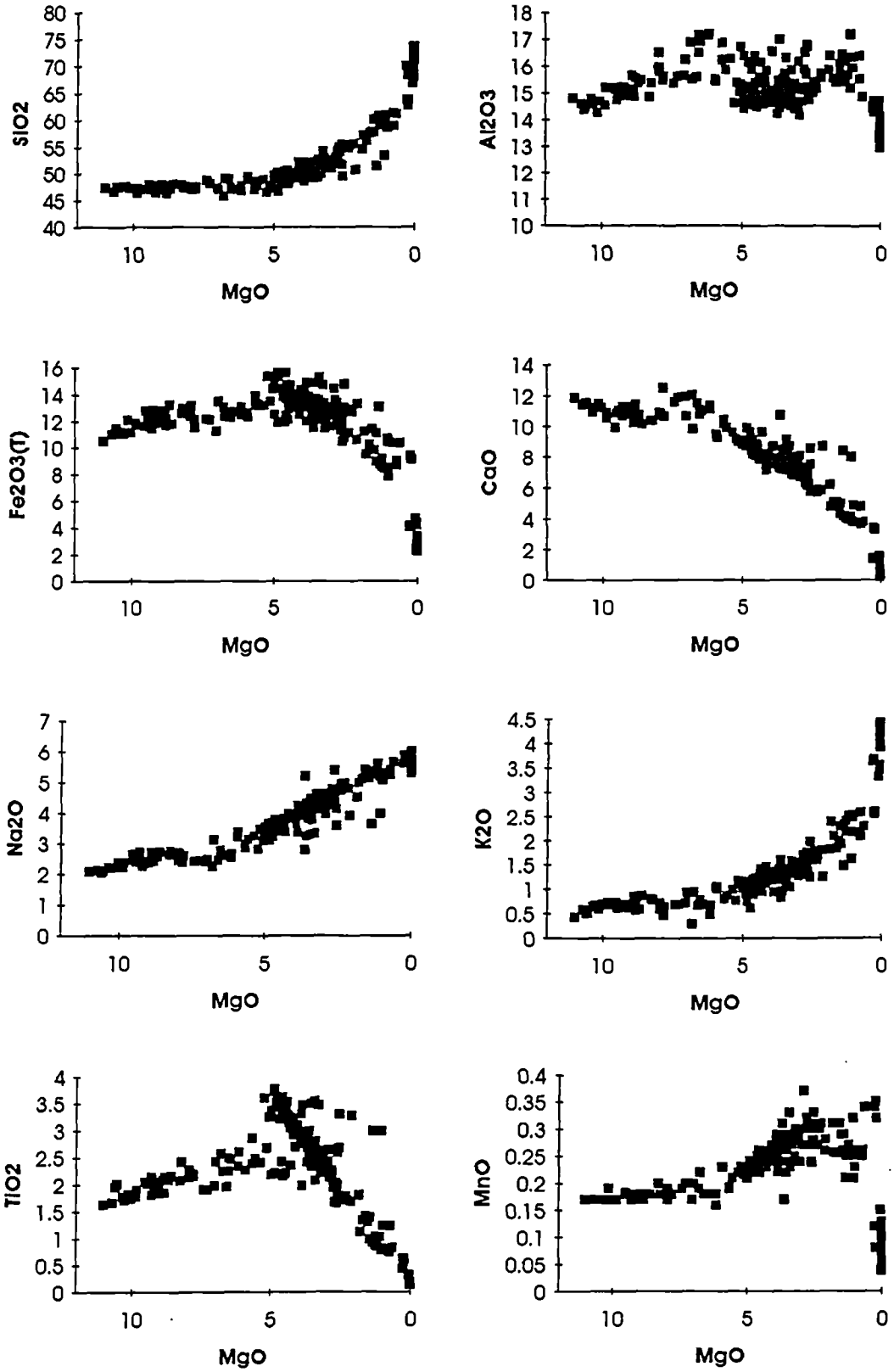

Figure 4.11 Variation diagrams, using MgO as the fractionation index, for elements analysed by X-ray fluorescence (XRF).

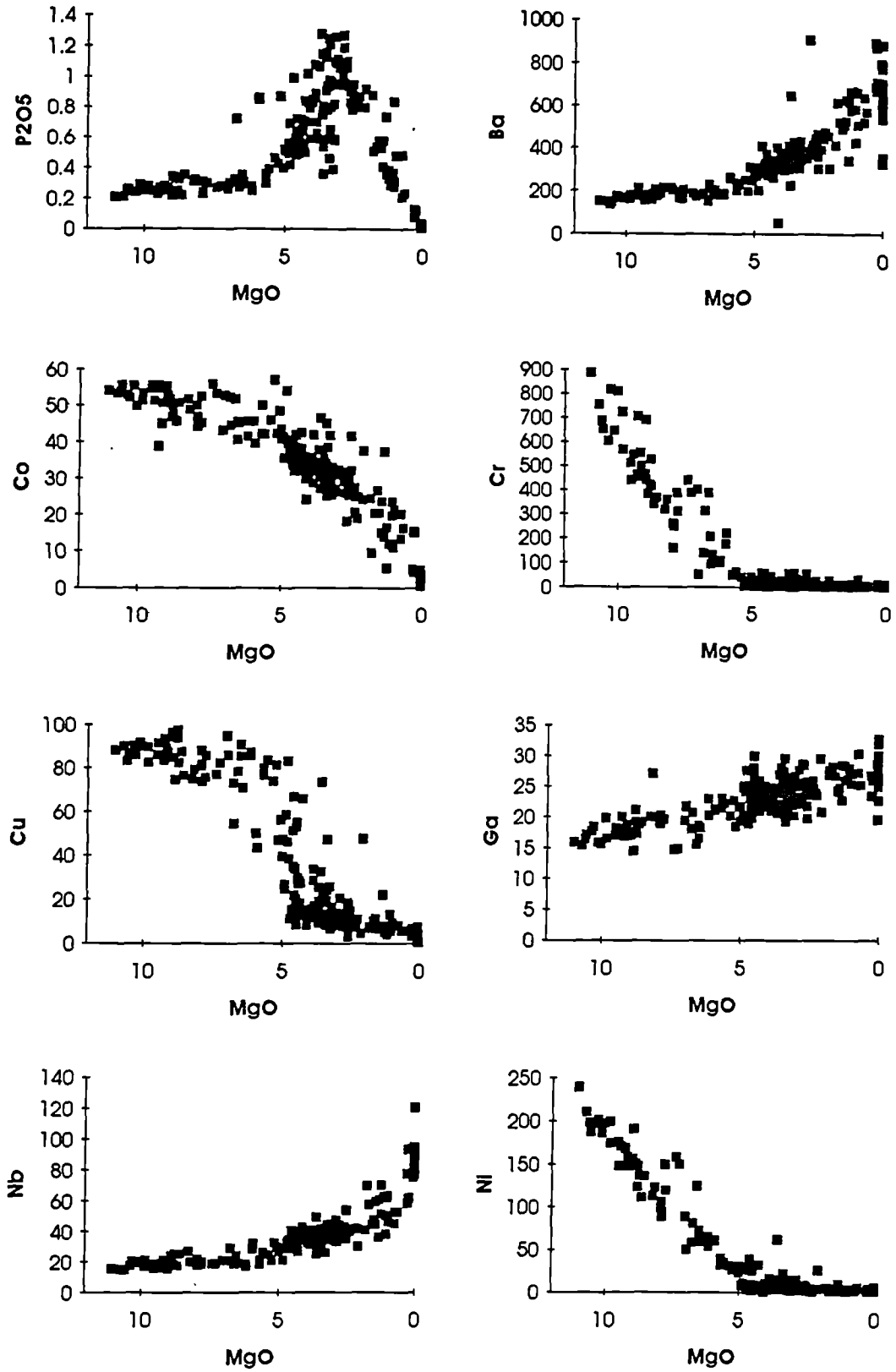

Figure 4.11 (Continued).

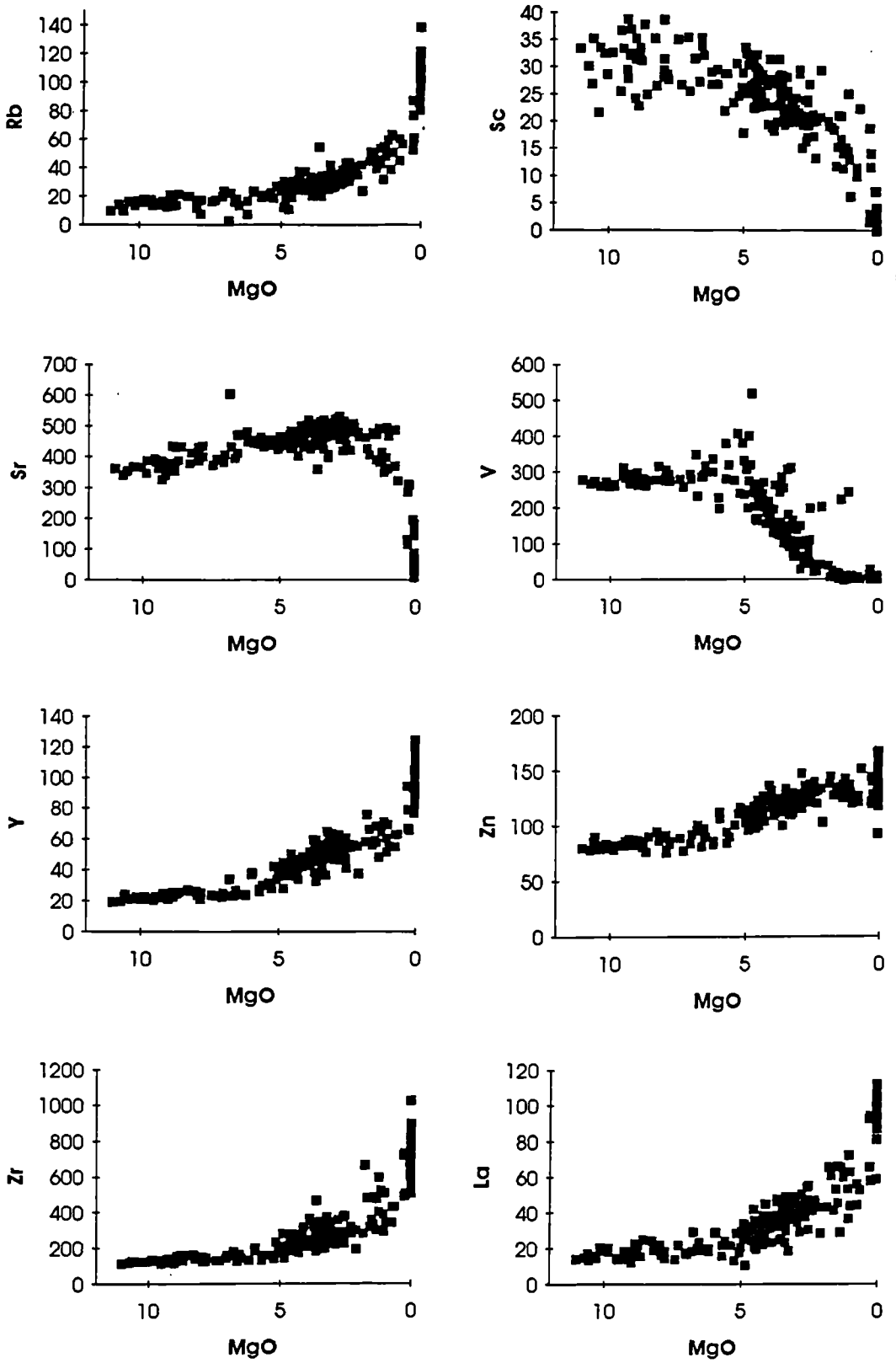

Figure 4.11 (Continued).

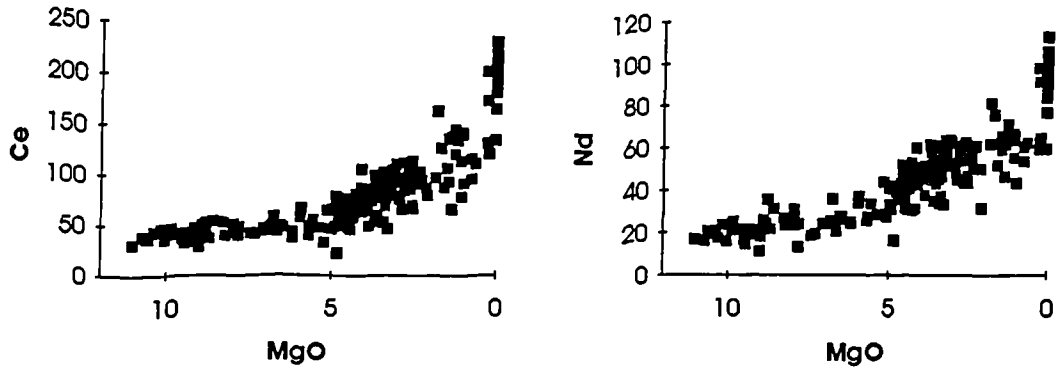

Figure 4.11 (Continued).

These observations correlate reasonably well with petrographic observations which indicate the following crystallisation sequence:

BASALT $\Rightarrow$ OL + PL + SP ($\pm$ CPX)† $\Rightarrow$ BASALTIC HAWAIITE $\Rightarrow$ PL + MGT + OL + CPX $\Rightarrow$ HAWAIITE $\Rightarrow$ PL + MGT + CPX + AP $\Rightarrow$ MUGEARITE

OL = olivine, PL = plagioclase, SP = Cr-spinel, CPX = clinopyroxene, MGT = magnetite, AP = apatite.

†Clinopyroxene phenocrysts are only present in a few basalts, despite compositional evidence for clinopyroxene crystallisation. This is a relatively common phenomenon (Basaltic Volcanism Study Project 1981).

This is reinforced by qualitative modelling, below, clarifying which parts of some of the more blurred trends can be accounted for by crystal fractionation alone.

In order to qualitatively model the crystallisation sequence, a primitive end-member composition - an approximation of the primary mantle melt - must be identified. It is clear from petrographic work, however, that all sampled compositions have undergone at least minor amounts of fractional crystallisation. Therefore the primitive end-member should be considered simply a *potential parental composition* as opposed to a *primary mantle melt.*

Selection of a parental magma composition

Compositionally there was one obvious candidate for a parental magma composition, VH10, which had the highest MgO at 11.0 wt%, Cr at 885ppm (which partitions into early spinels[6]) and Ni at 240ppm (which partitions into fosteritic olivines[6]) contents. Petrographically this sample also appears to be very primitive, it just contains euhedral olivine phenocrysts, along with plagioclase and chrome spinel microphenocrysts. Unlike most other samples, it appears that plagioclase was not actually on the liquidus. Care must be taken, however, to ensure that the olivines are not cumulus, there are three potential ways to check this:

1). To microprobe both groundmass and phenocryst olivines; if in equilibrium these should show no great differences in composition;
2). To use probe data of olivine compositions, glass or whole-rock compositions and look at the distribution coefficient (K_D; Roeder & Emslie 1970) relating the partitioning of Mg and Fe between olivine and liquid, which should give a value of 0.3 if equilibrium has been attained .
3). Using the computer program TRACE (Nielsen 1988), described below, to predict the equilibrium composition of the olivine and compare this with actual probe data.

The first method was impractical due to the very fine-grained nature of the groundmass. Therefore the other two methods were employed and the results recorded in table 4.1.

Observed range in olivine compositions	Fo_{89-87}
K_D (Roeder & Emslie 1970) using whole rock composition, as opposed to interstitial glass	0.27
Equilibrium olivine composition *calculated* by TRACE	$Fo_{87.5}$

Table 4.1 olivine composition in sample VH10.

Therefore it would appear that VH10 is a very good candidate for a parental magma to the series, the calculated olivine composition agrees reasonably well with probe data. The K_D value of 0.27 for an averaged olivine composition is also close to the equilibrium value.

[6]Partition coeficient for basaltic liquids (Rollinson 1993):
Spinel Cr=153
Olivine Ni= 5.9-29

The most magnesian olivine composition (Fo_{89}) found in sample VH10 is close to the maximum recorded in Icelandic lavas, Fo_{90} (Meyer et al. 1985), and lies within the mantle range Fo_{92-89} defined by Kostopoulos (1991), confirming the primitive nature of this sample.

Modelling of fractional crystallisation

Modelling of the effects of crystal fractionation on both major and trace element compositions was attempted using TRACE.FOR (Nielsen 1988). TRACE uses expressions for major and trace element partitioning between minerals and melt derived from experimental work, with the compositional dependence reduced to allow the temperature dependence to be expressed as a simple linear regression. The combination of these expressions with a model of major-element phase-equilibria has produced a model to calculate the differentiation paths of mafic and intermediate compositions as they undergo fractional crystallisation of the following mineral phases: olivine, plagioclase, clinopyroxene, orthopyroxene and spinel. fO_2 can be varied from +2 to -4 log units relative to the QFM buffer. The default crystallisation increment is 0.2% and output every 2% crystallisation.

TRACE is restricted to the study of *low-pressure* differentiation, since most of the experimental work on which it is based was conducted at 1atm. Compositionally, it is restricted to compositions with <65% SiO_2; although it is applicable to both alkalic and tholeiitic compositions. More evolved compositions produce meaningless results, since TRACE does not incorporate the mineral phases apatite and alkali feldspar - both of which are observed in more evolved members of the Snaefell suite. At oxygen fugacities close to the QFM buffer, compositions with >500ppm Cr also cause problems due to the high partition coefficient of Cr in spinel.

VH10 was input into TRACE as the starting composition, with fO_2 set at 1 log unit below the QFM buffer as indicated by Fe-Ti oxide compositions (section 3.2.4); Fe^{2+}:Fe^{3+} ratio was set following Middlemost (1989), and Cr at 500ppm. Recharge and eruption were set at zero, so that the modelling was for a closed system. Output was as default settings (see above). The results for selected major and trace elements are presented in figure 4.12 compared with the actual data. Crystallisation reached 90% (MgO = 2.5 wt%; i.e. mugearitic composition) before the program crashed.

Generally, the model predicts mineral compositions close to those observed in the suite and a liquid line of descent (LLD) that fits the overall trends in the Snaefell data fairly well down to ~4% MgO. At lower MgO contents, the model becomes increasingly unrealistic.

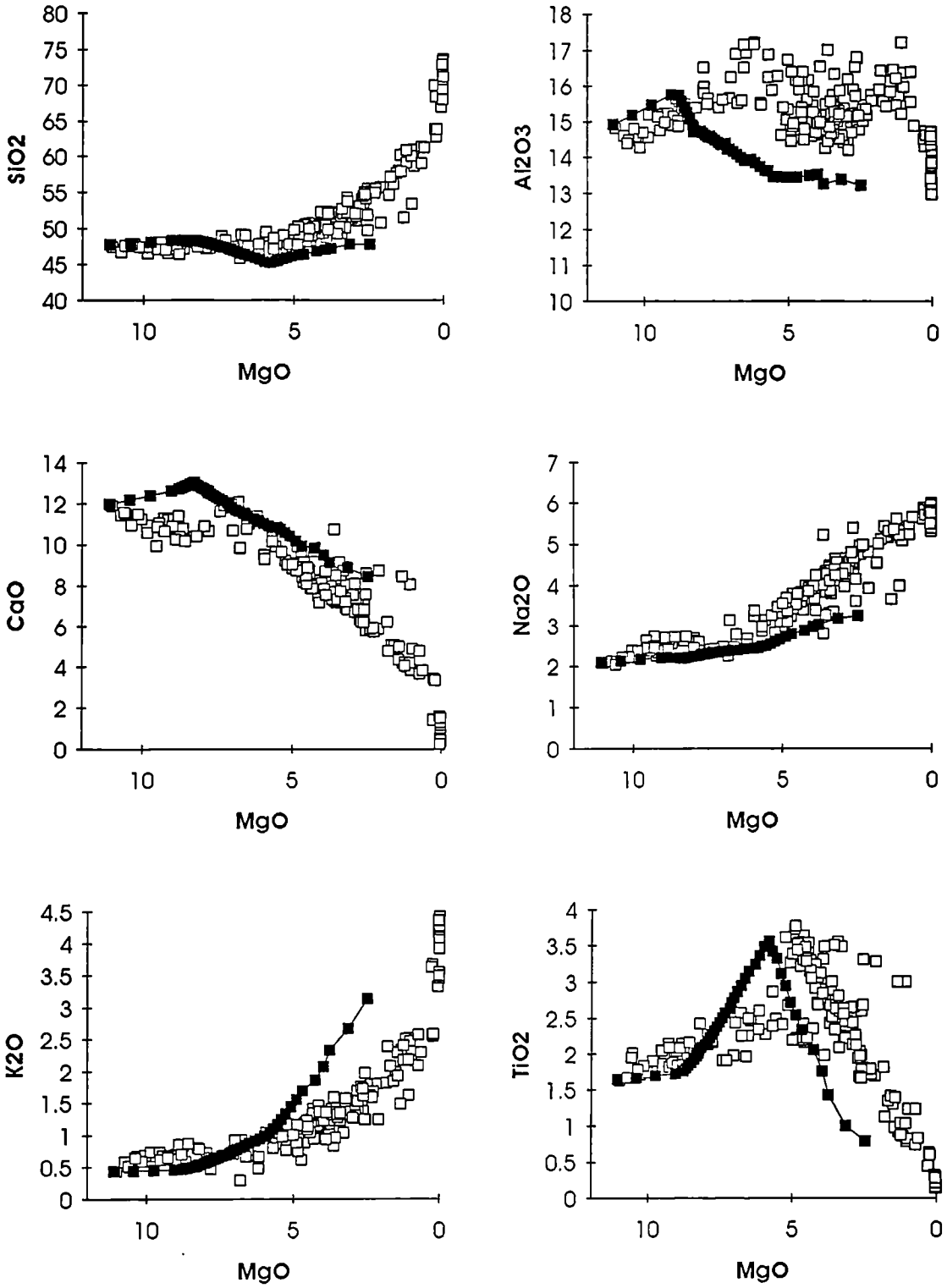

Figure 4.12 Plots of selected major and trace elements vs MgO. Closed symbols depict the liquid lines of descent (LLDs) predicted by the computer program TRACE, each symbol separated from the previous by 2% crystallisation. Open symbols are the Snaefell data.

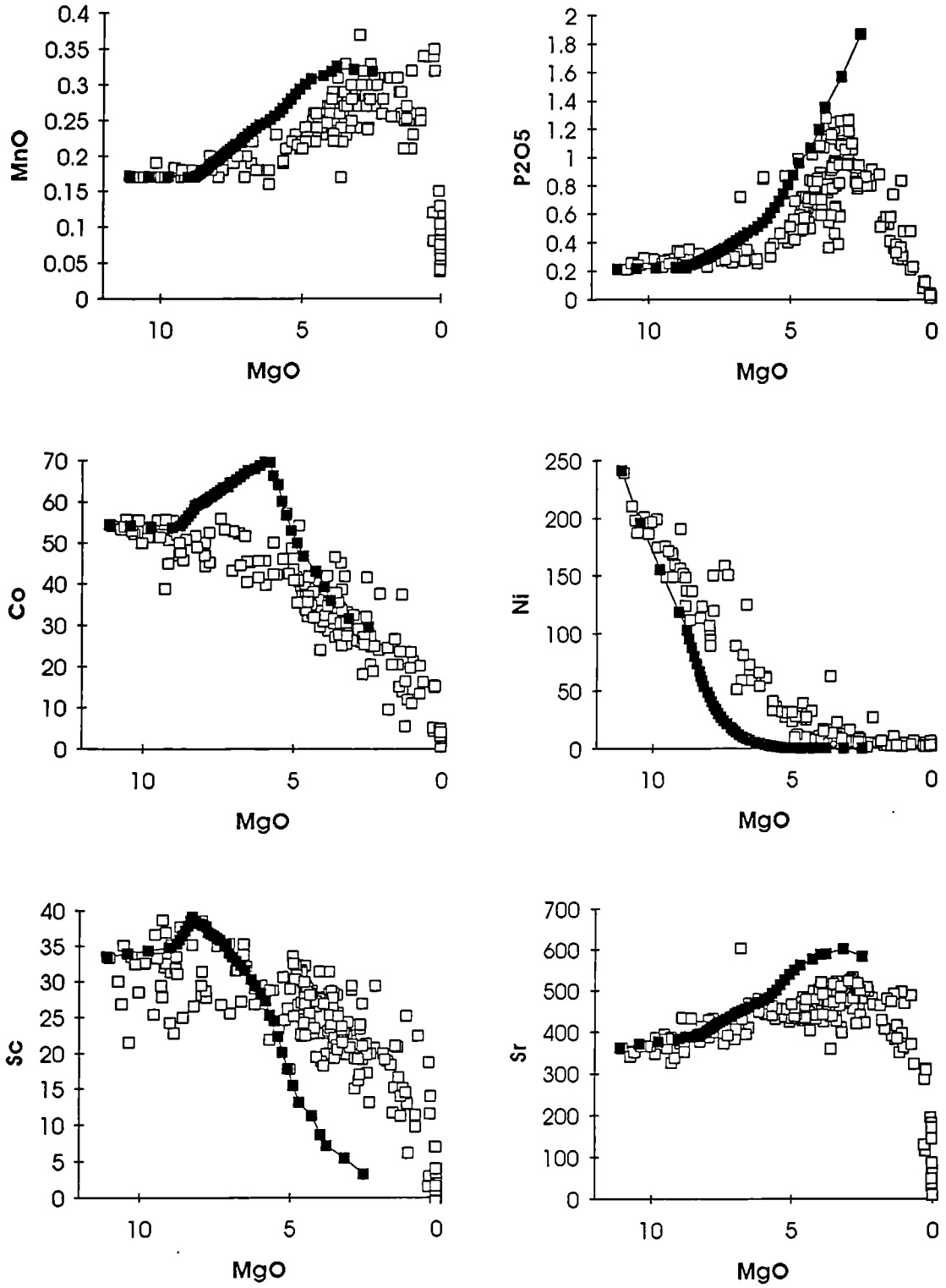

Figure 4.12 (Continued).

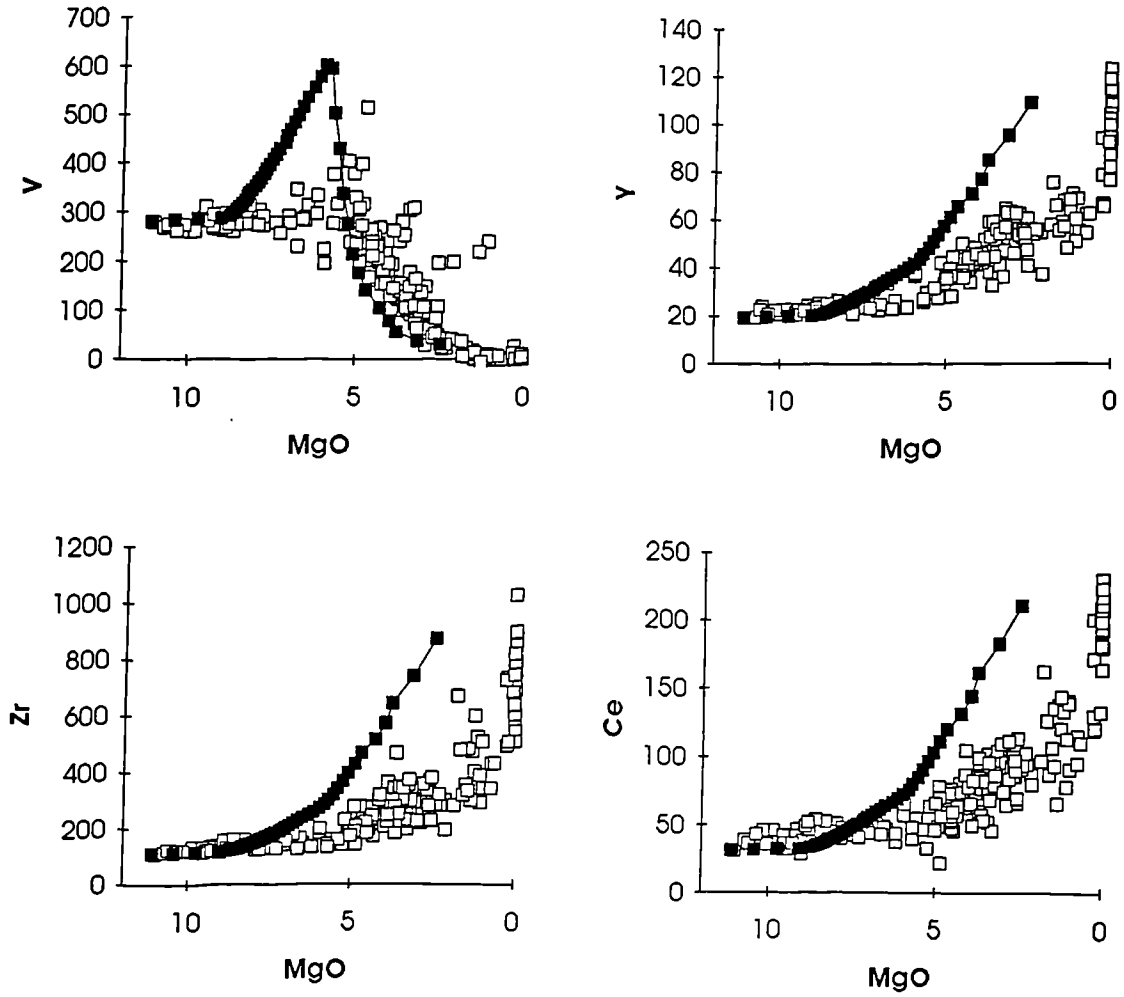

Figure 4.12 (Continued).

TRACE predicts that, at the input value of fO_2 and Cr abundance, initially only chrome-rich spinel with be in equilibrium with the chosen parental composition, joined almost immediately by forsteritic olivine ($Fo_{87.5}$, as already noted) as the magma cools. This will the be joined by plagioclase ($An_{70.2}$; plagioclase laths ranging $An_{72\text{-}77}$ were found in VH10) after 8% of the magma has crystallised, prior to spinel leaving the crystallising assemblage. Next clinopyroxene ($En_{49.5}Wo_{41.6}Fs_{8.9}$; VH106, 8.82% MgO - an ankaramitic sample, contained clinopyroxene $En_{46}Wo_{47}Fs_7$) begins to crystallise after 20% crystallisation and finally titanomagnetite after 62% crystallisation. Olivine is absent from the crystallising assemblage between 68 and 78% crystallisation (5.53-4.67% MgO), subsequently a more fayalite-rich composition is predicted to re-join the crystallising assemblage at lower MgO contents. While this sequence goes

quite a long way to explaining observed trends, there are several points where it fails noticeably and these are addressed in the following discussion.

Initially (11-8.78% MgO), with just olivine and Cr-spinel crystallising, TRACE predicts rapid decreases in Cr and Ni, along with less marked decreases in other elements compatible in olivine and spinel[7]. Predicted concentrations of other elements, incompatible in these phases, show a progressive increase until the onset of plagioclase crystallisation. At this stage, the only major discrepancy is in CaO content, which appears suppressed in the Snaefell suite.

As plagioclase, an MgO-free phase, begins to crystallise, subsequent crystallisation increments of the TRACE model have far less impact on the MgO content of the residual liquid, resulting in steeper trends on figure 4.12 for elements incompatible with the crystallising assemblage (Ti, V, Sc and Co). This is not borne out in the actual data where Ti, V and Co concentrations all appear suppressed and there is an excessive amount of scatter in Sc. All of these elements (V as V^{3+}, its lowest valence state) are compatible in clinopyroxene[7], implying that perhaps early crystallisation of this phase occurred. Nevertheless augite is relatively rare as a phenocryst phase. Thus it could be a case of the "missing clinopyroxene" phenomena seen in many oceanic basaltic suites (e.g. Basaltic Volcanism Study Project 1981). In the light of the discussion below this is, however, not the sole cause of the discrepancy between the predicted and actual trends in the data.

At 8.28% MgO clinopyroxene is predicted by TRACE to join the crystallising assemblage, resulting in falling CaO and Sc contents. The Snaefell data set shows these features quite well. Nevertheless TRACE predicts V, Ti and Co should still increase, while in the Snaefell data they are all still suppressed, with Co concentration actually falling. Over the range 8.28-5.97% MgO, until magnetite crystallisation begin, there are also further discrepancies in other elements. These include Ni which decreases less rapidly than predicted, and MnO and P_2O_5 which increase less rapidly than predicted. As titanomagnetite joins the crystallising assemblage at 5.97% MgO, maxima in V, Co, Ti and Fe_2O_3(T) - >17% - occur, and the concentrations of these elements begin to fall. The predicted trends re-join the Snaefell data at ~5.5% MgO.

TRACE simply predicts the LLD that would result from fractional crystallisation of the given parental magma composition *at 1atm.* As already noted, the Snaefell magmas equilibrated at slightly greater pressure, ~3.5kb and it is clear from figure 4.9 that

---

[7] Partition coefficients for basaltic liquids:

Olivine	Co= 6.6*, Mn=1.45*
Spinel	Co=7.4* Mn=1.4+
Clinopyroxene	Sc= 1.7-3.2*, Ti=0.8#, V=1.35*

*Rollinson 1993,+Ewart, pers. comm. to R. N. Thompson, 1988, #Henderson 1982.

augite was one of the major phases precipitating *throughout* their evolution. Nevertheless, this is insufficient to be the sole cause of all the observed discrepancies.

What is significant here is that members of the suite with >8.78% MgO and <5.5% MgO fall along the predicted LLD (this is probably most marked in the case of TiO_2), and are thus considered comagmatic. The intermediate compositions remain the problem for which the most plausible explanation stems from the observation that in many anorgenic lava suites around the world there is a compositional gap between basaltic and intermediate compositions (Thompson 1972). There are often abundant basalts and hawaiites in a comagmatic suite, while basaltic hawaiites are extremely scarce; whereas, if the hawaiites were derived by crystal fractionation from the basalts, basaltic hawaiites should theoretically be *more* abundant than hawaiites. An explanation for the existence of this gap in the Skye Main Lava Series (SMLS) in terms of the "non-eruptability" of basaltic hawaiites was proposed by Cattelll (1989). Fractional crystallisation of basalt to basaltic hawaiite involves the extraction of olivine, clinopyroxene and a large proportion of plagioclase. This Fe-poor assemblage is less dense than the liquid from which it separates and thereby generates an increasingly dense residual liquid. This process continues until magnetite (>4gcm^{-3}) starts to crystallise. Cattelll (op. cit.) has calculated that the crystallising assemblage in the SMLS, after magnetite saturates, was > 10% magnetite - well in excess of what is required to raise the density of the extract above that of the liquid. Thus the coincidence between the compositional gap and density maximum in the LLD suggests that liquid density controls "eruptibility". Sparks & Huppert (1984) point out that as differentiation proceeds it generates increasingly dense residual liquids. These would pond at the base of the chamber *beneath* a the less-dense parent magma. Subsequently, they might also be density-trapped beneath low density extreme differentiates. Thus, in a magma chamber system containing a range of compositions, this dense basaltic-hawaiite magma cannot be erupted without extensive mixing with the overlying magma, or extensive draining of the magma chamber - which is unlikely. The one lava suite cited by Thompson (1972) in which the compositional gap is lacking, comes from Kilauea volcano, Hawaii. Here there is clear evidence for extensive magma-mixing in the high-density portion of the LLD (Wright & Fiske 1971).

The members of the Snaefell suite with between 8.78 and 5.5% MgO are therefore probably hybrids. This is reinforced by the fact that none reaches the predicted Fe_2O_3(T) maximum of >17%, i.e. the density maximum. Petrographically, however, there is little support for these lavas being hybrid, except for the complex plagioclase phenocrysts/xenocrysts whose presence is ubiquitous throughout the suite. Experimental work (Biggar & Clarke 1976) on xenocryst reaction rates in basaltic melts suggests, however, that microphenocrysts at least are unlikely to survive for

more than a few days without either re-equilibrating or dissolving. Plagioclase is the most resistant mineral phase to this. This means that erupted lavas, unless magma mixing occurred a very short time prior to, or actually during eruption, are likely to give few direct clues to their hybrid nature.

As already mentioned, the onset of titanomagnetite crystallisation results in decreasing TiO_2, V and Co concentrations. Ti and V decreases predicted by TRACE, however, occur at higher MgO contents than observed in the actual data. Magnetite crystallisation is strongly affected by Fe^{3+}:Fe^{2+} ratio in the magma, which in turn is controlled by oxygen fugacity (fO_2) (Carmichael & Nicholls 1967). V compatibility in magnetite is also dependant on fO_2, and can vary by over two orders of magnitude, since V can exist in three common valence states under terrestrial conditions: V^{5+} which is essentially incompatible, V^{4+} substituting for Ti^{4+}, and V^{3+} for Fe^{3+} in minerals (Shervais 1982). The results of varying fO_2 in the TRACE program on the predicted LLD for V are shown in figure 4.13. The implication is that the fO_2 was actually *lower* than previously thought and perhaps closer to the Fe-Wü than the QFM buffer curve. This also fits the Cr data better, since VH10 actually contains >900ppm Cr, well above Cr-spinel saturation at fO_2s in the vicinity of the QFM buffer.

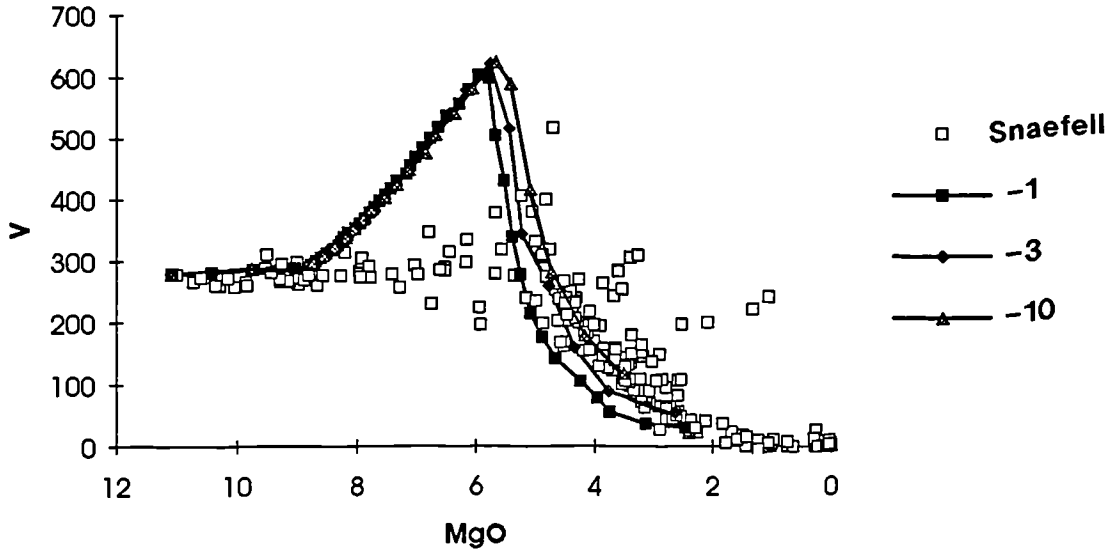

Figure 4.13 Plot of V vs MgO, showing the LLDs predicted by TRACE at varying oxygen fugacities, figures (-1,-3, -10) are the number of log units from the QFM buffer curve.

Below about 4% MgO the TRACE program becomes increasingly unrealistic (i.e. the last 6% of crystallisation modelled). This coincides with the inflection in the P variation diagram, i.e. the onset of apatite crystallisation.

This can explain discrepancies in Y and LREE[8] contents between the predicted LLD and the Snaefell data, where the concentration of these elements are suppressed. At this degree of fractionation it is likely that the feldspar crystallising would be ternary, rather than plagioclase, TRACE does not allow for this, which could account for the suppression of K in the Snaefell data.

Fractional crystallisation from hawaiite to mugearite.

The evolution of hawaiite to low-MgO mugearite can be further constrained qualitatively using a primitive-mantle-normalised spider diagram (figure 4.14). This diagram shows selected samples ranging from a high MgO basalt (VH10) through to a low, (~2%) MgO mugearite (VH170). Among the more-evolved samples, troughs reveal the nature and relative extent of the fractionating phases as crystal fractionation proceeds.

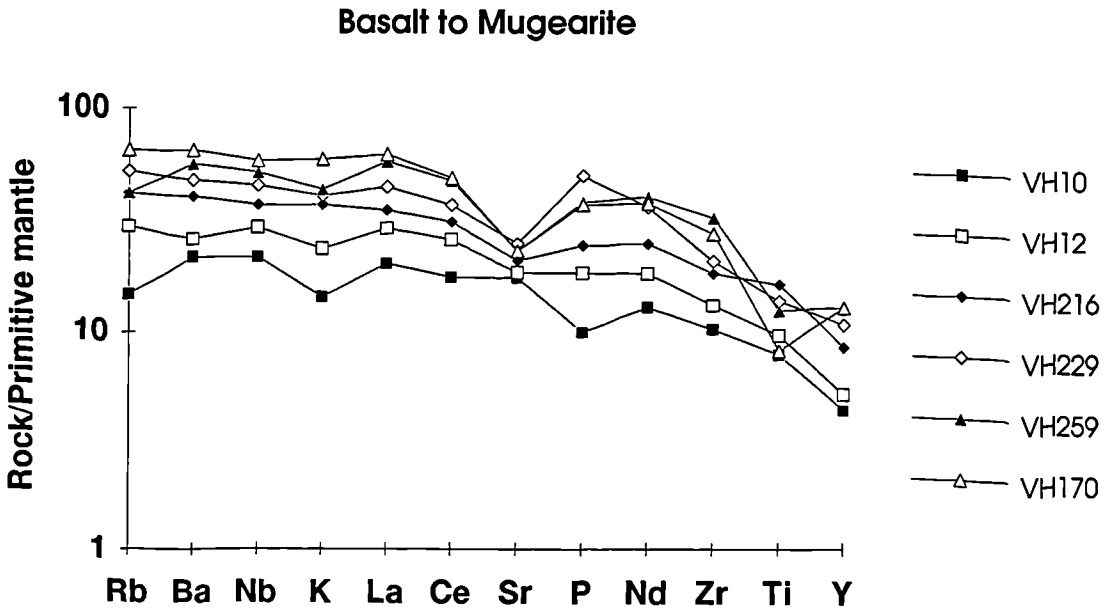

Figure 4.14 Primitive mantle normalised spider diagram showing a sequence of Snaefell lava compositions from high MgO basalt through to low MgO mugearite. VH10 = 11% MgO basalt, VH12 = 6% MgO basalt, VH216 = 5% MgO basaltic hawaiite, VH229 = 4% MgO hawaiite, VH259 = 3% MgO mugearite, VH170 = 2% MgO mugearite.

The scatter in the elements Rb and K is probably due to slight alteration and no petrogenetic significance has been attached to it. The trough at P in the pattern of basalt VH10, however, appears real, since P is not a particularly mobile element and

[8]Partition coefficients for rhyolitic liquids (Rollinson 1993). Where two were given, the lower one has been taken:

Apatite Y=40, La=14.5, Ce=21.1, Nd=32.8.

this sample has been repeatedly analysed (appendix 2). Only Ba and La appear incompatible throughout this compositional range, suggesting that alkali feldspar crystallisation does not commence until more-evolved compositions are reached. The first trough to appear in the patterns is at Sr in the low-MgO basalt. This becomes more and more pronounced with falling MgO, due to the increasing compatibility of Sr in sodic plagioclase; K_D^{Sr} in plagioclase varies from 1.83 in basaltic liquids to up to 15(!) in rhyolitic liquids (Rollinson 1993). The basaltic hawaiite pattern mirrors those of the low-MgO basalts, although element concentrations have increased. The hawaiite shows the highest P content and a lower Ti content than the previous sample, indicating the onset of titanomagnetite fractionation. The first mugearite (~3% MgO), displays a marked drop in P content, signifying the onset of apatite fractionation. The low-MgO mugearite shows a further drop in Ti, P, and Sr as expected along with little or no increase in the LREEs, and Y which partition in apatite[8]. Zr also shows a small decrease between the two mugearite samples, which could indicate zircon crystallisation; zircons, however, have not actually been observed in these lavas.

4.3.5 Higher differentiates

As already noted the Snaefell series shows a compositional (Daly) gap from low-MgO mugearite to low-silica rhyolite. With the possible exception of one low-silica benmoreite unit, all samples falling in this compositional range have, on closer examination, proved to be hybrid. This compositional gap is seen in many other Icelandic suites, e.g. Krafla (Jonasson 1994).

Central volcanoes producing rhyolite characteristically occur in Iceland's flank zones (Meyer et al. 1985), where they locally constitute up to 20% of the exposed volcanics (Johannesson 1975). New rift zones appear to begin life as flank zones, the present example began the eastern rift zone (ERZ, 2m.y.), which is gradually replacing the mature (7m.y.) western rift zone (WRZ). Notably, rhyolites are absent in the SW part of the WRZ (the Reykjanes peninsula), which cuts young crust. The relative abundance of rhyolites in the NRZ may also be related to its recent relocation. Thus their production appears to relate to the presence locally of older, thicker crust and a relatively low magma supply rate. The production of rhyolitic magmas in Iceland has been variously attributed to either fractional crystallisation from a basaltic parent (Carmichael 1964, Wood 1978, Sigurdsson & Sparks 1981, MacDonald et al. 1990, Furman et al. 1992), or partial melting of hydrated, metamorphosed basaltic crust (e.g. Oskarsson et al. 1982, Oskarsson et al. 1985, Sigmarsson et al. 1992b). Nevertheless it is recognised that these two processes need not be mutually exclusive; the products of

the 1875 Askja eruption were found to contain xenoliths; both derived from the crust, and with autogenic origins (MacDonald et al. 1987). Only the former possibility will be evaluated here, as the role of the crust in the generation of rhyolitic magmas is discussed in section 4.4.

Field evidence for the presence of rhyolites at different stratigraphic levels, indicates that, like the basaltic suite, they are not related to a single differentiation event. Instead they represent at least two cycles of differentiation, where the magma supply was low and residence time was sufficient to allow >90% crystallisation of the parental basaltic magma. Wood (1978) proposes ~93% crystallisation across a similar compositional range on the basis of least squares modelling. The compositional gap, and complexity of the basaltic suite makes it impossible to model fractional crystallisation *quantitatively* across this range for Snaefell. The genetic relationships can, however, be evaluated and fractional crystallisation constrained qualitatively.

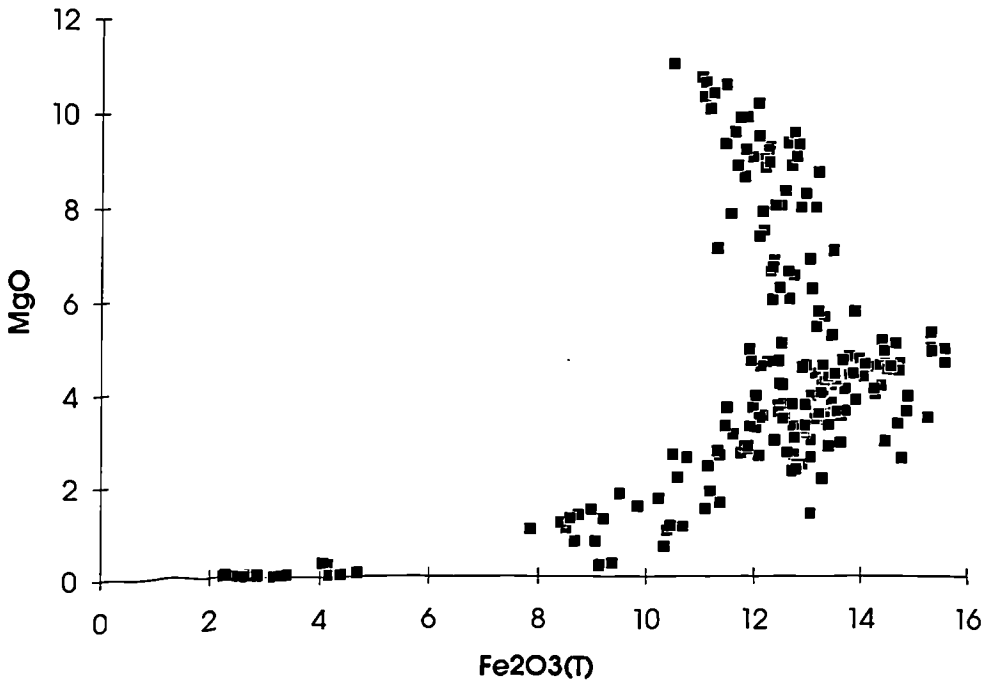

Figure 4.15 Plot of MgO vs $Fe_3O_3(T)$ clearly showing the compositional gap in the Snaefell series below 8% $Fe_2O_3(T)$.

Figure 4.15 shows a plot of $Fe_2O_3(T)$ vs MgO. This clearly shows the compositional gap from 4-6% $Fe_2O_3(T)$, but also shows that the rhyolites are not inconsistent with simple crystal fractionation origin, forming a coherent group with little internal variation. Inter-element relationships, such as those presented in figure 4.16, are characteristic of pairs of elements with similar, low, bulk distribution coefficients for the observed olivine + plagioclase + clinopyroxene + titanomagnetite assemblage, and are more consistent with a closed-system fractional crystallisation than

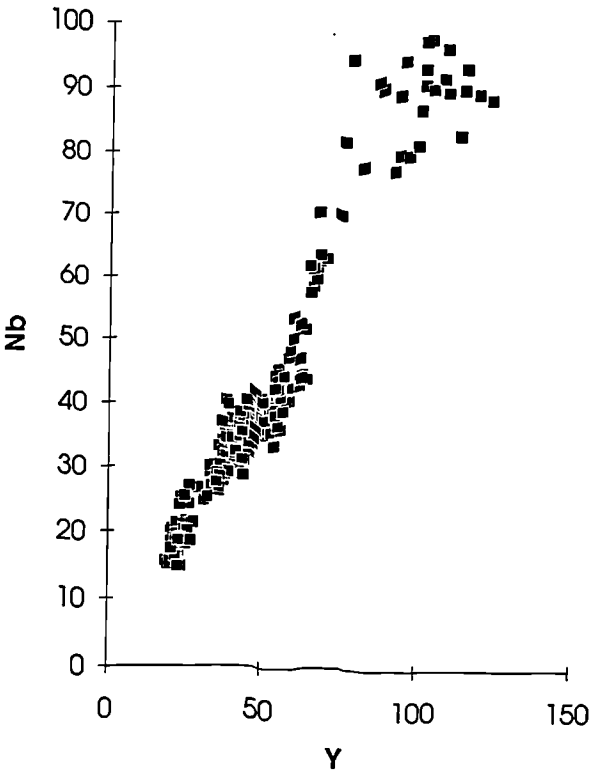

Figure 4.16 Plot of Nb against Y showing the coherence of the Snaefell basalt-rhyolite series, in terms of these elements.

separate origins for the basalts and rhyolites. The scatter in the rhyolites is most probably due to crystal (alkali feldspar) accumulation. A further important observation is the homogeneity of the isotopic ratios throughout the Snaefell suite:

$\delta^{18}O = +4.8\text{-}5.4‰$,
$^{143}Nd/^{144}Nd = 0.512983\text{-}0.513025$,
$^{206}Pb/^{204}Pb = 18.332\text{-}18.611$,
$^{207}Pb/^{204}Pb = 15.431\text{-}15.498$,
$^{208}Pb/^{204}Pb = 37.937\text{-}38.222$.

The entire range is encompassed by the basaltic compositions. Since there are small, but systematic regional isotopic variations in Iceland (Meyer et al. 1985), this is a strong argument for the basalts and rhyolites being co-magmatic. Only in the Sr isotopes do we see any difference between basalts and rhyolites (figure 4.17); the one high-silica rhyolite analysed has a significantly higher value.

Chondrite normalised REE patterns (figure 4.18) show an overall similarity between mafic, intermediate and silicic lavas. The increasing concentrations in the sequence basalt to rhyolite, and the appearance of a strong negative Eu anomaly in the rhyolites, is consistent with fractionation of a plagioclase-bearing assemblage. This has a low bulk partition coefficient for all REEs except Eu, which in the divalent state becomes

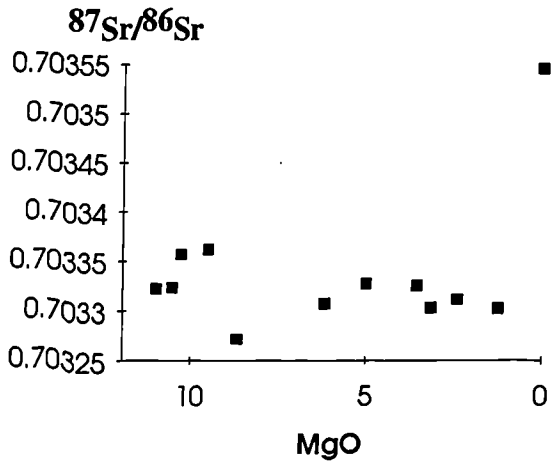

Figure 4.17 Plot of $^{87}Sr/^{86}Sr$ against MgO, showing the consistency of $^{87}Sr/^{86}Sr$ across the Snaefell series with the exception of one rhyolitic sample.

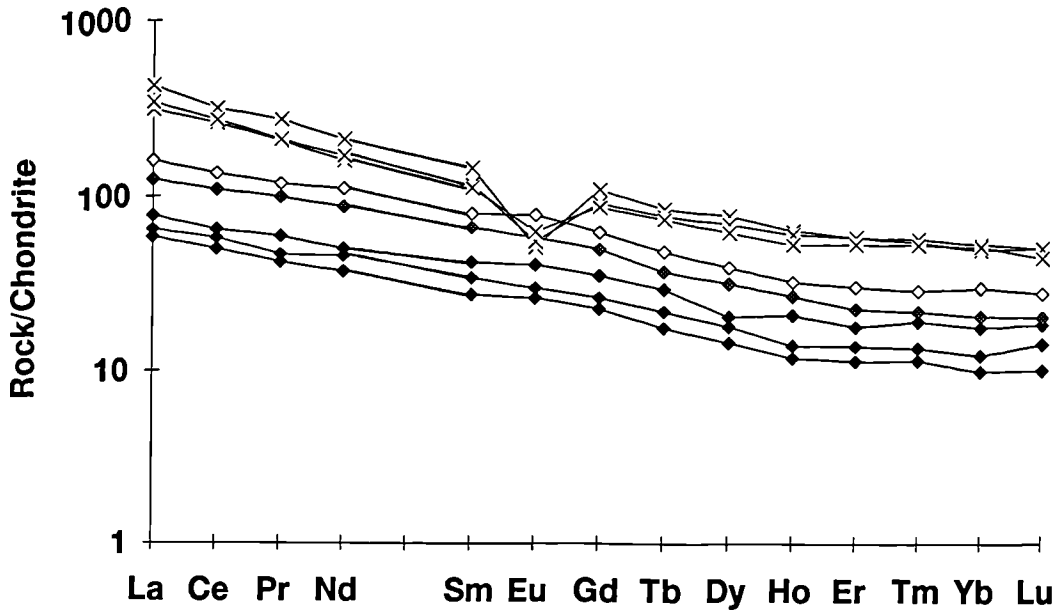

Figure 4.18 Chondrite normalised (Sun & McDonough 1989) rare-earth-element patterns of Snaefell lavas.
Key to symbols: solid diamonds = representative selection of basalts, lightly shaded diamonds = a hawaiite, open diamonds = a mugearite and crosses = rhyolites.

progressively more compatible in plagioclase as differentiation proceeds[9]. The slight change in the slope of the LREEs can be accounted for by fractionation of apatite, in which the middle REEs are most compatible. Looking at figure 4.19, a primitive-mantle-normalised spider diagram, the crystal fractionation sequence relating low-MgO mugearite, VH170, through to high (>73%) SiO_2 rhyolite, VH49, can be qualitatively assessed.

[9]Partition coefficient for Eu in plagioclase (Rollinson 1993):
In basaltic liquids = 0.34-1.12
In intermediate liquids = 0.31-1.21
In rhyolitic liquids = 2.11-5.42.

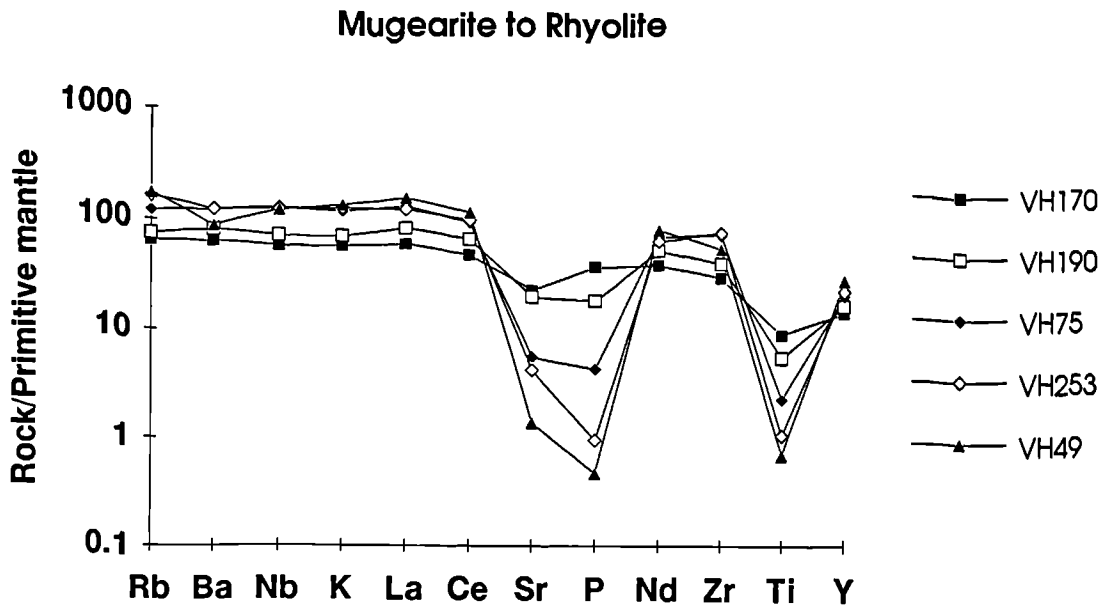

Figure 4.19 Primitive mantle normalised spider diagram showing a sequence of lava compositions from low-MgO mugearite to high-silica rhyolite.
VH170 = 2% MgO mugearite, VH190 = benmoreiite, VH75 = trachyte, VH253 = rhyolite, VH49 = high-silica rhyolite (>73% SiO_2).

From VH170 through to VH49 concentrations of Rb, La, Ce, Nd and Y all increase and, although the rate appears to slow down, all of these have very low bulk partition coefficients in the crystallising assemblage as a whole. The deepening troughs at Sr, P and Ti are consistent with the continuation of plagioclase, apatite and titanomagnetite fractionation, respectively. VH49, the most evolved rock found, also shows the development of a trough at Ba and a slight relative drop in K, due to the onset of alkali feldspar crystallisation. Nb also shows a decrease, which probably reflects its increasing compatibility in magnetite as differentiation proceeds[10]. Zr also appears to fall which, in a peraluminous magma (molar $[Na_2O + K_2O]/Al_2O_3 < 1$), would indicate the onset of zircon crystallisation. However, in a peralkaline magma such as this comendite, >500ppm Zr is required before zircon saturation will occur (Watson 1979). Thus zircon crystallisation is unlikely; on petrographic examination no zircon was found in any of the lavas.

The compositional gap between low-MgO mugearite and rhyolite, however, poses a problem to the fractional crystallisation scheme since abundant intermediates should be produced. One possible explanation lies in the fluid dynamics of the evolving magma

[10]Partition coefficients for Nb in magnetite (Rollinson 1993):
In intermediate liquids = 1.0
In rhyolitic liquids = 2.5.
Higher values are quoted elsewhere; e.g. Johnson 1989, in rhyolitic liquids = 10.

chamber. Sparks et al. (1984) considered the fluid dynamic effects of fractional crystallisation numerically.

They proposed that one of the main driving forces in fractional crystallisation was *convective fractionation;* buoyant convection of magma away from the site of crystallisation. This process should lead to both temperature and compositional gradients within a magma chamber. The implications of this are that silicic magma chambers should be vertically zoned, with low-density, volatile-rich silicic magmas overlying high-temperature mafic ones; separated by a double-diffusive interface, allowing the transfer of heat, but very little mass. Thus the rhyolitic liquids may evolve separately from the main magma body, explaining the lack of intermediates.

Therefore, in the light of the above discussion, the ultimate derivation of the Snaefell rhyolites by closed-system crystal fractionation from a basaltic parent is entirely plausible.

4.4 Crustal contributions

Even in the continental setting (Larsen et at. 1989), where the crust has a markedly different composition to the primary magmas, the degree to which the chemical and isotopic compositions of basalts are influenced by the crust as they pass through it or are stored in magma chambers has been a matter of much controversy. Detecting crustal input is therefore, potentially much more difficult in the case of Iceland, where the crust itself is basaltic and too young (at <16Ma) to have evolved a characteristic isotopic signature. The role played by the Icelandic crust in the formation of Icelandic magmas, and the lines of evidence for it, will first be reviewed in the light of current literature, before the Snaefell data are examined in detail.

4.4.1 Crustal contribution in the genesis of recent Icelandic volcanics

Detection of a crustal input to Icelandic magmatism

Numerous isotopic and geochemical studies of recent Icelandic volcanics have been undertaken over the past two decades, and opinions vary from those who believe the entire Icelandic regional geochemical anomaly to be the product of the Iceland hotspot reworking its own earlier products (e.g. Oskarsson et al. 1982, Oskarsson et al. 1985) to those who believe that most of the variation is due to mantle heterogeneity (e.g. Hemond et al. 1993). Studies of Pb and Nd (and to a lesser degree, Sr) isotopes generally emphasis mantle heterogeneity (Sun et al. 1975, Sigmarsson et al. 1992a,

Hemond et al 1993), while variations primarily in O and Th isotopes in young, *unaltered* lavas support crustal contamination (e.g. Nicholson et. 1991, Sigmarsson et al. 1991, Sigmarsson et al. 1992b).

Pb and Nd isotopic ratios in the crust are likely to be little different to those in the fresh lavas due to the low age of the Icelandic crust; although small increases in $^{87}Sr/^{86}Sr$ can occur within the Icelandic timescale in high Rb/Sr lavas. Additionally interaction with sea spray can also raise the Sr isotope ratio (Hemond et al. 1993). $\delta^{18}O$ as low as -10‰ have been found in *hydrothermally altered* basalts from depths of up to 3km, in the region of the Krafla central volcano (Hattori & Muehlenbachs 1982). These authors attributed the observed "oxygen shift" to interaction with the light meteoric waters present at high latitudes.

The use of ^{238}U-^{230}Th disequilibria as a tracer in magmatic processes is reviewed in Condomines et al. (1988), and a brief resume is presented here. ^{230}Th is the longest-lived of a chain of daughter nuclides in the radioactive decay series of ^{238}U:

$$^{238}U \Rightarrow {}^{234}Th \Rightarrow {}^{234}Pa \Rightarrow {}^{234}U \Rightarrow {}^{230}Th \Rightarrow\Rightarrow\Rightarrow {}^{206}Pb$$

In the mantle this decay chain should have attained secular equilibrium unless there has been any recent (<300ka) disturbances, such as a partial melting event. During partial melting, fractionation will occur between the various daughter nuclides, resulting in disequilibrium. Equilibrium will quickly re-establish between ^{238}U and the first two daughter nuclides, and in fresh rocks, $(^{234}U) = (^{238}U)$, therefore ^{230}Th may be regarded as the direct daughter of ^{238}U. In most mid-ocean ridge basalts (MORBs) and ocean island basalts (OIBs) $(^{230}Th) > (^{238}U)$ where () = activity. Th-U fractionation is commonly recorded using the "isochron plot" (figure 4.20) where values of ^{230}Th and ^{238}U are both normalised to ^{232}Th, which has a sufficiently long half-life to be regarded as a stable isotope over the timescale concerned. Secular equilibrium exists when $(^{230}Th) = (^{238}U)$ the "equiline", and will re-establish after ~300ka. Whereas $^{87}Sr/^{86}Sr$ may be considered a tracer on the time-integrated Rb/Sr of the source material, $^{230}Th/^{232}Th$ acts as a tracer on the U/Th ratio of the source at the time of magma genesis.

In recent axial tholeiites a negative correlation between $^{87}Sr/^{86}Sr$ and $\delta^{18}O$, and a positive correlation between $^{230}Th/^{232}Th$ and $\delta^{18}O$ has been shown (Hemond et al. 1988). In case studies of Askja (MacDonald et al. 1987) and Krafla (Nicholson et al. 1991) lower $\delta^{18}O$ and $^{230}Th/^{232}Th$ (Krafla), accompanied by selective enrichments in highly incompatible elements, Rb, Th and U, were observed in more evolved compositions, while Sr and Nd isotopic ratios were more or less constant for all compositions.

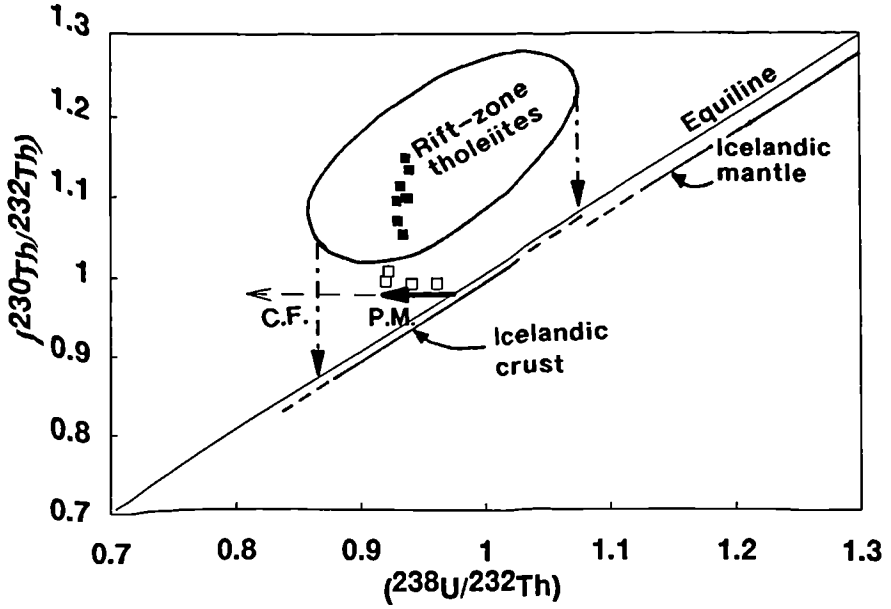

Figure 4.20 ($^{230}Th/^{232}Th$) isochron diagram. Samples plotting on the equiline would have (^{230}Th) = (^{238}U), i.e. be in secular equilibrium. Rift-zone tholeiite field, and mantle and crust fields on the equiline (inferred from data on rift-zone tholeiites) from Sigmarsson et al. (1991).Data plotted on are from Krafla (Nicholson et al. 1991).
Key to symbols: closed squares = tholeiitic basalts, open squares = intermediates and rhyolites. Vectors marked on: P.M. = partial melting, C.F. = crystal fractionation,
dotted and dashed lines = re-establishment of secular equilibrium.

On the (Th/U) isochron diagram (figure 4.20) all the Krafla data (Nicholson et al. 1991) can be seen to plot left of the equiline, indicating disequilibrium; the lowest $^{230}Th/^{232}Th$ were found in the silicic rocks, which is consistent with input from crustal partial melts *or* possibly the longer repose time necessary to generate rhyolitic magmas by fractional crystallisation (Furman et al. 1992), discussed below. Similar results were obtained from Hekla in the ERZ - an example of a flank zone volcanic centre - except that the $\delta^{18}O$ values were almost constant, at between 4.8‰ and 5.1‰ (Sigmarsson et al. 1992b). The lack of O-isotopic variation, however, could be due to the lack of extensive hydrothermal activity associated with flank-zone central volcanoes, in contrast to those in the ARZs. Hence the $\delta^{18}Os$ of the older lava pile - forming the crust - may be unaltered. These isotopic and elemental variations described and discussed in this paragraph have been interpreted in terms of either assimilation accompanied by crystal fractionation (AFC; DePaolo 1981)(MacDonald et al. 1987, Nicholson et al. 1991) or derivation of silicic magmas by partial melting of the crust alone (e.g. Sigmarsson et al. 1992b).

Fluid dynamic modelling of AFC

Recent laboratory modelling of assimilation at the top of a basaltic magma chamber (Campbell & Turner 1986) has cast doubt on the viability of AFC in many magma chambers. The heat required for assimilation comes from the latent heat of crystallisation, and the resulting partial melt goes to form a light roof-layer which may *initially* mix with some of the underlying basalt magma, but is likely subsequently to be separated from it by a double-diffusive interface; consequently separating assimilation from crystal fractionation in space and time. When partial melting occurs along the walls of the chamber, the efficiency of mixing depends on the steepness of the walls; the steeper they are, the more efficiently the mixing (i.e. AFC) can occur. The resulting stratified magma chambers also explain the bimodal nature of the Icelandic volcanics; many intermediate compositions containing clear petrographic evidence for magma mixing (Sigurdsson & Sparks 1981).

Derivation of Icelandic rhyolites by partial melting of the crust

Many authors have suggested that rhyolitic magmas in Iceland are produced by partial melting of hydrothermally altered, metamorphosed basaltic crust (e.g. Oskarsson et al. 1982, Sigmarsson et al. 1991, Sigmarsson et al. 1992b). This has been reinforced by a review of existing experimental work (Thy et al. 1990), which showed that partial melts of basalts and their metamorphic equivalents under water-undersaturated conditions resemble Icelandic dacites and rhyolites in terms of major element composition.

A detailed geochemical study of Hekla (Sigmarsson et al. 1992b) cites $^{230}Th/^{232}Th$ and Th/U ratios as possibly the most important tracers of magmatic processes. The differences between the basalts and basaltic andesites, and silicic rocks - dacites and rhyolites - were thought by Sigmarsson et al. (op. cit.) to preclude fractional crystallisation as the main differentiation process. Instead, partial melting of the crust, in response to the injection of basaltic magma is proposed, forming a dacitic melt. The basaltic magma evolves by fractional crystallisation, to form basaltic andesite magma and this can mix with the dacitic melt to form andesitic compositions. At higher levels in the magma chamber, the dacitic magma sometimes undergoes further differentiation, if the repose period is sufficient, to form rhyolitic magmas. An alternative interpretation of the $^{230}Th/^{232}Th$ and Th/U data was, however, proposed by Furman et al. (1992); who suggested that the low $^{230}Th/^{232}Th$ in the silicic samples simply reflects the time necessary to create evolved lavas by crystal fractionation (~10,000yrs), and that the higher Th/U ratios result from zircon fractionation.

The Krafla rhyolites have recently been re-examined by Jonasson (1994), who, focusing on their *occurrence* and *elemental* compositions, proposes them to be pure

crustal melts. He stated that compositionally they are minimum melts on the quartz-plagioclase cotectic plane in the granitic system (Qz-Or-Ab-An), and they appear to have "evolved by near-solidus as opposed to near-liquidus fractionation". The two main emplacement phases were related to the formation of the caldera and a ring dyke. The deformation accompanying these events was invoked to provide the extraction mechanism for the rhyolitic melts from the heated region around the basaltic magma body in the crustal chamber.

Melting of pre-existing plagiogranites and rhyolitic segregation veins (Sigurdsson 1977, Marsh et al. 1991) in older crust, soon after a rift-jump, has also been suggested. The evidence for this is the existence of plagiogranite (trodhjemite) xenoliths in many lava suites (e.g. Askja, where partially assimilated examples of such xenoliths were found; Sigurdsson & Sparks 1981, MacDonald et al. 1987). These plagiogranites are thought by Sigurdsson (op. cit.) to be derived from oceanic layer 3 in the Icelandic crust, where they formed by fractional crystallisation of basaltic magmas in the lower crust. Thus, as already noted, rhyolitic volcanism is confined to central volcanoes underlain by older crust that contains differentiated gabbro sequences and/or segregation veins. The sheer volume of rhyolitic extrusives poses a problem to the latter explanation, but the low density of these may result in their being over-represented in the exposed upper crust.

4.4.2 The case against *significant* crustal input in the Snaefell volcanics

Has AFC a role?

As has already been noted, Nd, Pb and O isotope ratios are fairly constant right across the Snaefell series; the entire range being seen in the basaltic compositions. These variations correlate with changes in REE patterns and can be accounted for in terms of source heterogeneity and different degrees of partial melting (discussed in section 5.3.3). The constant nature of $\delta^{18}O$ does not, however, rule out AFC, since fractional crystallisation alone has been seen to *increase* $\delta^{18}O$ (Muehlenbachs & Byerly 1982), and this process could therefore conceivably counterbalance the effect of assimilating low $\delta^{18}O$ crust. The implication of the high $^{87}Sr/^{86}Sr$ found in the rhyolitic sample, VH49, is that there could have been some crustal input to the rhyolites alone from an old, high Rb/Sr crustal rock; possibly an earlier rhyolite with normal $\delta^{18}O$ - i.e. which had not been subject to hydrothermal alteration. This possibility is discussed in more detail below.

Most trace element variations throughout the series, appear accountable by crystal fractionation and magma mixing (section 4.5). Previous authors (above) have focused

on highly incompatible elements: Rb, Th and U; suggesting them to be selectively enriched by crustal assimilation, and that this also results in fractionation of their ratios. Across the Snaefell series Rb rises steadily, undergoing a 13-fold increase from basalt to rhyolite (the one rhyolite found with a greater increase than this, VH284, also had a high LOI indicating alteration, and should therefore be ignored since Rb is extremely mobile), implying that if this was the result of fractional crystallisation alone, crystallisation must have reached >92%, which is not unrealistic. Th and U show 9- and 7.5-fold increases respectively, resulting in an increase from ~3 to >4 in Th/U. This is not entirely regular, and an exceptionally high ratio of >5 is seen in one rhyolite (figure 4.21).

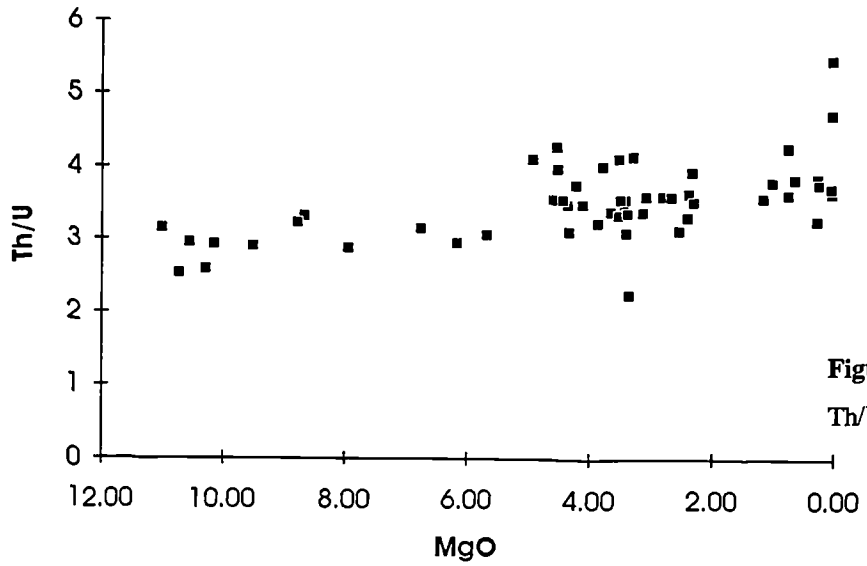

Figure 4.21 Plot of Th/U vs MgO.

A similar range is observed in the Hekla volcanic suite (Sigmarsson et al. 1992b), which, in conjunction with Th isotope data, was interpreted by these authors to show that the silicic magmas were crustally derived. In this study, Th isotope data are not available and, due to the peralkaline nature of the rhyolites, zircon fractionation (as suggested by Furman et al. (1992) as an alternative reason for U/Th fractionation) is unlikely. However, looking at available partition coefficient data[11] apatite crystallisation could also bring about this increase over a similar compositional range.

The discussion so far has indicated that there is little evidence for the occurrence of AFC throughout the series, however, it is does not rule out the possibility that the rhyolites are partial crustal melts, which is addressed below.

[11]Partition coefficients for apatite in silicic liquids (Ewart, pers. comm. to R. N. Thompson, 1988): Th = 1.1-1.3, U = 2.9-6.3.

The rhyolites - the result of crustal anatexis?

As first highlighted by Sigurdsson (1977), Icelandic rhyolites are unlikely to be the result of partial melting of hydrothermally altered basalts since they are often almost dry, containing only anhydrous phenocryst phases. The Snaefell rhyolites are no exception and show a marked absence of any hydrous phenocrysts. Some samples are, however, notably vesicular, suggesting significant volatile contents. In the light of the recent review of experimental work (Thy et al. 1990), indicating that melts resembling Icelandic rhyolites and dacites can be generated by dehydration melting of metabasalts (P_{H_2O}<1kbar), the possibility of Snaefell rhyolites being generated in this way should be evaluated.

Figure 4.22 shows the compositions of the rhyolites, compared with results of melting experiments conducted by Beard & Lofgren (1991) in water undersaturated conditions over a pressure range 1atm to 3kb (included in Thy et. al.'s (1990) study). There is an overlap in Al_2O_3 between natural and experimental data sets, although the bulk of the natural data lie beneath the experimental ones and show a monotonic decrease, in contrast to the rise and subsequent fall in Al_2O_3, with rising SiO_2, seen in the experimental set. CaO is markedly lower in the natural than the synthetic rhyolites. Thy et al. (1990) suggest that CaO is insensitive to water pressure during melting. Therefore, the observed differences must result from a difference in genetic process; possibly clinopyroxene crystallisation occurred during fractional crystallisation forming the Snaefell rhyolites. FeO* is indistinguishable in the two data sets while MgO, TiO_2 and P_2O_5 are all significantly lower and Na_2O and K_2O significantly higher in the natural rhyolites. The relative depletion of P_2O_5 in the natural rhyolites would necessitate the presence of apatite in the restite, if they were produced by partial melting. This is, of course, impossible if the source was basaltic. K_2O and Na_2O are both higher in the Snaefell rhyolites; which is not surprisingly since all the experimental melts were peraluminous and the Snaefell rhyolites are peralkaline. Thy et al. (op. cit.) suggest that K_2O content especially, is primarily a function of the source material, thus one possible source for the rhyolites would be a fairly strongly alkaline basalt. Since dissected older crust beneath Snaefell is uniformly tholeiitic, this is difficult to envisage.

A further way to describe the composition of the Snaefell rhyolites is by using the system $NaAlSi_3O_8$-$KAlSi_3O_8$-SiO_2-H_2O (figure 4.23). In this projection the Snaefell rhyolites can be seen to form a tight group, falling within the feldspar field and just on the albite side of the axis of the thermal valley. The synthetic melts of Beard & Lofgren (1991), in contrast mostly fall on the opposite side of the quartz-feldspar divide and encompass a large range.

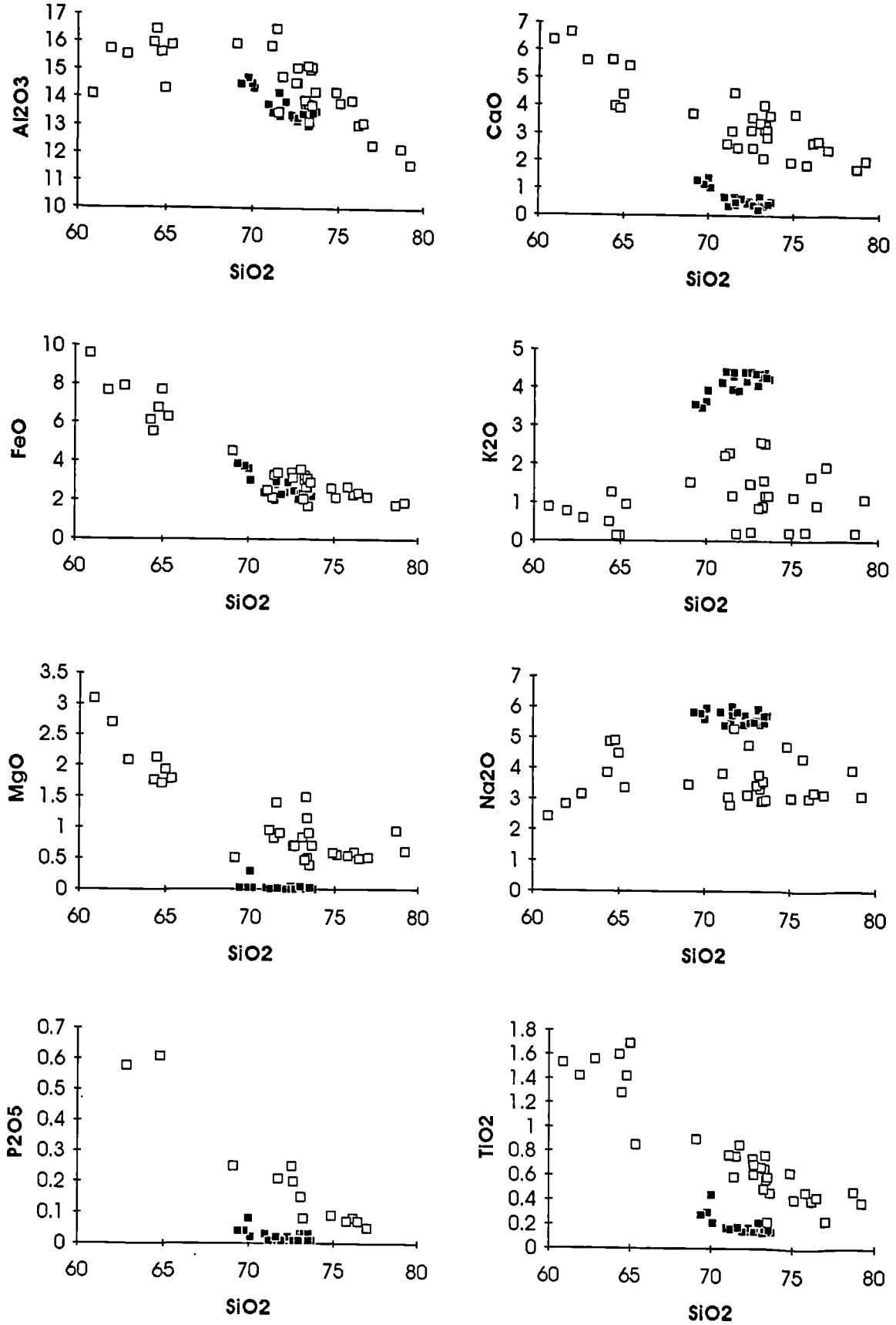

Figure 4.22 Comparison of major element oxides in Snaefell rhyolites (closed symbols) with water under saturated experimental melts of metabasalts at pressures ranging from 1atm to 3kb (open symbols; Beard and Lofgren 1991).

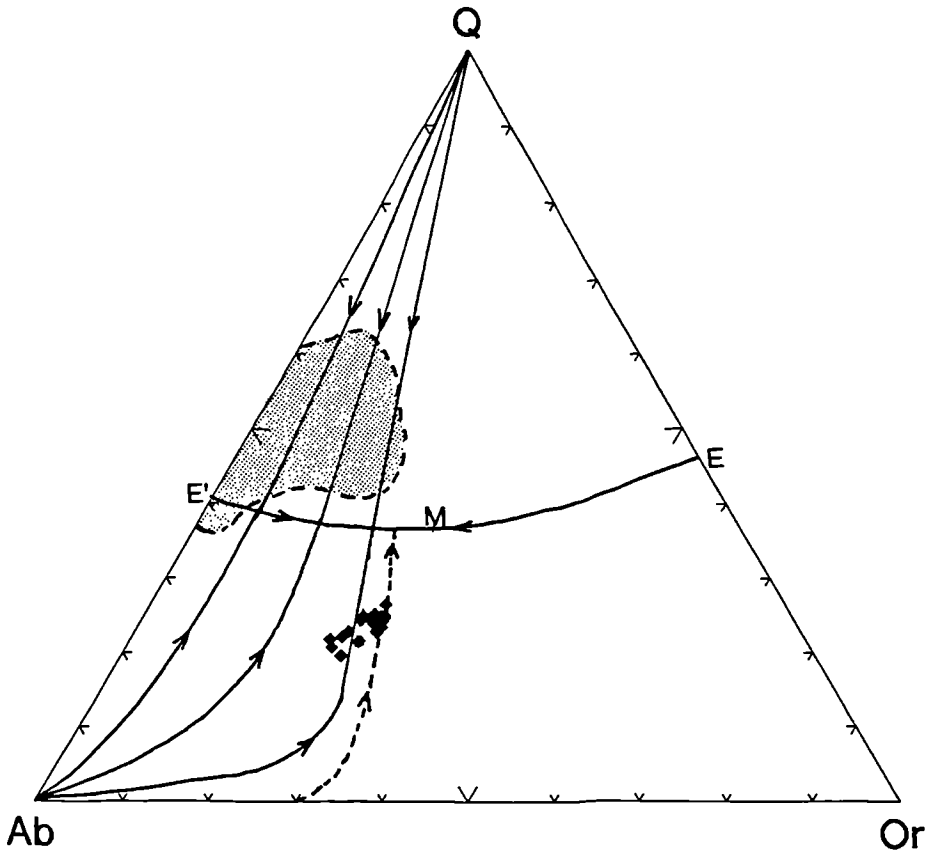

Figure 4.23 Normative *ab*, *or* and *q* of the Snaefell rhyolites (closed diamonds) and experimental melts (stippled area; Beard & Lofgren 1991) plotted on a projection of the system $NaAlSi_3O_8$-$KAlSi_3O_8$-SiO_2-H_2O onto the anhydrous base of the tetrahedron. The quartz-feldspar boundary (E-E'), thermal valley (dotted line) and minimum (M) at P_{H_2O} = 1kb are from Tuttle & Bowen (1958).

Petrologically, the minimum on an isobaric diagram is probably the most important feature of the system, since this is the composition towards which liquids will evolve as the crystallise. The exact position of this minimum is dependant on both P_{H_2O} and absolute pressure. Nevertheless, it is apparent that trend delineated by the Snaefell rhyolites is consistent with control by crystal-liquid equlibria. This is apparent in any diagram involving K_2O; the concentration of this oxide ceases to rise in the most-evolved peralkaline rhyolites, which precipitate alkali feldspar of a constant composition (Or_{30} - the thermal valley). The synthetic melts, however, show little relationship to the cotectics or fractionation curves. In partial melting experiments (Thompson 1981), the resultant melts have been found to fall on or near these cotectics only if the parent rock composition was close to the system's minimum. This, would thus appear to argue strongly *against* the Snaefell rhyolites being derived by partial melting of a basaltic parent.

As an alternative, Sigurdsson (1977) proposes melting of plagiogranites in layer 3 of the Icelandic crust, and such xenoliths were certainly found in three spatially separate eruption units within the Snaefell volcanic system, although peripheral to the central volcano. None of these units, however, was rhyolitic. A final possibility is the melting of pre-existing rhyolite segregation veins (Marsh et al. 1991) although there is no further evidence to suggest this. Finally, it is the author's opinion that the association of alkaline basalts with peralkaline rhyolites and tholeiitic basalts with peraluminous ones argues against the rhyolites being the product of partial melting of the crust.

The high $^{87}Sr/^{86}Sr$ determined in one Snaefell rhyolite still remains to be explained. One possibility is the introduction of a component derived from pre-existing rhyolites (i.e. selective crustal contamination in the rhyolites). There are abundant silicic rocks associated with the Tertiary central volcano at Geldingafell to the SE of Snaefell (Johannesson & Saemundsson 1989), which could have evolved high $^{87}Sr/^{86}Sr$ ratios during a few million years. This central volcano would presumably, while active, have had an extensive hydrothermal field associated with it, like present-day axial volcanic centres. Such activity would have resulted in extensive hydrothermal alteration of the rocks and, hence a significant oxygen isotope shift.

It can therefore only be concluded that the Snaefell rhyolites are the product of crystal fractionation, with little or no contribution from the crust.

4.5 Magma mixing and open magma chambers

Magma mixing is increasingly viewed as a fundamental process in the compositional diversification (differentiation) in volcanic rock suites (e.g. Anderson 1976, Sparks & Marshal 1986). Magma *co-mingling* - where incomplete mixing between two magma types has occurred - has been recognised in all environments. Where magma mixing has produced a homogeneous product it is referred to as a *hybrid*, although on close examination it still may be found to contain a disequilibrium phenocryst assemblage (Sparks & Marshal 1986). Magma mixing and comingling at Snaefell has been described in field studies (section 2.4), petrographic studies (section 3.1.6) and cited as the reason for data points falling away from the main or predicted trends in compositional data (section 4.3.4). In the following sections, the occurrence of magma mixing, the physical constraints on it, and the resultant compositional affects will be reviewed; and the evidence in the Snaefell suite described and discussed.

4.5.1 Magma mixing

Linear compositional variations in suites of volcanic rocks are best explained by the mixing of two *genetically related* magmas (McBirney 1980). Modelling by the same author indicates that, at shallow levels, the magma columns should become vertically zoned during the repose period between eruptions. This results from crystal fractionation and collection of buoyant evolved liquid under the roof of the magma chamber; since the compositional change and density decrease have a greater effect on the boundary layer than thermal contraction. The stable upper zone becomes smoothly graded, with the most silicic material at the top, while the lower convecting zone remains better mixed. A dense basal layer may also form since, as differentiation of a basaltic magma proceeds, it can generate increasingly dense residual liquids in the basaltic hawaiite compositional range (Sparks & Huppert 1984). As already mentioned (section 4.3.4), the eruption of this magma would result in extensive mixing with the overlying magma. Thus, at any given stage of magmatic evolution there should be two or more magma types available to mix in the magma chamber; and the magma body should become increasingly zoned with time.

Eruptions from stratified magma chambers can result in extensive magma mixing, the key consideration being the pattern of magma removal. Blake (1981) has analysed this mathematically and comes to the following conclusions:

1). Magma from widely separate horizons may be erupted simultaneously.
2). From analysis of the flow field, about half the sample erupted will come from the deepest part of the chamber tapped during that eruption.
3). Magma hybridisation is dependant on the flow behaviour in the conduit (as well as other factors, see below).

The ability of two magmas to mix is controlled by their physical properties after thermal equilibration, which in turn are controlled by the compositions of the two magmas, their temperature contrast, water contents and the overall cooling rate (Sparks & Marshal 1986). Their compositions and relative proportions are critical, to mix both must be liquid and basaltic magma in contact with a cooler silicic magma will tend to "freeze". Therefore complete hybridisation of silicic and basaltic magmas is unlikely, although commingling may occur if there is a high proportion of basaltic magma. Nevertheless, recent work by Grasset & Alberede (1994) has indicated that mafic enclaves in silicic magmas are likely to be substantially hybridised by the host magma, due to buoyancy-forced convection within the enclaves, implying the basic

melt must remain liquid for a significant amount of time. Thus contamination of silicic melts by mafic ones is possible.

Turning to the Snaefell suite; as previously described, magma co-mingling on all scales has been observed and many of the variation diagrams (figure 4.11) show linear variations which could well correspond to mixing chords. Certainly the linear variation on the TAS diagram (figure 4.5) from mugearite to rhyolite can be demonstrated to be a mixing chord - samples of benmoreitic and trachytic composition nearly all show the tell-tale disequilibrium phenocryst assemblages (section 3.1.6). Major and trace element concentrations in the basaltic hawaiites require them to be hybrid; the result of mixing between a relatively primitive and evolved liquids. Both of these are likely to lie above the dense basaltic hawaiite magma in the chamber (section 4.3.4).

4.5.2 Open magma chambers

O'Hara (1977) drew attention to the fact that most volcanic systems are *open systems* that undergo repeated tappings and fillings, and this concept is now accepted as geological common sense. In some cases, if the period between replenishments is extended, magma mixing between the new influx of primitive magma and pre-existing magma body may be inhibited by density differences. In this case, the new magma will form a layer at the chamber base until it fractionated sufficiently to mix, resulting in compositional mixing chords between two evolved compositions as described above. Injection of primitive magma into bodies of silicic magma is also thought to cause violent plinian eruptions as a result of interaction between the two different magma types (Sparks et al. 1977); indeed many rhyolitic ignimbrites and tephra deposits have been found to contain 1-40% basic material.

O'Hara & Mathews (1981) quantitatively analysed the processes that occur in periodically refilled, repeatedly tapped continuously fractionating (RTF) magma chambers. They showed how trace elements may become "decoupled" from major elements, and that both incompatible and compatible trace elements were enriched - by factors of up to 100(!) - in the magma relative to their concentration during fractional crystallisation alone. The ratios of incompatible elements can also be altered significantly. Such effects would previously have been attributed to varying degrees of *partial melting* within a *heterogeneous* source; but can now in many cases be attributed to open system effects on a *single primary magma* type, derived from a homogeneous source material. Maximum changes in trace element concentrations and ratios are attained when the ratio X (the mass fraction crystallising in each cycle)/Y (mass fraction escaping) is large.

Trace element variations, such as enrichment in compatible trace elements (e.g. Ni) and less compatible ones (e.g. Ti or V) in the Snaefell suite cannot be reconciled with simple crystal fractionation alone. This, and the degree of scatter can best be accounted for by open system processes acting on a single parental magma type. This has been modelled (figure 4.24) using the periodic mixing option in the computer program TRACE (Nielsen 1988). This allows the crystallisation increment (X) between magma chamber replenishment events and the replenishment factor (R; as a factor of the system remaining) to be set. X was varied between 0.2 and 0.7, and R between 0.5 and 0.9. The eruption factor (Y) was set at zero. These values are extreme, but similar effects could be produced by smaller X values and Y>0 during a greater number of cycles. Setting Y at zero means the magma chamber must expand. This along with considerable fractionation between replenishments is most representative of the beginning of the magmatic episode when magma chambers are developing (Larsen et al. 1989), or in an extensional environment such as might have been present in the Snaefell region at the onset of magmatism. Y is in any case likely to be small, since Blake (1981) calculated that eruption of a mass fraction of just 0.001 of the magma body was required to compensate for the overpressure resulting from over inflation.

As when simple closed-system fractional crystallisation was modelled (above) the parental magma composition used was basalt VH10. Looking further at figure 4.24, it is evident that mixing must have occurred between primitive basalts and highly evolved material, which is beyond the scope of TRACE to model, but compositions lie in the array of sub-parallel to mixing chords produced by TRACE when X=0.7 and R=0.9. The whole suite, with the exception of the rhyolites, contain complexly zoned plagioclases, often showing oscillatory zoning, which would tend to support the operation of open system processes (Hibbard 1981).

X = 0.2, R = 0.5

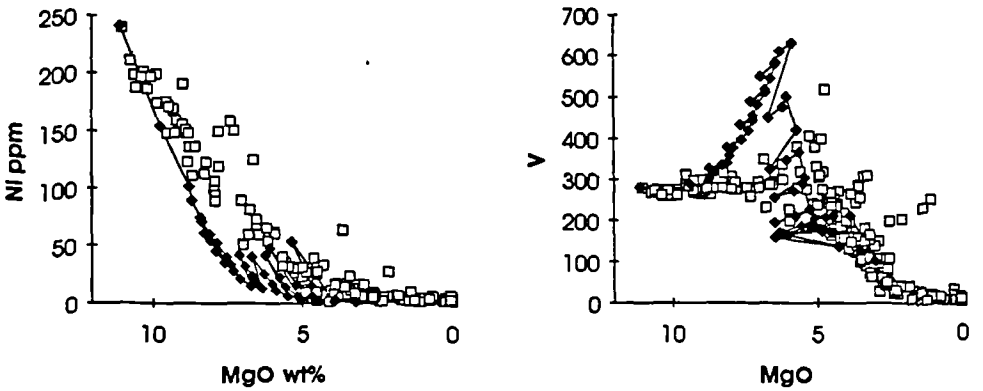

X = 0.5, R = 0.5.

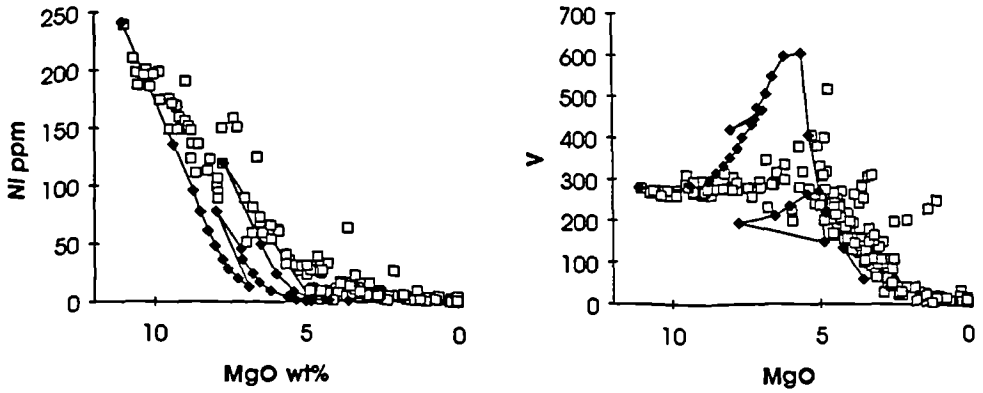

X = 0.7, R = 0.9.

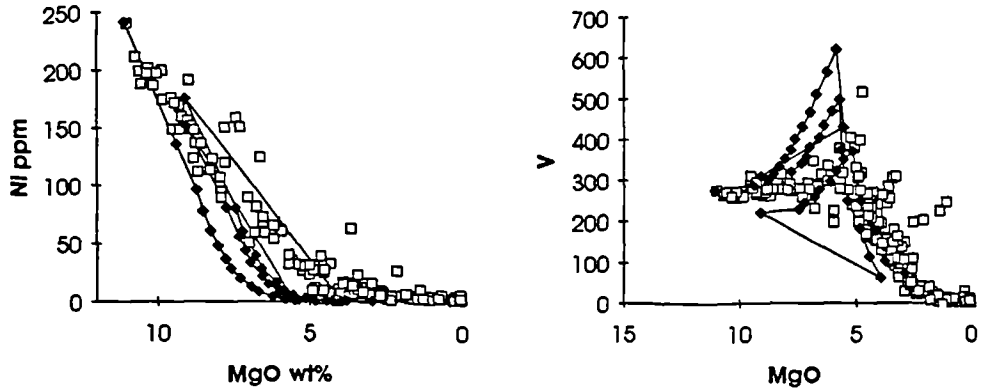

Figure 4.24 Results of modelling a periodically replenished, continuously fractionating magma chamber using the computer program TRACE (Nielsen 1988), explaining the excessive *enrichment* in Ni (compatible), and relative *depletion* in V(much less compatible in terms of bulk D) compared to that resulting from simple crystal fractionation. The degree of fractionation between replenishments (X) was put at 0.2-0.7, the replenishment factor (R) at 0.5-0.9, data output was set at 5% crystallisation (closed symbols). These values are extreme, but less extreme fractionation demands a higher number of cycles to obtain the same results. The most extreme situation modelled, X = 0.7, R = 0.9 might however be realistic in a dying magma chamber, when the volumes involved are relatively small.

4.6 Summary

1). Both the Snaefell suite and the topmost lavas from the underlying pile show few signs of alteration. Thus even mobile element concentrations may be considered primary and can be used to ascertain petrogenetic processes with relative confidence.

2). Compositionally the Snaefell suite is mildly alkalic, ranging from nepheline-normative basalt to peralkaline, comenditic rhyolites (IUGS systematics). As is typical of Icelandic volcanic suites, the suite is bimodal with few intermediate (benmoreiitic to trachytic) compositions in evidence. The underlying Plio-Pleistocene lava pile is tholeiitic, ranging from tholeiitic basalt to peraluminous rhyolite.

3). The basaltic members of the suite appear to have fractionated at a pressure of ~3.5kb, which corresponds to the magma chamber lying at ~15km (approximately the thickness of the Icelandic crust off-axis). Thus it appears, that as is often thought to happen in the continental setting, the magma accumulated at the base of the crust as a result of the density contrast there, although this is likely to be much less marked in the case of Iceland.

4). The dominant compositional variations across the suite appear to have resulted from crystal fractionation of the observed mineral assemblages, as follows:

BASALT ⇒ OL + PL + SP (± CPX)† ⇒ **Low MgO BASALT** ⇒ PL + OL + CPX ⇒ **BASALTIC HAWAIITE** ⇒ PL + MGT + OL + CPX ⇒ **HAWAIITE** ⇒ PL + MGT + CPX + AP ⇒ **MUGEARITE** ⇒ PL + CPX + MGT + AP ⇒ **BENMOREIITE** ⇒ Na-rich PL + AF + CPX + OL + AP + (MGT) ⇒ **TRACHYTE ⇒ RHYOLITE.**

OL= olivine, PL= plagioclase, SP= Cr-spinel, CPX= clinopyroxene, MGT= magnetite, AP = apatite, AF = alkali feldspar.

† CPX is not observed in many basalts, although from compositional trends, it was present in the crystallising assemblage of all but the most magnesian basalts. This lack of CPX phenocrysts is a common phenomenon in basaltic suites (Basaltic Volcanism Study Project 1981).

The final section of the fractionation sequence is poorly constrained due to the lack of benmoreiites and especially trachytes in the eruptive products of the volcano.

5). Most of the samples of basaltic hawaiite composition fall off the trends predicted for simple crystal fractionation, and this is most evident in the variation diagram for TiO_2, which shows a very disjointed trend. Basaltic hawaiite corresponds to a density maxima in the LLD, thus these liquids pond at the base of the magma chamber. This reduces substantially their "eruptibilty"; their eruption would result in extensive mixing with the overlying liquids, which may be primitive or more evolved.

6). There appears to have been little or no crustal input to the suite, isotope ratios are consistent throughout, and almost the entire range is encountered in the basalts. Trace element variation also is consistent with crystal fractionation. In many other Icelandic suites the rhyolites are thought to be the result of anatexis. In the Snaefell suite they appear cogenetic with the basalts, showing marked evidence for control by liquid-crystal equilibria in the system *ab-or-q*.

7). Magma mixing accounts for the linear compositional trends in the series, and reinforces the view that the magma chamber was strongly compostionally zoned. Much of the scatter in the data, and excessive enrichments in compatible trace elements can be reconciled if the system was open, undergoing repeated tappings and fillings while continuously fractionating. Thus, the whole series could easily have been derived from a single parent magma type, the result of partial melting of a homogeneous source material. This also means that the data cannot be inverted to uniquely define the magma chamber parameters without sweeping assumptions, possibly invalidating any results obtained.

Chapter 5
Petrogenesis II: Magma Genesis

5.1 Melting the mantle

5.1.1 Background

The processes involved in generating basaltic magma from the mantle have been the subject of serious discussion for some 30 years. Most attention has been given to mid-ocean ridge basalts, since these are the most abundant type of volcanic rocks on Earth and their genesis avoids the extra complexities introduced by subduction zones and/or continental settings. In this section I shall resist *even attempting* to present a full appraisal of the history of the evaluation of the subject, and simply present a very brief overview of what are now generally accepted principles, together with recent developments that are relevant to this work.

Our knowledge of upper mantle structure, physical properties, composition and melting behaviour is limited by lack of direct access. What knowledge we do have comes primarily from the study of the ultramafic xenoliths found in kimberlite and alkali basalt suites, and outcrops within orogenic ultramafic massifs, ophiolites and abyssal peridotites. Extensive high pressure experimental studies have provided evidence for the relationship between spinel and garnet lherzolite mineralogies (Wilson 1989, Grutter 1994). In addition, such studies have provided constraints on the conditions necessary for the onset of partial melting, and leave no doubt as to the wide range of silicate liquids that can be generated by varying both temperature and pressure (figure 5.1), and mantle source composition (e.g. Jaques & Green 1980, Falloon et al. 1988, Baker & Stolper 1994, Baker et al. 1995 to name but a few). There is now a substantial published database, although it must be remembered that all experimental studies are confined to *isobaric batch melting*, and fraught with experimental difficulties such as quenching problems which are only now being resolved (Baker & Stolper 1994). Many earlier interpretations applied simplified isobaric phase diagrams and standard phase equilibria techniques to the analysis of basaltic magma genesis. Clearly this approach can only be entirely successful if *mantle convection did not occur*. Nevertheless, they are still a useful tool (see Hess 1992), but need to be

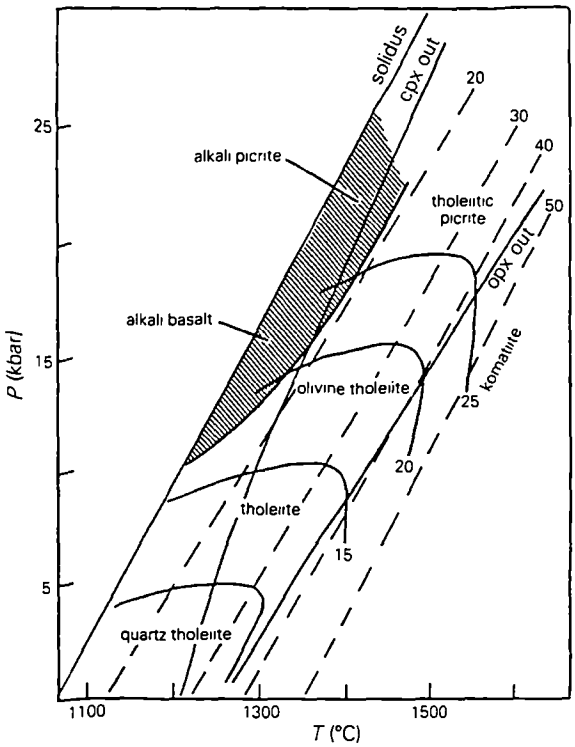

Figure 5.1 Experimentally determined partial melting characteristics of an enriched lherzolite source. Dashed lines are partial melting contours for 20, 30, 40 and 50% partial melting. The shaded area represents the conditions necessary for the generation of alkalic basaltic magmas (after Jaques & Green 1980).

carefully adapted to melting in a convecting mantle, as emphasised by Langmuir et al. (1992). They point out that:

1). There are no mantle eutectics, even on a pseudo-ternary phase diagram. Therefore mantle melting produces a *range* of compositions. It is now recognised that mantle melting is primarily controlled by *solid solution* and not *eutectic* behaviour (Kostopoulos 1991).

2). Mantle melting is a *polybaric* process; melts form and probably also segregate over a range of pressures.

5.1.2 Mantle melting in response to adiabatic ascent

Overview

It is now generally accepted that basaltic magmatism at oceanic spreading centres results from adiabatic decompression of ascending mantle (Ahern & Turcotte 1979). A thesis on Icelandic magmatism has no need to enter the controversies surrounding basaltic magma genesis in other environments - e.g. continents. Ascending mantle will follow an adiabatic gradient of 1-2°C/kb, whereas the mantle solidus has a markedly different temperature gradient of 13°C/kb. Three major processes affect the chemistry of the resultant basalts:

1). The temperature and pressure of melting, together with modes of melt segregation and migration - i.e. physical processes.
2). Mantle source composition in terms of major and trace elements - i.e. the chemistry factor.
3). Crystallisation and differentiation processes at shallow levels (considered in chapter 4).

Obviously, the higher the mantle temperature, the deeper the solidus is intersected, the greater the extent of partial melting that results and hence the greater the thickness of oceanic crust (McKenzie 1984). Many quantitative studies of the physical processes associated with melting in ascending mantle have been undertaken (e.g. Ahern & Turcotte 1979, McKenzie 1984, 1985, Ribe 1985, Richardson & McKenzie 1994). The results of these have subsequently been taken in conjunction with the results of experimental studies in attempts to "parameterise" the melting process, relating physical processes and compositional parameters (e.g. Klein & Langmuir 1987, McKenzie & Bickle 1988, Langmuir et al. 1992, Kostopoulos & James 1992).

All studies of the physical processes involved in mantle melting emphasise: (a) the efficiency of melt extraction, even at very small degrees of melting; (b) that, due to the density contrast, these buoyant melts will then rise faster than the residual solid. The mean melt composition, and its relationship to mantle temperature and crustal thickness can be envisioned simply by considering the "residual mantle column" (Langmuir et al. 1992), that emerges outside the melting regime for each increment of spreading at a passive plate margin (figure 5.2).

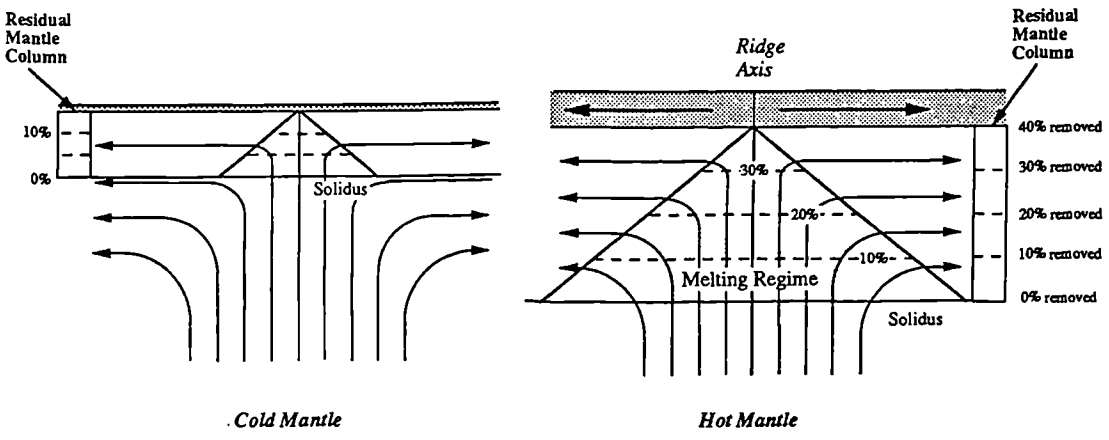

Figure 5.2 Idealised steady state melting regimes produced by diverging plates. Solid arrows are mantle flow paths through the melting regime. Dashed lines are contours of the extent of melting in the regime or extent of melt removed in the residual melting column. The two melting regimes are for two mantle temperatures, the hotter the mantle, the deeper it intersects its solidus, leading to greater extents of melting, a taller melting column and a thicker crust. (From Langmuir et al. 1992)

This column reflects what has happened during basaltic magma genesis within the melting regime. In the 2D analysis of Langmuir et al. (1992), the deeper portions of the residual column are produced at the outer corners of the melting regime, while the shallowest are produced at its axis. This residual column shows an increasing depletion in melt upwards, reflecting the increasing extent of melting. Crustal thickness simply reflects the total amount of melt extracted, as discussed in detail by White et al. (1992). Parameterisations (McKenzie & Bickle 1988, Kostopoulos & James 1992) indicate that the formation of the ~7km of basaltic crust on "normal" mid-ocean ridges requires a mantle potential temperature (Tp[1]) of 1280°C, i.e. a solidus temperature (Ts) of around 1320°C. In contrast thick intraplate lava sequences, such as those of Hawaii (depth to Moho beneath Kilauea and Mauna Loa ~17-19km) require Tp ~1480°C, i.e. Ts of the order of 1500-1550°C, supporting the presence of "hot jets" (mantle plumes), thought to originate at the core-mantle boundary (Loper 1991). Beneath Iceland, Tp is thought to be elevated by some 200°C above normal (White & McKenzie 1989, White et al. 1992), resulting in voluminous tholeiitic (and picritic) magmatism along the axial rift zone and the production of a crust ~20km thick. Off-axis, where the lithosphere is thicker (such as beneath Snaefell), magmatism is dominantly alkalic and much less voluminous since the solidus overstep is significantly reduced.

It also follows that, as emphasised by O'Hara (1985), the mean composition of magma erupted at the surface is a rather complex weighted average of all the diverse melts extracted of at various depths. McKenzie & Bickle (1988) define a *point average* composition as the average composition of melt generated as an instantaneous melt at constant pressure, while the *point and depth average* composition was defined as the weighted average generated over the entire melting interval. Another important aspect of the mantle melting column concept is that simultaneous tappings of melt from different depths within a single column may result in interdigitation of lavas showing the effects of low degrees of mantle fusion at high pressures with lavas attesting to the reverse scenario (Kostopoulos & James 1992), if these contrasting liquids can reach the surface *without* mixing.

Major elements

Klein & Langmuir (1987) were the first to attempt to systematise available high pressure experimental data and to generalise how *major elements* varied in the liquid with changing pressure during isobaric batch melting of spinel lherzolite (table 5.1). Their critical observation from regionally averaged MORBs is that the *total extent of*

[1]Tp = potential temperature, the temperature of the mantle corrected for decompression to 1 atmosphere (equation 5: McKenzie & Bickle 1988).

melting (inferred from Na_2O corrected for low pressure crystal fractionation to $Na_{8.0}$[2]) and the *pressure of melting* (inferred from FeO*, similarly corrected - $Fe_{8.0}$) correlate positively, resulting in the so-called *global trend* (Klein & Langmuir 1987, 1989).

Oxide	General systematics of melt compositions	Point average	Point & depth average
SiO_2†	for constant MgO, increases with F increase, decreases with increasing P	increases with F	decreases with Po
Al_2O_3	decreases with F, decreases with P (or possibly P independent).	decreases with F	decreases with Po
MgO	increases with F at constant P, increases with P	approximately constant	increases with Po
FeO^t	constant with F at constant P, increases with P (or decreases with F while CPX* residual, then increases)	decreases with F	increases with Po
CaO	increases with F while CPX residual*	increases with F while CPX residual*	increases with Po, while CPX residual*
Na_2O & TiO_2†	decrease with F, behave as moderately incompatible elements (do not appear to be P dependant)	decrease with F	decrease with Po
K_2O	decreases with F, behaves as a highly incompatible element	decreases with F	decreases with Po

Table 5.1 Systematics of melting spinel lherzolite from F = 0-0.30, from Klein & Langmuir (1987), with additional inferences from McKenzie & Bickle (1988) in brackets.
F = melt fraction, P = pressure, Po = mean pressure of melting.
* Although clinopyroxene-out curves from peridotite isobaric equilibrium melting experiments suggest that it will be consumed at F = 22%, during adiabatic upwelling it should not disappear *completely* until F = 42% (Kostopoulos 1991).
† Recent experimental work (Baker et al. 1995) at low degrees of fusion of *anhydrous* peridotite at 10kb appears to contradict previous experimental results, suggesting that the initial melts will be richer in SiO_2 and poorer in TiO_2 than melts resulting from higher degrees of fusion

The reverse is observed if separate MORB samples are taken over an individual ridge segment, and was termed the *local trend* (Klein & Langmuir 1989). These observations require a model in which higher extents of melting occur at higher mean pressures, to accomplish this requires efficient extraction of deep melts *without* their re-equilibrating at shallow levels.

[2]MORBs from different areas, when plotted together, were observed to form sub-parallel trends; such that, at a given value of MgO, they showed markedly different Na_2O. 8% MgO was selected as a reference value, and samples with MgO between 5 and 8.5 wt% were corrected for the effects of crystal fractionation, back to the reference value (Klein & Langmuir 1987).

Certain hotspots (e.g. Galapagos) have a marked influence on the chemical composition of local MORBs; as the crust thickens and the ridge axis shallows, so $Na_{8.0}$ increases and $Fe_{8.0}$ drops - the reverse of the global trend. Not all hotspots, however, exhibit this anomalous relationship. Along the Reykjanes Ridge $Na_{8.0}$ decreases while $Fe_{8.0}$ increases towards Iceland, in line with the global trend (although $Na_{8.0}$ is rather higher than would be expected on a normal ocean ridge). Nevertheless, $Ti_{8.0}$, which normally correlates positively with $Na_{8.0}$, increases towards Iceland (Langmuir et al. 1992). This suggests that *the mantle source of Icelandic magmatism may differ from MORB source in its major element composition.*

The debate over the composition of primary magmas has raged for the last three decades, with many suggesting in the light of experimental data that they should be picritic (e.g. Jaques & Green 1980). An important result of parameterisation (McKenzie & Bickle 1988) is that wholesale (as opposed to incipient) melting beneath a normal mid-ocean ridge, beginning at ~40km is calculated to generate magmas with overall compositions similar to those of MgO-rich MORBs, containing ~10% MgO. (But, see Baker & Stolper (1994), the debate goes on...). Picrites, as would be expected, are found in Iceland, where the solidus is intersected much deeper.

Trace element systematics

Trace elements, especially rare-earth elements (REEs), have often been used to investigate melting processes since their ratios, at least, are unchanged up to moderate degrees of crystal fractionation. LREEs may be considered incompatible in the principal mantle minerals and thus the mantle source is depleted, relative to the melts derived from it. Therefore the relative LREE depletion of normal MORBs requires a LREE depleted source (termed depleted MORB mantle or DMM; Kostopoulos & James 1992). The presence of hotspots results in long wavelength enrichments in the LREE element content of the basalts (e.g. Schilling et al. 1983), consistent with their source being relatively undepleted.

The magma composition is controlled not only by the source composition, but also the *source mineralogy*. The mantle is now accepted to be composed of garnet lherzolite below ~80km, the spinel-to-garnet transition zone spans ~60-80km, and spinel lherzolite gives way to plagioclase lherzolite in the region 30-20km (Ellam 1992). HREE are compatible in garnet, and thus preferentially retained during melting, if this phase remains in the residual mantle. Thus, in the case of the hot solidus intersection (Ts = 1550°C, ~120km, Ps >25kb), REE patterns show pronounced relative depletion in the HREE, regardless of how enriched or depleted the source material may be. In the case of the cooler solidus (Ts = 1350°C, <20kb), thought to produce most normal MORBS, there is now a convergence of views based on both

trace and major elements, that melting occurs at <70km (Klein & Langmuir 1987, McKenzie & Bickle 1988). Thus, melting may occur almost exclusively in the spinel lherzolite stability field, so that the REE patterns should be controlled solely by the source composition, as indicated by the modelling of Kostopoulos & James (1992). The preservation of the REE patterns in the resultant basalts emphasises both the efficiency of melt extraction and the lack of re-equilibration occurring at shallow depths. It also emphasises the importance of low degree melts. REEs reside almost exclusively in the aluminous phase, which, since melting is non-modal, is first to disappear after ~8% of partial melting; that is equivalent to a pressure decrease of 4kb, or ~12km ascent (Kostopoulos 1991).

5.1.3 Partial melting processes

There are essentially two end-member processes of melting and melt extraction (Wilson 1989):

1). *Equilibrium* or *batch melting*, where the melt formed continuously reacts and equilibrates with the crystalline residue until segregation; until then the bulk composition remains constant.
2). *Fractional* or *Raleigh melting*, where melt is instantaneously removed from the system as each increment is generated. In this case, the bulk composition of the system is continuously changing.

Whichever occurs could potentially have a profound effect on the composition and volume of the melt generated. Fractional melting requires a significantly greater temperature increase for a given melt fraction, and perfect fractional melting should theoretically terminate as clinopyroxene leaves the residue (Langmuir et al. 1992). It will thus result in a thinner crust (lower volume of melt) for a given pressure of intersection of the solidus. Fractional melting results in the extraction of most of the incompatible elements into the first few melt increments. The pooled results of fractional melting, will, nevertheless strongly resemble those of an equivalent amount of batch melting, with the exception of the concentrations of elements for which partition coefficients are pressure dependent (e.g. transition elements; Langmuir et al. op. cit.).

Neither model is realistic; the critical parameter being the ability of magma to separate from the matrix (i.e. the permeability threshold of the lherzolite). It was realised relatively early on (Ahern & Turcotte 1979) that large melt fractions cannot

remain in the asthenosphere. Small degrees of partial melt will result in the formation of an interconnecting network and *excess* magma will migrate rapidly upwards, in response to the buoyancy of the magma, relative to the residual solid. Thus the actual partial melting process is probably intermediate between the two extremes outlined above, and is now generally referred to as *dynamic melting* (Langmuir et al. 1977). The geochemical effects are also intermediate, since flow of melt through the system allows a substantial amount to interact with the residual solid. Thus, contrary to popular belief, the enrichment of more incompatible elements over less incompatible elements are not always greater in dynamic melting than for an equivalent amount of batch melting. This has implications for modelling, as detailed below.

5.1.4 Segregation and ascent of magma

Melt segregation and extraction processes are poorly constrained. Nevertheless, it appears that melt fractions <1% can separate from the solid matrix and be extracted from the upwelling column of mantle (McKenzie 1985, Richardson & McKenzie 1994). The question remains, as to the extent that the ascending magma interacts with the surrounding mantle peridotite. There are two end-member melt migration processes:

1). *Homogeneous porous flow* or *percolation,* where there is extensive interaction and re-equilibration of the mantle with through-going melts.
2). *Channellised flow,* where there is little or no interaction between melt and mantle, so that "deep characteristics" may be preserved.

Study of harzburgite xenoliths from western Samoa (Hauri & Hart 1994) revealed the existence of substantial intergranular trace element heterogeneity, and clinopyroxene distribution that suggested a diffuse channel network in many samples. This implies that melt migration within the Samoan plume occurred substantially by channellised flow. This reinforces the theories of Sleep (1988), who suggested that veins and dykes - such as observed in ophiolites - were important in melt segregation and focusing. Thus in dynamic melting, if lateral migration of melts takes place relative to the matrix, the volume of mantle supplying small melt fractions in equilibrium with residual garnet may exceed that supplying the more extensive melt fractions at shallower levels. This accounts for the apparent "decoupling" between trace and major element systematics, apparent in some suites, such as some Hawaiian lavas (Eggins 1992). As a result of modelling, Eggins (op. cit.) concluded that primary dynamic melts

are particularly sensitive to the mechanism of melt segregation, and channellised flow can result in incompatible element abundances up to 40% greater than an equivalent amount of batch melting, whereas percolation result in very similar trace element abundances. Trace element *ratios* are, however, very similar - regardless of melting and segregation mechanisms.

5.2 Generation of the Snaefell magmas

5.2.1 Constraints on the degree of melting and length of the melting column beneath Snaefell

Thermal structure of the mantle beneath Iceland

The formation of the anomalously thick Icelandic crust - for which estimates from seismic studies range between ~8km along the axial rift and ~15km off-axis (Palmason 1981, Flovenz & Gunnarsson 1991), to 20-24km in a recent study of SW Iceland (Bjarnsson et al. 1993) - requires the presence of hot mantle, i.e. a "hot jet" or "plume". The geophysical evidence for this phenomenon was discussed in chapter 1. This was modelled by McKenzie & Bickle (1988) to be ~200°C hotter than MORB source (i.e. Tp = ~1500°C), and to intersect the solidus at around 120km. Beneath the axial rift zone, the mantle continues to upwell to within a few km of the surface, resulting in a long melting column that allows it to undergo large degrees of melting. The maximum mean is 20%, which should theoretically result in a crustal thickness of 22.5 km (McKenzie & Bickle op. cit.). The modelled thermal structure of plumes (Courtney & White 1986) shows strong lateral temperature gradients. Thus mantle rising away from the immediate vicinity (i.e. within 100km or even less) of the core of the plume is likely to be significantly cooler, and hence to intersect its solidus at shallower depths. That the thicker crust is formed along the entire length of the rift zone, at even greater distances from the plume centre than some of the low productivity flank volcanic zones, can be explained by channelling along the rift zones of upwelling plume material. This was first suggested by Vogt (1974) to account for the V-shaped basement structure on the Reykjanes Ridge, to the south of Iceland. The peripheral (flank) volcanic zones additionally lie on older (up to 15Ma), thicker crust, and possibly some associated lithospheric mantle. Thus the level to which the mantle can adiabatically decompress is limited, further reducing the degree of melting (figure 5.3).

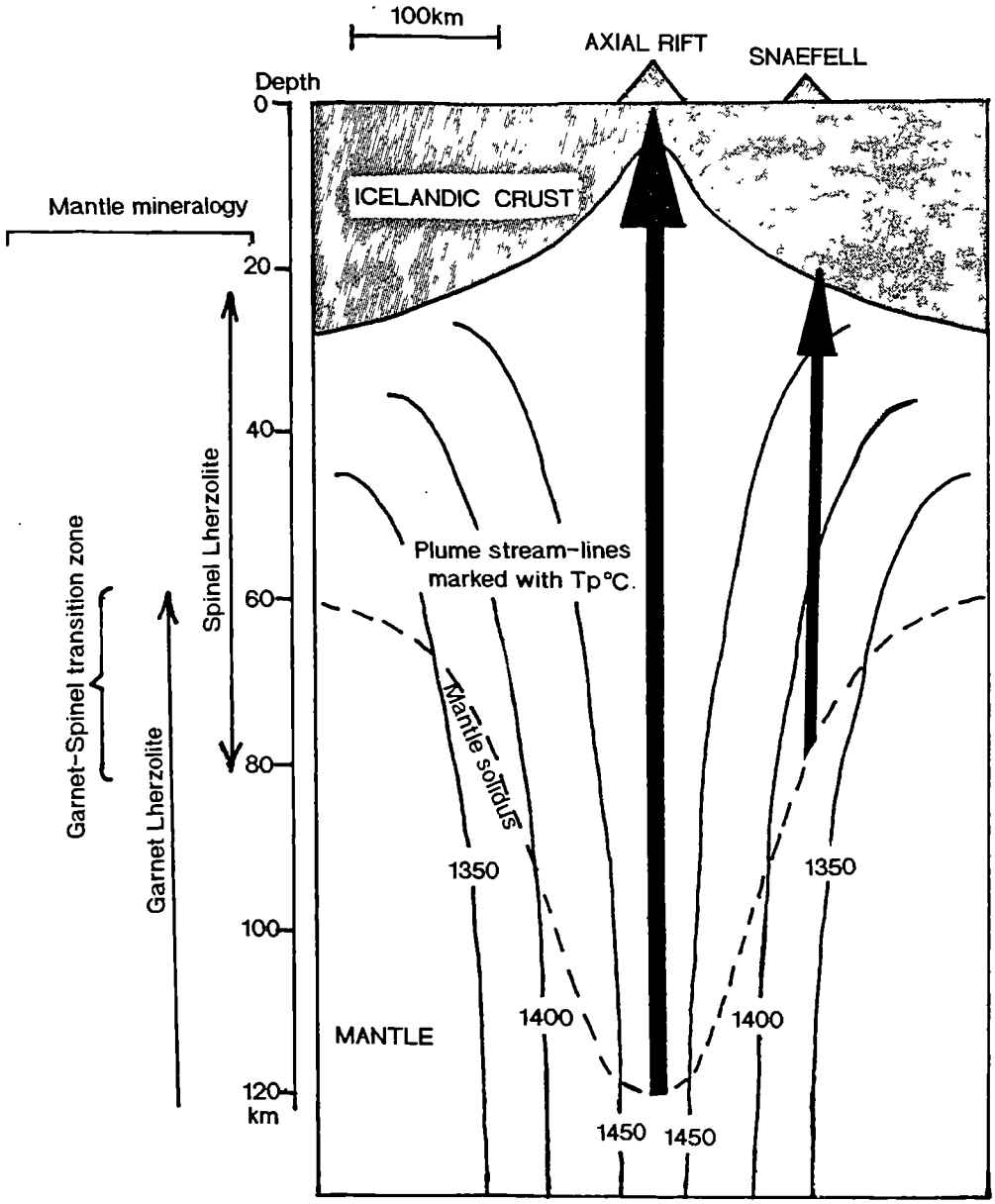

Figure 5.3 Sketch of the thermal structure of the mantle beneath Iceland, modified from the diagram constructed by Elliott (1991) from the results of modelling data from the Cape Verde hotspot (Courtney & White 1986). Since this hotspot has a similar buoyancy flux to the Iceland hotspot, it is probably for this specific purpose a reasonable analogue. The thermal structure of the upwelling plume determines the depth of the mantle solidus, whilst the thickness of the overlying crust (and lithosphere) also affects the melting column lengths, as indicated by arrows. The thickness of the arrows reflects the overall degree of melting.

The thickness of the lithospheric plate beneath Snaefell can be estimated from the following equation (Fowler 1990):

$$1100 = Tp.erf(L/2\sqrt{kt})$$

where Tp is the potential temperature of the asthenosphere, L is the lithospheric (plate) thickness, k is the thermal diffusivity and t is the age of the plate. The temperature at the base of the lithosphere is assumed to be 1100°C. Assuming Tp beneath the whole of Iceland to be between 1300°C (normal asthenosphere) and 1500°C, and the age of the plate beneath Snaefell - the underlying lava pile is Plio-Pleistocene in age - to be a maximum of 3Ma; the formula gives a lithospheric thickness of between 19 and 15km. This is approximately in agreement with seismic studies (e.g. Flovenz & Gunnarsson 1991, Bjarnsson et al. 1993).

Implied degree of melting and estimates of potential temperature

McKenzie & Bickle's (1988) parameterisation of published experimental peridotite melting data was presented as a series of equations. These allow an estimate to be made of the Tp range and extent of melting that produced a given suite of magmas. Such an approach has been used, with some success, on the West Greenland picrites by Gill (1992). As already emphasised, the temperature-dependence of the degree of fusion is complicated; natural peridotites melt over a range of temperatures (the melting interval) and this range is, in turn, pressure dependant. McKenzie & Bickle (1988) simplify things by normalising the temperature of melting to the melting interval at a given pressure to define a dimensionless temperature parameter, *T'*. T' varies from -0.5 at the liquidus to 0.5 at the solidus, and can be related directly to the melt fraction (*F*). These authors went on to derive empirical equations relating melt composition to T', predicting major element oxide concentrations in the melt. For many oxides the resultant curves are pressure independent. Nevertheless, SiO_2 (especially), MgO and FeO* were found to depend on the melting pressure.

As in chapter 4 the chosen parental magma composition for the Snaefell suite was sample VH10, which contains 11% MgO and shows little evidence of crystal fractionation. The value of 11% MgO gives values of T' of -0.42 to -0.48 over the pressure range 1-2Gpa (10-20kbars). Additionally, SiO_2 is perhaps more strongly pressure dependant, and the relatively low silica content of VH10, 47.43wt%, implies that the pressure was in excess of 1Gpa. Taking a pressure range of 1.5-2Gpa, and T' = -0.45 to -0.48 for 11wt% MgO, these calculations indicate that 4-9% fusion is required to produce a primary alkalic basalt of this composition. This corresponds to Tp between 1340 and 1380°C, depending on whether the entropy of melting (ΔS) is taken

as 250 $JK^{-1}kg^{-1}$ (McKenzie & Bickle op. cit.), or 400 $JK^{-1}kg^{-1}$ (Watson & McKenzie 1991)[3]. Prior to any discussion of the potential significance of these results, it must be emphasised that these estimates may only be considered semi-quantitative. The parameterisation concerned, and therefore the resultant Tp and F estimates, assume isobaric (*point average*) melt compositions. Whereas in reality mantle fusion is a polybaric process and the composition erupted at the surface represents a weighted average of melts pooled from that portion of the mantle ascent path in which melting occurs (the *point and depth average*). Thus the onset of melting will occur at a greater pressure than estimated here.

The Tp estimate, although perhaps lower than might have been expected for plume derived magmas, is in reasonable agreement with figure 5.3. Additionally, the F estimated tallies with the earlier calculations of Meyer et al. (1985), which accounted for the Icelandic alkali basalts (such as these from Snaefell, the subject of this study) as 1-6% batch melts. The evidence for polybaric melting beneath Snaefell is reviewed in the following section.

5.2.2 Evidence for the presence of a melting column beneath Snaefell

Major elements

The variation in major element composition of primary melts with changes in degree of mantle fusion (F) and pressure (P) was reviewed in section 5.1.2. Briefly, Klein & Langmuir (1987) realised that regional averages of the major element chemistry of ocean ridge basalts, corrected for low pressure fractionation, showed marked correlations which could be accounted for by regional variations in mantle potential temperature, i.e. length of the melting column (defining the so-called *global trend;* i.e. *inter*-melting column variations). Subsequently the same authors expanded on this work (Klein & Langmuir 1989) realising that, on slow-spreading ridges, data from *individual* ridge segments defined perpendicular trends (the so-called *local trend*; i.e. *intra*-melting column variations). Such trends are also seen in ocean-island-basalt (OIB) suites, although these may disrupt the global trends - indicating differences in major element composition of their source in comparison with MORBs (Langmuir et al. 1992). That these so-called local variations are preserved, indicates that melt is tapped from *all levels* in the melting column and imperfectly mixed. In order to compare primary characteristics in what are evidently variably and often fairly extensively fractionated basalts, corrections must first be made to remove the effects of this. Equations have been published (Klein & Langmuir 1987, Klein and Langmuir

[3]See Gill et al. (1992) figure 4.

1989, Langmuir et al. 1992), allowing correction of FeO*, Na_2O, SiO_2 and TiO_2 compositions for the effects of low pressure (1 atm) fractionation of olivine, plagioclase and clinopyroxene, back to an arbitrary value of 8% MgO in basalts containing between 5 and 8.5% MgO. Immediately, it must be noted that this approach has its limitations:

1). It has already been demonstrated (section 4.3.3) that the Snaefell lavas fractionated at pressures greater than 1atm.
2). It is likely that both primary MORB magmas and the those from Snaefell contained significantly more than 8% MgO. In a recent paper Kinzler & Langmuir (1995) corrected analyses to 10% MgO, which is probably more realistic for both MORBs and OIBs.
3). These relatively evolved compositions (5-8.5% MgO) may have been significantly influenced by open system processes (section 4.5), which can decouple the less compatible elements (e.g. TiO_2 & Na_2O) from the more compatible ones (FeO* & SiO_2), potentially destroying the expected correlations.

The results of correcting a suitable subset of the Snaefell data are presented in figure 5.4, and the expected trends (from the systematics presented in table 5.1), from low to high F and high to low pressure (P) of melting (the *local trends;* Klein & Langmuir 1989) are depicted with arrows. In some cases, despite the reservations outlined above, the trends are remarkably well preserved. As expected, there is a positive correlation between $Na_{8.0}$ and $Fe_{8.0}$, depicting a mixing line between high P, low F melts (high $Na_{8.0}$, high $Fe_{8.0}$) from the deeper parts of the melting column, and shallow, low P, high F melts (low $Na_{8.0}$, low $Fe_{8.0}$). The correlation between $Si_{8.0}$ and $Fe_{8.0}$ is poorer, but still negative as predicted; the lower F melts formed at higher pressures are Fe-rich and Si-poor, and SiO_2 content apparently increases with F. The plot of $Na_{8.0}$ against $Si_{8.0}$, however, shows a poorly defined trend that is perpendicular to what would have been predicted. The total variation in $Si_{8.0}$ displayed is only 4%, and the variation in the raw, uncorrected data is of approximately the same magnitude. These data were obtained by XRF analysis, a technique that generates significant errors in SiO_2 values. Nevertheless, as reported in appendix 2, the reproducibility was good, $2\sigma = 0.45$ for a repeatedly analysed basalt, VH10. Therefore the lack of the expected correlation of SiO_2 with $Na_{8.0}$ is real, and probably a clue to the melting processes. To further investigate this point, $Ti_{8.0}$ was also calculated for the Snaefell data. $Ti_{8.0}$ should show almost identical behaviour to $Na_{8.0}$, being another moderately incompatible element in the upper mantle. But when plotted against $Na_{8.0}$, $Ti_{8.0}$ shows no apparent correlation at all. Evidently the two elements are behaving very differently on melting.

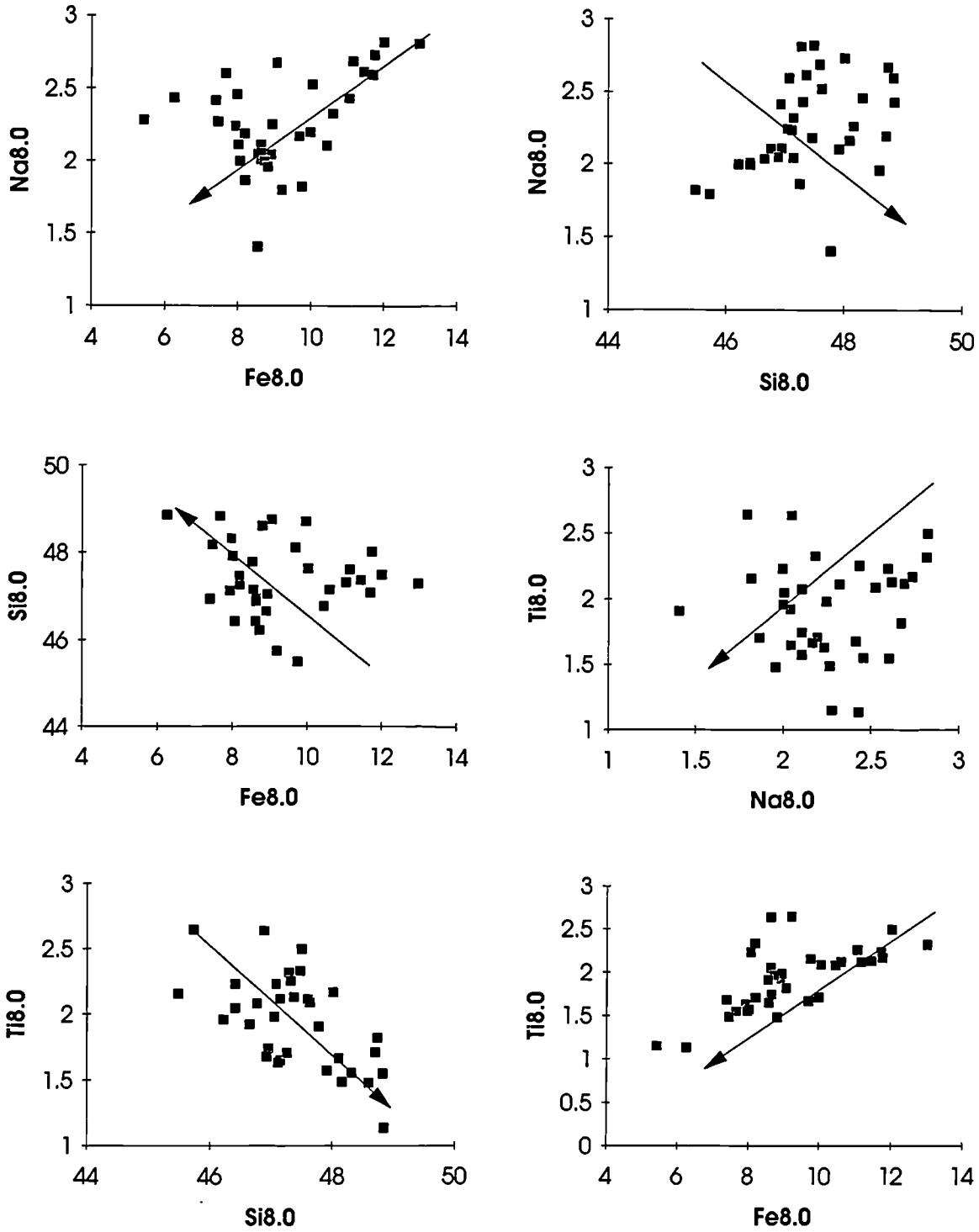

Figure 5.4 Plots of major element oxide abundances in Snaefell lavas containing between 5 and 8.5% MgO, corrected for fractionation of olivine, plagioclase and clinopyroxene back to an arbitrary value of 8% MgO. Algorithms for these corrections are from Klein & Langmuir (1987): $Na_{8.0}$, $Fe_{8.0}$, Klein & Langmuir (1989): $Si_{8.0}$ and Langmuir et al. 1992: $Ti_{8.0}$. Arrows depict the expected *intra-column* (local: Klein & Langmuir 1989) vectors.

Nevertheless, $Ti_{8.0}$ shows negative and positive correlations with $Si_{8.0}$ and $Fe_{8.0}$ that are exactly as predicted. Since $Na_{8.0}$ probably shows the poorest correlations with any of the other elements in figure 5.4, it is tempting to explain this phenomenon by post-magmatic alteration. In many other rock suites this is probably the case. It was, however, demonstrated in section 4.1 that, in the Snaefell suite, all elements may be considered to show magmatic distributions.

Therefore, the lack of correlation between $Na_{8.0}$ and $Ti_{8.0}$, and reverse correlation between $Na_{8.0}$ and $Si_{8.0}$ implies that either Na_2O, and/or TiO_2 and SiO_2 melting systematics beneath Snaefell were not as predicted. The database used to define the behaviour of the various oxides during mantle fusion (Klein and Langmuir 1987, McKenzie & Bickle 1988, Langmuir et al. 1992) is confined to melting in the spinel stability field, relevant to MORBs. As already indicated, in the presence of a hotspot, the melting column is likely to extend to greater depth and melting begin within the garnet stability field. The melting proportions of the various mantle phases changes with depth, and this has the most marked affect in the initial stages of fusion (seen here in alkalic basalts). In the garnet stability field the first few percent of melt are dominantly derived from garnet, whereas, in the spinel stability field, clinopyroxene is the main phase contributing to the melt (Kostopoulos & James 1992). This could affect the melting systematics of the oxides considered above, especially Na_2O, since at the relatively low pressures (1-2Gpa) of melting inferred in this case, Na is dominantly held in the clinopyroxene (Elthon 1992). Only at much higher pressures (>6Gpa, ~200km depth) is a significant amount of Na found in the garnet, due to a high-pressure garnet-pyroxene solid-solution (Moore et al. 1991). Therefore, at a given small degree of fusion, a small melt-fraction liquid formed in the garnet stability field could potentially contain markedly less Na_2O than one formed by an equivalent degree of fusion in the spinel stability field.

Trace elements

In an attempt to resolve the problems outlined above, two further elements, Ce and Y were considered. Ce may be considered essentially completely incompatible at all pressures of lherzolite melting and therefore should simply decrease with increasing F. As already mentioned, hotspots cause long wavelength regional variations in elements such as the LREEs. Nevertheless, within a single melting column (such as is assumed here), this scale of source variation is unlikely. Y on the other hand (an analogue for HREEs), is compatible in garnet, and therefore should behave in only a moderately incompatible manner during partial fusion at higher pressures (i.e. >20kb) where garnet is stable. In contrast, it will behave as a highly incompatible element, like Ce, at lower pressures (i.e. the spinel stability field).

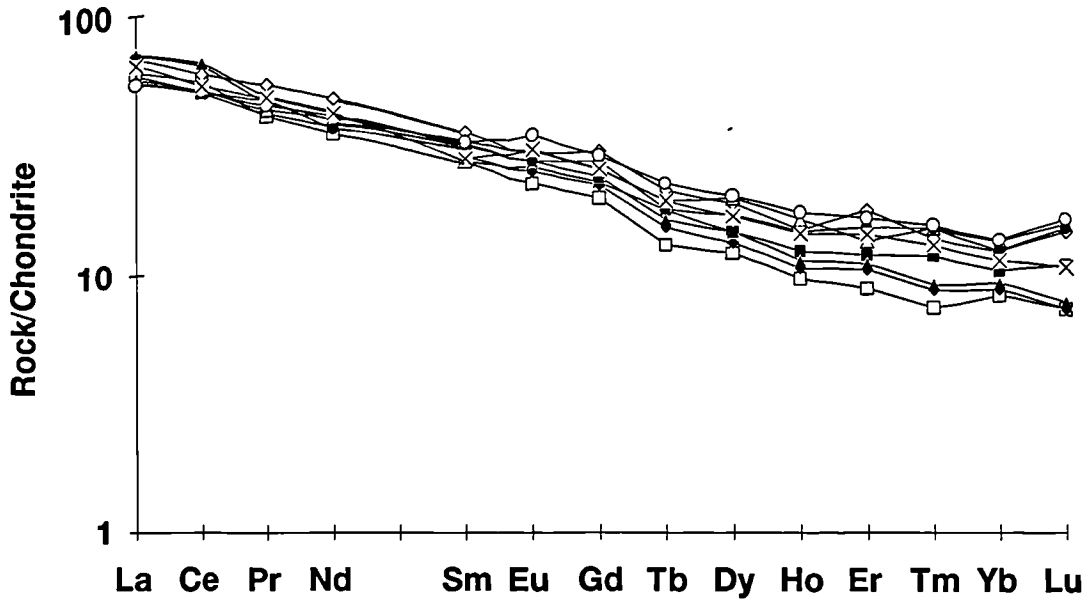

Figure 5.5 REE patterns normalised to chondritic abundance (Sun & McDonough 1989) for Snaefell high MgO (>9%) basalts.

The REE element patterns of the high MgO (>9wt %) Snaefell basalts are steeply inclined (figure 5.5), $[La/Yb]_n$[4] ranging from 4 to 9. The LREE-enrichment indicates that either relatively small degrees of melting were involved and/or the source mantle was relatively enriched in LREE. The low abundances of HREEs ($[Lu]_n$ as low as 11) indicate the presence of residual garnet in the source. This implies that the melting column extended down to at least 60-70km, into the garnet-spinel transition zone beneath Snaefell. The preservation of the "garnet signature" indicates that neither re-equilibration with the spinel facies lherzolite nor mixing with shallower, higher degree melts was sufficient to flatten out the REE patterns (section 5.1.2). In detail, the array of REE patterns appears to fan out at the HREE end. This could be due to variations in either the depth of melting and/or the proportions of deep and shallow melts that went to make up each erupted lava.

Therefore, in the light of the above discussion, if the lack of expected correlations in figure 5.4 are due to differing melting systematics between the spinel and garnet lherzolite, there should be some contrasts between the relationships of $Ce_{8.0}$[5] and $Y_{8.0}$[5] to elements already considered (figure 5.6). As in figure 5.4, the *expected* trends in figure 5.6 are marked with arrows.

[4]Normalised to C1 chondrite (Sun & McDonough 1989).

[5]The equation for $Ce_{8.0}$ is given by Plank & Langmuir (1992), and the same equation has been used to calculating $Y_{8.0}$, simply assuming Y to be completely incompatible during fractional crystallisation. This is obviously a simplification.

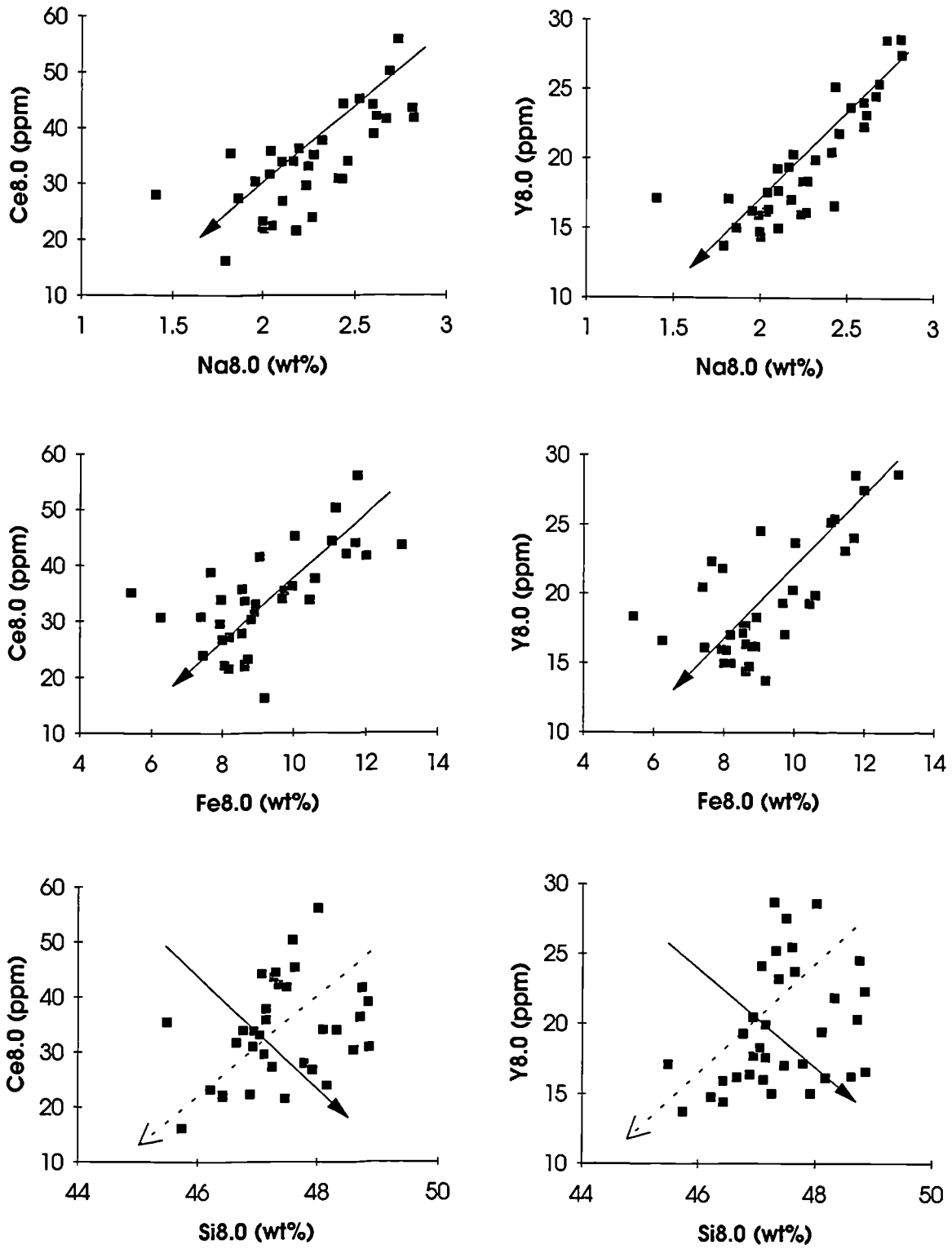

Figure 5.6 Plots of major element oxides, corrected as in figure 5.4, against $Ce_{8.0}$ and $Y_{8.0}$ using the algorithm for $Ce_{8.0}$ (Plank & Langmuir 1992). Again solid arrows indicate the expected local vector, dashed arrows pick out the main element of observed trends.

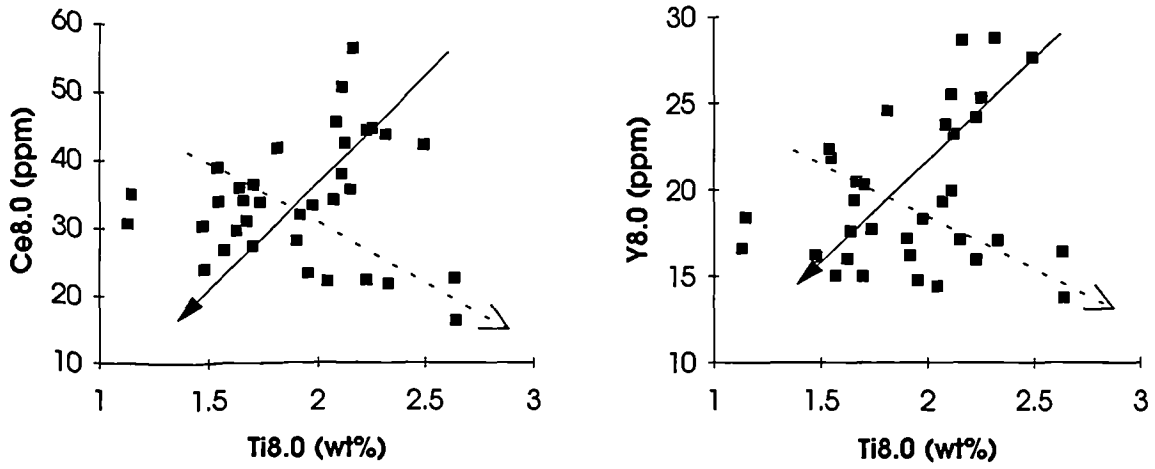

Figure 5.6 Continued.

First it is obvious that Ce and Y show almost identical behaviour. Thus the differing mantle mineralogy with depth cannot explain the deviation from expected behaviour. While $Ce_{8.0}$ varies by a factor of ~5, Y shows a more restricted range, varying by a factor of ~2.5. As expected, both $Ce_{8.0}$ and $Y_{8.0}$ correlate positively with $Na_{8.0}$ and $Fe_{8.0}$, indicating that Na_2O is behaving incompatibly (as expected). In contrast, $Si_{8.0}$ and $Ti_{8.0}$ show large amounts of scatter when plotted against either $Ce_{8.0}$ or $Y_{8.0}$. $Si_{8.0}$ shows a poor positive correlation with both incompatible elements, indicating that its concentration in the melt *decreased* at higher degrees of fusion. $Ti_{8.0}$ shows a more complex relationship with the incompatible elements, showing a "V-shaped" plot, with two almost perpendicular components. This suggests that in some melts, but not all, TiO_2 *decreased* as F *increased.*

Clues to the reason for the anomalous behaviour in SiO_2 and TiO_2 (described above, figure 5.4) at relatively low degrees of fusion are found in recent melting experiments on spinel peridotites, and thermodynamic calculations (Baker et al. 1995). Both experiments and calculations show that at 10kbars, in the *absence of volatiles*, near solidus melts (F = 0.02-0.05) are enriched in SiO_2 and Na_2O and depleted in FeO* and TiO_2, relative to higher degree melts. The increase in SiO_2 content of the melt is due to the high Na_2O contents of low F melts. This element is known to reduce the SiO_2 activity of the melt, resulting in an increase in weight percent SiO_2 content to compensate, since the coexistence of olivine and orthopyroxene essentially fix the silica activity. The decrease in TiO_2 of low degree melts can, however, be accounted for in two ways. First, as already mentioned, clinopyroxene is the dominant contributor to the melt phase at low F and this is the mineral with the largest partition coefficient for Ti.

Secondly and more importantly, $D_{Ti}^{cpx/liq}$ increases by a factor of 2.5-3.5 below F = 0.08 in both calculations and experiments (Baker et al. op. cit.). From preliminary work, the indications are that, at greater pressures similar compositional trends will be seen.

The trends originally predicted by Langmuir and colleagues are, nevertheless, seen in many alkali basalt suites (i.e. low degree melts), such as those from Loihi (Kinzler & Langmuir 1995) and the Tertiary basalts of Skye (Scarrow & Cox 1995). This is at odds with the observations of Baker et. al (1995). The answer probably lies in the role of volatiles, such as H_2O and especially CO_2, in the generation of low F melts in the Earth's mantle (Kinzler & Langmuir 1995).

Thus, it seems possible that the Snaefell basalts were generated by low degrees of fusion of a relatively *dry* peridotite source, with the "melting column" extending down into the garnet stability field. The position of the volcano at the periphery of a mantle plume - where low degree melts are erupted, rather than mixed more efficiently with higher degree melts - is probably responsible for the subtle variations of melting systematics of TiO_2 and SiO_2 being noticeable. Nevertheless, Snaefell is not the ideal site to investigate these phenomena, since the centre was underlain by an established magma chamber which was periodically tapped and refilled (chapter 4). To investigate this topic further is therefore beyond the scope of both this data set and this thesis. A more ideal setting to follow up this theme would be a series of related, monogenetic volcanoes, thus avoiding the overprint of magma chamber processes.

5.2.3 Modelling mantle melting

The previous sections have established that the Snaefell magmas were derived from their mantle source by relatively low degrees of fusion (F < 0.1), and that the melting column extended down into the garnet stability field. In this section an attempt has been made to constrain, by modelling, more precisely the source composition in terms of trace element composition, mineralogy (i.e. pressure of melting) and the degree of fusion. This was done using the non-modal batch melting equations of Shaw (1979) and modal mineralogies, melting proportions and distribution coefficients derived from the parameterisation of physical and chemical processes in mantle melting (Kostopoulos & James 1992). Virtually all current physical models of melting processes involve mixing of melts from near solidus to the maximum extent of melting attained in the melting regime. Therefore, given the boundary conditions, even complex melting regimes should theoretically lead to results that are similar to those produced by an equivalent amount of batch melting (Plank & Langmuir 1992). Additionally, as

noted earlier, even if absolute element abundances vary with the melting process, trace element ratios will remain constant (Eggins 1992). Thus batch melting may approximate the effects of *whatever melting process actually occurs* remarkably well. The source compositions used; *Depleted MORB Mantle* (DMM) and an estimate of *Bulk Silicate Earth* (BSE) - an enriched composition relative to DMM, are also from Kostopoulos & James (1992). Modelling with six different source compositions was attempted, representing three different depths (or pressures) in the mantle and two different chemical compositions, DMM and BSE (Table 5.2).

Number	Source composition	Modal mineralogy
1	undepleted mantle (BSE)	gt lherzolite
2	undepleted mantle	sp lherzolite
3	undepleted mantle	sp/gt lherzolite
4	depleted mantle (DMM)	gt lherzolite
5	depleted mantle	sp lherzolite
6	depleted mantle	sp/gt lherzolite

Table 5.2 Mantle compositions and modal mineralogies used in non-modal batch melt modelling. gt = garnet, sp = spinel, sp/gt = a 50/50 mixture of garnet and spinel lherzolite. (An attempt to model the result of melting in the garnet-spinel transition zone).

For garnet lherzolite, the melting proportions chosen are for 30kb, the lower of the two pressures given by Kostopoulos & James (op. cit.). At greater pressures, the garnet contribution drops and clinopyroxene becomes more important. For both spinel and garnet lherzolite sources, "fertile" modal mineralogies were employed, despite the fact that this may not be appropriate for chemically depleted compositions.

Previous estimates, both in this study and others, require <10% mantle fusion to produce Icelandic alkali basalts such of those of Snaefell. The modelling, therefore, was run up to 8% fusion, since within this range the source mineralogy may be assumed to remain *constant.* At higher degrees of fusion, phases leave the melting assemblage, necessitating the calculation of new melting proportions and distribution coefficients. The results of modelling are first looked at in terms of ratios. $[La/Ce]_n$ was selected first in an effort to determine which source mantle composition was appropriate, since these two elements may be considered completely incompatible. Thus, even at low degrees of melting their ratio should not change, and the source mineralogy should be of no importance. $[La/Ce]_n$ was plotted against $[La/Yb]_n$, i.e. the slope of the resultant REE patterns, to look at the effects of source mineralogy (figure 5.7).

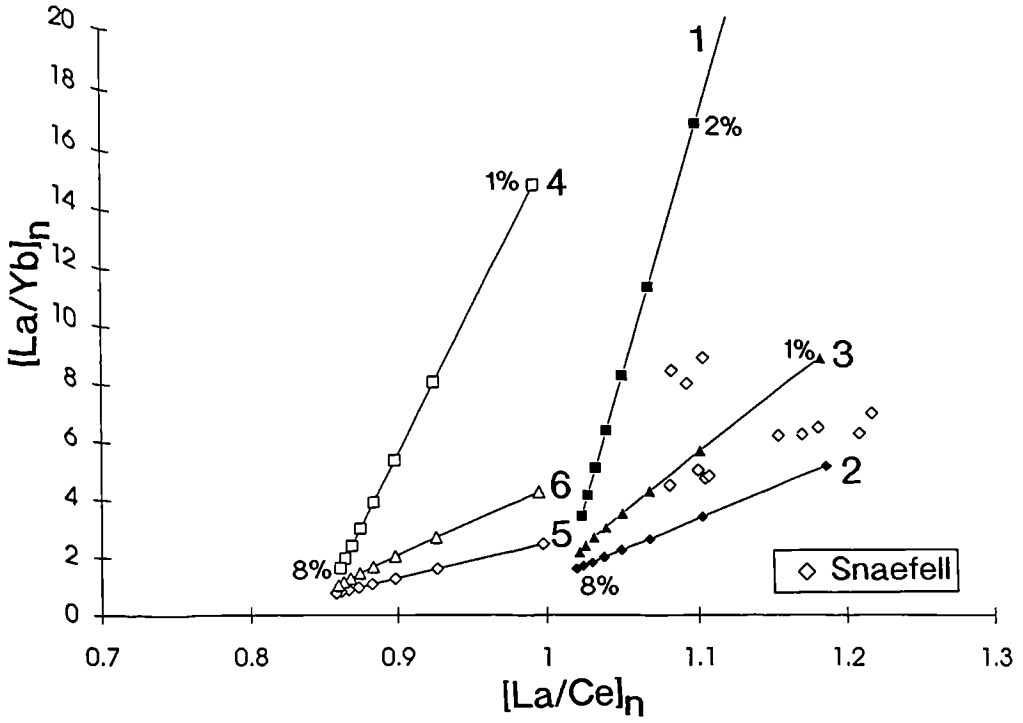

Figure 5.7 $[La/Ce]_n$ - a measure of source enrichment - plotted against $[La/Yb]_n$ - a measure of depth and degree of melting - for the results of modelling non-modal batch melting (as described in text); varying both the aluminous phase and the source composition to give six separate melting curves. Sources 1-6 are defined in Table 5.2. The range of partial melting considered is 1-8%. The high MgO (>9%) Snaefell lavas appear to represent small degrees of melting of an undepleted garnet-bearing source material.

From this it appears that the Snaefell basalts are the result of low degree melting (1-4%) in the garnet-spinel transition zone, of an undepleted or slightly enriched[6] source material. This conclusion is reinforced when absolute element abundances are considered (figures 5.8 & 5.9). Only samples containing >9% MgO were used, and these form a relatively tight group on most variation diagrams. Obviously the absolute abundances could have been increased by crystal fractionation and open system processes. If so the data would indicate a *lower* degree of fusion. Looking at figure 5.8, the Snaefell basalts form a tight group, modelled by around 3-5% melting of a BSE source composition. In figure 5.9 La is plotted against Yb and Nb against Zr. La and Nb are in each case the more incompatible element and thus act as a measure of mantle fusion, whereas Yb and Zr are more sensitive to the source mineralogy. In both of these plots the Snaefell data fall between the curves for mantle source types 1 and 3, at 3-5 and 2-5% fusion respectively.

[6]In the rest of this study, the terms *enriched* and *depleted* are relative to the composition of Bulk Earth (or estimates thereof).

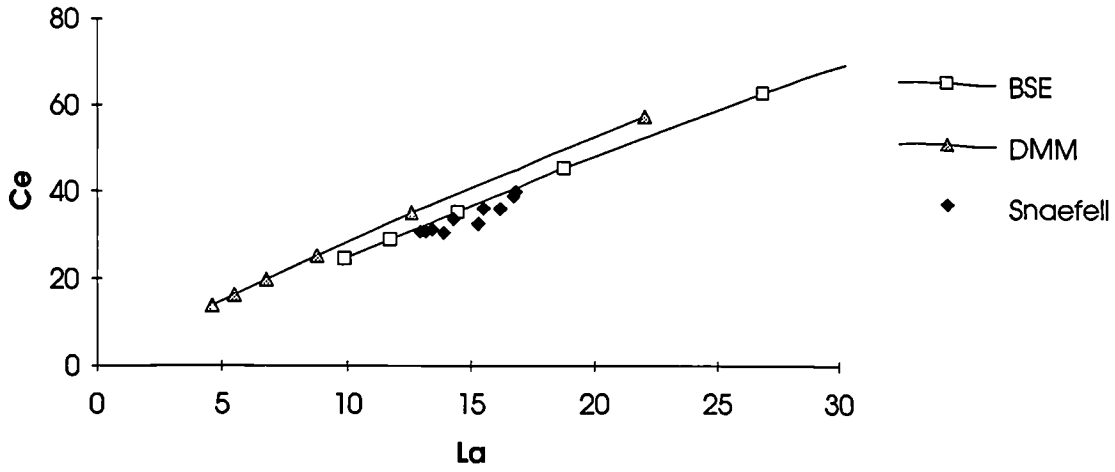

Figure 5.8 Plot of Ce vs La. Shows melting curves for BSE and DMM and data from high MgO Snaefell lavas. The abundances of these two highly incompatible elements the melt phase is unaffected by the mantle mineralogy, therefore the sole control is the bulk chemical composition of the source.

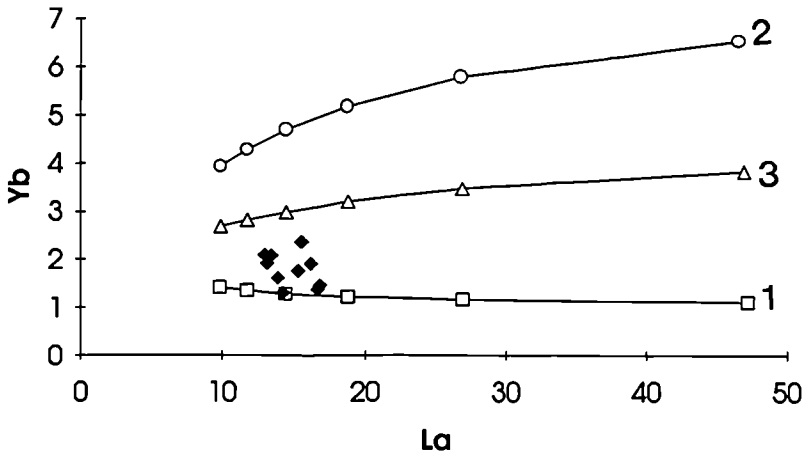

Figure 5.9 Further trace variation diagrams, showing melting curves for a BSE-type source varying the aluminous phase (sources 1-3 defined in table 5.2). Closed diamonds = high MgO Snaefell lavas. Yb and La determined by ICP-MS, while Nb and Zr data are from XRF analysis.

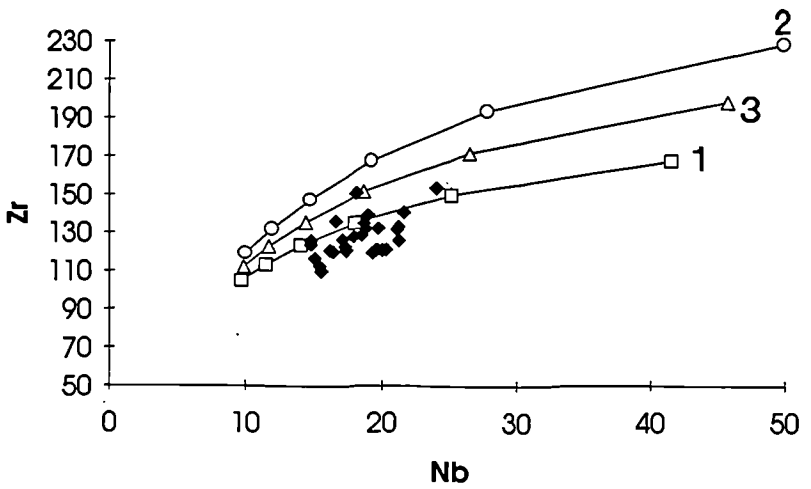

When complete REE patterns are considered, the sample with steepest pattern (VH104, $[La/Yb]_n$ = 8.50) is consistent with 3-4% melting of source type 1 (figure 5.10a), while the shallowest pattern obtained (VH212, $[La/Yb]_n$ = 4.5) requires a slightly higher degree of melting, 4-5%, of source type 3 (figure 5.10b). Again it must be remembered that the actual

lava compositions erupted represent pooled melts from various levels in the melting column, so these two extremes here are probably composed of different proportions of deep and shallow melts.

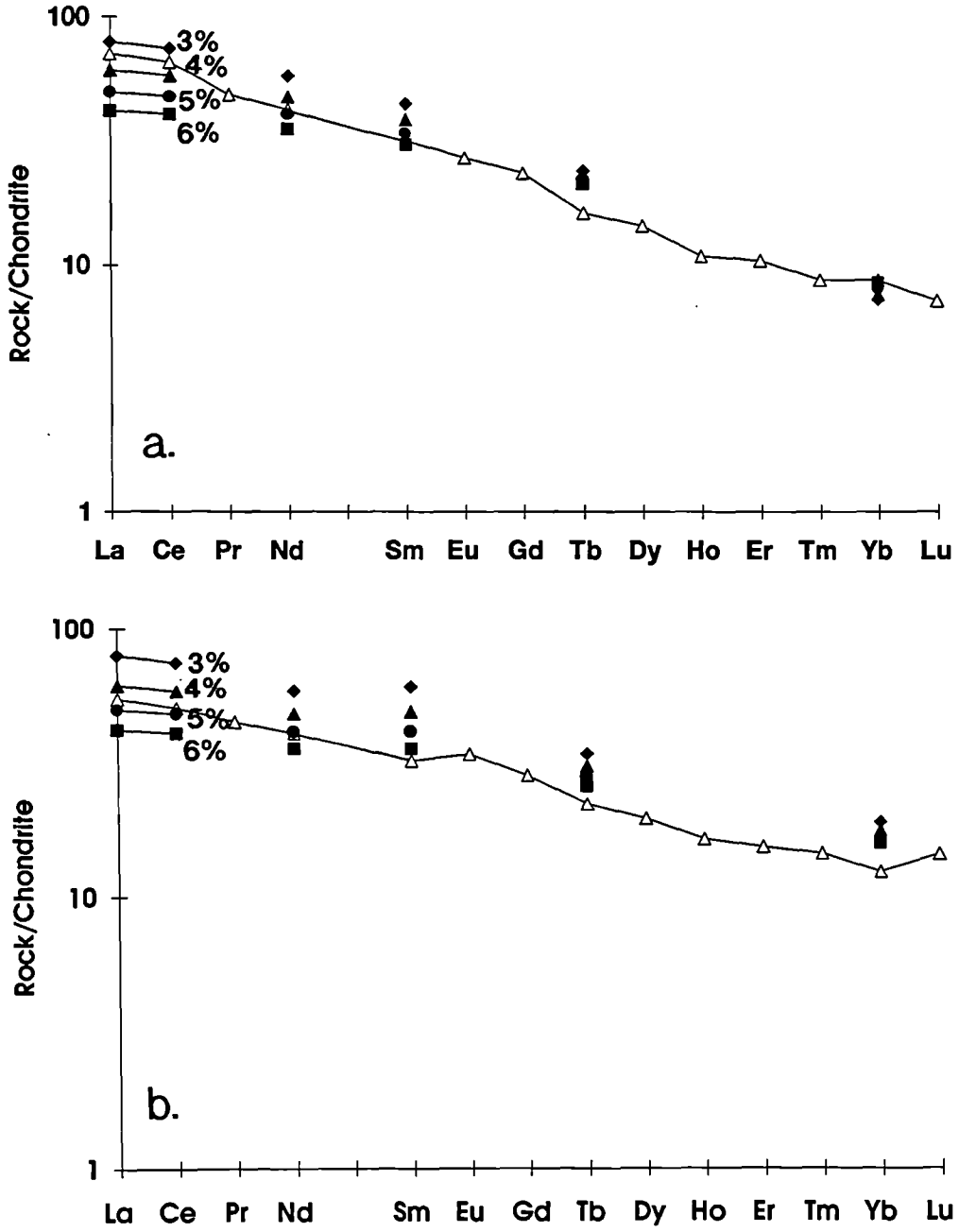

Figure 5.10 Chondrite normalised REE patterns showing the compositions of modelled batch melts 3-6% compared with the two end member REE patterns seen among the Snaefell basalts. (a). Open triangles = VH104, $[La/Yb]_n$ ~8.5, solid symbols = 3-6% melting undepleted garnet lherzolite.
(b). Open triangles = VH212, $[La/Yb]_n$ ~4.5, solid symbols - 3-6% undepleted 50/50 mixture garnet and spinel lherzolite.

In summary, the erupted lava compositions from Snaefell represent pooled melts from a melting column extending down ~80km into the mantle, sampling melts in equilibrium with garnet lherzolite. The average degree of melting evidently ranged from 1% to perhaps as high as 5%. The chemical signature of residual garnet in the source is preserved, despite extraction and ascent to shallower levels, where these melts tend to be mixed with shallower higher degree melts. The bulk chemical composition of the source is modelled moderately well using Kostopolous & James's (1992) BSE, or undepleted mantle. La/Ce ratios, however, imply *lower* degrees of fusion than absolute element abundances. This is the opposite from what would be expected, since no true primary magma composition was sampled, and differentiation processes increase incompatible element concentrations. This then suggests that the mantle source composition beneath Snaefell must have been enriched in terms of trace elements. This is unsurprising, when it is considered that, in the oceanic realm, plumes are accepted to have enriched signatures in terms of trace elements(Weaver 1991).

The isotopic characteristics of the Snaefell lavas, in terms of Sr and Nd, are show in figure 5.11. Relative to bulk Earth (Faure 1986), they appear depleted, but they are still significantly enriched over basalts derived from depleted or N-MORB source upper mantle, indicating that the source of the Snaefell magmas must have been isolated from the convecting upper mantle for a significant period in geological time.

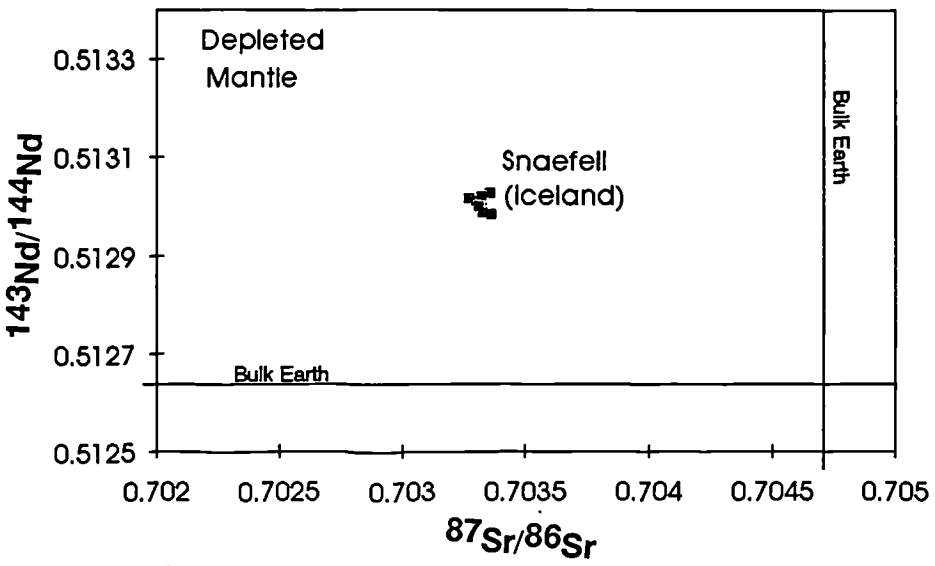

Figure 5.11 Plot of $^{87}Sr/^{86}Sr$ vs $^{143}Nd/^{144}Nd$ showing Snaefell basalts relative to the field of depleted mantle, and bulk earth (Faure 1986).

5.3 Implications for the mantle source of Icelandic basalt types

5.3.1 Comparison of the Snaefell basalts with basalts from the rest of Iceland

In this section, the mildly alkalic Snaefell lavas are looked at in conjunction with published data for the other lava types erupted in Iceland. It demonstrates firstly that in most ways the Snaefell basalts are typical of Icelandic alkali basalts. Secondly, that although alkalic volcanism in Iceland is volumetrically insignificant, accounting for just 15% of the lava erupted within the Neovolcanic zones and plays little role in crustal accretion, it can afford significant insights into the melting processes and the nature of the mantle source material beneath Iceland. This, in turn, has fairly major implications for plume theory.

Major elements

Looking at figure 5.3, it is obvious that lavas erupted along the axial rift zone, where the lithospheric thickness is minimal, should be the result of higher degrees of melting from a longer melting column than off-axis equivalents. If the plume is truly ridge-centred, or if plume material is channelled along the rift zones, then melting should also commence at greater depths as already discussed. This should be reflected in the composition of the resultant magmas, and to assess this a mature axial volcano - Krafla - for which a comprehensive data set (Nicholson 1990) was available to the author, was selected and compared and contrasted to Snaefell. In terms of major element composition, Krafla is tholeiitic, and the high MgO basalts show a large range in FeO* content (Nicholson & Latin 1992), suggesting a wide range of melting depths. Compared to Snaefell (figure 5.12), Krafla lavas appear to be dominantly the result of higher mean degrees of melting - reflected in lower $Na_{8.0}$ values - over a wider pressure interval - reflected in a wider range in $Fe_{8.0}$, than the Snaefell lavas. This is exactly as expected, and necessitates *no difference* in source material for the tholeiitic and alkalic basalts.

Trace elements

In terms of trace elements, this melting model also appears to apply. The contrasting REE patterns for the various Icelandic lava types (figure 5.13) and their geographical distribution can be explained as follows. At the centre of the plume, the mantle material crosses its solidus at ~120km, and ceases at <20 km beneath the axial rift, easily generating the 15-20% partial melt that theoretical calculations indicate to be required to form the voluminous tholeiitic magmas (e.g. Meyer et al. 1985).

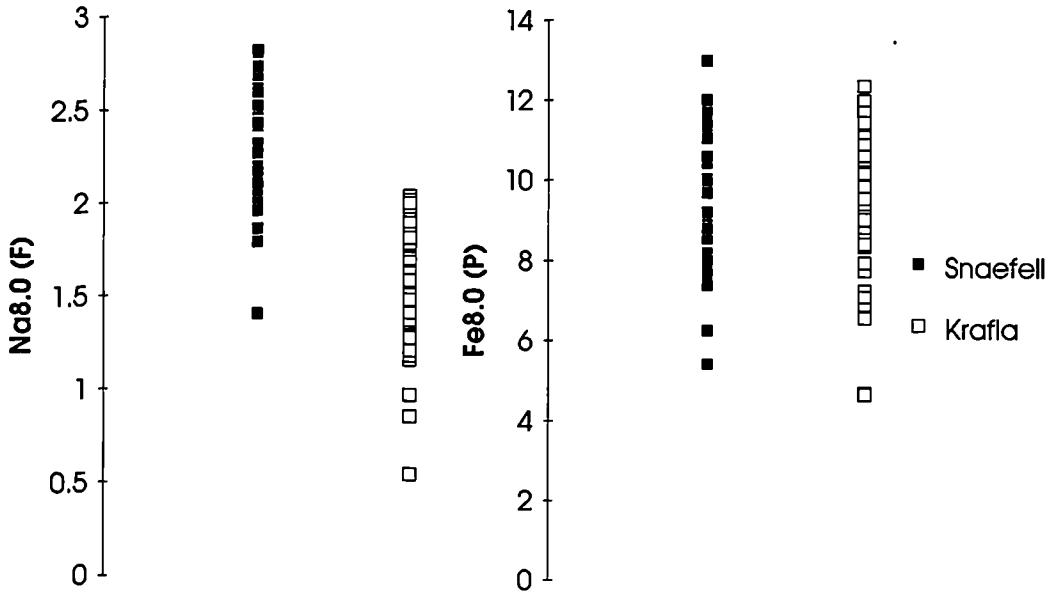

Figure 5.12 Snaefell compared with Krafla - a mature axial volcanic centre - in terms of $Na_{8.0}$ (F) and $Fe_{8.0}$ (P). The Krafla basalts are evidently the result of more extensive partial melting over a larger pressure interval than the Snaefell basalts.

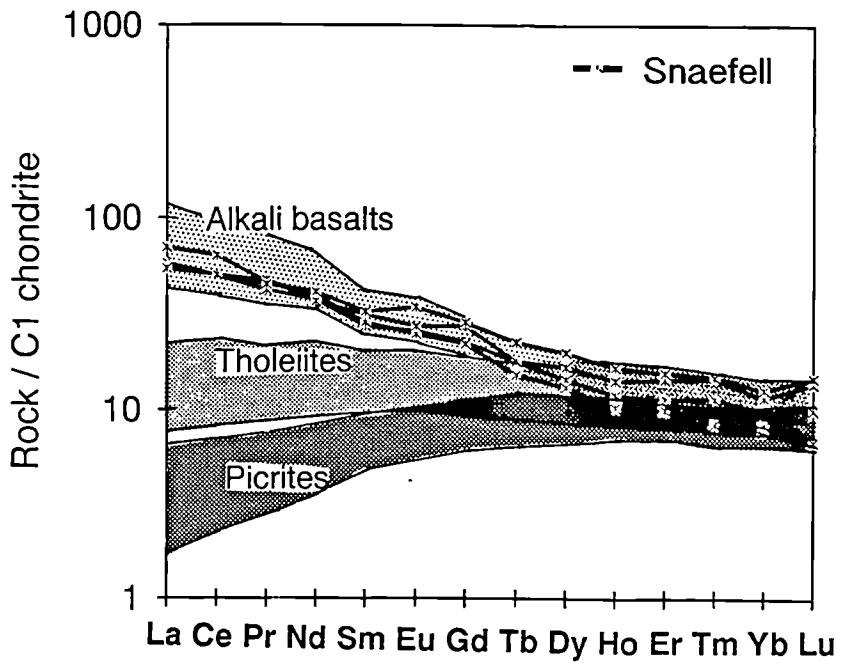

Figure 5.13 Chondrite normalised (Sun & McDonough 1989) REE abundance ranges in the various lava types found in Iceland (reproduced from Hards et al. 1995, Fig. 1).

At such high degrees of melting, most of the aluminous phase in the source material should be consumed; hence the flat REE patterns of the tholeiites should reflect those of their source region. Off-axis, at the plume peripheries beneath volcanic centres such as Snaefell, melting should commence at significantly shallower levels, although

potentially still within the garnet stability field (or the garnet-spinel transition zone, ~60-80km). It should also cease at greater depths, due to the thicker lithosphere. This results in lower degrees of melting and hence the preservation of the chemical "garnet signature". In detail, these contrasts may be less marked than this simplified model, due to the possibility of mixing between end-member compositions, as observed in the lava suites. It is also implicit in this conclusion that re-equilibration with the spinel facies was insufficient to flatten the REE patterns. Nevertheless, the Icelandic picrites, with their convex upwards REE patterns, appear to require a depleted source.

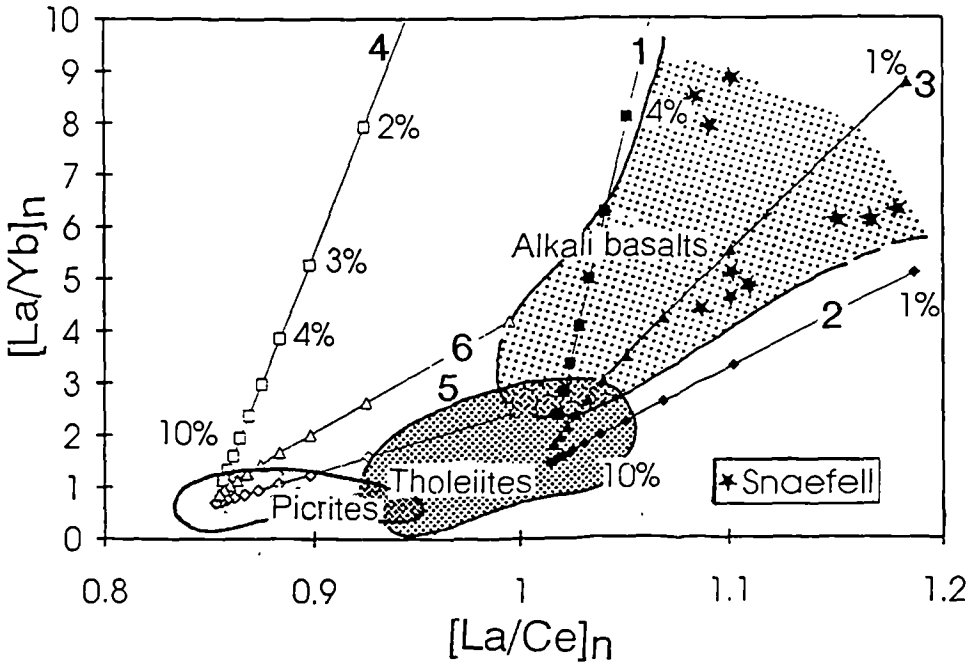

Figure 5.14 Results of modelling non-modal batch melting, melting curves as in figure 5.7. The melting interval here is extended; 1-10%, Sources 1-6 are defined in table 5.2 (modified from Hards et al. 1995; Fig. 2).

The above scenario can be modelled, using the non-modal batch melting equations of Shaw (1979) and parameters from Kostopoulos & James (1992) as previously (section 5.2.3), and the results are summarised in figure 5.14. A gradation may be seen in the data from the alkali basalts (Snaefell and published examples), which appear to represent small degrees (1-6%) of melting of an undepleted garnet-bearing mantle source, to the tholeiites, which represent higher degrees of melting of both the same source, and a progressively more *depleted* one (as indicated by a drop in $[La/Ce]_n$). The picrites also grade into the tholeiites, although requiring a significantly more *depleted source* that overlaps DMM in terms of $[La/Ce]_n$. This could be a second mantle component, or the picrites could simply represent a second phase of melting, *after* the extraction of the alkali basalts.

Isotopes

Isotopic data immediately rule out a single-component source model for the Icelandic volcanics because the different lava types show different isotopic characteristics. In general, the alkali basalts show a relatively restricted range, with the highest $^{87}Sr/^{86}Sr$ and lowest $^{143}Nd/^{144}Nd$ of Icelandic mafic rocks (figure 5.15).

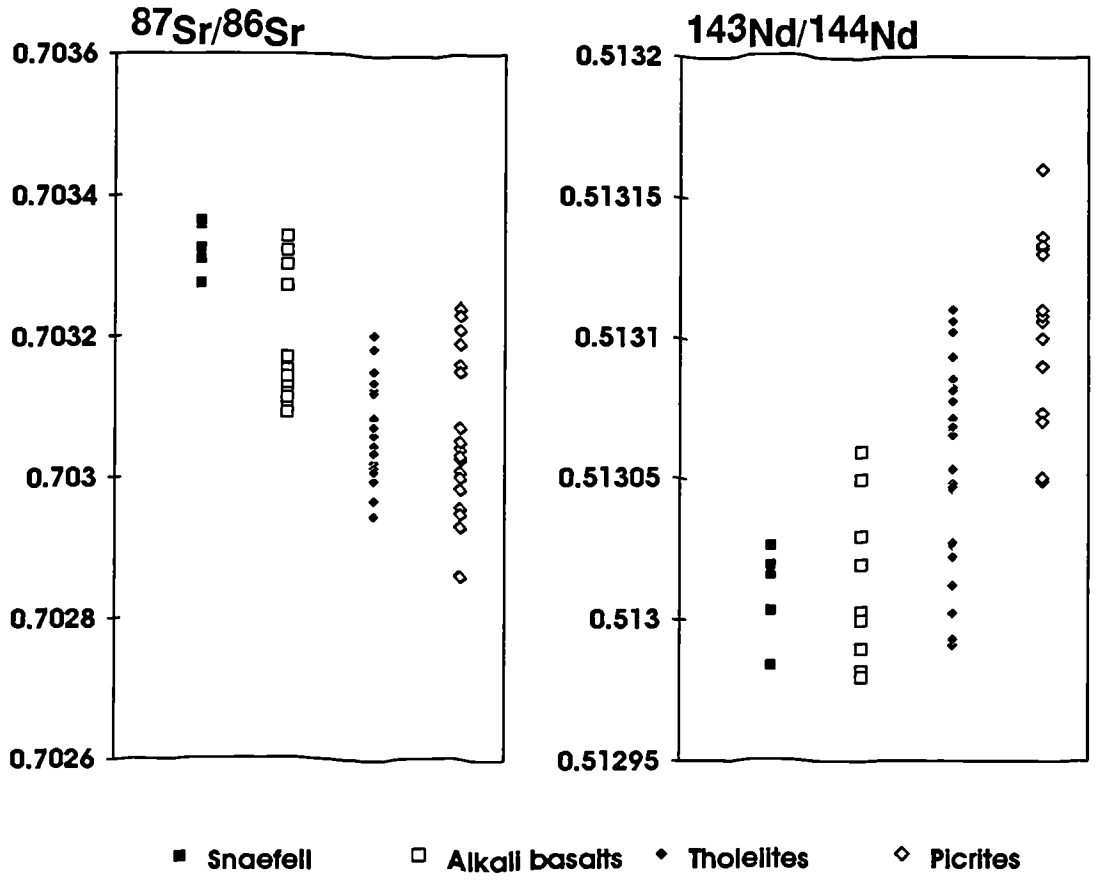

Figure 5.15 Variations in $^{86}Sr/^{87}Sr$ and $^{143}Nd/^{144}Nd$ in Icelandic volcanics.

The picrites, in contrast, cover most of the Sr-Nd isotopic range of Icelandic lavas, including members at the opposite end of the spectrum to the alkalic rocks. Pb isotope systematics are rather more complex (figure 5.16), and only a limited amount of data are available. Therefore data from the transitional volcanic centres of the ERZ - not used in figure 5.15 - have been included. It is immediately obvious that the most radiogenic Pb is to be found in the lavas from the transitional volcanic centre, Katla. The alkalic lavas of Vestmannaeyjar show rather *less* radiogenic Pb isotopes, and those overlap the transitional lavas from Hekla. Snaefell shows still more unradiogenic Pb isotopes and overlaps the field of tholeiitic lavas of the Veidivotn fissure swarm and some of the high MgO lavas from the Reykjanes peninsula. As might have been expected, the least radiogenic Pb isotopic ratios are found in picritic lavas, specifically those from the Theistareykir volcanic centre in the NRZ.

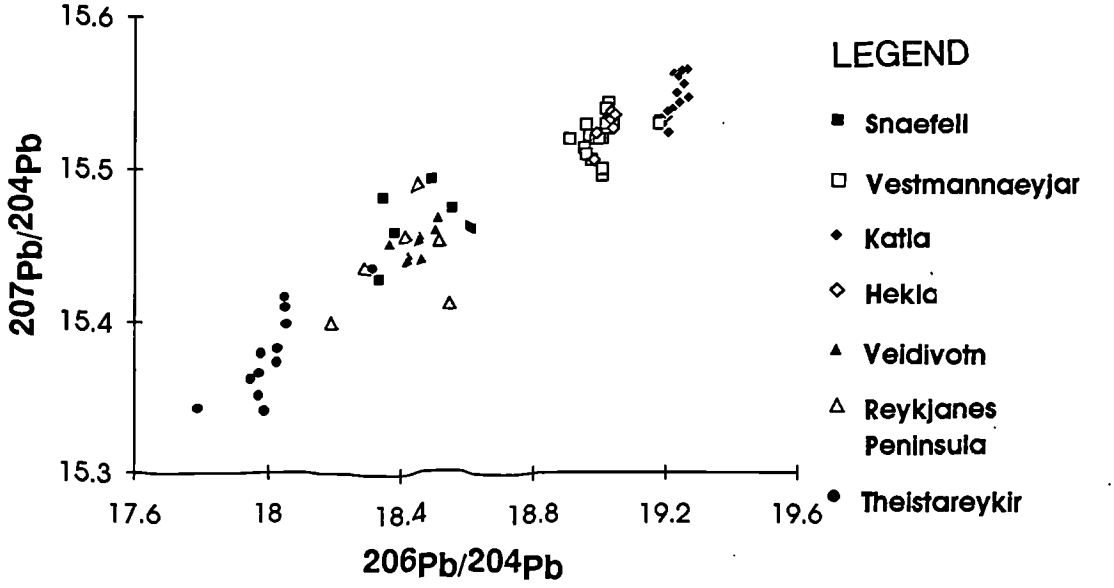

Figure 5.16 $^{206}Pb/^{204}Pb$ vs $^{207}Pb/^{204}Pb$ for all volcanic centres in Iceland for which good data are available. Data Sources: Furman et al. 1991, Elliott et al. 1991, Park 1989 and the present study.

These overlap with the MORB isotopic field and show some of the least radiogenic Pb isotopes recorded in Atlantic oceanic lavas (Elliott et al. 1991). The Katla volcanic centre, however, does not show the correspondingly high $^{87}Sr/^{86}Sr$ or low $^{143}Nd/^{144}Nd$ but is intermediate between the alkali basalts and tholeiites, exactly as might be expected from the emerging patterns. $^{3}He/^{4}He$ ratios are enriched 8 to 26 times over atmospheric ratios in rocks from the neovolcanic zones that have been analysed (Kurz et al. 1986). The highest value so far was obtained from the ERZ and no analyses of rocks from the Snaefellsnes volcanic zone (or Oraefajokull-Snaefell zone) were included in this study.

5.3.2 Mantle source characteristics

It has been proposed that the variations in isotope systematics of Icelandic mafic lavas are the result of the interaction between melts from a relatively homogeneous mantle plume (that yields relatively unenriched magmas), with old, hydrothermally altered Icelandic crust during ascent and eruption. Effectively the plume re-cycles its own older products (Oskarsson et al. 1982, 1985, Steinthorsson et al. 1985, Hemond et al. 1988). The alkalic basalts in this scheme were proposed to be derived from relatively small degrees of partial melting of amphibolite facies lower crust, while the tholeiites and picrites, although showing some crustal contamination, were considered more representative of the plume composition.

The basis of the model outlined above was the abnormally low O-isotope values of tholeiitic basalts, which pointed to the important role played by meteoric waters hydrothermal alteration of the crust (Hattori & Muehlenbachs 1982). This model has now been invalidated with consideration of Nd (and Pb) isotopes in addition to Sr and O. The variation in $^{143}Nd/^{144}Nd$, from 0.51314 in Icelandic picrites to 0.51295 in the alkali basalts ($^{147}Sm/^{144}Nd$ = 0.12-0.28), requires the isolation of the crustal reservoir for >200Ma - which greatly exceeds the maximum age of any Icelandic rocks (~16Ma), and indeed the entire North Atlantic! Thus the Nd and Pb isotopic variations must directly reflect the *mantle source composition* (Hemond et al. 1993).

The Sr (and Pb) isotopic ratios can be seen to correlate positively with other measures of source enrichment, such as incompatible trace-element ratios (e.g. La/Sm), while similar negative correlations occur with $^{143}Nd/^{144}Nd$. Perhaps more significantly, there appear to be similar correlations with the *degree of partial melting* (increasing from alkali basalts to tholeiites and picrites) inferred from $[Sm/Yb]_n$ (figure 5.17). Unfortunately, the database available is insufficient to use $Na_{8.0}$ as a measure of degree of melting. It then follows that the source region of the Icelandic volcanics must be *heterogeneous*, a conclusion reached by several previous authors (Zindler et al. 1979, Elliott et al. 1991, Hemond et al. 1993). There must be at least two components, a less refractory one which is geochemically undepleted and fusible, and would therefore dominate initial melts (to produce alkali basalts), and a more refractory one that is depleted (relative to estimates of bulk Earth). During progressive decompression fusion, melts from the more refractory component should gradually dilute the early, enriched liquids to form the tholeiites and most picrites. The most extremely depleted picrites in this model would result from a second phase of melting after the extraction of basaltic magmas. Their depleted isotopic systematics can therefore be considered to approach those of the depleted end-member component (Sobolev et al. 1994), but it beyond the scope of the present discussion to explore this possibility further.

The enriched component, best represented in the alkali basalts, appears complex. From the isotope systematics of the alkalic and transitional basalts it seems possible that there are *two* enriched components, or that the one is heterogeneous, since the most radiogenic Pb isotope ratios do not correspond with the most radiogenic Sr or least radiogenic Nd isotopic ratios.

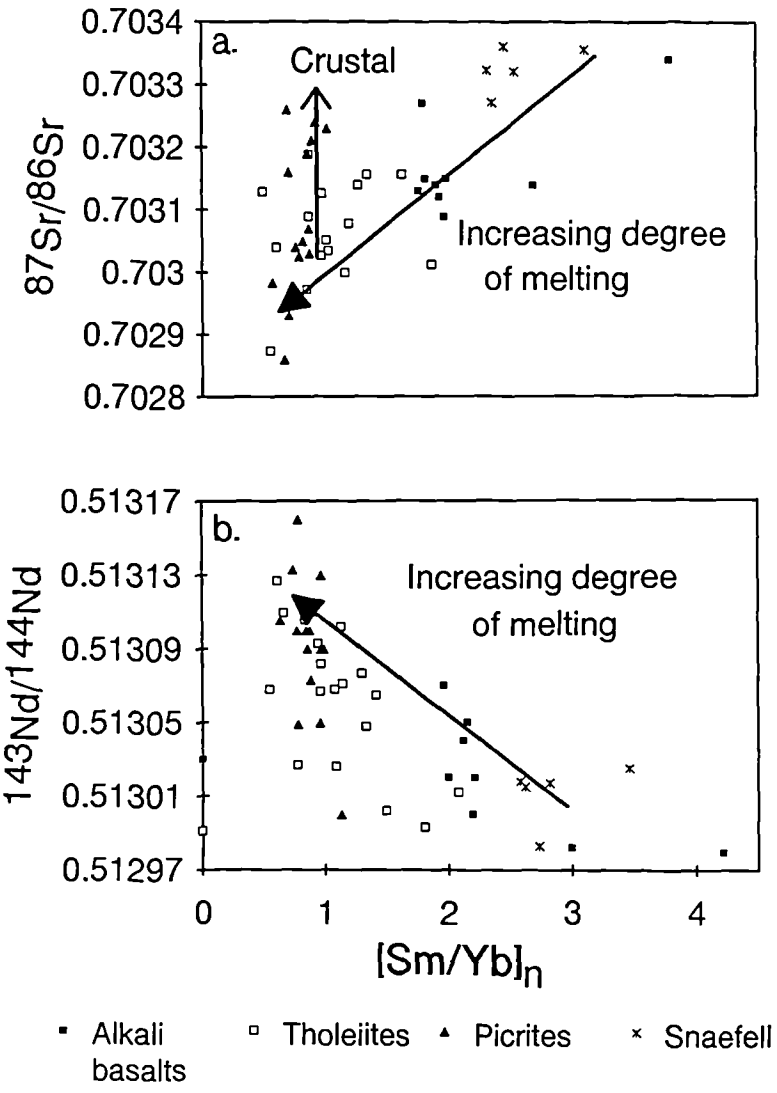

Figure 5.17
(a) $^{87}Sr/^{86}Sr$ vs $[Sm/Yb]_n$ for Icelandic volcanics, showing a reasonable positive correlation.
(b) $^{143}Nd/^{144}Nd$ vs $[Sm/Yb]_n$, showing a good negative correlation. (Reproduced from Hards et al. 1995).

5.3.3 Mantle heterogeneity beneath Iceland

It is now becoming accepted that the mantle source of the Icelandic volcanics is heterogeneous (Hemond et al. 1993). Essentially two models have been proposed to account for the heterogeneities. The first requires the chemically enriched lavas (alkali basalts) to be derived from a source within the plume itself, whereas the source of the less enriched lavas is dominated by *depleted local upper mantle* - the source of North Atlantic MORBs - that has somehow been incorporated into the plume (Sun & Jahn

1975, Langmuir et al. 1978, Schilling et al. 1983). The second proposes that both the enriched and depleted components are *integral* parts of the plume itself (Elliott et al. 1991, Thirwall et al. 1994, Hards et al. 1995). The following discussion attempts to evaluate the first option by considering the feasibility of incorporating local upper mantle into the plume itself.

Plume-Upper mantle mixing

Plume-upper mantle mixing has been accepted for some time to occur along the Reykjanes Ridge south of Iceland (Schilling 1973, Sun et al. 1975, Schilling et al. 1983). Geochemical studies show that $^{206}Pb/^{204}Pb$ and $^{87}Sr/^{86}Sr$ become more radiogenic towards Iceland, and an increase in $(La/Sm)_n$ has also been observed (figure 5.18).

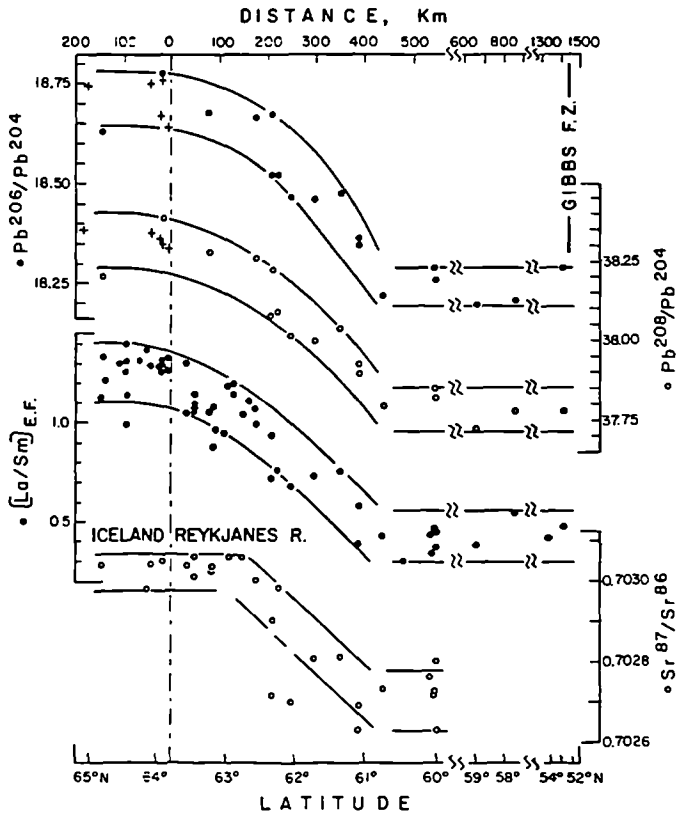

Figure 5.18
Variation of $^{206}Pb/^{204}Pb$, $^{208}Pb/^{204}Pb$, $[La/Sm]_{EF}$ and $^{87}Sr/^{86}Sr$ in basalts with latitude between 52°N and 65°N. $[La/Sm]_{EF}$ stands for La and Sm values normalised to chondrite. (Reproduced from Sun et al. 1975).

To evaluate the feasibility of this hypothesis, the thermal structure and scale of the Iceland plume must be taken into consideration.

General features of vertical, steady state plumes were listed by White & McKenzie (1989):

1). They consist of narrow (150-200 km wide) columnar upwellings.
2). The convected material spreads to form a mushroom head some 100-200°C above ambient mantle temperature.
3). The lateral extent of the hot asthenosphere in the head is 1000-2000 km.
4). The convecting mantle in the hotspot causes dynamic uplift, reaching a maximum of 1000-2000m in height.

The Iceland plume appears to fit this general model fairly well (section 1.2). Therefore, it would appear that *the whole of the Iceland block should be underlain by plume-derived material alone*, so that petrogenetic models requiring MORB-source (upper) mantle to be present in this region must be treated with caution.

Vigorous convection in the mushroom-like head that develops above a steady-state plume could potentially result in the entrainment of surrounding ambient mantle, and prevent ponding of the plume-derived material. However, the indications are, from a geophysical study of mid-plate mantle plumes, that such convection is sluggish (Sleep 1994). Thus there is no obvious mechanism for entrainment of *upper* mantle material into a *vertical plume conduit*, although Richards & Griffiths (1989) have demonstrated that significant entrainment of upper mantle material could occur when the plume conduit is deflected sideways by increased shear flow velocities.

Plume heterogeneity

Probably the most convincing piece of evidence for the hypothesis that *both dominant components in the mantle source of the Icelandic volcanics being distinct from local upper mantle* is a plot of $^{207}Pb/^{204}Pb$ vs $^{208}Pb/^{204}Pb$ (figure 5.19). This displays data from Iceland and North Atlantic N-MORB, the Reykjanes and the Kolbeinsey Ridges. The North Atlantic N-MORB field is defined using samples distant from known hotspots (Iceland, the Azores, Jan Mayen) and fracture zones. As previously noted by Thirwall et al. (1994), this diagram almost totally separates the fields for Iceland itself and North Atlantic N-MORB, and strongly militates against any *significant* contribution from the MORB source mantle to Icelandic magmatism. Therefore, although the depleted source component in Icelandic magmatism may *resemble* MORB source mantle in terms of trace elements, and Nd and Sr isotope systematics, it is distinct in $^{208}Pb/^{204}Pb$ - $^{207}Pb/^{204}Pb$ isotopic space. The data from the Reykjanes and Kolbeinsey Ridges, however, straddle both the MORB and Iceland

fields, thus confirming the proposed plume-MORB mixing there (Schilling 1973, Sun et al. 1975, Schilling et al. 1983, Mertz et al. 1991).

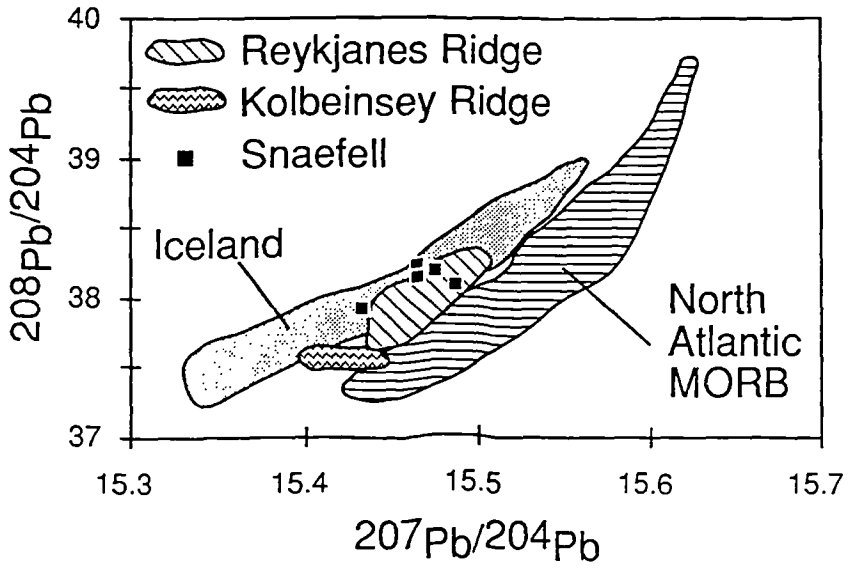

Figure 5.19 $^{207}Pb/^{204}Pb$ vs $^{208}Pb/^{204}Pb$ showing data fields for Iceland, North Atlantic MORB, the Reykjanes and Kolbeinsey Ridges and individual data points from Snaefell. Data sources for Iceland and North Atlantic MORB in Hards et al. (1995), Reykjanes Ridge (Sun et al. 1975), Kolbeinsey Ridge (Mertz et al. 1991).

To conclude, it would appear that the Iceland plume consists of undepleted streaks (a minor part of the plume volumetrically) set in a more refractory, geochemically depleted matrix. The streaks dominate the initial melts - alkali basalts - while the contribution to melts from the matrix increases with the degree of melting - forming the tholeiites and picrites. The proposal of a depleted component within the plume that is distinct from DMM has implications for the study of all plumes. It contradicts the generally accepted view that oceanic mantle plume melts have enriched isotopic signatures. It is, nevertheless significant that the most depleted signatures in Icelandic magmas are found in the highest degree melts (i.e. the picrites), since Iceland is unique among present-day plumes in its position beneath an oceanic spreading centre. This means that the upwelling plume material undergoes the maximum possible amount of decompression melting; the lithospheric "lid" being limited to just ~20km of crustal rocks at the plume axis (figure 5.20). At mid-plate hotspots (e.g. Cape Verde, Reunion, the Canaries, St. Helena) it therefore follows, that the amount of decompression melting of the plume material is greatly reduced (hence the lack of picrites), and thus only the enriched streaks may be sampled. Thus the depleted component may be barely sampled at all, and therefore remain undetected. Therefore a fourth, depleted plume component is suggested, in addition to the three components

(high U/Pb mantle: HIMU, and "enriched" components: EMI and EMII) that are usually postulated to account for the range of enriched geochemical signatures of OIBs in Sr-Nd-Pb isotopic space.

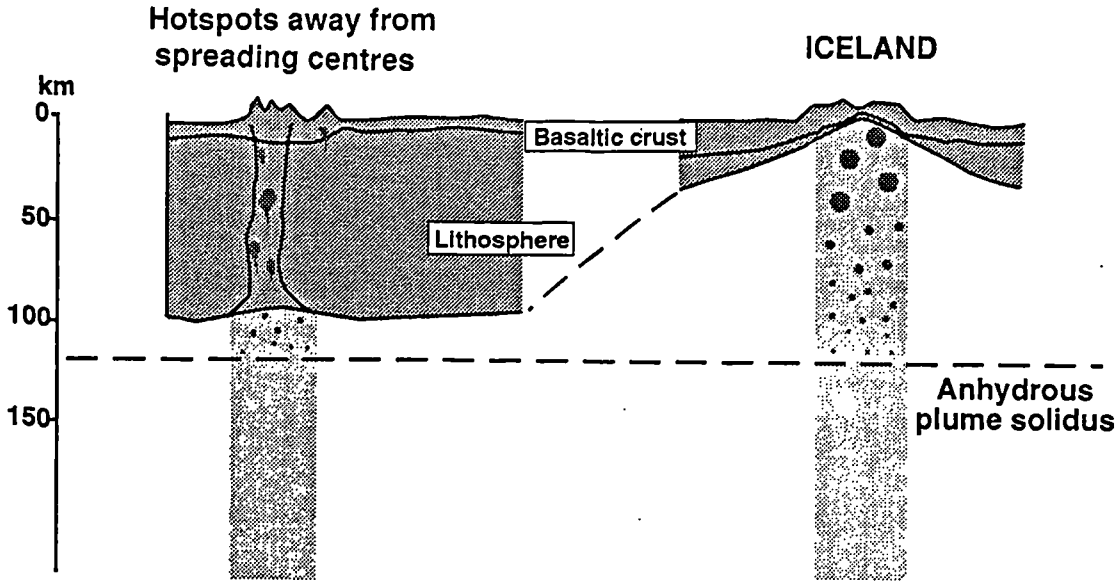

Figure 5.20 Cartoon showing the upwelling mantle plume beneath Iceland compared with other plumes that impinge on older, thicker lithosphere - the value used here is around the maximum thickness attained by oceanic lithosphere. The dark circles represent the increasing amount of partial melting as the plume ascends. It illustrates that, for a given potential temperature, a longer melting column and thus a higher degree of melting is attained where the lithosphere is thinner. (Reproduced from Hards et al. 1995).

5.3.4 Iceland - an immature HIMU plume?

The enriched streaks in the Iceland plume, best represented in the off-axis alkali basalts, must be composed of similar material to that which produces the enriched products of mid-plate hotspots (above). In order to explain the distinctive $^{208}Pb/^{206}Pb$ - $^{207}Pb/^{206}Pb$ of the Icelandic basalts, Thirwall et al. (1994) proposed that Iceland is underlain by an immature HIMU-type plume, bringing up material which has not been isolated from the convecting mantle for sufficient time to develop the Pb isotope signature that typifies HIMU plumes. Incompatible trace element ratios can also be used fairly successfully to characterise the various mantle components (Weaver 1991). While isotope systems evolve with time, incompatible trace element ratios remain constant, except at very low degrees of mantle fusion (<1%). Thus they can provide time-independent information as to the composition of the plume source region. Figure 5.21 shows Ba/La vs K/Nb for basalts from ocean islands considered representative of the mantle components EMI, EMII and HIMU, along with picritic, tholeiitic and

alkalic basalts (Snaefell) from Iceland. This plot clearly shows that the incompatible trace element ratios (particularly K/Nb) of the Icelandic volcanics are, with the exception of a few tholeiites, completely distinct from HIMU OIBs (Kerr & Hards, submitted). As already emphasised, it is probably the alkali basalts of Iceland that are most comparable with other OIBs, since most plumes impinge on thicker lithosphere, limiting the degree of melting that can occur. The Snaefell basalts are the furthest from HIMU characteristics on figure 5.21. Thus, if anything, the Iceland plume could be an immature EMII plume.

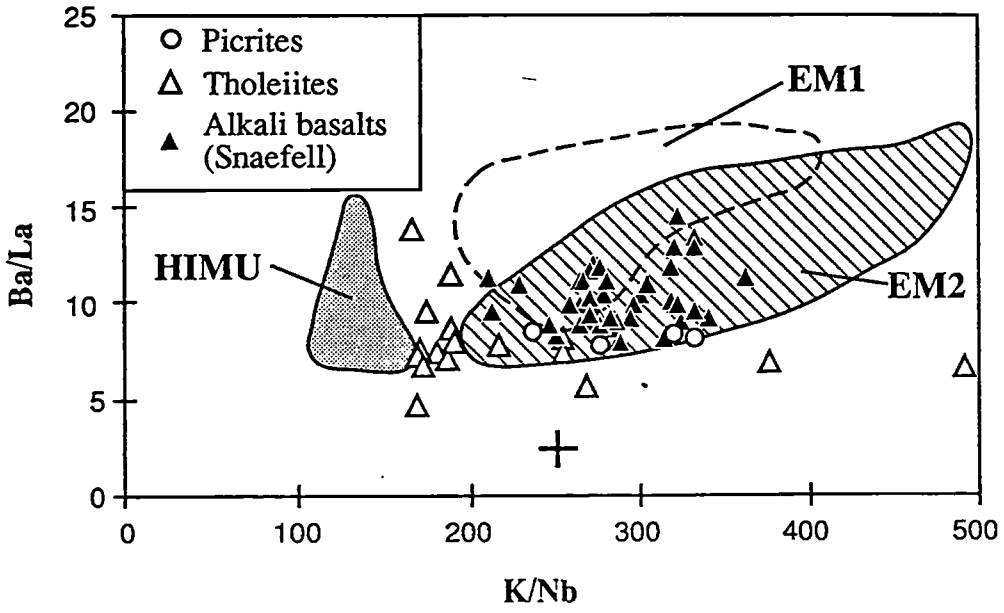

Figure 5.21 Plot of Ba/La vs K/Nb showing fields for EMI, EMII and HIMU-type OIBs, along with picrites, tholeiites and alkali basalts from Iceland. Cross represents N-MORB (Sun & McDonough 1989). Data sources: EMI - Pitcairn Islands (Woodhead & McCullough 1989), Walvis Ridge (Humphris & Thompson 1983): EMII - Samoa (Palacz & Saunders 1986, Devey et al. 1990); HIMU - St. Helena (Weaver et al. 1987, Chaffey et al. 1989); Icelandic picrites and tholeiites (Hemond et al. 1993). From Kerr & Hards (submitted).

5.4 Source of the mantle components expressed in Icelandic magmatism

There is now a growing acceptance, in both the geochemical and geophysical literature, that mantle plumes must rise from a thermal boundary layer within the Earth's mantle in order to gain the heat required to provide the buoyancy necessary for plume to rise. Both the 670km discontinuity (upper mantle-lower mantle boundary) and the core-mantle boundary (D" layer) have been considered as potential plume sources (Campbell & Griffiths 1992, Loper 1991). In the case of Iceland, the high (primordial) $^{3}He/^{4}He$ signatures found in many lavas (Condomines et al. 1983, Kurz et al. 1985), and the eruption of picritic lavas that require Tp at least 200°C above ambient mantle (McKenzie & Bickle 1988), are two strong lines of evidence for the latter.

5.4.1 Origin of the enriched plume components

Numerous models to explain the different *enriched* OIB source components have been proposed, although now a general consensus of opinion suggests that they are predominantly derived from ancient (>1Ga) recycled oceanic lithosphere, plus small amounts of sediment, (Hofmann & White 1982, Zindler & Hart 1986, Weaver 1991). Most OIBs show Nd-Sr isotope systematics close to HIMU OIB, suggesting that this is possibly the dominant source of chemical heterogeneity within the mantle (Wilson 1993). HIMU is thought to be derived from recycled subducted oceanic crust, its geochemical characteristics modified by hydrothermal alteration on the sea floor. EMI and EMII are thought to form from HIMU by contamination with small (<5%) amounts of pelagic and terriginous sediment, respectively (Weaver 1991). This concept is reinforced by the comparative rarity of what might be called a "pure HIMU chemical signature".

In the case of Iceland there appears to be an additional, depleted plume component, best represented in the highest degree melts (picrites) that are distinct from DMM. Anderson (1994) suggests that this is "a major paradox for plume theories". Nevertheless, in the following discussion it can be demonstrated that, contrary to Anderson's arguments, a depleted plume component requires no deviation from the conventional plume models.

5.4.2 Origins of the depleted plume component

There are two possible origins for the depleted component sampled in plume volcanism: either it is also present in the D" layer, or it is entrained as the plume rises through the lower mantle. Kerr et al. (1995) raise the first possibility, noting that the oceanic lithosphere consists of both MORB cumulates and the residues from the melting event that formed the oceanic crust. It would thus be depleted in terms of trace elements, relative to the oceanic crust. The present author considers this unlikely, since this material would still have an *upper mantle* isotopic signature, from which the depleted component in the Iceland plume is distinct. Further, it is suggested that the oceanic lithosphere separates from the crust attached to it, as the slabs pass through the mantle (Hofmann & White 1982, Weaver 1991). Thus if the D" layer consists of material entirely derived from subduction, then the depleted material must represent entrained lower mantle material.

Modelling (Griffiths & Campbell 1990) suggests that a starting plume rising from the core-mantle boundary should entrain material into its head as it rises, and that most of this entrainment should take place in the *lower* mantle. Similarly, Hauri et al. (1994) have show that significant entrainment of ambient mantle, driven by radial conduction of heat out from the plume, should occur in vertical, steady state mantle plume tails or conduits (such as the present-day Iceland plume). Considering a range of buoyancy fluxes from 0.1 to 10Mgs^{-1}, which encompasses all terrestrial plumes, the amount of entrainment of ambient mantle varies from >90% to <5%, and shows a negative correlation with the buoyancy flux. Detailed examination of the mantle streamlines indicates that most of the entrained fraction originates in the lower half of the layer traversed - i.e. the bulk of the entrainment should take place in the lower mantle and there should be little input from the upper mantle. Additionally, a layer of lower mantle material should be drawn up with the plume material by viscous coupling (Hauri et al. op. cit.). Thus on reaching the base of the lithosphere, a plume may only contain a very small proportion volumetrically of material from the D" layer (ultimate plume source). There are several independent lines of evidence to lend credibility to this model:

1). Os isotopes are perhaps the best tool for detecting the presence of old oceanic crust in the mantle source of basalt magmas (Roy-Barman & Allegre 1995). $^{187}Os/^{186}Os$ ratios of OIBs from Hawaii, Reunion and Mangaia are slightly more radiogenic than estimates of bulk silicate Earth (~1.06) and published peridotite analyses, ranging from 1.08-1.15 (Pegram & Allegre 1992, Roy-Barman & Allegre 1995). These authors found an ankaramite from Iceland to have a value of 1.07, and two picrites from the WRZ, values of 1.12 and 1.11. These values preclude the possibility that

these OIBs were derived either largely or totally by the fusion of ancient subducted oceanic crust, as such material would have a much higher $^{187}Os/^{186}Os$ (Pegram & Allegre 1992). These authors have subsequently used mixing calculations to show that a basalt with $^{186}Os/^{187}Os$ of 1.11 could be generated from a source containing just 8% of 3Ga crust, assuming the depleted component to have chondritic Re-Os systematics.

2). Available Sr-Nd-Pb-He isotopic data from OIBs form sublinear arrays converging on a volume characterised by MORB-like $^{87}Sr/^{86}Sr$ and $^{143}Nd/^{144}Nd$, and elevated $^{206}Pb/^{204}Pb$ and $^{3}He/^{4}He$. This common chemical "component" in oceanic basic magmas was termed "FOZO" by Hart et al.(1992) and appears, from its high (primordial) $^{3}He/^{4}He$, to have its origins in the lower mantle. If this is the case, in direct contradiction to previous theories, the lower mantle must also have undergone depletion at some time during the Earth 's history, *if* available estimates of BSE are valid. These authors and subsequently Hauri et al. (1994) point out, however, that the data arrays from Iceland and Galapagos overlap MORB in Sr-Nd-$^{206}Pb/^{204}Pb$ space, suggesting an upper mantle contribution. Thus, as has already been demonstrated (above) further isotopic systems need to be considered in order to separate MORBs from "depleted OIBs". It is also the opinion of the present author that, to fully investigate the nature of FOZO, OIBs from hotspots where *higher* degrees of melting occur - i.e. better sampling of depleted more refractory material - should be used. If this were done, then the "FOZO" compositional range might expand.

3). Diamonds have been found to contain syngenetic inclusions consisting of an assemblage of magnesiowüstite (Mg# ~85, NiO ~1 wt%) plus enstatite, En_{94-95}. If these inclusions were formed in the lower mantle as proposed, the enstatite would correspond to a retrogressive transformation product of perovskite (Kesson & Fitz Gerald 1991). These authors have investigated the partitioning behavior of selected elements between magnesiowüstite and perovskite at lower mantle pressures (30-50 Gpa), thus proving the observed partitioning behavior in the inclusions between enstatite and magnesiowüstite to be entirely consistant with equilibration in the lower mantle. These inclusions, therefore, can be used to assess the bulk composition of the lower mantle. Most significantly, Kesson and Fitz Gerald (op. cit.) conclude that these inclusions present no requirements for any profound compositional differences betwen the upper and lower mantle - i.e. the lower mantle must contain substantial depleted components.

5.5 Summary

1). There is now a general consensus that mantle melting occurs in response to adiabatic decompression and that melts erupted at the surface represent the pooled melts derived from a column of ascending mantle by varying degrees of partial melting over a range of pressures.

2). The composition of the resulting melts are controlled by, firstly, the pressure and temperature of melting (i.e. the degree of partial melting) and, secondly, the mantle source composition and mineralogy.

3). The actual melting process in operation is probably intermediate between the two theoretical end members - batch and fractional melting - although for the purpose of modelling non-modal batch melting can provide a reasonable approximation of the resultant *pooled* melt composition. The segregation and ascent of magma takes place by a process intermediate between homogeneous porous flow and channellised flow, thus allowing only *limited* interaction with the mantle through which it ascends.

4). The alkalic lavas of the Snaefell volcanic centre represent the pooled liquids from a melting column that extended down into the garnet stability field. Despite shallow level differentiation and open system processes, the intra-column variations that indicate varying extents of melting at different pressures - depths - in the melting column are still preserved in the erupted lava compositions.

5). The average extent of partial melting varied from 1 to 5%. This is, however, based on modelling which can only represent point-and-depth averages. Thus, in the actual melting column beneath Snaefell, the range is probably significantly greater.

6). The bulk composition of the mantle source region must be undepleted or slightly enriched, relative to estimates of bulk silicate Earth, to produce the observed range of trace element composition in the Snaefell volcanics..

7). There is considerable variation in isotopic and incompatible trace element composition in the Icelandic volcanics. These variations clearly correlate with differences in rock type and can best be explained by the existence of two distinct components in the source region and mixing between them or melts thereof. The alkalic volcanism is dominated by a fusible, enriched component, while the tholeiitic

and picritic volcanism shows a progressively greater contribution from a more refractory, depleted component.

8). Although many previous authors have suggested that the depleted component is derived from the local upper mantle, Pb isotope systematics (especially) would appear to preclude this. Rather, it appears that this component is an integral part of the plume itself.

9). The enriched component is thought to have its origins at the D'' layer (core-mantle boundary) and be dominantly composed of ancient, re-cycled oceanic crust, while the depleted component is proposed to be *lower* mantle material entrained by the plume on ascent.

10). The implication of this work is that all plumes are *heterogeneous*, but that only those which impinge on sufficiently thin lithosphere to allow extensive melting are likely to display it (this point is explored further in section 6.3). This is highlighted by the correlation of the depleted geochemical signature with Icelandic *picritic* lava compositions.

Chapter 6
Concluding Remarks

6.1 The evolution of the Snaefell volcano

6.1.1 Intentions

This chapter intends to draw together inferences from the rest of the thesis in order to outline the tectonomagmatic development of the Snaefell volcano. Its magmatic plumbing and the petrogenesis of its lavas are also reviewed. Subsequently, insights into the melting processes within the Icelandic mantle plume afforded by this study are presented, together with a model to explain the compositional variability of Icelandic mafic lavas in general. The unique position of the Iceland plume beneath an oceanic spreading centre makes it an ideal place to study plume magmas, because the plume material is allowed to decompress to shallow levels, attaining a higher degree of fusion than intraplate plumes. This situation permits sampling of more of the plume material, and the lack of lithospheric material above the plume means that there is no possibility of contamination (i.e. the magmas must be plume-derived, and not lithospheric melts). Other plumes are then reviewed, from the published literature, and it will be shown that variations in the compositions of their products can be seen to fit the "Iceland model" proposed in this thesis.

6.1.2 Snaefell, tectonics and volcanology

The Snaefell volcano is located in central-east Iceland, at the northern end of a short flank or lateral volcanic zone. This zone comprises three recognised volcanic centres: Oraefajokull which is still active, Esjufjoll which is possibly still active, and Snaefell, which is presumed extinct, although its activity is confined to the last 0.7-0.8 Ma by the Bruhnes magnetic signature of its products (Kristjansson et al. 1988). The lavas of Snaefell are mildly alkalic, ranging from hypersthene normative basalts to peralkaline (comenditic) rhyolites; thus bridging the gap between Jakobsson's (1979a) alkalic and transitional alkalic series. The Oraefajokull volcanics are similarly mildly alkalic and range from basalt to rhyolite (Prestvik 1985). This suggests that the tectonic setting of

the zone was similar to the present-day ERZ - a propagating rift. It appears then, that the zone represents a spreading centre, frozen in the early stages of development. Perhaps it was the result of a relatively small-scale failed rift-jump. Activity in the axial rift zone (ARZ) itself, NW of Snaefell, appears to have refocused westwards within the last 0.7Ma, with the rift-jump from the Fjallgardur volcanic centre to its present position. As suggested in chapter 1, this could be the result of a waning in plume activity, such as was tentatively suggested from the geochemical studies of Schilling et al. (1982) to account for the less enriched nature of younger lavas compared to the Tertiary ones. There is no further evidence for this, and this is indeed disputed by Hardason & Fitton (1994).

Snaefell itself forms an elongate, fissure-parallel stratovolcano reaching 1833m, typical of flank zone volcanoes (Saemundsson 1979). Its products unconformably overly the Plio-Pleistocene plateau basalts at 700-800m. The central mountain was built up by repeated eruptions from an established magma chamber, the products of which become highly evolved with the production of rhyolitic magmas towards the end of its lifetime. The surrounding hills are basaltic and monogenetic; the products of eruptions along the system's poorly developed fissure system. Little crustal accretion would have occurred as a result of this activity.

Although the onset of activity occurred during an interglacial period, with the production of two extensive subaerial lava flows, the bulk of its eruptions took place beneath the Upper-Pleistocene ice sheet. Hence most of its products belong to the lithologically complex *moberg* formation (described in detail in section 2.2). Morphologically, Snaefell resembles the table mountains of northern Iceland, with steep sides up to a plateau at ~1600m, then rising more gently to its summit. From this it is possible to estimate the thickness of the ice sheet; given the height of the plateau, this must have attained a maximum thickness of around 900m. Intercalations of red, oxidised cinder horizons indicate, however, that the ice sheet varied in thickness over time.

6.1.3 Conclusions from petrographic work

As is typical of Icelandic volcanics, the products of the Snaefell volcano are bimodal, lacking true intermediates. Petrographic examination confirms the hybrid nature of the few compositionally intermediate examples found. These are banded and streaky, with mixed phenocryst populations that include both plagioclase and alkali feldspar. Rounded partially resorbed phenocrysts are also present. Complex plagioclase xenocrysts are a ubiquitous feature of the series, showing oscillatory zoning, mantling,

dendritic growth zones and sieve textures, suggesting magma mixing played a key role in the evolution of the series (Hibbard 1981). This is in marked contrast with the ARZ lavas, which more often contain tabular, euhedral plagioclases (Meyer et al. 1985). It implies longer residence times in the magma chambers and longer time intervals between chamber replenishments in the flank zone volcanic systems such as Snaefell - as would be expected from their lower volcanic productivity. The compositional range seen in clinopyroxene echoes the bimodality, with a gap between Fs_{25} and Fs_{45}; the few intermediate examples were contained in markedly hybrid samples. The failure of the clinopyroxene compositional trend to culminate in aegirine (section 3.2.3), coupled with the complete lack of hydrous minerals, suggests that the magma was relatively dry. This conclusion is reinforced by the FeTi-oxide equilibria (section 3.2.4) which indicate a relatively low fO_2.

6.1.4 Petrogenesis

Magma chamber processes

Both the Snaefell suite and the topmost lavas of the underlying lava pile show few signs of alteration (section 4.1). Hence even mobile elements - such as Rb and K - are considered to show a magmatic distribution. Compositionally the Snaefell lavas form an enriched (in large ion lithophile elements) sodic alkalic series, in contrast to the less enriched tholeiitic basalts of the underlying lava pile. The basaltic members of the suite appear to have fractionated at ~3.5kb pressure prior to eruption. On a normative plot of diopside, hypersthene, olivine, nepheline and quartz, the bulk of the Snaefell lavas plot mid-way between the 1atm and 9kb cotectics, delineating an intermediate cotectic (section 4.3.3). This suggests that, as commonly occurs in the continental setting, the magma chamber lay at the crust-mantle boundary. This further contrasts with the magmatic plumbing in the ARZs, where seismic studies indicate that magma bodies exist at depths of ~3km (Brandsdottir 1994), i.e. the buoyant equilibrium depth of basaltic magmas in the Icelandic crust.

Geochemical studies indicate that the dominant compositional trends in the suite, from basalt to rhyolite, can be accounted for by the fractionation of the following mineral assemblages:

BASALT $\Rightarrow$ OL + PL + SP ($\pm$ CPX)† $\Rightarrow$ **Low-MgO BASALT** $\Rightarrow$ PL + OL + CPX $\Rightarrow$ **BASALTIC HAWAIITE** $\Rightarrow$ PL + MGT + OL + CPX $\Rightarrow$ **HAWAIITE** $\Rightarrow$ PL + MGT + CPX + AP $\Rightarrow$ **MUGEARITE** $\Rightarrow$ PL + CPX + MGT + AP $\Rightarrow$ **BENMOREITE** $\Rightarrow$ Na-rich PL + AF + CPX + OL + AP + (MGT) $\Rightarrow$ **TRACHYTE** $\Rightarrow$ **RHYOLITE.**

OL= olivine, PL= plagioclase, SP= Cr-spinel, CPX= clinopyroxene, MGT= magnetite, AP = apatite, AF = alkali feldspar.

† CPX is not observed as a phencryst in many basalts although, from the compositional trends, it was present in the crystallising assemblage of all but the most magnesian basalts. This lack of CPX phenocrysts is a common phenomenon in basaltic suites (section 4.3).

The section of the fractionation sequence from basalt through to hawaiite can be modelled using the computer program TRACE (Nielsen 1988), and the all of it can be qualitatively constrained using variation diagrams (sections 4.3.4 and 5). The final section is perhaps the most poorly constrained, due to the lack of true benmoreiites - and especially trachytes - in the eruptive products of the volcano. Most of the samples of basaltic hawaiite composition fall off the trends predicted by TRACE for simple crystal fractionation. This is most evident in the variation diagram for TiO_2, which shows a very disjointed trend. Basaltic hawaiite corresponds to a density maximum in the liquid line of descent, and these liquids would therefore pond at the base of the magma chamber. This reduces substantially their "eruptibilty" (Cattell 1989) because their eruption would result in extensive mixing with the overlying liquids, which may be either more primitive or more evolved. This appears to have occurred, both in this compositional range and between more and less evolved members of the suite. Magma mixing can also account for the linear compositional trends in the series. Additionally it reinforces the view that the magma chamber was strongly compostionally zoned. Much of the scatter in the geochemical data, and excessive enrichments in compatible trace elements, can be reconciled if the system was open and undergoing repeated tappings and fillings while continuously fractionating. Thus, the whole series could probably have been derived from a single parent magma type. This magmatic plumbing also means that the geochemical data cannot be inverted to uniquely define the magma chamber parameters without making sweeping assumptions, possibly invalidating any results obtained.

There appears to have been little or no crustal input to the suite, despite the common suggestion in the literature that Icelandic rhyolites are derived by partial melting of the crust around the long-lived magma chambers that typify central volcanoes (e.g. Krafla; Jonasson 1994). Isotope ratios (Nd, Pb, O) are consistent throughout the suite, and almost the entire range is encountered in the basalts. The Snaefell rhyolites thus appear cogenetic with the basalts, showing marked evidence for control by liquid-crystal equilibria in the system *ab-or-q*.

Magma genesis

The formation of Iceland's anomalously thick crust requires the presence of anomalously hot mantle, a "hot jet" or mantle plume. This was modelled by McKenzie & Bickle (1988) to be ~200°C hotter than ambient mantle (i.e. Tp ~1500°C), resulting in the mantle solidus being intersected at ~120km at the plume core. Beneath the ARZs, the thin crust permits the mantle to continue decompressing to within a few kilometres of the surface, resulting in up to 20% average melting. Moving off-axis, and away from the immediate vicinity of the plume centre, the melting column length will quickly shorten. The modelled thermal structure of plumes (Courtney & White 1986) indicates strong lateral temperature gradients. Thus the depth at which the upwelling mantle intersects its solidus will rapidly rise away from the immediate vicinity of the plume centre. Additionally, the increasing crust (and lithosphere) thickness with the age of the plate limits the level to which the mantle material can decompress off-axis. The plate thickness beneath Snaefell has been calculated at between 15 and 19km thick, using the equations of Fowler (1990). Subsequently, using the parameterisation of McKenzie & Bickle (1988), and taking VH10 (a basalt containing 11 wt% MgO) as the primary magma for the Snaefell suite (the merits of this are discussed in section (4.3.4), Tp was estimated at between 1340 and 1380°C. The composition of the parental basalt indicates that most of the melting occurred over the pressure range 1.5-2Gpa and that the mean extent of melting was 4-9%, which is reasonable for a low-silica alkalic basalt. These estimates, however, assume isobaric melting and therefore represent only a *point average*.

The variation in Na_2O, FeO*, SiO_2, TiO_2 contents of the basalts, when corrected for low pressure fractionation, suggests that melting beneath Snaefell occurred over a range of pressures and that mixing between melts from the various depths was incomplete. Some of the correlations were not either as clear as expected, or the reverse of those expected from published studies (Klein & Langmuir 1987). SiO_2 for instance appeared to *decrease* as the degree of fusion (F) increased, while in some melts TiO_2 appeared to *increase* with F. Nevertheless, recent experimental work on near-solidus melts and thermodynamic calculations (Baker et al. 1995), predicts exactly these trends under anhydrous conditions. That they are not seen in many oceanic alkalic suites is probably due to the role of volatiles (Kinzler & Langmuir 1995). Therefore the source of the Snaefell volcanic appears to have been unusually dry.

Trace elements can further constrain the mantle source, and the steep REE patterns of the Snaefell basalts indicate the presence of residual garnet: a feature that has survived magma extraction and potential mixing with shallower melts. Modelling (section 5.2.3), using non-modal batch melting equations (Shaw 1979) and mantle composition and distribution coefficients from Kostopoulos & James (1992), confirms

this. It suggests that the range of REE abundances can be accounted for by 1-5% melting of mantle varying from fertile garnet lherzolite to a 50:50 mixture of garnet and spinel lherzolite (i.e. the garnet-spinel transition zone). The bulk composition appears to be best modelled using the estimate of Bulk Silicate Earth given by Kostopoulos & James (1992). In summary, the erupted lava compositions appear to represent the pooled melts of a column of mantle extending down to ~80km, sampling melts in equilibrium with garnet lherzolite.

6.2 A model to explain the chemical variability in Icelandic mafic lavas

In comparison to the tholeiitic lavas of the ARZs, the alkalic basalts of the Snaefell volcano are volumetrically minor but can still afford significant insights into the melting processes within the Iceland plume. Comparisons have been confined to the mafic lavas to avoid, so far as possible, the complications introduced by magma chamber processes. The Snaefell basalts and other Icelandic alkalic basalts are poorer in SiO_2 and richer in Na_2O and incompatible elements than the ARZ tholeiites, reflecting the fact that they are derived from a lower degrees of partial melting of their mantle source. They display steeply dipping REE patterns, contrasting with the flat patterns of the axial tholeiitic basalts and convex-upwards ones of the picrites. While these differences may be explained by differing degrees of partial fusion, the isotopic characteristics require differences also in the sources of the various lava types. The alkalic lavas display the most restricted range, having high $^{87}Sr/^{86}Sr$ and $^{206}Pb/^{204}Pb$, and low $^{143}Nd/^{144}Nd$. The picrites show a larger range, extending to some partial overlap with the MORB isotopic field. The tholeiites are intermediate.

At first sight, the simplest explanation for these variations is that depleted local upper mantle (MORB source) has somehow become incorporated into the plume. It can be argued that the undepleted plume material is more fusible and thus melts first to form the alkalic basalts. At higher degrees of melting the early enriched liquids become progressively diluted with melts from the more refractory depleted material. This line of reasoning, however, does not follow when $^{207}Pb/^{204}Pb$ and $^{208}Pb/^{204}Pb$ are considered. The Iceland data form a separate field from North Atlantic N-MORB, suggesting that the depleted component *is an integral part of the plume*. As discussed in chapter 5, the most plausible potential source of this is the lower mantle; implying that this, too, is depleted. Thus, on arrival at the base of the plate the plume is heterogeneous, comprising streaks of enriched material derived from the D" layer (the ultimate origins of which are discussed in section 5.4), set in a more depleted matrix of

material entrained in the lower part of the mantle as the plume rose, and with a further carapace of this material dragged up by viscous coupling (cf. Hauri et al. 1994).

Figure 6.1 shows a cartoon illustrating the melting processes that are envisaged to result as the plume material decompresses.

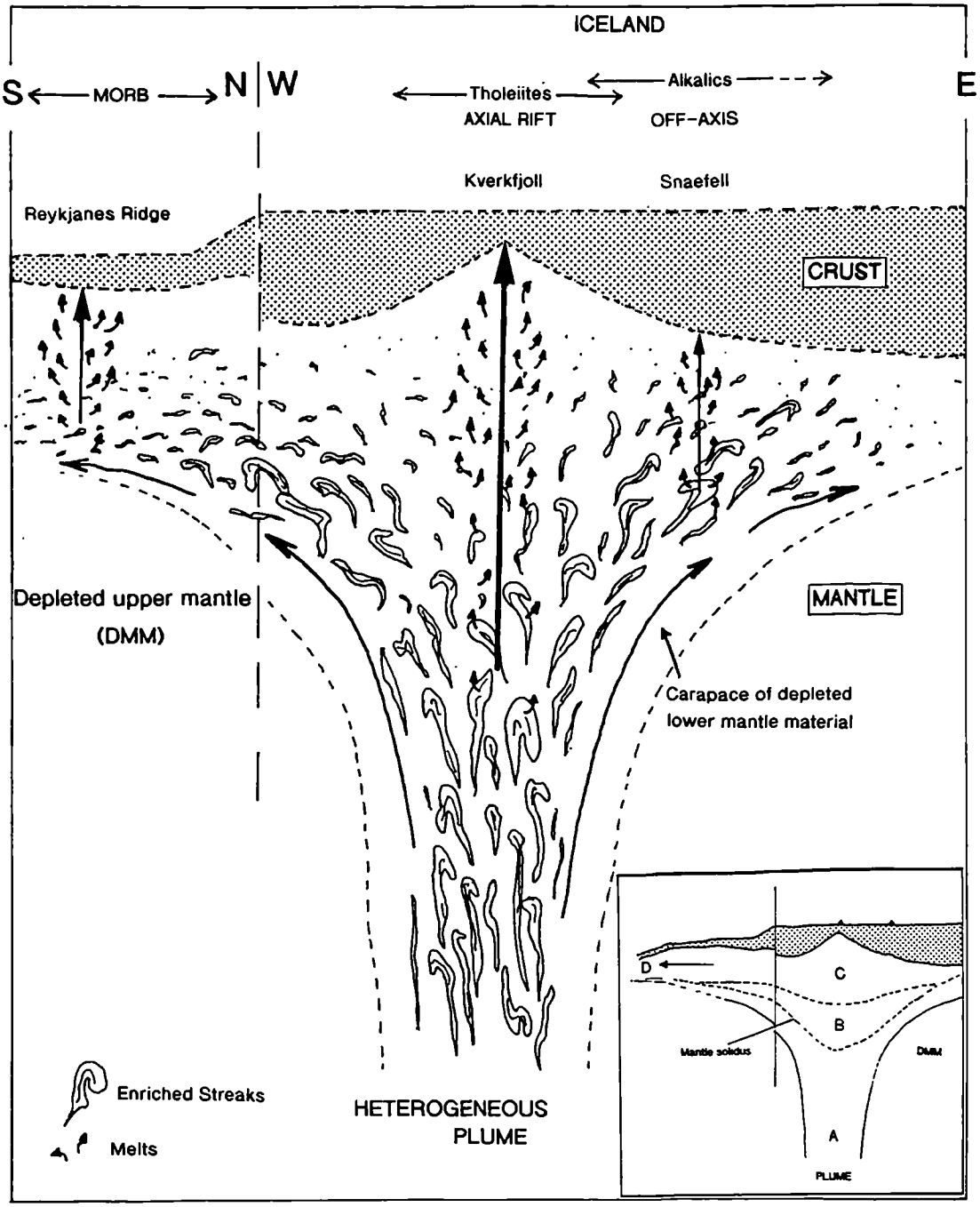

Figure 6.1. Cartoon of the heterogeneous plume proposed in this study. This shows the melting processes, whereby the enriched streaks contribute most to the early, deep melts and the melts erupted at the plume periphery, while the entrained lower mantle material (matrix and carapace dragged up with the plume by viscous coupling) melts later, at shallower levels. Melting columns are indicated by arrows; the thickness of each is proportional to the mean extent of melting achieved. Inset shows the zones in which the different melting regimes operate, as discussed in text.

In zone A (see inset, figure 6.1) the plume mantle has yet to intersect its solidus. In zone B, just the fusible enriched streaks are melting - if these melts were erupted they should be enriched and alkalic. In zone C most of the enriched streaks have already been consumed and the refractory matrix is now undergoing wholesale melting. Zone D underlies the Reykjanes ridge, where the geochemistry of the lavas is clear testimony to the fact that part of the plume flux leaks sideways within the uppermost convecting mantle. The north-south gradients observed (Sun et al. 1975, Schilling et al. 1983) may, to some extent, reflect systematic extraction by subaxial decompression melting of the remaining fusible enriched streaks as the plume mantle flows south. Presumably some of the peripheral mantle upwelling within Iceland evades decompression melting and may escape into the convecting mantle, making it geochemically streaky. Then this model could equally well apply to the axial MORB and flanking OIB seamounts at 9-14°N on the East Pacific Rise (Zindler et al. 1984). This model presented above, relating the varied lava types within Iceland and along the Mid-Atlantic ridge to the south (and north) requires no great shift from accepted plume theory, and therefore could reconcile observations of "anomalous" characteristics in the composition of some hotspot lavas, as discussed below.

6.3 "Anomalous" plume magmas reconciled

6.3.1 Manifestations of plume heterogeneity

Of particular significance in the arguments above is the correlation of the depleted (MORB-like) signature in the Icelandic mafic lavas with the picritic compositions - the highest degrees of melting. It has been accepted for some time that plumes in the oceanic realm generally give rise to geochemically enriched lavas (e.g. Zindler & Hart 1986, Weaver 1991). While this may be true of weaker plumes, and plumes that impinge on thick lithosphere (e.g. Cape Verde, Reunion, Canaries and St. Helena), plumes which impinge on the lithosphere at or near a spreading centre, or beneath a pre-existing thinspot (Thompson & Gibson 1991) produce more voluminous melts of more varied compositions, including *MORB-like* ones. Examples of this are briefly reviewed below and can be shown to fit the proposed Iceland model.

The Galapagos hotspot and Gorgona

The Galapagos archipelago has long been cited as an example of plume volcanism. A number of features, however, conflict with the accepted plume model. The chemistry of the lavas seems to require two source components, with the most depleted trace element and isotopic signatures found in lavas at the centre of the archipelago. These are in some cases indistinguishable from MORB (Geist et al. 1988, Geist 1992). This plume impinges on young and relatively thin lithosphere, close to a spreading centre, where the effects of plume - upper mantle mixing can be clearly seen in the chemistry of the lavas (Geist et al. 1988). If the chemical variations within the archipelago itself were simply due to such mixing, then the most depleted lavas would perhaps be expected at the peripheries. What is actually observed is perhaps better explained by the Iceland model.

Gorgona Island is known for its unique Cretaceous komatiititic lavas, which result from very high degrees of melting (≥20%), possibly during the initial activity of the Galapagos plume within a pre-existing ocean basin (Hill 1993). The komatiites are spatially associated with tholeiitic lavas, although they have distinctive trace element and isotope signatures (Dupre & Echeverria 1984, Aitken & Echeverria 1984). The komatiites are very depleted in terms of trace elements, with Sr, Nd and $^{6/4}$Pb isotope ratios within the MORB field, while the tholeiites vary from almost indistinguishable in terms of trace elements from N-MORB to more enriched ones which are comparable with the Icelandic tholeiites. These chemical features can be explained by mixing between two distinct source components as in the Iceland model. The small size of the island (8 x 2.5 km) suggests a small scale of mantle heterogeneity. It has also been suggested that the very depleted komatiites are the result of a second-stage of melting of the mantle source region (Aitken & Echeverria 1984), as suggested in this thesis as a possible mechanism of formation of the Icelandic picrites.

The Marquesas hotspot

The lavas show compositions which are thought to reflect the mixing of two chemically distinct sources. The tholeiites could be derived from MORB-source mantle, were it not for their radiogenic Pb, while the peripheral alkalic lavas require a more enriched source (Desonie et al. 1993). This suggests involvement of FOZO - lower mantle (Hart et al. 1992). It is significant that the Marquesas archipelago lies on a region of thinner-than-normal lithosphere, termed the South Pacific isotopic and thermal anomaly [SOPITA] (McNutt & Judge 1990).

Hawaii

Most of the lavas erupted on Hawaii show enriched trace element signatures and radiogenic isotope ratios exactly as expected. Nevertheless, various authors have noted that, despite their origin in a hot mantle plume, a significant number of Hawaiian basalts appear to have been derived from a relatively depleted source region (e.g. Stille et al. 1986). These authors account for the depletion in terms of plume-upper mantle interaction. In the light of this study, an explanation in terms of plume heterogeneity seems more plausible.

The Iceland plume over time

It would appear that this heterogeneity is not a transient feature, and this can be demonstrated by looking at the products of the Iceland plume over the last ~64Ma (Kerr & Hards submitted). This appears to have contained a depleted component throughout its history. Many of the early Tertiary picrites erupted in West Greenland and Baffin Bay are both elementally and isotopically depleted (Holm et al. 1993). Because of rifting between west Greenland and Labrador in the late Cretaceous, the lithosphere was significantly thinned towards SW Greenland by 64Ma (Hill 1991). This allowed the plume to upwell to shallow levels, hence generate the abundant picrites. In addition, Gariepy et al. (1983) have proposed the source region of the Faeroese lavas to have contained a depleted mantle component, in the light of trace element and isotopic studies.

In all cases the explanation proposed in published accounts is that the source of the depleted component was upper mantle material somehow incorporated into the top of the plume. Figure 6.2a shows a plot of $^{207}Pb/^{204}Pb$ vs $^{208}Pb/^{204}Pb$ showing data fields for Iceland, North Atlantic N-MORB, and the North Atlantic Tertiary Igneous Province (NATIP). This diagram militates strongly against any significant contribution of a MORB component to Icelandic magmas, and likewise to most of the NATIP lavas. As would be expected from lavas that have passed through continental lithosphere, their Pb isotope ratios have been significantly modified and most of the samples lie along a linear mixing array, trending from the Icelandic array towards less radiogenic values characteristic of Archean crust in the North Atlantic area (Kerr et al. 1995b). Some MORB source input to some of the NE Greenland lavas from Hold With Hope cannot, however, be ruled out. This possibility can, however, be eliminated using a plot of $^{143}Nd/^{144}Nd$ vs $^{206}Pb/^{204}Pb$, figure 6.2b. In this the NE Greenland lavas appear simply to lie on a mixing line between the Icelandic lavas and a low $^{143}Nd/^{144}Nd$ component, probably derived from the lower lithosphere (Thirwall et al. 1994). It appears therefore, that the model presented in this thesis to reconcile the

trace element and isotopic differences between the various Icelandic lava types, can also reconcile the apparent anomalies in the products of the plume during its ~64Ma history.

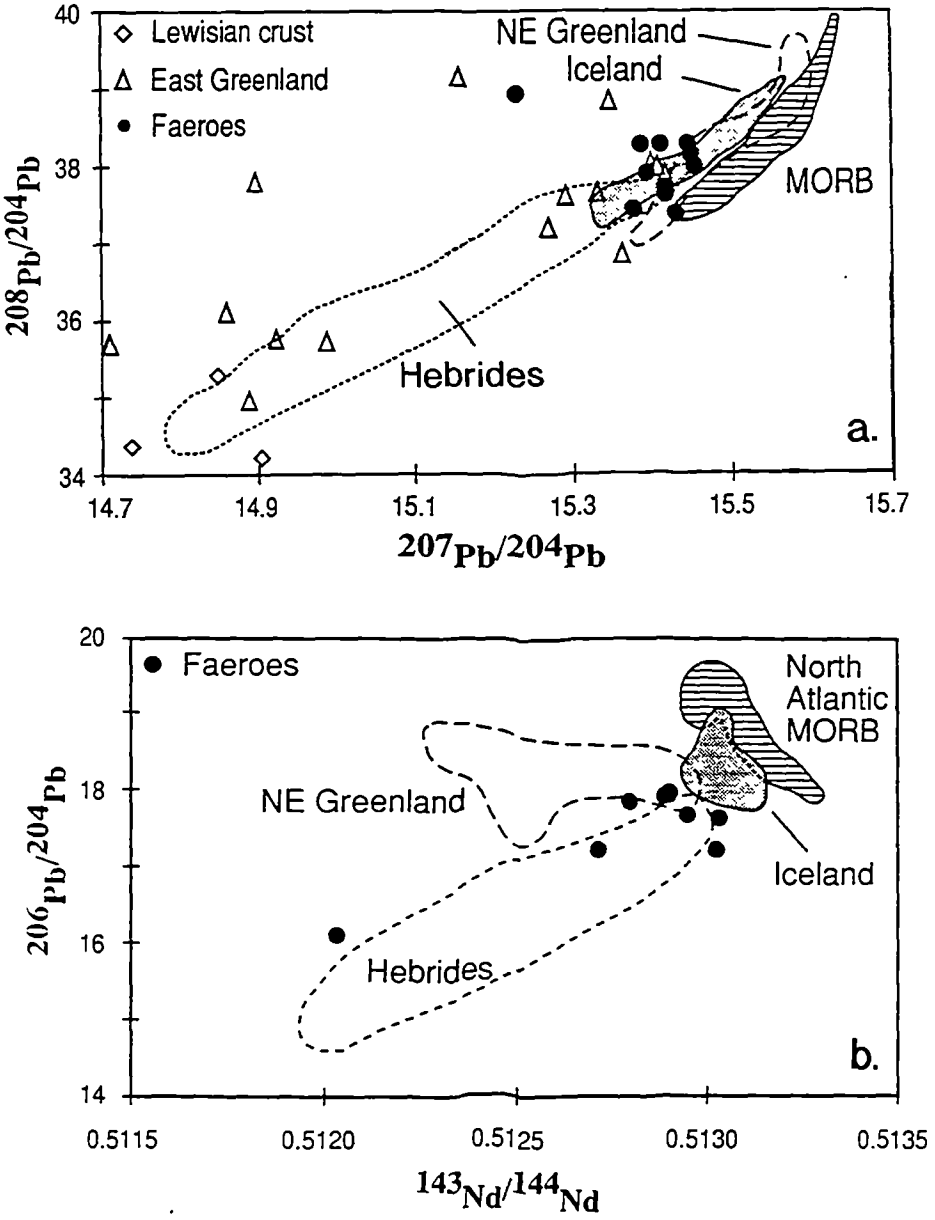

Figure 6.2.
.(a). Plot of $^{208}Pb/^{204}Pb$ vs $^{207}Pb/^{204}Pb$ showing basalts from the North Atlantic Province and North Atlantic MORB. (Modified from Kerr & Hards submitted.)
(b). Plot of $^{206}Pb/^{204}Pb$ vs $^{143}Nd/^{144}Nd$ showing basalts from the North Atlantic Province and North Atlantic MORB. (From Kerr & Hards submitted.)
Data for the NATIP are taken from Dickin (1981), Gariepy et al. (1983), Dickin et al. (1987), Holm et al. (1988), Thirwall et al. (1994) and Kerr et al.(1995a). Data sources for Iceland and North Atlantic MORB are given in Hards et al. (1995).

6.3.2 An updated view of "FOZO"

When the composition of FOZO - proposed to represent the lower mantle - was defined (Hart et al. 1992), plumes producing lavas thought of as MORB-like were evidently not included. Hauri et al. (1994) cite Iceland and the Galapagos as showing a distinct MORB component in Sr-Nd-$^{6/4}$Pb space. The model presented above proposes a fourth (depleted) component in mantle plumes, in addition to the three accepted enriched ones (Weaver 1991). It is the opinion of the present author that, if it is the depleted component that is of interest, surely plumes which undergo the highest degrees of decompression melting are those that sample it best and would therefore be the best place to study it. With such data, the gap between MORB and FOZO, in Sr-Nd-$^{6/4}$Pb space, would merge and more isotopic "dimensions" would be required to separate the two.

6.4 Possible future work

6.4.1 Snaefell

- Detailed unit-by-unit mapping at Snaefell still remains to be attempted. Given the shallow level of erosion and heavy scree cover on most of the area, this would be an arduous task.

- No attempt was made in this study to establish any stratigraphy. Snaefell is an example of *"heap geology"*, but some stratigraphic constraints may lead to a better understanding of the centre's evolution. It could be that melting processes in operation beneath the centre changed over time.

- Finally, the centre remains to be dated, at present all that is known of its lifespan is that it was active <0.7Ma.

6.4.2 Iceland

- Despite the massive amount of analytical work done on Icelandic rocks, there is still a woeful lack of a really comprehensive elemental and isotopic database. Thus geochemical models, such as proposed in this study, cannot really be fully tested and evaluated. As already mentioned, the ridge-centred position is the ideal place to study *all* of the plume components.

- Additional insights could be gained from looking at further isotopic systems. For instance $^{176}Hf/^{177}Hf$ might especially aid the characterisation of the non-MORB depleted mantle component detected in Icelandic volcanics which currently hinges on $^{207}Pb/^{204}Pb$ and $^{208}Pb/^{204}Pb$. In OIBs, Hf isotopes correlate with Nd, and the enriched OIB components have now been characterised in terms of Hf-isotopic ratios (Salters & Hart 1991). These authors have also observed that in MORBs the Hf-Nd correlation appears to break down, and the variation in Hf isotope ratios is much greater than would be expected from the OIB array. In the second of the two models proposed to account for this, Salters & Hart (op. cit.) suggest that the MORB source mantle underwent initial depletion in the garnet stability field, and has subsequently been contaminated with high $^{176}Hf/^{177}Hf$ material. This, in the model proposed in this thesis, could be material derived from plumes, this was indistinguishable from depleted MORB source in terms of Nd isotope ratios.

- Further Os isotope analysis could, in turn, help characterise the depleted component. Subsequently, such data might possibly be used to determine the origins of the enriched component and the proportion of the source of the various Icelandic volcanic suites that it constitutes (Roy-Barman & Allegre 1995).

References cited

Ahern, J. L. & Turcotte, D. L. 1979. Magma migration beneath an ocean ridge. *Earth and Planetary Science Letters,* **45,** 115-122.

Aitkin, B. G. & Echeverria, L. M. 1984. Petrology and geochemistry of komatiites and tholeiites from Gorgona island, Colombia. *Contributions to Mineralogy and Petrology,* **86,** 94-105.

Allen, C. C. 1980. Icelandic subglacial volcanism; thermal and physical studies. *Journal of Geology,* **88,** 108-117.

Anderson, A. T. 1976. Magma mixing: petrological process and volcanological tool. *Journal of Volcanology and Geothermal Research,* **1,** 3-33.

Anderson, D. L. 1994. Komatiites and picrites: evidence that the plume source is depleted. *Earth and Planetary Science Letters,* **128,** 303-311.

Baker, M. B. & Stolper, E. M. 1994. Determining the composition of high pressure mantle melts using diamond aggregates. *Geochimica et Cosmochimica Acta,* **58,** 2,811-2,827.

Baker, M. B., Hirschmann, M. M., Ghiorso, M. S. & Stolper, E. M. 1995. Compositions of near-solidus peridotite melts from experiments and thermodynamic calculations. *Nature,* **375,** 308-311.

Basaltic Volcanism Study Project. 1981. Basaltic volcanism on terrestrial planets. *Pergamon Press, 1286pp.*

Beard, J. S. & Lofgren, G. E. 1991. Dehydration melting and water-saturated melting of basaltic and andesitic greenstones and amphibolites. *Journal of Petrology,* **32,** 365-401.

Beblo, M. & Bjornsson, A. 1978. Magnetotelluric investigation of the lower crust and upper mantle beneath Iceland. *Journal of Geophysics,* **45.** 1-16.

Beblo, M. & Bjornsson, A. 1980. A model of electrical resistivity beneath NE Iceland, correlation with temperature. *Journal of Geophysics,* **47,** 184-190.

Beblo, M., Bjornsson, A., Arnaso, K., Stein, B. & Wolfgram, P. 1983. Electrical Conductivity beneath Iceland - constraints imposed by magnetotelluric results on temperature, partial melt, crust- and mantle-structure. *Journal of Geophysics,* **53,** 16-23.

Biggar, G. M. & Clarke, D. B. 1976. Reaction rate of xenocrysts in synthetic basalt melts. *In NERC Progress in experimental petrology, Series D,* **6,** 227-230.

Bjarnsson, I.T., Menke, W., Flovenz, O. G. & Caress, D. 1993. Tomographic image of the mid-Atlantic plate boundary in SW Iceland. *Journal of Geophysical Research,* **98,** 6,607-6,622.

Bjornsson, A. 1985. Dynamics of crustal rifting in NE Iceland. *Journal of Geophysical Research,* **90,** 10,151-10,162.

Bjornsson, H. & Einarsson, P. 1990. Volcanoes beneath Vatnajokull, Iceland: evidence from radio echo-sounding, earthquakes and jokulhlaups. *Jokull,* **40,** 147-167.

Blake, S. 1981. Eruptions from zoned magma chambers. *Journal of the Geological Society of London,* **138,** 281-287.

Borthwick, J. & Harmon, R. S. 1982. A note regarding ClF3 as an alternative to BrF_5 for oxygen isotope analysis. *Geochemica et Cosmochimica Acta,* **46,** 1665-1668.

Bott, M. H. P. 1988. A new look at the causes and consequences of the Iceland hotspot. *In,* Morton, A. C. & Parson, L. M. (eds.), *Early Tertiary volcanism and the opening of the NE Atlantic,* Geological Society Special Publication, **39,** 15-23.

Brandsdottir, B. 1994. The crustal magma chambers at Katla, Krafla and Askja, Iceland. *Arthur Holmes European Research Conference, The Icelandic plume and its influence on the evolution of the NE Atlantic, Reykjavik, Iceland, 4-8 July 1994, abstract volume,* 10.

Brooks, C. K. 1976. The Fe_2O_3/FeO ratio of basalt analyses: an appeal for a standardized procedure. *Bulletin of the Geological Society of Denmark,* **25,** 117-120.

Bryan, W. B. 1983. Systematics of modal phenocryst assemblages in submarine basalts: Petrological implications. *Contributions to Mineralogy and Petrology,* **83,** 62-74.

Buddington, A. F. & Lindsley, D. H. 1964. Iron-titanium oxide minerals and synthetic equivalents. *Journal of Petrology,* **5,** 310-357.

Bunsen, R. 1847. Beitrag zur kenntnis des islandischen tuffgebirges. *Annal. Chem. Pharm.* **61,** 265-279.

Campbell, I. H. & Griffiths, R. W. 1992. The changing nature of mantle hotspots through time: implications for the chemical evolution of the mantle. *Journal of Geology,* **92,** 497-523.

Campbell, I. H. & Turner, J. S. 1987. A laboratory investigation of assimilation at the top of a basaltic magma chamber. *Journal of Geology,* **95,** 155-172.

Carlise, D. 1963. Pillow breccias and their aquagenetuffs, Quadra Island, British Columbia. *Journal of Geology,* **71,** 48-71.

Carmichael, I. S. E. 1964. The petrology of Thingmuli, a Tertiary volcano in E Iceland. *Journal of Petrology,* **5,** 435-460.

Carmichael, I. S. E. 1967. The mineralogy of Thingmuli, a Tertiary volcano in eastern Iceland. *American Mineralogist,* **52,** 1815-1841.

Carmichael, I. S. E & Nicholls, J. 1967. Iron-Titanium Oxides and Oxygen Fugacities in Volcanic Rocks. *Journal of Geophysical Research,* **72,** 4665-87

Carr, J. M. 1954. Zoned plagioclases in the layered gabbros of the Skaergaard intrusion, East Greenland. *Mineralogical Magazine,* **30,** 367-375.

Cattell, A. C. 1989. The Skye Main Lava Series: liquid density and the absence of basaltic hawaiites. *Geological Magazine,* **126,** 681-684.

Cas, R. A. F. & Wright, J. V. 1987. Volcanic successions modern and ancient. *Chapman & Hall, 528pp.*

Chaffey, D. J., Cliff, R. A. & Wilson B. M. 1989. Characterisation of the St. Helena magma source. *In* Saunders, A. D., & Norry, M. J. (eds.) *Magmatism in ocean basins.* Geological Socirty Special Publication, **42,** 257-276.

Christie, D. M., Carmichael, I. S. E. & Langmuir, C. H. 1986. Oxidation states of mid-ocean ridge basalts. *Earth and Planetary Science Letters,* **79,** 397-411.

Clayton, R. N. & Mayeda, T. K. 1963. The use of bromine pentafluoride in the extraction of oxygen from oxides and silicates for isotopic analysis. *Geochimica, et Cosmochimica Acta,* **27,** 43-52.

Condomines, M., Gronvold, K., Hooker, P. J., Muehlenbachs, K., O'Nions, R. K., Oskarsson, N. & Oxburgh, E. R. 1983, He, O, Sr and Nd isotopic relationships in Icelandic volcanics. *Earth and Planetary Science Letters,* **66,** 125-136.

Condomines, M., Hemond, C. & Allegre, C. J. 1988. U-Th-Ra disequilibria and magmatic processes. *Earth and Planetary Science Letters,* **90,** 243-262.

Courtney, R. C. & White, R. S. 1986. Anomalous heat flow and geoid across the Cape Verde rise: evidence for dynamic support from a thermal plume in the mantle. *Geophysical Journal of the Royal Astronomical Society,* **87,** 815-867.

Cox, K. G. 1980. A model for flood basalt volcanism. *Journal of Petrology,* **21,** 629-650.

Cox, K. G., Bell, J. D. & Pankhurst, R. J. 1979. The interpretation of the igneous rocks. *Unwin Hyman, 450pp.*

Daux, V., Crovisier, J.L., Hemond, C. & Petit, J. C. 1994. Geochemical evolution of basaltic rocks subjected to weathering; fate of major elements, rare-earth elements, and thorium. *Geochimica et Cosmochimica Acta,* **58,** 4,941-4,954.

Deer, W. A., Howie, R. A. & Zussman, J. 1992. An Introduction to The Rock-Forming Minerals. 2nd Edition. *Longman Scientific & Technical 696pp.*

DePaolo, D. J. 1981. Trace element and isotopic effects of combined wall rock assimilation and fractional crystallisation. *Earth and Planetary Science Letters,* **53,** 189-202.

Desonie, D. L., Duncan, R. A. & Natland, J. H. 1993. Temporal and geochemical variability of volcanic products of the Marquesas hotspot. *Journal of Geophysical Research,* **98,** 17,469-17,665.

Devey, C. W., Albarede, F., Cheminee, J.-L., Michard, A., Muhe, R. & Stoffers, P. 1990. Active submarine volcanism on the Society Hotspot swell (west Pacific): a geochemical study. *Journal of Geophysical Research,* **95,** 5,049-5,066.

Dickin, A. P. 1981. Isotope geochemistry of Tertiary igneous rocks from the Isle of Skye, NW Scotland. *Journal of Petrology*, **22**, 155-189.

Dickin, A. P., Jones, N. W., Thirwall, M. F. & Thompson, R. N. 1987. A Ce/Nd isotope study of crustal contamination processes affecting Palaeocene magmas in Skye, NW Scotland. *Contributions to Mineralogy and Petrology*, **96**, 455-464.

Drever, H. I. & Johnston, R. 1957. Crystal growth of fosteritic olivine in magmas and melts. *Transactions of the Royal Society of Edinburgh*, **63,2**, 289-314.

Droop, G. T. P. 1987. A general equation for estimating Fe^{3+} concentrations in ferromagnesian silicates and oxides from microprobe analyses using stoichiometric criteria. *Mineralogical Magazine*, **51**, 431-435,

Dowty, E. 1980. Synneusis reconsidered. *Contributions to Mineralogy and Petrology*, **74**, 75-84.

Dupre, B. & Echeverria, L. M. 1984. Pb isotopes of Gorgona island (Colombia): isotopic variations correlated with magma type. *Earth and Planetary Science Letters*, **67**, 186-190.

Eggins, S. M. 1992. Petrogenesis of Hawaiian tholeiites: 2, aspects of dynamic melt segregation. *Contributions to Mineralogy and Petrology*, **110**, 398-410.

Einarsson, P. 1991. Earthquakes and present-day tectonism in Iceland. *Tectonophysics*, **189**, 261 - 279.

Eldholm, O. & Grue, K. 1994. North Atlantic Volcanic margins; dimensions and production rate. *Journal of Geophysical Research*, **99**, 2,955-2,968.

Ellam, R. M. 1992. Lithospheric thickness as a control on basalt geochemistry. *Geology*, **20**, 153-156.

Elliott, T. R. 1991. Element fractionation in the petrogenesis of ocean island basalts. *Unpublished Ph.D thesis, The Open University.*

Elliott, T. R., Hawkesworth, C. J. & Gronvold, K. 1991. Dynamic melting of the Iceland plume. *Nature*, **351**, 201-206.

Elthon, D. 1992. Chemical trends in abyssal peridotites: refertilisation of depleted suboceanic mantle. *Journal of Geophysical Research,* **97,** 9,015-9,025.

Falloon, T. J., Green, D. H., Hatton, C. J. & Harris, K. L. 1988. Anhydrous partial melting of a fertile and depleted peridotite from 2 to 30kb and application to basalt petrogenesis. *Journal of Petrology,* **29,** 1,257-1,282.

Faure, G. 1986. Principles of isotope geology. *John Wiley & Sons Incs. 589pp.*

Fisher, R. V. & Schminke, H.-U. 1984. Pyroclastic rocks. *Springer-Verlag, 472pp.*

Flovenz, O. G. & Gunnarsson, K. 1991. Seismic crustal structure in Iceland and the surrounding area. *Tectonophysics,* **189,** 1-17.

Foulger, G. & Long, R. E. 1984. Anomalous focal mechanisms: tensile crack formation on an accreting plate boundary. *Nature,* **310,** 43-45.

Foulger, G. R., Beutler, G., Bilham, R., Einarsson, P., Fankhauser, S., Gurter, W., Hugentobler, U., Morgan, W. J., Rothacher, M., Thorbergsson, G. & Wild, U. 1993. The Iceland GPS geodetic survey: tectonic goals and data processing results. *Bulletin Geodesique,* **67,** 148-172.

Fowler, C. M. R. 1990. The solid earth, an introduction to global geophysics. *Cambridge University Press, 472pp.*

Furman, T., Frey, F. A. & Park, K.-H. 1991. Chemical constraints on the petrogenesis of mildly alkaline lavas from Vestmannaeyjar, Iceland: the Eldfell (1973) and Surtsey (1963-1967) eruptions. *Contributions to Mineralogy and Petrology,* **109,** 19-37.

Furman, T., Frey, F. A. & Meyer, P. S. 1992. Petrogenesis of evolved basalts and rhyolites at Austurhorn, Southeast Iceland: the role of fractional crystalisation. *Journal of Petrology,* **33,** 1405-1445.

Furnes, H. 1978. Element mobility during palagonitization of a subglacial hyaloclastite in Iceland. *Chemical Geology,* **22,** 249-264.

Furnes, H. 1984. Chemical changes during progressive subaerial palagonitisation of a subglacial olivine tholeiite hyaloclastite: a microprobe study. *Chemical Geology,* **43,** 271-285.

Furnes, H., Fridleifsson, I. B. & Atkins, F. B. 1980. Subglacial volcanics - on the formation of acid hyaloclastites. *Journal of Volcanology and Geothermal Research,* **8,** 95-110.

Garcia, M. O., Jorgenson, B., Mahoney, J. J., Ito, E. & Irving, A. J. 1993. An evaluation of temporal geochemical evolution of Loihi summit lavas: results from *Alvin* submersible dives. *Journal of Geophysical Research,* **98,** 537-550.

Gariepy, C., Ludden, J. & Brooks, C. 1983. Isotopic and trace element constraints on the genesis of the Faeroe lava pile. *Earth and Planetary Science Letters,* **63,** 257-272.

Geist, D. J. 1992. An appraisal of melting processes and the Galapagos hotpot: major- and trace-element evidence. *Journal of Volcanology and Geothermal Research,* **52,** 65-82.

Geist, D. J., White, W. M. & McBirney, A. R. 1988. Plume-asthenosphere mixing beneath the Galapagos archipelago. *Nature,* **333,** 657-660.

Gibb, F. G. F. 1973. The zoned clinopyroxenes of the Shiant Isles Sill, Scotland. *Journal of Petrology,* **14,** 203-230.

Gill, R. C. O., Pedersen, A. K. & Larsen, J. G. 1992. Tertiary picrites in West Greenland: melting at the periphery of a plume? *In* Story, B. C., Alabaster, T. & Pankhurst, R. J. (eds.) *Magmatism and continental break-up,* Geological Socirty Special publication, **68,** 335-348.

Govindaraju, K. 1989. Compilation of working values and sample description for *272 geostandards. Geostandards Newsletter,* **XII, Special Issue.**

Grasset, O. & Albarede, F. 1994. Hybridisation of mingling magmas with different densities. *Earth and Planetary Science Letters,* **121,** 327-332.

Gribble, C. D. & Hall, A. J. 1985. A practical introduction to optical mineralogy. *George Allen & Unwin, 249pp.*

Griffiths, R. W. & Campbell, I. H. 1990. Stirring and structure in mantle starting plumes. *Earth and Planetary Science Letters,* **99,** 66-78.

Grutter, H. S. 1994. Spinel-garnet-carbon phase relations in coarse Kaapvaal-type peridotites and implications for garnet-orthopyroxene equlibration. *International Symposium on the physics and chemistry of the upper mantle, Sao Paulo, Brazil, 14-19 August, Extended abstracts* 5-7.

Gudmundsson, A. 1986. Formation of crustal magma chambers in Iceland. *Geology*, **14**, 164-166.

Gudmundsson, A. 1995. Infrastructure and mechanics of volcanic systems in Iceland. *Journal of Volcanology and Geothermal Research*, **64**, 1-22.

Gustafsson, L. E., Lapp, B., Thomas, L. & Lapp, M. 1989. Tertiary silicic rocks in the area of the Kaekjuskord rhyolitic volcano, eastern Iceland. *Jokull*, **39**, 75-89.

Hardarson, B. & Fitton, J. G. 1994. Geochemical variations in the Tertiary basalts of Iceland. *Mineralogical Magazine*, **58A**, 372-373.

Hards, V. L., Kempton, P. D. & Thompson, R. N. 1995. The heterogeneous Iceland plume: new insights from the alkali basalts from the Snaefell volcanic centre. *Journal of the Geological Society, London* **152**, in press.

Hart, S. R., Hauri, E. H. Oschmann, L. A. & Whitehead, J. A. 1992. Mantle plumes and entrainment: isotopic evidence. *Science*, **256**, 517-520.

Hattori, K. & Muehlenbachs, K. 1982. Oxygen isotope ratios of the Icelandic crust. *Journal of Geophysical Research*, **87**, 6,559-6,565.

Hauri, E. H. & Hart, S. R. 1994. Constraints on melt migration from mantle plumes: a trace element study of peridotite xenoliths from Savai'i, western Samoa. *Journal of Geophysical Research*, **99**, 24,301-24,321.

Hauri, E. H., Whitehead, J. A. & Hart, S. R. 1994. Fluid dynamic and geochemical aspects of entrainment in mantle plumes. *Journal of Geophysical Research*, **99**, 24,275-24,300.

Hawkesworth, C. J. & Morrison, M. A. 1978. A reduction in $^{87}Sr/^{86}Sr$ during basalt altertation. *Nature*, **276**, 381-383.

Helgason, J. 1984. Frequent shifts of the volcanic zones in Iceland. *Geology*, **12**, 212-216.

Helgason, J. 1985. Shifts of the plate boundary in Iceland: some aspects of Tertiary volcanism. *Journal of Geophysical Research*, **90**, 10084-10092.

Helz, R. T. 1980. Chemical and experimental study of the Ice Harbour member of the Yakima basalt subgroup: evidence for intracrust storage and contamination. *EOS, Transactions of the American Geophysical union,* **61,** 68.

Hemond, C., Condomines, M., Fourcade, S., Allegre, C. J., Oskarsson, N. & Javoy, M. 1988. Th, Sr and O isotopic geochemistry in recent tholeiites from Iceland: crustal influence on mantle-derived magmas. *Earth and Planetary Science Letters,* **87,** 273-285.

Hemond, C., Arndt, N. T., Lichtenstein, U., Hofmann, A. W., Oskarsson, N. & Steinthorsson, S. 1993. The heterogeneous Iceland plume: Nd-Sr-O isotopes and trace element constraints. *Journal of Geophysical Research,* **98,** 15,833-15,850.

Henderson, P. 1982. Inorganic Geochemistry. *Pergamon Press. 353pp.*

Hertzberg, C. T. & Chapman, N. A. 1976. Clinopyroxene geothermometry of spinel lherzolites. *The American Mineralogist,* **61,** 626-637.

Hess, P. C. 1992. Phase equilibria constraints on the origin of ocean floor basalts, *In* Mantle flow and melt generation at mid-ocean ridges. *In;* Morgan, J. P., Blackman, D. K. & Sinton, J. M. (eds.) *Mantle Flow and melt generation at mid-ocean ridges,* American Geophysical Union, Geophysical Monograph, **71,** 67-102.

Hibbard, M. J., 1981. The magma mixing origin of mantled feldspars. *Contributions to Mineralogy and Petrology,* **76,** 158-170.

Hill, R. I. 1991. Starting plumes and continental break-up. *Earth and Planetary Science Letters,* **104,** 398-416.

Hill, R. I. 1993. Mantle plumes and continental tectonics. *Lithos,* **30.** 193-206.

Hofmann, A. W. & White, W. M. 1982. Mantle plumes from ancient oceanic crust. *Earth and Planetary Science Letters,* **57,** 421-436.

Holm, P. M. 1988. Nd, Sr and Pb isotope geochemistry of the lower lavas, E Greenland Tertiary Igneous Province. *In:* Morton, A. C. & Parson, L. M. (eds.), *Early Tertiary volcanism and the opening of the NE Atlantic,* Geological Society Special Publication, **39,** 181-195.

Holm, P. M., Gill, R. C. O., Pederson, A. K., Larsen, J. G., Hald, N., Nielsen, T. F. D. & Thirwall, M. F. 1993. The Tertiary picrites of W Greenland: contributions from "Icelandic" and other sources. *Earth and Planetary Science Letters*, **115**, 227-244.

Honnorez, J. & Kirst, P. 1975. Submarine basaltic volcanism: morphometric parameters for discriminating between hyaloclastites and hyalotuffs. *Bulletin of Volcanology*, **39**, 1-25.

Humphris, S. E., Morrison, A. & Thompson, R. N. 1978. Influence of rock crystallisation history upon subsequent lanthanide mobility during hydrothermal alteration of basalts. *Chemical Geology*, **23**, 125-137.

Humphris, S. E. & Thompson, G. 1983. Geochemistry of rare earth elements in basalts from the Walvis ridge: implications for its origin and evolution. *Earth and Planetary Science Letters*, **66**, 223-242.

Hunter, R. H. 1987. Textural equilibrium in layered igneous rocks. *In* Parsons, I, (ed.) *Origins of Igneous Layering, NATO advanced study institute series, Series C: Mathematical and Physical Sciences*, **196**, 473-503.

IOC, IHO & BODC. 1994. GEBCO digital atlas (CD-ROM). *Published on behalf of the Intergovernment Oceanographic Commission (of Unesco) and the International Hydrographic Organisation as part of the general bathymetric chart of the oceans (GEBCO); British Oceanographic data centre, Birkenhead.*

Ito, E., White, W. M. & Gopel, C. 1987. The O, Sr, Nd and Pb isotope geochemistry of MORB. *Chemical Geology*, **62**, 157-176.

Jakobsson, S. P. 1972. Chemistry and distribution pattern of recent basaltic rocks in Iceland. *Lithos* **5**, 365-386.

Jakobsson, S. P. 1979a. Outline of the petrology of Iceland. *Jokull* **29**, 57-73.

Jakobsson, S. P. 1979b. Petrology of recent basalts of the Eastern Volcanic Zone, Iceland. *Acta Naturalia Islandica*, **26**, 1-103.

Jakobsson, S. P. & Moore, J. G. 1985. Hydrothermal minerals and alteration rates at Surtsey volcano, Iceland. *Geological Society of America Bulletin.* **97**, 648-659.

Jakobsson, S. P., Jonsson, J. & Shido, F. 1978. Petrology of the Western Reykjanes Peninsula. *Journal of Petrology*, **19**, 669-705.

Jaques, A. L. & Green, D. H. 1980. Anhydrous melting of peridotite at 0-15kb pressure and the genesis of tholeiitic basalts. *Contributions to Mineralogy and Petrology*, **73**, 287-310.

J.C.P.D.S., International centre for diffraction data. 1986. Mineral Powder Diffraction File Search Manual and Data Book.

Jennings, J. N. 1952. Snaefell, East Iceland. *Journal of Glaciology*, **2**, 132-137.

Johannesson, H. 1975. Structure and Petrochemistry of the Reykjadalur central volcano and the surrounding areas, midwest Iceland. *Unpublished Ph.D thesis, University of Durham. 273pp.*

Johannesson, H. 1980. Jardlagaskipan og throun rekbelta a Vesturlandi. *Natturufraedingurinn*, **50**, 13-31. (In Icelandic with English summary.)

Johannesson, H. & Saemundsson, K. 1989. Geological map of Iceland, 1:500,000, bedrock geology. *pub. Icelandic Natural History Museum and Icelandic Geodetic Survey.*

Johnson, R. W. 1989. Intraplate volcanism in Eastern Australia and New Zealand. *Cambridge University Press, 408pp.*

Jonasson, K. 1994. Rhyolite volcanism in the Krafla central volcano NE Iceland. *Bulletin of Volcanology*, **56**, 516-528.

Jones, J. G. 1966. Intraglacial volcnoes of SW Iceland and their significance in the interpretation of the form of marine basaltic volcanoes. *Nature*, **212**, 586-588.

Jones, J. G. 1968. Pillow lava and pahoehoe. *Journal of Geology*, **76**, 485-488.

Jones, J. G. 1969a. Intraglacial volcanoes of the Laugarvatn region SW Iceland, I. *Quarterly Journal of the Geological Society of London*, **124**, 197-211.

Jones, J. G. 1969b. Pillow lavas as depth indicators. *American Journal of Science*, **267**, 181-195.

Jones, J. G. 1970. Intraglacial volcanoes of the Laugarvatn region, SW Iceland, II. *Journal of Geology*, **78**, 127-140.

Jones, J. G. & Nelson, P. H. H. 1970. The flow of basalt lava from air into water - its structural expression and stratigraphic significance. *Geological Magazine,* **107,** 13-19.

Kerr, A. C. 1993. The geochemistry and petrogenesis of the Mull and Morvern Tertiary lava sucession, Argyll, Scotland. *Unpublished Ph.D thesis, University of Durham, 357pp.*

Kerr, A. C. & Hards, V. L. 1995. Geochemical evidence against plume-upper mantle mixing in the source region of the North Atlantic Igneous Province. *Submitted to Journal of the Geological Society, London.*

Kerr, A. C. & Hardy, R. 1993. Na contamination of fused X-ray fluorescence discs. *Journal of the Arthur Holmes Society,* **7 (New Series),** 38.

Kerr, A. C., Kempton, P. D. & Thompson, R. N. 1995a. Crustal assimilation during turbulent magma ascent (ATA); new isotopic evidence from the Mull Tertiary lava sucession, NW Scotland. *Contributions to Mineralogy and Petrology,* **119,** 142-154.

Kerr, A. C., Saunders, A. D., Tarney, J., Berry, N. H. & Hards, V. L. 1995b. Depleted mantle plume geochemical signatures: no paradox for plume theories. *Geology,* in press.

Kesson, S. E. & Fitz Gerald, J. D. 1991. Partitioning of MgO, FeO, NiO, MnO and Cr_2O_3 between magnesian silicate perovskite and magnesiowustite: implications for the origin of inclusions in diamond and the composition of the lower mantle. *Earth and Planetary Science Letters,* **111,** 229-240.

Kinzler, R. J. & Langmuir, C. H. 1995. Minute mantle melts. *Nature,* **375,** 274-275.

Kjartansson, G. 1959. The moberg formation. *In* Thorarinsson, S., Einarsson, T & Kjartansson, G. On the geology and geomorphology of Iceland. *Geogr. Annlr.* **41,** 135-169.

Klein, E. M. & Langmuir, C. H. 1987. Global correlations of ocean ridge basalt chemistry with axial depth and crustal thickness. *Journal of Geophysical Research,* **92,** 8,089-8,115.

Klein, E. M. & Langmuir, C. H. 1989. Local verses global variations in ocean ridge basalt composition: a reply. *Journal of Geophysical Research,* **94,** 4,241-4,252.

Kokelaar, P. 1986. Magma-water interactions in subaqueous and emergent volcanism. *Bulletin of Volcanology*, **48**, 275-289.

Kostopoulos, D. K. 1991. Melting of the shallow upper mantle: A new perspective. *Journal of Petrology*, **32**, 671-699.

Kostopoulos, D. K. & James, S. D. 1992. Parameterisation of the melting regime of the shallow upper mantle and the effects of variable lithospheric stretching on mantle modal stratification and trace-element concentrations in magmas. *Journal of Petrology*, **33**, 665-691.

Kristjansson, L., Johannesson, H., Eiriksson, J. & Gudmundsson, A. I. 1988. Bruhnes-Matuyama paleomagnetism in three lava sections in Iceland. *Canadian Journal of Earth Sciences*, **25**, 215-225.

Kurz, M. D., Meyer, P. S. & Sigurdsson, H. 1986. He isotopic systematics within the neovolcanic zones of Iceland. *Earth and Planetary Science Letters*, **74**, 291-301.

La Breque, J. L., Kent, D. V. & Cande, S. C. 1977. Revised magnetic polarity timescale for late Cretaceous and Cenozoic time. *Geology*, **5**, 330-335.

Lackschewitz, K. S., Dehn, J. & Wallrabe-Adams, H,-J. 1994. Volcaniclastic sediments from mid-oceanic Kolbeinsey ridge, north of Iceland: evidence for submarine volcanic fragmentation processes. *Geology*, **22**, 975-978.

Langmuir, C. H., Bender, J. F., Bence, A. E., Hanson, G. N. & Taylor, S. R. 1977. Petrogenesis of basalts from the FAMOUS area: Mid Atlantic Ridge, *Earth and Planetary Science Letters*, **36**, 133-156.

Langmuir, C. H., Voche, R. D., Hanson, G. N. & Hart, S. R. 1978. A general mixing equation with applications to Icelandic basalts. *Earth and Planetary Science Letters*, **37**, 380-392.

Langmuir, C. H., Klein, E. M. & Plank, T. 1992. Petrological systematics of mid-ocean ridge basalts: constraints on melt generation beneath ocean ridges. *In;* Morgan, J. P., Blackman, D. K. & Sinton, J. M. (eds.) *Mantle Flow and melt generation at mid-ocean ridges*, American Geophysical Union, Geophysical Monograph, **71**, 183-280.

Larsen, L. M., Watt, W. S. & Watt, M. 1989. Geology and Petrology of the lower Tertiary plateau basalts of the Scoresby Sund region, East Greenland. *Bulletin 157, Greenland Geological Survey. 162pp.*

Lawver, L. A. & Muller, R. D. 1994. Iceland hotspot track. *Geology,* **22,** 311-314.

Le Bas, M. J. & Streckeisen, A. L. 1991. The IUGS systematics of igneous rocks. *Journal of the Geological Society, London.* **148,** 825-833.

Le Maitre, R. W. 1976. The chemical variability of some common igneous rocks. *Journal of Petrology,* **17,** 589-673.

Le Maitre, R. W. (ed.) 1989. A classification of igneous rocks and a glossary of terms, recomendations of the I.U.G.S. on the systematic of igneous rocks. *Blackwell Scientific Publications, 193pp.*

Loomis, T. P. 1982. Numerical simulations of crystalization processes of plagioclase in complex melts: the origin of major and oscillatory zoning in plagioclase. *Contributions to Mineralogy and Petrology,* **81,** 219-229.

Loper, D. E. 1991. Mantle plumes. *Tectonophysics,* **187,** 373-384.

Ludden, J., Gelinas, L. & Trudel, P. 1982. Archean metavolcanics from the Rouyn-Noranda district, Abitibi greenstone belt, Quebec. 2. Mobility of trace elements and petrogenetic constraints. *Canadian Journal of Earth Sciences,* **19,** 2,276-2,287.

Macdonald, G. A. & Katsura, T. 1964. Chemical composition of Hawaiian lavas. *Journal of Petrology,* **5,** 82-133.

MacDonald, R., Sparks, R. S., Sigurdsson, H., Mattey, D. P., McGarvie, D. W. & Smith, R. L. 1987. The 1875 eruption of Askja volcano, Iceland: combined fractional crystallisation and selective contamination in the generation of rhyolitic magma. *Mineralogical Magazine,* **51,** 183-202.

MacDonald, R., McGarvie, D. W., Pinkerton, H., Smith, R. L. & Palacz, Z. A. 1990. Petrogenetic evolution of the Torfajokull volcanic complex, Iceland I. Relationship between the magma types. *Journal of Petrology,* **31,** 429-459.

MacKenzie, W. S., Donaldson C. H. & Guilford, C. 1982. Atlas of igneous rocks and their textures. *Longman Scientific & Technical, 148pp.*

Marsh, B. D., Gunnarsson, B., Congdon, R. & Carmody, R. 1991. Hawaiian basalt and Icelandic rhyolite: indicators of differentiation and partial melting. *Geologishe Rundschau,* **80,** 481-510.

Mathews, W. H. 1947. "Tuyas", flat-topped volcanoes in northern British Columbia. *American Journal of Science,* **245,** 560-570.

McBirney, A. R. 1980. Mixing and unmixing of magmas. *Journal of Volcanological and Geothermal Research,* **7,** 357-371.

McKenzie, D. 1984. The generation and compaction of partially molten rock. *Journal of Petrology,* **25,** 713-765.

McKenzie, D. 1985. The extraction of magma from the crust and mantle. *Earth and Planetary Science Letters,* **74,** 81-91.

McKenzie, D. & Bickle, M. J. 1988. The volume and composition of melt generated by extension of the lithosphere. *Journal of Petrology,* **29,** 625-679.

McNutt, M. K. & Judge, A. V. 1990. The superswell and mantle dynamics beneath the south Pacific, *Science,* **248,** 969-975.

Menke, W. & Levin, V. 1994. Cold crust in a hotspot. *Geophysical Research Letters,* **21,** 1967-1970.

Mertz, D. F., Devey, C. W., Todt, W., Stoffers, P. & Hofmann, A. W. 1991. Sr-Nd-Pb isotope evidence against plume-asthenosphere mixing north of Iceland. *Earth and Planetary Science Letters,* **107,** 243-255.

Meyer, P. S., Sigurdsson, H. & Schilling, J,-G. 1985. Petrological and geochemical variations along Iceland's neovolcanic zones. *Journal of Geophysical Research,* **90,** 10,043-10,072.

Middlemost, E. A. K. 1989. Iron oxidation ratios, norms and the classification of volcanic rocks. *Chemical Geology,* **77,** 19-26.

Mills, A. A. 1984. Pillow lavas and the Leidenfrost effect. *Journal of the Geological Society of London,* **141,** 183-186.

Miyashiro, A. 1978. Nature of alkalic volcanic rock series. *Contributions to Mineralogy and Petrology,* **66,** 91-104.

Moorbath, S. H., Sigurdsson, H. & Goodwin, R. 1968. K-Ar ages of the oldest exposed rocks in Iceland. *Earth and Planetary Science Letters,* **4,** 197-205.

Moore, J. G. 1970. Water content of basalt erupted on the ocean floor. *Contributions to Mineralogy and Petrology,* **28,** 272-279.

Moore, J. G. 1975. Mechanism of formation of pillow lava. *American Scientist,* **63,** 269-277.

Moore, J. G. & Evans, B. W. 1967. The role of olivine in the crystalisation of the prehistoric Makaopuhi tholeiitic lava lake, Hawaii. *Contributions to Mineralogy and Petrology,* **15,** 202-223.

Moore, R. O., Gurney, J. J., Griffin, W. L. & Shimizu, N. 1991. Ultra high pressure garnet inclusions in Monastery diamonds: trace element abundance patterns and conditions of origin. *European Journal of Mineralogy,* **3,** 213-230.

Morgan, W. J. 1971. Convection plumes in the lower mantle, *Nature,* **230,** 42-43.

Morimoto, N., Fabries, J., Ferguson, A. K., Ginzburg, I. V., Ross, M., Seifert, F. A., Zussman, J., Aoki, K. & Gottardi, G. 1988. Nomenclature of pyroxenes. *Mineralogical Magazine,* **52,** 535-550.

Muehlenbachs, K. & Byerly, G. 1982. ^{18}O-Enrichment of silicic magmas caused by crystal fractionation at the Galapagos spreading centre. *Contributions to Mineralogy and Petrology,* **79,** 76-79.

Nelson, S. T. & Montana, A. 1992. Sieve-textured plagioclase in volcanic rocks produced by rapid decompression. *American Mineralogist,* **77,** 1242-1249.

Nicholson, H. 1990. The magmatic evolution of Krafla, NE Iceland. *Unpublished Ph.D Thesis, University of Edinburgh.*

Nicholson, H. & Latin, D. 1992. Olivine tholeiites from Krafla, Iceland: evidence for variations in melt fraction within a plume. *Journal of Petrology,* **33,** 1,105-1,124.

Nicholson, H., Condomines, M., Fitton, J. G., Fallick, A. E., Gronvold, K. & Rogers, G. 1991. Geochemical and isotopic evidence for crustal assimilation beneath Krafla, Iceland. *Journal of Petrology,* **32,** 1,005-1,020.

Nielson, R. L. 1988. TRACE.FOR: A program for the calculation of combined major and trace-element liquid lines of descent for natural magmatic systems. *Computers & Geosciences,* **14,** 15-35.

Noe-Nygaard, A. 1940. Subglacial volcanic activity in ancient and recent times - studies in the palagonite system of Iceland, No. 1. *Folia Geographica Danica, 1, no. 2. Kongelige Danske Geografisk Selskab.*

O'Hara, M. J. 1977. Geochemical evolution during fractional crystallisation of a periodically refilled magma chamber. *Nature,* **266,** 503-507.

O'Hara, M. J. 1985. The importance of the "shape" of the melting regime during partial melting of the mantle. *Nature,* **314,** 58-62.

O'Hara, M. J. & Mathews, R. E. 1981. Geochemical evolution in an advancing periodically replenished, periodically tapped, continuously fractionating magma chamber. *Journal of the Geological Society, London,* **138,** 237-227.

Oskarsson, N., Sigvaldason, G. E. & Steinthorsson, S. 1982. A dynamic model of rift zone petrogenesis and regional petrology of Iceland. *Journal of Petrology,* **23,** 28-74.

Oskarsson, N., Steinthorsson, S. & Sigvaldason, G. E. 1985. Iceland geochemical anomaly: origin, volcanotectonics, chemical fractionation and isotope evolution of the crust. *Journal of Geophysical Research,* **90,** 10,011-10,025.

Palacz, Z. A. & Saunders, A. D. 1986. Coupled trace element and isotope enrichment in the Cook-Austral-Samoa islands, southwest Pacific. *Earth and Planetary Science Letters,* **79,** 270-280.

Palmason, G. 1971. Crustal structure of Iceland from explosion seismology: *Societas Scientiarum Islandica, Reykjavik,* **40,** *187pp.*

Palmason, G. 1981. Crustal rifting and related thermo-mechanical proeesses in the lithosphere beneath Iceland. *Geologische Rundschau,* **70,** 244-260.

Palmason, G. 1986. Model of crustal formation in Iceland and application to submarine mid-ocean ridges. *In* Vogt, P. R. & Tucholke, B. E. (eds.), *The Geology of North America,* **Volume M,** *The Western N. Atlantic Region: Geological Society of America.* 87-97.

Park, K. H. 1989. *Unpublished Ph.D thesis, Lamont-Doherty University Geological Observatory, Columbia University, U.S. A.*

Peacock, M. A. 1926. The vulcano-glacial palagonite formation of Iceland. *Geological Magazine,* **63,** 385-399.

Peacock M. A. *In,* Peacock, M. A. & Tyrell. 1926. The petrology of Iceland. Part 1. The basic tuffs. *Transactions of the Royal Society of Edinburgh,* **55,** 51-76.

Pegram, W. J. & Allegre, C.-J. 1992. Osmium isotopic compositions from oceanic basalts. *Earth and Planetary Science Letters,* **111,** 59-68 .

Plank, T. & Langmuir, C. H. 1992. Effects of the melting regime on the composition of oceanic crust. *Journal of Geophysical Research,* **97,** 19,749-19,770.

Powell, R. & Powell, M. 1977. Geothermometry and oxygen barometry using coexisting iron-titanium oxides: a reappraisal. *Mineralogical Magazine,* **41,** 257-63.

Preston, J. 1982. Eruptive Volcanism. *In* Sutherland, D. S. (ed.) *Igneous rocks of the British Isles,* Part 7: The British Tertiary igneous province, Chapter 28, 351-368, John Wiley & Sons Ltd.

Prestvik, T, 1982. Petrography, chemical characteristics and nomenclature of Oraefajokull rocks. *Jokull,* **32,** 69-76.

Prestvik, T, 1985. Petrology of Quarternary volcanic rocks from Oraefi, SE Iceland. *Geologisk Insititutt, Norges Tekniske Hogskole, Universitetet i Trondheim, Report* **21,** *81pp.*

Ribe, N. M. 1985. The generation and composition of partial melts in the earth's mantle. *Earth and Planetary Science Letters,* **73,** 361-376.

Richards, M. A. & Griffiths, R. W. 1989. Thermal entrainment by deflected plumes. *Nature,* **342,** 900-902.

Richardson, C. & McKenzie, D. 1994. Radioactive disequilibria from 2D models of melt generation by plumes and ridges. *Earth and Planetary Science Letters,* **128,** 425-437.

Rittman, A. 1962. Volcanoes and their activity. *John Wiley & Sons, New York, 305pp.*

Roeder, P. L. & Emslie, R. F. 1970. Olivine-liquid equilibria. *Contributions to Mineralogy and Petrology,* **29,** 275-289.

Rollinson, H. 1993. Using geochemical data: evaluation, presentation, interpretation. *Longman Scientific & Technical, 352pp.*

Roy-Barman, M. & Allegre, C. J. 1995. $^{187}Os/^{186}Os$ in oceanic island basalts: tracing oceanic crust recycling in the mantle. *Earth and Planetary Science Letters,* **129,** 145-161.

Ryan, M. P. 1990. The physical nature of the Icelandic magma transport system. *In* Ryan, M. P. (ed.), *Magma transport and storage, J. Wiley & Sons Ltd.* 175-223.

Saemundsson, K. 1974. Evolution of the axial rifting zone in N Iceland and the Tjornes fracture zone. *Geological Society of America Bulletin,* **85,** 495-504.

Saemundsson, K. 1978. Fissure swarms and central volcanoes of the neovolcanic zones in Iceland. *In: Crustal evolution in NW Britain and adjacent regions, Geological JournalSpecialIssue,* **10,** 415-432.

Saemundsson, K. 1979. Outline of the Geology of Iceland. *Jokull,* **29,** 7-28.

Saemundsson, K. 1986. Subaerial volcanism in the western N Atlantic. *In* Vogt, P. R. & Tucholke, B. E. (eds.), *The Geology of North America,* **Volume M,** *The Western N. Atlantic Region: Geological Society of America.* 69-86.

Salters, V. J. M. & Hart, S. R. 1991. The mantle sources of ocean ridges, islands and arcs: the Hf-isotope connection. *Earth and Planetary Science Letters,* **104,** 364-380.

Sato, H., Sacks, I. S. & Murase, T. 1989. The use of laboratory velocity data for estimating temperature and partial melt fraction in the low velocity zone: comparison with heat flow and electrical conductivity studies. *Journal of Geophysical Research,* **94,** 5689-5704.

Scarrow, J. H. & Cox, K. G. 1995. Basalts generated by decompressive adiabatic melting of a mantle plume: a case study from the Isle of Skye, NW Scotland. *Journal of Petrology*. **36,** 3-22.

Schilling, J.-G. 1973. Iceland mantle plume, geochemical evidence along the Reykjanes ridge, *Nature,* **246,** 141-143.

Schilling, J.-G. 1986. Geochemical and isotopic variation along the mid-Atlantic Ridge axis from 79°N to 0°N. *In* Vogt, P. R. & Tucholke, B. E. (eds.), *The Geology of North America,* **Volume M,** *The Western N. Atlantic Region: Geological Society of America.* 137-156.

Schilling, J,-G., Meyer, P. S. & Kingsley, R. H. 1982. Evolution of the Iceland hotspot. *Nature,* **296,** 313-320.

Schilling, J.-G., Zajac, M., Evans, R., Johnston, T., White, W., Devine, J. D. & Kingsley, R. 1983. Petrologic and geochemical variations along the Mid-Atlantic Ridge from 29N to 73N. *American Journal of Science,* **283,** 510-586.

Schmeling, H. 1985. Partial melt below Iceland: a combined interpretation of seismic and conductivity data. *Journal of Geophysical Research,* **90,** 10,105-10,116.

Schminke, H.-U., Rautenschelein, M., Robinson, P. T. & Mehegan, J. M. 1983. Troodos extrusive series of Cyprus: a comparison with oceanic crust. *Geology,* **11,** 405-409.

Shaw, D. M. 1979. Trace element melting models. *In* Ahrens, L. H. (ed.) *Origin and distribution of the elements.* Physics and Chemistry of the Earth. **11,** 577-586.

Shervais, J. W. 1982. Ti-V plots and the petrogenesis of modern and ophiolitic lavas. *Earth and Planetary Science Letters,* **59,** 101-118.

Sigmarsson, O., Hemond, C., Condomines, M. Fourcade, S. & Oskarsson, N. 1991. Origin of silicic magma in Iceland revealed by Th isotopes. *Geology,* **19,** 621-624.

Sigmarsson, O., Condomines, M. & Fourcade, S. 1992a. Mantle and crustal contribution in the genesis of recent basalts from off-rift zones in Iceland: constraints from Th, Sr and O isotopes. *Earth and Planetary Science Letters,* **110.** 149-162.

Sigmarsson, O., Condomines, M. & Fourcade, S. 1992b. A detailed Th, Sr and O isotope study of Hekla: differentiation processes in an Icelandic volcano. *Contributions to Mineralogy and Petrology*. **112,** 20-34.

Sigurdsson, H. 1970. Structural origin and plate tectonics of the Snaefellsnes volcanic zone, western Iceland. *Earth and Planetary Science Letters,* **10,** 129-135.

Sigurdsson, H. 1977. Generation of Icelandic rhyolites by melting of plagiogranites in the oceanic layer. *Nature,* **269,** 25-28.

Sigurdsson, H. & Sparks, R. S. 1981. Petrology of rhyolitic and mixed magma ejecta from the 1875 eruption of Askja, Iceland. *Journal of Petrology,* **22,** 41-84.

Sigurdsson, H., Schilling, J.,-G. & Meyer, P. S. 1978. The Skagi and Langjokull volcanic zones in Iceland. *Journal of Geophysical Research,* **83,** 3,971-3,982.

Sigvaldason, G. E. 1968. Structure and products of subaquatic volcanoes in Iceland. *Contributions to Mineralogy and Petrology,* **18,** 1-16.

Sigvaldason, G. E., Steinthorsson, S., Oskarsson, N. & Imsland, P. 1974. Compositional variation in recent Icelandic tholeiites and the Kverkfjoll hotspot. *Nature,* **251,** 579-582.

Simkin, T. & Smith, J. V. 1970. Minor element distribution in olivines. *Journal of Geology,* **78,** 304-325.

Sleep, N. H. 1988. Tapping of melt by veins and dykes. *Journal of Geophysical Research,* **93,** 10,255-10,272.

Sleep, N. H. 1990. Hotspots and mantle plumes: Some phenomenology. *Journal of Geophysical Research,* **95,** 6,715-6,736.

Sleep, N. H. 1994. Lithospheric thinning by midplate mantle plumes and the thermal history of hot plume material ponded at sublithospheric depths. *Journal of Geophysical Research,* **99,** 9,327-9,343.

Smellie, J. L., Hole, M. J. & Nell, P. A. R. 1993. Late Miocene valley-confined subglacial volcanism in northern Alexander Island, Antarctic Penninsula. *Bulletin of Volcanology,* **55,** 273-288.

Smith, D. & Lindsley, D. H. 1971. Stable and metastable augite crystallization trends in single basalt flow. *American Mineralogist,* **56,** 225-233.

Smith, J. V. 1974. Feldspar Minerals, Volume. 1 Crystal Structure and Physical Properties. *Springer-Verlag, 627pp.*

Smith, R. E. & Smith, S. E. 1976. Comments on the use of Ti, Zr, Y, Sr, K, P and Nb in classification of basaltic magmas. *Earth and Planetary Science Letters,* **32,** 114-120.

Smith, R. F. 1967. Segregation vesicles in basaltic lava. *American Journal of Science,* **265,** 696-713.

Sobolev, A. V., Gurenko, A. A. & Shimizu, N. 1994. Ultra-depleted melts from Iceland: data from melt inclusion studies. *Mineralogical Magazine,* **58A,** 860-861.

Sparks, R. S. J. & Huppert, H. E, 1984. Density changes during fractional crystallisation of basaltic magmas: fluid dynamical implications. *Contributions to Mineralogy and Petrology,* **85,** 300-309.

Sparks, R. S. J. & Marshal, L. A. 1986. Thermal and mechanical constraints on mixing between mafic and silicic magmas. *Journal of Volcanology and Geothermal Research,* **29,** 99-124.

Sparks, R. S. J., Sigurdsson, H. & Wilson, L. 1977. Magma mixing: a mechanism for triggering acid explosive eruptions. *Nature,* **267,** 315-318.

Sparks, R. S. J., Huppert, H. E. & Turner, J. S. 1984. The fluid dynamics of evolving magma chambers. *Philosophical Transactions of the Royal Society, London,* **A 310,** 511-534.

Steinthorsson, S., Oskarsson, N. & Sigvaldason, G. E. 1985. Origin of alkali basalts in Iceland: a plate tectonic model. *Journal of Geophysical Research,* **90,** 10,027-10,042.

Stille, P., Unruh, D. M. & Tatsumoto, M. 1986. Pb, Sr, Nd and Hf isotopic constraints on the origin of Hawaiian basalts and evidence for a unique mantle source, *Geochimica et Cosmochimica Acta,* **50,** 2,303-2,319.

Sun, S.-s. & Jahn, B. M. 1975. Pb and Sr isotopes in post-glacial basalts from Iceland. *Nature,* **255,** 527-530.

Sun, S.-s. & McDonough, W. F. 1989. Chemical and isotopic systematics of oceanic basalts: implications for mantle compositions and processes. *In* Saunders, A. D. & Norry, M. J. (eds.), *Magmatism in Ocean Basins*. Special Publication of the Geological Society, **42,** 313-345.

Sun, S,-s., Tatsumoto, M. & Schilling, J. G. 1975. Mantle plume mixing along the Reykjanes Ridge axis: lead isotopic evidence, *Science,* **190,** 143-147.

Sweatman, T. R. & Long, J. P. 1969. Quantitative electron microprobe microanalysis of rock-forming minerals. *Journal of Petrology,* **10,** 332-380.

Thirwall, M. F., Upton, B. G. J. and Jenkins, C. 1994. Interaction between continental lithosphere and the Iceland plume: Sr-Nd-Pb isotope geochemistry of Tertiary basalts, NE Greenland. *Journal of Petrology,* **35,** 839-879.

Thompson, R. N. 1972. Evidence for a chemical discontinuity near the basalt-"andesite" transition in many anorogenic volcanic suites. *Nature,* **236,** 106-110.

Thompson, R. N. 1973. One-atmosphere melting behaviour and nomenclature of terrestrial lavas. *Contributions to Mineralogy and Petrology,* **41,** 197-204

Thompson, R. N. 1981. Thermal aspects of the origin of Hebridean Tertiary acid magmas. I. An experimental study of partial fusion of Lewisian gneisses and Torridonian sediments. *Mineralogical Magazine,* **44,** 161-170.

Thompson, R. N. 1982. Magmatism of the British Tertiary Igneous province. *Scottish Journal of Geology,* **18,** 49-107.

Thompson, R. N. 1987. Phase-equilibria constraints in the genesis and magmatic evolution of oceanic basalts. *Earth-Science Reviews,* **24,** 161-210.

Thompson, R. N. & Gibson, S. A. 1991. Subcontinental mantle plumes, hotspots and pre-existing thinspots. *Journal of the Geological Society, London,* **148,** 973-977.

Thompson, R. N. & MacKenzie, W. S. 1967. Feldspar-liquid equilibria in peralkaline acid liquids: an experimental study. *American Journal of Science,* **265,** 714-734.

Thorarinsson, S. 1958. The Oraefajokull eruption 1362. *Acta Naturalia Islandica,* **II, 2,** *100pp.*

Thorarinson, S., Saemundsson, K. & Williams, R. S. 1973. ERTS-1 image of Vatnajokull: analysis of glaciological structural and volcanic features. *Jokull,* **23,** 7-17.

Thoroddsen, Th. 1905. Island, grundriss der geographie und geologie. *Petermanns Geographische Mitteilungen, Erganzungsheft,* **152-3,** 274.

Thy, P. 1983. Phase relations in transitional and alkali basaltic glasses from Iceland. *Nordic Volcanic Institute Report No. 8202. University of Iceland.*

Thy, P. 1991. High and low pressure phase equilibria of a mildly alkalic lava from the 1965 Surtsey eruption: Experimental results. *Lithos,* **26,** 226-243.

Thy, P., Beard, J. S. & Lofgren, G. E. 1990. Experimental constraints on the origins of Icelandic rhyolites. *Journal of Geology,* **98,** 417-421.

Todt, W., Cliff, R. A., Hanser, A. & Hofmann, A. W. 1984. ^{202}Pb and ^{205}Pb double spike for lead isotopic analyses. *Terra Cognita,* **4,** 209.

Torfason, H. 1979. Investigations into the structure of SE Iceland. *Unpublished Ph.D thesis, University of Liverpool,* 587pp.

Torfason, H. 1992. Structure of sub-volcanic intrusions in SE Iceland. *Joint meeting of the Volcanic and Tectonic studies groups, University of Liverpool, 13 May, 1992.* Abstract.

Tryggvasson, K., Husebye, E. S. & Stefansson, R. 1983. Seismic image of the Icelandic hotspot. *Tectonophysics,* **100,** 97-118.

Tuttle, O. F. & Bowen, N. L. 1958. Origin of granite in the light of experimental studies in the system $NaAlSi_3O_8$-$KAlSi_3O_8$-SiO_2-H_2O. *Geological Society of America, Memoir* **74,** *153pp.*

Vink, G. E. 1984. A hotspot model for Iceland and the Voring plateau. *Journal of Geophysical Research,* **89,** 9,949-9,959.

Vogt, P. R. 1974. The Iceland phenomena: imprints of a hotspot on ocean crust and implications for flow below the plates. *In* Kristjansson, L. (ed.) *Geodynamics of Iceland and the North Atlantic area, NATO advanced study institutes series, Series C,* **11,** 105-126.

Walker, G. P. L. 1965. Some aspects of Quarternary volcanism. *Transactions of the Leicester Literary and Philosophical Society,* **59,** 25-40.

Walker, G. P. L. 1971. Compound and simple lava flows. *Bulletin of Volcanology,* **82,** 2991-3012.

Walker, G. P. L. 1973. Explosive volcanic eruptions - a new classification scheme. *Geologische Rundschau,* **62,** 431-446.

Walker, G. P. L. 1974. The structure of Eastern Iceland, *In* Kristjansson, L. (ed.) *Geodynamics of Iceland and the North Atlantic area, NATO advanced study institutes series, Series C,* **11,** 177-188.

Walker, G. P. L. 1975. Excess spreading axes and spreading rate in Iceland. *Nature,* **255,** 468-471.

Walker, G. P. L. & Blake, D. H. 1966. The formation of a palagonite breccia mass beneath a valley glacier in Iceland. *Quarterly Journal of the Geological Society of London,* **122,** 45-61.

Watkins, N. D. & Walker, G. P. L. 1977. Magnetostratigraphy of east Iceland. *American Journal of Science,* **277,** 513-584.

Watson, E. B. 1979. Zircon saturation in felsic liquids: experimental results and applications to trace element geochemistry. *Contributions to Mineralogy and Petrology,* **70,** 407-419.

Watson, S. & McKenzie, D. 1991. Melt generation by plumes: a study of Hawaiian volcanism. *Journal of Petrology,* **35,** 501-537.

Weaver, B. L. 1991. The origin of ocean island basalt end-member compositions: trace element and isotopic constraints. *Earth and Planetary Science Letters,* **104,** 381-397.

Weaver, B. L., Wood, D. A. & Tarney, J. 1987. Geochemistry of ocean island basalts from the South Atlantic, Ascension, Bouvet, St. Helena, Gough and Tristan da Cunha. *In* Fitton, J. G. & Upton, B. G. J. (eds.) *Alkaline igneous rocks,* Geological Socirty Special publication, **30,** 253-267.

Wessel, P. & Smith, W. H. F. 1991. Free software helps map and display data, *EOS Transactions of the American Geophysical union,* **72,** 441, 445-446.

White, R. S. 1988. A hotspot model for early Tertiary volcanism in the N Atlantic. *In* Morton, A. C. & Parson, L. M. (eds.), *Early Tertiary volcanism and the openning of the NE Atlantic,* Geological Society Special Publication, **39,** 3-13.

White, R. S. & McKenzie, D. 1989. Magmatism at rift zones: the generation of volcanic continental margins and flood basalts. *Journal of Geophysical Research,* **94,** 7,685-7,729.

White, R. S., McKenzie, D. & O'Nions, R. K. 1992. Oceanic crustal thickness from seismic measurements and rare earth element inversions. *Journal of Geophysical Research,* **97,** 19,683-19,715.

Whitten, D. G. A. & Brooks, J. R. V. 1972. Dictionary of Geology, *Penguin Group, London.*

Williams, R. S., Thorarinsson, S. & Morris, E. 1983. Geomorphic classification of Icelandic volcanoes. *Jokull,* **33,** 19-24.

Wilson, J. T. 1963. A possible origin of the Hawaiian Islands, *Canadian Journal of Physics,* **41,** 863-870.

Wilson, M. 1989. Igneous petrogenesis: a global tectonic approach. *Harper Collins Academic, 465pp.*

Wilson, M. 1993. Geochemical signatures of oceanic and continental basalts: a key to mantle dynamics? *Journal of the Geological Society, London,* **150,** 977-990.

Winchester, J. A. & Floyd, P. A. 1977. Geochemical discrimination of different magma series and their differentiation products using immobile elements. *Chemical Geology,* **20,** 325-343.

Wood, D. A. 1978. Major and trace element variations in the Tertiary lavas of eastern Iceland and their significance with respect to the Iceland geochemical anomaly. *Journal of Petrology,* **19,** 393-436.

Wood, D. A., Gibson, I. L. & Thompson, R. N. 1976. Elemental mobility during zeolite facies metamorphism of the Tertiary basalts of eastern Iceland. *Contributions to Mineralogy and Petrology,* **55,** 241-254.

Woodhead, J. D. & McCullough, M. T. 1989. Ancient seafloor signals in Pitcairn Island lavas and evidence for large amplitude, small length-scale mantle heterogeneities. *Earth and Planetary Science Letters,* **94,** 257-273.

Wright, T. L. & Fiske, R. S. 1971. Origin of differentiated and hybrid lavas of the Kilauea volcano, Hawaii. *Journal of Petrology*, **12**, 1-65.

Zindler, A. & Hart, S. R. 1986. Chemical Geodynamics, *Annual Reviews in Earth and Planetary Sciences*, **14**, 493-571.

Zindler, A., Hart, S. R., Frey, F. A. & Jakobsson, S. P. 1979. Nd and Sr isotope ratios and REE abundances in the Reykjanes Peninsula basalts: evidence for mantle heterogeneity beneath Iceland. *Earth and Planetary Science Letters*, **45**, 249-262.

Zindler, A., Staudigel, H. & Batiza, R. 1984. Isotope and trace element geochemistry of young Pacific seamounts: implications for the scale of upper mantle heterogeneity. *Earth and Planetary Science Letters*, **70**, 175-195.

Appendix 1
Sample Localities and Descriptions

For all samples collected, in order of acquisition, a brief description of the outcrop locality, form and the rock type is given, followed by the classification (following the guidelines put forward by the IUGS subcommision; LeMaitre 1989) of samples analysed. Unless otherwise stated, all samples have alkalic affinities. A grid reference referring to the grid on map A1 - to be found in the back of the thesis - is also given, to eight figures. Where no grid reference is given, it is the same as for the previous sample.

Most units were erupted subglacially, and the terms - feeder dyke, breccia, pillows, tuff - used are those defined in chapter 2. Where nothing beyond the locality and/or description and classification of the sample are given, it was unclear as to the mode of emplacement; whether subaerially or subglacially, as intrusive (or pseudointrusive) or extrusive body.

	Locality, sample description and classification	**Grid reference**
	South Western Snaefell	
VH1	Plagioclase, olivine and clinopyroxene phyric basalt, taken from breccia deposit.	[3881,4786]
VH2	Very fine grained vitric tuff.	
VH3	Coarse vitric tuff, more heavily palagonitised than VH2.	
VH4	Pillow lavas, fine grained plagioclase phyric basalt.	[3879,4784]
VH5	Zeolitic vug infill from VH4.	
VH6	Breccia deposit, Plagioclase, olivine and clinopyroxene phyric basalt. Late stage segregations of glassy material visible in vesicles.	[3877,4784]
VH7	Vitric tuff.	
VH8	Feeder dyke at centre of subglacial eruption unit, plagioclase phyric basalt.	[3873,4786]
VH9	Pillow lavas, plagioclase phyric mugearite.	[3869,4789]
	Hamar	
VH10	Breccia, fine grained olivine phyric basalt, very fresh.	[3869,4793]
VH11	Vitric tuff	[3871,4794]
VH12	Lava flow? Poorly exposed, poorly developed jointing. Olivine phyric basalt.	

VH13	Lava flow or sill, fairly well developed cube jointing, practically aphyric basalt.	[3874,4794]
	Western Snaefell	
VH14	Breccia, cidery, aphyric basalt.	[3874,4805]
VH15	Vitric tuff, fairly heavily palagonitised.	
VH16	Breccia, olivine phyric basalt.	[3870,4806]
VH17	Porous, gabbroic xenolith, glass lining cavities.	
VH18	Coarse, poorly sorted tuff, abundant lithic lappilli.	[3866,4804}
VH19	Breccia, very fine grained cindery basalt, small fresh olivine phenocrysts.	[3862,4801]
VH20	Porous, gabbroic xenolith, glass lined cavities	[3860,4800]
VH21	Small feeder tube, fresh, olivine phyric basalt.	[3859,4800]
	Co-mingling magmas, Steep cliff-like outcrop ~1400m	
VH22	Contact between glassy hybrid and basic (mugearitic) end member.	[3851,4799]
VH23	Glassy hybrid, compositionally a trachyte.	
VH24	Basic end-member, fine grained, plagioclase phyric mugearite.	
VH25	Blebs of the acidic (rhyolitic) end-member enclosed in the mugearite.	
VH26	Scree, glassy hybrid containing partially resorbed feldspar phenocrysts.	
VH27	~100m to the south. Pillow lava, plagioclase phyric mugearite.	[3851,4798]
VH28	Highly vesicular material from contact between mugearitic lava and the glassy hybrid.	[3851,4799]
VH29	Discarded.	
VH30	Large (~3m) feeder dyke. Fine grained mugearite, flow aligned plagioclase laths.	
VH31	Lower horizon of pillow lavas below feeder dyke (VH30), fine grained, few plagioclase laths.	[3851,4798]
VH32	Breccia, medium gained mugearite, plagioclase phyric.	[3860,4801]
VH33	Breccia, olivine phyric basalt.	
VH34	Discarded.	
	South western Snaefell	
VH35	Poorly exposed stony rhyolite flow showing platy weathering, impossible to estimate thickness.	[3875,4776]
VH36	Very fine grained vitric tuff above rhyolite flow.	
VH37	Small, <50cm, pillow lavas, very fine grained aphyric basalt.	[3870,4780]
VH38	Second sample of stony rhyolite, same flow as VH35, here showing well developed columnar jointing.	[3870,4781]
VH39	Heavily palagonitised lapilli tuff.	[3865,4781]

VH40	Feeder tube showing radial columnar jointing, ~2.5m diameter. Basalt.	[3864,4777]
VH41	Summit of small hill, 1325m. Subaerial, columnar jointed lava flow ~3m thick grading down into fragmental deposits. Plagioclase phyric basalt.	[3861,4780]
VH42	Tuff, abundant fresh, glassy lapilli.	[3860,4780]
VH43	Lava flow showing platy weathering, beneath lappilli tuff horizon. Plagioclase and olivine phyric basalt.	
	Eastern flank of Snaefell	
VH44	Heavily palagonitised tuff showing signs of re-working, bedding parallel to scree slope.	[3824,4799]
VH45	Pillow lavas, fine grained mugearite, few phenocrysts of plagioclase and olivine.	[3825,4799]
VH46	Small dyke ~1m wide. Fine grained, plagioclase phyric mugearite.	[3826,4799]
VH47	Lava flow ~2m thick, overlain by tuff. Olivine and plagioclase phyric mugearite.	[3827,4799]
VH48	Rhyolite, Very thick unit >15m.	
VH49	Second sample of rhyolite.	
VH50	Plagioclase rich basalt, overlying rhyolite unit.	
VH51	Scree, feldspar phyric obsidian.	
	Laugara river	
VH52	V10 in Walker's profiles through the plateau basalts of E. Iceland.	[3744,4898]
VH53	V11	
VH54	V12	
VH55	Zeolite taken from V12.	
VH56	Topmost flow of Plio-Pleistocene lava pile.	[3750,4894]
	Laugarfell	
VH57	Platy weathering mugearite flow, probably subaerial, 2-3m thick.	[3766,4895]
VH58	Pillow breccia, plagioclase phyric mugearite, some vesicles infilled by secondary minerals.	[3765,4894]
VH59	Top of Laugarfell, feeder dyke. Plagioclase phyric mugearite.	[3766,4889]
	North of Snaefell	
VH60	Small subaerial hawaiite flow unit ~2m thick, fairly well developed columnar jointing. Alteration evident, vugs infilled with secondary minerals. Almost aphyric, just a few plagioclase laths visible.	[3804,4887]
VH61	Second subaerial hawaiite unit, few meters north of first.	

VH62	Third subaerial hawaiite unit, ~20m to the south of the first.	
VH63	Vitric tuff	[3805,4890]
VH64	Fourth small, columnar jointed hawaiite flow.	[3816,4878]
	Saudahnjukur East	
VH65	Benmoreite ?dome. Sparsely feldspar phyric.	[3902,4792]
VH66	Second sample of benmoreite from hill top.	[3908,4790]
VH67	Small subglacial unit on western flank, breccia, finely vesicular, aphyric basalt.	[3916.4791]
VH68	Third sample of benmoreite.	[3919,4795]
	Saudahnjukur West	
VH69	Feeder dyke, ~3m wide, showing chilled margins and showing a concentration of vesicles at its centre, fine grained, aphyric hawaiite.	[3919,4795]
VH70	Second feeder dyke, ~2m wide. Fine grained aphyric hawaiite.	[3914,4794]
VH71	Third feeder dyke, ~2m wide. Fine grained aphyric hawaiite.	[3920,4796]
VH72	Small feeder dyke, ~30cm, wide. Fine grained, abundant tabular plagioclase phenocrysts. Hawaiite.	[3921,4795]
VH73	Fourth larger feeder dyke, showing well-developed columnar jointing. Aphyric hawaiite.	
VH74	Feeder dyke, ~2m, aphyric basalt.	[3919,4800]
	Western flank of Snaefell	
VH75	Aphyric foliated trachyte flow.	[3874,4811]
VH76	?Lava flow, well developed small-scale columnar jointing, olivine and plagioclase phyric hawaiite.	[3873,4811]
VH77	Lava flow, fresh, glassy, highly vesicular olivine phyric basalt.	[3860,4804]
VH78	Subaerial lava flow ~2m thick (top eroded away), well developed columnar jointing. Olivine, plagioclase and clinopyroxene phyric basalt.	[3854,4804]
VH79	Pillow lava from underlying subglacial eruption unit. Olivine and plagioclase phyric mugearite.	
VH80	Second section of subaerial lava flow, olivine, plagioclase and clinopyroxene phyric basalt.	[3855,4805]
VH81	Gabbroic xenolith.	
	Thordafell	
VH82	Central feeder dyke, plagioclase, olivine and ?clinopyroxene phyric basalt.	[3886,4771]
VH83	Basaltic pillow lava, vugs infilled with secondary minerals (calcite).	

VH84	Vitric tuff, fairly coarse grained and palagonitised.	
VH85	Bedded, fine grained vitric tuff.	[3889,4777]
	Bj'alfafell	
VH86	Subaerial cap flow, grading down into fragmental deposites. Plagioclase phyric, tholeiitic basalt.	[3903,4717]
VH87	Second subaerial flow, plagioclase phyric tholeiitic basalt.	[3905,4716]
VH88	Pillow breccia, again plagioclase phyric tholeiitic basalt.	[3906,4715]
	Litla-Snaefell	
VH89	Pillow lava, olivine and plagioclase phyric basalt.	[3891,4715]
VH90	Columnar jointed feeder dyke, olivine phyric basalt.	[3890,4716]
VH91	Dyke, fine grained, rare plagioclase phenocrysts. basalt.	[3890,4722]
	Kentilhnjukur	
VH92	~1050m up, sill. Aphyric hawaiite.	[3887,4735]
VH93	~1100m, dyke-like body. Hawaiite, rare plagioclase laths.	[3888,4737]
VH94	Feeder dyke, Hawaiite, flow-aligned plagioclase laths.	[3890,4738]
VH95	~900m, pillow-like body. Hawaiite, few plagioclase phenocrysts.	[3886,4743]
	Tiutiu	
VH96	Gully below Tiutiu. Lava flow/sill, well developed columnar jointing. Feldspar phyric basalt.	[3869,4821]
VH97	Feeder dyke, small-scale columnar jointing. Plagioclase phyric benmoreite.	[3865,4827]
VH98	Summit, dyke. Plagioclase phyric hawaiite.	[3864,4830]
	Western Snaefell	
VH99	Lava flow, plagioclase and pyroxene phyric mugearite.	[3877,4801]
VH100	Bedded, fine grained vitric tuff.	[3876,4800]
VH101	?Lava tubes? plagioclase and olivine phyric basalt.	[3875,4840]
	North of Snaefell	
VH102	Dyke, ~2.5m wide. Plagioclase and olivine phyric basalt.	[3835,4869]
	Grabergshnjukur	
VH103	Bedded, vitric tuff, fairly heavily palagonitised.	[3835,4869]
VH104	First summit, 1050m. Plagioclase, olivine and clinopyroxene phyric basalt.	[3856,4866]

VH105	Second summit, 1001m, fine grained, aphyric hawaiite.	[3861,4850]
	Sandar	
VH106	Ankaramitic lava flow, exposure in stream bed.	[3895,4812]
	Langihnjukur	
VH107	Olivine and plagioclase phyric basalt.	[3908,4820]
VH108	Vitric tuff.	[3906,4816]
	Grjotarhnjukur	
VH109	Summit, feeder dyke. Plagioclase phyric hawaiite.	[3891,4845]
VH110	Bedded vitric tuff.	[3889,4343]
VH111	Discarded.	
VH112	Discarded.	
VH113	Mugearite flow, occasional tabular plagioclases, platy weathering. Represents the onset of alkalic activity in the area.	[3802,4810]
VH114	As VH113.	[3791,4790]
VH115	As VH113.	[3780,4872]
VH116	As VH113.	[3765,4896]
VH117	As VH113.	[3792,4900]
VH118	Columnar jointed lava flow. Topmost of the underlying plateau basalts. Plagioclase and olivine phyric tholeiitic basalt. Olivines completely oxidised to iddingsite.	[3810,4917]
	West of Thordafell	
VH119	Massive ankaramitic lava flow.	[3905,4775]
VH120	Ankaramitic lava flow.	[3905,4761]
VH121	Ankaramitic lava flow.	[3911,4760]
	Fitjahnjukur	
VH122	Feeder dyke, olivine and plagioclase phyric basalt.	[3914,4743]
VH123	Boulder, basaltic.	
	Geldaerhnjukur	
VH124	Lava flow, platy weathering, tholeiitic basalt.	[3842,4897]
VH125	Feeder dyke, plagioclase phyric basalt.	[3852,4887]

VH126	Feeder dyke, plagioclase phyric basalt.	[3861,3864]
	Thjofahnjukur	
VH127	Feeder dyke, fine-grained plagioclase phyric hawaiite.	[3877,4735]
VH128	Friable, felsic xenoliths.	
VH129	Feeder dyke, fine-grained plagioclase phyric hawaiite.	[3872,4742]
VH130	Basalt lava, ~10% phenocrysts of olivine, plagioclase and clinopyroxene.	[3869,4781]
VH131	As 130, showing well-developed curved columnar jointing.	[3862,4756]
	South Western ridge of Snaefell	
VH132	Pillow system, 1160m summit. Aphyric basalt.	[3866,4773]
VH133	Narrow dyke, clear chill margins, fine grained mugearite.	[3865,4768]
VH134	Large pillow/feeder tube, radial jointing. Plagioclase and olivine phyric basalt.	
VH135	1150m summit. Feeder dyke. Flinty, olivine phyric mugearite.	[3871,4759]
VH136a	Small rhyolite ?dome, reaching ~1000m. Pyroxene and abundant tabular feldspar phenocrysts, platy jointing.	[3858,4764]
VH136b	Large pillow structure, plagioclase phyric basalt.	[3861,4784]
VH137	Feeder complex, plagioclase and clinopyroxene phyric mugearite.	[3851,4785]
VH138	Scree, obsidian, feldspar phyric.	
VH139	Feldspar phyric obsidian.	[3853,4783]
VH140	Basaltic tuff, heavily palagonitised.	[3851,4782]
VH141	Pitchstone breccia.	[3854,4782]
VH142	Stony rhyolite, pyroxene and feldspar phyric.	[3854,4774]
VH143	Basaltic tuff, heavily palagonitised.	[3855,4772]
VH144	Stony rhyolite, pyroxene and feldspar phyric.	[3856,4770]
	Hamar	
VH145	Porous gabbroic xenoliths.	[3867,4792]
	Saudafell	
VH146	Rather altered (rusty staining due to Fe oxidation), aphyric basalt.	[3819,4891]
	Hafursfell	
VH147	Fragmental deposit, composed of aphyric mugearite lava.	[3803,4860]
VH148	Feeder dyke ~960m, aphyric mugearite.	[3799,4860]
VH149	Friable, felsic xenolith.	
VH150	Feeder dyke, aphyric mugearite.	[3793,4858]

Thraelaalda

VH151	Subaerial cap-flow, well developed columnar jointing. Basaltic, abundant (~15%) plagioclase phenocrysts.	[3805,4954]

Thraelahals

VH152	Subaerial ?spatter deposit. Basaltic, abundant (~15%) plagioclase, with rarer olivines.	[3782,4971]
VH153	?Feeder dyke, as VH152, not very fresh appearance.	[3783,4966]
VH154	Aphyric lava, platy weathering. Tholeiitic basalt.	[3785,4972]
VH155	Second tholeiitic basalt, abundant plagioclase phenocrysts and red iddingsite after olivine.	[3789,4974]

Nalhushnjukur

VH156	Feeder dyke, aphyric hawaiite, showing signs of secondary alteration - rusty staining.	[3810,4882]
VH157	As VH156.	[3812,4879]

North west flanks of Snaefell

VH158	Pillow complex. Aphyric basalt, altered.	[3837,4854]
VH159	As VH158, lower unit?	
VH160	Feeder dyke. Fine grained basalt, abundant small, fresh olivine phenocrysts.	[3831,4855]
VH161	Pillows. As VH160.	[3834,4849]
VH162	Small hill, 1010m. Plagioclase and olivine phyric basalt.	[3842,4844]
VH163	Stony rhyolite.	[3844,4825]
VH164	Pumice-rich rhyolite breccia.	
VH165	Top of rhyolite flow. Pitchstone with stony horizons.	[3845,4818]
VH166	Vitric tuff.	[3842,4825]
VH167	?Lower rhyolite unit. Porphyritic obsidian.	[3841,4832]
VH168	Beneath rhyolite and tuff, basalt, abundant plagioclase phenocrysts.	[3878,4835]

Nalhushnjukur

VH169	Feeder dyke, plagioclase phyric mugearite, platy weathering.	[3820,4867]
VH170	As VH169.	[3822,4865]
VH171	Fine grained tuff.	
VH172	More massive mugearite lava, plagioclase and olivine phenocrysts. Mugearite.	[3825,4865]
VH173	Feeder dyke, fine grained, vesicular basalt full of small fresh olivines.	[3823,4862]

VH174	Sheet of basalt lava intercalated with bedded tuffs. As VH173.	[3824,4856]
VH175	Stream bed, large pillow lobes. Benmoreite, rare plagioclase and pyroxene phenocrysts.	[3808,4875]
	North eastern flanks of Snaefell	
VH176	Reddened, oxidised subaerial deposit of cinders and spatter, near to summit at ~1775m. Mugearite composition.	[3841,4799]
VH177	Feeder dyke, rather altered hawaiite with abundant large plagioclase phenocrysts.	[3839,4806]
VH178	Coarse tuff.	[3838,4809]
VH179	Basalt, vesicular, abundant plagioclase and rarer olivine phenocrysts.	
VH180	~1500m, fine grained hawaiite, rare plagioclase phenocrysts.	[3837,4810]
VH181	~1420m, aphyric hawaiite.	[3836,4814]
VH182	Dyke, as VH181.	
VH183	~1200m, scree sample. Mugearite, plagioclase phyric.	[3831,4824]
VH184	~1260m, break in slope. Plagioclase phyric mugearite.	
	Vatnsdalur	
VH185	Tuff	[3834,4833]
VH186	Altered, basaltic unit, large plagioclase phenocrysts.	[3834,4384]
VH187	Upper unit, aphyric, flinty mugearite.	
VH188	Altered, fragmental basalt.	[3825,4836]
	Sandfell	
VH189	Benmoreite, Platy weathering, few feldspar phenocrysts.	[3818,4841]
VH190	~3m wide feeder dyke, feldspar phyric benmoreite.	[3816,4843]
VH191	Friable, very felsic xenoliths.	[3816,4844]
VH192	Calcite/aragonite vein in tuffs.	
VH193	Feeder dyke at summit, benmoreite, containing partially resorbed feldspar megacrysts.	[3815,4846]
VH194	Feeder dyke, feldspar phyric benmoreite.	[3815,4849]
VH195	Large ?pillow lobe, fine grained, olivine phyric basalt.	[3828,4844]
	Thjofahnjukur	
VH196	Eastern most hill. Feeder dyke, plagioclase and pyroxene phyric basalt.	[3840,4736]
VH197	1122m, Flinty, subaerial lava flow, or series of flows, each ~3m thick. Basal flow, tholeiitic basalt, few small phenocrysts of olivine, plagioclase and pyroxene.	[3864,4731]

VH198	Topmost flow in series. As VH197.	
VH199	Fine grained hawaiite, few plagioclase phenocrysts.	[3880,4731]
	Ha'alda. *(Not show on map, lies to the south of B'jalfafell).*	
VH200	Breccia, olivine, plagioclase and pyroxene phyric tholeiitic basalt.	-
VH201	Columnar jointed subaerial basalt flow, exposed in stream bed. Pyroxene and plagioclase phyric tholeiitic basalt.	-
VH202	Second exposure in stream bed. Plagioclase phyric tholeiitic basalt.	[3912,4725]
	North west flank Snaefell	
VH203	Breccia, basaltic, abundant large plagioclase phenocrysts.	[3849,4816]
VH204	Stony rhyolite, rich in feldspar and acicular pyroxene phenocrysts.	[3843,4812]
VH205	Very edge of corrie, fine grained aphyric mugearite lava.	[3844,4812]
VH206	Rhyolite ridge between corries. Soft and evidently heavily hydrated.	[3850,4810]
VH207	Mugearite block caught up in rhyolite.	
VH208	Moraine sample, hawaiite, olivine, plagioclase and clinopyroxene phenocrysts.	[3849,4811]
VH209	Second moraine sample, hawaiitic, abundant plagioclase phenocrysts, rare clinopyroxenes.	
VH210	Third moraine sample, as VH208.	
	Eastern Snaefell	
VH211	Dyke in stream bed, hard and flinty, plagioclase phyric, basaltic andesite.	[3811,4804]
VH212	Lobate outcrop, olivine and pyroxene phyric basalt.	
VH213	Pillow complex, plagioclase and pyroxene phyric basalt.	[3813,4784]
VH214	Pillow rind.	
VH215	Lappilli tuff.	[3818,4781]
VH216	Small dyke cutting tuffs. Fine grained, vesicular plagioclase phyric basalt.	[3819,4779]
VH217	Breccia. Dark, fine grained, olivine phyric hawaiite.	[3822,4775]
VH218	Flinty, banded hybrid dome, benmoreitic composition.	[3825,4771]
VH219	Dyke? below dome. Fine grained, almost aphyric hawaiite.	
VH220	Scree, Fine grained plagioclase (and olivine) phyric mugearite.	
VH221	Dyke, very fine grained almost aphyric mugearite.	[3830,4773]
VH222	~1150m, feeder dyke, very fine grained plagioclase phyric mugearite.	[3829,4776]
VH223	1200m, mugearite lava.	[3827,4786]

	North of Nalhushnjukur	
VH224	Fine grained plagioclase and pyroxene phyric tholeiitic basalt, showing platy weathering, .	[38124884]
VH225	Large irregular body of lava, possibly marking the vent for a subglacial eruption. Benmoreite, few plagioclase and pyroxene phenocrysts. Not very fresh, rusty staining.	[3808,4878]
VH226	More distal facies, pillow-like lobes. Mugearite, few plagioclase and pyroxene phenocrysts.	[3805,4873]
VH227	Coarse lappilli tuff.	[3805,4873]
	Hafursfell	
VH228	Feeder dyke, plagioclase phyric mugearite.	[3796,4870]
VH229	Feeder traceable from here to summit, plagioclase phyric hawaiite.	[3785,4867]
	East of Snaefell	
VH230	Aphyric basalt.	[3810,4776]
VH231	Feeder dyke system grading up into breccias. Olivine phyric basalt.	[3809,4793]
VH232	Tuff, low density, black and glassy. Notable lack of palagonite.	
VH233	Breccia, messy altered rock, vesicles showing infilling of secondary minerals. Basaltic, abundant large, stained plagioclase and ?pyroxene phenocrysts.	[3813,4790]
VH234	Breccia, plagioclase phyric mugearite.	[3813,4784]
VH235	Dyke, fine grained, aphyric, flinty basaltic andesite.	[3810,4781]
VH236	Subaerial lava flow top, small scale jointing. As VH235.	[3811,4779]
VH237	Altered (rusty staining), aphyric basaltic andesite, same unit as VH235.	[3814,4766]
VH238	Platy jointed lava flow - as VH235.	[3815,4762]
VH239	Rhyolitic lava overlying basaltic andesite, flow banding picked out by alteration. Tholeiitic.	
VH240	Fine grained aphyric, tholeiitic basalt.	[3827,4749]
VH241	Second, fine grained aphyric tholeiitic basalt.	[3839,4741]
VH242	Breccia, appears altered, fine grained tholeiitic basalt, rare plagioclase phenocrysts.	[3841,4742]
VH243	Feeder dyke, sparsely plagioclase phyric mugearite.	[3842,4744]
VH244	1-2m thick, ?subaerial columnar jointed lava flow. Fine grained, sparsely plagioclase phyric mugearite.	[3844,4745]
	Snaefellshals	
VH245	Breccia, fairly altered appearance, aphyric hawaiite.	[3841,4755]

VH246	Feeder dyke at summit, basaltic, abundant plagioclase and rare clinopyroxene phenocrysts.	[3839,4755]
	South eastern flank of Snaefell	
VH247	Feeder system in subglacial unit, fine grained basalt with fairly abundant small fresh olivine phenocrysts.	[3835,4781]
VH248	Top of unit, as VH247.	[3836,4786]
VH249	Overlying olivine-phyric unit, streaky hybrid. Compositionally a trachyte.	[3836,4787]
	Co-mingling magmas	
VH250	Highly vesicular, cindery fine grained aphyric benmoreite.	[3836,4788]
VH251	Streaky hybrid, fairly glassy, compositionally a benmoreite.	
VH252	?Basic end-member, compositionally a benmoreite.	
VH253	Acid end member, highly porphyritic obsidian.	
VH254	Overlying zone of magma co-mingling, separated from it by a red, oxidised cinder horizon, Fine grained plagioclase phyric mugearite.	
VH255	Fine grained, platy weathering, sparsely plagioclase phyric mugearite, lower of ?two subaerial flows, separated from each other by a cinder and rubble horizon.	[3833,4787]
VH256	Upper flow unit.	
VH257	Dark, rather cindery olivine phyric basalt.	[3838,4770]
VH258	Fine grained, plagioclase phyric mugearite.	[3844,4775]
	Around Hafursfell	
VH259	Fine grained, platy weathering mugearite lava flow.	[3802,4844]
VH260	Stream section, columnar jointed lava flow, tholeiitic basalt.	[3822,4877]
	Hamar	
VH261	Feeder dyke, fine grained, vesicular basalt with abundant small, fresh olivine phenocrysts.	[3866,4798]
VH262	Feeder dyke, as VH261, but more abundant larger olivines.	[3859,4794]
VH263	Small, isolated pillows and breccia, fine grained mugearite, abundant small tabular plagioclases and rarer clinopyroxenes	[3853,4788]
VH264	Feeder dyke, platy weathering, sample as VH263.	[3851,4789]
VH265	Altered, very vesicular mugearite.	[3848,4789]
VH266	As VH13.	[3874,4794]

	Western Flank of Snaefell	
VH267	Outcrop with well developed radiating columnar jointing, fine grained basalt, just a few largish feldspar phenocrysts.	[3873,4792]
VH268	Fine grained, platy, aphyric rhyolite flow, ~10m thickness visible.	[3869,4815]
VH269	Fine grained, mugearite flow, few plagioclase phenocrysts.	
	Grjotahnjukur	
VH270	Dyke, fine grained almost aphyric tholeiitic basalt.	[3886,4855]
VH271	Fine grained plagioclase phyric basalt.	[3888,4860]
VH272	Platy, altered plagioclase rich tholeiitic basalt.	[3881,4853]
VH273	Top of waterfall, aphyric tholeiitic basalt flow.	[3877,4881]
VH274	Next flow up succession, platy, aphyric tholeiitic basalt.	[3875,4880]
VH275	Lava flow beneath VH273, also a tholeiitic basalt.	[3878,4882]
	Thordafell	
VH276	Feeder dyke, olivine, plagioclase and clinopyroxene phyric basalt.	[3891,4763]
VH277	Porous gabbroic xenoliths.	
VH278	Red "bole" horizon from between lavas from the Plio-Pleistocene lava pile - between VH273 and VH275.	[3900,4881]
	Hamar	
VH279	Vitric tuff.	[3864,4793]
VH280	Tuff, large (cms) glassy lappilli set in a very fine grained, palagonitised matrix.	
VH281	Porous, gabbroic xenolith with glass lined cavities.	
	Saudahnjukur West	
VH282	Cindery pillow basalt.	[3914,4794]
VH283	Columnar jointed outcrop of basalt.	[3922,4805]
	South of Snaefell itself	
VH284	Vesicular, porphyritic pitchstone.	[3852,4775]
VH285	Columnar jointed basaltic lava flow, ~2m thickness visible.	[3843,4750]
	Saudahnjukur East	
VH286	Fresh, glassy feldspar phyric benmoreite.	[3903,4787]

Nalhushnjukur

VH287	Tuff, fine grained and very well consolidated - unusually resistant to erosion.	[3814,4866]

Moraines

MA1-14	Moraine of "Creeping Glacier" ("C" in figure 2.3).	[3868,4815]
	Range of compositions, basalt to rhyolite inclusive.	
MB1-11	Moraine of Halsjokull ("A" in figure 2.3).	[3820,4810]
	Range of compositions, basalt to rhyolite inclusive.	

Most samples described as "altered" have been excluded from all geochemical and petrogenetic discussions completely, but are included in the data set - if analysed - just for completeness. These include: VH83, VH158, VH159, VH186 and VH207..

Appendix 2
Analytical Geochemistry

A2.1 Sample preparation

Whole rock samples weighing ~1 kg were collected in the field, where every effort was made to take only fresh rock. Weathered edges were mostly removed with a hammer. Back in Durham these samples were split using a clipper saw and all remaining weathered edges trimmed off. After washing to remove surface contamination (e.g. rock flour from the saw), the samples were coarsely crushed to ~5mm grainsize using a *Fritsch Pulverisette* jaw crusher (type 01-704). At this stage visibly altered particles/vein materials (rare) were removed by hand. The jaw crusher plates were carefully cleaned between samples, using a wire brush and absolute alcohol. Approximately 150g of sample was then ground to a fine powder using an agate ball mill, run for 30 minutes. This was then bagged, labelled and stored under dry conditions. Most of the samples in this study were very fine grained; thus this sample size was considered sufficient to give a representative analysis.

A2.2 X-ray fluorescence (XRF) analysis

All XRF work was carried out at Durham and the results are presented in appendix 3. 10 major elements were analysed for, and the results expressed in oxide form, along with 17 trace elements (including 3 REEs), expressed as parts per million. Fused discs (30mm in diameter) were used for major element analysis and pressed powder pellets for trace elements.

Fusion disc preparation

First the loss on ignition (LOI - H_2O+) was determined. About 4g of dry rock powder was accurately weighed out into a pre-weighed porcelain crucible, then heated in a furnace at 900°C for 2 hours. The ignited powders were then allowed to cool in a desiccator before being re-weighed, and then put into air-tight sample bottles for storage.

Approximately 0.45g of ignited powder was then accurately weighed out and exactly five times this amount of lithium tetraborate flux (Johnson Matthey "Spectroflux 100B") added. This was then thoroughly mixed in a pestle and mortar before being placed in a Pt-Au crucible (with lid) and heated in a furnace at 1050°C for 20 minutes. The molten glass was then poured into graphite moulds on a hotplate set at 250°C and the disc formed using a stainless steel plunger. The discs were allowed to cool slowly before being bagged and labelled, then stored in a desiccator prior to analysis. Great care was taken to avoid touching the analytical surface, since this results in contamination from sweat, especially affecting Na_2O, K_2O and P_2O_5 in the resulting analysis (Kerr & Hardy 1993).

Powder pellet preparation

Approximately 8g of rock powder was thoroughly mixed with about 13 drops of PVA "Mowiol" organic binder solution in a small beaker, then placed in a mould. This was then subjected to 10 tonnes pressure in a hydraulic press for 2 minutes. The resulting pellet was dried overnight in an oven at 100°C, before being labelled and bagged.

XRF analysis

XRF analysis was carried out using a Philips PW1400 X-ray spectrometer incorporating a PW1500/10 72 sample changer with a 3 kW rhodium anode tube as the X-ray source (accelerating potential =80 kV, 30na or 55kV, 50 na for REEs). For some of the major element analyses in this study a chromium anode tube was used due to Rh tube failure. A Cr tube is as good if not better than a Rh one for major elements, but does not give good results for trace elements; whereas a Rh tube gives good results for both. Therefore a Rh tube is normally used to avoid changing tubes, and thus the need for more calibrations (potentially bringing in errors), between major and trace element analysis. Philips X40 software was used to process the raw count rates.

Calibration was carried out using international standard materials of "known" composition (Govindaraju 1989). For each element (after correction for inter-element effects etc.) the X40 program generates a plot of count rates vs known concentration of each element, and then calculates a best-fit line. The calibration may be improved by deleting points (samples) which fall far from the regression line.

Data accuracy and precision

To assess the accuracy of each calibration and the overall data set (which was created over a two-year period using more than one calibration), international standards were run as unknowns. An overall average value and standard deviation for

three such standards - BHVO-1, AGV-1 and G2, which encompass the compositional range displayed by the Snaefell suite - are presented in table A2.1, along with accepted values (Govindaraju 1989).

Sample	BHVO-1			AGV-1			G-2		
	rec	x (n=7)	2σ	rec	x (n=7)	2σ	rec	x (n=7)	2σ
SiO2	**49.94**	49.64	0.45	**58.79**	59.98	0.62	**69.08**	69.04	0.76
Al2O3	**13.80**	13.66	0.31	**17.14**	17.49	0.29	**15.38**	15.44	0.33
Fe2O3(T)	**11.70**	12.24	0.12	**8.80**	6.86	0.11	**3.62**	2.63	0.11
MgO	**7.23**	7.37	0.22	**1.53**	1.66	0.06	**0.75**	0.78	0.04
CaO	**11.40**	11.38	0.06	**4.94**	4.95	0.05	**1.96**	1.92	0.02
Na2O	**2.26**	2.33	0.11	**4.26**	4.39	0.06	**4.08**	4.12	0.12
K2O	**0.52**	0.52	0.01	**2.91**	2.96	0.01	**4.48**	4.45	0.02
TiO2	**2.71**	2.72	0.02	**1.05**	1.06	0.01	**0.48**	0.48	0.00
MnO	**0.17**	0.17	0.00	**0.09**	0.10	0.00	**0.03**	0.03	0.00
P2O5	**0.27**	0.27	0.01	**0.49**	0.50	0.02	**0.14**	0.14	0.02
Total	**100.00**	100.33	0.41	**100.00**	100.10	0.72	**100.00**	99.25	0.93
		(n=5)			(n=6)			(n=6)	
Nb	**19.00**	17.38	2.56	**15.00**	15.83	0.85	**12.00**	14.72	2.60
Zr	**179.00**	172.82	14.91	**227.00**	225.00	11.35	**309.00**	307.60	7.61
Y	**27.60**	26.48	1.69	**20.00**	21.35	1.00	**11.00**	10.42	1.58
Sr	**403.00**	386.02	9.70	**662.00**	671.30	9.06	**478.00**	473.58	11.68
Ga	**21.00**	21.00	3.72	**20.00**	19.50	3.51	**23.00**	20.23	1.32
Zn	**105.00**	100.36	3.32	**88.00**	84.82	3.16	**86.00**	86.80	5.82
Cu	**136.00**	135.48	7.56	**60.00**	62.00	1.33	**11.00**	12.97	3.21
Ni	**121.00**	120.10	8.09	**16.00**	18.13	3.12	**5.00**	5.77	2.13
Co	**45.00**	42.76	2.96	**15.30**	14.50	3.28	**4.60**	3.52	0.87
Cr	**289.00**	285.46	17.86	**10.10**	14.23	3.12	**8.70**	8.82	7.27
V	**317.00**	313.34	11.50	**121.00**	129.90	3.26	**36.00**	40.77	5.31
Rb	**11.00**	10.44	2.06	**67.30**	68.55	2.07	**170.00**	165.00	7.96
Ba	**139.00**	141.14	13.05	**1226.00**	1231.80	17.89	**1882.00**	1889.85	34.57
Sc	**31.80**	31.72	7.41	**12.20**	13.03	3.08	**3.50**	3.45	2.32
		(n=5)			(n=5)			(n=5)	
La	**15.80**	16.76	2.53	**38.00**	38.33	1.29	**89.00**	86.74	4.45
Ce	**39.00**	41.24	2.85	**67.00**	71.17	2.84	**160.00**	153.34	9.38
Nd	**25.20**	25.92	2.78	**33.00**	35.90	1.60	**55.00**	51.20	4.34

Table A2.1 International standard materials analysed by XRF as unknowns among the samples in this study. rec = recommended value (Govindaraju 1989), x = arithmetic mean of analyses and 2σ = twice the standard deviation.

Precision and reproducibility were assessed using internal monitors. Three samples - VH10, VH35 and VH94 - were included in all runs. In larger runs, more than one of each - ie. more than one pellet or disc. The results of this are presented in table A2.2 and it can be seen that precision and reproducibility are fairly good.

Sample	VH10		VH94		VH35	
	x (n=16)	2σ	x (n=7)	2σ	x(n=14)	2σ
SiO2	47.20	0.45	49.90	0.49	71.61	0.71
Al2O3	14.74	0.27	14.89	0.20	14.17	0.51
Fe2O3(T)	10.80	0.46	13.73	0.57	2.20	0.12
MgO	11.02	0.22	4.11	0.10	0.02	0.03
CaO	11.87	0.07	7.99	0.05	0.69	0.02
Na2O	2.09	0.21	4.08	0.15	5.61	0.21
K2O	0.43	0.02	1.20	0.00	3.98	0.03
TiO2	1.62	0.02	3.01	0.02	0.16	0.01
MnO	0.16	0.01	0.26	0.01	0.07	0.00
P2O5	0.21	0.01	0.84	0.02	0.03	0.02
Total	100.18	0.86	100.07	0.74	98.52	0.73
	(n=10)		(n=13)		(n=13)	
Nb	15.40	1.51	39.04	4.08	96.55	17.22
Zr	100.88	62.93	242.30	29.00	582.98	39.99
Y	19.02	1.87	44.00	5.53	83.22	16.56
Sr	356.53	12.24	476.02	28.63	57.32	16.57
Ga	16.43	4.09	22.83	2.77	28.02	3.90
Zn	79.65	4.98	126.33	6.66	117.75	3.00
Cu	91.29	8.82	12.71	3.71	1.80	2.86
Ni	237.90	4.95	4.15	2.31	1.70	3.35
Co	56.45	9.31	31.33	5.96	2.59	2.16
Cr	885.03	37.66	4.93	4.53	0.85	2.13
V	274.94	8.53	164.42	6.36	2.61	3.09
Rb	8.91	1.46	28.32	4.36	91.52	17.67
Ba	150.77	7.42	311.32	22.13	683.35	23.93
Sc	33.84	4.90	25.95	5.04	1.15	2.18
	(n=8)		(n=8)		(n=7)	
La	13.55	2.56	37.32	4.54	90.82	9.12
Ce	30.01	4.85	74.64	17.46	190.57	16.03
Nd	17.17	3.80	48.30	4.49	86.81	4.77

Table A2.2 Internal standards analysed repeatedly in every XRF run. Abreviations as in table A2.1

A2.3 Inductively coupled plasma mass spectrometry (ICP-MS)

A subset of samples was chosen to cover the compositional and stratigraphic range of the suite. These were then analysed by ICP-MS for REEs and selected trace elements (Ba, Nb, Rb, Sr, Y, Th, U and Pb). The results are presented in appendix 6. Analysis was carried out in 2 visits to the NERC facility at the Centre for Analytical Research in the Environment (CARE), Imperial College at Silwood Park, Ascot.

Sample preparation

The powdered samples were first dried at 100°C overnight. Then 0.1 ± 0.001g was weighed out and digested by boiling in 4ml of 48% ARISTAR grade HF and 1ml of ARISTAR grade HNO_3 in a sealed Savillex bomb for 24 hours. The lid was then removed, washed in HNO_3 and the washings added to the sample, which was subsequently allowed to evaporate down to leave nitrate salts. 1ml of HNO_3 was then added and the sample allowed to evaporate down again; this was then repeated. After cooling for 10 minutes, 2.5 ml HNO_3 and ~20 ml deionised water was added to each,

the bombs sealed, and boiled for 30 minutes to dissolve the salts. The cooled solutions were then made up to 50 ml in volumetric flasks with more deionised water and stored in plastic bottles prior to analysis. Along with each batch of samples a reagent blank and three international standards were prepared in the same manner. Prior to analysis aliquots of the solutions were diluted by a further factor of 10.

ICP-MS analysis

Analysis was carried out using a FI Elemental PlasmaQuad STE, with a detection limit of <0.01 $ngml^{-1}$ for most elements. It was calibrated using solutions of known elemental concentrations. Corrections for drift over the run were made by analysing one such solution - a "drift monitor" - after every 5 samples. Raw counts were corrected for drift and converted to ppm values using "in house" software at the facility. The values obtained for the preparation blank were then subtracted and finally correction was made for the dilution factor.

Data accuracy

To assess the data accuracy the international reference materials (BHVO-1, AGV-1 and G2) were analysed in both analytical runs. The average values along with the accepted values (Govindaraju 1989) are given in table A2.3. From this it can be seen that the results compare favourably with accepted values.

	BHVO-1	av	AGV-1	av	G2	av
Ba	**139.00**	126.99	**1226.00**	1165.98	**1882.00**	1801.21
Nb	**19.00**	18.46	**15.00**	14.25	**12.00**	11.99
Rb	**11.00**	9.47	**67.30**	64.54	**180.00**	161.40
Sr	**403.00**	400.90	**662.00**	656.62	**478.00**	468.32
Y	**27.60**	24.92	**20.00**	18.07	**11.00**	8.61
La	**15.80**	15.71	**38.00**	37.70	**89.00**	87.88
Ce	**39.00**	37.52	**67.00**	66.42	**160.00**	159.66
Pr	**5.70**	5.51	**7.60**	8.42	**18.00**	16.33
Nd	**25.20**	25.94	**33.00**	32.67	**55.00**	56.47
Sm	**6.20**	6.21	**5.90**	6.17	**7.20**	7.27
Eu	**2.06**	2.35	**1.64**	1.86	**1.40**	1.73
Gd	**6.40**	7.19	**5.00**	5.95	**4.30**	7.16
Tb	**0.96**	1.07	**0.70**	0.78	**0.48**	0.76
Dy	**5.20**	5.61	**3.60**	3.81	**2.40**	2.29
Ho	**0.99**	1.09	**0.67**	0.76	**0.40**	0.64
Er	**2.40**	2.91	**1.70**	2.12	**0.92**	0.96
Tm	**0.33**	0.41	**0.34**	0.34	**0.18**	0.16
Yb	**2.02**	2.27	**1.72**	1.99	**0.80**	1.03
Lu	**0.29**	0.37	**0.27**	0.35	**0.11**	0.24
Pb	**2.60**	2.47	**36.00**	36.19	**30.00**	29.34
Th	**1.08**	1.31	**6.50**	6.22	**24.70**	23.17
U	**0.42**	0.45	**1.92**	1.87	**2.07**	1.77

Table A2.3
International standards prepared along with samples and analysed as unknowns by ICP-MS. Vales for standards are from Govindaraju (1989), av = average value obtained from the 2 analytical runs.

Comparison with XRF

Ba, Nb, Rb, Sr, Y, La, Ce and Nd were analysed for by both XRF and ICP-MS, allowing a comparison between the two analytical methods. Figure A2.1 shows plots comparing the results, and it can be see that they compare fairly well. There is however quite a lot of scatter in the results for Sr at higher concentrations (>400ppm), Y appears to give systematically higher results by XRF, compared with those obtained by ICP-MS, and Nb gives higher results by ICP-MS. Such comparisons have also allowed poor analyses to be picked out. (Low concentrations from ICP-MS, for instance, could mean incomplete dissolution of the rock powder.)

A2.4 Electron microprobe analysis

Polished thin sections were made at Durham. These were mounted on glass slides 48 x 25 mm and ~30μm thick; ie.a standard rock thin-section, allowing petrographic study. These were then carbon coated and stored in a desiccator. Results are given in mineral groupings in appendix 5.

Analysis was carried out mostly at the NERC facility at Manchester, although in the early part of the project a few samples were analysed using Durham's own microprobe. The microprobe at Manchester is a modified Cambridge Instruments Geoscan and uses Energy Dispersive Spectrometry (EDS). The beam diameter was about 2μm and the beam current 5nA at 15kV. A "live time" of 60 seconds was used for each analysis and data processing was carried out using a LINK-290 package. Standard spectra are stored on the hard disc of the on-line computer and these are compared with unknowns. A Co metal standard is used as a monitor sample to correct for any long-term drift. The Durham machine is a Cambridge Instruments Geoscan Mark 2 (bought in 1965) and although fitted with both Wavelength Dispersive spectrometers and Energy dispersive spectrometers (WDS and EDS), only the EDS system is currently used. The electron beam diameter is larger than that on the Manchester machine at 5-10μm; thus it is less good for analysing groundmass minerals. Again the beam current was 5nA at 15kV. A "live time" of 100 seconds was used and data processing carried out on a LINK-AN10/55S package using the ZAF-4/FLS program.

Three mineral standards of known composition (Sweatman & Long 1969) were analysed on both microprobes to check the calibrations, and to allow comparison between the two microprobes. These were jadeite, for Na, wollastonite for Ca and Si, and olivine for Mg, Si and Fe.

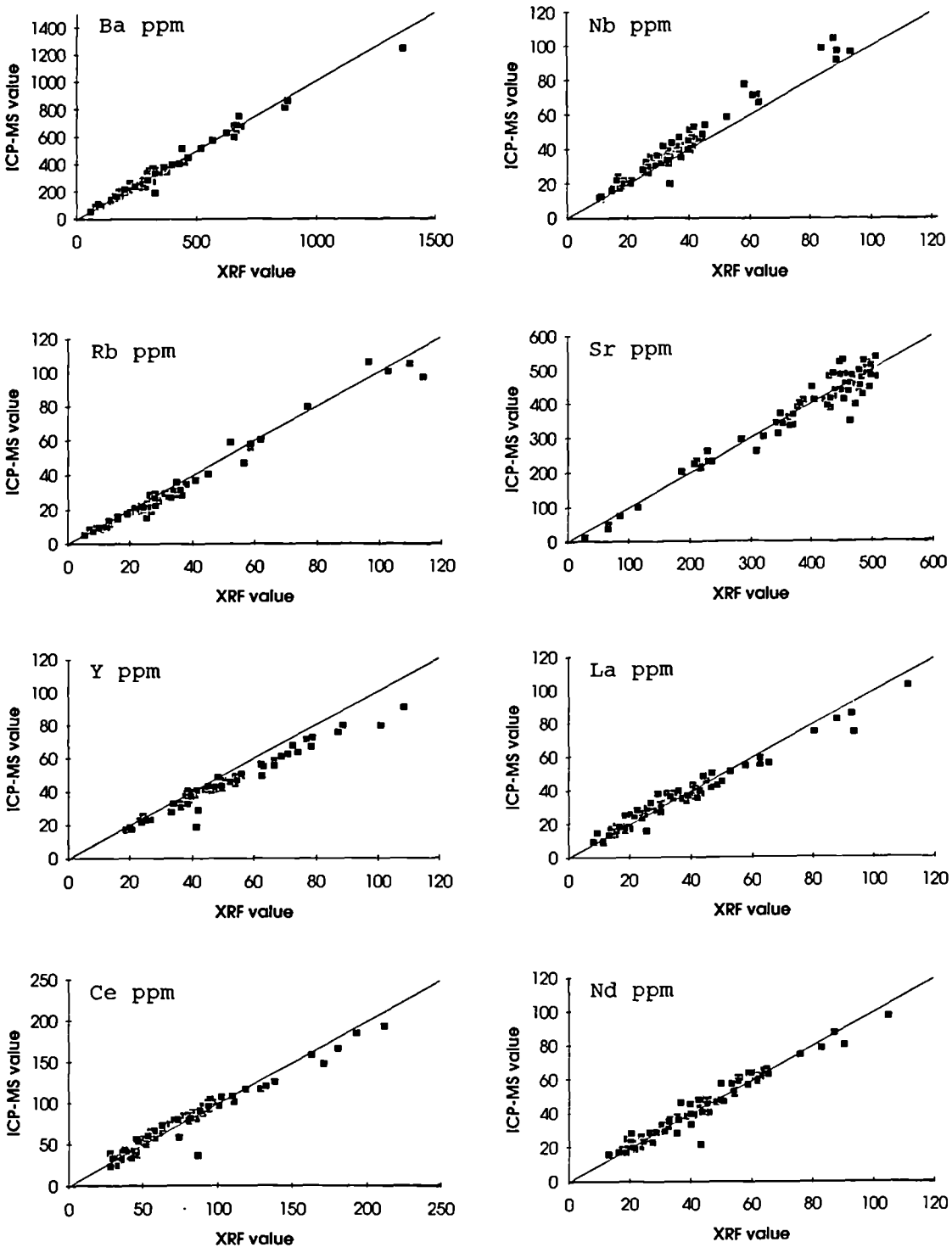

Figure A2.1 Results obtained by ICP-MS plotted against those obtained by XRF for selected elements.

Mineral	Wolastonite			Olivine			Jadeite		
standard	rec	Dur	Man	rec	Dur	Man	rec	Dur	Man
SiO2	**51.350**	50.293	51.503	**40.820**	41.270	41.320	**59.430**	59.454	59.518
TiO2	**0.000**	0.161	0.000	**0.000**	0.062	0.046	**0.000**	0.000	0.012
Cr2O3	**0.000**	0.197	0.226	**0.000**	0.000	0.032	**0.000**	0.000	0.000
Al2O3	**0.000**	0.000	0.263	**0.000**	0.229	0.000	**25.000**	25.022	25.219
FeO	**0.390**	0.365	0.369	**9.800**	9.404	9.770	**0.220**	0.109	0.059
MnO	**0.000**	0.124	0.239	**0.140**	0.000	0.071	**0.000**	0.031	0.025
MgO	**0.000**	0.000	0.123	**48.840**	49.487	49.496	**0.000**	0.000	0.000
CaO	**48.020**	48.583	47.071	**0.000**	0.049	0.000	**0.000**	0.087	0.037
Na2O	**0.000**	0.072	0.117	**0.000**	0.068	0.225	**15.290**	15.001	15.129
K2O	**0.000**	0.030	0.000	**0.000**	0.000	0.028	**0.000**	0.000	0.000
NiO	**0.000**	0.000	0.000	**0.350**	0.000	0.000	**0.000**	0.000	0.000
Total	**99.760**	99.960	99.911	**99.950**	100.997	100.988	**99.940**	99.705	99.999

Table A2.4 Mineral standards, rec = accepted compositons (Sweatman & Long 1969), Dur and Man = values obtained for analysis of standard materials at Durham and Manchester respectively.

Table A2.4 gives the accepted compositions for the three mineral standards and the results of analysis from both instruments. Both give very similar results, close to the accepted standard compositions.

A2.5 X-ray diffraction (XRD)

<0.5g of sample was required for each analysis. This was finely ground in a pestle and mortar and mounted on a glass slide using acetone. Clay samples were sedimented through distilled water, rather than mounted directly in acetone, to orient the fragments and hence produce better peak resolution in the resultant trace. Analysis was done at Durham using a Philips PW1130 2kW X-ray diffractometer assembly with a Cu anode tube as the X-ray source. The power was set at 40kW at 25nA and the scanning rate 1° of 2Θ per minute. The chart recorder was set at 10mm per minute (i.e. 1cm = 1° of 2Θ)

Traces were interpreted using the JCPDS mineral powder diffraction file data book and cards.

A2.6 Radiogenic isotope analysis

Sr, Nd and Pb analyses were carried out in collaboration with P. D. Kempton at the NERC Isotope Geoscience laboratory (NIGL), Keyworth, Nottingham. Results are presented in appendix 7.

Sample preparation

0.1- 0.2g of dried rock powder was weighed out, the amount depending on the sample composition. Less is needed for rhyolitic compositions, which have a higher Pb content and are difficult to dissolve. Sr, Nd and Pb were all extracted from the same dissolution. The samples were first leached in 6M HCl to remove secondary minerals such as carbonates, thought to be present in one or two of the samples. This could particularly effect the results for Sr. Lack of laboratory time prevented any further work on unleached samples that could have quantified such effects. After dissolution using 1ml of HNO_3 combined with 3 to 5ml of HF, residues were converted to nitrate and finally chloride; 1ml of HBr was then added to the residue. Pb was separated by passing the samples through columns prepared from PVP disopsible pipette tips fitted with a 2mm diameter polyethylene frit and containing Dowex 1 x 8 200-400 mesh resin. The Sr and Nd fractions were then collected in 2mls of 1M HBr and Pb collected in 1ml 6M HCl. Sr and Nd fractions were then purified using standard one and two-column cation exchange techniques respectively. A reagent blank was prepared at the same time.

Analysis

Sr, Pb and Nd were run as the metal species on single Ta, single Re and double Re-Ta filaments, respectively, using a Finnegan MAT 262 multicollector mass spectrometer at NERC Isotope Geoscience Laboratory (NIGL). Nd analyses for a few samples were also determined using triple Re-Ta filament assemblies using a VG354 multicollector mass spectrometer, also at NIGL. The agreement between the data from the two machines was very good.

Data accuracy

Blanks for Nd and Pb were less than 130pg and 110pg respectively. The Sr blank failed, but the maximum obtained by other users at the lab over the same time period was 500pg. Reference standards throughout the course of the analysis averaged values of $^{87}Sr/^{86}Sr = 0.710217 \pm 32$ (2σ) for NBS 987 standard. For the Johnson Matthey Nd standard, $^{143}Nd/^{144}Nd = 0.511127 \pm 34$ (2σ) for analyses on the Finnegan MAT 262 and 0.511129 ± 12 (2σ) for those on the VG 354. $^{87}Sr/^{86}Sr$ was normalised to

$^{86}Sr/^{88}Sr = 0.1194$; $^{143}Nd/^{144}Nd$ was normalised to a value of $^{146}Nd/^{144}Nd = 0.7219$. Pb mass fractionation was 0.08% per a.m.u. Based on repeated runs of NBS 981 common Pb standard, the reproducibility is better than 0.1%. Pb isotopic ratios were corrected relative to the average standard Pb isotopic compositions of Todt et al. (1984). Internal errors on individual isotope measurements were always much smaller than the standard reproducibility reported here, and therefore the ability to reproduce the standards should be taken as the limiting factor in interpreting the uncertainty of any given analysis.

A2.7 Oxygen isotope analysis

O-isotope ratios in samples were also determined at the NIGL, by P. B. Greenwood. Results are presented in appendix 7.

Sample preparation

Sample aliquots of approx. 6mg were weighed out without further drying or loss on ignition. Carbonate bearing samples were acid treated. Samples were then outgassed under high vacuum at 250°C for 2 hours after loading under dry nitrogen flow.

The oxygen liberation technique of Clayton & Mayeda (1963) employed but using ClF_3 at 600°C as a reagent instead of BrF_5 as described by Borthwick & Harmon (1982). The samples were cleaned-up pre-fluorination by heating to 250°C for 2 minutes with ClF_3 at 100mb absolute pressure, and the clean-up products removed. The oxygen liberation reaction was carried out by heating samples in high purity nickel reaction vessels at 600°C for 14 hours (overnight) with ClF_3 in excess of stoichiometric requirements.

The oxygen yields were converted to CO_2 by reaction with a platinized graphite rod heated to 675°C by an induction furnace. CO_2 yields were measured by a capacitance manometer. The yield for the above process were consistently lower than theoretical expectations. This is the usual case for volcanic rocks, and is generally regarded as a valid precaution to minimise the effects of alteration products on the results. There were, however, some variable yields between replicates in this batch of samples.

Analysis

CO_2 isotopic ratios were measured on a CJS Sciences Ltd. Phoenix 390 mass spectrometer (re-built VG 903 automated triple collector machine) and reported here

in the usual δ notation as per mil deviations relative to the SMOW standard for $^{18}O/^{16}O$ ratios (R) were;

$$\delta_X = [(R_X/R_{std}) - 1] \times 10^3$$

Data accuracy

The ^{18}O SMOW results are normalised through the NIGL laboratory whole rock standard pyroxenite (XRC) and quoted relative to the international standard quartz NBS#28 (African glass sand) at a value of 9.6(3)‰. Currently determined value for NBS#28 is 9.5‰. During the course of this work 4n determinations of the LQS laboratory standard gave 1σ reproducibility of ± 0.1(2)‰. Few replicates were run, but the differences appear generally to be <0.1‰. The overall determinative error for this work is taken to be ± 0.1‰ (1σ), and the interpretations made accordingly.

Appendix 3
XRF Data

In the following tables all XRF data obtained during this study is reported. For sample localities and descriptions see appendix 1.

Major element analyses are presented in weight percent (wt%) and have been recalculated on a volatile-free basis. Analyses were done on fused discs (see appendix 2). Totals between 98 and 102% were deemed acceptable.

Trace element analyses are given in parts per million (ppm) and were carried out on powder pellets (see appendix 2).

	VH1	VH2	VH4	VH6	VH8	VH9	VH10	VH12	VH13	VH14	VH16	VH19	VH20	VH21	VH23	VH24	VH27	VH28	VH30
SiO2	45.85	47.67	48.12	47.13	47.40	54.88	47.43	47.45	49.41	46.49	46.52	47.37	49.89	48.06	63.82	51.56	51.90	51.95	51.79
Al2O3	16.90	16.42	15.42	16.93	17.17	15.02	14.82	15.67	15.24	15.04	14.56	15.24	24.67	14.92	14.45	14.84	14.83	15.26	14.84
Fe2O3*	13.04	13.37	14.15	12.74	12.30	12.09	10.50	11.29	13.99	12.28	11.87	11.45	5.30	11.96	9.38	13.15	13.41	12.74	13.36
MgO	6.81	7.00	4.49	6.46	6.54	2.59	11.01	7.04	4.52	9.20	9.86	9.28	3.83	8.99	0.27	3.40	3.42	2.60	3.34
CaO	12.05	10.36	8.35	11.00	11.10	6.27	11.87	11.95	8.21	10.95	10.95	11.29	12.15	10.80	3.42	7.25	7.28	7.34	7.14
Na2O	2.26	0.88	3.46	2.61	2.65	4.50	2.08	2.40	3.64	2.26	2.22	2.73	3.27	2.41	5.77	4.48	4.43	4.27	4.34
K2O	0.29	0.19	1.14	0.68	0.67	1.72	0.43	0.71	1.08	0.62	0.67	0.68	0.25	0.70	2.58	1.41	1.37	1.37	1.368
TiO2	2.57	2.63	3.27	2.46	2.25	1.98	1.63	1.98	3.31	1.96	1.78	1.82	0.95	1.91	0.63	2.57	2.58	2.59	2.55
MnO	0.19	0.20	0.24	0.18	0.18	0.31	0.17	0.17	0.23	0.17	0.17	0.17	0.07	0.18	0.34	0.29	0.29	0.28	0.27
P2O5	0.32	0.34	0.54	0.31	0.29	0.78	0.21	0.26	0.51	0.26	0.25	0.25	0.08	0.34	0.13	0.98	0.96	0.93	0.97
Total	100.29	99.06	99.19	100.50	100.55	100.14	100.15	98.92	100.21	99.22	98.86	100.28	100.53	100.26	100.79	99.93	100.54	99.41	100.01
LOI	1.93	27.28	0.34	-0.26	-0.06	0.50	0.43	0.15	-0.10	0.69	-0.20	-0.26	0.93	-0.35	-0.29	-0.02	0.51	1.63	0.02
Ba	152.1	191.2	271.2	186.1	183.4	407.1	152.0	183.3	297.1	161.5	163.0	157.9	76.6	175.2	689.6	359.8	352.8	369.7	349.0
Co	52.3	50.1	41.9	45.2	45.5	28.6	54.1	43.2	36.2	55.0	51.4	38.8	26.7	51.7	15.4	32.0	34.2	30.8	32.7
Cr	138.5	93.0	3.3	132.1	94.7	20.1	884.5	401.0	56.9	552.7	723.1	704.1	208.7	690.2	11.9	21.1	56.8	23.9	34.6
Cu	73.1	52.2	8.4	70.7	90.7	3.0	88.3	94.8	20.2	89.4	89.5	83.4	70.4	96.2	5.1	9.1	8.5	7.1	9.3
Ga	18.1	14.7	23.0	18.3	16.6	25.4	16.0	19.5	26.1	16.8	19.8	18.1	21.1	17.3	23.5	20.1	20.5	19.8	20.9
Nb	21.0	19.6	40.4	19.0	19.2	43.0	15.6	21.1	33.5	19.0	17.1	16.6	7.0	19.3	58.4	38.8	38.1	39.8	38.5
Ni	59.0	38.8	5.2	59.1	67.6	3.7	239.6	89.3	5.8	159.4	199.2	168.0	54.6	190.8	2.3	5.1	3.9	9.0	6.2
Rb	2.7	2.0	27.5	12.9	15.3	43.5	9.4	19.1	23.9	14.8	15.4	15.2	4.5	16.6	52.4	31.5	30.4	31.2	31.6
Sc	31.5	32.6	32.2	32.1	33.8	24.0	33.3	35.4	28.3	32.0	32.5	38.7	14.0	31.3	18.7	21.3	20.1	23.4	19.8
Sr	602.3	339.8	479.9	470.7	468.0	454.2	360.9	381.5	457.4	379.3	346.3	325.7	766.7	358.4	284.5	492.5	489.3	505.5	501.4
V	347.8	341.4	238.9	315.8	290.7	56.9	277.6	293.1	243.3	279.8	265.0	266.4	124.0	262.6	1.2	100.1	98.4	107.8	91.6
Y	23.1	21.7	38.8	23.9	25.6	59.6	19.1	22.4	38.7	22.4	20.9	22.7	6.3	20.9	66.7	47.4	46.8	49.1	47.5
Zn	95.3	83.4	122.4	89.3	89.5	137.6	79.5	83.3	115.9	82.1	78.0	82.9	36.7	82.6	144.2	128.0	128.9	133.2	126.9
Zr	156.8	129.6	223.6	143.9	151.6	368.9	109.6	140.9	226.9	138.9	126.3	135.9	20.5	119.3	488.4	246.4	242.7	257.5	251.8
La	18.3	18.5	34.6	18.7	23.1	54.2	13.84	17.6	27.1	17.4	18.1	17.1	3.8	16.9	65.5	43.5	37.8	43.4	40.7
Ce	47.9	38.9	68.1	46.8	48.8	108.8	30.78	45.6	55.9	42.5	40.1	33.4	8.9	35.5	129.6	76.8	78.7	85.4	75.8
Nd	25.3	24.2	41.8	27.6	27.5	62	16.9	24	38.8	20.9	20.9	19.1	50.4	20.5	59	54.2	52.6	54.7	45.8

	VH31	VH32	VH33	VH35	VH36	VH37	VH38	VH40	VH41	VH43	VH45	VH46	VH47	VH48	VH49	VH50	VH52	VH53	VH54
SiO2	51.11	51.10	46.67	71.57	49.86	49.46	70.96	48.90	48.72	48.37	52.03	51.88	51.17	72.40	73.69	47.87	47.33	46.64	48.49
Al2O3	14.70	14.42	14.60	14.19	15.97	14.77	13.77	14.57	14.60	14.65	15.43	15.43	15.21	13.33	13.52	15.89	14.77	14.76	15.82
Fe2O3*	12.92	13.06	11.02	2.27	12.33	14.05	2.68	14.69	14.72	14.64	12.09	12.54	12.44	2.68	2.46	13.31	12.49	14.18	11.63
MgO	3.08	2.92	10.72	0.01	6.97	4.28	0.03	4.53	4.57	4.45	3.36	3.69	3.65	0.04	0.00	5.57	9.30	9.25	7.19
CaO	7.07	7.38	11.43	0.68	11.22	8.28	0.68	8.77	8.79	8.79	8.28	7.83	7.80	0.51	0.49	9.90	11.22	10.57	12.65
Na2O	4.43	4.65	2.13	5.49	1.11	3.8	5.82	3.68	3.72	3.62	3.78	4.06	4.05	5.73	5.73	3.14	2.09	2.27	1.95
K2O	1.40	1.49	0.58	3.96	0.40	1.121	4.13	1.03	1.04	1.05	1.38	1.41	1.35	4.18	4.22	0.87	0.22	0.26	0.09
TiO2	2.45	2.38	1.67	0.16	2.16	3.25	0.17	3.51	3.51	3.48	2.57	2.68	2.68	0.14	0.14	2.48	1.83	2.26	1.66
MnO	0.29	0.30	0.17	0.07	0.20	0.256	0.08	0.26	0.26	0.25	0.28	0.26	0.27	0.08	0.05	0.21	0.18	0.20	0.18
P2O5	0.96	1.00	0.21	0.02	0.39	0.84	0.03	0.72	0.72	0.72	0.80	0.75	0.75	0.02	0.01	0.39	0.18	0.23	0.15
Total	98.42	98.70	99.20	98.54	100.62	100.15	98.35	100.66	100.66	100.02	100.17	100.54	99.36	99.11	100.37	99.62	99.61	100.63	99.80
LOI	0.27	1.82	-0.30	0.39	29.96	-0.39	0.28	-0.72	-0.59	-0.24	1.21	1.13	2.35	0.22	0.27	-0.38	-0.19	-0.56	2.22
Ba	353.4	384.3	149.8	679.2	209.0	300.5	707.9	371.6	280.9	287.8	320.9	302.7	374.9	674.3	629.2	228.9	58.3	89.9	46.3
Co	31.9	31.0	53.3	2.1	45.0	38.3	3.5	32.1	39.3	38.4	27.8	37.8	30.3	3.5	2.7	42.2	52.5	53.2	50.3
Cr	7.0	10.9	752.9	0.6	264.5	4.3	10.1	56.3	3.0	3.0	34.2	5.5	2.3	2.0	2.2	62.7	461.7	305.5	234.7
Cu	11.2	8.2	89.9	1.6	66.9	14.9	7.2	15.1	21.9	29.1	24.1	25.3	14.9	2.6	1.2	83.4	97.5	132.5	125.2
Ga	20.3	25.2	15.4	27.2	15.6	23.8	26.5	20.8	19.8	24.7	25.6	20.6	22.1	28.6	26.7	22.2	21.4	20.2	19.2
Nb	39.2	39.2	15.1	88.1	23.6	36.6	91.8	40.5	33.9	35.7	41.4	34.9	40.6	94.9	88.9	26.6	11.4	13.8	9.1
Ni	5.2	3.5	210.5	1.8	54.0	2.9	1.5	6.2	8.0	9.3	12.9	8.3	4.4	2.7	1.8	35.6	192.1	153.0	81.1
Rb	31.2	32.9	13.9	96.6	8.1	26.7	92.7	28.7	24.9	27.3	34.5	25.0	28.3	108.7	109.8	19.4	5.5	4.6	1.8
Sc	19.8	21.7	30.0	1.5	32.6	28.7	3.2	25.8	29.9	29.4	25.6	31.4	23.1	1.3	0.7	28.8	30.0	30.9	35.4
Sr	507.8	496.2	340.2	66.6	342.8	475.5	65.6	448.7	453.9	454.7	465.1	453.6	454.8	31.9	28.4	430.4	229.5	271.4	192.3
V	90.1	65.2	266.3	2.6	304.8	200.2	2.1	163.0	245.3	242.9	149.5	242.9	159.2	1.0	0.4	318.3	258.1	281.7	288.3
Y	48.8	49.9	19.5	88.8	23.7	40.4	95.9	49.9	37.7	38.5	50.2	38.4	48.0	104.5	108.5	29.6	24.5	26.6	24.3
Zn	128.4	127.9	77.8	117.5	84.1	121.9	141.9	123.0	113.8	117.4	125.7	112.3	122.2	148.7	124.9	89.2	89.2	86.4	88.1
Zr	251.8	263.4	116.7	565.9	147.5	219.6	624.8	275.4	221.6	201.7	302.9	218.9	276.8	612.7	542.0	158.9	100.7	117.5	83.8
La	41.6	43.8	14.8	92.92	23.6	30.9	90.4	41.7	29.2	29.3	39.6	31.9	38.6	99.4	111.5	24	8.4	13.1	8.2
Ce	78.9	91.2	38.5	193.48	54.4	80.5	190.6	76.4	61.6	58.9	84.8	59.9	80.9	208.9	211.9	54.7	27.8	36.6	26.2
Nd	50.9	52.5	16.2	87.4	26.8	52.9	90	50.3	45.9	43	49.7	48.9	48.3	95	105	33.5	13.1	19.1	11.3

	VH56	VH57	VH58	VH59	VH60	VH61	VH62	VH64	VH65	VH66	VH67	VH68	VH69	VH70	VH71	VH72	VH73	VH74	VH75
SiO2	46.46	51.35	48.71	49.67	51.04	51.77	51.54	51.53	60.34	60.17	48.04	60.40	49.49	50.08	49.71	49.43	49.37	47.77	68.40
Al2O3	13.41	14.42	14.65	14.78	15.50	15.75	15.75	15.88	16.22	16.15	16.16	15.97	15.20	14.93	15.09	15.22	15.20	14.59	14.32
Fe2O3*	17.66	12.95	14.26	14.76	12.71	12.56	12.16	12.03	8.75	8.98	13.79	8.52	13.45	13.49	13.66	13.97	14.08	11.07	4.15
MgO	5.35	3.07	3.91	2.53	3.69	3.40	3.44	3.19	1.32	1.44	4.71	1.03	4.10	4.39	4.62	4.67	4.54	10.29	0.26
CaO	9.20	6.94	8.66	8.60	7.74	7.83	8.53	8.06	4.18	4.34	9.66	3.83	7.78	7.90	8.19	8.42	8.40	11.24	1.46
Na2O	2.88	4.54	3.66	3.60	3.92	3.92	4.03	4.11	5.37	5.15	3.22	5.33	3.96	3.73	3.68	3.78	3.49	2.20	5.88
K2O	0.71	1.36	1.31	1.25	1.36	1.34	1.26	1.42	2.34	2.30	0.61	2.53	1.29	1.25	1.17	1.13	1.02	0.66	3.67
TiO2	4.39	2.26	3.31	3.30	2.42	2.38	2.36	2.43	0.92	0.98	3.21	0.78	2.98	3.14	3.30	3.43	3.41	1.71	0.44
MnO	0.25	0.28	0.29	0.33	0.28	0.28	0.33	0.28	0.25	0.26	0.23	0.25	0.24	0.24	0.24	0.24	0.24	0.17	0.08
P2O5	0.51	1.10	0.89	0.88	1.15	1.21	1.25	1.26	0.36	0.41	0.99	0.28	0.59	0.56	0.53	0.54	0.51	0.24	0.09
Total	100.82	98.26	99.64	99.78	99.80	100.45	100.63	100.20	100.15	100.27	100.62	98.93	99.08	99.71	100.19	100.83	100.32	99.98	98.73
LOI	0.85	0.34	1.12	2.54	0.97	1.88	2.81	1.42	0.77	0.85	4.28	1.33	0.12	-0.21	0.21	-0.09	0.44	-0.02	0.65
Ba	166.9	381.7	312.8	306.9	338.1	350.8	361.9	341.8	621.4	629.9	406.8	659.9	321.8	334.5	320.1	299.4	298.9	166.7	874.6
Co	51.5	27.2	35.8	41.5	32.5	32.4	31.3	33.1	13.8	15.0	37.7	11.9	34.3	32.9	34.3	35.4	37.1	52.2	4.2
Cr	35.1	5.3	8.1	4.8	24.8	32.6	24.5	26.8	5.1	10.6	26.9	1.8	8.2	11.0	23.7	16.6	8.7	815.7	2.9
Cu	44.1	9.8	13.4	14.5	19.1	19.2	18.4	16.5	7.9	6.9	11.1	5.6	8.2	12.4	13.1	15.1	14.2	86.0	3.4
Ga	22.6	26.7	21.0	23.6	22.1	21.2	27.4	23.5	28.5	24.1	18.9	25.4	24.7	24.0	27.5	22.9	25.1	18.4	26.7
Nb	25.8	44.7	36.9	37.6	40.5	41.3	42.0	41.1	60.7	59.6	33.0	62.3	38.2	36.9	34.8	34.3	34.5	20.3	93.6
Ni	34.7	3.6	3.8	7.3	13.2	11.8	9.4	15.2	4.3	4.7	4.4	1.5	6.2	2.9	5.7	3.4	3.1	201.2	1.6
Rb	11.5	25.9	31.4	32.5	30.9	27.1	28.1	29.3	54.6	53.2	10.7	62.8	29.2	30.8	27.8	25.5	23.8	15.6	76.9
Sc	30.8	22.3	27.8	26.9	28.3	28.1	24.7	24.2	16.6	15.2	26.7	13.1	27.8	24.8	31.6	30.8	24.7	33.5	2.9
Sr	342.3	473.7	477.3	483.4	481.2	492.6	495.9	509.2	381.4	389.9	1183.4	358.9	460.0	448.7	444.6	451.2	452.4	367.0	114.7
V	371.8	70.7	195.1	197.9	136.6	135.3	132.9	145.8	2.7	1.0	517.8	0.5	217.8	226.9	241.7	253.5	256.7	258.7	26.5
Y	49.3	63.3	42.4	40.9	50.6	50.5	50.1	51.6	68.1	67.9	36.2	68.9	43.8	43.2	40.4	38.6	38.9	21.1	78.9
Zn	129.9	127.5	123.0	123.2	119.5	126.6	123.1	123.8	137.0	134.7	111.5	130.0	117.7	117.3	112.8	117.1	112.2	81.7	119.8
Zr	239.6	339.8	210.6	223.9	245.7	251.5	245.6	248.7	471.5	481.5	209.8	506.7	246.7	229.5	226.7	212.4	223.4	120.9	731.4
La	24.2	46.7	31.4	30.4	47.6	45.6	43.8	41.6	65.4	65.9	30	71.9	33.6	31.2	29.1	29	29.9	14.3	93.8
Ce	58.4	101	63.6	65.9	95.9	88.9	101.7	87.6	137.4	134.8	58.9	140.4	62.8	61.3	62.4	49.9	63.6	42.3	171.17
Nd	41	63	47.6	43	57.1	48.9	56	51.3	61	65	40.8	63	42.4	44.2	43.2	37.1	44.8	17.6	90.77

	VH76	VH77	VH78	VH79	VH80	VH82	VH83	VH86	VH87	VH88	VH89	VH90	VH91	VH92	VH93	VH94	VH95	VH96	VH97
SiO2	50.09	47.34	47.31	59.68	47.86	47.50	45.08	49.62	49.67	48.21	48.95	49.13	49.48	49.8	49.09	49.93	49.33	47.55	60.97
Al2O3	15.39	14.70	14.91	15.72	15.22	16.53	16.36	13.74	13.92	14.49	15.53	15.53	15.48	15.12	14.59	14.74	14.73	15.15	16.37
Fe2O3*	13.48	11.18	12.26	8.43	11.83	12.63	12.58	15.16	15.06	14.76	12.65	12.36	12.34	13.3	14.35	14.37	13.70	12.17	7.86
MgO	4.35	10.04	9.14	1.16	9.16	6.54	6.69	5.37	5.37	5.17	5.95	6.76	5.93	3.91	4.52	4.08	4.02	8.97	1.01
CaO	8.28	11.23	11.30	4.00	11.21	10.76	12.26	10.28	10.28	10.52	9.48	9.84	9.30	7.98	8.80	7.97	8.03	11.23	3.85
Na2O	3.82	2.39	2.34	5.62	2.41	2.79	2.43	2.71	2.73	2.56	3.22	3.13	3.37	3.92	3.67	3.93	3.98	2.37	5.14
K2O	1.25	0.68	0.66	2.51	0.67	0.77	0.52	0.45	0.44	0.35	1.00	0.93	1.04	1.169	1.04	1.20	1.22	0.64	2.48
TiO2	3.19	1.74	1.89	0.86	1.88	2.49	2.399	2.76	2.74	2.63	2.27	2.25	2.27	2.99	3.52	3.00	3.03	1.84	0.82
MnO	0.23	0.17	0.18	0.25	0.17	0.18	0.182	0.22	0.22	0.21	0.23	0.22	0.23	0.247	0.25	0.27	0.27	0.17	0.23
P2O5	0.51	0.25	0.25	0.29	0.27	0.35	0.44	0.28	0.27	0.27	0.85	0.72	0.86	0.86	0.72	0.84	0.85	0.25	0.31
Total	100.59	99.71	100.24	98.52	100.66	100.55	99	100.62	100.72	99.17	100.14	100.88	100.30	99.32	100.56	100.32	99.16	100.34	99.04
LOI	1.60	-0.07	0.08	1.04	-0.10	0.08	2.22	-0.17	0.09	1.23	-0.03	-0.16	0.02	-0.25	-0.10	-0.20	0.01	-0.24	1.73
Ba	318.5	171.9	179.2	668.1	181.6	204.2	188.2	70.9	80.6	74.8	263.6	227.8	256.2	315.8	300.8	311.4	312.9	186.8	660.9
Co	33.8	49.9	50.7	11.9	45.0	40.5	44.5	60.4	59.6	54.2	45.6	44.5	39.7	35.4	34.4	32.2	35.5	52.8	11.0
Cr	12.8	808.1	465.9	2.9	500.9	206.7	113	63.0	53.6	79.8	176.0	312.5	217.5	25.8	21.6	5.6	4.8	440.9	30.9
Cu	28.4	89.8	87.4	4.2	86.0	85.4	84.4	166.1	164.4	158.5	50.0	54.6	43.5	11.6	13.1	12.0	14.6	84.8	6.9
Ga	23.6	15.6	18.8	26.2	17.9	18.7	19.4	21.8	24.2	20.2	21.3	20.7	21.1	24.8	22.5	22.2	21.8	17.0	27.0
Nb	36.9	20.0	21.2	62.7	21.1	24.1	21.6	16.0	16.1	16.1	28.4	29.0	32.1	38.8	38.3	38.1	38.7	19.7	63.3
Ni	5.7	196.8	149.5	3.0	148.4	72.7	65.4	47.4	46.4	44.1	62.3	81.3	60.7	3.3	1.8	4.3	3.5	149.2	3.6
Rb	30.1	16.5	16.5	58.9	16.1	18.0	8.8	10.4	9.3	8.7	22.5	21.7	22.9	25.8	28.6	28.6	28.6	16.2	62.1
Sc	22.6	28.5	32.5	15.1	36.9	35.3	27.1	38.2	38.0	34.7	29.5	31.6	26.9	22.8	24.2	27.7	27.5	35.2	12.9
Sr	467.0	365.9	363.1	349.5	337.4	409.7	441.9	217.2	211.7	228.0	453.3	430.5	442.1	494.2	480.6	465.0	484.6	372.9	361.8
V	236.2	258.3	266.2	-0.5	267.4	285.4	308.9	412.4	391.9	389.5	225.8	231.3	197.4	159.9	169.4	165.0	171.6	272.7	4.8
Y	37.5	20.9	24.5	70.9	24.3	26.5	23.1	40.0	38.6	38.9	36.7	33.6	37.7	43.7	43.5	44.5	43.3	23.2	68.9
Zn	111.2	79.4	86.9	128.4	84.9	96.7	91.3	119.5	118.2	113.6	111.8	100.1	106.4	121.3	120.6	124.2	127.7	86.5	127.3
Zr	242.5	120.6	125.7	521.8	131.6	163.8	149.5	156.9	156.3	151.6	182.6	176.7	196.7	223.4	216.7	230.1	221.3	132.3	505.0
La	33.1	18.6	18.1	62.7	18.3	23.3	17.8	12.5	9.5	11.5	28.5	29	28.9	34.9	35.6	35.86	36.6	18.1	62.6
Ce	60.7	35.2	46.4	132.9	41.9	47.9	54.1	31.8	33.8	30.4	57	56.9	65.7	69.4	70.1	68.52	70.6	37.9	138.6
Nd	46.7	16.1	21.2	64	21.2	26.3	28.4	18.5	19.3	16.7	33.8	35.6	36.7	50.4	48.3	48.38	49.3	18.1	65

	VH98	VH99	VH101	VH102	VH104	VH105	VH106	VH107	VH109	VH113	VH114	VH115	VH116	VH117	VH118	VH119	VH120	VH121	VH122
SiO2	49.89	52.27	47.38	47.14	47.39	49.51	47.21	47.61	50.51	50.40	53.13	51.89	51.16	53.06	48.73	47.39	47.1	47.08	47.08
Al2O3	15.52	14.74	15.20	16.25	14.27	14.85	15.03	15.89	15.47	14.26	14.71	14.62	14.53	14.93	14.58	15.98	15.8	15.38	16.26
Fe2O3*	13.79	13.07	11.73	13.88	12.08	13.54	12.70	12.48	12.47	13.45	13.41	12.93	12.73	12.89	12.05	12.86	13.14	13.20	13.48
MgO	4.32	3.86	9.84	5.68	10.15	4.21	8.82	7.96	4.13	3.71	2.79	3.13	3.21	3.16	6.94	7.93	7.93	8.67	6.99
CaO	8.18	7.71	10.56	10.42	11.47	7.94	10.97	10.74	7.51	7.97	6.96	7.02	6.92	6.83	12.20	10.84	10.83	10.78	10.69
Na2O	3.63	4.01	2.38	2.87	2.23	3.98	2.45	2.70	3.83	4.15	4.56	4.50	4.63	4.55	2.14	2.64	2.62	2.56	2.48
K2O	1.41	1.31	0.73	0.80	0.59	1.15	0.57	0.72	1.46	1.18	1.38	1.34	1.36	1.36	0.15	0.592	0.594	0.59	0.92
TiO2	3.20	2.89	1.90	2.86	1.83	2.91	2.14	2.13	2.70	2.84	2.20	2.30	2.24	2.21	1.89	2.151	2.253	2.08	2.43
MnO	0.23	0.25	0.17	0.19	0.19	0.26	0.18	0.19	0.24	0.31	0.31	0.28	0.29	0.28	0.19	0.179	0.184	0.18	0.20
P2O5	0.54	0.63	0.28	0.30	0.29	1.02	0.25	0.31	0.79	1.28	1.06	1.12	1.10	1.09	0.17	0.24	0.23	0.22	0.30
Total	100.68	100.80	100.19	100.44	100.49	99.38	100.37	100.73	99.10	99.54	100.60	99.14	98.17	100.35	99.04	100.83	100.71	100.76	100.84
LOI	1.21	0.87	-0.14	0.20	-0.31	-0.65	-0.45	-0.30	0.13	0.57	0.93	0.41	-0.31	0.45	2.69	-0.51	0.01	-0.24	1.39
Ba	321.7	379.9	179.6	203.0	166.8	308.5	175.9	191.1	401.6	326.8	389.1	369.3	370.6	390.0	64.8	190.3	194.5	186.9	189.5
Co	33.8	28.7	53.5	50.1	55.5	34.0	46.9	50.0	29.7	32.1	29.1	27.0	28.1	27.2	52.3	46.6	44.3	45.7	52.8
Cr	1.9	12.7	567.1	51.3	644.5	8.3	421.6	261.5	21.7	10.2	17.5	8.1	11.1	21.9	174.9	256.7	249.9	339.8	50.7
Cu	27.2	17.0	82.6	79.8	91.7	13.8	97.2	80.8	13.5	9.9	7.8	9.5	7.7	11.5	104.3	73.8	81.6	87.2	86.0
Ga	20.9	23.5	16.5	23.0	15.9	22.4	19.2	19.4	25.1	24.6	23.0	21.9	24.4	25.6	19.4	19.0	20.3	18.8	21.7
Nb	39.8	40.6	21.2	21.4	19.6	39.8	18.7	21.6	42.5	40.9	44.3	43.0	44.0	44.2	9.4	18.6	17.8	17.9	21.0
Ni	3.5	4.7	174.4	32.6	186.3	8.2	123.4	99.6	2.9	6.9	5.0	2.0	2.8	4.5	75.0	94.5	89.3	111.5	50.8
Rb	34.9	28.8	18.0	20.2	13.4	23.8	13.2	17.1	37.0	24.7	29.4	27.8	27.5	28.5	2.3	13.1	13.7	13.6	23.2
Sc	24.5	22.8	32.6	28.8	32.4	22.8	31.8	28.1	26.5	23.1	20.3	24.1	24.0	22.7	36.2	31.4	38.6	37.7	25.5
Sr	464.7	424.4	385.9	440.5	364.9	498.2	352.0	409.7	431.1	463.8	454.4	467.9	476.5	471.7	206.1	397.8	386.8	388.2	406.2
V	239.8	158.9	259.9	379.4	271.5	155.0	279.2	284.3	183.1	123.4	45.8	71.9	72.8	63.8	298.4	297.5	305.1	261.2	278.5
Y	39.5	51.6	22.5	25.9	22.4	46.2	25.3	25.7	48.3	59.1	62.6	62.4	64.7	63.1	27.3	23.6	24.5	24.2	24.9
Zn	111.6	114.2	82.2	93.7	83.5	115.5	80.2	88.7	118.2	124.5	133.4	126.9	129.4	123.9	95.0	77.7	75.3	76.4	91.6
Zr	269.8	360.9	132.9	143.8	120.9	238.9	134.7	140.2	298.7	318.4	354.6	340.9	345.3	342.8	99.6	121.8	131.8	127.8	154.6
La	31.4	38.4	19.8	15.8	20.3	38.4	16.9	21.8	44.7	45.8	50.1	48.7	48.2	48.3	10	17	16.4	15.6	16.7
Ce	57.8	85.6	45.6	39.5	45.8	71	46.1	50.8	86.9	99	96.7	96.7	97.5	104.2	25.6	42.9	44.9	36.7	43.7
Nd	41.6	49.9	25.2	25.7	23.6	50.6	24.4	30.8	59.5	60.8	60.3	62	62.8	58	14.8	24.2	23.8	21.8	23.9

	VH123	VH124	VH125	VH126	VH127	VH128	VH129	VH130	VH131	VH132	VH133	VH134	VH135	VH136a	VH136b	VH137	VH138	VH139	VH142
SiO2	48.15	48.96	47.84	47.33	49.52	61.54	50.48	47.15	47.70	49.27	55.51	47.93	52.20	72.63	48.86	51.56	71.63	72.31	71.63
Al2O3	14.78	13.28	14.79	15.06	14.98	18.29	15.27	15.20	15.65	14.60	15.16	14.87	14.21	13.18	14.50	14.68	13.34	13.39	13.36
Fe2O3*	15.59	15.76	15.31	14.40	13.16	5.48	13.28	11.63	11.54	13.32	10.75	12.57	14.45	2.73	14.48	13.63	3.19	3.27	3.27
MgO	4.60	6.27	4.91	5.06	4.35	0.74	4.11	9.54	7.79	4.18	2.54	8.27	2.90	0.00	4.43	3.43	0.00	0.00	0.00
CaO	8.83	10.84	9.10	9.07	8.23	4.11	7.91	9.94	10.67	8.24	5.78	10.40	6.69	0.37	8.77	7.17	0.44	0.46	0.40
Na2O	3.47	2.50	3.20	3.09	3.66	6.23	3.93	2.64	2.60	3.83	4.73	2.63	4.37	5.48	3.56	4.33	6.01	5.42	5.73
K2O	0.89	0.24	0.95	1.10	1.11	1.85	1.126	0.73	0.65	1.15	1.97	0.80	1.36	4.36	1.04	1.33	4.30	4.40	4.30
TiO2	3.63	2.46	3.72	3.26	3.29	0.70	3.055	2.05	2.16	3.23	1.80	2.07	2.13	0.14	3.46	2.59	0.17	0.17	0.17
MnO	0.25	0.23	0.23	0.21	0.25	0.19	0.251	0.18	0.18	0.26	0.27	0.20	0.37	0.08	0.25	0.28	0.09	0.10	0.10
P2O5	0.64	0.23	0.51	0.40	0.64	0.21	0.79	0.25	0.30	0.83	0.86	0.31	1.19	0.01	0.72	0.94	0.01	0.02	0.02
Total	100.87	100.76	100.56	99.01	99.21	99.46	100.24	99.33	99.25	98.96	99.42	100.08	99.90	98.99	100.09	99.97	99.23	99.59	99.02
LOI	-0.62	0.17	0.88	0.45	-0.21	1.03	0.37	-0.25	0.57	-0.21	0.60	0.05	0.13	0.05	0.07	-0.14	0.72	8.14	0.28
Ba	284.6	69.9	267.1	245.5	296.7	1367.0	330.0	211.1	205.3	302.3	465.9	214.3	372.2	355.1	299.4	362.3	603.6	591.5	554.0
Co	34.6	58.8	41.6	48.6	34.8	7.9	33.4	54.6	45.2	36.1	25.3	51.7	31.5	2.5	34.9	32.9	3.2	3.5	3.5
Cr	5.7	86.4	7.7	22.3	6.8	3.1	4.5	512.6	310.9	4.9	6.1	317.8	4.5	1.0	4.4	13.7	1.0	1.1	0.7
Cu	34.9	171.0	24.8	56.4	17.3	7.2	14.1	86.1	85.8	15.3	11.0	74.9	8.1	3.7	29.9	13.2	2.2	0.5	3.2
Ga	23.2	19.6	20.1	21.6	22.3	26.4	24.3	17.0	19.6	22.3	23.8	20.0	24.9	32.7	21.6	29.5	30.1	22.7	25.9
Nb	30.5	13.3	28.6	30.0	31.8	33.2	33.9	18.8	20.2	34.6	53.8	26.9	47.2	86.6	31.5	35.3	93.5	88.0	90.4
Ni	8.8	57.2	8.3	30.0	5.1	3.9	2.7	175.7	119.5	4.4	2.7	113.0	3.6	1.2	7.0	4.2	3.6	1.9	3.1
Rb	18.6	5.4	24.6	26.4	26.0	28.3	25.5	17.4	16.9	26.5	42.8	19.6	28.6	114.2	26.5	31.3	116.7	138.7	102.4
Sc	31.3	39.7	33.6	26.2	27.5	11.4	27.2	25.4	27.7	23.5	19.1	35.2	28.8	0.4	29.1	22.1	4.0	0.0	1.0
Sr	427.2	190.8	440.8	423.6	456.0	438.7	474.0	393.3	399.5	477.6	440.0	377.5	516.8	35.1	444.8	489.1	47.6	51.5	46.3
V	239.7	359.5	305.9	380.1	234.9	17.8	196.6	287.9	273.7	184.8	49.1	277.2	27.7	1.0	241.8	104.2	1.0	1.0	1.0
Y	43.0	37.3	35.8	33.5	39.1	33.5	41.4	21.3	25.0	42.3	60.6	26.7	62.7	94.3	38.8	47.7	109.6	102.5	102.5
Zn	97.4	108.7	113.5	110.3	115.3	77.6	119.6	82.8	85.5	119.7	130.5	94.1	147.0	138.6	119.1	129.6	167.3	162.2	158.1
Zr	220.5	135.7	196.5	193.4	210.5	409.4	221.3	131.9	144.0	208.4	378.3	159.7	269.7	748.4	188.1	224.7	884.5	843.9	893.2
La	24.1	9.6	25	17.6	30.3	36.1	25.6	14.5	18.4	21.9	54.9	24.2	42.7	86.6	19.5	32.4	101.2	102.6	102.1
Ce	50	30	48.9	46.7	58	79.9	86.7	42.1	47.7	64.9	113.1	52.3	95.8	179.4	45.6	77.6	205.8	207.7	214.3
Nd	36	15.8	30.7	26.9	43.8	39.8	43.3	21.5	24.4	31.1	59	26.7	51.6	85	30.7	44.8	95	95	112

	VH144	VH145	VH146	VH147	VH148	VH149	VH150	VH151	VH152	VH153	VH154	VH155	VH156	VH157	VH158	VH159	VH160	VH161	VH162
SiO2	72.67	50.18	49.35	54.99	51.82	71.53	51.07	46.79	47.82	47.21	53.93	48.82	51.36	51.64	55.31	53.54	47.61	48.05	48.87
Al2O3	13.28	25.21	14.95	15.77	14.98	15.44	14.82	17.23	17.18	15.50	13.23	15.99	15.57	16.20	15.74	15.45	14.97	14.76	15.27
Fe2O3*	2.78	4.67	15.25	11.76	13.70	2.82	13.89	13.08	12.48	12.14	14	10.89	12.46	12.39	9.94	10.62	12.64	12.08	14.45
MgO	0.00	2.84	3.41	2.65	3.55	0.18	3.78	6.17	6.18	7.81	3.4	6.52	3.52	2.91	3.87	5.52	9.30	9.44	4.77
CaO	0.39	12.49	9.13	6.38	7.28	1.36	7.65	11.13	11.36	12.51	7.33	12.89	7.70	8.10	8.35	8.41	10.70	11.06	8.81
Na2O	5.49	3.28	3.30	4.56	4.33	5.48	4.14	2.68	2.54	2.39	3.62	2.01	3.83	3.96	3.40	3.20	2.49	2.39	3.47
K2O	4.40	0.23	1.09	1.56	1.32	3.70	1.23	0.66	0.48	0.47	1.13	0.15	1.42	1.39	1.71	1.54	0.63	0.67	1.10
TiO2	0.14	0.85	3.55	2.03	2.52	0.20	2.76	2.60	2.34	2.18	2.86	1.60	2.33	2.43	2.01	2.02	2.14	2.01	3.54
MnO	0.08	0.07	0.23	0.27	0.29	0.12	0.28	0.18	0.16	0.18	0.24	0.16	0.26	0.37	0.17	0.17	0.18	0.18	0.23
P2O5	0.01	0.12	0.46	0.90	1.13	0.05	1.07	0.25	0.28	0.30	1.06	0.13	1.16	1.27	0.27	0.27	0.28	0.27	0.50
Total	99.27	99.95	100.76	100.92	100.95	100.95	100.73	100.79	100.83	100.73	100.82	99.16	99.66	100.70	100.81	100.78	100.97	100.94	101.02
LOI	0.48	1.88	4.06	0.40	0.01	2.11	-0.09	0.10	2.72	1.83	1.29	0.79	2.18	2.61	2.03	2.12	-0.31	-0.17	0.24
Ba	326.7	113.1	310.5	428.3	376.1	779.6	338.3	182.3	188.6	164.3	226.1	47.5	348.2	373.1	406.1	370.1	165.8	178.7	286.5
Co	2.5	12.3	45.1	28.3	30.6	3.5	34.4	41.5	45.6	52.5	36.6	40.8	30.4	31.2	32.4	37.1	54.6	51.4	39.5
Cr	1.0	184.5	1.0	1.3	1.7	1.0	3.1	108.7	99.5	389.0	5.8	219.7	16.7	19.4	234.5	221.6	462.5	544.3	1.9
Cu	1.7	48.3	24.3	18.3	13.5	3.9	14.6	85.4	87.0	75.7	14.1	105.5	18.5	20.3	62.3	63.2	84.1	86.0	38.6
Ga	29.3	18.7	26.5	24.6	28.0	30.0	22.2	20.3	22.9	19.6	27.6	18.7	26.0	27.7	18.9	21.4	20.0	17.9	27.6
Nb	90.5	4.1	27.7	39.0	36.1	65.4	33.5	17.0	18.7	18.5	31.4	5.9	37.1	38.7	29.0	27.2	16.4	17.3	28.7
Ni	1.8	41.6	4.4	5.8	6.0	1.8	4.3	53.9	65.3	150.0	11.3	74.4	15.3	15.3	78.2	81.9	169.3	171.3	10.1
Rb	121.4	1.0	25.7	36.2	30.6	85.7	28.9	16.1	7.1	7.4	25.4	1.7	32.6	29.1	43.1	38.6	13.7	15.1	25.5
Sc	1.0	18.9	22.3	19.3	26.6	2.6	19.9	29.0	26.8	28.6	25.4	40.6	28.3	29.4	24.4	23.9	29.4	33.3	31.5
Sr	34.8	758.8	448.6	501.3	506.8	142.2	506.8	447.8	479.4	432.0	344.7	212.8	497.0	515.8	345.5	350.9	387.3	360.9	438.8
V	0.5	101.3	306.2	56.3	100.8	6.4	127.6	335.4	298.7	292.0	177.2	274.7	143.5	149.1	251.9	256.4	270.5	281.1	318.7
Y	115.9	8.7	38.0	51.7	50.7	67.6	46.2	23.4	23.8	20.9	77.2	24.1	49.8	50.3	35.0	34.4	22.3	22.6	35.9
Zn	138.1	39.9	113.8	126.9	118.6	93.7	121.0	85.8	82.6	83.2	136.0	80.4	120.1	128.6	92.4	91.9	87.6	85.5	109.0
Zr	788.7	48.7	194.6	266.9	232.2	342.1	212.0	131.6	130.8	124.6	318.4	87.5	243.3	248.3	184.7	176.4	120.0	122.6	199.4
La	98.9	1.4	23.4	37.2	35.7	68.1	34.1	18.4	19.8	14.5	37.3	10.7	41.1	38.3	30.7	28.9	14	13.8	26
Ce	192	5.1	52.3	85.6	82.7	134.9	73.6	36.9	43.2	39.5	83.4	26.3	82.6	75.3	62.1	65.8	35.3	31.9	60.4
Nd	94	20.1	33.3	43	49	61	44.9	24.4	24.7	13.4	55.5	15.1	54.1	47.2	33.8	33.8	21.6	14.6	38.3

	VH164	VH165	VH167	VH168	VH169	VH170	VH171	VH172	VH173	VH174	VH175	VH176	VH177	VH179	VH180	VH181	VH182	VH183	VH184
SiO2	73.45	73.04	73.16	50.54	54.92	55.69	48.23	54.07	47.12	47.07	58.67	52.21	51.08	49.92	51.38	50.78	50.22	52.64	51.54
Al2O3	13.76	13.73	13.59	15.91	15.46	15.75	15.84	15.90	14.91	15.13	15.98	14.60	16.35	16.18	14.96	15.59	14.71	15.38	14.79
Fe2O3*	2.78	2.63	2.64	12.46	11.15	10.60	12.16	11.88	12.79	12.76	10.40	13.52	12.53	13.39	13.34	13.29	14.23	11.61	12.98
MgO	0.00	0.02	0.01	4.61	2.37	2.12	6.56	2.73	9.01	9.51	0.98	3.53	3.38	4.28	3.50	2.09	4.02	3.04	3.65
CaO	0.45	0.68	0.43	9.15	5.88	5.87	11.27	6.33	10.90	10.88	4.89	7.17	8.51	9.66	7.73	8.73	8.14	7.50	7.67
Na2O	5.70	5.55	5.92	3.41	4.75	4.81	1.94	4.58	2.39	2.46	5.09	4.07	3.86	3.39	4.09	3.92	3.91	4.26	4.00
K2O	4.39	4.06	4.37	1.195	1.79	1.80	0.65	1.66	0.62	0.616	2.17	1.33	1.23	0.95	1.36	1.25	1.22	1.54	1.36
TiO2	0.14	0.16	0.13	2.413	1.71	1.69	2.41	1.94	2.04	2.043	1.23	2.50	2.08	2.35	2.73	3.27	3.12	2.63	2.89
MnO	0.08	0.09	0.08	0.249	0.27	0.26	0.19	0.27	0.18	0.183	0.26	0.29	0.24	0.23	0.27	0.28	0.26	0.24	0.26
P2O5	0.02	0.03	0.02	0.48	0.81	0.80	0.30	0.94	0.22	0.23	0.48	0.91	0.65	0.50	0.94	0.92	0.83	1.06	0.81
Total	100.80	100.04	100.40	100.5	99.15	99.44	99.58	100.32	100.20	100.9	100.19	100.16	99.96	100.90	100.34	100.14	100.70	99.95	99.98
LOI	1.11	0.66	0.86	1.11	0.48	0.80	7.91	0.55	-0.05	-0.21	2.50	1.30	3.20	2.19	0.91	2.76	0.43	0.61	0.11
Ba	538.9	659.9	542.3	298.2	450.4	459.1	186.4	419.5	159.1	177.0	508.6	366.0	322.8	263.8	330.3	306.9	374.9	386.1	346.2
Co	3.0	3.8	2.2	36.9	24.8	24.0	47.8	26.0	55.4	55.5	21.3	32.9	38.6	42.5	29.5	37.6	31.0	26.2	30.4
Cr	0.4	1.3	2.3	57.2	6.6	1.9	190.7	2.4	465.9	440.9	0.5	1.3	29.0	42.7	10.8	27.4	4.1	3.4	3.6
Cu	4.1	2.2	2.6	66.7	9.7	4.7	75.6	9.7	94.1	91.3	9.3	25.2	47.3	65.8	9.2	47.8	15.0	13.9	14.2
Ga	28.3	26.8	27.1	21.9	24.6	29.5	14.4	28.4	17.6	18.3	25.4	25.7	19.3	21.9	21.2	20.8	23.7	22.9	21.1
Nb	86.9	84.2	87.4	31.4	41.1	42.0	17.7	39.5	15.5	15.4	46.3	36.3	34.6	26.9	37.0	30.2	34.8	43.3	36.6
Ni	2.8	2.7	2.4	38.8	4.8	4.4	56.5	4.3	156.2	148.4	4.3	5.0	22.0	32.0	6.1	26.3	10.3	5.4	3.4
Rb	115.6	114.3	121.4	27.0	40.9	41.7	14.2	38.7	12.4	13.4	50.6	34.1	26.7	23.9	32.7	23.5	29.3	35.7	32.9
Sc	1.0	2.6	0.6	27.0	17.2	20.7	31.4	23.9	24.2	36.6	6.1	21.3	25.0	28.3	19.9	29.4	31.4	24.3	23.5
Sr	38.9	66.1	38.9	432.3	479.7	479.9	393.5	486.6	379.5	381.7	467.2	491.5	486.9	454.8	436.8	465.3	501.7	473.6	471.1
V	1.0	0.0	1.0	263.0	42.3	41.1	321.2	65.5	297.3	309.9	10.8	110.5	180.2	270.4	131.0	201.6	197.7	137.4	156.6
Y	110.1	101.1	105.0	40.6	54.0	55.0	24.7	53.1	20.9	20.4	55.5	47.2	40.9	33.9	49.7	37.5	43.5	56.0	46.8
Zn	129.8	152.3	152.8	107.2	129.8	133.8	82.2	130.8	86.7	81.9	120.4	123.9	109.4	103.6	128.2	102.6	131.8	119.8	124.5
Zr	685.6	601.0	718.8	230.1	290.2	298.2	124.2	270.3	113.6	112.3	341.2	235.8	208.1	171.2	252.6	192.9	230.0	298.1	248.1
La	106.2	80.8	93.5	30.9	40.8	42.8	16.9	43	11.9	13.7	43.5	34.6	29.4	25.7	33.3	28.2	32.9	47.2	32.4
Ce	207	163.3	192	62	90.2	86.7	40.2	92.8	28.1	36.3	90.7	80.2	80.8	73.8	81.8	79.7	77.8	109.5	82.7
Nd	99	76	90	39.1	49.9	49.8	19.2	53.4	11.2	16.5	43	42.5	36.7	30.2	45.5	31.2	49	62	44.2

	VH186	VH187	VH188	VH189	VH190	VH191	VH192	VH193	VH194	VH195	VH196	VH197	VH198	VH199	VH200	VH201	VH202	VH203	VH204
SiO2	52.05	52.45	46.59	57.99	59.09	66.74		46.66	61.41	46.99	49.02	49.56	49.98	49.37	48.57	49.81	49.73	50.06	71.93
Al2O3	16.81	15.13	14.64	15.52	15.46	15.44		14.88	15.56	14.98	14.80	13.09	13.19	15.14	14.13	13.95	13.89	15.01	13.87
Fe2O3*	11.29	11.83	15.33	9.85	9.21	3.72		15.34	8.68	12.83	14.71	15.85	15.48	14.56	14.70	15.28	14.86	14.68	2.59
MgO	2.32	2.80	5.24	1.50	1.24	0.65		4.83	0.74	9.27	4.42	5.42	5.45	4.50	6.36	5.44	5.31	3.28	0.00
CaO	9.63	7.15	9.21	4.92	4.22	3.69		9.91	3.66	10.67	8.59	9.93	9.82	8.22	11.61	10.40	10.21	8.73	0.63
Na2O	3.40	4.27	2.82	5.18	5.29	5.28		3.09	5.43	2.45	3.61	2.79	2.8	3.75	2.34	2.80	2.67	3.34	5.83
K2O	1.21	1.69	0.77	1.99	2.18	2.65		0.75	2.58	0.65	1.05	0.51	0.521	1.09	0.24	0.49	0.45	1.04	3.92
TiO2	2.53	2.26	3.61	1.30	1.04	0.40		3.52	0.74	2.09	3.53	3.14	3.113	3.31	2.40	2.80	2.79	3.48	0.14
MnO	0.32	0.27	0.23	0.29	0.27	0.14		0.23	0.26	0.18	0.25	0.23	0.224	0.26	0.20	0.23	0.22	0.24	0.08
P2O5	0.56	1.10	0.43	0.53	0.39	0.07		0.42	0.21	0.25	0.65	0.33	0.35	0.64	0.22	0.28	0.28	0.39	0.01
Total	100.15	99.01	98.90	99.12	98.45	98.84		99.65	99.34	100.39	100.66	100.86	100.93	100.87	100.78	101.49	100.44	100.26	99.07
LOI	3.92	2.39	1.08	1.24	-0.26	1.68	44.19	0.59	0.56	-0.29	0.21	0.09	0.19	-0.17	2.32	0.23	0.43	4.06	0.23
Ba	292.3	400.1	198.1	509.7	579.6	657.1	16.1	202.3	638.7	172.1	320.1	96.8	104.2	284.6	63.0	82.1	90.5	306.0	694.1
Co	34.2	29.0	57.2	20.5	16.4	5.8	2.9	54.2	13.3	55.6	38.4	60.1	57.5	37.9	59.6	55.5	53.1	41.8	3.1
Cr	59.5	4.8	3.5	1.9	3.9	6.2	48.5	11.4	2.2	452.5	-0.1	57.2	57.2	7.7	132.1	41.7	33.8	21.3	0.9
Cu	62.0	13.9	81.4	6.7	7.8	15.5	19.7	83.1	8.2	93.5	26.9	122.3	126.4	17.2	156.6	169.0	174.5	25.5	1.2
Ga	22.0	22.1	22.7	24.3	28.4	22.6	0.6	20.2	27.2	17.6	24.2	19.2	27.4	27.5	21.4	22.2	23.3	23.9	28.7
Nb	33.5	44.5	21:2	47.8	51.7	49.5	4.2	21.3	52.7	16.2	28.7	18.2	17.9	28.6	11.4	14.6	15.6	26.1	80.5
Ni	24.1	3.1	26.7	2.6	2.1	8.7	24.2	30.1	2.5	148.4	5.7	50.3	47.2	9.2	68.8	45.6	44.9	11.7	3.0
Rb	26.9	38.0	18.3	45.5	47.8	64.5	0.2	15.3	60.1	13.9	25.5	13.0	12.7	25.7	5.2	10.7	10.4	24.6	102.3
Sc	24.6	15.0	30.6	11.7	14.0	3.8	0.3	30.3	9.8	27.8	28.5	38.5	40.7	27.8	37.6	42.7	34.8	21.9	2.0
Sr	465.3	481.2	436.0	471.1	413.3	263.4	792.9	440.0	368.4	383.8	452.7	233.0	230.2	454.8	213.1	216.3	220.1	462.8	59.6
V	277.1	95.9	406.4	18.6	10.3	31.9	11.6	399.8	0.8	294.4	251.7	430.8	425.7	241.5	383.4	402.1	433.7	309.8	0.0
Y	42.0	56.3	27.6	58.9	64.2	56.1	6.9	27.9	62.5	22.0	38.5	41.6	41.6	37.6	32.3	39.6	39.7	36.4	114.1
Zn	117.7	128.8	110.2	128.6	126.2	69.8	16.0	101.8	126.7	83.9	114.7	127.9	122.5	111.7	109.1	115.5	120.1	109.3	135.4
Zr	231.5	289.8	139.8	352.4	401.6	433.9	32.6	140.3	427.4	120.7	194.6	174.9	175.8	200.1	122.5	149.8	154.8	195.5	505.8
La	30.2	50.1	13.4	53	59.7	58.9	1.2	10.6	56.1	18.2	25.8	12.6	14	20.6	14.3	14.3	13.9	18.6	96.6
Ce	74.3	111.3	32.6	106	120.1	126.5	21.7	21.8	115.2	36.2	58.3	28.5	28.3	47.4	32.7	30	30.4	45.6	208.3
Nd	40.2	56	28.3	62	68	53	11.2	16.1	60	21.1	40	21.4	20.7	33.6	20.5	20.5	22	32.8	93

	VH205	VH206	VH207	VH208	VH209	VH210	VH211	VH212	VH213	VH216	VH217	VH218	VH219	VH220	VH221	VH222	VH223	VH224	VH225
SiO2	56.16	73.27	51.90	50.48	50.66	50.45	56.25	47.48	48.98	48.40	50.14	61.26	50.20	55.20	55.47	54.92	53.60	48.69	59.02
Al2O3	15.58	12.99	14.46	16.17	16.17	16.15	13.96	14.48	16.29	15.34	15.61	14.89	15.63	15.03	15.19	15.36	15.72	13.24	16.40
Fe2O3*	10.24	2.43	11.50	12.23	12.12	11.95	11.26	11.46	13.17	14.65	13.85	10.35	13.51	12.91	12.71	12.80	12.62	13.98	9.07
MgO	1.68	0.01	3.61	4.58	4.50	4.63	3.23	10.55	5.36	5.00	4.35	0.64	4.33	2.40	2.26	2.39	2.66	5.62	0.74
CaO	5.08	0.37	7.24	8.51	8.93	8.68	7.11	11.47	9.63	8.84	8.00	3.82	7.87	5.87	5.74	5.88	6.21	10.53	4.79
Na2O	5.11	5.44	5.22	3.73	3.78	3.79	3.65	2.11	3.25	3.30	3.58	5.66	3.73	4.96	4.98	4.94	4.71	2.80	5.24
K2O	2.087	4.28	1.59	1.17	1.19	1.14	1.47	0.50	0.98	1.13	1.31	2.30	1.34	1.63	1.68	1.62	1.54	0.39	2.09
TiO2	1.341	0.16	3.00	2.16	2.19	2.19	2.49	2.01	2.41	3.38	3.15	0.83	3.04	1.78	1.71	1.78	1.97	2.70	1.23
MnO	0.255	0.06	0.24	0.23	0.23	0.22	0.29	0.17	0.22	0.22	0.24	0.34	0.24	0.31	0.31	0.31	0.30	0.23	0.25
P2O5	0.54	0.03	0.36	0.58	0.58	0.59	1.12	0.26	0.46	0.52	0.68	0.23	0.71	0.85	0.80	0.86	0.93	0.27	0.48
Total	98.12	99.09	99.17	99.87	100.39	99.82	100.86	100.51	100.79	100.81	100.94	100.39	100.62	100.98	100.88	100.88	100.30	98.45	99.36
LOI	2.75	0.37	1.05	1.32	4.37	1.88	0.49	1.43	-0.04	-0.27	0.37	-0.26	0.18	0.28	0.26	0.05	-0.07	0.31	2.41
Ba	523.2	550.8	647.2	328.2	305.4	303.4	268.3	148.8	249.7	285.7	345.8	570.5	330.6	394.6	476.9	467.1	430.1	96.4	521.4
Co	20.4	1.9	27.2	33.7	38.7	39.9	27.5	55.6	46.0	43.5	38.0	16.2	31.9	20.5	24.9	27.4	27.1	50.5	20.1
Cr	5.7	2.8	3.7	5.8	30.5	27.6	7.2	653.0	40.5	10.6	1.0	5.5	5.4	8.5	0.4	2.9	9.3	32.5	7.0
Cu	10.1	1.4	32.4	15.7	52.9	51.3	5.9	86.3	74.0	39.6	18.3	5.7	14.8	7.2	10.8	11.0	9.4	114.2	8.1
Ga	28.2	32.0	26.9	23.7	21.4	21.2	24.6	17.1	20.2	19.4	25.6	25.2	25.9	25.9	23.5	23.9	25.7	21.9	30.3
Nb	57.6	85.7	48.9	32.8	29.5	29.5	31.0	14.8	24.7	26.7	32.1	52.5	31.8	39.6	41.5	40.4	40.0	13.7	45.4
Ni	2.1	1.4	12.7	5.5	24.5	26.3	3.6	187.4	31.7	23.1	6.7	5.9	6.7	1.9	4.2	1.3	3.5	39.2	3.4
Rb	47.6	118.8	54.3	29.5	25.3	27.8	29.3	9.4	22.0	26.8	31.6	56.6	36.8	39.3	34.5	38.1	36.2	5.0	45.0
Sc	18.9	0.0	28.6	22.4	26.9	22.6	21.5	35.1	23.4	28.9	25.5	22.4	28.1	21.3	20.0	19.8	16.2	36.2	11.4
Sr	405.5	35.5	358.2	483.5	473.2	471.0	370.0	353.5	455.1	432.2	445.9	321.6	402.5	421.0	495.8	498.3	498.6	209.1	485.1
V	23.9	4.5	284.8	169.1	203.4	203.6	130.1	273.1	276.4	331.8	233.1	1.0	207.8	21.7	22.3	25.7	42.8	390.7	8.1
Y	66.0	124.0	59.3	43.5	38.0	36.6	74.4	23.9	31.4	36.4	41.5	62.8	44.2	56.4	55.9	54.1	52.5	42.4	54.7
Zn	127.3	160.1	535.9	117.9	99.8	101.4	139.4	89.4	100.6	114.2	118.8	151.6	126.8	139.5	131.4	131.0	131.1	109.1	121.2
Zr	476.5	768.9	463.4	213.8	189.4	183.0	276.3	125.6	159.1	197.0	231.2	430.5	243.8	290.2	279.5	282.0	259.1	147.4	340.2
La	60.6	104.7	36	31.9	26.7	26.1	42.1	13.4	21.5	20.5	24.5	52.8	27	43.7	45.4	45.1	41.4	13.2	44.1
Ce	125.8	229.5	76.9	73.5	52.6	59.6	90.2	36	46.8	46.1	56.7	109.9	63.4	90.9	94.2	93.5	94.3	28.4	94.7
Nd	75	102	51.6	51.5	31.4	35.1	65.6	19.4	28	32.9	40.7	62	45.4	54.6	60.5	55.6	58.8	19	53.4

	VH226	VH228	VH229	VH230	VH231	VH233	VH234	VH235	VH236	VH237	VH238	VH239	VH240	VH241	VH242	VH243	VH244	VH245	VH246
SiO2	54.64	53.03	50.37	47.81	47.60	50.08	53.42	55.21	55.12	56.72	56.65	72.56	49.12	49.30	49.02	52.06	52.03	51.52	47.33
Al2O3	15.91	15.23	14.96	15.4	14.39	17.03	17.23	14.01	13.70	14.34	14.21	13.41	13.06	13.27	13.62	15.19	15.22	16.47	16.53
Fe2O3*	11.20	11.89	13.26	13.47	11.10	11.98	10.69	12.47	12.62	11.99	12.17	3.98	16.35	15.53	15.52	12.96	13.26	13.06	12.38
MgO	1.83	2.79	3.94	5.16	10.60	3.61	1.06	3.31	3.27	2.75	2.84	0.01	4.84	4.81	4.77	3.67	3.49	1.34	7.95
CaO	6.20	6.82	7.85	9.02	11.56	10.74	8.04	7.04	7.17	6.25	6.22	1.26	9.76	9.90	10.16	7.32	7.24	8.44	10.89
Na2O	4.54	4.34	3.97	3.47	2.04	2.80	3.98	3.68	3.66	3.93	3.92	4.84	2.95	3.06	2.96	4.25	4.34	3.65	2.45
K2O	1.82	1.53	1.24	1.168	0.51	0.83	1.62	1.30	1.37	1.44	1.45	3.05	0.65	0.49	0.47	1.32	1.28	1.48	0.59
TiO2	1.81	2.12	2.84	2.67	1.95	2.51	2.99	2.50	2.49	2.11	2.07	0.30	3.63	3.86	3.73	2.67	2.67	2.99	2.27
MnO	0.31	0.32	0.28	0.216	0.17	0.17	0.21	0.23	0.24	0.24	0.24	0.04	0.23	0.22	0.24	0.26	0.27	0.21	0.17
P2O5	0.88	1.10	1.08	0.87	0.25	0.54	0.84	1.10	1.09	1.02	1.00	0.04	0.41	0.40	0.42	0.77	0.78	0.74	0.31
Total	99.19	99.21	99.80	99.28	100.19	100.30	100.15	100.87	100.76	100.82	100.81	99.54	100.99	100.85	100.90	100.50	100.62	99.93	100.88
LOI	2.03	2.38	0.79	1.65	0.37	2.89	2.97	0.85	1.82	0.73	1.00	1.06	0.91	0.95	2.06	0.23	0.03	3.51	0.95
Ba	416.0	402.2	336.2	309.4	136.6	227.2	425.8	230.6	249.2	279.3	281.3	528.9	134.0	123.9	130.9	412.6	430.9	343.0	167.9
Co	24.5	31.8	32.4	42.4	53.9	46.5	23.5	29.1	29.1	29.5	27.5	3.3	48.6	38.2	48.8	31.7	27.7	37.3	46.9
Cr	2.4	2.4	2.9	14.8	685.7	54.5	4.3	2.6	5.5	5.2	10.6	3.6	22.2	22.9	19.5	3.7	2.9	0.1	160.0
Cu	7.4	11.5	15.6	47.1	83.5	73.4	12.9	4.7	5.0	9.1	5.2	0.8	133.2	124.7	122.0	9.1	10.6	22.0	88.0
Ga	26.9	28.6	24.5	18.5	16.4	21.8	28.0	23.5	24.6	26.2	27.5	21.8	23.1	26.6	23.3	23.8	24.1	22.8	19.3
Nb	40.9	39.9	32.6	32.5	14.8	25.2	38.4	31.4	30.5	34.1	32.8	50.4	18.8	17.8	17.8	36.4	36.6	36.6	18.1
Ni	4.7	6.0	6.9	30.4	198.2	62.0	4.3	2.2	5.6	3.7	6.0	3.6	36.1	30.8	36.6	3.5	5.3	9.8	106.8
Rb	44.2	31.2	33.6	26.6	10.1	19.8	38.5	28.8	28.1	32.1	33.2	72.1	19.4	9.7	10.4	26.8	26.5	31.7	11.6
Sc	20.0	19.3	18.8	24.6	26.8	24.0	25.1	24.0	20.9	19.8	18.1	4.6	34.7	38.4	36.7	25.3	22.2	20.9	29.4
Sr	461.6	530.1	518.1	454.1	351.3	435.7	494.5	371.5	370.6	359.8	345.9	161.7	291.7	285.7	339.2	473.3	470.7	489.9	427.4
V	37.6	62.2	130.5	240.6	272.2	282.9	242.7	128.6	123.0	93.0	86.4	1.1	385.4	393.6	464.4	139.8	129.1	221.9	274.9
Y	58.0	53.6	46.0	42.0	22.7	32.7	51.1	74.5	72.8	78.9	78.6	96.2	44.5	46.4	42.8	53.2	56.1	48.1	25.5
Zn	138.0	136.2	108.4	116.0	84.7	100.0	130.5	135.1	130.2	137.9	142.1	112.2	114.8	116.2	122.3	124.5	121.6	124.5	91.2
Zr	280.1	248.6	205.1	228.9	123.6	180.6	291.5	273.6	269.5	334.9	334.5	683.5	204.1	198.1	183.1	342.3	345.6	298.4	150.4
La	43.1	38.1	30.6	28.2	17.3	24.6	36.5	38.4	39.1	44	42.9	80.3	15.3	17.4	15.8	35	35.5	28.8	18.6
Ce	96.7	83.6	65.5	63.5	36.3	57.7	77.8	84	88	95.2	93.7	183	28.2	40	39.8	84.7	82.9	65.7	44.9
Nd	61.5	56.6	47.9	43.3	20.5	34.5	54.9	63.4	61.1	68.2	65.5	90	26.5	34.2	31.9	56.8	53.8	46.2	27.5

	VH247	VH248	VH249	VH250	VH251	VH252	VH253	VH254	VH255	VH256	VH257	VH258	VH259	VH260	VH261	VH262	VH263	VH264	VH265
SiO2	47.81	47.50	62.77	57.69	60.02	57.88	70.12	54.95	51.94	51.67	48.13	52.01	52.16	48.96	46.35	47.71	50.18	52.19	52.02
Al2O3	15.56	15.65	14.74	15.44	15.22	15.84	14.36	15.36	15.16	14.96	15.50	15.08	15.15	13.63	14.87	14.80	14.68	15.23	15.17
Fe2O3*	12.20	12.27	9.15	11.38	10.47	11.11	3.40	12.79	13.62	13.32	11.81	13.13	13.41	13.70	11.67	11.23	13.21	12.95	12.76
MgO	8.77	8.89	0.24	1.58	1.07	1.43	0.03	2.30	2.87	3.42	8.58	3.37	3.24	6.77	8.81	10.36	3.49	3.23	2.96
CaO	10.40	10.27	3.37	5.08	4.18	4.98	1.03	5.92	7.38	7.28	10.18	7.25	7.34	11.79	11.41	10.94	7.33	7.22	7.54
Na2O	2.65	2.71	5.83	5.43	5.22	5.32	5.95	4.98	4.41	4.35	2.72	4.34	4.31	2.41	2.41	2.22	4.28	4.39	4.28
K2O	0.83	0.85	2.55	1.84	2.19	1.93	3.93	1.59	1.30	1.32	0.87	1.34	1.32	0.27	0.70	0.64	1.32	1.39	1.27
TiO2	2.09	2.08	0.61	1.41	1.03	1.39	0.21	1.79	2.65	2.62	2.16	2.59	2.57	2.41	1.85	1.78	2.63	2.60	2.64
MnO	0.18	0.18	0.35	0.31	0.32	0.29	0.12	0.30	0.30	0.29	0.18	0.28	0.28	0.21	0.17	0.17	0.29	0.30	0.27
P2O5	0.32	0.33	0.12	0.58	0.37	0.58	0.02	0.87	0.96	0.96	0.35	0.96	0.82	0.22	0.24	0.24	0.93	0.95	0.95
Total	100.84	100.74	99.80	100.80	100.16	100.82	99.25	100.90	100.63	100.21	100.49	100.39	100.65	100.37	98.51	100.13	98.37	100.47	99.89
LOI	0.19	-0.09	-0.18	0.47	-0.33	0.89	0.31	-0.05	0.97	-0.08	0.36	-0.29	1.46	1.22	2.50	0.09	-0.20	0.44	2.58
Ba	205.1	206.4	671.1	492.2	584.7	530.7	885.6	443.2	909.2	383.7	213.6	352.3	397.5	60.3	179.2	174.9	344.1	377.3	352.6
Co	47.7	51.9	14.9	26.6	19.7	23.6	4.8	18.9	31.6	30.6	50.7	33.6	30.4	52.8	50.0	52.9	35.6	30.7	32.5
Cr	413.6	380.9	10.8	3.7	7.2	2.3	6.7	6.7	3.7	3.7	366.8	2.8	3.2	184.4	525.7	603.8	6.5	4.1	54.1
Cu	82.3	74.7	6.6	11.1	6.5	7.4	1.5	8	12.2	12.5	76.4	8.1	6.5	161.7	93.6	90.3	11.7	10.6	12.0
Ga	17.3	14.5	26.0	26.7	27.4	24.8	19.6	23.9	23.3	21.7	19.2	22.9	23.5	21.3	21.1	17.7	24.9	23.2	25.6
Nb	25.1	24.0	61.3	44.5	50.5	44.9	89.3	41.7	33.1	33.9	25.3	34.3	37.3	11.0	18.5	17.4	34.2	34.4	34.0
Ni	136.6	151.3	4.0	2.2	1.1	1.7	5.5	0.6	4.7	4.5	136.4	4.8	3.4	72.5	148.2	196.4	6.1	3.7	5.0
Rb	19.4	20.6	58.9	38.9	50.3	42.4	102.8	34.9	27.8	32.5	20.8	30.2	26.9	5.9	16.9	16.3	30.5	32.7	31.2
Sc	31.1	22.8	11.5	18.4	14.5	21.0	0	13.1	21.2	21.1	24.9	25.1	23.7	31.9	33.5	21.5	19.3	22.3	20.8
Sr	431.8	433.8	309.9	478.2	395.6	471.5	85.8	506.7	524.6	512.2	432.5	519.7	480.0	218.0	376.6	365.4	514.3	508.1	521.5
V	282.0	269.0	0.4	11.4	6.1	15.4	1.6	30.2	108.1	105.0	276.5	109.3	108.5	329.5	276.4	260.0	105.7	109.8	106.7
Y	23.9	23.6	66.7	55.6	60.3	57.2	87.3	56.1	46.1	46.3	25.1	46.7	55.1	33.8	22.2	20.9	46.4	47.2	46.0
Zn	85.2	83.5	139.8	135.1	137.1	134.7	134.6	120.2	115.4	115.4	89.6	123.3	123.1	96.3	80.7	78.7	133.2	118.5	119.9
Zr	157.4	153.1	494.5	316.0	386.3	331.8	763.4	317.4	219.2	225.8	158.7	221.7	352.3	119.8	128.3	120.6	223.5	229.9	224.1
La	21.6	22.5	57.8	41.3	53.2	45.4	88.3	46.9	29.1	35.5	24.5	32.4	39.7	11.7	22.1	15.9	35.6	35.9	34.3
Ce	47.3	49.1	119.2	86.7	112.6	92.7	180.7	102.3	64.8	76.7	53.7	68.3	84.7	32.8	51.7	42.7	82	79.2	74.6
Nd	35.6	26	62	51.3	66	58.6	83	60	44.6	52	31.3	48.3	53.4	21.7	24.2	21	54.8	54.9	52

	VH266	VH267	VH268	VH269	VH270	VH271	VH272	VH273	VH274	VH275	VH276	VH281	VH282	VH283	VH284	VH285	VH286
SiO2	49.38	48.91	70.01	54.24	49.20	49.12	48.90	48.64	48.65	48.83	47.43	62.46	52.2	57.16	71.64	47.7	60.86
Al2O3	15.40	15.27	14.53	15.32	13.08	14.96	13.20	13.54	12.56	13.41	15.39	23.38	15.84	16.43	13.56	14.45	16.22
Fe2O3*	12.98	13.29	4.07	11.46	16.00	14.43	15.56	15.23	17.62	15.86	12.96	0.57	12.53	9.51	3.32	15.59	8.59
MgO	4.51	4.53	0.29	3.22	5.65	4.82	6.17	6.81	5.32	6.45	8.21	0.36	4.1	1.78	0.02	4.89	1.24
CaO	8.10	8.49	1.40	7.37	9.93	8.78	10.69	11.37	9.78	10.85	10.41	13.13	7.17	4.79	0.5	8.89	4.05
Na2O	3.55	3.52	5.62	4.24	2.77	3.36	2.55	2.38	2.71	2.42	2.74	1.05	3.85	5.01	5.31	3.57	5.36
K2O	1.19	1.23	3.63	1.53	0.45	0.938	0.40	0.26	0.39	0.29	0.78	0.183	1.363	2.389	4.404	0.889	2.41
TiO2	3.28	3.47	0.44	2.63	3.17	3.432	2.74	2.31	3.29	2.42	2.42	0.095	2.683	1.125	0.172	3.77	0.873
MnO	0.23	0.22	0.12	0.25	0.22	0.235	0.22	0.22	0.24	0.23	0.18	0.012	0.247	0.256	0.096	0.241	0.253
P2O5	0.52	0.49	0.08	0.59	0.35	0.69	0.27	0.20	0.34	0.23	0.32	0.02	0.7	0.51	0.02	0.49	0.33
Total	99.18	99.45	100.27	100.90	100.83	100.8	100.71	100.97	100.90	100.98	100.86	101.28	100.77	99.06	99.1	100.54	100.29
LOI	0.13	0.60	0.86	1.98	0.23	0.46	0.20	0.09	0.10	0.25	-0.23	0.77	2.9	0.99	4.22	-0.33	-0.01
Ba	302.0	306.2	896.3	421.7	94.9	306.7	79.4	60.0	93.2	54.3	202.0	3.8	51.7	615.1	617.5	302	665.8
Co	37.1	35.6	5.0	25.4	48.3	40.6	47.6	58.0	55.4	63.7	48.9	6	24	9.5	0.5	35.5	5.4
Cr	4.9	4.7	3.8	6.1	66.7	5.0	91.5	91.2	41.9	78.4	359.4	25.3	7.6	10.6	2	3.2	15.4
Cu	18.3	33.9	6.0	14.6	140.8	46.3	176.5	144.1	154.8	156.3	79.2	14.8	13.6	6.8	0.5	26.8	4.9
Ga	29.9	28.0	26.8	24.8	24.0	24.1	22.4	21.3	23.2	19.5	27.1	13.3	21.6	27.6	25.4	24.8	26
Nb	29.9	30.1	77.7	39.0	18.3	28.8	13.7	11.4	16.5	11.7	20.1	2.6	40.7	69.9	120.7	29.2	70
Ni	8.1	9.2	2.4	5.9	60.8	11.5	55.3	57.7	45.9	59.2	122.9	7.5	0.1	6	1.7	9.4	2
Rb	28.2	30.3	87.0	41.3	10.1	20.6	7.8	5.6	8.3	7.2	19.7	21.8	25.9	50.8	287.7	12.1	52.5
Sc	29.9	24.2	1.5	21.8	33.7	32.3	39.1	44.9	37.0	36.1	26.5	7.3	19.4	19.1	3.3	32.5	11.2
Sr	433.0	462.9	129.4	409.1	236.1	441.4	204.3	186.8	207.0	195.2	411.9	66	439.5	427.1	8.4	437.3	382.9
V	232.3	266.9	12.7	152.0	405.2	274.8	383.7	347.9	415.1	384.9	314.0	16.1	156.5	6.1	0.8	310.4	-4.9
Y	38.6	36.9	94.4	54.4	45.2	44.5	37.8	34.1	48.3	35.2	26.1	0.5	45.5	75.6	98.6	39.7	68.4
Zn	120.1	105.0	122.0	111.5	119.4	110.9	108.3	99.5	124.3	111.4	86.2	9.2	136.5	144.2	161	111.6	142.4
Zr	204.4	219.6	721.0	370.7	182.9	207.2	142.2	120.3	171.6	121.5	139.2	13.8	315.2	665	1023.4	275	597.3
La	22.5	25.1	92.2	40.8	18.5	26.6	15.7	11.5	16.7	13.6	18.7	3.1	44.4	65.4	86.6	33.7	60.9
Ce	54.1	56.7	199.9	88.3	39.1	56.7	34.6	28.6	38.2	31.1	39.6	3.1	104.7	161.8	207.7	78.2	143.6
Nd	36.1	37.7	97	56.2	31.6	41.7	24.8	18.9	28.8	20.6	23.4	20.2	44.2	80.6	88.6	40	70.5

	MA1	MA2	MA3	MA4	MA5	MA6	MA7	MA8	MA9	MA10	MA11	MA12	MA13	MA14
SiO2	49.90	49.03	48.89	54.15	48.32	52.67	54.46	73.52	53.75	63.81	71.20	73.52	51.81	49.22
Al2O3	16.41	15.61	15.39	16.78	15.62	15.28	16.55	13.50	15.23	14.64	13.48	13.46	15.18	14.86
Fe2O3*	12.91	12.34	12.16	11.37	12.08	12.1	11.33	2.89	11.92	9.14	2.86	2.88	13.06	14.85
MgO	4.48	6.62	7.42	2.60	7.29	3.39	2.68	0.03	3.21	0.22	0.01	0.03	2.54	3.55
CaO	8.88	11.52	11.61	6.83	11.90	7.74	6.25	0.44	7.22	3.33	0.36	0.42	7.57	8.49
Na2O	3.78	2.47	2.41	4.67	2.43	4.1	4.80	5.49	4.23	5.71	5.39	5.72	4.14	3.26
K2O	1.13	0.66	0.68	1.61	0.69	1.35	1.76	4.25	1.57	2.59	4.42	4.281	1.25	0.96
TiO2	2.22	1.96	1.91	1.77	1.91	2.802	1.68	0.17	2.55	0.60	0.16	0.159	2.67	3.50
MnO	0.24	0.18	0.19	0.24	0.20	0.27	0.27	0.07	0.28	0.32	0.07	0.075	0.28	0.22
P2O5	0.57	0.27	0.27	0.80	0.28	0.64	0.83	0.03	0.58	0.12	0.01	0.01	0.95	0.59
Total	100.53	100.68	100.93	100.86	100.74	100.37	100.65	100.45	100.58	100.55	98.02	100.56	99.48	99.52
LOI	0.98	0.76	1.37	2.22	2.06	1.17	1.31	0.27	0.45	1.24	2.83	0.74	1.24	0.74
Ba	281.6	191.8	189.7	423.9	175.3	418.2	391.4	572.3	432.4	712.5	623.3	558.7	360.6	307.6
Co	41.7	51.7	55.9	27.1	53.3	25.1	18.1	3.1	27.4	15.1	3.3	2.5	32.0	37.8
Cr	33.2	387.6	440.2	7.0	387.8	4.1	4.8	1.0	11.2	3.6	1.0	3.7	5.4	4.1
Cu	55.0	78.3	77.1	17.2	82.4	19.4	7.4	6.9	13.4	6.4	4.1	0.8	11.5	22.3
Ga	22.9	15.6	14.7	21.8	14.9	24.9	25.0	27.1	23.6	23.4	26.8	27.3	25.1	27.3
Nb	28.8	18.7	18.9	41.3	18.7	34.2	42.9	77.4	39.4	61.7	87.3	86.6	35.2	31.1
Ni	27.0	124.5	158.4	7.3	150.5	9.6	5.6	1.3	7.7	1.3	3.8	2.6	4.9	12.7
Rb	25.8	15.8	15.8	32.0	16.7	32.0	43.1	112.8	37.1	60.7	107.3	117.1	29.8	19.9
Sc	22.5	27.2	35.0	23.9	26.7	20.5	19.2	1.0	21.5	14.0	1.0	-0.6	21.0	27.7
Sr	477.9	394.0	371.7	503.4	391.0	425.1	419.3	40.8	397.5	307.2	46.3	37.3	499.2	437.3
V	213.4	286.2	279.1	83.6	257.6	149.9	45.5	3.5	164.6	1.0	1.1	0.7	108.8	255.0
Y	35.9	23.0	23.5	50.6	23.2	54.0	55.5	97.3	56.9	65.6	115.3	119.9	47.5	44.6
Zn	102.8	80.9	88.5	120.8	77.4	115.3	127.8	137.3	111.4	128.4	147.2	153.1	132.7	113.5
Zr	181.3	125.4	129.4	261.5	126.5	340.5	288.7	650.8	371.0	504.6	786.5	816.3	227.8	249.3
La	26.3	20	14	42.9	21.7	48.9	46.4	104.9	41.4	58	101.4	105.9	30.5	25.3
Ce	59.7	43	42	89.8	40.7	95.7	99.8	229.5	86.4	120.1	216.8	222.9	69.5	53.4
Nd	36	20.7	18.8	54.2	19.6	60.5	60.3	105	53.4	64	98	101	46.4	45.1

	MB1	MB2	MB3	MB4	MB5	MB6	MB7	MB8	MB9	MB10	MB11
SiO2	66.94	50.23	69.77	49.79	72.94	54.71	48.64	69.37	52.07	68	49.75
Al2O3	14.58	16.41	14.73	16.73	13.43	16.82	16.89	14.51	16.56	14.6	15
Fe2O3*	4.69	11.91	4.19	12.52	2.30	10.5	13.2	4.35	12.03	4.39	14.88
MgO	0.07	4.87	0.03	4.99	0.04	2.62	5.68	0.03	3.87	0.03	3.87
CaO	1.60	8.73	1.17	9.03	0.23	6.18	10.16	1.3	7.53	1.51	8.72
Na2O	5.81	3.68	5.8	3.55	5.50	5.4	2.97	5.82	4.24	5.76	3.37
K2O	3.33	1.16	3.464	1.008	4.37	1.726	0.797	3.556	1.356	3.502	0.937
TiO2	0.32	2.22	0.299	2.189	0.21	1.661	2.386	0.276	1.976	0.275	3.48
MnO	0.15	0.22	0.038	0.21	0.04	0.238	0.193	0.104	0.231	0.129	0.221
P2O5	0.04	0.56	0.04	0.51	0.01	0.82	0.36	0.04	0.7	0.03	0.59
Total	98.11	100.02	99.61	100.56	99.12	100.73	100.88	99.43	100.59	98.31	100.83
LOI	0.23	2.73	1.82	0.33	0.44	1.69	0.50	1.21	0.73	1.78	0.79
Ba	800.0	307.9	791.5	280.4	605.8	445.4	238.4	781.7	353.1	776.5	296.4
Co	4.5	40.9	4.7	40.9	3.0	25.3	42.3	4.8	34.6	3.9	41.9
Cr	1.1	28.5	0.4	41.5	-0.2	10.5	48.9	4.3	27.2	1.1	4.0
Cu	6.3	58.5	4.8	47.5	2.1	12.1	76.7	2.2	33.6	4.0	28.6
Ga	28.6	25.1	27.9	21.7	26.6	21.7	21.5	24.9	24.8	26.9	23.7
Nb	75.5	28.4	77.2	27.4	81.3	43.2	18.6	94.6	35.7	78.9	31.3
Ni	2.4	27.1	4.1	31.1	1.9	4.5	40.3	5.8	16.1	2.3	14.6
Rb	85.7	30.0	80.7	23.2	115.2	40.4	18.9	87.9	28.4	88.6	20.0
Sc	7.0	25.1	7.0	17.8	1.0	17.0	21.9	1.6	18.2	3.9	26.9
Sr	192.8	457.3	179.7	465.5	47.1	516.5	462.8	143.1	489.4	169.3	440.9
V	1.0	199.4	0.4	236.4	8.3	51.2	279.4	9.7	147.0	4.2	263.7
Y	92.8	36.6	82.5	35.6	76.7	54.4	27.0	102.8	44.0	100.2	44.1
Zn	130.3	95.4	121.8	102.1	92.2	121.4	83.7	165.9	110.4	141.8	118.3
Zr	677.5	186.0	639.7	172.8	739.6	279.7	131.1	740.6	222.1	634.1	245.6
La	92.7	32.8	92.4	29.2	58.8	47.1	21.7	93	38.4	92.4	23.4
Ce	200.7	70.1	192.8	65.9	132.2	97.4	48.2	201.3	82.7	198.4	49.3
Nd	96	41.7	94	40.3	59	60.7	27.3	92	51.3	90	37.2

Appendix 4
CIPW norms

CIPW norms calculating using the computer program "IGPET 3"© of M. J. Carr (1990) are presented in the following tables, separated into basalts, hawaiites, mugearites, benmoreites, trachytes and rhyolites on the basis of bulk composition, following the recommendations of the IUGS subcommission (LeMaitre 1989).

In XRF analysis, iron is simply expressed as Fe_2O_3*, thus for normative calculations the Fe^{3+}/Fe^{2+} ratio must be set arbitrarily. The Fe_2O_3/FeO ratio has a significant influence on the abundance and nature of normative minerals. It increases with both the differentiation state of the rock in question, and the amount of late stage deuteric oxidation or subsequent post-magmatic alteration. Various schemes have been proposed (e.g. Brooks 1976, LeMaitre 1976), based on wet-chemical data, but most either failed by failing to exclude highly oxidised samples or failing to take the differentiation state into account. This study follows the recommendations of Middlemost (1989), using the following standard ratios: basalt 0.2, hawaiite 0.3, mugearite 0.35, benmoreite 0.4 and trachytes and rhyolites 0.5.

Basalts

	VH1	VH4	VH6	VH8	VH10	VH12	VH13	VH14	VH16	VH19	VH21	VH33
%AN	64.74	44.19	59.52	59.53	62.89	59.54	41.73	60.31	59.66	57.2	57.71	61.31
Q												
or	1.71	6.74	4.02	3.96	2.54	4.2	6.38	3.66	3.96	4.02	4.14	3.43
ab	19.12	29.28	22.09	22.42	17.6	20.31	30.8	19.12	18.79	20.45	20.39	18.02
an	35.11	23.18	32.47	32.98	29.83	29.89	22.06	29.06	27.79	27.32	27.83	28.57
ne										1.44		
di	18.48	12.23	16.45	16.54	22.27	22.58	12.73	19.12	20.16	21.9	19.09	21.57
hy	4.61	10.1	4.66	3.92	4.3	4.15	13.12	4.11	3.16	0	8.33	1.82
ol	11.38	5.6	11.29	11.79	16.62	9.77	3.03	15.84	17.18	17.4	12.19	18.56
mt	3.15	3.42	3.07	2.97	2.54	2.73	3.38	2.97	2.87	2.77	2.89	2.67
il	4.88	6.21	4.67	4.27	3.1	3.76	6.29	3.72	3.38	3.46	3.63	3.17
ap	0.74	1.25	0.72	0.67	0.49	0.6	1.18	0.6	0.58	0.58	0.79	0.49

	VH37	VH40	VH41	VH43	VH50	VH58	VH59	VH67	VH70	VH71	VH72	VH73
%AN	38.27	39.34	38.93	40.24	50.12	38.85	40.2	50.54	39.15	40.51	39.89	43.57
Q							1.65					
or	6.62	6.09	6.15	6.21	5.14	7.74	7.39	3.6	7.39	6.91	6.68	6.03
ab	32.15	31.14	31.48	30.63	26.57	30.97	30.46	27.25	31.56	31.14	31.99	29.53
an	19.94	20.2	20.07	20.63	26.7	19.68	20.48	27.84	20.31	21.2	21.23	22.8
di	13.02	15.47	15.65	15.2	16.4	14.59	13.95	11.28	12.64	13.23	14.1	12.9
hy	12.82	9.52	7.57	8.5	4.69	9.39	12.68	16.16	14.87	12.69	8.37	15.67
ol	2.87	5.14	6.62	5.82	10.19	4.31		1.61	1.3	3.09	6.17	1.1
mt	3.39	3.55	3.55	3.54	3.22	3.45	3.57	3.33	3.26	3.31	3.38	3.41
il	6.17	6.67	6.67	6.61	4.71	6.29	6.27	6.1	5.96	6.27	6.51	6.48
ap	1.95	1.67	1.67	1.67	0.9	2.06	2.04	2.29	1.3	1.23	1.25	1.18

	VH74	VH77	VH78	VH80	VH82	VH89	VH90	VH91	VH93	VH96c	VH101	VH102
%AN	60.05	57.51	58.78	58.49	56.21	47.82	49.13	45.74	39.49	58.96	58.71	54.51
Q												
or	3.9	4.02	3.9	3.96	4.55	5.91	5.5	6.15	6.15	3.78	4.31	4.73
ab	18.62	20.22	19.8	20.39	23.61	27.25	26.49	28.52	31.05	20.05	20.14	24.29
an	27.99	27.38	28.23	28.73	30.31	24.97	25.58	24.04	20.27	28.81	28.64	29.1
di	21.14	21.56	21.26	20.36	17.02	13.58	15.17	13.54	15.51	20.52	17.73	17.02
hy	5.94	1.09	3.11	4.36	3.42	11.28	9.41	11.32	10.52	4.32	4.59	3.67
ol	14.95	17.94	15.79	14.83	11.98	6.76	8.77	6.42	4.03	14.83	16.69	10.96
mt	2.68	2.7	2.96	2.86	3.06	3.06	2.99	2.99	3.47	2.94	2.84	3.35
il	3.25	3.3	3.59	3.57	4.73	4.31	4.27	4.31	6.69	3.49	3.61	5.43
ap	0.56	0.58	0.58	0.63	0.81	1.97	1.67	1.99	1.67	0.58	0.65	0.7

	VH104	VH105	VH106	VH107	VH119	VH120	VH121	VH122	VH123	VH125	VH126	VH127
%AN	59.03	36.38	57.75	56.03	57.32	57.18	57.02	59.26	42.97	46.13	47.83	40.6
Q												
or	3.49	6.8	3.37	4.26	3.5	3.51	3.49	5.44	5.26	5.61	6.5	6.56
ab	18.87	33.68	20.73	22.85	22.34	22.17	21.66	20.99	29.36	27.08	26.15	30.97
an	27.19	19.26	28.33	29.11	30.01	29.6	28.73	30.52	22.13	23.19	23.98	21.17
di	22.51	11.21	19.88	18.04	18.11	18.47	18.99	16.85	14.57	15.45	15.24	12.83
hy	3.76	12.67	4.34	2.45	2.96	2.29	1.79	4.12	10.63	10.92	8.09	15.22
ol	16.61	3.48	14.91	15.21	15.07	15.57	17.33	13.23	5.44	5.08	7.23	0.44
mt	2.91	3.28	3.07	3.02	3.1	3.18	3.19	3.26	3.77	3.7	3.48	3.18
il	3.48	5.53	4.06	4.05	4.09	4.28	3.95	4.62	6.89	7.07	6.19	6.25
ap	0.67	2.36	0.58	0.72	0.56	0.53	0.51	0.7	1.48	1.18	0.93	1.48

Basalts

	VH130	VH131	VH132	VH134	VH136A	VH146	VH151	VH152	VH153	VH160	VH161	VH162
%AN	55.15	56.96	37.26	54.27	40.51	44.91	59.3	61.31	59.88	56.9	57.68	43.76
Q						0.71						
or	4.31	3.84	6.8	4.73	6.15	6.44	3.9	2.84	2.78	3.72	3.96	6.5
ab	22.34	22	32.41	22.25	30.12	27.92	22.68	21.49	20.22	21.07	20.22	29.36
an	27.47	29.11	19.25	26.41	20.51	22.76	33.04	34.06	30.18	27.81	27.57	22.84
di	16.34	17.77	13.46	18.86	15.21	16.41	16.87	16.79	24.37	19.02	20.69	14.59
hy	3.22	7.69	12.45	6.03	12.23	13.71	1.34	9.51	1	4.88	5.95	9.55
ol	17.36	10.29	2.16	13.03	2.91		13.17	6.98	13.37	15.62	14.16	5.6
mt	2.81	2.78	3.22	3.04	3.49	3.68	3.16	3.02	2.93	3.06	2.91	3.49
il	3.89	4.1	6.13	3.93	6.57	6.74	4.94	4.44	4.14	4.06	3.82	6.72
ap	0.58	0.7	1.92	0.72	1.67	1.07	0.58	0.65	0.7	0.65	0.63	1.16

	VH168	VH174	VH179	VH188	VH193	VH195	VH196	VH199	VH208	VH209	VH210	VH212
%AN	45.39	57.73	47.67	51.18	48.39	57.42	40.83	40.12	43.12	42.5	42.49	61.54
Q												
or	6.91	3.64	5.61	4.55	4.43	3.84	6.21	6.44	6.91	7.03	6.74	2.95
ab	28.69	20.82	28.69	23.86	26.15	20.73	30.55	31.73	31.56	31.99	32.07	17.85
an	23.84	28.42	26.13	25.02	24.52	27.96	21.08	21.26	23.92	23.64	23.69	28.56
di	15.01	19.52	15.44	14.8	18.2	18.96	14.38	12.76	12.02	13.99	12.84	21.48
hy	8.73	1.23	11.91	13.97	5.45	2.9	11.78	11.14	11.89	9.11	10.21	6.87
ol	5.12	18.7	3.1	3.84	8.24	17.26	3.64	5.01	4.1	5.16	4.83	14.63
mt	3.02	3.09	3.23	3.71	3.71	3.1	3.55	3.52	2.96	2.93	2.89	2.77
il	4.43	3.88	4.46	6.86	6.69	3.97	6.7	6.29	4.1	4.16	4.16	3.82
ap	1.02	0.53	1.16	1	0.97	0.58	1.51	1.48	1.34	1.34	1.37	0.6

	VH213	VH216	VH217	VH230	VH231	VH233	VH246	VH247	VH248	VH257	VH259	VH261
%AN	49.51	45.92	42.79	43.92	62.36	57.03	60.96	55.63	55	54.45	33.16	58.66
Q						2.68					0.72	
or	5.79	6.68	7.74	6.9	3.01	4.91	3.49	4.91	5.02	5.14	7.8	4.14
ab	27.5	27.92	30.29	29.36	17.26	23.69	20.73	22.42	22.93	23.02	36.47	19.52
an	26.97	23.71	22.66	23	28.6	31.45	32.37	28.11	28.03	27.52	18.1	27.69
ne												0.48
di	14.71	13.88	10.47	13.29	21.84	15.25	15.98	17.37	16.86	16.79	10.9	22.18
hy	7.6	9.62	16.73	4.87	8.15	12.41	6.75	3.19	0.98	5.08	15.48	
ol	8.26	6.59	0.97	10.37	13.42		12.51	16.13	18.21	14.18		16.61
mt	3.19	3.54	3.35	3.26	2.68	2.9	2.99	2.94	2.97	2.86	3.25	2.83
il	4.58	6.42	5.98	5.07	3.7	4.77	4.31	3.97	3.95	4.1	4.88	3.51
ap	1.07	1.2	1.58	2.02	0.58	1.25	0.72	0.74	0.76	0.81	1.9	0.56

	VH262	VH266	VH269	VH271	VH276	MA1	MA2	MA3	MA5	MA14	MB2	MB4
%AN	60.3	42.9	42.74	44.69	54.16	43.35	58.58	58.85	59.07	45.55	44.37	47.09
Q										2.11		
or	3.78	7.03	7.27	5.54	4.61	6.68	3.9	4.02	4.08	5.67	6.86	5.96
ab	18.79	30.04	29.79	28.43	23.19	31.99	20.9	20.39	20.56	27.59	31.14	30.04
an	28.53	22.57	22.23	22.97	27.39	24.47	29.56	29.17	29.68	23.08	24.83	26.74
di	19.51	11.76	13.8	13.33	18.05	13.18	21.17	21.77	22.49	12.73	12.24	12.18
hy	6.84	14.9	10.63	16.69	2.03	6.24	12.08	10	5.9	15.49	9.87	9.27
ol	15.06	1.19	3.66	0.99	16.03	8.23	4.7	7.37	9.82	0	5.67	6.94
mt	2.71	3.13	3.22	3.49	3.13	3.12	2.99	2.94	2.91	3.6	2.89	3.03
il	3.38	6.23	6.59	6.52	4.6	4.22	3.72	3.63	3.63	6.65	4.22	4.16
ap	0.56	1.2	1.14	1.6	0.74	1.32	0.63	0.63	0.65	1.37	1.3	1.18

	Basalts		Hawaiites								
	MB7	MB11	VH47	VH60	VH61	VH62	VH64	VH69	VH76	VH92	VH94
%AN	54.75	44.69	36.07	38.41	39.24	38.3	37.3	37.25	39.56	37.86	36.4
Q		1.34	1.2	1.72	2.84	1.71	1.78			0.49	
or	4.71	5.54	7.98	8.04	7.92	7.45	8.39	7.62	7.39	6.91	7.09
ab	25.13	28.52	34.27	33.17	33.17	34.1	34.78	33.51	32.32	33.17	33.25
an	30.4	23.04	19.34	20.68	21.42	21.17	20.69	19.89	21.16	20.21	19.04
di	14.56	13.69	11.98	8.47	7.92	10.8	9.21	12.28	13.68	11.39	12.46
hy	8.74	15.89	12.66	15.24	14.67	13.05	12.86	10.5	11.74	13.99	14.61
ol	8.08							2.72	1.52		0.32
mt	3.19	3.6	4.16	4.25	4.2	4.07	4.03	4.49	4.51	4.45	4.81
il	4.53	6.61	5.09	4.6	4.52	4.48	4.62	5.66	6.06	5.68	5.7
ap	0.83	1.37	1.74	2.66	2.8	2.9	2.92	1.37	1.18	1.99	1.95

	VH95	VH98	VH109	VH113	VH129	VH150	VH156	VH157	VH177	VH180	VH181	VH182
%AN	35.73	41.61	38.99	32.36	38.37	34.22	39.43	39.98	42	34.77	39.05	36.46
Q			0.78	1.11	0.9	1.03	2.64	2.65	0.77	1.49	3.12	0.29
or	7.21	8.33	8.63	6.97	6.65	7.27	8.39	8.21	7.27	8.04	7.39	7.21
ab	33.68	30.72	32.41	35.12	33.25	35.03	32.41	33.51	32.66	34.61	33.17	33.09
an	18.73	21.89	20.71	16.8	20.7	18.22	21.1	22.32	23.66	18.45	21.25	18.99
di	12.89	12.52	9.4	11.95	11.05	10.59	7.92	8	11.94	11.46	13.55	13.25
hy	11.56	13.24	15.1	13.72	14.54	15.1	14.91	13.31	13	13.41	7.84	14.14
ol	1.74	1										
mt	4.58	4.61	4.18	4.49	4.44	4.65	4.18	4.15	4.19	4.47	4.45	4.76
il	5.75	6.08	5.13	5.39	5.8	5.24	4.43	4.62	3.95	5.18	6.21	5.93
ap	1.97	1.25	1.83	2.97	1.83	2.48	2.69	2.94	1.51	2.18	2.13	1.92

						Mugearites					
	VH184	VH219	VH229	VH245	VH263	VH9	VH24	VH27	VH28	VH30	VH31
%AN	35.2	41.02	36.54	43.92	31.88	29.2	29.97	30.61	33.77	31.61	30.04
Q	2.15	0.19	0.97	5.05	0.06	5.33	1.24	1.76	3.75	2.39	1.79
or	8.04	7.92	7.33	8.75	7.8	10.16	8.33	8.1	8.1	8.08	8.27
ab	33.85	31.56	33.59	30.89	36.22	38.08	37.91	37.49	36.13	36.72	37.49
an	18.39	21.95	19.34	24.19	16.95	15.71	16.22	16.54	18.43	16.97	16.09
di	11.92	10.28	10.4	11	11.11	8.61	11.05	11.03	9.93	10.04	10.56
hy	12.89	15.72	14.82	7.27	13.61	10.76	11.57	11.87	9.67	12.1	10.99
mt	4.35	4.52	4.44	4.36	4.42	6.13	6.67	6.8	6.47	6.79	6.55
il	5.49	5.77	5.39	5.68	5	3.76	4.88	4.9	4.92	4.85	4.65
ap	1.88	1.64	2.5	1.71	2.15	1.81	2.27	2.22	2.15	2.25	2.22

	VH32	VH45	VH46	VH57	VH99	VH114	VH115	VH116	VH117	VH133	VH137	VH147
%AN	26.35	39.7	36.46	28.02	35.1	28.78	29.24	27.48	29.74	26.35	31.3	31.76
Q	0.44	4.01	2.23	2	3.24	3.52	2.57	1.19	3.32	5.14	2.12	5.39
or	8.81	8.16	8.33	8.04	7.74	8.16	7.92	8.04	8.04	11.64	7.86	9.22
ab	39.35	31.99	34.35	38.42	33.93	38.59	38.08	39.18	38.5	40.02	36.64	38.59
an	14.07	21.06	19.72	14.95	18.35	15.6	15.74	14.85	16.3	14.32	16.69	17.96
di	13.33	12.2	11.71	10.22	12.97	10.04	9.78	10.2	8.69	7.28	10.56	6.51
hy	9.45	9.93	11.2	11.45	11.14	11.41	11.74	11.65	12.46	10.29	12.28	11.49
mt	6.63	6.13	6.37	6.57	6.63	6.8	6.57	6.47	6.54	5.45	6.92	5.97
il	4.52	4.88	5.09	4.29	5.49	4.18	4.37	4.25	4.2	3.42	4.92	3.86
ap	2.32	1.85	1.74	2.55	1.46	2.46	2.59	2.55	2.53	1.99	2.18	2.09

Mugearites

	VH148	VH169	VH170	VH172	VH176	VH183	VH187	VH220	VH221	VH222	VH223	VH226
%AN	32.38	27.93	28.31	31.63	33.87	33.67	32.16	24.93	25.12	26.35	30.15	31.49
Q	2.12	4.7	5.56	3.85	3.85	3.77	3.59	4.02	4.24	3.73	3.14	5.65
or	7.8	10.58	10.64	9.81	7.86	9.1	9.99	9.63	9.93	9.57	9.1	10.76
ab	36.64	40.19	40.7	38.76	34.44	36.05	36.13	41.97	42.14	41.8	39.86	38.42
an	17.54	15.58	16.07	17.93	17.64	18.3	17.13	13.93	14.13	14.95	17.21	17.66
di	9.27	6.94	6.56	6.11	9.93	9.89	9.27	8.1	7.68	7.23	6.3	6.2
hy	13.42	10.53	9.6	12.15	12.92	9.65	10.2	11.59	11.38	11.91	12.57	9.49
mt	6.96	5.65	5.38	6.03	6.86	5.89	6	6.55	6.45	6.5	6.41	5.68
il	4.79	3.25	3.21	3.68	4.75	5	4.29	3.38	3.25	3.38	3.74	3.44
ap	2.62	1.88	1.85	2.18	2.11	2.46	2.55	1.97	1.85	1.99	2.15	2.04

	VH228	VH234	VH243	VH244	VH254	VH255	VH256	VH258	VH264	VH265	VH268	MA4
%AN	32.35	41.98	33.94	33.22	26.07	32.21	32.09	32.54	32.33	33.73	33.72	33.68
Q	4.49	7.31	2.34	2.21	3.8	2.59	2.07	2.5	2.48	3.46	4.8	2.71
or	9.04	9.57	7.8	7.56	9.4	7.68	7.8	7.92	8.21	7.51	9.04	9.51
ab	36.72	33.68	35.96	36.72	42.14	37.32	36.81	36.72	37.15	36.22	35.88	39.52
an	17.56	24.37	18.47	18.27	14.86	17.73	17.4	17.71	17.75	18.43	18.25	20.07
di	7.56	8.51	10.56	10.38	7.43	10.51	10.31	9.92	9.83	10.6	11.9	7.16
hy	11.38	3.78	12.12	12.05	11.53	10.82	12.08	11.99	11.54	10.16	9	11.05
mt	6.03	5.42	6.58	6.73	6.5	6.92	6.76	6.67	6.57	6.48	5.81	5.77
il	4.03	5.68	5.07	5.07	3.4	5.03	4.98	4.92	4.94	5.01	5	3.36
ap	2.55	1.95	1.78	1.81	2.02	2.22	2.22	2.22	2.2	2.2	1.37	1.85

	MA6	MA7	MA9	MA13	MB6	MB9
%AN	35.75	31.2	33.38	35.34	26.6	38.17
Q	3.78	2.52	4.17	4.47	0.32	0.75
or	7.98	10.4	9.28	7.39	10.2	8.01
ab	34.69	40.62	35.79	35.03	45.69	35.88
an	19.3	18.42	17.93	19.15	16.56	22.15
di	12.27	5.98	11.64	10.19	7.27	8.76
hy	9.57	12	9.69	9.54	10.42	13.73
mt	6.15	5.76	6.05	6.63	5.34	6.1
il	5.32	3.19	4.84	5.07	3.15	3.75
ap	1.48	1.92	1.34	2.2	1.9	1.62

Benmoreites

	VH65	VH66	VH68	VH79	VH97
%AN	22.57	24.52	21.26	17.74	24.71
Q	8.07	8.79	8.54	6.37	10.35
or	13.83	13.59	14.95	14.83	14.66
ab	45.44	43.58	45.1	47.56	43.49
an	13.24	14.16	12.18	10.26	14.27
di	4.37	3.98	4.27	6.56	2.39
hy	8.27	8.91	7.61	6.55	7.78
mt	3.62	3.73	3.52	3.49	3.26
il	1.75	1.86	1.48	1.63	1.56
ap	0.83	0.95	0.65	0.67	0.72

	VH175	VH189	VH190	VH194	VH205	VH218	VH225	VH250	VH251	VH252
%AN	24.99	23.17	21.14	18.55	23.67	14.97	25.35	21.15	20.84	23.26
Q	7.87	7.12	8.16	9.56	4.76	8.88	8.54	5.33	9.21	5.97
or	12.82	11.76	12.88	15.25	12.33	13.59	12.35	10.87	12.94	11.41
ab	43.07	43.83	44.76	45.95	43.24	47.89	44.34	45.95	44.17	45.02
an	14.35	13.22	12	10.47	13.41	8.43	15.06	12.32	11.63	13.64
di	5.83	6.55	5.44	5.46	6.98	7.85	4.81	7.73	5.75	6.2
hy	7.71	8.11	7.8	6.48	8.57	6.54	6.36	8.99	8.49	9.14
mt	4.31	4.07	3.81	3.6	4.25	4.29	3.76	4.71	4.34	4.6
il	2.34	2.47	1.98	1.41	2.55	1.58	2.34	2.68	1.96	2.64
ap	1.11	1.23	0.9	0.49	1.25	0.53	1.11	1.34	0.86	1.34

	Trachytes							Rhyolites			
	VH23	VH75	VH193	VH249	MA10	MB1	MB10	VH35	VH38	VH48	VH49
%AN	10.8	3.57	19.18	11.67	12.13	7.3	6.95	4.88			
Q	11.88	16.63	17.55	10.61	12.26	16.15	17.13	22.46	19.78	22.01	23.11
or	15.25	21.69	15.66	15.07	15.31	19.68	20.7	23.4	24.41	24.7	24.94
ab	48.82	49.76	44.68	49.33	48.32	49.16	48.74	46.46	47.84	45.3	46.05
an	5.91	1.84	10.6	6.52	6.67	3.87	3.64	2.38			
di	8.98	4.17	6.1	8.29	7.99	3.37	3.25	0.77	2.82	2.13	2.11
hy	3.3	1.34	1.22	3.44	3.49	2.02	1.76	1.35	1.03	1.85	1.39
ac	4.54								1.24	2.57	2.15
mt	1.2	2	1.8	4.42	4.42	2.26	2.12	1.1	0.67		0.11
il	0.3	0.84	0.76	1.16	1.14	0.61	0.52	0.3	0.32	0.27	0.27
ap		0.21	0.16	0.28	0.28	0.09	0.07	0.05	0.07	0.05	0.02
NMS										0.06	

	VH136a	VH138	VH139	VH142	VH144	VH164	VH165	VH167	VH204	VH206	VH253	VH267
%AN							1.18		0.2		1.7	7.22
Q	23.02	20.55	22.46	20.74	22.78	22.25	23.43	21.85	21.4	24.55	17.94	19.51
or	25.77	25.41	26	25.41	26	25.94	23.99	25.83	23.17	25.29	23.23	21.45
ab	43.52	44.68	44.38	44.78	43.81	46.34	46.96	45.58	49.33	42.99	50.35	47.56
an							0.56		0.1		0.87	3.7
di	1.58	1.89	1.92	1.65	1.67	1.87	2.32	1.78	2.64	1.46	3.65	2.35
hy	2.05	2.39	1.96	2.63	1.99	1.7	0.9	1.91	0.65	1.78	0.83	2.36
ac	2.51	3.07	1.31	3.15	2.33	1.67		2.55		2.34		
mt	0.06		0.93		0.18	0.51	1.28		1.25		1.64	1.97
il	0.27	0.32	0.32	0.32	0.27	0.27	0.3	0.25	0.27	0.3	0.4	0.84
ap	0.02	0.02	0.05	0.05	0.02	0.05	0.07	0.05	0.02	0.07	0.05	0.19
NMS		0.63		0.03				0.38		0.09		

	MA8	MA11	MA12	MB3	MB5	MB8
%AN				7.41		5.68
Q	23.91	21.62	22.7	19.3	23.39	18.37
or	25.12	26.12	25.3	20.47	25.83	21.02
ab	45.78	44.73	45.4	49.08	44.75	49.25
an				3.93		2.97
di	1.76	1.53	1.79	1.43	0.95	2.86
hy	1.54	1.67	2.14	2.34	1.67	1.89
ac	0.59	0.77	2.64		1.57	
mt	1.09	0.99	0.07	2.03	0.33	2.1
il	0.32	0.3	0.3	0.57	0.4	0.52
ap	0.07	0.02	0.02	0.09	0.02	0.09

Appendix 5
Electron Microprobe Analyses

The following abbreviations have been used in the data tables:

Rock types: B - basalt, BH - basaltic hawaiite, H - hawaiite, M - mugearite, Ben - benmoreite, T - trachyte, R - rhyolite and X - xenolith.

core - phenocryst core
rim - phenocryst rim

For clinopyroxenes and FeTi oxides, Fe^{3+} concentrations were estimated using a general equation based on stoichiometric criteria (Droop 1987).

A5.5 Olivine-Liquid equilibria

Average olivine and glass analyses are presented in where possible, where glass was absent, whole rock analyses are considered in its place and the K_Ds calculated.

$$K_D = \frac{(X^{ol}_{FeO})(X^{liq}_{MgO})}{(X^{liq}_{FeO})(X^{ol}_{MgO})}$$

Where the liquid (glass) and olivine are in equilibrium a value of 0.3 should be obtained (Roeder & Emslie 1970).

A5.1 Olivine analyses

	VH1	VH1 core	VH1 rim	VH1	VH10	VH10 resorbed	VH10	VH10	VH10	VH10	VH10	VH10 core	VH10 rim	VH10 core	VH10	VH20	VH20	VH20	VH20
	B	B	B	B	B	B	B	B	B	B	B	B	B	B	B	X	X	X	X
SiO2	40.00	38.93	39.30	38.97	40.60	40.15	40.98	41.17	40.68	41.38	41.23	40.24	39.87	40.43	41.21	40.15	38.72	37.13	37.13
TiO2	0.00	0.09	0.00	0.00	0.00	0.00	0.00	0.00	0.00	0.00	0.00	0.00	0.00	0.00	0.00	0.00	0.00	0.00	0.00
Cr2O3	0.00	0.20	0.00	0.00	0.00	0.00	0.20	0.00	0.00	0.00	0.00	0.00	0.00	0.00	0.00	0.00	0.00	0.00	0.00
Al2O3	0.00	0.00	0.00	0.00	0.00	0.00	0.00	0.00	0.00	0.00	0.00	0.00	0.00	0.00	0.00	0.34	0.00	0.30	0.30
FeO	19.37	21.19	20.65	19.43	11.66	13.36	11.12	11.08	10.72	10.48	10.02	10.00	11.26	10.98	11.11	16.44	14.29	26.99	26.99
MnO	0.00	0.00	0.00	0.00	0.14	0.00	0.00	0.00	0.00	0.00	0.00	0.00	0.00	0.00	0.00	0.00	0.25	0.55	0.55
MgO	41.86	39.34	41.04	40.85	47.38	46.14	48.21	48.22	47.75	48.51	48.55	48.06	46.74	47.33	48.21	43.95	42.67	35.11	35.01
CaO	0.29	0.13	0.27	0.34	0.29	0.36	0.27	0.21	0.25	0.22	0.27	0.22	0.34	0.23	0.25	0.37	0.25	0.00	0.00
Na2O	0.44	0.56	0.55	0.46	0.20	0.58	0.45	0.22	0.30	0.35	0.26	0.28	0.51	0.23	0.36	0.00	0.00	0.00	0.00
K2O	0.00	0.00	0.00	0.00	0.00	0.00	0.00	0.00	0.00	0.00	0.00	0.00	0.00	0.00	0.00	0.00	0.00	0.00	0.00
NiO	0.00	0.00	0.00	0.00	0.17	0.00	0.31	0.18	0.00	0.00	0.00	0.00	0.00	0.00	0.00	0.00	0.00	0.00	0.00
Total	101.95	100.43	101.82	100.04	100.44	100.59	101.54	101.08	99.70	100.93	100.33	98.79	98.72	99.20	101.14	101.25	96.17	100.08	99.99
per 4 oxygens																			
Si	1.00	1.00	1.00	1.00	1.00	1.00	1.00	1.00	1.00	1.01	1.01	1.00	1.00	1.00	1.00	1.00	1.01	0.99	0.99
Ti	0.00	0.00	0.00	0.00	0.00	0.00	0.00	0.00	0.00	0.00	0.00	0.00	0.00	0.00	0.00	0.00	0.00	0.00	0.00
Cr	0.00	0.00	0.00	0.00	0.00	0.00	0.00	0.00	0.00	0.00	0.00	0.00	0.00	0.00	0.00	0.00	0.00	0.00	0.00
Al	0.00	0.00	0.00	0.00	0.00	0.00	0.00	0.00	0.00	0.00	0.00	0.00	0.00	0.00	0.00	0.01	0.00	0.01	0.01
Fe	0.41	0.46	0.44	0.42	0.24	0.28	0.23	0.23	0.22	0.21	0.20	0.21	0.24	0.23	0.23	0.34	0.31	0.60	0.60
Mn	0.00	0.00	0.00	0.00	0.00	0.00	0.00	0.00	0.00	0.00	0.00	0.00	0.00	0.00	0.00	0.00	0.01	0.01	0.01
Mg	1.57	1.51	1.55	1.56	1.74	1.71	1.75	1.75	1.76	1.76	1.77	1.78	1.75	1.75	1.75	1.63	1.66	1.39	1.39
Ca	0.01	0.00	0.01	0.01	0.01	0.01	0.01	0.01	0.01	0.01	0.01	0.01	0.01	0.01	0.01	0.01	0.01	0.00	0.00
Na	0.02	0.03	0.03	0.02	0.01	0.03	0.02	0.01	0.01	0.02	0.01	0.01	0.02	0.01	0.02	0.00	0.00	0.00	0.00
K	0.00	0.00	0.00	0.00	0.00	0.00	0.00	0.00	0.00	0.00	0.00	0.00	0.00	0.00	0.00	0.00	0.00	0.00	0.00
Ni	0.00	0.00	0.00	0.00	0.00	0.00	0.01	0.00	0.00	0.00	0.00	0.00	0.00	0.00	0.00	0.00	0.00	0.00	0.00
Total	3.01	3.00	3.02	3.01	3.00	3.02	3.01	3.00	3.00	3.00	3.00	3.01	3.01	3.00	3.00	2.99	2.99	3.01	3.01
%Fo	78.31	75.41	77.50	78.13	87.02	85.34	87.47	87.62	87.84	87.97	88.40	89.00	87.27	87.61	87.54	81.61	82.90	69.71	69.58

Olivines

	VH24	VH24	VH24	VH24	VH24	VH41	VH41	VH41	VH41	VH41	VH41	VH41	VH50	VH50	VH50	VH50	VH51	VH51	VH51
	M	M	M	M	M	BH	BH	BH	BH	BH	BH	BH	BH	BH	BH	BH	R	R	R
SiO2	35.57	36.36	36.15	35.78	37.84	35.63	35.73	35.86	35.60	35.80	36.06	35.61	36.16	38.74	38.56	38.16	28.96	29.49	29.18
TiO2	0.00	0.00	0.00	0.00	0.00	0.00	0.00	0.19	0.00	0.00	0.16	0.00	0.00	0.00	0.00	0.00	0.00	0.00	0.00
Cr2O3	0.00	0.00	0.00	0.00	0.00	0.00	0.00	0.00	0.00	0.00	0.00	0.00	0.00	0.00	0.00	0.00	0.00	0.00	0.00
Al2O3	0.00	0.00	0.00	0.00	0.00	0.00	0.00	0.00	0.00	0.00	0.00	0.00	0.00	0.00	0.00	0.00	0.00	0.00	0.00
FeO	37.42	30.56	33.22	35.35	31.78	40.39	38.90	39.62	36.13	38.17	38.64	37.92	30.99	21.88	20.39	22.27	64.40	63.92	67.05
MnO	0.30	0.00	0.32	0.00	0.24	0.45	0.35	0.31	0.17	0.30	0.26	0.23	0.00	0.00	0.00	0.00	3.13	3.22	2.29
MgO	25.91	31.74	29.47	27.83	30.91	24.52	25.21	24.93	25.68	26.11	25.97	26.19	30.74	39.21	39.94	38.28	0.27	0.21	0.19
CaO	0.35	0.42	0.23	0.29	0.48	0.29	0.26	0.34	0.38	0.32	0.28	0.33	0.27	0.26	0.26	0.17	0.32	0.23	0.24
Na2O	0.53	0.59	0.56	0.62	0.65	0.58	0.52	0.51	0.60	0.62	0.63	0.64	0.80	0.40	0.63	0.41	0.64	0.41	0.44
K2O	0.00	0.00	0.00	0.00	0.00	0.00	0.00	0.00	0.00	0.00	0.00	0.00	0.00	0.00	0.00	0.00	0.00	0.00	0.00
NiO	0.00	0.00	0.00	0.00	0.00	0.00	0.00	0.00	0.00	0.00	0.00	0.00	0.00	0.00	0.00	0.00	0.00	0.00	0.00
Total	100.09	99.67	99.96	99.87	101.88	101.85	100.96	101.74	98.55	101.34	101.98	100.92	98.96	100.49	99.77	99.28	97.72	97.48	99.38
per 4 oxygens																			
Si	1.00	0.99	1.00	1.00	1.00	1.00	1.00	1.00	1.01	1.00	1.00	1.00	1.00	1.00	1.00	1.00	1.00	1.01	0.99
Ti	0.00	0.00	0.00	0.00	0.00	0.00	0.00	0.00	0.00	0.00	0.00	0.00	0.00	0.00	0.00	0.00	0.00	0.00	0.00
Cr	0.00	0.00	0.00	0.00	0.00	0.00	0.00	0.00	0.00	0.00	0.00	0.00	0.00	0.00	0.00	0.00	0.00	0.00	0.00
Al	0.00	0.00	0.00	0.00	0.00	0.00	0.00	0.00	0.00	0.00	0.00	0.00	0.00	0.00	0.00	0.00	0.00	0.00	0.00
Fe	0.88	0.70	0.77	0.82	0.70	0.94	0.91	0.92	0.86	0.89	0.89	0.89	0.71	0.47	0.44	0.49	1.86	1.83	1.90
Mn	0.01	0.00	0.01	0.00	0.01	0.01	0.01	0.01	0.00	0.01	0.01	0.01	0.00	0.00	0.00	0.00	0.09	0.09	0.07
Mg	1.09	1.29	1.21	1.16	1.22	1.02	1.05	1.04	1.08	1.08	1.07	1.09	1.26	1.51	1.54	1.50	0.01	0.01	0.01
Ca	0.01	0.01	0.01	0.01	0.01	0.01	0.01	0.01	0.01	0.01	0.01	0.01	0.01	0.01	0.01	0.00	0.01	0.01	0.01
Na	0.03	0.03	0.03	0.03	0.03	0.03	0.03	0.03	0.03	0.03	0.03	0.03	0.04	0.02	0.03	0.02	0.04	0.03	0.03
K	0.00	0.00	0.00	0.00	0.00	0.00	0.00	0.00	0.00	0.00	0.00	0.00	0.00	0.00	0.00	0.00	0.00	0.00	0.00
Ni	0.00	0.00	0.00	0.00	0.00	0.00	0.00	0.00	0.00	0.00	0.00	0.00	0.00	0.00	0.00	0.00	0.00	0.00	0.00
Total	3.01	3.02	3.02	3.02	2.98	3.01	3.01	3.01	3.00	3.02	3.02	3.02	3.02	3.01	3.02	3.01	3.02	2.99	3.01
%Fo	54.32	64.55	60.56	57.81	61.07	51.10	52.69	51.83	54.22	54.12	53.58	54.56	63.15	75.47	77.03	74.80	0.70	0.54	0.48

Olivines

	VH51	VH51	VH65	VH65	VH65	VH65	VH65	VH65	VH80 core	VH80 rim	VH80	VH80	VH80	VH80	VH81	VH81	VH81 melt	VH81 melt	VH89
	R	R	Ben	Ben	Ben	Ben	Ben	Ben	B	B	B	B	B	B	X	X	X	X	BH
SiO2	29.63	29.59	33.84	33.32	30.95	32.39	32.71	31.21	39.01	37.89	39.91	39.59	37.99	40.17	35.27	34.55	40.01	40.14	40.22
TiO2	0.00	0.00	0.00	0.00	0.00	0.00	0.00	0.00	0.00	0.00	0.00	0.00	0.00	0.00	0.00	0.00	0.00	0.00	0.00
Cr2O3	0.00	0.00	0.00	0.00	0.00	0.00	0.00	0.00	0.00	0.00	0.00	0.00	0.00	0.00	0.00	0.00	0.00	0.00	0.00
Al2O3	0.00	0.00	0.00	0.00	0.00	0.00	0.00	0.00	0.00	0.00	0.00	0.00	0.00	0.00	0.00	0.00	0.00	0.00	0.00
FeO	66.75	67.30	50.14	49.00	58.48	51.43	48.24	59.07	20.13	26.56	16.27	17.20	25.71	14.41	42.30	41.56	15.61	13.60	13.79
MnO	2.15	2.39	1.10	1.12	2.05	1.29	1.15	1.99	0.00	0.00	0.00	0.00	0.00	0.00	0.46	0.37	0.00	0.00	0.00
MgO	0.00	0.00	15.72	16.14	7.29	12.88	16.14	7.23	41.25	35.02	43.91	43.60	36.42	44.84	22.72	22.01	44.06	46.20	46.14
CaO	0.19	0.28	0.37	0.83	0.31	0.44	0.39	0.23	0.25	0.30	0.22	0.23	0.27	0.25	0.16	0.15	0.26	0.27	0.27
Na2O	0.63	0.53	0.57	0.70	0.51	0.63	0.75	0.46	0.64	0.64	0.48	0.43	0.69	0.30	0.62	0.62	0.49		0.53
K2O	0.00	0.00	0.00	0.00	0.00	0.00	0.00	0.00	0.00	0.00	0.00	0.00	0.00	0.00	0.00	0.00	0.00	0.00	0.00
NiO	0.00	0.00	0.00	0.00	0.00	0.00	0.00	0.00	0.00	0.00	0.00	0.00	0.00	0.00	0.00	0.00	0.00	0.00	0.00
Total	99.36	100.09	101.73	101.09	99.58	99.06	99.36	100.19	101.28	100.41	100.79	101.05	101.07	99.97	101.51	99.25	100.44	100.21	100.95
per 4 oxygens																			
Si	1.00	1.00	1.00	0.99	1.00	1.00	0.99	1.00	0.99	1.00	1.00	0.99	0.99	1.01	1.00	1.00	1.00	1.00	0.99
Ti	0.00	0.00	0.00	0.00	0.00	0.00	0.00	0.00	0.00	0.00	0.00	0.00	0.00	0.00	0.00	0.00	0.00	0.00	0.00
Cr	0.00	0.00	0.00	0.00	0.00	0.00	0.00	0.00	0.00	0.00	0.00	0.00	0.00	0.00	0.00	0.00	0.00	0.00	0.00
Al	0.00	0.00	0.00	0.00	0.00	0.00	0.00	0.00	0.00	0.00	0.00	0.00	0.00	0.00	0.00	0.00	0.00	0.00	0.00
Fe	1.89	1.90	1.24	1.22	1.57	1.33	1.22	1.58	0.43	0.59	0.34	0.36	0.56	0.30	1.00	1.01	0.33	0.28	0.28
Mn	0.06	0.07	0.03	0.03	0.06	0.03	0.03	0.05	0.00	0.00	0.00	0.00	0.00	0.00	0.01	0.01	0.00	0.00	0.00
Mg	0.00	0.00	0.69	0.72	0.35	0.59	0.73	0.34	1.56	1.38	1.64	1.63	1.42	1.67	0.96	0.95	1.65	1.71	1.70
Ca	0.01	0.01	0.01	0.03	0.01	0.01	0.01	0.01	0.01	0.01	0.01	0.01	0.01	0.01	0.00	0.00	0.01	0.01	0.01
Na	0.04	0.03	0.03	0.04	0.03	0.04	0.04	0.03	0.03	0.03	0.02	0.02	0.03	0.01	0.03	0.03	0.02	0.00	0.03
K	0.00	0.00	0.00	0.00	0.00	0.00	0.00	0.00	0.00	0.00	0.00	0.00	0.00	0.00	0.00	0.00	0.00	0.00	0.00
Ni	0.00	0.00	0.00	0.00	0.00	0.00	0.00	0.00	0.00	0.00	0.00	0.00	0.00	0.00	0.00	0.00	0.00	0.00	0.00
Total	3.01	3.02	3.01	3.02	3.02	3.02	3.03	3.02	3.02	3.01	3.01	3.02	3.02	3.00	3.02	3.01	3.01	3.00	3.01
%Fo	0.00	0.00	34.66	35.79	17.49	29.74	36.47	17.25	78.23	69.09	82.03	81.65	71.10	83.66	48.07	47.64	82.36	85.65	84.92

Olivines

	VH89	VH89	VH89	VH89	VH94	VH94	VH94	VH94	VH105	VH105	VH105	VH105	VH105	VH106	VH106 core	VH106 rim	VH106	VH106	VH106
	BH	BH	BH	BH	H	H	H	H	H	H	H	H	H	B	B	B	B	B	B
SiO2	39.83	38.34	37.87	32.70	38.10	36.76	37.09	36.79	39.20	38.21	38.04	38.26	38.24	38.68	38.91	38.89	39.99	39.64	39.07
TiO2	0.00	0.00	0.00	1.02	0.00	0.11	0.00	0.00	0.00	0.00	0.00	0.00	0.00	0.00	0.00	0.00	0.00	0.14	0.00
Cr2O3	0.00	0.00	0.00	3.14	0.00	0.00	0.00	0.00	0.00	0.00	0.00	0.00	0.00	0.00	0.00	0.00	0.00	0.00	0.00
Al2O3	0.00	0.00	0.00	0.00	0.00	0.00	0.00	0.00	0.00	0.00	0.00	0.00	0.00	0.00	0.00	0.00	0.00	0.00	0.00
FeO	13.63	21.16	22.59	24.90	28.52	28.26	27.73	28.92	20.50	25.08	24.89	24.22	24.46	22.75	19.60	18.18	15.45	18.30	19.83
MnO	0.00	0.12	0.00	0.00	0.00	0.17	0.00	0.14	0.00	0.00	0.00	0.00	0.00	0.00	0.00	0.00	0.00	0.00	0.00
MgO	45.50	39.16	37.44	34.99	34.89	32.84	34.06	33.00	40.59	36.55	36.01	37.52	36.72	39.15	40.73	41.40	44.82	41.94	41.38
CaO	0.28	0.20	0.30	0.15	0.16	0.26	0.17	0.20	0.24	0.30	0.30	0.23	0.27	0.28	0.23	0.25	0.25	0.37	0.31
Na2O	0.40	0.42	0.53	0.41	0.44	0.63	0.62	0.55	0.53	0.47	0.70	0.51	0.64	0.60	0.57	0.46	0.45	0.45	0.71
K2O	0.00	0.00	0.00	0.00	0.00	0.00	0.00	0.00	0.00	0.00	0.00	0.00	0.00	0.00	0.00	0.00	0.00	0.00	0.00
NiO	0.00	0.00	0.00	0.00	0.00	0.00	0.00	0.00	0.00	0.00	0.00	0.00	0.00	0.00	0.00	0.00	0.00	0.00	0.00
Total	99.64	99.39	98.73	97.30	102.11	99.02	99.66	99.60	101.05	100.60	99.93	100.75	100.33	101.46	100.04	99.18	100.96	100.84	101.30
per 4 oxygens																			
Si	1.00	1.00	1.00	0.89	1.00	1.00	1.00	1.00	1.00	1.00	1.00	1.00	1.00	0.99	1.00	1.00	1.00	1.00	0.99
Ti	0.00	0.00	0.00	0.02	0.00	0.00	0.00	0.00	0.00	0.00	0.00	0.00	0.00	0.00	0.00	0.00	0.00	0.00	0.00
Cr	0.00	0.00	0.00	0.07	0.00	0.00	0.00	0.00	0.00	0.00	0.00	0.00	0.00	0.00	0.00	0.00	0.00	0.00	0.00
Al	0.00	0.00	0.00	0.00	0.00	0.00	0.00	0.00	0.00	0.00	0.00	0.00	0.00	0.00	0.00	0.00	0.00	0.00	0.00
Fe	0.29	0.46	0.50	0.57	0.62	0.64	0.62	0.65	0.44	0.55	0.55	0.53	0.54	0.49	0.42	0.39	0.32	0.39	0.42
Mn	0.00	0.00	0.00	0.00	0.00	0.00	0.00	0.00	0.00	0.00	0.00	0.00	0.00	0.00	0.00	0.00	0.00	0.00	0.00
Mg	1.70	1.52	1.48	1.42	1.36	1.33	1.36	1.33	1.54	1.43	1.42	1.46	1.44	1.50	1.56	1.58	1.67	1.58	1.57
Ca	0.01	0.01	0.01	0.00	0.00	0.01	0.00	0.01	0.01	0.01	0.01	0.01	0.01	0.01	0.01	0.01	0.01	0.01	0.01
Na	0.02	0.02	0.03	0.02	0.02	0.03	0.03	0.03	0.03	0.02	0.04	0.03	0.03	0.03	0.03	0.02	0.02	0.02	0.04
K	0.00	0.00	0.00	0.00	0.00	0.00	0.00	0.00	0.00	0.00	0.00	0.00	0.00	0.00	0.00	0.00	0.00	0.00	0.00
Ni	0.00	0.00	0.00	0.00	0.00	0.00	0.00	0.00	0.00	0.00	0.00	0.00	0.00	0.00	0.00	0.00	0.00	0.00	0.00
Total	3.01	3.01	3.01	2.99	3.01	3.02	3.02	3.02	3.01	3.01	3.01	3.02	3.01	3.02	3.01	3.00	3.01	3.01	3.02
%Fo	84.95	76.08	73.79	70.92	68.09	66.47	68.19	66.56	77.17	71.40	70.83	72.91	71.76	74.93	77.99	79.16	83.31	79.06	78.37

Olivines

	VH106	VH106	VH117	VH117	VH137	VH137	VH137	VH137	VH137	VH137	VH151	VH151	VH151 rim	VH151 core	VH151	VH189	VH189	VH189	VH262
	B	B	M	M	M	M	M	M	M	M	B	B	B	B	B	Ben	Ben	Ben	B
SiO2	39.48	38.32	34.94	34.18	36.89	37.03	36.05	35.30	30.79	35.14	39.28	39.08	39.36	39.60	37.88	33.45	33.41	25.69	40.75
TiO2	0.00	0.00	0.49	0.00	0.09	0.00	0.00	0.00	6.57	0.09	0.00	0.00	0.00	0.08	0.80	0.00	0.00	4.56	0.00
Cr2O3	0.22	0.00	0.00	0.00	0.00	0.00	0.00	0.00	0.00	0.00	0.00	0.00	0.00	0.00	0.00	0.00	0.00	0.00	0.00
Al2O3	0.00	0.00	0.00	0.00	0.00	0.00	0.00	0.00	0.00	0.00	0.00	0.00	0.00	0.00	0.00	0.00	0.00	0.00	0.00
FeO	17.88	24.77	41.36	44.60	32.56	32.15	36.03	38.57	38.93	38.52	19.25	21.87	18.97	19.28	25.09	47.24	47.49	51.24	14.53
MnO	0.00	0.00	0.00	0.72	0.00	0.12	0.30	0.00	0.20	0.27	0.00	0.00	0.00	0.00	0.00	0.76	0.79	0.50	0.00
MgO	42.68	36.48	21.00	20.56	30.87	31.16	28.27	25.50	22.29	25.23	41.50	39.02	41.47	41.78	35.68	17.59	16.94	12.55	46.52
CaO	0.18	0.35	1.44	0.20	0.24	0.26	0.20	0.31	0.37	0.32	0.25	0.26	0.30	0.23	0.30	0.60	0.54	1.46	0.24
Na2O	0.45	0.38	0.64	0.68	0.74	0.59	0.51	0.42	0.45	0.63	0.45	0.48	0.72	0.65	0.54	0.72	0.71	0.63	0.50
K2O	0.00	0.00	0.00	0.00	0.00	0.00	0.00	0.00	0.00	0.00	0.00	0.00	0.00	0.00	0.00	0.00	0.00	0.00	0.00
NiO	0.00	0.00	0.00	0.00	0.00	0.00	0.00	0.00	0.00	0.00	0.00	0.00	0.00	0.00	0.00	0.00	0.00	0.00	0.00
Total	100.89	100.29	99.87	100.94	101.38	101.30	101.36	100.09	99.59	100.21	100.72	100.72	100.81	101.62	100.27	100.35	99.88	96.63	102.54
per 4 oxygens																			
Si	1.00	1.01	1.00	0.99	0.99	1.00	0.99	1.00	0.89	0.99	1.00	1.01	1.00	1.00	1.00	0.99	1.00	0.83	0.99
Ti	0.00	0.00	0.01	0.00	0.00	0.00	0.00	0.00	0.14	0.00	0.00	0.00	0.00	0.00	0.02	0.00	0.00	0.11	0.00
Cr	0.00	0.00	0.00	0.00	0.00	0.00	0.00	0.00	0.00	0.00	0.00	0.00	0.00	0.00	0.00	0.00	0.00	0.00	0.00
Al	0.00	0.00	0.00	0.00	0.00	0.00	0.00	0.00	0.00	0.00	0.00	0.00	0.00	0.00	0.00	0.00	0.00	0.00	0.00
Fe	0.38	0.54	0.99	1.08	0.73	0.72	0.83	0.91	0.94	0.91	0.41	0.47	0.40	0.41	0.55	1.17	1.19	1.39	0.30
Mn	0.00	0.00	0.00	0.02	0.00	0.00	0.01	0.00	0.00	0.01	0.00	0.00	0.00	0.00	0.00	0.02	0.02	0.01	0.00
Mg	1.61	1.43	0.89	0.89	1.24	1.25	1.16	1.07	0.96	1.06	1.57	1.50	1.57	1.57	1.40	0.78	0.75	0.61	1.69
Ca	0.00	0.01	0.04	0.01	0.01	0.01	0.01	0.01	0.01	0.01	0.01	0.01	0.01	0.01	0.01	0.02	0.02	0.05	0.01
Na	0.02	0.02	0.04	0.04	0.04	0.03	0.03	0.02	0.03	0.03	0.02	0.02	0.04	0.03	0.03	0.04	0.04	0.04	0.02
K	0.00	0.00	0.00	0.00	0.00	0.00	0.00	0.00	0.00	0.00	0.00	0.00	0.00	0.00	0.00	0.00	0.00	0.00	0.00
Ni	0.00	0.00	0.00	0.00	0.00	0.00	0.00	0.00	0.00	0.00	0.00	0.00	0.00	0.00	0.00	0.00	0.00	0.00	0.00
Total	3.01	3.00	2.97	3.03	3.02	3.02	3.02	3.01	2.97	3.02	3.01	3.01	3.02	3.02	3.00	3.03	3.02	3.04	3.01
%Fo	80.33	71.34	44.75	44.49	62.05	62.63	58.00	53.70	48.01	53.19	78.70	74.89	78.55	78.53	70.00	38.96	37.70	30.33	84.58

Olivines

	VH262	VH262	VH262	VH262 rim
	B	B	B	B
SiO2	40.93	40.49	40.73	39.45
TiO2	0.00	0.00	0.00	0.00
Cr2O3	0.00	0.00	0.00	0.00
Al2O3	0.00	0.00	0.00	0.00
FeO	13.52	14.58	13.08	16.36
MnO	0.00	0.00	0.00	0.00
MgO	46.66	45.53	45.11	43.06
CaO	0.22	0.29	0.29	0.14
Na2O	0.45	0.42	0.37	0.42
K2O	0.00	0.00	0.00	0.00
NiO	0.00	0.00	0.00	0.00
Total	101.78	101.30	99.57	99.42
per 4 oxygens				
Si	1.00	1.00	1.01	1.00
Ti	0.00	0.00	0.00	0.00
Cr	0.00	0.00	0.00	0.00
Al	0.00	0.00	0.00	0.00
Fe	0.28	0.30	0.27	0.35
Mn	0.00	0.00	0.00	0.00
Mg	1.70	1.68	1.67	1.63
Ca	0.01	0.01	0.01	0.00
Na	0.02	0.02	0.02	0.02
K	0.00	0.00	0.00	0.00
Ni	0.00	0.00	0.00	0.00
Total	3.01	3.01	2.98	3.00
%Fo	85.05	83.92	83.63	81.53

A5.2 Feldspar analyses

	VH1 rim B	VH1 core B	VH1 core B	VH1 rim B	VH1 lath B	VH1 lath B	VH1 B	VH9 M	VH9 M	VH9 M	VH9 M	VH9 M	VH9 M	VH10 lath B	VH10 lath B	VH10 lath B	VH20 X	VH20 X	VH20 X
SiO2	47.35	47.57	47.88	49.19	50.78	51.27	48.34	54.76	55.19	57.52	55.93	56.53	57.43	49.44	50.23	48.93	53.03	53.63	53.34
TiO2	0.00	0.00	0.00	0.18	0.00	0.20	0.20	0.00	0.00	0.29	0.00	0.00	0.18	0.34	0.17	0.18	0.00	0.00	0.00
Cr2O3	0.00	0.00	0.00	0.00	0.00	0.00	0.00	0.00	0.00	0.00	0.00	0.19	0.00	0.00	0.00	0.00	0.00	0.00	0.00
Al2O3	32.72	33.09	33.32	31.80	31.54	30.56	31.59	26.53	27.80	25.33	27.29	27.29	26.17	30.71	30.71	31.86	29.65	29.30	29.65
FeO	0.53	0.60	0.60	0.64	0.76	1.11	1.32	1.33	0.72	1.13	0.59	0.97	0.89	1.30	1.15	0.79	0.00	0.40	0.00
MnO	0.00	0.00	0.00	0.00	0.00	0.00	0.00	0.00	0.00	0.00	0.11	0.00	0.00	0.00	0.00	0.00	0.00	0.00	0.00
MgO	0.34	0.21	0.22	0.37	0.36	0.38	0.26	0.38	0.12	0.12		0.13		0.40	0.56	0.46	0.00	0.00	0.00
CaO	16.54	16.84	16.84	15.46	14.64	14.24	15.59	9.84	10.73	8.32	10.10	9.97	8.97	14.97	14.86	15.92	12.48	11.97	12.48
Na2O	2.05	1.92	2.07	2.73	3.10	3.55	2.46	5.36	5.41	6.29	5.58	5.78	6.11	2.76	3.04	2.53	4.73	4.55	4.73
K2O		0.10		0.14	0.05	0.13	0.07	0.20	0.19	0.46	0.25	0.27	0.31	0.20	0.15	0.05	0.17	0.19	0.17
NiO	0.00	0.00	0.00	0.00	0.00	0.00	0.00	0.00	0.00	0.00	0.00	0.00	0.00	0.00	0.00	0.00	0.00	0.00	0.00
Total	99.80	100.33	101.37	100.50	101.33	101.42	99.82	98.52	100.16	99.45	100.21	101.21	100.16	100.12	100.87	100.90	100.06	100.05	100.59
per 8 oxygens																			
Si	2.18	2.18	2.18	2.25	2.29	2.32	2.23	2.52	2.49	2.60	2.52	2.52	2.58	2.27	2.29	2.23	2.40	2.43	2.41
Ti	0.00	0.00	0.00	0.01	0.00	0.01	0.01	0.00	0.00	0.01	0.00	0.00	0.01	0.01	0.01	0.01	0.00	0.00	0.00
Cr	0.00	0.00	0.00	0.00	0.00	0.00	0.00	0.00	0.00	0.00	0.00	0.01	0.00	0.00	0.00	0.00	0.00	0.00	0.00
Al	1.78	1.79	1.79	1.71	1.68	1.63	1.72	1.44	1.48	1.35	1.45	1.44	1.39	1.66	1.65	1.71	1.58	1.56	1.58
Fe	0.02	0.02	0.02	0.02	0.03	0.04	0.05	0.05	0.03	0.04	0.02	0.04	0.03	0.05	0.04	0.03	0.00	0.02	0.00
Mn	0.00	0.00	0.00	0.00	0.00	0.00	0.00	0.00	0.00	0.00	0.00	0.00	0.00	0.00	0.00	0.00	0.00	0.00	0.00
Mg	0.02	0.01	0.01	0.03	0.02	0.03	0.02	0.03	0.01	0.01	0.00	0.01	0.00	0.03	0.04	0.03	0.00	0.00	0.00
Ca	0.82	0.83	0.82	0.76	0.71	0.69	0.77	0.48	0.52	0.40	0.49	0.48	0.43	0.74	0.72	0.78	0.61	0.58	0.60
Na	0.18	0.17	0.18	0.24	0.27	0.31	0.22	0.48	0.47	0.55	0.49	0.50	0.53	0.25	0.27	0.22	0.42	0.40	0.41
K	0.00	0.01	0.00	0.01	0.00	0.01	0.00	0.01	0.01	0.03	0.01	0.02	0.02	0.01	0.01	0.00	0.01	0.01	0.01
Ni	0.00	0.00	0.00	0.00	0.00	0.00	0.00	0.00	0.00	0.00	0.00	0.00	0.00	0.00	0.00	0.00	0.00	0.00	0.00
Total	5.01	5.01	5.00	5.02	5.00	5.02	5.02	5.00	5.01	5.00	4.99	5.01	4.99	5.02	5.02	5.01	5.02	5.00	5.01
%Or	0.00	0.58	0.00	0.82	0.29	0.73	0.41	1.21	1.11	2.73	1.45	1.53	1.80	0.00	0.89	0.29	0.94	1.08	0.94
%Ab	18.33	17.00	18.16	24.02	27.63	30.83	22.15	49.06	47.16	56.17	49.29	50.41	54.24	0.03	26.81	22.29	40.31	40.31	40.31
%An	81.67	82.42	81.84	75.17	72.08	68.43	77.43	49.73	51.72	41.10	49.27	48.06	43.96	99.97	72.30	77.42	58.75	58.60	58.75

Feldspars

	VH20	VH20 core	VH20 rim	VH20 core	VH20 rim	VH24 core	VH24 rim	VH24	VH24 coroded	VH24	VH24 lath	VH24 skeletal	VH35	VH35	VH35	VH35	VH41	VH41	VH41
	X	X	X	X	X	M	M	M	M	M	M	M	R	R	R	R	BH	BH	BH
SiO2	53.63	52.53	47.73	52.46	49.11	47.02	53.69	55.12	57.74	53.57	54.49	55.58	67.65	66.55	67.71	67.84	52.55	52.57	52.24
TiO2	0.00	0.00	0.19	0.00	0.51	0.00	0.17	0.00	0.00	0.00	0.00	0.00	0.00	0.17	0.00	0.18	0.18	0.14	0.00
Cr2O3	0.00	0.11	0.00	0.00	0.00	0.00	0.00	0.00	0.00	0.00	0.00	0.00	0.00	0.00	0.00	0.00	0.00	0.00	0.00
Al2O3	29.34	29.14	31.70	28.45	29.55	33.30	28.39	28.78	26.24	28.26	28.69	27.21	20.94	20.96	20.51	20.36	30.07	29.94	30.49
FeO	0.40	0.43	0.62	0.28	1.09	0.46	0.70	0.38	0.66	0.62	0.56	0.76	0.00	0.00	0.29	0.36	0.68	1.02	0.63
MnO	0.00	0.00	0.00	0.10	0.00	0.00	0.00	0.00	0.00	0.00	0.00	0.00	0.00	0.00	0.00	0.00	0.00	0.00	0.00
MgO	0.00	0.29	0.27	0.13	0.35	0.32	0.00	0.00	0.00	0.26	0.00	0.21	0.00	0.00	0.00	0.00	0.20	0.19	0.22
CaO	11.97	11.85	15.32	11.75	13.61	16.93	11.59	10.70	8.88	11.56	11.55	9.98	1.66	2.04	1.27	0.91	13.00	13.07	13.58
Na2O	4.55	4.55	2.62	4.62	3.41	1.86	4.86	5.32	6.38	4.76	4.95	5.73	9.81	9.84	9.75	9.31	4.15	4.03	4.01
K2O	0.19	0.17	0.00	0.09	0.07	0.00	0.16	0.15	0.34	0.12		0.25	1.54	1.43	1.96	2.69	0.20	0.27	0.09
NiO	0.00	0.00	0.16	0.00	0.00	0.00	0.00	0.00	0.00	0.00	0.00	0.00	0.00	0.00	0.00	0.00	0.00	0.00	0.00
Total	100.46	99.06	98.60	97.87	97.68	99.89	99.56	100.45	100.23	99.14	100.23	99.71	101.60	100.98	101.48	101.65	101.02	101.35	101.39
per 8 oxygens																			
Si	2.43	2.41	2.22	2.43	2.30	2.17	2.45	2.48	2.59	2.45	2.46	2.52	2.93	2.91	2.94	2.95	2.37	2.37	2.35
Ti	0.00	0.00	0.01	0.00	0.02	0.00	0.01	0.00	0.00	0.00	0.00	0.00	0.00	0.01	0.00	0.01	0.01	0.00	0.00
Cr	0.00	0.00	0.00	0.00	0.00	0.00	0.00	0.00	0.00	0.00	0.00	0.00	0.00	0.00	0.00	0.00	0.00	0.00	0.00
Al	1.56	1.57	1.74	1.55	1.63	1.81	1.52	1.52	1.39	1.52	1.53	1.45	1.07	1.08	1.05	1.04	1.60	1.59	1.62
Fe	0.02	0.02	0.02	0.01	0.04	0.02	0.03	0.01	0.02	0.02	0.02	0.03	0.00	0.00	0.01	0.01	0.03	0.04	0.02
Mn	0.00	0.00	0.00	0.00	0.00	0.00	0.00	0.00	0.00	0.00	0.00	0.00	0.00	0.00	0.00	0.00	0.00	0.00	0.00
Mg	0.00	0.02	0.02	0.01	0.02	0.02	0.00	0.00	0.00	0.02	0.00	0.01	0.00	0.00	0.00	0.00	0.01	0.01	0.01
Ca	0.58	0.58	0.76	0.58	0.68	0.84	0.57	0.51	0.43	0.57	0.56	0.48	0.08	0.10	0.06	0.04	0.63	0.63	0.65
Na	0.40	0.40	0.24	0.41	0.31	0.17	0.43	0.46	0.55	0.42	0.43	0.50	0.82	0.83	0.82	0.78	0.36	0.35	0.35
K	0.01	0.01	0.00	0.01	0.00	0.00	0.01	0.01	0.02	0.01	0.00	0.01	0.09	0.08	0.11	0.15	0.01	0.02	0.00
Ni	0.00	0.00	0.01	0.00	0.00	0.00	0.00	0.00	0.00	0.00	0.00	0.00	0.00	0.00	0.00	0.00	0.00	0.00	0.00
Total	5.00	5.01	5.02	5.01	5.02	5.01	5.01	5.00	5.00	5.01	5.00	5.02	4.99	5.00	5.00	4.99	5.01	5.01	5.01
%Or	1.08	0.97	0.00	0.52	0.39	0.00	0.94	0.89	1.93	0.73	0.00	1.42	8.65	7.89	10.96	15.26	1.15	1.54	0.49
%Ab	40.31	40.62	23.60	41.35	31.10	16.58	42.75	46.91	55.41	42.38	43.66	50.26	83.52	82.64	83.06	80.38	36.22	35.25	34.65
%An	58.60	58.41	76.40	58.13	68.51	83.42	56.31	52.20	42.66	56.90	56.34	48.33	7.83	9.47	5.97	4.36	62.63	63.21	64.86

Feldspars

	VH41 core BH	VH41 rim BH	VH41 BH	VH41 BH	VH41 BH	VH41 BH	VH41 rim BH	VH41 core BH	VH41 rim BH	VH41 core BH	VH50 BH	VH50 BH	VH50 core BH	VH50 rim BH	VH50 BH	VH50 core BH	VH50 rim BH	VH50 BH	VH51 R
SiO2	55.02	53.19	52.53	52.86	52.33	52.41	53.93	53.80	51.97	53.46	48.04	50.74	54.26	51.50	52.81	48.42	50.75	49.78	66.25
TiO2	0.16	0.00	0.24	0.21	0.00	0.00	0.28	0.29	0.00	0.00	0.00	0.00	0.00	0.00	0.00	0.00	0.00	0.00	0.00
Cr2O3	0.00	0.19	0.00	0.00	0.00	0.00	0.00	0.00	0.00	0.00	0.00	0.00	0.00	0.00	0.00	0.00	0.00	0.00	0.00
Al2O3	28.87	30.19	29.46	30.47	29.83	29.72	29.47	27.62	29.52	9.03	33.32	31.33	29.15	30.83	30.37	32.92	30.77	30.78	19.44
FeO	0.87	0.79	0.99	0.90	0.77	0.92	0.93	1.66	0.72	0.95	0.58	0.76	0.41	0.71	0.41	0.64	0.70	0.80	0.00
MnO	0.00	0.00	0.16	0.00	0.00	0.00	0.00	0.00	0.00	0.09	0.00	0.00	0.00	0.00	0.00	0.00	0.00	0.00	0.00
MgO	0.14	0.29	0.16	0.18	0.19	0.21	0.34	0.84	0.18	0.20	0.28	0.28	0.23	0.37	0.28	0.30	0.34	0.38	0.00
CaO	11.58	13.07	12.54	12.91	12.93	12.86	12.18	12.24	12.96	12.12	16.67	14.62	11.69	14.17	13.39	16.43	14.27	14.47	0.44
Na2O	5.04	4.19	4.29	4.03	4.13	4.11	4.70	4.30	4.06	4.42	1.97	3.19	4.78	3.65	4.24	2.38	3.28	3.13	8.23
K2O	0.30	0.22	0.24	0.20	0.25	0.18	0.28	0.56	0.26	0.25			0.16	0.11	0.18		0.13	0.11	4.21
NiO	0.00	0.00	0.00	0.00	0.00	0.00	0.00	0.00	0.00	0.00	0.00	0.00	0.00	0.00	0.00	0.00	0.00	0.00	0.00
Total	101.99	102.14	100.60	101.75	100.42	100.55	102.11	101.31	99.66	100.66	100.85	100.92	100.67	101.34	101.68	101.09	100.24	99.46	98.57
per 8 oxygens																			
Si	2.45	2.37	2.38	2.37	2.37	2.38	2.40	2.43	2.38	3.02	2.19	2.30	2.44	2.32	2.37	2.20	2.31	2.29	2.98
Ti	0.01	0.00	0.01	0.01	0.00	0.00	0.01	0.01	0.00	0.00	0.00	0.00	0.00	0.00	0.00	0.00	0.00	0.00	0.00
Cr	0.00	0.01	0.00	0.00	0.00	0.00	0.00	0.00	0.00	0.00	0.00	0.00	0.00	0.00	0.00	0.00	0.00	0.00	0.00
Al	1.51	1.59	1.57	1.61	1.59	1.59	1.55	1.47	1.59	0.60	1.79	1.67	1.54	1.64	1.60	1.76	1.65	1.67	1.03
Fe	0.03	0.03	0.04	0.03	0.03	0.03	0.03	0.06	0.03	0.04	0.02	0.03	0.02	0.03	0.02	0.02	0.03	0.03	0.00
Mn	0.00	0.00	0.01	0.00	0.00	0.00	0.00	0.00	0.00	0.00	0.00	0.00	0.00	0.00	0.00	0.00	0.00	0.00	0.00
Mg	0.01	0.02	0.01	0.01	0.01	0.01	0.02	0.06	0.01	0.02	0.02	0.02	0.02	0.02	0.02	0.02	0.02	0.03	0.00
Ca	0.55	0.62	0.61	0.62	0.63	0.62	0.58	0.59	0.63	0.73	0.81	0.71	0.56	0.68	0.64	0.80	0.70	0.71	0.02
Na	0.43	0.36	0.38	0.35	0.36	0.36	0.41	0.38	0.36	0.48	0.17	0.28	0.42	0.32	0.37	0.21	0.29	0.28	0.72
K	0.02	0.01	0.01	0.01	0.01	0.01	0.02	0.03	0.02	0.02	0.00	0.00	0.01	0.01	0.01	0.00	0.01	0.01	0.24
Ni	0.00	0.00	0.00	0.00	0.00	0.00	0.00	0.00	0.00	0.00	0.00	0.00	0.00	0.00	0.00	0.00	0.00	0.00	0.00
Total	5.01	5.01	5.02	5.00	5.02	5.01	5.02	5.03	5.02	4.92	5.00	5.01	5.00	5.02	5.02	5.02	5.01	5.02	4.99
%Or	1.72	1.25	1.39	1.18	1.41	1.07	1.60	3.21	1.50	1.47	0.00	0.00	0.90	0.65	0.98	0.00	0.74	0.66	24.65
%Ab	43.28	36.26	37.71	35.67	36.14	36.24	40.48	37.62	35.65	39.18	17.61	28.34	42.16	31.56	36.08	20.75	29.15	27.97	73.17
%An	55.01	62.50	60.90	63.15	62.45	62.69	57.93	59.17	62.86	59.35	82.39	71.66	56.94	67.79	62.93	79.25	70.11	71.37	2.18

Feldspars

	VH51	VH51 rim	VH51 core	VH51	VH51 small	VH51	VH51	VH65	VH65 core	VH65 rim	VH65 rim	VH65 core	VH65 lath	VH65 lath	VH65 rim	VH65 core	VH75	VH75	VH75
	R	R	R	R	R	R	R	Ben	Ben	Ben	Ben	Ben	Ben	Ben	Ben	Ben	T	T	T
SiO2	67.47	67.78	65.90	67.59	66.84	65.72	65.82	57.92	59.77	56.50	56.55	56.10	57.10	58.50	57.96	57.24	55.90	54.32	52.40
TiO2	0.21	0.00	0.00	0.18	0.18	0.00	0.00	0.00	0.00	0.00	0.00	0.00	0.00	0.00	0.00	0.00	0.20	0.00	0.17
Cr2O3	0.00	0.00	0.00	0.00	0.00	0.00	0.00	0.00	0.00	0.00	0.00	0.00	0.00	0.00	0.00	0.00	0.00	0.00	0.00
Al2O3	19.37	19.24	20.31	20.23	18.58	19.03	18.72	25.77	24.58	26.63	27.50	26.96	26.05	26.04	26.39	27.26	28.27	27.62	28.63
FeO	0.00	0.28	0.00	0.21	0.41	0.00	0.33	0.32	0.23	0.28	0.42	0.44	0.44	0.45	0.26	0.54	0.72	0.85	0.65
MnO	0.00	0.00	0.00	0.00	0.00	0.00	0.00	0.00	0.00	0.00	0.00	0.00	0.00	0.00	0.00	0.00	0.00	0.00	0.00
MgO	0.00	0.00	0.00	0.00	0.00	0.00	0.00	0.00	0.00	0.00	0.00	0.00	0.00	0.00	0.00	0.19	0.00	0.00	0.00
CaO	0.30	0.20	1.58	0.90	0.14	0.32	0.00	7.90	6.45	9.16	9.48	9.38	8.57	8.01	8.78	9.63	10.63	10.77	11.84
Na2O	8.37	8.00	9.34	8.90	8.14	8.07	7.53	6.83	7.68	5.88	6.02	5.92	6.52	6.86	6.55	6.17	5.49	5.41	4.65
K2O	4.39	4.89	1.82	3.03	4.40	4.11	4.97	0.34	0.40	0.27	0.22	0.25	0.33	0.38	0.25	0.27	0.26	0.19	0.18
NiO	0.00	0.00	0.00	0.00	0.00	0.00	0.00	0.00	0.00	0.00	0.00	0.00	0.00	0.00	0.00	0.00	0.00	0.00	0.00
Total	100.09	100.38	98.94	101.05	98.68	97.26	97.37	99.08	99.10	98.73	100.19	99.05	99.02	100.23	100.18	101.13	101.47	99.15	98.52
per 8 oxygens																			
Si	2.99	3.00	2.94	2.96	3.00	2.99	3.00	2.62	2.69	2.57	2.54	2.55	2.59	2.62	2.59	2.54	2.49	2.48	2.42
Ti	0.01	0.00	0.00	0.01	0.01	0.00	0.00	0.00	0.00	0.00	0.00	0.00	0.00	0.00	0.00	0.00	0.01	0.00	0.01
Cr	0.00	0.00	0.00	0.00	0.00	0.00	0.00	0.00	0.00	0.00	0.00	0.00	0.00	0.00	0.00	0.00	0.00	0.00	0.00
Al	1.01	1.00	1.07	1.04	0.98	1.02	1.01	1.37	1.30	1.43	1.45	1.44	1.39	1.37	1.39	1.43	1.48	1.49	1.56
Fe	0.00	0.01	0.00	0.01	0.02	0.00	0.01	0.01	0.01	0.01	0.02	0.02	0.02	0.02	0.01	0.02	0.03	0.03	0.03
Mn	0.00	0.00	0.00	0.00	0.00	0.00	0.00	0.00	0.00	0.00	0.00	0.00	0.00	0.00	0.00	0.00	0.00	0.00	0.00
Mg	0.00	0.00	0.00	0.00	0.00	0.00	0.00	0.00	0.00	0.00	0.00	0.00	0.00	0.00	0.00	0.00	0.00	0.00	0.00
Ca	0.01	0.01	0.08	0.04	0.01	0.02	0.00	0.38	0.31	0.45	0.46	0.46	0.42	0.38	0.42	0.46	0.51	0.53	0.58
Na	0.72	0.69	0.81	0.75	0.71	0.71	0.67	0.60	0.67	0.52	0.52	0.52	0.57	0.59	0.57	0.53	0.47	0.48	0.42
K	0.25	0.28	0.10	0.17	0.25	0.24	0.29	0.02	0.02	0.02	0.01	0.01	0.02	0.02	0.01	0.02	0.01	0.01	0.01
Ni	0.00	0.00	0.00	0.00	0.00	0.00	0.00	0.00	0.00	0.00	0.00	0.00	0.00	0.00	0.00	0.00	0.00	0.00	0.00
Total	4.98	4.98	4.99	4.98	4.98	4.98	4.97	5.00	5.01	4.99	5.00	5.00	5.01	5.01	5.00	5.01	5.01	5.02	5.01
%Or	25.27	28.42	10.48	17.51	26.04	24.71	30.28	1.94	2.28	1.61	1.28	1.44	1.92	2.17	1.41	1.54	1.49	1.07	1.04
%Ab	73.30	70.60	81.86	78.14	73.27	73.68	69.72	59.84	66.73	52.87	52.78	52.55	56.81	59.45	56.61	52.87	47.59	47.09	41.11
%An	1.43	0.98	7.67	4.35	0.69	1.61	0.00	38.22	30.99	45.52	45.94	46.01	41.28	38.37	41.98	45.59	50.92	51.84	57.85

Feldspars

	VH75	VH80 core	VH80 rim	VH80 core	VH80 rim	VH80	VH80 core	VH80 rim	VH80 core	VH80 rim	VH80	VH81	VH81	VH81	VH81 melt	VH80 lath	VH89	VH89	VH89
	T	B	B	B	B	B	B	B	B	B	B	X	X	X	X	B	BH	BH	BH
SiO2	66.35	48.24	47.62	47.41	46.78	47.02	56.00	51.37	50.50	49.67	58.04	52.91	52.91	54.18	50.68	49.55	50.96	50.51	51.00
TiO2	0.00	0.00	0.00	0.00	0.00	0.00	0.00	0.00	0.00	0.16	0.00	0.00	0.00	0.00	0.46	0.25	0.33	0.00	0.13
Cr2O3	0.00	0.00	0.00	0.00	0.00	0.00	0.00	0.00	0.27	0.00	0.00	0.00	0.00	0.00	0.00	0.00	0.00	0.00	0.00
Al2O3	19.63	33.39	32.68	32.59	32.65	32.46	27.35	29.01	31.19	31.09	26.31	29.60	29.62	29.46	24.47	30.71	27.65	29.80	29.52
FeO	0.45	0.71	0.73	0.49	0.60	0.45	0.00	1.12	0.24	0.85	0.31	0.00	0.28	0.34	3.25	1.01	2.72	0.68	0.85
MnO	0.00	0.00	0.00	0.00	0.00	0.00	0.00	0.00	0.00	0.00	0.00	0.00	0.00	0.00	0.00	0.00	0.00	0.00	0.00
MgO	0.00	0.26	0.27	0.30	0.00	0.25	0.00	0.00	0.00	0.37	0.00	0.26	0.00	0.00	3.25	0.26	0.31	0.33	0.23
CaO	0.78	16.89	16.25	16.36	16.21	16.57	9.78	12.86	14.38	14.48	8.46	11.61	12.13	11.92	14.73	14.54	11.85	13.73	13.26
Na2O	8.18	2.22	2.32	2.17	1.90	1.92	5.70	3.85	3.29	3.04	6.46	4.72	4.72	4.81	3.03	2.96	3.92	3.54	3.78
K2O	3.90	0.00	0.00	0.00	0.00	0.00	0.24	0.21	0.12	0.10	0.29	0.14	0.00	0.16	0.18	0.16	0.28	0.07	0.15
NiO	0.00	0.00	0.00	0.00	0.00	0.00	0.00	0.00	0.00	0.00	0.00	0.00	0.00	0.00	0.00	0.00	0.00	0.00	0.00
Total	99.28	101.71	99.88	99.32	98.14	98.66	99.07	98.42	99.97	99.75	99.86	99.24	99.66	100.87	100.05	99.44	98.12	98.76	98.91
per 8 oxygens																			
Si	2.96	2.18	2.19	2.19	2.19	2.19	2.54	2.38	2.30	2.28	2.60	2.41	2.41	2.43	2.36	2.28	2.39	2.33	2.35
Ti	0.00	0.00	0.00	0.00	0.00	0.00	0.00	0.00	0.00	0.01	0.00	0.00	0.00	0.00	0.02	0.01	0.01	0.00	0.00
Cr	0.00	0.00	0.00	0.00	0.00	0.00	0.00	0.00	0.01	0.00	0.00	0.00	0.00	0.00	0.00	0.00	0.00	0.00	0.00
Al	1.03	1.78	1.77	1.78	1.80	1.78	1.46	1.58	1.68	1.68	1.39	1.59	1.59	1.56	1.34	1.67	1.53	1.62	1.61
Fe	0.02	0.03	0.03	0.02	0.02	0.02	0.00	0.04	0.01	0.03	0.01	0.00	0.01	0.01	0.13	0.04	0.11	0.03	0.03
Mn	0.00	0.00	0.00	0.00	0.00	0.00	0.00	0.00	0.00	0.00	0.00	0.00	0.00	0.00	0.00	0.00	0.00	0.00	0.00
Mg	0.00	0.02	0.02	0.02	0.00	0.02	0.00	0.00	0.00	0.03	0.00	0.02	0.00	0.00	0.23	0.02	0.02	0.02	0.02
Ca	0.04	0.82	0.80	0.81	0.81	0.83	0.48	0.64	0.70	0.71	0.41	0.57	0.59	0.57	0.74	0.72	0.59	0.68	0.66
Na	0.71	0.19	0.21	0.19	0.17	0.17	0.50	0.35	0.29	0.27	0.56	0.42	0.42	0.42	0.27	0.26	0.36	0.32	0.34
K	0.22	0.00	0.00	0.00	0.00	0.00	0.01	0.01	0.01	0.01	0.02	0.01	0.00	0.01	0.01	0.01	0.02	0.00	0.01
Ni	0.00	0.00	0.00	0.00	0.00	0.00	0.00	0.00	0.00	0.00	0.00	0.00	0.00	0.00	0.00	0.00	0.00	0.00	0.00
Total	4.98	5.02	5.02	5.02	5.00	5.01	4.99	5.01	5.00	5.01	4.99	5.01	5.01	5.00	5.09	5.01	5.02	5.01	5.01
%Or	22.94	0.00	0.00	0.00	0.00	0.00	1.38	1.27	0.67	0.60	1.66	0.81	0.00	0.91	1.07	0.94	1.70	0.44	0.86
%Ab	73.22	19.22	20.54	19.38	17.52	17.36	50.61	34.67	29.07	27.36	57.08	42.02	41.31	41.82	26.86	26.65	36.83	31.68	33.71
%An	3.84	80.78	79.46	80.62	82.48	82.64	48.01	64.06	70.26	72.04	41.26	57.17	58.69	57.27	72.07	72.41	61.48	67.89	65.43

Feldspars

	VH94	VH94	VH94	VH94 core	VH94	VH102	VH102 core	VH102 rim	VH102 lath	VH105 core	VH105 rim	VH105	VH105	VH105 lath	VH105 lath	VH105 coroded	VH105	VH105	VH106
	H	H	H	H	H	B	B	B	B	H	H	H	H	H	H	H	H	H	B
SiO2	53.68	52.89	53.25	52.96	52.83	53.72	48.36	50.56	51.66	48.51	47.94	47.24	52.62	52.74	51.12	49.82	48.23	53.30	51.09
TiO2	0.00	0.17	0.00	0.00	0.18	0.00	0.00	0.00	0.00	0.00	0.00	0.00	0.00	0.00	0.16	0.00	0.00	0.00	0.00
Cr2O3	0.00	0.00	0.00	0.00	0.00	0.00	0.00	0.00	0.00	0.00	0.00	0.21	0.00	0.00	0.00	0.00	0.00	0.00	0.00
Al2O3	28.58	28.37	28.47	28.28	28.31	29.47	32.75	30.54	29.06	33.13	33.11	32.41	29.80	28.47	29.75	30.85	32.02	30.42	30.78
FeO	0.72	0.88	0.75	0.78	0.87	0.59	0.47	0.95	0.86	0.60	0.49	0.41	0.64	1.02	0.88	0.63	0.54	0.51	0.86
MnO	0.00	0.00	0.00	0.09	0.00	0.00	0.00	0.00	0.00	0.00	0.00	0.00	0.00	0.00	0.00	0.00	0.00	0.00	0.00
MgO	0.24	0.25	0.12	0.19	0.21	0.15	0.36	0.32		0.33	0.43	0.26	0.15	0.28	0.25	0.24	0.40	0.29	0.33
CaO	11.34	11.75	11.67	11.30	11.64	12.13	16.09	14.34	13.31	16.46	16.41	16.23	12.59	12.25	13.28	14.39	15.74	12.93	13.76
Na2O	4.74	4.87	4.61	4.69	4.58	4.50	2.37	3.41	3.85	2.10	2.28	2.20	4.23	4.48	3.81	3.22	2.52	4.39	3.52
K2O	0.17	0.16	0.14	0.12	0.16	0.16	0.08	0.08	0.13	0.10	0.00	0.00	0.15	0.18	0.13	0.00	0.12	0.13	0.20
NiO	0.00	0.00	0.00	0.00	0.00	0.00	0.00	0.00	0.00	0.00	0.00	0.00	0.00	0.00	0.00	0.00	0.00	0.00	0.00
Total	99.67	99.33	99.11	98.40	98.79	100.71	100.55	100.20	98.86	101.23	100.66	98.95	100.17	99.41	99.39	99.14	99.57	101.97	100.54
per 8 oxygens																			
Si	2.44	2.42	2.44	2.44	2.43	2.42	2.21	2.31	2.38	2.20	2.19	2.19	2.39	2.42	2.35	2.30	2.22	2.38	2.32
Ti	0.00	0.01	0.00	0.00	0.01	0.00	0.00	0.00	0.00	0.00	0.00	0.00	0.00	0.00	0.01	0.00	0.00	0.00	0.00
Cr	0.00	0.00	0.00	0.00	0.00	0.00	0.00	0.00	0.00	0.00	0.00	0.01	0.00	0.00	0.00	0.00	0.00	0.00	0.00
Al	1.53	1.53	1.54	1.54	1.53	1.56	1.76	1.64	1.58	1.77	1.78	1.77	1.59	1.54	1.61	1.68	1.74	1.60	1.65
Fe	0.03	0.03	0.03	0.03	0.03	0.02	0.02	0.04	0.03	0.02	0.02	0.02	0.02	0.04	0.03	0.02	0.02	0.02	0.03
Mn	0.00	0.00	0.00	0.00	0.00	0.00	0.00	0.00	0.00	0.00	0.00	0.00	0.00	0.00	0.00	0.00	0.00	0.00	0.00
Mg	0.02	0.02	0.01	0.01	0.01	0.01	0.02	0.02	0.00	0.02	0.03	0.02	0.01	0.02	0.02	0.02	0.03	0.02	0.02
Ca	0.55	0.58	0.57	0.56	0.57	0.58	0.79	0.70	0.66	0.80	0.80	0.81	0.61	0.60	0.65	0.71	0.78	0.62	0.67
Na	0.42	0.43	0.41	0.42	0.41	0.39	0.21	0.30	0.34	0.18	0.20	0.20	0.37	0.40	0.34	0.29	0.22	0.38	0.31
K	0.01	0.01	0.01	0.01	0.01	0.01	0.00	0.00	0.01	0.01	0.00	0.00	0.01	0.01	0.01	0.00	0.01	0.01	0.01
Ni	0.00	0.00	0.00	0.00	0.00	0.00	0.00	0.00	0.00	0.00	0.00	0.00	0.00	0.00	0.00	0.00	0.00	0.00	0.00
Total	5.00	5.03	5.00	5.01	5.01	5.00	5.01	5.02	5.00	5.01	5.02	5.01	5.01	5.02	5.02	5.01	5.02	5.02	5.02
%Or	0.99	0.90	0.80	0.71	0.96	0.93	0.44	0.44	0.73	0.58	0.00	0.00	0.89	1.06	0.78	0.00	0.72	0.72	1.18
%Ab	42.63	42.45	41.36	42.57	41.17	39.80	20.94	29.98	34.07	18.65	20.09	19.69	37.45	39.40	33.89	28.81	22.27	37.76	31.26
%An	56.39	56.65	57.83	56.72	57.87	59.27	78.62	69.58	65.20	80.77	79.91	80.31	61.67	59.54	65.33	71.19	77.01	61.51	67.57

Feldspars

	VH106	VH106	VH106	VH117	VH117	VH117	VH117	VH137	VH137	VH137	VH137 core	VH137 rim	VH137	VH151	VH151 lath	VH151 rim	VH151 core	VH151 core	VH151 rim
	B	B	B	M	M	M	M	M	M	M	M	M	M	B	B	B	B	B	B
SiO2	52.12	51.07	50.39	57.37	55.45	55.59	61.72	56.03	53.31	55.24	53.73	53.79	54.47	49.98	49.21	49.78	46.99	47.87	49.42
TiO2	0.00	0.00	0.15	0.00	0.00	0.00	0.23	0.00	0.00	0.00	0.00	0.16	0.00	0.15	0.18	0.00	0.00	0.00	0.00
Cr2O3	0.00	0.00	0.00	0.00	0.00	0.00	0.00	0.00	0.00	0.00	0.00	0.00	0.00	0.00	0.00	0.00	0.00	0.00	0.00
Al2O3	30.69	29.63	29.90	27.52	27.18	27.01	22.28	27.23	27.94	27.23	28.06	28.10	28.49	31.19	30.34	31.03	33.15	31.92	30.69
FeO	0.75	0.71	0.74	0.86	0.59	0.62	0.91	0.99	0.99	0.70	0.65	0.63	0.68	0.73	0.77	0.77	0.50	0.56	0.85
MnO	0.00	0.00	0.00	0.00	0.00	0.00	0.00	0.00	0.00	0.00	0.00	0.00	0.00	0.00	0.00	0.00	0.00	0.00	0.00
MgO	0.37	0.23	0.26	0.00	0.00	0.00	0.00	0.20	0.45	0.00	0.11	0.00	0.29	0.37	0.24	0.37	0.26	0.25	0.30
CaO	13.86	13.40	13.95	9.80	10.18	10.00	5.02	10.01	11.49	10.45	11.24	11.37	10.97	14.90	14.39	14.73	16.79	15.98	14.50
Na2O	3.82	3.85	3.43	5.93	5.58	5.45	7.46	5.60	4.81	5.40	4.95	4.81	4.97	3.11	3.06	3.02	1.85	2.30	3.12
K2O	0.16	0.20	0.16	0.31	0.23	0.22	1.14	0.23	0.16	0.31	0.18	0.15	0.21	0.14	0.12	0.10	0.00	0.00	0.07
NiO	0.00	0.00	0.00	0.00	0.00	0.00	0.00	0.00	0.00	0.00	0.00	0.00	0.00	0.00	0.00	0.00	0.00	0.00	0.00
Total	102.10	99.08	98.97	101.79	99.21	98.88	98.76	100.59	99.15	99.56	99.20	99.00	100.18	100.59	98.30	99.87	99.74	99.04	99.03
per 8 oxygens																			
Si	2.33	2.35	2.33	2.54	2.52	2.53	2.79	2.52	2.44	2.51	2.46	2.46	2.46	2.28	2.29	2.28	2.17	2.22	2.29
Ti	0.00	0.00	0.01	0.00	0.00	0.00	0.01	0.00	0.00	0.00	0.00	0.01	0.00	0.01	0.01	0.00	0.00	0.00	0.00
Cr	0.00	0.00	0.00	0.00	0.00	0.00	0.00	0.00	0.00	0.00	0.00	0.00	0.00	0.00	0.00	0.00	0.00	0.00	0.00
Al	1.62	1.61	1.63	1.44	1.46	1.45	1.18	1.44	1.51	1.46	1.51	1.51	1.52	1.68	1.67	1.68	1.80	1.74	1.67
Fe	0.03	0.03	0.03	0.03	0.02	0.02	0.03	0.04	0.04	0.03	0.02	0.02	0.03	0.03	0.03	0.03	0.02	0.02	0.03
Mn	0.00	0.00	0.00	0.00	0.00	0.00	0.00	0.00	0.00	0.00	0.00	0.00	0.00	0.00	0.00	0.00	0.00	0.00	0.00
Mg	0.02	0.02	0.02	0.00	0.00	0.00	0.00	0.01	0.03	0.00	0.01	0.00	0.02	0.03	0.02	0.03	0.02	0.02	0.02
Ca	0.66	0.66	0.69	0.46	0.50	0.49	0.24	0.48	0.56	0.51	0.55	0.56	0.53	0.73	0.72	0.72	0.83	0.79	0.72
Na	0.33	0.34	0.31	0.51	0.49	0.48	0.65	0.49	0.43	0.48	0.44	0.43	0.44	0.27	0.28	0.27	0.17	0.21	0.28
K	0.01	0.01	0.01	0.02	0.01	0.01	0.07	0.01	0.01	0.02	0.01	0.01	0.01	0.01	0.01	0.01	0.00	0.00	0.00
Ni	0.00	0.00	0.00	0.00	0.00	0.00	0.00	0.00	0.00	0.00	0.00	0.00	0.00	0.00	0.00	0.00	0.00	0.00	0.00
Total	5.01	5.02	5.01	5.00	5.00	4.99	4.97	5.00	5.02	4.99	5.00	5.00	5.00	5.02	5.01	5.01	5.00	5.00	5.01
%Or	0.88	1.17	0.94	1.78	1.32	1.30	6.85	1.31	0.94	1.76	1.06	0.86	1.25	0.82	0.68	0.59	0.00	0.00	0.41
%Ab	32.98	33.78	30.47	51.36	49.14	49.00	67.90	49.66	42.69	47.47	43.89	42.98	44.49	27.21	27.60	26.93	16.63	20.67	27.90
%An	66.14	65.05	68.59	46.86	49.54	49.69	25.25	49.02	56.37	50.77	55.06	56.15	54.26	71.98	71.72	72.49	83.37	79.33	71.69

Feldspars

	VH151 core	VH151 rim	VH151	VH189	VH189	VH189	VH189	VH189 core	VH189 rim	VH191 core	VH191 rim	VH191 core	VH191 rim	VH229	VH229	VH229	VH262 lath	VH262	VH262
	B	B	B	Ben	Ben	Ben	Ben	Ben	Ben	X	X	X	X	M	M	M	B	B	B
SiO2	46.92	49.54	49.41	62.64	59.28	58.50	59.73	61.57	58.92	63.97	63.20	65.47	65.80	54.57	54.38	54.38	52.61	48.39	49.69
TiO2	0.00	0.00	0.00	0.00	0.31	0.24	0.23	0.00	0.00	0.00	0.00	0.26	0.18	0.00	0.26	0.17	0.00	0.00	0.00
Cr2O3	0.00	0.00	0.00	0.00	0.00	0.00	0.00	0.00	0.00	0.00	0.00	0.00	0.00	0.00	0.00	0.00	0.00	0.00	0.00
Al2O3	32.53	31.40	30.21	22.74	22.00	24.12	22.24	22.96	24.28	21.60	22.62	19.96	19.78	28.02	27.57	27.63	28.64	31.24	30.40
FeO	0.61	0.75	0.77	0.43	3.06	1.24	1.88	0.29	0.49	0.00	0.25	0.00	0.00	0.71	0.51	0.62	0.96	0.53	0.64
MnO	0.00	0.00	0.00	0.00	0.00	0.00	0.17	0.00	0.00	0.00	0.00	0.00	0.00	0.00	0.10	0.21	0.00	0.00	0.00
MgO	0.22	0.35	0.21	0.00	0.49	0.17	0.18	0.25	0.16	0.00	0.00	0.00	0.00	0.20	0.00	0.17	0.22	0.33	0.48
CaO	16.28	14.88	14.27	4.79	9.49	7.18	6.62	4.57	7.06	3.11	4.21	1.37	1.50	10.83	10.83	10.76	12.38	15.57	14.65
Na2O	1.95	2.73	3.23	8.48	6.56	6.92	6.96	8.45	6.99	8.71	8.37	9.14	8.35	5.26	5.04	5.12	4.15	2.57	2.98
K2O	0.00	0.14	0.11	0.70	0.92	0.60	0.87	0.62	0.52	1.35	0.70	2.27	2.91	0.22	0.21	0.31	0.29	0.08	0.15
NiO	0.00	0.00	0.00	0.00	0.00	0.00	0.00	0.00	0.00	0.00	0.00	0.00	0.00	0.00	0.00	0.00	0.00	0.00	0.00
Total	98.49	99.79	98.43	99.97	100.11	98.98	98.87	98.80	98.42	98.74	99.35	98.47	98.52	99.92	98.91	99.50	99.33	98.94	99.15
per 8 oxygens																			
Si	2.19	2.27	2.30	2.79	2.66	2.66	2.72	2.77	2.68	2.86	2.81	2.93	2.95	2.47	2.49	2.48	2.41	2.25	2.29
Ti	0.00	0.00	0.00	0.00	0.01	0.01	0.01	0.00	0.00	0.00	0.00	0.01	0.01	0.00	0.01	0.01	0.00	0.00	0.00
Cr	0.00	0.00	0.00	0.00	0.00	0.00	0.00	0.00	0.00	0.00	0.00	0.00	0.00	0.00	0.00	0.00	0.00	0.00	0.00
Al	1.79	1.70	1.66	1.19	1.16	1.29	1.19	1.22	1.30	1.14	1.19	1.05	1.05	1.50	1.49	1.48	1.55	1.71	1.65
Fe	0.02	0.03	0.03	0.02	0.11	0.05	0.07	0.01	0.02	0.00	0.01	0.00	0.00	0.03	0.02	0.02	0.04	0.02	0.02
Mn	0.00	0.00	0.00	0.00	0.00	0.00	0.01	0.00	0.00	0.00	0.00	0.00	0.00	0.00	0.00	0.01	0.00	0.00	0.00
Mg	0.01	0.02	0.01	0.00	0.03	0.01	0.01	0.02	0.01	0.00	0.00	0.00	0.00	0.01	0.00	0.01	0.01	0.02	0.03
Ca	0.81	0.73	0.71	0.23	0.46	0.35	0.32	0.22	0.34	0.15	0.20	0.07	0.07	0.53	0.53	0.53	0.61	0.77	0.72
Na	0.18	0.24	0.29	0.73	0.57	0.61	0.61	0.74	0.62	0.75	0.72	0.79	0.73	0.46	0.45	0.45	0.37	0.23	0.27
K	0.00	0.01	0.01	0.04	0.05	0.03	0.05	0.04	0.03	0.08	0.04	0.13	0.17	0.01	0.01	0.02	0.02	0.00	0.01
Ni	0.00	0.00	0.00	0.00	0.00	0.00	0.00	0.00	0.00	0.00	0.00	0.00	0.00	0.00	0.00	0.00	0.00	0.00	0.00
Total	5.01	5.00	5.01	5.00	5.06	5.01	5.00	5.00	5.00	4.97	4.97	4.99	4.97	5.01	4.99	5.00	5.00	5.01	5.01
%Or	0.00	0.86	0.63	4.00	4.85	3.49	5.11	3.61	3.03	7.82	4.15	13.13	17.24	1.28	1.24	1.79	1.70	0.46	0.91
%Ab	17.80	24.73	28.85	73.17	52.89	61.33	62.20	74.23	62.23	76.87	75.09	80.13	75.17	46.18	45.14	45.44	37.09	22.87	26.65
%An	82.20	74.41	70.52	22.83	42.26	35.17	32.69	22.16	34.74	15.31	20.76	6.73	7.59	52.54	53.63	52.77	61.21	76.67	72.44

Feldspars

	MB8	MB8 core	MB8 rim	MB8	MB8
	R	R	R	R	R
SiO2	62.95	63.97	64.08	62.48	61.41
TiO2	0.00	0.00	0.00	0.00	0.00
Cr2O3	0.00	0.00	0.00	0.00	0.00
Al2O3	23.22	21.88	22.71	22.93	23.31
FeO	0.35	0.14	0.25	0.19	0.26
MnO	0.00	0.10	0.00	0.00	0.00
MgO	0.00	0.00	0.00	0.00	0.00
CaO	4.37	3.45	3.93	4.40	5.11
Na2O	8.57	8.74	8.76	8.66	8.17
K2O	0.70	0.88	0.79	0.61	0.49
NiO	0.00	0.00	0.00	0.00	0.00
Total	100.17	99.15	100.51	99.39	98.84
per 8 oxygens					
Si	2.79	2.85	2.82	2.79	2.76
Ti	0.00	0.00	0.00	0.00	0.00
Cr	0.00	0.00	0.00	0.00	0.00
Al	1.21	1.15	1.18	1.21	1.23
Fe	0.01	0.01	0.01	0.01	0.01
Mn	0.00	0.00	0.00	0.00	0.00
Mg	0.00	0.00	0.00	0.00	0.00
Ca	0.21	0.16	0.19	0.21	0.25
Na	0.74	0.76	0.75	0.75	0.71
K	0.04	0.05	0.04	0.03	0.03
Ni	0.00	0.00	0.00	0.00	0.00
Total	4.99	4.98	4.99	4.99	4.99
%Or	4.05	5.18	4.51	3.51	2.84
%Ab	74.86	77.86	76.50	75.35	72.19
%An	21.09	16.96	18.98	21.14	24.97

A5.3 Clinopyroxene analyses

	VH9	VH9	VH9	VH9	VH9	VH9	VH9	VH20	VH20	VH20	VH20	VH24	VH35	VH35	VH50	VH50	VH51	VH51	VH51
	M	M	M	M	M	M	M	X	X	X	X	M	R	R	BH	BH	R	R	R
SiO2	51.10	48.96	49.99	49.77	49.63	50.16	51.73	49.24	48.95	51.13	49.22	48.80	48.90	47.72	48.69	48.01	48.33	47.84	48.20
TiO2	1.16	1.77	1.05	0.68	1.11	0.94	0.72	1.14	1.15	1.28	1.13	1.97	0.28	0.45	2.04	1.71	0.00	0.26	0.18
Cr2O3	0.09	0.00	0.00	0.10	0.00	0.00	0.00	0.00	0.00	0.00	0.00	0.00	0.00	0.00	0.00	0.19	0.00	0.00	0.00
Al2O3	2.87	3.72	2.71	2.05	2.78	2.35	2.01	3.70	3.97	4.76	4.21	4.17	0.54	1.02	5.39	4.44	0.41	0.37	0.51
Fe2O3	2.49	3.74	3.11	1.76	3.37	1.95	1.63	3.01	3.59	0.00	0.00	3.25	0.00	0.74	4.63	5.73	3.25	2.68	3.36
FeO	9.73	12.45	9.86	14.50	8.50	13.73	11.27	6.84	6.07	10.91	8.43	8.21	26.88	27.76	6.19	3.94	26.69	28.46	27.60
MnO	0.21	0.60	0.40	0.55	0.38	0.47	0.38	0.13	0.43	0.34	0.28	0.00	0.98	1.01	0.00	0.00	0.82	0.84	0.82
MgO	13.13	11.49	13.18	9.75	12.94	10.43	13.89	14.90	14.30	15.67	14.25	13.00	1.75	0.64	13.49	13.65	1.00	0.00	0.22
CaO	20.42	18.03	18.66	18.88	19.39	19.51	18.38	18.13	19.65	16.26	20.12	19.89	19.09	18.43	21.04	21.03	19.12	18.84	19.49
Na2O	0.57	0.76	0.66	0.75	0.77	0.65	0.55	0.68	0.52	0.77	0.74	0.70	0.61	0.85	0.62	0.81	0.86	0.86	0.87
K2O	0.00	0.00	0.00	0.00	0.00	0.00	0.00	0.00	0.00	0.00	0.00	0.00	0.00	0.00	0.00	0.00	0.00	0.00	0.00
NiO	0.00	0.00	0.00	0.00	0.00	0.00	0.00	0.00	0.00	0.00	0.00	0.00	0.00	0.00	0.00	0.00	0.00	0.00	0.00
Total	101.76	101.52	99.62	98.78	98.86	100.19	100.56	97.50	98.32	11.20	97.93	99.99	99.02	98.61	102.09	99.51	100.48	100.14	101.24
per 6 oxygens																			
Si	1.89	1.84	1.89	1.93	1.89	1.92	1.93	1.87	1.85	1.88	1.86	1.83	2.01	1.98	1.79	1.80	1.97	1.98	1.97
Ti	0.03	0.05	0.03	0.02	0.03	0.03	0.02	0.03	0.03	0.04	0.03	0.06	0.01	0.01	0.06	0.05	0.00	0.01	0.01
Cr	0.00	0.00	0.00	0.00	0.00	0.00	0.00	0.00	0.00	0.00	0.00	0.00	0.00	0.00	0.00	0.01	0.00	0.00	0.00
Al	0.13	0.16	0.12	0.09	0.12	0.11	0.09	0.17	0.18	0.21	0.19	0.18	0.03	0,05	0.23	0.20	0.02	0.02	0.02
Fe3+	0.07	0.11	0.09	0.05	0.10	0.06	0.05	0.09	0.10	0.00	0.00	0.09	0.00	0.02	0.13	0.16	0.10	0.08	0.10
Fe2+	0.30	0.39	0.31	0.47	0.27	0.44	0.35	0.22	0.19	0.33	0.27	0.26	0.92	0.96	0.19	0.12	0.91	0.98	0.94
Mn	0.01	0.02	0.01	0.02	0.01	0.02	0.01	0.00	0.01	0.01	0.01	0.00	0.03	0.04	0.00	0.00	0.03	0.03	0.03
Mg	0.72	0.64	0.74	0.56	0.73	0.59	0.77	0.84	0.80	0.86	0.80	0.73	0.11	0.04	0.74	0.76	0.06	0.00	0.01
Ca	0.81	0.73	0.76	0.79	0.79	0.80	0.74	0.74	0.79	0.64	0.82	0.80	0.84	0.82	0.83	0.84	0.84	0.83	0.85
Na	0.04	0.06	0.05	0.06	0.06	0.05	0.04	0.05	0.04	0.05	0.05	0.05	0.05	0.07	0.04	0.06	0.07	0.07	0.07
K	0.00	0.00	0.00	0.00	0.00	0.00	0.00	0.00	0.00	0.00	0.00	0.00	0.00	0.00	0.00	0.00	0.00	0.00	0.00
Ni	0.00	0.00	0.00	0.00	0.00	0.00	0.00	0.00	0.00	0.00	0.00	0.00	0.00	0.00	0.00	0.00	0.00	0.00	0.00
Total	4.00	4.00	4.00	4.00	4.00	4.00	4.00	4.00	4.00	4.01	4.04	4.00	4.00	4.00	4.00	4.00	4.00	4.00	4.00
En	39.47	36.57	41.04	30.99	40.89	32.45	41.56	46.91	44.92	46.81	42.61	40.75	5.74	2.16	42.04	44.07	3.36	0.00	0.73
Wo	44.12	41.22	41.74	43.15	44.04	43.60	39.53	41.01	44.37	34.91	43.24	44.82	44.91	44.97	47.14	48.79	46.25	45.89	47.16
Fs	16.41	22.22	17.21	25.86	15.07	23.95	18.92	12.08	10.70	18.28	14.15	14.44	49.35	52.87	10.83	7.14	50.39	54.11	52.12

Clinopyroxenes

	VH51	VH65	VH65	VH65	VH65	VH65	VH65	VH75	VH75	VH75	VH80	VH80	VH80	VH80	VH81	VH81	VH81 core	VH81 rim	VH81
	R	Ben	Ben	Ben	Ben	Ben	Ben	T	T	T	B	B	B	B	X	X	X	X	X
SiO2	45.59	49.48	49.25	49.68	49.07	51.99	46.55	52.50	51.13	48.81	49.03	49.34	48.61	49.10	52.76	52.54	51.92	51.70	50.53
TiO2	0.27	0.78	0.89	0.88	0.94	0.53	0.73	0.94	0.98	1.92	1.63	1.61	1.61	1.26	0.42	0.34	0.67	0.75	1.09
Cr2O3	0.00	0.00	0.20	0.00	0.00	0.00	0.14	0.00	0.18	0.00	0.00	0.24	0.18	0.25	0.00	0.00	0.00	0.00	0.43
Al2O3	0.31	2.25	2.98	3.42	2.94	3.01	1.06	1.96	2.14	3.97	4.51	4.79	4.91	4.83	1.83	1.38	2.07	2.12	4.51
Fe2O3	3.08	2.62	3.14	2.21	2.44	0.00	3.42	2.52	4.30	3.74	2.87	4.08	3.10	3.48	3.38	2.23	2.56	2.32	2.40
FeO	26.04	14.45	13.36	12.87	16.93	18.23	22.49	9.48	6.99	8.87	6.77	5.36	6.11	4.42	7.98	9.68	10.10	9.93	5.50
MnO	1.15	0.59	0.36	0.33	0.65	0.45	0.78	0.32	0.27	0.22	0.00	0.00	0.00	0.00	0.35	0.40	0.30	0.32	0.00
MgO	0.00	9.90	11.36	11.26	9.97	7.47	2.65	16.34	15.39	13.57	13.97	14.44	14.02	14.67	14.58	13.57	13.57	13.35	15.26
CaO	18.55	18.83	17.83	18.09	16.47	17.30	20.01	17.22	18.38	18.16	19.77	20.28	19.90	20.55	19.86	20.01	19.51	19.59	20.08
Na2O	0.82	0.66	0.62	0.81	0.66	1.20	0.58	0.57	0.82	0.77	0.67	0.73	0.64	0.64	0.80	0.69	0.67	0.72	0.65
K2O	0.00	0.00	0.00	0.00	0.00	0.45	0.00	0.00	0.00	0.00	0.00	0.00	0.00	0.00	0.00	0.00	0.00	0.00	0.00
NiO	0.00	0.00	0.00	0.00	0.00	0.00	0.00	0.00	0.00	0.00	0.00	0.00	0.00	0.00	0.00	0.00	0.00	0.00	0.00
Total	95.80	99.56	99.96	99.55	100.07	100.63	98.40	101.85	100.56	100.03	99.21	100.86	99.09	99.19	101.65	100.65	101.13	100.60	100.22
per 6 oxygens																			
Si	1.97	1.91	1.88	1.90	1.89	1.99	1.92	1.92	1.89	1.83	1.84	1.82	1.82	1.83	1.93	1.95	1.92	1.93	1.86
Ti	0.01	0.02	0.03	0.03	0.03	0.02	0.02	0.03	0.03	0.05	0.05	0.04	0.05	0.04	0.01	0.01	0.02	0.02	0.03
Cr	0.00	0.00	0.01	0.00	0.00	0.00	0.00	0.00	0.01	0.00	0.00	0.01	0.01	0.01	0.00	0.00	0.00	0.00	0.01
Al	0.02	0.10	0.13	0.15	0.13	0.14	0.05	0.08	0.09	0.18	0.20	0.21	0.22	0.21	0.08	0.06	0.09	0.09	0.19
Fe3+	0.10	0.08	0.09	0.06	0.07	0.00	0.11	0.07	0.12	0.11	0.08	0.11	0.09	0.10	0.09	0.06	0.07	0.07	0.07
Fe2+	0.94	0.47	0.43	0.41	0.55	0.58	0.78	0.29	0.22	0.28	0.21	0.16	0.19	0.14	0.24	0.30	0.31	0.31	0.17
Mn	0.04	0.02	0.01	0.01	0.02	0.01	0.03	0.01	0.01	0.01	0.00	0.00	0.00	0.00	0.01	0.01	0.01	0.01	0.00
Mg	0.00	0.57	0.65	0.64	0.57	0.43	0.16	0.89	0.85	0.76	0.78	0.79	0.78	0.81	0.80	0.75	0.75	0.74	0.84
Ca	0.86	0.78	0.73	0.74	0.68	0.71	0.88	0.67	0.73	0.73	0.79	0.80	0.80	0.82	0.78	0.80	0.77	0.78	0.79
Na	0.07	0.05	0.05	0.06	0.05	0.09	0.05	0.04	0.06	0.06	0.05	0.05	0.05	0.05	0.06	0.05	0.05	0.05	0.05
K	0.00	0.00	0.00	0.00	0.00	0.02	0.00	0.00	0.00	0.00	0.00	0.00	0.00	0.00	0.00	0.00	0.00	0.00	0.00
Ni	0.00	0.00	0.00	0.00	0.00	0.00	0.00	0.00	0.00	0.00	0.00	0.00	0.00	0.00	0.00	0.00	0.00	0.00	0.00
Total	4.00	4.00	4.00	4.00	4.00	3.98	4.00	4.00	4.00	4.00	4.00	4.00	4.00	4.00	4.00	4.00	4.00	4.00	4.00
En	0.00	31.39	35.88	35.76	31.86	24.79	8.94	48.02	47.33	42.94	43.69	45.10	44.16	45.96	43.74	40.66	40.80	40.45	46.56
Wo	47.72	42.90	40.46	41.30	37.81	41.27	48.51	36.36	40.62	41.31	44.44	45.52	45.04	46.28	42.83	43.07	42.16	42.67	44.02
Fs	52.28	25.71	23.66	22.93	30.33	33.94	42.56	15.62	12.05	15.76	11.87	9.38	10.80	7.76	13.43	16.27	17.03	16.88	9.42

Clinopyroxenes

	VH89	VH94	VH94	VH94	VH94	VH94	VH102 gm	VH102	VH102 gm	VH105 rim	VH105 ophitic	VH105	VH105	VH105	VH105 core	VH105 rim	VH105 gm	VH105 core	VH106
	BH	H	H	H	H	H	B	B	B	H	H	H	H	H	H	H	H	H	B
SiO2	47.59	51.64	51.26	49.72	50.33	49.34	47.13	49.00	50.73	49.52	50.49	50.15	51.48	49.07	44.83	45.53	46.27	50.36	50.65
TiO2	2.05	1.09	0.91	1.30	0.97	1.55	3.60	1.80	1.24	1.70	1.23	1.26	1.20	1.28	3.21	3.10	3.26	1.37	1.34
Cr2O3	0.52	0.00	0.00	0.00	0.09	0.00	0.17	0.16	0.00	0.00	0.00	0.00	0.00	0.00	0.00	0.00	0.00	0.00	0.51
Al2O3	5.64	2.06	1.90	3.15	2.30	3.76	5.76	4.53	2.27	4.45	2.81	3.46	2.76	3.56	7.33	7.13	5.26	4.02	2.85
Fe2O3	3.69	1.77	3.85	3.82	1.97	2.80	2.57	2.88	2.65	2.99	3.22	3.40	2.40	3.98	2.97	5.71	3.76	3.26	2.30
FeO	5.35	9.04	7.00	7.29	7.93	7.05	11.10	6.03	7.47	6.30	6.38	6.86	7.51	9.03	8.16	5.33	8.74	6.34	6.04
MnO	0.00	0.18	0.23	0.41	0.11	0.15	0.00	0.00	0.11	0.00	0.00	0.00	0.00	0.37	0.00	0.00	0.00	0.00	0.00
MgO	13.79	15.31	15.36	14.10	14.49	13.77	10.41	14.19	14.71	14.01	15.22	14.44	15.99	12.65	11.35	12.48	11.43	14.64	14.85
CaO	20.03	18.52	19.01	19.13	19.45	20.10	19.57	20.18	19.84	21.12	19.22	19.35	18.85	18.89	19.96	20.33	20.18	20.15	21.20
Na2O	0.68	0.54	0.68	0.71	0.49	0.63	1.05	0.66	0.55	0.52	0.72	0.80	0.54	0.79	0.54	0.78	0.71	0.69	0.45
K2O	0.00	0.00	0.00	0.00	0.00	0.00	0.00	0.00	0.00	0.00	0.00	0.00	0.00	0.00	0.00	0.00	0.00	0.00	0.00
NiO	0.00	0.00	0.00	0.00	0.00	0.00	0.00	0.00	0.00	0.00	0.00	0.00	0.00	0.00	0.00	0.00	0.00	0.00	0.00
Total	99.33	100.13	100.19	99.62	98.12	99.14	101.37	99.42	99.56	100.62	99.28	99.71	100.71	99.62	98.35	100.38	99.61	100.82	100.19
per 6 oxygens																			
Si	1.78	1.92	1.90	1.87	1.91	1.86	1.77	1.83	1.90	1.83	1.88	1.87	1.89	1.86	1.72	1.70	1.76	1.85	1.88
Ti	0.06	0.03	0.03	0.04	0.03	0.04	0.10	0.05	0.03	0.05	0.03	0.04	0.03	0.04	0.09	0.09	0.09	0.04	0.04
Cr	0.02	0.00	0.00	0.00	0.00	0.00	0.01	0.00	0.00	0.00	0.00	0.00	0.00	0.00	0.00	0.00	0.00	0.00	0.01
Al	0.25	0.09	0.08	0.14	0.10	0.17	0.25	0.20	0.10	0.19	0.12	0.15	0.12	0.16	0.33	0.31	0.24	0.17	0.12
Fe3+	0.10	0.05	0.11	0.11	0.06	0.08	0.07	0.08	0.07	0.08	0.09	0.10	0.07	0.11	0.09	0.16	0.11	0.09	0.06
Fe2+	0.17	0.28	0.22	0.23	0.25	0.22	0.35	0.19	0.23	0.20	0.20	0.21	0.23	0.29	0.26	0.17	0.28	0.20	0.19
Mn	0.00	0.01	0.01	0.01	0.00	0.00	0.00	0.00	0.00	0.00	0.00	0.00	0.00	0.01	0.00	0.00	0.00	0.00	0.00
Mg	0.77	0.85	0.85	0.79	0.82	0.77	0.58	0.79	0.82	0.77	0.85	0.80	0.88	0.71	0.65	0.70	0.65	0.80	0.82
Ca	0.80	0.74	0.76	0.77	0.79	0.81	0.79	0.81	0.80	0.84	0.77	0.77	0.74	0.77	0.82	0.81	0.82	0.79	0.84
Na	0.05	0.04	0.05	0.05	0.04	0.05	0.08	0.05	0.04	0.04	0.05	0.06	0.04	0.06	0.04	0.06	0.05	0.05	0.03
K	0.00	0.00	0.00	0.00	0.00	0.00	0.00	0.00	0.00	0.00	0.00	0.00	0.00	0.00	0.00	0.00	0.00	0.00	0.00
Ni	0.00	0.00	0.00	0.00	0.00	0.00	0.00	0.00	0.00	0.00	0.00	0.00	0.00	0.00	0.00	0.00	0.00	0.00	0.00
Total	4.00	4.00	4.00	4.00	4.00	4.00	4.00	4.00	4.00	4.00	4.00	4.00	4.00	4.00	4.00	4.00	4.00	4.00	4.00
En	44.22	45.43	46.62	44.14	44.01	42.80	33.90	44.25	44.36	42.81	46.67	44.85	47.39	40.44	37.51	41.49	37.07	44.80	44.36
Wo	46.15	39.51	41.46	43.05	42.47	44.90	45.82	45.21	43.01	46.38	42.35	43.20	40.14	43.38	47.38	48.58	47.02	44.31	45.52
Fs	9.63	15.06	11.92	12.81	13.52	12.29	20.29	10.54	12.63	10.80	10.98	11.95	12.48	16.19	15.11	9.93	15.91	10.89	10.12

Clinopyroxenes

	VH106	VH106	VH106	VH106	VH137	VH137	VH137	VH137	VH151 gm	VH151 gm	VH151 gm	VH151 gm	VH151 gm	VH229	VH229	VH262 gm	MB8	MB8	MB8
	B	B	B	B	M	M	M	M	B	B	B	B	B	M	M	B	R	R	R
SiO2	49.59	50.29	50.82	51.51	51.48	50.13	50.95	48.88	45.27	47.93	50.52	45.53	51.26	48.51	48.86	48.71	47.40	48.06	47.24
TiO2	1.35	1.45	1.33	1.04	1.07	1.68	1.51	1.99	4.04	2.28	1.39	3.64	1.25	2.66	1.62	2.74	0.34	0.57	0.27
Cr2O3	0.83	0.93	0.75	0.59	0.09	0.15	0.00	0.12	0.10	0.20	0.23	0.13	0.25	0.09	0.00	0.17	0.13	0.00	0.00
Al2O3	3.66	4.22	3.55	2.84	1.44	3.60	2.93	3.89	6.25	4.91	2.92	5.92	2.58	3.22	2.65	5.27	0.60	0.98	0.66
Fe2O3	3.69	2.11	2.90	1.27	2.58	3.68	1.89	3.47	4.81	3.41	2.97	4.50	2.07	2.90	3.87	2.82	3.33	3.71	1.94
FeO	4.23	5.11	5.38	6.09	11.20	7.90	11.07	8.07	7.60	6.67	6.93	7.31	6.45	10.97	12.75	8.21	25.24	24.86	26.55
MnO	0.00	0.00	0.00	0.00	0.31	0.13	0.22	0.25	0.00	0.00	0.00	0.13	0.00	0.21	0.33	0.00	0.92	0.94	0.95
MgO	14.95	14.93	14.78	15.96	14.19	14.04	12.89	13.58	11.33	12.83	14.42	11.28	14.96	11.25	10.15	13.01	1.59	1.98	1.02
CaO	21.04	20.94	20.98	19.96	17.99	19.50	17.99	19.09	20.94	21.02	20.53	20.67	20.90	19.96	19.60	20.39	19.55	19.37	19.48
Na2O	0.58	0.62	0.73	0.52	0.58	0.74	1.00	0.70	0.68	0.63	0.59	0.80	0.55	0.77	0.78	0.69	0.63	0.83	0.53
K2O	0.00	0.00	0.00	0.00	0.00	0.00	0.11	0.00	0.00	0.00	0.00	0.00	0.00	0.00	0.00	0.00	0.00	0.00	0.00
NiO	0.00	0.00	0.00	0.00	0.00	0.00	0.00	0.00	0.00	0.00	0.00	0.00	0.00	0.00	0.00	0.00	0.00	0.00	0.00
Total	99.91	100.60	101.21	99.78	100.91	101.56	100.57	100.03	101.01	99.86	100.50	99.91	100.27	100.55	100.60	101.99	99.72	101.29	98.65
per 6 oxygens																			
Si	1.84	1.85	1.86	1.90	1.92	1.85	1.91	1.83	1.70	1.80	1.87	1.73	1.90	1.84	1.87	1.79	1.95	1.94	1.97
Ti	0.04	0.04	0.04	0.03	0.03	0.05	0.04	0.06	0.11	0.06	0.04	0.10	0.03	0.08	0.05	0.08	0.01	0.02	0.01
Cr	0.02	0.03	0.02	0.02	0.00	0.00	0.00	0.00	0.00	0.01	0.01	0.00	0.01	0.00	0.00	0.00	0.00	0.00	0.00
Al	0.16	0.18	0.15	0.12	0.06	0.16	0.13	0.17	0.28	0.22	0.13	0.26	0.11	0.14	0.12	0.23	0.03	0.05	0.03
Fe3+	0.10	0.06	0.08	0.04	0.07	0.10	0.05	0.10	0.14	0.10	0.08	0.13	0.06	0.08	0.11	0.08	0.10	0.11	0.06
Fe2+	0.13	0.16	0.16	0.19	0.35	0.24	0.35	0.25	0.24	0.21	0.21	0.23	0.20	0.35	0.41	0.25	0.87	0.84	0.92
Mn	0.00	0.00	0.00	0.00	0.01	0.00	0.01	0.01	0.00	0.00	0.00	0.00	0.00	0.01	0.01	0.00	0.03	0.03	0.03
Mg	0.83	0.82	0.81	0.88	0.79	0.77	0.72	0.76	0.64	0.72	0.80	0.64	0.82	0.64	0.58	0.71	0.10	0.12	0.06
Ca	0.84	0.82	0.82	0.79	0.72	0.77	0.72	0.77	0.84	0.85	0.82	0.84	0.83	0.81	0.80	0.80	0.86	0.84	0.87
Na	0.04	0.04	0.05	0.04	0.04	0.05	0.07	0.05	0.05	0.05	0.04	0.06	0.04	0.06	0.06	0.05	0.05	0.06	0.04
K	0.00	0.00	0.00	0.00	0.00	0.00	0.01	0.00	0.00	0.00	0.00	0.00	0.00	0.00	0.00	0.00	0.00	0.00	0.00
Ni	0.00	0.00	0.00	0.00	0.00	0.00	0.00	0.00	0.00	0.00	0.00	0.00	0.00	0.00	0.00	0.00	0.00	0.00	0.00
Total	4.00	4.00	4.00	4.00	4.00	4.00	4.00	4.00	4.00	4.00	4.00	4.00	4.00	4.00	4.00	4.00	4.00	4.00	4.00
En	46.09	45.46	44.95	47.33	42.49	43.23	40.24	42.68	36.98	40.49	43.61	37.30	44.53	35.44	32.33	40.31	5.34	6.65	3.41
Wo	46.60	45.81	45.86	42.53	38.70	43.14	40.37	43.09	49.10	47.70	44.63	49.14	44.70	45.18	44.88	45.42	47.15	46.64	46.81
Fs	7.31	8.73	9.18	10.14	18.81	13.63	19.39	14.22	13.91	11.81	11.75	13.57	10.78	19.38	22.79	14.26	47.51	46.72	49.78

A5.4 FeTi Oxide analyses *Magnetites*

	VH9	VH9	VH9	VH24	VH24	VH24	VH24	VH24	VH24	VH41	VH41	VH41	VH41	VH65	VH65	VH65	VH65	VH94	VH94
	M	M	M	M	M	M	M	M	M	BH	BH	BH	BH	Ben	Ben	Ben	Ben	H	H
SiO2	0.67	0.43	0.79	0.82	0.45	0.31	0.37	0.38	0.31	0.48	0.35	0.41	0.49	0.37	0.41	0.36	0.40	0.33	0.34
TiO2	21.68	21.94	21.81	23.05	23.91	21.81	19.64	20.29	20.81	19.47	20.11	22.89	22.53	21.82	21.40	21.03	21.44	19.69	19.78
Cr2O3	0.26	0.13	0.13	0.12	0.17	0.00	0.23	0.00	0.00	0.19	0.11	0.12	0.18	0.00	0.00	0.00	0.11	0.00	0.12
Al2O3	2.42	2.33	2.44	2.92	2.36	3.16	3.71	3.27	3.10	2.64	2.37	2.16	2.08	2.10	1.72	2.57	2.42	4.12	3.79
Fe2O3	26.61	26.86	24.67	22.64	23.22	26.59	30.22	27.13	27.28	29.21	29.55	24.92	24.84	27.98	27.33	27.62	27.14	29.71	28.22
FeO	46.87	45.40	46.54	47.40	47.71	45.60	42.62	44.00	44.54	46.13	44.94	47.65	47.43	48.02	47.13	46.96	47.77	43.33	42.39
MnO	0.00	0.00	0.00	0.00	0.00	0.00	0.00	0.00	0.00	0.00	0.00	0.00	0.00	0.00	0.00	0.00	0.00	0.00	0.00
MgO	2.77	2.97	2.77	3.15	2.71	3.12	3.70	3.25	3.09	2.45	2.39	2.70	2.76	1.69	1.52	1.70	1.62	3.74	3.43
CaO	0.11	0.00	0.10	0.31	0.10	0.06	0.00	0.00	0.00	0.60	0.00	0.06	0.00	0.10	0.06	0.00	0.00	0.08	0.09
Na2O	0.42	0.62	0.41	0.40	0.62	0.51	0.57	0.37	0.44	0.00	0.49	0.42	0.36	0.53	0.53	0.51	0.49	0.41	0.55
K2O	0.00	0.00	0.00	0.00	0.00	0.00	0.00	0.00	0.00	0.00	0.00	0.00	0.00	0.00	0.00	0.00	0.00	0.00	0.00
Total	101.78	100.68	99.66	100.80	101.23	101.14	101.07	98.70	99.56	101.16	100.30	101.32	100.67	102.61	100.10	100.75	101.38	101.41	98.70
per 4 oxygens																			
Si	0.02	0.02	0.03	0.03	0.02	0.01	0.01	0.01	0.01	0.02	0.01	0.01	0.02	0.01	0.01	0.01	0.01	0.01	0.01
Ti	0.58	0.59	0.60	0.62	0.64	0.58	0.52	0.56	0.57	0.53	0.55	0.62	0.61	0.59	0.59	0.57	0.58	0.52	0.54
Cr	0.01	0.00	0.00	0.00	0.00	0.00	0.01	0.00	0.00	0.01	0.00	0.00	0.01	0.00	0.00	0.00	0.00	0.00	0.00
Al	0.10	0.10	0.10	0.12	0.10	0.13	0.15	0.14	0.13	0.11	0.10	0.09	0.09	0.09	0.07	0.11	0.10	0.17	0.16
Fe3+	0.71	0.73	0.67	0.61	0.62	0.71	0.81	0.74	0.74	0.79	0.81	0.67	0.67	0.75	0.75	0.75	0.74	0.79	0.77
Fe2+	1.39	1.36	1.41	1.41	1.42	1.36	1.26	1.34	1.35	1.39	1.36	1.43	1.43	1.43	1.44	1.42	1.44	1.28	1.29
Mn	0.00	0.00	0.00	0.00	0.00	0.00	0.00	0.00	0.00	0.00	0.00	0.00	0.00	0.00	0.00	0.00	0.00	0.00	0.00
Mg	0.15	0.16	0.15	0.17	0.14	0.17	0.20	0.18	0.17	0.13	0.13	0.14	0.15	0.09	0.08	0.09	0.09	0.20	0.19
Ca	0.00	0.00	0.00	0.01	0.00	0.00	0.00	0.00	0.00	0.02	0.00	0.00	0.00	0.00	0.00	0.00	0.00	0.00	0.00
Na	0.03	0.04	0.03	0.03	0.04	0.03	0.04	0.03	0.03	0.00	0.03	0.03	0.03	0.04	0.04	0.04	0.03	0.03	0.04
K	0.00	0.00	0.00	0.00	0.00	0.00	0.00	0.00	0.00	0.00	0.00	0.00	0.00	0.00	0.00	0.00	0.00	0.00	0.00
Total	3.00	3.00	3.00	3.00	3.00	3.00	3.00	3.00	3.00	3.00	3.00	3.00	3.00	3.00	3.00	3.00	3.00	3.00	3.00
Mgt	38.04	37.98	36.14	32.94	32.69	37.88	43.49	40.08	39.61	42.87	42.36	35.26	35.54	39.07	38.98	39.65	38.77	43.01	41.65
Ulv	61.96	62.02	63.86	67.06	67.31	62.12	56.51	59.92	60.39	57.13	57.64	64.74	64.46	60.93	61.02	60.35	61.23	56.99	58.35

Magnetites

	VH102	VH102	VH102	VH105	VH106	VH106	VH137	VH137	VH151	VH151	VH229	VH229	VH229	VH229	MB8
	B	B	B	H	B	B	M	M	B	B	M	M	M	M	R
SiO2	0.75	0.31	0.46	0.29	0.37	0.36	0.40	0.32	0.47	0.40	0.34	0.27	0.91	0.91	0.39
TiO2	19.13	19.73	20.19	16.71	23.62	21.27	24.78	24.42	20.51	20.26	22.25	22.25	22.43	22.04	22.74
Cr2O3	0.84	0.24	0.44	0.43	0.30	0.20	0.14	0.00	0.30	0.23	0.13	0.21	0.11	0.14	0.00
Al2O3	3.72	3.80	3.57	4.55	1.56	1.58	2.57	2.40	3.32	3.05	1.68	2.53	1.26	2.51	0.84
Fe2O3	28.77	29.89	27.77	35.18	23.27	26.96	21.09	22.08	27.75	28.09	26.02	25.32	24.28	24.97	24.14
FeO	42.85	42.90	44.61	38.39	48.97	46.66	47.95	46.81	44.21	44.03	47.50	46.19	48.58	46.33	48.56
MnO	0.00	0.00	0.00	0.00	0.00	0.00	0.00	0.00	0.00	0.00	0.00	0.00	0.00	0.00	0.00
MgO	3.36	3.92	3.36	4.62	1.54	1.32	3.34	3.12	2.80	3.03	1.33	2.82	1.56	2.40	0.13
CaO	0.12	0.00	0.13	0.09	0.00	0.06	0.00	0.07	0.06	0.00	0.00	0.00	0.07	0.10	0.00
Na2O	0.55	0.41	0.33	0.56	0.58	0.58	0.52	0.67	0.64	0.49	0.67	0.47	0.41	0.65	0.72
K2O	0.00	0.05	0.00	0.00	0.00	0.00	0.00	0.00	0.00	0.00	0.00	0.00	0.14	0.10	0.09
Total	100.08	101.26	100.85	100.80	100.22	99.00	100.79	99.89	100.06	99.58	99.92	100.07	99.74	100.14	97.61
per 4 oxygens															
Si	0.03	0.01	0.02	0.01	0.01	0.01	0.01	0.01	0.02	0.01	0.01	0.01	0.03	0.03	0.01
Ti	0.51	0.52	0.54	0.44	0.65	0.59	0.66	0.66	0.56	0.55	0.61	0.61	0.62	0.60	0.65
Cr	0.02	0.01	0.01	0.01	0.01	0.01	0.00	0.00	0.01	0.01	0.00	0.01	0.00	0.00	0.00
Al	0.16	0.16	0.15	0.19	0.07	0.07	0.11	0.10	0.14	0.13	0.07	0.11	0.05	0.11	0.04
Fe3+	0.77	0.79	0.74	0.93	0.64	0.75	0.57	0.60	0.75	0.77	0.72	0.69	0.67	0.68	0.69
Fe2+	1.28	1.27	1.33	1.13	1.50	1.45	1.43	1.41	1.33	1.33	1.46	1.40	1.49	1.40	1.54
Mn	0.00	0.00	0.00	0.00	0.00	0.00	0.00	0.00	0.00	0.00	0.00	0.00	0.00	0.00	0.00
Mg	0.18	0.21	0.18	0.24	0.08	0.07	0.18	0.17	0.15	0.16	0.07	0.15	0.09	0.13	0.01
Ca	0.00	0.00	0.00	0.00	0.00	0.00	0.00	0.00	0.00	0.00	0.00	0.00	0.00	0.00	0.00
Na	0.04	0.03	0.02	0.04	0.04	0.04	0.04	0.05	0.04	0.03	0.05	0.03	0.03	0.05	0.05
K	0.00	0.00	0.00	0.00	0.00	0.00	0.00	0.00	0.00	0.00	0.00	0.00	0.01	0.00	0.00
Total	3.00	3.00	3.00	3.00	3.00	3.00	3.00	3.00	3.00	3.00	3.00	3.00	3.00	3.00	3.00
Mgt	42.93	43.11	40.75	51.29	33.01	38.80	29.87	31.15	40.36	40.95	36.91	36.28	35.13	36.17	34.68
Ulv	57.07	56.89	59.25	48.71	66.99	61.20	70.13	68.85	59.64	59.05	63.09	63.72	64.87	63.83	65.32

Ilmenites

	VH24	VH65	VH106	VH106	VH106	VH106	VH106	VH106	VH229	VH229
	M	Ben	B	B	B	B	B	B	M	M
SiO2	0.23	0.31	0.35	0.36	0.25	0.34	0.27	0.35	0.73	0.76
TiO2	49.80	50.32	49.66	49.39	51.02	49.44	51.29	50.56	49.34	48.78
Cr2O3	0.00	0.00	0.00	0.12	0.10	0.12	0.00	0.00	0.00	0.00
Al2O3	0.45	0.16	0.18	0.15	0.16	0.16	0.14	0.09	0.14	0.19
Fe2O3	10.45	7.05	5.42	8.33	5.70	5.90	4.12	6.15	5.20	5.63
FeO	34.62	39.02	39.90	40.25	41.43	40.03	42.49	39.97	41.39	41.39
MnO	0.00	0.48	0.00	0.00	0.00	0.00	0.00	0.00	0.24	0.00
MgO	4.86	2.22	2.01	1.38	1.87	1.90	1.75	2.29	1.08	1.02
CaO	0.00	0.00	0.10	0.16	0.08	0.00	0.00	0.00	0.06	0.08
Na2O	0.39	0.47	0.32	0.42	0.29	0.31	0.18	0.35	0.31	0.28
K2O	0.00	0.00	0.00	0.00	0.00	0.00	0.00	0.08	0.06	0.06
Total	100.80	100.04	97.95	100.56	100.89	98.20	100.25	99.82	98.55	98.20
per 3 oxygens										
Si	0.01	0.01	0.01	0.01	0.01	0.01	0.01	0.01	0.02	0.02
Ti	0.90	0.94	0.94	0.92	0.94	0.94	0.96	0.94	0.94	0.93
Cr	0.00	0.00	0.00	0.00	0.00	0.00	0.00	0.00	0.00	0.00
Al	0.01	0.00	0.01	0.00	0.00	0.00	0.00	0.00	0.00	0.01
Fe3+	0.19	0.13	0.10	0.16	0.11	0.11	0.08	0.11	0.10	0.11
Fe2+	0.70	0.81	0.84	0.83	0.85	0.85	0.88	0.83	0.88	0.88
Mn	0.00	0.01	0.00	0.00	0.00	0.00	0.00	0.00	0.01	0.00
Mg	0.17	0.08	0.08	0.05	0.07	0.07	0.06	0.08	0.04	0.04
Ca	0.00	0.00	0.00	0.00	0.00	0.00	0.00	0.00	0.00	0.00
Na	0.02	0.02	0.02	0.02	0.01	0.02	0.01	0.02	0.02	0.01
K	0.00	0.00	0.00	0.00	0.00	0.00	0.00	0.00	0.00	0.00
Total	2.00	2.00	2.00	2.00	2.00	2.00	2.00	2.00	2.00	2.00
ilm	90.50	93.45	94.82	92.22	94.71	94.37	96.14	94.26	95.00	94.55
hem	9.50	6.55	5.18	7.78	5.29	5.63	3.86	5.74	5.00	5.45

A5.5 Olivine -Liquid K_{Ds}

Sample	VH1	VH10	VH80	VH106	VH151	VH262	VH137	VH65	VH11	VH84	VH100	VH44	VH15
Lithology	B	B	B	B	B	B	M	Ben	Hy	Hy	Hy	Hy	Hy
	XRF whole rock analyses						Average microprobe glass analyses						
SiO2	45.85	47.43	47.86	47.21	46.79	47.71	53.06	65.87	48.93	48.95	48.09	56.15	47.39
Al2O3	16.90	14.82	15.22	15.03	17.23	14.80	12.15	15.14	15.08	16.31	14.49	15.17	15.93
FeO	11.74	9.45	10.65	11.43	11.77	10.11	13.91	4.76	10.79	11.16	13.14	9.81	9.48
MgO	6.81	11.01	9.16	8.82	6.17	10.36	2.85	0.45	6.93	4.91	5.53	2.91	5.98
CaO	12.05	11.87	11.21	10.97	11.13	10.94	6.56	2.59	11.71	10.86	10.60	6.75	11.85
Na2O	2.26	2.08	2.41	2.45	2.68	2.22	4.09	4.54	2.83	3.19	3.20	3.89	2.58
K2O	0.29	0.43	0.67	0.57	0.66	0.64	1.94	3.32	0.71	0.81	0.90	1.94	0.74
TiO2	2.57	1.63	1.88	2.14	2.60	1.78	3.11	0.71	2.30	2.81	3.36	2.74	2.08
MnO	0.19	0.17	0.17	0.18	0.18	0.17	0.18	0.15	0.00	0.00	0.00	0.00	0.23
Total	98.66	98.89	99.23	98.80	99.21	98.73	97.89	97.45	99.28	99.00	99.30	99.36	96.09
Average olivine composition.													
SiO2	39.30	40.72	39.09	39.12	39.04	40.47	35.20	32.40	40.09	39.84	39.38	38.05	39.54
TiO2	0.02	0.00	0.00	0.02	0.18	0.00	2.25	0.00	0.23	0.00	0.00	0.00	0.00
FeO	20.16	11.07	20.05	19.59	20.89	14.41	36.13	52.73	15.13	15.11	19.31	24.75	18.18
MnO	0.00	0.01	0.00	0.00	0.00	0.00	0.22	1.45	0.00	0.00	0.00	0.00	0.30
MgO	40.77	47.74	40.84	41.07	39.89	45.37	27.22	12.56	44.57	44.52	41.41	36.04	36.53
CaO	0.26	0.27	0.26	0.28	0.27	0.24	0.28	0.43	0.36	0.22	0.19	0.27	0.22
Na2O	0.50	0.34	0.53	0.51	0.57	0.43	0.55	0.60	0.46	0.43	0.40	0.65	0.00
Total	101.01	100.15	100.76	100.59	100.83	100.92	101.86	100.17	100.84	100.12	100.70	99.77	94.77
KD	**0.29**	**0.27**	**0.42**	**0.37**	**0.27**	**0.33**	**0.27**	**0.40**	**0.22**	**0.15**	**0.20**	**0.20**	**0.31**
(Roeder & Emslie 1971)													

Appendix 6
ICP-MS Data

	VH10	VH13	VH23	VH24	VH33	VH35	VH41	VH45	VH47	VH49	VH52	VH56
Rb	7.86	18.95	58.79	29.44		105.63	20.86	28.47	24.04	104.54	4.57	9.76
Sr	353.91	458.08	294.88	520.28		47.86	487.85	460.06	411.83	9.37	260.48	343.06
Y	16.70	35.61	58.24	42.99		79.54	34.86	46.31	41.12	90.14	25.10	46.28
Nb	15.70	37.41	77.71	42.27	16.78	104.50	35.61	41.95	39.22	91.75	10.84	26.69
Ba	131.05	305.63	671.22	360.73	127.83	744.99	275.94	312.86	332.75	622.71	58.16	144.43
La	13.88	29.63	55.65	37.99	14.28	84.93	28.28	35.91	33.55	102.08	8.74	22.42
Ce	30.61	64.79	115.87	82.57	33.74	183.85	62.77	83.91	76.79	192.53	22.32	56.70
Pr	3.96	8.55	14.64	11.16	3.87	22.53	8.64	11.23	10.58	25.69	3.27	8.26
Nd	17.25	37.50	63.14	50.84	16.33	86.72	39.90	47.70	45.85	96.72	15.28	38.15
Sm	4.11	8.08	14.24	11.86	4.10	19.16	9.25	11.32	10.77	21.46	4.34	9.83
Eu	1.48	3.04	5.10	4.41	1.28	3.42	3.31	3.91	3.76	2.87	1.75	3.51
Gd	4.56	9.25	14.20	12.36	3.98	19.42	9.80	12.58	12.52	21.68	5.88	11.71
Tb	0.65	1.34	2.28	1.76	0.48	2.98	1.38	1.86	1.78	3.09	0.96	1.75
Dy	3.61	8.19	12.67	9.66	2.99	17.15	7.72	10.04	9.69	19.16	5.19	10.33
Ho	0.66	1.45	2.29	1.78	0.52	3.22	1.45	2.00	1.92	3.53	1.02	1.95
Er	1.84	4.09	7.16	4.85	1.38	8.96	4.01	5.52	5.36	9.29	2.85	5.54
Tm	0.28	0.41	1.06	0.70	0.18	1.31	0.55	0.75	0.69	1.32	0.42	0.76
Yb	1.62	3.45	6.53	4.81	1.31	7.92	3.36	4.43	4.45	7.93	2.59	4.85
Lu	0.25	0.45	1.14	0.67	0.17	1.15	0.48	0.70	0.63	1.21	0.39	0.65
Pb	1.62	2.82	6.48	2.81	1.29	8.98	0.77	3.48	2.24	4.68	0.95	1.19
Th	1.29	2.81	6.44	3.10	1.09	12.19	2.53	3.36	3.33	10.80	0.93	1.55
U	0.41	0.66	1.98	1.00	0.43	2.58	0.71	1.49	0.98	1.98	0.24	0.49

	VH57	VH59	VH73	VH74	VH75	VH78	VH79	VH87	VH90	VH97	VH99	VH102
Rb	22.79	28.98	21.97		79.44	14.33	55.44	8.48	20.79	60.00	24.11	18.16
Sr	454.64	475.46	529.67		100.01	359.19	368.81	232.81	479.29	347.63	408.67	438.25
Y	54.70	37.50	40.19		71.97	20.84	62.31	38.79	32.31	60.57	45.24	23.61
Nb	46.59	35.16	39.88	19.29	96.64	21.10	71.70	16.65	33.12	67.07	42.30	21.63
Ba	364.37	353.21	334.76	143.42	809.36	152.34	640.39	86.52	259.86	674.88	340.91	190.64
La	41.53	32.30	31.72	16.72	74.06	16.20	54.80	14.17	27.76	58.52	34.84	18.48
Ce	96.24	73.10	68.89	39.12	147.30	36.23	120.02	33.90	60.95	125.14	79.75	42.09
Pr	13.32	9.58	9.31	4.38	19.71	5.11	15.09	4.86	8.55	16.14	10.77	5.51
Nd	60.98	44.16	41.73	18.29	79.76	22.26	64.62	24.59	37.36	65.05	47.06	23.90
Sm	13.32	9.85	9.12	4.30	16.67	5.35	14.15	6.40	8.61	13.36	10.26	5.44
Eu	5.00	3.92	3.35	1.42	3.56	1.65	4.53	2.17	2.91	4.51	3.73	2.19
Gd	15.19	12.88	10.21	4.45	16.06	6.00	14.53	8.01	9.50	15.09	12.58	6.94
Tb	2.13	1.79	1.51	0.56	2.59	0.78	2.15	1.34	1.28	2.23	1.79	0.95
Dy	12.01	8.89	8.69	3.27	15.93	4.66	13.20	8.55	6.82	12.82	10.61	5.44
Ho	2.23	1.84	1.56	0.57	2.80	0.79	2.47	1.60	1.35	2.48	1.96	1.12
Er	6.08	4.58	4.36	1.62	8.61	2.72	6.76	4.43	3.36	6.96	5.36	2.78
Tm	0.77	0.62	0.63	0.21	1.25	0.33	1.00	0.67	0.47	0.87	0.75	0.41
Yb	5.06	4.07	3.77	1.38	7.95	1.91	6.52	3.85	3.28	6.41	4.91	2.61
Lu	0.80	0.64	0.57	0.17	1.09	0.33	0.93	0.62	0.43	0.94	0.67	0.37
Pb	2.39	1.72	2.08	1.53	6.09	0.95	4.10	1.84	1.57	5.56	1.96	1.35
Th	3.33	2.64	2.80	1.27	9.19	1.79	6.10	1.26	2.31	6.35	3.29	1.98
U	0.93	0.84	0.79	0.49	2.39	0.43	1.71	0.39	0.73	1.68	1.02	0.64

	VH104	VH106	VH115	VH121	VH122	VH125	VH127	VH128	VH129	VH130	VH134	VH137
Rb		20.89	24.87	11.14	20.15	19.97	23.61	29.28	15.01	15.01	16.75	28.89
Sr		502.23	482.41	408.50	409.65	432.31	485.22	419.48	397.05	397.05	387.09	510.34
Y		40.52	56.07	20.17	22.38	31.95	34.49	27.33	18.39	18.39	22.95	42.44
Nb	20.02	39.77	46.08	17.70	20.31	30.19	36.85	38.17	19.84	19.84	26.23	41.33
Ba	145.22	294.81	358.39	164.17	193.65	243.59	288.02	1236.97	191.86	191.86	218.73	361.98
La	16.83	34.66	42.49	13.42	18.43	25.32	29.73	39.00	15.41	15.41	22.97	37.53
Ce	40.13	78.51	100.07	31.39	41.33	56.36	66.61	80.07	35.41	35.41	48.72	83.70
Pr	4.61	10.79	13.91	4.10	5.85	7.45	9.36	9.90	4.38	4.38	6.48	11.66
Nd	19.82	46.57	61.47	18.63	25.90	32.93	40.27	44.76	21.09	21.09	28.15	48.07
Sm	4.82	10.45	13.87	4.91	6.15	7.31	9.95	8.92	5.12	5.12	5.64	11.22
Eu	1.56	3.87	5.12	1.70	2.33	2.74	3.26	6.43	1.68	1.68	2.06	4.27
Gd	4.80	12.50	17.06	5.11	6.92	8.70	9.91	8.53	5.23	5.23	6.38	12.51
Tb	0.60	1.65	2.48	0.71	1.03	1.29	1.35	1.23	0.81	0.81	0.95	1.65
Dy	3.61	9.76	13.11	4.87	5.47	7.12	7.85	6.21	4.45	4.45	5.60	10.00
Ho	0.61	1.79	2.59	0.87	1.00	1.39	1.48	1.19	0.78	0.78	1.03	1.78
Er	1.71	5.03	6.94	2.08	2.84	3.63	3.61	3.19	2.24	2.24	2.65	4.52
Tm	0.22	0.60	0.91	0.36	0.31	0.41	0.54	0.54	0.33	0.33	0.29	0.61
Yb	1.46	3.82	6.07	2.08	2.34	3.25	3.35	3.23	2.00	2.00	2.38	4.32
Lu	0.18	0.56	0.88	0.35	0.35	0.43	0.49	0.59	0.35	0.35	0.34	0.60
Pb	1.66	1.92	2.02	0.91	3.94	2.51	1.85	2.29	1.04	1.04	2.35	2.01
Th	1.29	3.25	3.61	1.36	2.00	2.42	2.60	3.14	1.56	1.56	2.46	3.38
U	0.44	0.87	1.07	0.41	0.44	0.59	0.75	0.74	0.45	0.45	0.56	0.99

	VH146	VH150	VH151	VH152	VH154	VH156	VH165	VH169	VH174	VH176	VH177	VH180
Rb	23.40	25.39	15.38	8.25	21.13	27.33	96.46	36.92	13.09	30.99	28.36	27.19
Sr	482.66	478.10	522.43	498.17	341.79	447.38	34.67	441.89	398.07	488.30	526.60	488.17
Y	36.84	40.04	22.47	20.54	70.73	41.59	79.09	44.46	18.20	42.68	39.48	43.10
Nb	35.54	40.10	23.85	21.82	34.80	39.71	98.77	46.84	16.72	41.67	43.43	46.68
Ba	272.74	330.16	196.01	177.71	209.21	334.41	593.90	410.83	159.61	373.33	366.95	351.47
La	26.38	34.78	18.41	17.60	34.64	38.03	74.23	42.51	13.15	37.86	37.52	35.94
Ce	56.28	78.82	39.65	38.76	87.75	84.92	158.49	96.04	30.87	84.30	79.09	81.02
Pr	7.98	10.59	5.58	5.13	13.15	11.91	19.41	13.00	4.48	11.70	10.63	11.28
Nd	35.73	46.97	23.18	23.01	60.40	52.96	73.88	56.92	16.98	47.50	45.63	47.50
Sm	8.54	9.89	6.26	5.86	15.99	11.41	17.43	11.61	4.73	11.15	10.10	11.87
Eu	3.08	4.04	2.29	2.02	5.21	4.15	3.09	4.26	1.56	3.90	3.73	3.97
Gd	8.57	12.01	7.03	5.51	19.00	13.14	18.15	13.71	5.50	12.27	10.96	11.39
Tb	1.37	1.75	1.08	0.76	2.73	1.74	2.81	1.90	0.66	1.65	1.67	1.64
Dy	8.40	9.79	5.06	4.91	16.13	10.33	17.08	10.37	4.18	9.80	8.92	9.60
Ho	1.37	1.69	1.15	0.90	2.96	1.90	3.35	1.97	0.79	1.86	1.81	1.72
Er	3.72	4.88	2.89	2.25	8.55	5.12	9.30	5.64	2.33	4.86	4.70	4.89
Tm	0.62	0.51	0.47	0.35	1.16	0.56	1.39	0.76	0.36	0.65	0.65	0.70
Yb	3.31	3.96	2.88	2.40	7.08	4.06	8.55	4.74	1.92	4.17	3.93	3.85
Lu	0.47	0.57	0.45	0.35	1.01	0.54	1.22	0.71	0.34	0.62	0.66	0.52
Pb	1.79	2.73	1.30	1.60	1.82	2.49	7.52	2.84	30.55	1.54	3.08	2.22
Th	2.56	2.93	1.70	1.65	3.34	3.20	10.96	4.39	1.29	3.28	3.15	3.27
U	0.72	0.73	0.57	0.32	0.94	0.78	3.02	1.21	0.44	0.98	0.93	0.92

	VH186	VH187	VH196	VH198	VH201	VH203	VH211	VH212	VH216	VH218	VH219	VH222
Rb	18.64	34.57	20.70	9.25	8.31	21.46	24.63	9.18	21.57	46.81	28.22	34.53
Sr	346.63	453.25	438.13	230.18	216.35	435.97	335.26	339.77	387.20	302.03	447.28	512.99
Y	28.61	49.31	34.38	40.51	36.77	32.67	63.52	21.03	30.31	49.11	40.94	48.76
Nb	31.30	48.41	34.91	19.29	15.52	32.26	31.69	15.75	29.57	58.63	41.27	51.15
Ba	233.57	391.47	271.38	94.72	88.11	275.82	228.58	139.04	287.62	569.16	329.29	445.16
La	26.48	44.61	28.98	15.88	13.13	24.70	35.08	12.94	25.11	50.56	32.29	45.24
Ce	57.63	101.02	65.22	38.38	32.34	54.82	86.06	30.91	55.00	107.44	72.09	100.04
Pr	7.85	13.44	8.86	5.90	4.68	7.29	12.39	4.26	7.88	13.88	9.91	13.45
Nd	32.77	60.35	39.19	27.76	22.72	31.49	62.00	18.97	34.59	58.39	44.97	58.24
Sm	7.36	12.58	9.13	7.30	6.33	7.47	14.22	4.88	7.66	12.05	9.58	13.08
Eu	2.67	4.26	3.41	2.53	2.23	2.80	4.61	1.96	2.90	4.56	3.40	5.04
Gd	8.65	13.87	9.24	8.90	8.03	8.42	16.55	5.77	9.43	12.78	10.60	13.23
Tb	1.28	1.92	1.41	1.43	1.30	1.20	2.61	0.82	1.36	2.01	1.50	1.81
Dy	7.12	10.81	7.69	8.42	7.49	7.43	14.46	4.96	7.43	11.32	8.73	11.27
Ho	1.31	2.02	1.54	1.65	1.58	1.29	2.79	0.93	1.38	2.20	1.72	1.99
Er	3.66	5.37	4.04	4.90	4.14	3.77	7.66	2.53	3.94	6.18	4.55	5.65
Tm	0.43	0.62	0.53	0.59	0.61	0.44	1.02	0.37	0.43	0.74	0.55	0.79
Yb	3.06	4.50	3.41	4.28	3.70	3.05	6.45	2.10	3.04	5.29	3.62	4.91
Lu	0.45	0.68	0.53	0.60	0.64	0.48	0.87	0.37	0.48	0.84	0.52	0.69
Pb	2.31	4.25	3.00	1.30	0.95	1.60	2.39	0.82	2.28	3.81	2.11	2.65
Th	2.76	3.75	2.69	1.49	1.20	2.71	3.31	1.15	2.35	5.88	2.75	4.06
U	0.70	1.04	0.76	0.30	0.34	0.65	1.07	0.39	0.54	1.53	0.88	1.22

	VH223	VH225	VH236	VH238	VH246	VH247	VH249	VH253	VH254	VH260	VH262	VH266
Rb	31.32	40.27	26.68	26.77	9.68	17.24	57.35	99.80	35.59	4.62	13.99	22.29
Sr	482.55	426.71	366.86	310.24	393.94	417.39	259.52	73.61	536.11	211.26	334.40	413.74
Y	45.67	46.79	67.20	66.55	22.52	21.38	55.26	75.17	50.24	32.01	17.04	32.47
Nb	44.97	53.80	35.70	33.54	18.16	27.89	71.17	97.04	52.89	11.75	17.17	36.12
Ba	399.25	510.29	232.88	254.62	162.85	211.16	680.97	855.64	509.04	51.38	161.83	281.61
La	40.94	47.84	36.47	39.26	15.52	24.12	54.08	81.83	49.64	9.43	15.32	27.70
Ce	91.73	103.66	90.14	96.08	36.20	52.70	115.81	165.63	106.32	23.85	32.71	59.32
Pr	12.27	13.50	12.70	13.73	5.15	6.66	14.62	19.82	14.46	3.72	4.56	8.13
Nd	56.34	56.76	60.11	62.46	22.62	27.58	59.48	77.85	63.17	18.76	19.43	35.61
Sm	12.55	12.37	14.71	15.33	4.74	6.06	12.49	16.72	13.78	4.88	4.23	7.77
Eu	4.67	4.23	4.66	4.74	1.93	2.12	4.69	3.51	5.22	1.89	1.72	3.06
Gd	12.99	12.13	16.00	16.91	6.38	7.46	13.55	17.25	14.80	6.96	5.15	9.19
Tb	1.81	1.88	2.30	2.58	0.92	0.83	2.10	2.69	2.15	1.09	0.71	1.42
Dy	10.41	10.44	14.60	14.86	5.63	5.52	11.92	15.35	11.20	6.94	4.14	7.98
Ho	1.96	2.11	2.64	2.80	0.95	0.97	2.38	2.92	2.20	1.33	0.77	1.45
Er	5.14	5.87	7.26	7.94	2.84	2.59	6.91	8.44	5.71	3.81	2.20	3.98
Tm	0.65	0.71	1.04	1.00	0.27	0.44	0.84	1.28	0.84	0.48	0.20	0.48
Yb	4.22	6.93	6.13	6.76	2.37	2.70	6.33	8.29	5.13	3.42	1.76	3.44
Lu	0.62	0.79	0.89	0.96	0.31	0.34	0.95	1.15	0.71	0.56	0.24	0.48
Pb	2.71	4.27	2.16	4.50	1.24	1.72	4.05	7.15	2.98	1.98	1.22	2.70
Th	3.65	5.53	3.33	3.91	1.41	2.53	6.63	11.35	4.38	0.73	1.57	2.79
U	1.02	1.52	1.02	1.11	0.49	0.78	1.77	3.06	1.25	0.17	0.38	0.70

	VH270	VH273	VH274
Rb	9.06	4.57	6.80
Sr	230.59	201.28	223.83
Y	42.77	32.42	48.29
Nb	20.11	12.40	21.86
Ba	101.74	50.62	106.36
La	16.83	8.48	17.62
Ce	40.63	22.85	42.09
Pr	6.04	3.44	6.11
Nd	28.86	16.69	28.27
Sm	7.24	5.53	8.34
Eu	2.49	2.01	2.73
Gd	9.03	6.51	10.18
Tb	1.47	1.14	1.60
Dy	8.69	6.78	9.58
Ho	1.74	1.26	2.12
Er	5.12	3.91	5.41
Tm	0.65	0.55	0.80
Yb	4.36	3.03	5.78
Lu	0.62	0.49	0.81
Pb	3.33	0.48	0.82
Th	1.45	0.77	1.38
U	0.35	0.25	0.43

Appendix 7
Isotope Data

The following data tables give radiogenic isotope ratios - with 2σ errors - for Sr, Nd and Pb and stable isotope ratios for O - without errors, $\delta^{18}O$ values are simply averages calculated from one to three analyses run on each sample. Since the Snaefell lavas are <1Myrs. old, no age correction on the radiogenic isotopes was deemed necessary.

The samples analysed represent the complete compositional range seen in the series and include one of the underlying Plio-Pleistocene tholeiites, VH52 (V10).

	87Sr/86Sr	error	144Nd/143Nd		206Pb/204Pb		207Pb/204Pb		208Pb/204Pb		δ18O
VH10	0.703322	7	0.513017	5	18.553	2	15.473	2	38.181	5	5.1
VH49	0.703549	7	0.513005	4	18.453	1	15.467	1	38.141	2	5.3
VH52	0.703187	7	0.513019	5	18.43	2	15.447	2	38.062	5	4.8
VH74	0.703357	7	0.513025	5	18.611	2	15.463	2	38.219	4	4.9
VH115	0.703303	7	0.513003	5	18.447	2	15.466	2	38.119	4	5.1
VH121	0.703272	7	0.513015	5	18.345	2	15.485	2	38.08	4	5.2
VH151	0.703307	7	0.513002	5	18.492	3	15.492	3	38.222	6	5.3
VH174	0.703362	7	0.512983	4	18.379	2	15.462	2	38.133	4	4.9
VH176	0.703325	7	0.513002	5	18.432	2	15.498	2	38.177	4	5.1
VH190	0.703302	7	0.51301	6	18.486	1	15.474	1	38.202	2	5.1
VH212	0.703323	7	0.513018	5	18.332	5	15.431	4	37.937	10	5.4
VH216	0.703327	6	0.512987	4	18.347	1	15.451	1	38.059	2	4.7
VH222	0.703311	7	0.512999	5	18.475	1	15.474	1	38.188	2	5.2

Map A1.

The Snaefell Volcanic System

x = 392000 390 388 386 384 382 380 378

y = 496000 494 492 490 488 486 484 482 480 478 476 474 472

Thraelaalda
Thraelahals
878
Laugara
Saudafell
900
832
Laugarfell
Thuridarstadadalur
Geldaerhnjukur
Grjota
Vesturoraefi
900
600
Jokulsa i Fljotsdal
1050
Grabergshnjukur
1001
Nalhushnjukur
1210
Hafursfell
1098
Vatnsdalur
Sandfell
1120
Hafursa
1010
(Tiutiu)
Langihnjukur
900
Saudahnjukur
1004
1035
Snaefell
1833
Hamar
1338
Dimmagil
Eyabakkar
1150
1325
1006
Thordafell
1160
Snaefellshals
1008
Thjofadalir
Thjofagilsa
1008
Fifjahnjukur
Kentilhnjukur
1160
1230
Thjofahnjukur
1122
Litla-Snaefell
1060
Bjalfafell

Scale
0 1 2 3 4km
Heights in meters.

392 390 388 386 384 382 380 378 x = 376000

Journal of the Geological Society, London, Vol. 152, 1995, pp. 000–000, 5 figs, 1 table. Printed in Northern Ireland

The heterogeneous Iceland plume: new insights from the alkaline basalts of the Snaefell volcanic centre

V. L. HARDS[1], P. D. KEMPTON[2] & R. N. THOMPSON[1]

[1]*Department of Geological Sciences, University of Durham, South Road, Durham, DH1 3LE, UK*

[2]*NERC Isotope Geosciences Laboratory, Keyworth, Nottingham, NG12 5GG, UK*

Abstract: It has been accepted for some time that mixing between MORB-source mantle and the Iceland plume (geochemically relatively 'enriched' mantle) occurs along the Reykjanes Ridge. The composition of the basalts becomes progressively more enriched in lithophile elements towards Iceland. Within Iceland itself, there is significant variation in the composition of the mafic volcanic rocks. Although variations in degree of melting of a single source could have produced the elemental compositions of the Icelandic picritic, tholeiitic and alkalic basalts, their isotope systematics are not consistent with this model and require differences in source chemistry. Therefore, either MORB-source mantle has been mixed into the plume or the plume itself is heterogeneous. The clearest indications come from Pb isotopic data, which suggest that MORB-source mantle was *excluded* from the generation of Icelandic volcanic rocks.

Keywords: Iceland, mantle, plumes, basalts, isotopes.

In comparison with tholeiitic volcanism, alkaline volcanism in Iceland is volumetrically insignificant, accounting for only 15% of the lava erupted within the Neovolcanic zones (Jakobsson 1972). Its small volume means that it plays a minor role in crustal accretion. Nevertheless, its occurrence is important, since it can afford significant insights into mantle heterogeneity and melting processes beneath Iceland. Alkaline volcanism is limited to the flank or lateral volcanic zones (Saemundsson 1979), which are peripheral to the axial rift zones where the more voluminous tholeiitic (and minor picritic) volcanism occurs. The flank zones are Snaefellsnes to the west, Vestmannaeyjar to the south and Oraefajokull–Snaefell to the east. The new data, presented below, come from the Snaefell volcanic centre, at the northernmost end of the eastern flank zone. These will be used, along with published data, to evaluate the partial melting processes and the nature of compositional variations in the mantle beneath Iceland.

The geology of the Snaefell volcanic centre

Snaefell is typical of a flank-zone central volcano, having formed a large, elongate, fissure-parallel, volcanic edifice which lies unconformably on the older volcanic pile. The associated fissure swarm is short and has not seen the voluminous out-pourings associated with the axial volcanic zones of Iceland. Large-scale extensional faults and graben formation are also absent, indicating that local crustal separation was small.

Compositionally, the Snaefell lavas are mildly alkaline; the suite spans the entire range from basalt to peralkaline rhyolite. Since the objective of this paper is to focus on mantle processes and composition, further discussions of both these rocks and published data sets will be confined to basalts with >8% MgO. This should minimize complications introduced by fractional crystallization and crustal assimilation.

Results

Chemical analyses of five representative Snaefell basalts are listed in Table 1. It should be noted that SN10 contains olivine of Fo_{89}—close to the maximum (Fo_{90}) found in Icelandic lavas (Meyer *et al.* 1985)—and therefore could be considered as a possible primary magma.

The Snaefell lavas are typical of Icelandic alkali basalts. They are distinct from the axial tholeiites in that they have lower contents of SiO_2 (<48%), higher Al_2O_3, alkalis and large-ion lithophile elements (LILE) (Hémond *et al.* 1993). They also show steeply inclined rare-earth element (REE) patterns with $[La/Yb]_n \geq 5$ and $[Lu]_n$ as low as 11. This indicates the presence of residual garnet in the source, retaining heavy REE. The steep normalised REE patterns of the Snaefell lavas contrast markedly both with the flat REE patterns of the axial tholeiites, which have $[La/Yb]_n \approx 1$ and also with the convex upward LREE-depleted, $[La/Yb]_n < 1$, patterns of the axial picrites (Fig. 1). Isotopically there is little variation within the Snaefell suite. In comparison with the rest of Iceland, $^{87}Sr/^{86}Sr$ is high (0.70327–0.70336), and $^{143}Nd/^{144}Nd$ low (0.51298–0.51303). These values are similar to results obtained for Snaefellsjokull in the west (B. Hardason, pers. comm. 1994). Pb isotopic ratios from Snaefell basalts plot in the middle of the Iceland field defined by published data (Fig. 4), $^{206}Pb/^{204}Pb$ ranges from 18.332 to 18.611, $^{207}Pb/^{204}Pb$ from 15.431 to 15.485 and $^{208}Pb/^{204}Pb$ from 37.937 to 38.219.

Table 1. *Representative analyses of high MgO Snaefell Basalts*

Sample	SN10	SN74	SN121	SN174	SN212
SiO_2	47.43	47.77	47.08	47.07	47.48
TiO_2	1.63	1.71	2.08	2.04	2.01
Al_2O_3	14.82	14.59	15.38	15.13	14.48
$Fe_2O_3^T$	10.50	11.07	13.20	12.76	11.46
MnO	0.17	0.17	0.18	0.18	0.17
MgO	11.01	10.29	8.67	9.51	10.55
CaO	11.87	11.24	10.78	10.88	11.47
Na_2O	2.08	2.20	2.56	2.46	2.11
K_2O	0.43	0.66	0.59	0.62	0.50
P_2O_5	0.21	0.24	0.22	0.23	0.26
Total	100.15	99.98	100.76	100.90	100.51
LOI	0.43	−0.02	−0.24	−0.21	1.43
Ba	152	167	187	177	149
Cr	885	816	340	441	653
Nb	16	20	18	15	15
Ni	240	201	112	148	187
Rb	9	16	14	13	9
Sc	33	34	38	37	35
Sr	361	367	388	382	354
V	278	259	261	310	273
Y	19	21	24	20	24
Zr	110	121	128	112	126
La	13.9	16.7	13.4	13.2	12.9
Ce	30.6	39.1	31.4	30.9	30.9
Pr	4.0	4.4	4.1	4.5	4.3
Nd	17.3	18.3	18.6	17.0	19.0
Sm	4.1	4.3	4.9	4.7	4.9
Eu	1.5	1.4	1.7	1.6	2.0
Gd	4.6	4.5	5.1	5.5	5.8
Tb	0.7	0.6	0.7	0.7	0.8
Dy	3.6	3.3	4.9	4.2	5.0
Ho	0.7	0.6	0.9	0.8	0.9
Er	1.8	1.6	2.1	2.3	2.5
Tm	0.3	0.2	0.4	0.4	0.4
Yb	1.6	1.4	2.1	1.9	2.1
Lu	0.3	0.2	0.4	0.3	0.4
Pb	1.6	1.5	0.9	3.1	0.8
Th	1.3	1.3	1.4	1.3	1.2
U	0.4	0.5	0.4	0.4	0.4
Rb/Sr	0.03	0.04	0.04	0.04	0.03
Sm/Nd	0.24	0.24	0.26	0.28	0.26
$^{87}Sr/^{86}Sr$	0.703322 ± 7	0.703357 ± 7	0.703272 ± 7	0.703362 ± 7	0.703323 ± 7
$^{143}Nd/^{144}Nd$	0.513017 ± 5	0.513025 ± 5	0.513015 ± 5	0.512983 ± 4	0.513018 ± 5
$^{206}Pb/^{204}Pb$	18.533 ± 3	18.611 ± 2	18.345 ± 2	18.379 ± 2	18.332 ± 5
$^{207}Pb/^{204}Pb$	15.473 ± 2	15.463 ± 2	15.485 ± 2	15.462 ± 2	15.431 ± 4
$^{208}Pb/^{204}Pb$	38.181 ± 5	38.219 ± 4	38.080 ± 4	38.133 ± 4	37.937 ± 10

Major and trace element data obtained by XRF at Durham, using fused discs and powder pellets respectively. REEs were obtained by ICP-MS at the NERC facility at CARE, Imperial College at Silwood Park, Ascot; and isotopic data at the NIGL, Keyworth, Nottingham. All samples for isotopic analysis were leached in hot 6M HCl prior to dissolution. Reference standards throughout the course of analysis averaged values of $^{87}Sr/^{86}Sr = 0.710217 \pm 32$ (2σ) for NBS 987 standard. For the Johnson Matthey Nd standard, $^{143}Nd/^{144}Nd = 0.511129 \pm 12$ (2σ). $^{87}Sr/^{86}Sr$ was normalised to $^{86}Sr/^{88}Sr = 0.1194$; $^{143}Nd/^{144}Nd$ was normalized to a value of $^{146}Nd/^{144}Nd = 0.7219$. Pb massfractionation was 0.8% per a.m.u. Based on repeated runs of NBS 981 common Pb standard, the reproducibility is better than 0.1%. Blanks for Sr, Nd and Pb were less than 500 pg, 130 pg and 110 pg, respectively.

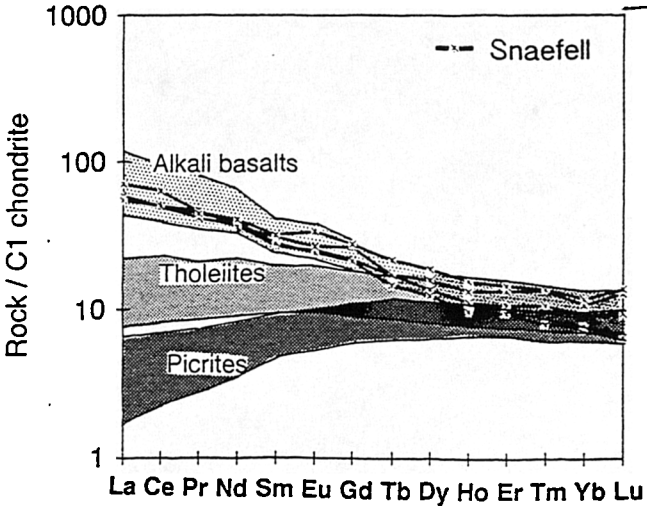

Fig. 1. REE abundance ranges in the various lava types found in Iceland. Data from Elliott (1991); Furman *et al.* (1991); Hémond *et al.* (1993) and the present study. Normalization factors from Sun & McDonough (1989).

Discussion

Origin of the alkaline suites

Trace-element evidence. In terms of trace elements, it is theoretically possible to derive both the Icelandic alkaline and tholeiitic magmas from a single source region, by varying degrees of partial melting. More specifically (Meyer *et al.* 1985), the tholeiites are calculated to result from higher degrees of melting (*c.* 10–15%) than the alkaline magmas (*c.* 1–6%). When combined with the envisaged thermal structure of the plume (see below), this melting model can explain the contrasting REE patterns and the geographical distribution of the lavas. Within the hot plume centre, decompression melting commences at a depth of about 120 km and ceases at <20 km beneath the axial rift, to produce the axial tholeiites (White & McKenzie in press). Due to the pronounced lateral thermal gradient, indicated by seismic studies and heat-flow measurements (Tryggvasson *et al.* 1983; Courtney & White 1986), melting commences at 70–80 km (within the garnet stability field) at the periphery of the upwelling Iceland plume stem, i.e. beneath the flank zones. Melting should also cease at greater depth, due to thicker lithosphere beneath the flank zones. This suggests that, in the peripheral zone, the resultant 'melting column' should be shorter than within the axial zone, resulting in the lower degrees of melting needed to produce the alkali basalts (such as those seen at Snaefell). The chemical 'signature' of residual garnet is preserved in the alkali basalts, whilst the flat REE patterns in the tholeiites should approach those of the source region, since at higher degrees of melting most of the aluminous phase would have been consumed. In detail, these contrasts may be less marked than in the simplified model, due to the possibility of mixing between end members in the observed lava suites. It is also implicit in this conclusion that re-equilibration with spinel facies lherzolite was insufficient to flatten the REE patterns.

The above scenario can be modelled, in terms of trace elements, using simple non-modal batch melting equations (Shaw 1970) and the results of this are summarized in Fig. 2. The Snaefell basalts appear to be small degree melts of an undepleted mantle source in the garnet–spinel transition zone. A gradation may be seen in the published data from the Icelandic alkaline lavas, which are produced by small-degrees of melting of a garnet-bearing source, to the tholeiites which model as higher-degree melts of this same source (Fig. 2). The picrites also show a gradation into the tholeiites; although they also seem to require a progressively more *depleted* source.

Isotopic evidence. The isotopic data are not, however, consistent with this simple model, because different lava types show different isotopic characteristics (Fig. 3). In general the alkaline lavas have a relatively restricted range, with the highest $^{87}Sr/^{86}Sr$ and $^{206}Pb/^{204}Pb$, and the lowest $^{143}Nd/^{144}Nd$ of Icelandic mafic rocks. The picrites, in contrast, cover most of the Icelandic Sr–Nd–Pb ratio range, and include members at the opposite end to the alkaline rocks. They overlap with the MORB isotopic field and show some of the least radiogenic Pb isotopes recorded in Atlantic MORBs (Elliott *et al.* 1991). The tholeiites have intermediate radiogenic isotope systematics.

It has been proposed that the alkaline basalts are the result of small degrees of partial melting of amphibolite-facies lower crust (e.g. Oskarsson *et al.* 1985, Steinthorsson *et al.* 1985). This could conceivably account for trace-element abundances and even Sr isotopes, but it cannot explain variations in Nd and Pb isotope ratios, since all Icelandic crust is not of sufficient age for these systems to have changed significantly. Although crustal assimilation can add to the elemental and oxygen isotopic variability, especially in more-evolved lavas (Nicholson *et al.* 1991), Nd and Pb isotopic variations within the basalts necessitate variations in *source composition*. Sr (and Pb) isotopic ratios

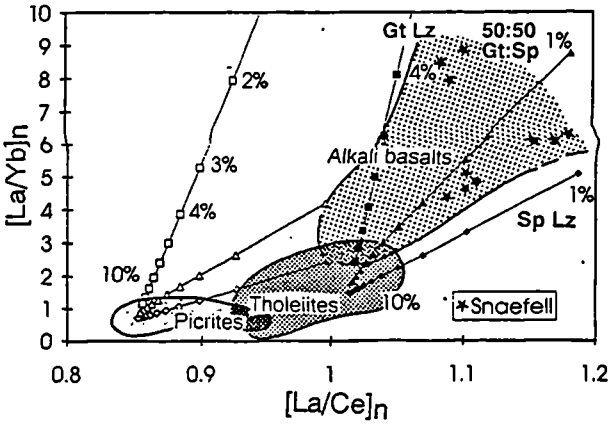

Fig. 2. Results of modelling non-modal batch melting; varying both the aluminous phase and the source composition to give six separate melting curves (parameters from Kostopoulos & James 1992). The filled symbols are used when the source composition was taken as the Bulk Silicate Earth of Kostopolous & James (1992) and open symbols have been used when the source composition was the same authors' Depleted MORB Mantle; 'Gt Lz' is garnet lherzolite, 'Sp Lz' is spinel lherzolite and '50:50 Gt:Sp' is a 50:50 mixture to simulate the garnet–spinel transition zone. Numbers along the melting curves are percentages of melting that the source would have to undergo, in order to produce a melt of that composition. The apparent intersection at <15% partial melting of the curves for each source composition is a feature of the original equations employed. Data fields from the same sources as in Fig. 1.

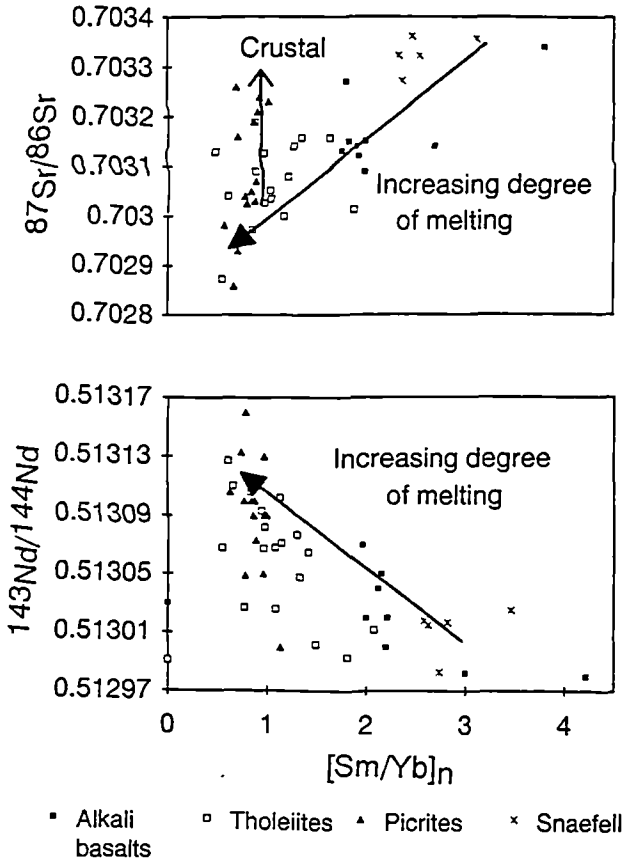

Fig. 3. (a) $^{87}Sr/^{86}Sr$ v. $[Sm/Yb]_n$ showing a fairly clear positive correlation, although some scatter may be due to crustal contamination (as indicated). (b). $^{143}Nd/^{144}Nd$ v. $[Sm/Yb]_n$. Data sources as in Fig. 1.

correlate positively with other measures of relative source enrichment, such as incompatible trace-element abundances and ratios, while similar negative correlations occur with $^{143}Nd/^{144}Nd$. Perhaps more significantly, there appear to be similar correlations (Fig. 3), with the degree of mantle partial melting (increasing from alkali basalts to tholeiites) inferred from $[Sm/Yb]_n$. The source region of the Icelandic volcanic suites must therefore be heterogeneous, a conclusion reached by several previous authors (Zindler *et al.* 1979; Elliott *et al.* 1991; Hémond *et al.* 1993). There must be at least two components, a less-refractory one that is relatively geochemically undepleted and fusible, and which would therefore dominate the initial melts (to produce the alkali basalts) and one that is depleted (relative to estimates of bulk earth). During progressive decompression fusion, melts from this more-refractory component should dilute the early enriched liquids to form the tholeiites. The picrites in this model would result from a second phase of decompression melting, after the extraction of the basaltic magmas. Their relatively depleted isotopic systematics approach those of the depleted component (Sobolev *et al.* 1994; Slater *et al.* 1994), but it is beyond the scope of this paper to explore this matter further.

Origins of source heterogeneity

There are two possible origins of the observed source heterogeneity in Icelandic magmatism, either mixing occurs between the Iceland plume and local upper mantle (MORB-source) or the plume itself is heterogeneous; or a indeed a combination of the two. The following discussion will explore these options.

It has been accepted for some time that mixing between MORB-source mantle and the Iceland plume (or melts of both) occurs along the Reykjanes Ridge (Schilling 1973; Sun *et al.* 1975; Schilling *et al.* 1983). The same model has also been proposed to account for geochemical variations within Iceland (Schilling 1973; Langmuir *et al.* 1978; Elliott *et al.* 1991). To evaluate the feasibility of this hypothesis, the thermal structure and scale of the Iceland plume must be taken into consideration. General features of steady-state plumes are listed by White & McKenzie (1989):

(1) they consist of narrow (150–200 km wide) columnar upwellings;
(2) the convected material spreads to form a mushroom head some 100–200 °C above ambient mantle temperature;
(3) the lateral extent of the hot asthenosphere in the head is 1000–2000 km;
(4) the convecting mantle in the hotspot causes dynamic uplift, reaching a maximum of 1000–2000 m height.

The Iceland plume fits this general model fairly well. Seismic studies point to a low-velocity columnar structure with a diameter of around 175 km at depths >175 km beneath Iceland (Ryan 1990). The swell associated with the plume has a diameter of 2000 km, with a maximum residual depth anomaly of *c.* 2000 m at its centre (White & McKenzie 1989). From this it would appear that the whole of Iceland is underlain by plume-derived material alone, so that petrogenetic models requiring MORB-source (upper) mantle beneath this region must be considered with caution.

Vigorous convection in the mushroom head of the plume would potentially result in entrainment of surrounding mantle and prevent a ponding of plume-derived material, but indications from the study of mid-plate mantle plumes are that such convection is sluggish (Sleep 1994). It would therefore appear that any entrainment that takes place must do so as the plume material rises up from the deep mantle in the narrow conduit.

Modelling by Hauri *et al.* (1994) of vertical, steady-state mantle plume conduits (such as the present-day Iceland plume) shows a range of entrainment of <5% to >90% of the surrounding material (mantle). This is driven by radial conduction of heat from the plume axis, which raises the buoyancy and lowers the viscosity of the surrounding material, thus facilitating entrainment; the bulk of which occurs in the *lower* part of the layer traversed. Additionally, further material from the surrounding mantle is dragged up alongside the plume conduit by viscous coupling. This model is independently supported by available Sr–Nd–Pb–He isotopic data from ocean-island basalts (OIBs). These form sublinear arrays converging on a volume characterized by MORB-like $^{87}Sr/^{86}Sr$ and $^{143}Nd/^{144}Nd$, and elevated $^{206}Pb/^{204}Pb$ and $^{3}He/^{4}He$. This common chemical 'component' in oceanic basic magmas was termed 'FOZO' by Hart *et al.* (1992) and appears, from its high $^{3}He/^{4}He$, to have its origins in the lower mantle. If this is the case, it appears that the lower mantle is characterized by long-term geochemical depletion, relative to estimates of bulk-earth composition.

The Iceland data fit this model reasonably well, except that they appear to intersect the global MORB field in

Sr–Nd–Pb isotopic space, thereby implying a significant amount of upper mantle entrainment, in terms of the Hart *et al.* (1992) model. Nevertheless, a plot of $^{207}Pb/^{204}Pb$ against $^{208}Pb/^{204}Pb$ (Fig. 4) would seem to rule this out, since the Iceland data and North Atlantic N-MORB form separate, sub-parallel arrays. It would thus seem that the plume itself is heterogeneous, consisting of: (1) streaks or blobs of relatively enriched material derived from an ancient geochemical source that was isolated from the convecting mantle for a significant amount of time, probably within the core–mantle boundary layer (CMBL); (2) a less-enriched host material dominantly derived from the lower mantle. Component (1) is best represented in the alkali basalts. The origination of the Iceland plume from the CMBL (Campbell & Griffiths 1992) is indicated by the elevated $^{3}He/^{4}He$ ratios (Condomines *et al.* 1983) and by the large heat flux required to support the topographic swell which spans most of the North Atlantic region (Bott 1988).

Comparisons with other hotspot volcanism

The maximum percentage of melting achieved by an upwelling mantle plume is determined by its potential temperature (T_P) and the thickness of the overlying lithospheric 'lid'. In the case of Iceland, the melting interval reaches a maximum in the axial rift zone, where the 'lid' consists of *c.* 20 km of crustal rocks, thus allowing melting to reach 20% (White & McKenzie in press). In the case of other oceanic islands such as Hawaii, where the plume impinges on older and thicker lithosphere (Watson & McKenzie 1991), the melting column is much shorter (Fig. 5). This results in much lower degrees of melting than in Iceland. Where plumes impinge on young or pre-thinned lithosphere, allowing higher degrees of melting to occur (Thompson & Gibson 1991), some of their volcanic products show more depleted (relative to bulk earth) signatures (like the Icelandic picrites). Ocean-basin examples of this are as follows:

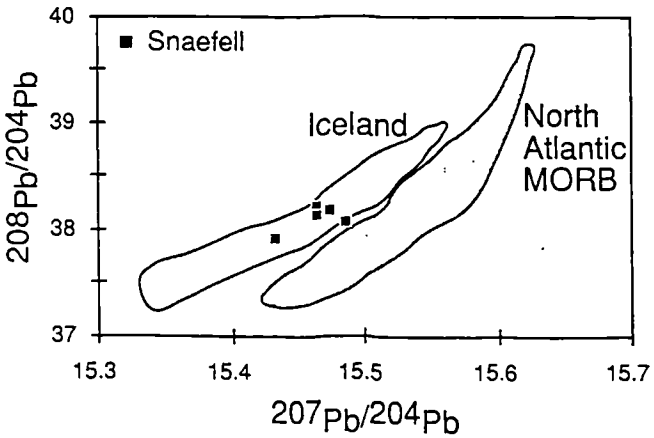

Fig. 4. $^{207}Pb/^{204}Pb$ v. $^{208}Pb/^{204}Pb$ of all available modern data for Iceland (Sun & Jahn 1975; Furman *et al.* 1991; Elliott 1991 and the present study) compared with North Atlantic N-MORB distant from plume influence (Dupré & Allègre 1980; Cohen & O'Nions 1982; Ito *et al.* 1987).

(1) The Galapagos plume, which produced both the elementally/isotopically depleted Cretaceous komatiites on Gorgona, and their spatially associated, less-depleted tholeiites (Aitken & Echeverria 1984). Within the currently active Galapagos archipelago, MORB-like basalts as well as relatively enriched ones can also be found (White *et al.* 1993).

(2) The Marquesas hotspot, the products of which are thought to reflect the mixing of two chemically distinct components. The tholeiites could be derived from a MORB-like source, but the peripheral alkali basalts require a relatively more geochemically and isotopically enriched one (Desonie *et al.* 1993).

Thus it would appear to be a hypothesis worth serious consideration; that all plumes consist of enriched streaks derived from the ultimate plume-source, in a matrix of less-enriched material probably entrained during ascent. The geochemically enriched component in all cases is thought to be from an ancient source, deep in the mantle, the dominant component of which may be recycled (subducted) basaltic oceanic crust (Zindler & Hart 1986). From the reasoning above, it should be clear that the enriched component is best represented in the alkali basalts of oceanic plume-related lava suites. Compared with global OIB data, the Icelandic examples have relatively low $^{87}Sr/^{86}Sr$ and high $^{144}Nd/^{143}Nd$, implying either that the Iceland plume-source material has only been isolated from the convecting mantle for a relatively short time, or that its Rb/Sr and Sm/Nd ratios differ little from those of the MORB source, or both. It is crucially important to remember that Iceland, alone amongst hotspot volcanic centres, both straddles an oceanic spreading centre and is subaerial. Therefore there is no question of invoking contamination of the upwelling plume-derived melts, by either 'enriched' veins within relatively old lithospheric mantle or thick sediments in an old ocean-basin site, as possible sources of the distinctive Nd–Pb isotope variations.

The geochemistry of Reykjanes Ridge magmatism is clear testimony that part of the Iceland plume flux leaks *away sideways within the uppermost convecting mantle.* The north–south isotopic gradients in Reykjanes Ridge basalts (Sun *et al.* 1975; Schilling *et al.* 1983) may, to some extent, reflect systematic early extraction, by subaxial decompression melting, of the more-fusible, relatively enriched streaks within the plume-head mantle, as it flows south. Presumably some of the peripheral mantle upwelling within the Iceland and other plumes avoids decompression fusion entirely and eventually escapes into the convecting upper mantle, making the latter geochemically 'streaky'. Then the model that we have described above, for relating axial picrites and tholeiites to flank alkaline basalts in Iceland, could apply equally well to the axial MORB and flanking OIB small seamounts at 9–14°N on the East Pacific Rise (Zindler *et al.* 1984). Thus our model can reconcile their observations with current views about the nature and sources of mantle plumes.

Conclusions

There is considerable variation in isotopic and incompatible trace-element composition within the Icelandic basic volcanics. The variations clearly correlate with differences in rock type (picrite-tholeiite-alkali basalt) and can best be explained by the existence of two distinct source regions and

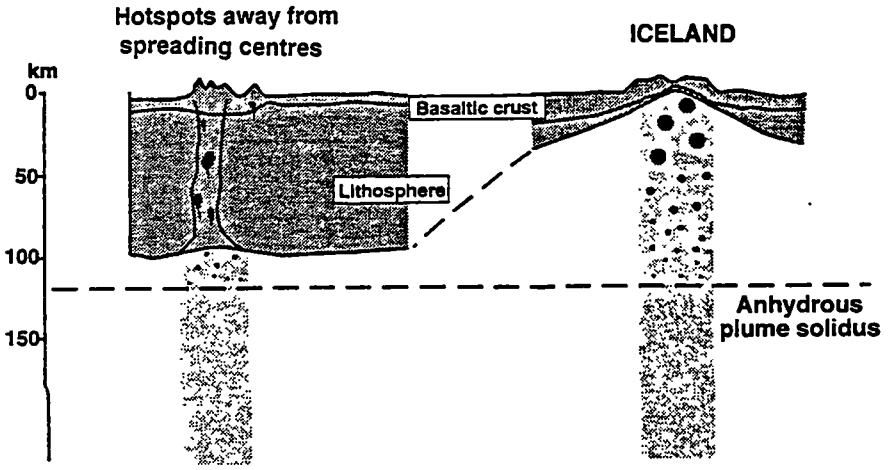

Fig. 5. Schematic diagram of the upwelling mantle plumes, comparing the Iceland plume with plumes that impinge on older, thicker lithosphere, shown here with the maximum thickness attained by oceanic lithosphere. The darker circles represent the increasing amounts of melting as the plume ascends. This shows that, for a given potential temperature, the 'melting column' beneath Iceland is much longer and therefore that much higher degrees of melting can be attained.

mixing between them, or melts derived from them. We deduce that the alkaline volcanism appears to be dominated by the more geochemically enriched component. We support the view that this has its origins deep in the mantle, where it has been isolated from the convecting mantle for sufficient time to evolve characteristic isotope systematics. The 'depleted' component, on the other hand, predominates in the picrite magmas and was probably derived from the convecting lower mantle, having being entrained by thermal conduction as the plume rose. Therefore this 'heterogeneity' should be present in all mantle plumes, but will only become obvious in those where lithospheric mantle (± crust) input is negligible, (e.g. at or near oceanic spreading centres) and where a sufficiently high degree of melting is attained axially, so that the more-enriched components are diluted. It follows from our conclusions that attempts to model basic magma genesis by inverting geochemical data, in relation to postulated single mantle compositions, may need further refinement.

The fieldwork in Iceland benefited greatly from the cooperation and assistance of S. P. Jakobsson, K. Saemundsson, K. Grönvold and N. Oskarsson. Our thanks must also go to A. C. Kerr and C. H. Emeleus for their encouragement and constructive criticisms of this manuscript during preparation; also to A. D. Saunders and J. G. Fitton for their thoughtful reviews. This work was supported in part by NERC, studentship GT4/92/145 to V.L.H. This paper represents NIGL publication series No. 123.

References

Aitken, B. G. & Echeverría, L. M. 1984. Petrology and geochemistry of komatiites and tholeiites from Gorgona island, Colombia. *Contributions to Mineralogy and Petrology*, **86**, 94–105.

Bott, M. H. P. 1988. A new look at the causes and consequences of the Iceland hot-spot. *In:* Morton, A. C. & Parson, L. M. (eds) *Early Tertiary Volcanism and the opening of the NE Atlantic.* Geological Society London, Special Publications, **39**, 15–23.

Campbell, I. H. & Griffiths, R. W. 1992. The changing nature of mantle hotspots through time: implications for the chemical evolution of the mantle. *Journal of Geology*, **92**, 497–523.

Cohen, R. S. & O'Nions, R. K. 1982. The Pb, Nd and Sr isotopic structure of ocean ridge basalts. *Journal of Petrology*, **23**, 299–324.

Condomines, M., Grönvold, K., Hooker, P. J., Muehlenbachs, K., O'Nions, R. K., Oskarsson, N. & Oxburgh, E. R. 1983. He, O, Sr and Nd isotopic relationships in Icelandic volcanics. *Earth Science and Planetary Letters*, **66**, 125–136.

Courtney, R. C. & White, R. S. 1986. Anomalous heat flow and geoid across the Cape Verde rise: evidence for dynamic support from a thermal plume in the mantle. *Geophysical Journal of the Royal Astrological Society*, **87**, 815–867.

Desonie, D. L., Duncan, R. A. & Natland, J. H. 1993. Temporal and geochemical variability of volcanic products of the Marquesas Hotspot. *Journal of Geophysical Research*, **98**, 17 649–17 665.

Dupré, B. & Allègre, C. J. 1980. Pb-Sr-Nd isotopic correlation and the chemistry of the North Atlantic Mantle. *Nature*, **286**, 17–22.

Elliott, T. R. 1991. *Element fractionation in the petrogenesis of ocean island basalts.* PhD Thesis, The Open University.

——, Hawkesworth, C. J. & Grönvold, K. 1991. Dynamic melting of the Iceland Plume. *Nature*, **351**, 201–206.

Furman, T., Frey, F. A. & Park, K.-H. 1991. Chemical constraints on the petrogenesis of mildly alkaline lavas from Vestmannaeyjar, Iceland: the Eldfell (1973) and Surtsey (1963-1967) eruptions. *Contributions to Mineralogy and Petrology*, **109**, 19–37.

Hart, S. R., Hauri, E. H., Oschmann, L. A. & Whitehead, J. A. 1992. Mantle plumes and entrainment: isotopic evidence. *Science*, **256**, 517–520.

Hauri, E. H., Whitehead, J. A. & Hart, S. R. 1994. Fluid dynamics and geochemical aspects of entrainment in mantle plumes. *Journal of Geophysical Research*, **99**, 24 275–24 300.

Hémond, C., Arndt, N. T., Lichtenstein, U. & Hofmann, A. W. 1993. The heterogeneous Iceland Plume: Nd-Sr-O Isotopes and trace element constraints. *Journal of Geophysical Research*, **98**, 15 833–15 850.

Ito, E., White, W. M. & Göpel, C. 1987. The O, Sr, Nd & Pb isotope geochemistry of MORB. *Chemical Geology*, **62**, 157–176.

Jakobsson, S. P. 1972. Chemistry and distribution pattern of recent basaltic rocks in Iceland. *Lithos*, **5**, 365–385.

Kostopoulos, D. K. & James, S. D. 1992. Parameterization of the melting regime of the shallow upper mantle and the effects of variable lithospheric stretching on mantle modal stratification and trace element concentration in magmas. *Journal of Petrology*, **33**, 665–691.

Langmuir, C. H., Vocke, R. D. Hanson, G. N. & Hart, S. 1978. A general mixing equation with application to Icelandic basalts. *Earth Science and Planetary Letters*, **37**, 380–392.

Meyer, P. S., Sigurdsson, H. & Schilling, J.-G. 1985. Petrological and geochemical variations along Iceland's volcanic zones. *Journal of Geophysical Research*, **90**, 10 043–10 072.

Nicholson, H., Condomines, M., Fitton, J. G., Fallick, A. E., Grönvold, K. & Rogers, G. 1991. Geochemical and isotopic evidence for crustal assimilation beneath Krafla, Iceland. *Journal of Petrology*, **32**, 1005–1020.

Oskarsson, N., Steinthorsson, S. & Sigvaldason, G. E. 1985. Iceland geochemical anomaly: volcanotectonics, chemical fractionation and evolution of the crust. *Journal of Geophysical Research*, **90**, 10 011–10 025.

Ryan, M. P. 1990. The physical nature of the Icelandic magma transport system. *In:* Ryan M. P. (ed.) *Magma Transport and Storage*, 175–220.

Saemundsson, K. 1979. Outline of the geology of Iceland. *Jokull*, **29**, 7–28.

Schilling, J.-G. 1973. Iceland mantle plume: geochemical study of the Reykjanes Ridge. *Nature*, **242**, 565–571.

——, Zajac, M., Evans, R., Johnston, T., White, W., Devine, J. D. & Kingsley, R. 1983. Petrologic and geochemical variations along the Mid-Atlantic Ridge from 29°N to 73°N. *American Journal of Science*, **283**, 510–586.

Shaw, D. M. 1970. Trace element fractionation during anatexis. *Journal of Petrology*, **34**, 237–243.

SLATER, L., GRÖNVOLD, K., SHIMIZU, N. & MCKENZIE, D. 1994. Melting beneath the Theistareykir region, NE Iceland. *Mineralogical Magazine*, **58A**, 848–849.

SLEEP, N. H. 1994. Lithospheric thinning by midplate mantle plumes and the thermal history of hot plume material ponded at sublithospheric depths. *Journal of Geophysical Research*, **99**, 9 327–9 343.

SOBOLEV, A. V., GURENKO, A. A. & SHIMIZU, N. 1994. Ultra-depleted melts from Iceland: data from melt inclusion studies. *Mineralogical Magazine*, **58A**, 860–861.

STEINTHORSSON, S., OSKARSSON, N. & SIGVALDASON, G. E. 1985. Origin of alkali basalts in Iceland: a plate tectonic model. *Journal of Geophysical Research*, **90**, 10 027–10 042.

SUN, S.-s. & JAHN, B.-M. 1975. Pb and Sr isotopes in post-glacial basalts from Iceland, *Nature*, **255**, 527–530.

—— & MCDONOUGH, W. F. 1989. Chemical and isotopic systematics of oceanic basalts: implications for mantle composition and processes. *In:* SAUNDERS, A. D. & NORRY, M. J. (eds) *Magmatism in the Ocean Basins. Geological Society, London, Special Publications*, **42**, 313–345.

——, TATSUMOTO, M. & SCHILLING, J.-G. 1975. Mantle plume mixing along the Reykjanes Ridge. *Science*, **190**, 143–147.

THOMPSON, R. N. &. GIBSON S. A. 1991 Subcontinental mantle plumes, hot spots and pre-existing thinspots. *Journal of the Geological Society, London*, **148**, 973–977.

TRYGGVASSON, K., HUSEBYE, E. S. & STEFANSSON, R. 1983. Seismic image of the Iceland hotspot. *Tectonophysics*, **100**, 97–118.

WATSON, S. & MCKENZIE, D. 1991. Melt generation by plumes: a study of Hawaiian volcanism. *Journal of Petrology*, **32**, 501–537.

WEAVER, B. L. 1991. The origin of ocean island basalt end-member compositions: trace element and isotopic constraints. *Earth Science and Planetary Letters*, **104**, 381–397.

WHITE, R. S. & MCKENZIE, D. 1989. Magmatism at rift zones: the generation of volcanic continental margins and flood basalts. *Journal of Geophysical Research*, **94**, 7 685–7 729.

—— & ——. Mantle plumes and flood basalts. *Journal of Geophysical Research*, in press.

WHITE, W. M., MCBIRNEY, A. R. & DUNCAN, R. A. 1993. Petrology and geochemistry of the Galapagos islands: portrait of a pathological mantle plume. *Journal of Geophysical Research*, **98**, 19 533–19 563.

ZINDLER, A. & HART, S. 1986. Chemical geodynamics. *Annual Review of Earth and Planetary Sciences*, **14**, 493–571.

——, FREY, F. A. & JAKOBSSON, S. P. 1979. Nd and Sr Isotope ratios and rare earth element abundances in Reykjanes peninsula basalts: evidence for mantle heterogeneity beneath Iceland. *Earth Science and Planetary Letters*, **45**, 249–262.

——, STAUDIGEL, H. & BATIZA, R. 1984. Isotope and trace element geochemistry of young Pacific seamounts: implications for the scale of upper mantle heterogeneity. *Earth and Planetary Science Letters*, **70**, 175–195.

Received 24 September 1994; revised typescript accepted 1 February 1995.

Depleted mantle plume geochemical signatures: No paradox for plume theories

Andrew C. Kerr
Andrew D. Saunders
John Tarney
Neil H. Berry
Department of Geology, University of Leicester, University Road, Leicester, LE1 7RH, UK

Victoria L. Hards
Department of Geological Sciences, University of Durham, South Rd. Durham, DH1 3LE, UK

ABSTRACT

High-MgO liquids erupted in ocean island settings and in some continental flood basalt provinces commonly preserve a 'depleted' composition, in terms of both highly incompatible trace elements and isotope ratios. These observations strongly imply that their source is also compositionally depleted. However, in at least one case (Iceland and the North Atlantic volcanic province) it can be shown that this depleted source is not the same as that feeding the present-day North Atlantic mid-ocean ridge. It must also have been much hotter than the mid-ocean ridge basalt (MORB) source, to account for the volume of melt and primitive composition of some magmas that were generated. This depleted character, then, is an intrinsic component of mantle plumes, originating from the deep mantle. We propose that mantle plumes consist of a mixture of enriched or fusible streaks in a depleted, refractory matrix; preferential extraction of the enriched component occurs close to the plume axis. The depleted residue from this melting remains in the upper mantle and may therefore be a major contributor to the source region of MORB.

INTRODUCTION

It is widely accepted in the geochemical literature that thermally buoyant mantle plumes which rise from a boundary layer within the mantle (e.g., White and McKenzie, 1989; Campbell and Griffiths, 1990) have trace element contents and Sr-Nd isotope signatures that are enriched relative to the source region of mid-ocean ridge basalt (MORB). It is observed that the decompression melt products of these plumes are commonly more enriched in incompatible trace elements and have Sr-Nd and Pb isotope ratios distinct from those of MORB. As a result, several chemically distinctive enriched[1] plume components have been postulated in order to explain the geochemical signatures of intraplate oceanic basalts (e.g. White 1985; Zindler and Hart, 1986; Weaver, 1991). One additional component, depleted MORB mantle, is generally regarded to be the source of MORB.

In this paper we challenge the assumption that all plumes are enriched (cf. Anderson 1994), and we present evidence that strongly supports the existence of plumes having substantial depleted component(s). These melt to produce magmas with compositional similarities to normal (N-type) MORB. We review the possible origins of this depleted endmember and probable mechanisms for its incorporation into an upwelling plume. Anderson (1994) suggested that the existence of depleted mantle plume signatures "is a major paradox for plume theories"; however, we show that this is not the case and that depleted plume geochemical signatures are entirely explicable within the framework of conventional plume models.

---

[1] In the remainder of the paper the terms "enriched" and "depleted" are relative to bulk earth, in terms of trace element contents and isotopic ratios.

DEPLETED MANTLE IN OCEANIC PLUME SOURCES

The Icelandic mantle plume has been producing basaltic melts for the past 63 m.y. (White 1988) and possibly longer (Lawver and Müller 1994). Today this plume impinges on the base of the lithosphere below the mid-Atlantic Ridge. Two main magma types are found on Iceland; on-axis tholeiites and picrites that erupt above relatively thin lithosphere, and off-axis alkalic basalts that form below thicker lithosphere (Hémond et al., 1993; Hards et al., 1995). The tholeiites and picrites are generally much more depleted ($La_N/Sm_N < 1$ and $\varepsilon_{Nd} > +7.1$) than the alkalic basalts ($La_N/Sm_N > 1$ and $\varepsilon_{Nd} < +7.8$; Hémond et al., 1993). Some authors attribute this depletion to the melting of MORB-source asthenosphere that has been entrained into the plume (Schilling et al., 1982; Elliott et al., 1991; Hart et al., 1992). More recently, Hémond et al. (1993) and Hards et al. (1995) showed that there are subtle elemental and isotopic differences between Icelandic volcanics and North Atlantic MORB. Pb isotopes, particularly $^{207}Pb/^{204}Pb$ and $^{208}Pb/^{204}Pb$ ratios (Fig. 1) clearly show these compositional differences (Thirlwall et al., 1994). Although Fig. 1 supports plume-MORB mixing along the Reykjanes Ridge (Schilling, 1973), it also precludes the involvement of any significant volume of local depleted N-type MORB mantle in the source region of Icelandic volcanic rocks, because Icelandic basalts and North Atlantic MORB define two, subparallel arrays. Contamination of N-type MORB basalts with altered Icelandic crust cannot explain this difference in Pb isotope systematics simply because Icelandic crust is too young (Hards et al. 1995). Therefore, it would seem that rather than entrained MORB source mantle, the depleted source region of the Icelandic picrites and olivine tholeiites is an integral part of a heterogeneous plume (Hards et al., 1995).

The late Cretaceous age komatiites and picrites of Gorgona Island, Colombia, have $\varepsilon_{Nd} > 10$ and $La_N/Sm_N << 1$ and are derived from primary magmas with >18% MgO; there is little evidence to suggest that the mantle source region was 'wet' (Kerr et al. 1995). Therefore, Kerr et al. (1995) argued that the depleted source of the Gorgona ultramafic lavas was much too hot to represent ambient upper (= MORB source) mantle. They propose that the plume responsible for the magmatism on Gorgona was itself markedly heterogeneous, containing both depleted and more enriched components.

Many of the lavas erupted on Hawaii have enriched trace element signatures and radiogenic isotope ratios. Nevertheless, various authors have noted that despite their origin in a hot mantle plume, a significant number of Hawaiian basalts have been derived from a relatively depleted source region (Budahn and Schmitt, 1985; Stille et al., 1986). It has been proposed that this depletion could be due to interaction of plume melts with depleted MORB-like lithosphere (e.g. Stille et al., 1986).

CONTINENTAL FLOOD BASALT PROVINCES

Although many lavas erupted in continental settings are contaminated by lithospheric material, most flood basalt provinces appear to have a few relatively uncontaminated lavas, which enable us to get some idea of the composition of the plume end member. MacDougall (1988) has noted that the radiogenic isotope signatures of many continental flood basalt (CFB) provinces show that at least one component in their source region has a long-term history of depletion.

The 250 Ma lavas of the Siberian Traps represent one of the largest outpourings of continental flood basalt during the Phanerozoic. Picrites with depleted signatures (ε_{Nd} +4 to +7.3 and $La_N/Sm_N < 1.3$: (Lightfoot et al., 1993) are found near the base of the succession. In contrast, the lowest ε_{Nd} so far reported from the basalts is +2 (Lightfoot et al., 1993). These observations strongly suggest that the picrites were derived from within the hot upwelling plume, and that this source contained a depleted component.

Within the early Tertiary Deccan CFB province, the lavas of the Ambenali Formation are generally regarded as being the least contaminated by lithospheric crust or mantle (maximum ε_{Nd} of +7.1; Mahoney, 1988). However, Mahoney (1988) showed that the Ambenali basalts, despite their depleted Nd isotope ratios, have $^{208}Pb/^{204}Pb$ and $^{207}Pb/^{204}Pb$ ratios that rule out a melt input from both Indian Ocean MORB source mantle and the present day Reunion plume.

The early Jurassic Karoo, South Africa, CFB province also contains examples of relatively depleted, plume-related, lavas and dikes. MORB-like dolerite dikes have been found at Rooi Rand, South Africa (ε_{Nd} up to +4; Duncan et al., 1990). Ellam and Cox (1991) proposed that the enriched picritic basalts from Nuanetsi were mixtures of enriched small melt fractions from the lithospheric mantle and a plume component with a depleted MORB-like composition ($\varepsilon_{Nd} = +10$).

The early Tertiary North Atlantic province is believed to result from decompression melting associated with the initial arrival of the head of the Icelandic plume below the lithosphere at 63 Ma (White, 1988). Kerr (1995) showed, that basalts from throughout the province, that are

uncontaminated with continental lithosphere, have a depleted signature and appear to have been derived from a depleted source region within the plume.

The picrites of West Greenland and Baffin Bay represent some of the most primitive lavas found in the North Atlantic Tertiary province. They are also some of the most depleted, with MORB-like light REE patterns and ε_{Nd} = +7 to +9 (O'Nions and Clarke, 1972; Holm et al., 1993). Holm et al. (1993) proposed that the enriched plume component in these lavas had been diluted by MORB-source mantle, during the ascent of the plume.

Depleted picrites are commonly found at the base of volcanic successions. This can be explained by poorly developed magma chambers in the early stages of volcanism; this will lead to high-MgO melts passing relatively quickly through the crust to be erupted as picrites. As the volcanic system evolves, more magma chambers will develop, so providing a greater chance for picrites to fractionate and, in the continental realm, become contaminated with (enriched) lithospheric material.

We have attempted to show above that lavas from both currently active plumes and from plume-related CFB provinces display evidence for depleted components in their source region(s). Moreover, it is the most-magnesian lavas within these provinces which display the greatest degree of depletion. This is true of Iceland, Gorgona, the Siberian traps and the North Atlantic Tertiary province. It is also significant that Archean komatiites, arguably the most magnesian lavas erupted in Earth's history, are also relatively depleted, having positive ε_{Nd} values and $La_N/Sm_N << 1$ (Campbell and Griffiths, 1992).

SOURCE OF THE DEPLETED COMPONENT AND ITS INCORPORATION INTO PLUMES

There is a growing acceptance in both the geochemical and geophysical literature that mantle plumes must rise from a boundary layer within Earth's mantle, either the 670 km discontinuity or from just above the core-mantle boundary (D"). Relatively high levels of primordial ^3He, in comparison to MORB, and the inferred mantle potential temperatures (up to 200 °C hotter than ambient upper mantle) suggest that at least some of the most vigorous present-day plumes (e.g., Iceland and Hawaii) must have a hot, deep, mantle source region (Davies and Richards 1992).

There are several possible models to explain where plumes acquire these depleted components:

1. Entrainment of MORB-source upper mantle. Although, as noted above, Pb isotopic constraints rule out this possibility for Iceland and the Deccan CFB province, it must be taken into account in any discussion of depleted-plume signatures. Griffiths and Campbell (1990), Hart et al. (1992), and Hauri et al. (1994) have shown that when starting plumes and steady-state plumes rise from the core-mantle boundary, the material entrained into the ascending plume head will be predominantly from the lower rather than the upper mantle. Richards and Griffiths (1989) have shown that significant entrainment of upper mantle material can occur when the plume conduit is deflected horizontally by larger than usual shear flow velocities in the upper mantle. It is also important to remember that smaller amounts of melt will be generated in the entrained mantle, relative to the rising plume. Even though the hot plume has the potential to heat up significant volumes of MORB-source mantle around its margins, this plume-heated upper mantle will not be as hot as the plume itself, and so at comparable pressures, will undergo only small-scale decompression melting. Although a possible explanation, this model does not explain why the hottest magmas erupted during plume-related volcanism are also the most depleted and why they sometimes have high $^3He/^4He$ ratios.

On the basis of evidence from Sr-Nd isotopes and rare earth elements, Anderson (1994) proposed that depleted picrites and komatiites come from the same depleted reservoir as MORB. He further suggested that melts from this depleted MORB-source could be contaminated with "shallow-level" enriched mantle to produce enriched plume signatures. However, both high ^3He signatures and the excess mantle heat required to produce high MgO (>15 wt%) magmas pose fundamental problems for Anderson's model. Hart et al. (1992) also showed that ocean island basalts have Sr-Nd-He-^{206}Pb isotopic systematics which, on the whole, do not require a significant input from MORB-source asthenosphere. Additionally, as noted above, the ^{207}Pb-^{208}Pb systematics of Icelandic (Fig. 1) and Deccan basalts (Mahoney 1988) rule out any contribution to their melts from MORB-source upper mantle.

2. Entrainment of depleted material from the lower mantle. We have already noted that the heat and the chemistry of most depleted, plume related lavas require a deeper source than the upper

mantle. Griffiths and Campbell (1990) and Hauri et al. (1994) suggested that plumes rising from the core-mantle boundary have the potential to entrain lower mantle material. The lower mantle thus represents a possible reservoir of this depleted mantle. Recent studies of diamond inclusions also lend support to the idea of the lower mantle containing substantial depleted components (Kesson and Fitzgerald, 1991).

3. Depletion in the mantle source. The plume source region could itself contain a depleted component as well as an enriched component. This source region could be the 670 km discontinuity, but for larger, high $^{3}He/^{4}He$, more powerful plumes, it is more likely that the source region is D". In the latter case D" can provide both the necessary heat and possibly ^{3}He, from degassing of the core. ^{3}He can also be derived from primitive undegassed lower mantle.

DISCUSSION

Thus far we have sought to show only that depleted plume signatures exist and that this depletion is not primarily caused by the incorporation of MORB-source mantle into the plume. We now turn to the ultimate origin of the depleted plume component(s). It has been proposed by several authors (Hofmann and White, 1982; White 1985; Zindler and Hart, 1986; Weaver, 1991) that the source region of mantle plumes (probably at the D" layer) is fed by subducted oceanic crust, with variable amounts of subducted abyssal or continental sedimentary material to account for the EM1 and EM2 signatures. The lower oceanic lithosphere consists of cumulate rocks and residues from melting which would be more trace element-depleted than the oceanic crust (Saunders et al., 1988). It has been suggested that this oceanic lithosphere separates from the overlying crust as the slab passes through the mantle (Hofmann and White, 1982; Weaver, 1991). However, if more depleted, refractory oceanic lithosphere is also transported down to the lower mantle, then this provides a possible explanation of how plumes obtain their depleted signatures.

Recent work suggests that some slabs do not pass through the 670 km discontinuity, but instead are deflected and flatten along it (Phipps-Morgan and Shearer, 1993; Tackley et al., 1993). Tackley et al. (1993) proposed that this slab material, which builds up at 670 km depths, eventually becomes gravitationally unstable and "avalanches" into the lower mantle, to accumulate at D". This mechanism also allows depleted oceanic lithospheric mantle to accumulate with the oceanic crust at the 670 km discontinuity, and so also be a part of the avalanche to the lower mantle and D" (Fig. 2).

Thus, all plumes have the potential to contain at least two components; a fertile component composed of oceanic crust and its associated sediments and a depleted component possibly derived from oceanic lithospheric mantle. In the oceanic realm many weaker plumes, and those that do not come up near a ridge, have enriched signatures (e.g., Cape Verde, Reunion, and St. Helena). In contrast, those plumes that impinge on the base of the lithosphere near a ridge (e.g., Iceland), or a lithospheric thin spot (e.g., West Greenland), result in more extensive partial melting. These higher degree melts are more depleted and more MgO-rich than ocean island basalt erupted in an intraplate setting (Fig. 2).

It is possible that the enriched components are dispersed in plumes as more fusible streaks or blobs set in a more depleted, refractory matrix (cf. Zindler et al. 1984; Fitton and James, 1986). Where the base of normal oceanic lithosphere restricts the degree of melting by placing a 'lid' on the melting column of a plume, a significant proportion of the melt will be derived from these more fusible, enriched components. In contrast, where the plume has a high mass/buoyancy flux (e.g., Hawaii), or where the plume comes up at a ridge (e.g., Iceland) higher degrees of melting will result, and the enriched component in the melt becomes progressively diluted by melting of the more depleted, refractory component. The fact that picrites (which are generally regarded as high-degree melts) are commonly the most depleted lavas in both the oceanic and continental realms provides support for this model.

The predominance of depleted lavas in the Archean and more enriched lavas at many present-day hotspots led Campbell and Griffiths (1992) to suggest that the plume source changed from depleted to enriched throughout geologic time. Our model does not, however, require any significant change in the composition of the plume source region with time. Because the correlation between depleted and high MgO (>18 wt.%) lavas extends into the Archean, we suggest that the fundamental factor in determining the nature of the erupted melt from the plume is in fact the degree of partial melting. In the Archean the ambient mantle temperature was most likely hotter than it is now, and so plumes in the past would have undergone more extensive melting than they do today (Campbell and Griffiths, 1990). It is therefore possible that the mantle source region of Archean plumes was similar

in composition to that of today, but more extensive partial melting in the Archean led to formation of relatively abundant high-MgO depleted lavas.

The point made by Anderson (1994) that "hotspots and MORB share a common depleted source" has no more meaning than saying that they both originate in the mantle. We propose that plumes can act as carriers of depleted material from the lower to the upper mantle; this depleted component may be isotopically distinct from the MORB reservoir, suggesting that it has had a distinct long-term history. Mixing into the upper mantle, of the residue left after melting this ancient depleted plume component at hotspots, *may* help to replenish the MORB source. The recognition of different depleted components has profound implications for geochemical mantle models.

ACKNOWLEDGMENTS

Supported by Natural Environment Research Council Grant GR3/8984 to Tarney and Saunders and NERC studentships to Hards and Berry. We thank Bob Thompson for discussions, and Ray Kent, Robert Duncan and an anonymous reviewer for helpful comments.

REFERENCES CITED

Anderson, D. L., 1994, Komatiites and picrites: Evidence that the 'plume' source is depleted: Earth and Planetary Science Letters, v. 128, p. 303-311.

Budahn, J. R., and Schmitt, R. A., 1985, Petrogenetic modelling of Hawaiian tholeiitic basalts: A geochemical approach: Geochimica et Cosmochimica Acta, v. 49, p. 67-87.

Campbell, I. H, and Griffiths, R. W., 1990, Implications of mantle plume structure for the evolution of flood basalts: Earth and Planetary Science Letters, v. 99, p. 79-93.

Campbell, I. H., and Griffiths, R. W., 1992, The changing nature of mantle hotspots through time: implications for the chemical evolution of the mantle: Journal of Geology, v. 92, p. 497-523.

Davies, G. F., and Richards, M. A., 1992, Mantle convection: Journal of Geology, v. 100, p. 151-206.

Duncan, A. R., Armstrong, R. A., Erlank, A. J., Marsh, J. S., and Watkins, R. T., 1990, MORB-related dolerites associated with the final phases of Karoo flood basalt volcanism in southern Africa, in Parker, A., et al., eds., Mafic dykes and emplacement mechanisms: Rotterdam, Netherlands, Balkema, p. 119-129.

Ellam, R. M., and Cox, K. G., 1991, An interpretation of Karoo picrite basalts in terms of interaction between asthenospheric magmas and the mantle lithosphere: Earth and Planetary Science Letters, v. 105, p. 330-342.

Elliott, T. R., Hawkesworth, C. J., and Grønvold, K., 1991, Dynamic melting of the Iceland plume: Nature, v. 351, p. 201-206.

Fitton, J. G. and James, D., 1986, Basic volcanism associated with intraplate linear features: Royal Society of London, Philosophical Transactions, v. A317, p. 253-266.

Griffiths, R. W., and Campbell, I. H., 1990, Stirring and structure in mantle starting plumes: Earth and Planetary Science Letters, v. 99, p. 66-78.

Hards, V. L., Kempton, P. D. and Thompson, R. N., 1995, The heterogeneous Iceland plume: new insights from the alkalic basalts from the Snaefell volcanic centre: Geological Society of London, Journal, v. 152, in press.

Hart, S. R., Hauri, E. H., Oschmann, L. A., and Whitehead, J. A., 1992, Mantle plumes and entrainment: isotopic evidence: Science, v. 256, p. 517-520.

Hauri, E. H., Whitehead, J. A., and Hart, S. R., 1994, Fluid dynamic and geochemical aspects of entrainment in mantle plumes: Journal of Geophysical Research, v. 99, p. 24, 275-24,300.

Hémond, C., Arndt, N. T., Lichtenstein, U., Hofmann, A. W., Oskarsson, N., and Steinthorsson, S., 1993, The heterogeneous Iceland plume; Nd-Sr-O isotopes and trace element constraints: Journal of Geophysical Research, v. 98, p. 15,833-15,850.

Hofmann, A. W., and White, W. M., 1982, Mantle plumes from ancient oceanic crust: Earth and Planetary Science Letters, v. 57, p. 421-436.

Holm, P. M., Gill, R. C., Pedersen, A. K., Larsen, J. G., Hald, N., Nielsen, T. F. D., and Thirlwall, M. F., 1993, The Tertiary picrites of West Greenland: Contributions from 'Icelandic' and other sources: Earth and Planetary Science Letters, v. 115, p. 227-244.

Kerr, A. C., 1995, The melting processes and composition of the North Atlantic (Icelandic) plume; geochemical evidence from the early Tertiary lavas: Geological Society of London, Journal, v. 152, in press.

Kerr, A. C., Marriner, G. F., Arndt, N. T., Tarney, J., Nivia, A., Saunders, A. D., Storey, M. J., and Duncan, R. A., 1995, The petrogenesis of komatiites, picrites and basalts from the Isle of Gorgona, Colombia; new field, petrographic and geochemical constraints: Lithos, in press.

Kesson, S. E. and Fitzgerald, J. D., 1991, Partitioning of MgO, FeO, NiO, MnO and Cr_2O_3 between magnesian silicate perovskite and magnesiowustite: Implications for the origin of inclusions in diamond and the composition of the lower mantle: Earth and Planetary Science Letters, v. 111, p. 229-240.

Lawver, L. A. and Müller, R. D., 1994, The Iceland hotspot track: Geology, v. 22, p. 311-314

Lightfoot, P. C., Hawkesworth, C. J., Hergt, J. M., Naldrett, A. J., Gorbachev, N. S., Fedorenko, V. A., and Doherty, W., 1993, Remobilisation of the continental lithosphere by a mantle plume: Major-, trace-element, and Sr-, Nd-, and Pb-isotopic evidence from picritic and tholeiitic lavas of the Noril'sk District, Siberian Trap, Russia: Contributions to Mineralogy and Petrology, v. 114, p. 171-188.

MacDougall, J. D., 1988, Continental flood basalts and MORB; a brief discussion of similarities and differences in their petrogenesis, in MacDougall, J. D., ed., Continental flood basalts: Dordrecht, Netherlands, Kluwer, p. 331-341.

Mahoney, J. J., 1988, Deccan Traps, in Macdougall, J. D. ed., Continental flood basalts: Dordrecht, Netherlands, Kluwer, p. 151-194.

O'Nions, R. K., and Clarke, D. B., 1972, Comparative trace element geochemistry of Tertiary basalts from Baffin Bay: Earth and Planetary Science Letters, v. 15, p. 436-446.

Phipps-Morgan, J., and Shearer, P. M., 1993, Seismic constraints on mantle flow and topography of the 660-km discontinuity: evidence for whole-mantle convection: Nature, v. 365, p. 506-511.

Richards, M. A., and Griffiths, R. W., 1989, Thermal entrainment by deflected plumes: Nature, v. 342, p. 900-902.

Saunders, A. D., Norry, M. J., and Tarney, J., 1988, Origin of MORB and chemically-depleted mantle reservoirs: trace element constraints, in Menzies, M. A. and Cox, K. G., eds., Oceanic and continental lithosphere: Similarities and differences: Journal of Petrology Special Lithosphere Issue, p. 415-445.

Schilling, J.-G., 1973, Icelandic mantle plume: Geochemical study of the Reykjanes Ridge: Nature, v. 242, p. 565-571.

Schilling, J.-G., Meyer, P. S., and Kingsley, R. H., 1982, Evolution of the Iceland hotspot: Nature, v. 296, p. 313-320.

Stille, P., Unruh, D. M., and Tatsumoto, M., 1986, Pb, Sr, Nd and Hf isotopic constraints on the origin of Hawaiian basalts and evidence for a unique mantle source: Geochimica et Cosmochimica Acta, v. 50, p. 2303-2319.

Sun, S.-s., Tatsumoto, M., and Schilling, J.-G., 1975. Mantle plume mixing along the Reykjanes Ridge axis: lead isotopic evidence: Science, v. 190, p. 13-17.

Thirlwall, M. F., Upton, B. G. J., and Jenkins, C., 1994, Interaction between continental lithosphere and the Iceland plume; Sr-Nd-Pb isotope geochemistry of Tertiary basalts, NE Greenland: Journal of Petrology, v. 35, p. 839-879.

Tackley, P. J., Stevenson, D. J., Glatzmaier, G. A. and Schubert, G., 1993, Effects of an endothermic phase transition at 670 km depth in a spherical model of convection in the Earth's mantle: Nature, v. 361, p. 699-704.

Weaver, B. L., 1991, The origin of ocean island basalt end-member compositions: Trace element and isotopic constraints: Earth and Planetary Science Letters, v. 104, p. 381-397.

White, R. S., 1988, A hot-spot model for the early Tertiary volcanism in the N Atlantic, in Morton, A. C., and Parson, L. M., eds., Early Tertiary volcanism and the opening of the NE Atlantic: Geological Society of London, Special Publication, 39, p. 3-13.

White, R. and McKenzie, D., 1989, Magmatism at rift zones: the generation of volcanic continental margins and flood basalts: Journal of Geophysical Research, v. 94, p. 7,685-7,729.

White, W. M., 1985, Sources of oceanic basalts and mantle evolution: Geology, v. 13, p. 115-118.

Zindler, A., and Hart, S. R., 1986, Chemical geodynamics: Annual Review in Earth and Planetary Sciences, v. 14, p. 493-571.

Zindler, A., Staudigel, H., and Batiza, R., 1984, Isotope and trace element geochemistry of young Pacific seamounts: implications for the scale of upper mantle heterogeneity: Earth and Planetary Science Letters, v. 70, p. 175-195.

Captions for Text-figures for Kerr et al.

Figure 1. $^{207}Pb/^{204}Pb$ vs. $^{208}Pb/^{204}Pb$ showing fields for Icelandic volcanic rocks and North Atlantic normal (N-type) MORB away from the influence transform faults and known mantle plumes. Data sources; Reykjanes Ridge - Sun et al. (1975), and referenced in Hards et al. (1995).

Figure 2. Schematic representation of plume involvement in mantle processes. A: Residual subducted slab accumulates in lower mantle D" layer and B: at 670 km discontinuity. C: Ascending plumes entrain surrounding mantle. D: Plumes impinge beneath thick oceanic lithosphere, generating ocean island basalt small-degree mantle melts, e.g., St. Helena. E: Passive upwelling of convecting upper mantle generates N-type MORB. F: Plume ascending beneath ridge forms oceanic plateau, including some depleted high-degree picritic melts (e.g., Iceland). G: Plume arising beneath rifted "thin-spot" continental lithosphere generates voluminous continental flood basalts with some depleted picritic melts (e.g., West Greenland).

Figure 1.

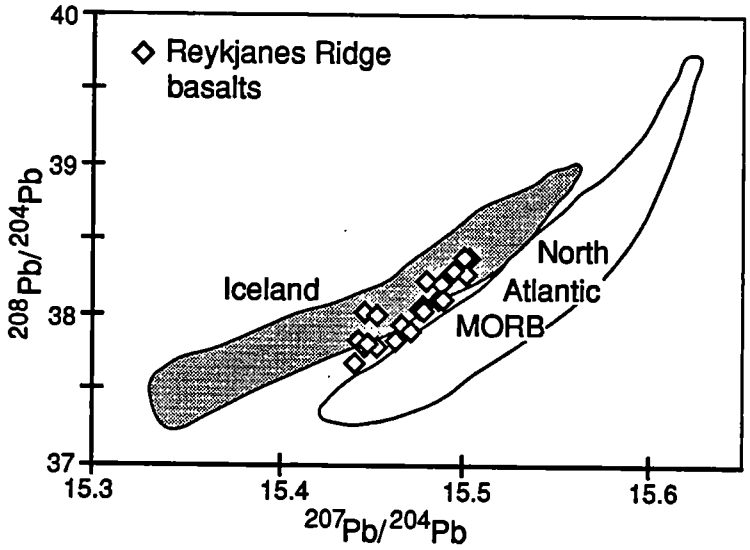

Figure 2.